DFG Deutsche Forschungsgemeinschaft

icdp

IODP INTERNATIONAL OCEAN DISCOVERY PROGRAM

IODP/ICDP Kolloquium 2014

GeoZentrum Nordbayern
17.-19.03.2014

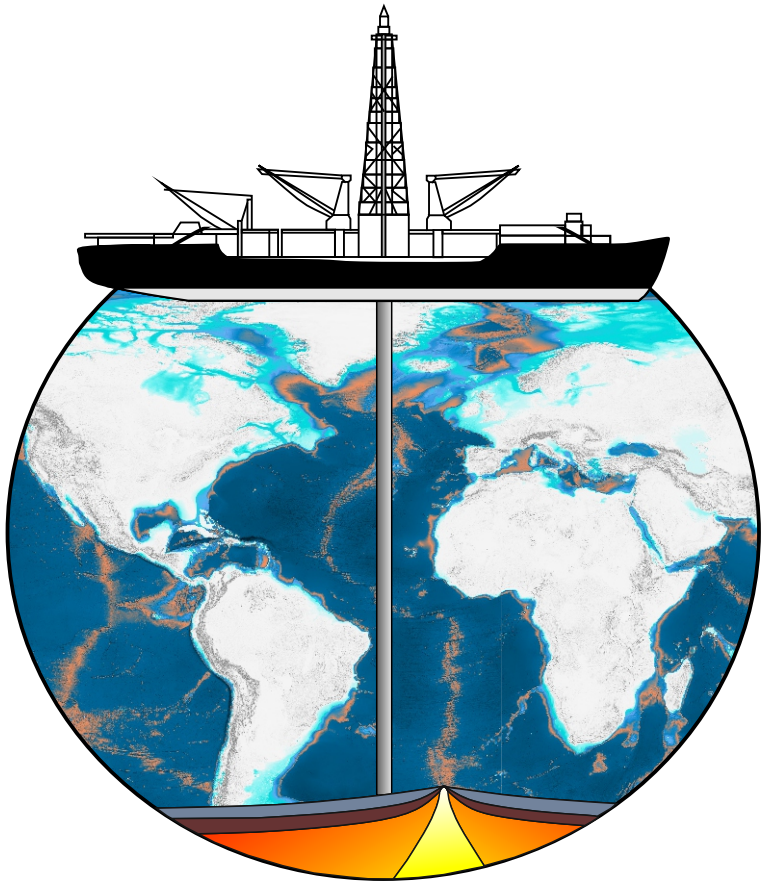

FAU FRIEDRICH-ALEXANDER UNIVERSITÄT ERLANGEN-NÜRNBERG

GeoZentrum Nordbayern

LEG LEHRSTUHL FÜR ENDOGENE GEODYNAMIK


Schloss (Tagungsort)
Alter Simpl
Hauptbahnhof
Brauerei Kitzmann
Goethestraße
Heuwaagstraße
Hauptstraße
Apfelstraße
Orangerie
House Of India
Sax
Da Pippo
Paulistraße
University of Erlangen-Nuremberg
Marktplatz
Schloßplatz
Helmstraße
Gaststätte Grüner Markt
Maalula
Sehzentrum Funk
Universitätsstraße
Trattoria Salento
Pizzeria Carpaccio
Obere Karlstraße
Beitter Friedrich-Wilhelm Dr. Zahnarzt
Untere Karlstraße
Hugenottenplatz
Hugenottenkirche
Bahnhofplatz
Calvinstraße
Erlangen
Bahnhof-Hotel
Weiße Herzstraße
Das neue Teehaus
Friedrichstraße
Fahrstraße
Holzgartenstraße
Frauenarztpraxis Dr. med. Peter Sasse
Neustädter Kirche
Gasthof Strauss
Schuhstraße
Lewandowski Eva
Innere Brucker Straße
Hotel Central
Gasthof
DJH Frankenhof Erlangen

Montag, 17. März 2014

10:00	13:00	**Registrierung**
13:00	13:30	**Begrüßung**
		Aktuelle Bohrungen
13:30	13:50	Alexander Francke **The ICDP SCOPSCO project at Lake Ohrid (Macedonia, Albania)**
13:50	14:10	Heinrich Bahlburg **IODP Expedition 341 Southern Alaska Margin Tectonics, Climate and Sedimentation**
14:10	14:30	Nina Kukowski **Drilling the centre of the Thuringian Basin, Germany, to decipher potential interrelation between shallow and deep fluid systems**
14:30	14:50	Jeroen Groeneveld **IODP Expedition 347 Baltic Sea Paleoenvironment**
14:50	17:00	**Posterpräsentation** **Kaffeepause**
		Paläoozeanographie/Paläoklima/Paläoumwelt
17:00	17:20	Steffen Kutterolf **Tephrochronology of lacustrine ash layers in Lake Petén Itzá sediments: Implications for regional volcanology and Central American palaeoclimate**
17:20	17:40	Antje Völker **Surface and upper Mediterranean Outflow Water signals during the Mid-Pleistocene Transition: the IODP Site U1387 record (Faro Drift)**
17:40	18:00	Marcus Gutjahr **Gulf of Mexico Pb isotopic evidence for temporally elevated deglacial freshwater runoff from the Laurentide Ice Sheet**
ab 19:00		**Gemeinsames Abendessen** **Alter Simpl, Bohlenplatz 2, Erlangen, und** **Kitzmann BräuSchänke, Südl. Stadtmauerstr. 25, Erlangen**

Dienstag, 18. März 2014

		Paläoozeanographie/Paläoklima/Paläoumwelt
9:00	9:20	Stephanie Pabich **´ 44/40Ca isotope fluctuations of the Cenozoic calcium isotope budget and investigations of benthic foraminifer test preservation**
9:20	9:40	Denise Banning **Resolving sedimentary sulfur cycling during the Shunga Event (early Palaeo-proterozoic) with sulfur isotopes**
9:40	10:00	Philipp Rammensee **A multiple isotope and trace element approach to constrain the oxygenation and metal cycling of 3.5 to 3.2 Ga paleo-oceans**
		Neue Projektvorschläge
10:00	10:15	Michael Weber **Late Neogene ice-sheet, ocean, and atmosphere history in the Drake Passage and the Weddell Sea – current drilling proposals within IODP**
10:15	10:30	Frank Preusser **Drilling overdeepened Alpine Valleys (DOVE)**
10:30	10:45	Christian Hübscher **Uncovering a Salt Giant. Deep-Sea Record of Mediterranean Messinian Events (DREAM) multi-phase drilling project**
10:45	12:00	**Posterpräsentation** **Kaffeepause**
		Neues aus den Programmen
12:00	12:20	Roland Oberhänsli **ICDP**
12:20	12:30	Jochen Erbacher & Rüdiger Stein **IODP**
12:30	13:00	Gilbert Camoin **A new ECORD in a new IODP**
13:00	17:00	**Mittagspause & Posterpräsentation**
		Parallel stattfindend:
15:00	16:30	**Geo-Show „unterirdisch“**
		Tiefe Biosphäre
17:00	17:20	Dirk Wagner **Insights into the deep biosphere of the El'gygytgyn Crater Lake**
17:20	17:40	Katja Fichtel **Hydrothermal fluids from the ocean crust support microbial life in deeply buried sediments (IODP Expedition 301)**
17:40	18:00	Bert Engelen **Viruses in subsurface sediments: predator or prey?**
18:00	18:20	Jens Kallmeyer **Putting age into the equation – A new look at microbial distribution in subseafloor sediments**
		Magmatische Petrologie
18:20	18:40	Aurelia Zirner **Experimental approach to form anorthositic melts: phase relations in the system $CaAl_2Si_2O_8$ – $CaMgSi_2O_6$ – Mg_2SiO_4 at 6 wt.% H_2O**
18:40	19:00	Anika Husen **Experimental petrology of the Shatsky Rise ocean plateau basalts**

Mittwoch, 19. März 2014		
Magmatische Petrologie		
08:40	09:00	Martin Oeser-Rabe **Time scales of magma evolution derived from diffusion modeling of Fe-Mg chemical and isotopic zoning in natural olivines**
09:00	09:20	Stefan Dultz **Mechanisms of palagonite formation on subsurface basaltic and rhyolithic glass alteration from ICDP sites Hawaii and Snake River Plain**
09:20	9:40	Tanja Mohr-Westheide **Petrographic and geochemical study of Archean spherule layer occurrences in the BARB 5 ICDP drill core, Barberton Greenstone Belt, South Africa**
9:40	11:30	**Posterpräsentation** **Kaffeepause**
Seismogene Zone		
11:30	11:50	Marco Bohnhoff **Downhole Seismic Monitoring in the Istanbul/Eastern Sea of Marmara Region: Recent Results from the ICDP-GONAF Project**
11:50	12:10	Michael Stipp **Preferred mineral alignment promotes great strength variability in soft sediments from the Nankai accretionary prism offshore SW-Japan**
12:10	12:30	Jan Behrmann **Fast response drilling and instrumentation of the 2011 Tohoku-Oki earthquake fault: a review of present accomplishments of IODP Expeditions 343 and 343T**
12:30	13:00	**Posterprämierungen und Schlussworte**
13:00		**Tagungsende**

Mittwoch, 19. März 2014	
Im Anschluss an das IODP/ICDP Kolloquium:	
13:00	**GESEP School 2014** Initial Drill-Core Processing, Analyses and Archiving “Hands-on introduction to initial core handling and measurements: from drilling rig to core repository”
<u>Ende:</u> Donnerstag, 20. März 2014, 14:30 Uhr	

Teilnehmerliste

Name	Vorname	Institution und Ort
Abratis	Michael	Institut für Geowissenschaften, Friedrich-Schiller-Universität, Jena
Almeev	Renat	Institut für Mineralogie, Leibniz Universität, Hannover
Andreev	Andrej	Institut für Geologie und Mineralogie, Universität Köln
Antz	Benny	Institut für Umweltphysik, Ruprecht-Karls-Universität, Heidelberg
Bahlburg	Heinrich	Institut für Geologie und Paläontologie, Westfälische Wilhelms-Universität, Münster
Bahr	André	Institut für Geowissenschaften, Goethe-Universität, Frankfurt
Banning	Denise	Institut für Geologie und Paläontologie, Westfälische Wilhelms-Universität, Münster
Bauersachs	Thorsten	Institut für Geowissenschaften, Christian-Albrechts-Universität, Kiel
Baumann-Wilke	Maria	Helmholtz-Zentrum Potsdam, Deutsches GeoForschungsZentrum GFZ, Potsdam
Baumgarten	Henrike	Leibniz-Institut für Angewandte Geophysik (LIAG), Hannover
Beermann	Oliver	Institut für Geowissenschaften, Christian-Albrechts-Universität, Kiel
Behrmann	Jan	GEOMAR, Helmholtz-Zentrum für Ozeanforschung, Kiel
Beier	Christoph	GeoZentrum Nordbayern, Friedrich-Alexander-Universität Erlangen-Nürnberg
Betzler	Christian	Institut für Geologie, Universität Hamburg
Bieseler	Bastian	Universität Bremen
Blaser	Patrick	Institut für Umweltphysik, Ruprecht-Karls-Universität, Heidelberg
Blöthe	Marco	BGR, Bundesanstalt für Geowissenschaften und Rohstoffe, Hannover
Böhm	Florian	GEOMAR, Helmholtz-Zentrum für Ozeanforschung, Kiel
Bohnhoff	Marco	Helmholtz-Zentrum Potsdam, Deutsches GeoForschungsZentrum GFZ, Potsdam
Bohrmann	Gerhard	MARUM - Zentrum für Marine Umweltwissenschaften, Universität Bremen
Bornemann	André	Institut für Geophysik und Geologie, Universität Leipzig
Bräuer	Karin	Helmholtz-Zentrum für Umweltforschung UFZ, Halle
Buske	Stefan	Institut für Geophysik und Geoinformatik, Technische Universität Bergakademie Freiberg
Camoin	Gilbert	CEREGE, Aix-en-Provence
Cavaleiro	Catarina	MARUM - Zentrum für Marine Umweltwissenschaften, Universität Bremen
Cohuo	Sergio	Technische Universität Braunschweig
Conze	Ronald	Helmholtz-Zentrum Potsdam, Deutsches GeoForschungsZentrum GFZ, Potsdam
Cukur	Deniz	GEOMAR, Helmholtz-Zentrum für Ozeanforschung, Kiel
Dersch-Hansmann	Michaela	Hessisches Ministerium der Justiz, für Integration und Europa, Wiesbaden
Deutsch	Alex	Institut für Planetologie, Westfälische Wilhelms-Universität, Münster
Diester-Haaß	Liselotte	Zentrum für Umweltforschung, Universität des Saarlandes, Saarbrücken
Drath	Gabriela	IODP, BGR, Bundesanstalt für Geowissenschaften und Rohstoffe, Hannover
Drury	Anna Joy	MARUM - Zentrum für Marine Umweltwissenschaften, Universität Bremen
Dullo	Wolf-Christian	GEOMAR, Helmholtz-Zentrum für Ozeanforschung, Kiel
Dultz	Stefan	Institut für Mineralogie, Leibniz Universität, Hannover
Dupont	Lydie	MARUM - Zentrum für Marine Umweltwissenschaften, Universität Bremen
Eder	Wolfgang	Universität München
Ehmann	Sebastian	Institut für Geophysik und extraterrestrische Physik, Technische Universität Braunschweig
Engelen	Bert	Institut für Chemie und Biologie des Meeres (ICBM), Carl-von-Ossietzky-Universität, Oldenburg
Erbacher	Jochen	IODP, BGR, Bundesanstalt für Geowissenschaften und Rohstoffe, Hannover
Erzinger	Jörg	Helmholtz-Zentrum Potsdam, Deutsches GeoForschungsZentrum GFZ, Potsdam
Faak	Kathrin	Ruhr-Universität, Bochum
Farber	Katja	RWTH, Aachen
Fenner	Juliane	BGR, Bundesanstalt für Geowissenschaften und Rohstoffe, Hannover
Fichtel	Katja	Institut für Chemie und Biologie des Meeres (ICBM), Carl-von-Ossietzky-Universität, Oldenburg
Förster	Verena	Universität Köln
Fraguas	Angela	Institut für Geowissenschaften, Goethe-Universität, Frankfurt
Francke	Alexander	Institut für Geologie und Mineralogie, Universität Köln
Friedrich	Oliver	Institut für Geowissenschaften, Universität Heidelberg
Friese	André	Helmholtz-Zentrum Potsdam, Deutsches GeoForschungsZentrum GFZ, Potsdam
Fritz	Jörg	Museum für Naturkunde, Berlin
Garbe-Schönberg	Dieter	Institut für Geowissenschaften, Christian-Albrechts-Universität, Kiel
García	Ángela	Institut für Erdwissenschaften, Karl-Franzens-Universität, Graz
Geldmacher	Jörg	GEOMAR, Helmholtz-Zentrum für Ozeanforschung, Kiel
Gohl	Karsten	Alfred-Wegener-Institut, Helmholtz-Zentrum für Polar- und Meeresforschung, Bremerhaven
Gose	Jürgen	GeoZentrum Nordbayern, Friedrich-Alexander-Universität Erlangen-Nürnberg
Groeneveld	Jeroen	Universität Bremen
Grunert	Patrick	Institut für Erdwissenschaften, Karl-Franzens-Universität, Graz
Grützner	Jens	Alfred-Wegener-Institut, Helmholtz-Zentrum für Polar- und Meeresforschung, Bremerhaven
Gussone	Nikolaus	Institut für Mineralogie, Westfälische Wilhelms-Universität, Münster
Gutjahr	Marcus	GEOMAR, Helmholtz-Zentrum für Ozeanforschung, Kiel
Haase	Karsten	GeoZentrum Nordbayern, Friedrich-Alexander-Universität Erlangen-Nürnberg
Haberland	Christian	Helmholtz-Zentrum Potsdam, Deutsches GeoForschungsZentrum GFZ, Potsdam
Hallmann	Nadine	CEREGE, Aix-en-Provence
Harms	Ulrich	Helmholtz-Zentrum Potsdam, Deutsches GeoForschungsZentrum GFZ, Potsdam
Hathorne	Ed	GEOMAR, Helmholtz-Zentrum für Ozeanforschung, Kiel
Heide	Klaus	Friedrich-Schiller-Universität, Jena
Herrle	Jens O.	Institut für Geowissenschaften, Goethe-Universität, Frankfurt
Hesse	Reinhard	Earth & Planetary Sciences, McGill University, Montreal
Hesse	Kirsten	GeoZentrum Nordbayern, Friedrich-Alexander-Universität Erlangen-Nürnberg
Heuer	Verena	MARUM - Zentrum für Marine Umweltwissenschaften, Universität Bremen
Hinz	Karl	Verwaltungsunion Hannover
Hofmann	Peter	Institut für Geologie und Mineralogie, Universität Köln
Holtz	François	Institut für Mineralogie, Leibniz Universität, Hannover
Holzheid	Astrid	Institut für Geowissenschaften, Christian-Albrechts-Universität, Kiel
Hübscher	Christian	Universität Hamburg
Husen	Anika	Institut für Mineralogie, Leibniz Universität, Hannover
Jakob	Kim	Institut für Geowissenschaften, Universität Heidelberg
Jehle	Sofie	Institut für Geophysik und Geologie, Universität Leipzig
Jöns	Niels	Universität Bremen
Jung	Gerlinde	MARUM - Zentrum für Marine Umweltwissenschaften, Universität Bremen
Kallmeyer	Jens	Helmholtz-Zentrum Potsdam, Deutsches GeoForschungsZentrum GFZ, Potsdam

Kämpf	Horst	Helmholtz-Zentrum Potsdam, Deutsches GeoForschungsZentrum GFZ, Potsdam
Karas	Cyrus	Institut für Geowissenschaften, Goethe-Universität, Frankfurt
Kollaske	Tina	BGR, Bundesanstalt für Geowissenschaften und Rohstoffe, Berlin
Kotthoff	Ulrich	Institut für Geologie, Universität Hamburg
Krastel	Sebastian	Institut für Geowissenschaften, Christian-Albrechts-Universität, Kiel
Kudraß	Hermann-Rudolf	MARUM - Zentrum für Marine Umweltwissenschaften, Universität Bremen
Kukowski	Nina	Institut für Geowissenschaften, Friedrich-Schiller-Universität, Jena
Kunkel	Cindy	Institut für Geowissenschaften, Friedrich-Schiller-Universität, Jena
Kunze	Sabine	IODP, BGR, Bundesanstalt für Geowissenschaften und Rohstoffe, Hannover
Kurz	Walter	Institut für Erdwissenschaften, Karl-Franzens-Universität, Graz
Kurzawski	Robert	GEOMAR, Helmholtz-Zentrum für Ozeanforschung, Kiel
Kutterolf	Steffen	GEOMAR, Helmholtz-Zentrum für Ozeanforschung, Kiel
Lazarus	David	Museum für Naturkunde, Leibniz-Institut für Evolutions- und Biodiversitätsforschung, Berlin
Lehnert	Oliver	GeoZentrum Nordbayern, Friedrich-Alexander-Universität Erlangen-Nürnberg
Lindhorst	Katja	Institut für Geowissenschaften, Christian-Albrechts-Universität, Kiel
Lippold	Jörg	Institut für Geowissenschaften, Universität Bern
Litt	Thomas	Steinmann-Institut für Geologie, Mineralogie und Paläontologie, Rheinische Friedrich-Wilhelms-Universität, Bonn
Loroch	Dominik	Institut für Mineralogie, Westfälische Wilhelms-Universität, Münster
Lübke	Nathalie	Ruhr-Universität, Bochum
Lückge	Andreas	BGR, Bundesanstalt für Geowissenschaften und Rohstoffe, Hannover
Lüniger	Guido	DFG Deutsche Forschungsgemeinschaft, Bonn
Macario	Laura	Technische Universität Braunschweig
Mangelsdorf	Kai	Helmholtz-Zentrum Potsdam, Deutsches GeoForschungsZentrum GFZ, Potsdam
Maronde	Dietrich	Universität Bonn
März	Christian	School of Civil Engineering and Geosciences (CEGS), Newcastle University
Meister	Patrick	Max-Planck-Institut für Marine Mikrobiologie (MPI), Bremen
Meschede	Martin	Institut für Geographie und Geologie, Ernst-Moritz-Arndt-Universität, Greifswald
Meyers	Philip A.	Department of Earth and Environmental Sciences, University of Michigan
Möbius	Iris	Institut für Geowissenschaften, Universität Heidelberg
Mohr-Westheide	Tanja	Museum für Naturkunde, Berlin
Mollenhauer	Gesine	Alfred-Wegener-Institut, Helmholtz-Zentrum für Polar- und Meeresforschung, Bremerhaven
Montinaro	Alice	Westfälische Wilhelms-Universität, Münster
Mousavi	Sima	Institut für Geophysik und Geologie, Universität Leipzig
Mulch	Andreas	Senckenberg Gesellschaft für Naturforschung, Biodiversität und Klima Forschungszentrum, Frankfurt
Müller	Juliane	Alfred-Wegener-Institut, Helmholtz-Zentrum für Polar- und Meeresforschung, Bremerhaven
Müller	Tim	Institut für Mineralogie, Leibniz Universität, Hannover
Mullick	Nirjhar	Institut für Geophysik und Geoinformatik, Technische Universität Bergakademie Freiberg
Neugebauer	Ina	Helmholtz-Zentrum Potsdam, Deutsches GeoForschungsZentrum GFZ, Potsdam
Neuhaus	Martin	Institut für Geophysik und extraterrestrische Physik, Technische Universität Braunschweig
Nowaczyk	Norbert R.	Helmholtz-Zentrum Potsdam, Deutsches GeoForschungsZentrum GFZ, Potsdam
Nowak	Marcus	Fachbereich Geowissenschaften, Eberhard Karls Universität, Tübingen
Nürnberg	Dirk	GEOMAR, Helmholtz-Zentrum für Ozeanforschung, Kiel
Oberhänsli	Hedwig	Museum für Naturkunde, Leibniz-Institut für Evolutions- und Biodiversitätsforschung, Berlin
Oberhänsli	Roland	ICDP, Universität Potsdam
O'Connor	John	VU Universität Amsterdam
Oeser-Rabe	Martin	Institut für Mineralogie, Leibniz Universität, Hannover
Osborne	Anne H.	GEOMAR, Helmholtz-Zentrum für Ozeanforschung, Kiel
Ostertag-Henning	Christian	BGR, Bundesanstalt für Geowissenschaften und Rohstoffe, Hannover
Pabich	Stephanie	Westfälische Wilhelms-Universität, Münster
Pälike	Heiko	MARUM - Zentrum für Marine Umweltwissenschaften, Universität Bremen
Pickarski	Nadine	Steinmann-Institut für Geologie, Mineralogie und Paläontologie, Rheinische Friedrich-Wilhelms-Universität, Bonn
Piller	Werner	Institut für Erdwissenschaften, Karl-Franzens-Universität, Graz
Preuß	Oliver	Eberhard Karls Universität, Tübingen
Preuß	Franziska	Institut für Chemie und Biologie des Meeres (ICBM), Carl-von-Ossietzky-Universität, Oldenburg
Preusser	Frank	Department for Physical Geography and Quaternary Geology, Stockholm University, Sweden
Pross	Jörg	Institut für Geowissenschaften, Universität Heidelberg
Raddatz	Jacek	GEOMAR, Helmholtz-Zentrum für Ozeanforschung, Kiel
Rammensee	Philipp	Institut für Geowissenschaften, Goethe-Universität, Frankfurt
Rausch	Svenja	Universität Bremen
Regelous	Anette	GeoZentrum Nordbayern, Friedrich-Alexander-Universität Erlangen-Nürnberg
Renaudie	Johan	Museum für Naturkunde, Leibniz-Institut für Evolutions- und Biodiversitätsforschung, Berlin
Röhl	Ursula	MARUM - Zentrum für Marine Umweltwissenschaften, Universität Bremen
Romero	Oscar Enrique	MARUM - Zentrum für Marine Umweltwissenschaften, Universität Bremen
Rüggeberg	Andres	GEOMAR, Helmholtz-Zentrum für Ozeanforschung, Kiel
Sarnthein	Michael	Institut für Geowissenschaften, Christian-Albrechts-Universität, Kiel
Schächinger	Steffen	Institut für Geowissenschaften, Christian-Albrechts-Universität, Kiel
Schindlbeck	Julie C.	GEOMAR, Helmholtz-Zentrum für Ozeanforschung, Kiel
Schippers	Axel	BGR, Bundesanstalt für Geowissenschaften und Rohstoffe, Hannover
Schmädicke	Esther	GeoZentrum Nordbayern, Friedrich-Alexander-Universität Erlangen-Nürnberg
Schmincke	Hans-Ulrich	GEOMAR, Helmholtz-Zentrum für Ozeanforschung, Kiel
Schmitt	Ralf Thomas	Museum für Naturkunde, Berlin
Schneider	Ralph	Institut für Geowissenschaften, Christian-Albrechts-Universität, Kiel
Schwalb	Antje	Institut für Geosysteme und Bioindikation, Technische Universität Braunschweig
Schwenk	Tilmann	Universität Bremen
Simon	Helge	Institut für Geophysik und Geoinformatik, Technische Universität Bergakademie Freiberg
Spiess	Volkhard	Universität Bremen
Stein	Rüdiger	Alfred-Wegener-Institut, Helmholtz-Zentrum für Polar- und Meeresforschung, Bremerhaven
Steinmann	Lena	Universität Bremen
Stipp	Michael	GEOMAR, Helmholtz-Zentrum für Ozeanforschung, Kiel
Strack	Dieter	International Oil & Gas Consultant, Ratingen
Strauß	Harald	Institut für Geologie und Paläontologie, Westfälische Wilhelms-Universität, Münster
Sumita	Mari	GEOMAR, Helmholtz-Zentrum für Ozeanforschung, Kiel
Teichert	Barbara	Institut für Geologie und Paläontologie, Westfälische Wilhelms-Universität, Münster
Thiede	Jörn	GEOMAR, Helmholtz-Zentrum für Ozeanforschung, Kiel
Timmerman	Martin	ICDP, Institut für Erd- und Umweltwissenschaften, Universität Potsdam
Vandieken	Verona	Institut für Chemie und Biologie des Meeres (ICBM), Carl-von-Ossietzky-Universität, Oldenburg

Virgil	Christopher	Institut für Geophysik und extraterrestrische Physik, Technische Universität Braunschweig
Voelker	Antje H. L.	Instituto Português do Mar e da Atmosfera (IPMA), Lissabon
Voigt	Janett	GEOMAR, Helmholtz-Zentrum für Ozeanforschung, Kiel
Vuillemin	Aurèle	Helmholtz-Zentrum Potsdam, Deutsches GeoForschungsZentrum GFZ, Potsdam
Wagner	Thomas	School of Civil Engineering and Geosciences, Newcastle University
Wagner	Bernd	Institut für Geologie und Mineralogie, Universität Köln
Wagner	Dirk	Helmholtz-Zentrum Potsdam, Deutsches GeoForschungsZentrum GFZ, Potsdam
Weber	Michael E.	Institut für Geologie und Mineralogie, Universität Köln
Wefer	Gerold	MARUM - Zentrum für Marine Umweltwissenschaften, Universität Bremen
Wehrmann	Laura M.	GEOMAR, Helmholtz-Zentrum für Ozeanforschung, Kiel
Westerhold	Thomas	MARUM - Zentrum für Marine Umweltwissenschaften, Universität Bremen
Wiersberg	Thomas	Helmholtz-Zentrum Potsdam, Deutsches GeoForschungsZentrum GFZ, Potsdam
Wiesmaier	Sebastian	Department für Geo- und Umweltwissenschaften, Ludwig-Maximilians-Universität, München
Wilke	Sören	Institut für Mineralogie, Leibniz Universität, Hannover
Will	Thomas	Lehrstuhl für Geodynamik & Geomaterialforschung, Universität Würzburg
Wonik	Thomas	Leibniz-Institut für Angewandte Geophysik (LIAG), Hannover
Yirgaw	Daniel G.	GEOMAR, Helmholtz-Zentrum für Ozeanforschung, Kiel
Zhang	Chao	Institut für Mineralogie, Leibniz Universität, Hannover
Zirner	Aurelia	Steinmann-Institut für Geologie, Mineralogie und Paläontologie, Rheinische Friedrich-Wilhelms-Universität, Bonn

AUTOR	TITEL	SPP	SEITE
H. Bahlburg, J. Müller, IODP Expedition 341 Science Party	Expedition Report - IODP Expedition 341 Southern Alaska Margin Tectonics, Climate and Sedimentation	IODP	16
A. Holbourn, M. Saavedra-Pellitero, R. Tada, R.W. Murray, C. Alvarez Zarikian & Expedition 346 Shipboard Scientists	Report from IODP Expedition 346 "Asian Monsoon": Onset and evolution of millennial-scale variability of Asian monsoon and its possible relation with Himalaya and Tibetan Plateau uplift	IODP	17
T. Andrén, B.B. Jorgensen, J. Groeneveld, T. Bauersachs, M. Kenzler, U. Kotthoff, C. Cotterill, D. McInroy, and Exp. 347 Scientists	IODP Expedition 347 – Baltic Sea Paleoenvironment	IODP	19
S.Hammerschmidt, H. Sone and the IODP Expedition 348 Scientists	Report from IODP Expedition 348: Nankai Trough Seismogenic Zone Experiment Stage 3 - Plate Boundary Deep Riser 3	IODP	21
M. Abratis, M. Aehnelt, C. Kunkel, D. Beyer, P. Methe, N. Kukowski, K. U. Totsche	Core processing during the INFLUINS scientific deep drilling campaign, Thuringian Basin, Germany	ICDP	22
M. Abratis, M. Görlitz, T. Wiersberg, N. Kukowski, K. U. Totsche	Online gas monitoring and sampling during drilling of the INFLUINS borehole EF-FB 1/12, Thuringian Basin, Germany	ICDP	22
A.A. Andreev, P.E. Tarasov, V. Wennrich, E. Raschke (Morozova), N.R. Nowaczyk, J. Brigham-Grette, M. Melles	Late Pliocene and Early Pleistocene environments inferred from the Lake El'gygytgyn pollen record	ICDP	23
B. Antz, J. Lippold, H. Schulz, N. Frank, A. Mangini	Comprehensive analysis of Atlantic Circulation during Heinrich-Event 1 & 2	IODP	25
H. Bahlburg, C. März, J. Müller, IODP Expedition 341 Science Party	Expedition Report - IODP Expedition 341 Southern Alaska Margin Tectonics, Climate and Sedimentation	IODP	26
A. Bahr, F. Jimenez-Espejo, N. Kolasinac, P. Grunert, U. Röhl, C. Escutia, J. Hernández-Molina, D.A.V. Stow, D. Hodell, C. Alvarez-Zarikian, IODP Exp. 339 Scientists	Highly variable MOW flow speed during MIS 1-5 inferred from XRF scanning of contourite deposits in the Gulf of Cadiz (IODP Exp. 339)	IODP	27
D. Banning, H. Strauss, V.A.Melezhik, A. Leppland, M.J. Whitehouse	Resolving sedimentary sulfur cycling during the Shunga Event (early Palaeoproterozoic) with sulfur isotopes	ICDP	28
S. Batenburg, S. Voigt, O. Friedrich, M. Frank	Evolution of deep-ocean circulation during the opening of the Atlantic Ocean in the latest Cretaceous and Paleocene	IODP	30
T. Bauersachs, A.S. Jonas, L. Schwark	Climate evolution and terrestrial vegetation changes in the NW Pacific from the Holcene to the late Miocene	IODP	31
M. Baumann-Wilke, Ch. Haberland, M. Stiller, L. Gibert, M. J. Jurado, G. Scott	Seismic reflection profiling of the Baza Basin (Southern Spain) – Preliminary results	ICDP	32

H. Baumgarten,T. Wonik, A. Francke, B. Wagner, K. Lindhorst, S. Krastel and the scopsco science team	First results from downhole logging in the ICDP project SCOPSCO at Lake Ohrid (Macedonia, Albania)	IODP	33
Jan H. Behrmann, Frederick M. Chester, Patrick M. Fulton, Kohtaro Ujiie, Weiren Lin, James J. Mori, Nobuisha Eguchi, Sean Toczko and Expedition 343 and 343T Scientists	Fast response drilling and instrumentation of the 2011 Tohoku-Oki earthquake fault: a review of present accomplishments of IODP Expeditions 343 and 343T	IODP	33
C. Beier , A.R.L. Nichols, P.A. Brandl, S. Krumm	Eruption environments and subsidence of Louisville seamounts	IODP	34
B. Bieseler, N. Jöns, W. Bach	Metasomatic epidote veins, diopsidite and rodingite dikes: witnesses of fluid flow in the history of formation and emplacement of the Oman Ophiolite	ICDP	35
P. Blaser, N. Frank, J. Lippold, E. Böhm	Ocean circulation in transition between glacial and interglacial – measurements of neodymium isotopes on Atlantic IODP/ODP cores.	IODP	36
Marco Blöthe, Anja Breuker and Axel Schippers	Characterization of metabolically active microorganisms in an active hydrothermal field in the Okinawa Trough (IODP Exp. 331)	IODP	37
Marco Bohnhoff, Georg Dresen, Fatih Bulut, Christina Raub, Tugbay Kilic, Recai F. Kartal, Filiz Tuba Kadirioglu, Murat Nurlu, Peter E. Malin , Hisao Ito	Downhole Seismic Monitoring in the Istanbul/Eastern Sea of Marmara Region: Recent Results from the ICDP-GONAF Project	ICDP	37
André Bornemann, Iris Möbius, Oliver Friedrich, Diederik Liebrand, Paul A. Wilson, Expedition 342 Scientists	A new surface-water temperature record for the Oligocene-Miocene Transition from the western North Atlantic (IODP Site U1405	IODP	38
Catarina Cavaleiro, Michael Kucera , Karl-Heinz Baumann, Antje Voelker, Heather Stoll	Coccolithophores paleoproductivity for Marine Isotopic Stages 11 and 12 in the North Atlantic	IODP	38
D. Cukur, S. Krastel, N. Cagatay, D. Winkelmann, and Bathyvan scientific team	New insights into the formation of shallow sedimentary structures in Lake Van, eastern Turkey: A joint analysis of high-resolution seismic and hydroacoustic data	ICDP	39
C. Dullo, A. Rüggeberg, S. Flögel, J. Raddatz	Seawater densities and cold-water coral carbonate mounds in the northeast Atlantic through time	IODP	40
S. Dultz, H. Behrens, C. Dupont and M. Plötze	Mechanisms of palagonite formation on subsurface basaltic and rhyolithic glass alteration from ICDP sites Hawaii and Snake River Plain	ICDP	40
S. Ehmann, A. Hördt, M. Leven, M.Neuhaus, C. Virgil	Bestimmung der Magnetostratigraphie aus Bohrlochmessungen	IODP	42
B. Engelen, T. Engelhardt, J. Kallmeyer, H. Cypionka,	Viruses in subsurface sediments: predator or prey?	IODP	42

K. Faak, K. Gillis and the IODP Expedition 345 Science Party	IODP Expedition 345: Slow cooling of the lowermost gabbroic crust from the fast-spreading East Pacific Rise determined from Mg-in-Pl and Ca-in-Ol geospeedometry	IODP	43
M. Fallahi, M. Korn, C. Sens-Schoenfelder	Investigation and monitoring of seismic velocity change related to earthquake swarms in West Bohemia/Vogtland	ICDP	44
K.Farber, A. Dziggel, F.M. Meyer,W. Prochaska	Fluid inclusion record of chert and quartz vein formation in ultramafic crust of the Mesoarchaean Barberton Greenstone Belt, South Africa	ICDP	44
K. Fichtel, H. Cypionka, B. Engelen	Hydrothermal fluids from the ocean crust support microbial life in deeply buried sediments (IODP Exp. 301)	IODP	46
David Fischer, Gerhard Bohrmann, Thomas Pape, Stephan A. Klapp, Frieder Enzmann, Werner F. Kuhs, Thomas Huthwelker	Sub-millimeter structure and internal architecture of ODP 204 (Hydrate Ridge) gas hydrates revealed by Synchroton Radiation X-Ray Cryo-Tomographic Microscopy	IODP	47
V. Foerster, A. Junginger, R. Vogelsang, A. Asrat,H.F. Lamb, V. Wennrich, M. Weber, J. Rethemeyer, U. Frank,M.C. Brown, M.H. Trauth, and F. Schaebitz	Wet-dry shifts in the source region of modern man: A Late Quaternary climate record from Chew Bahir, southern Ethiopia	ICDP	47
A. Fraguas, J. Zirkel, J.O. Herrle, J. Bollmann, H. Pälike	Calcareous nannofossil response to paleoceanographic changes recorded during the Mid-Oligocene in the Central Eastern Pacific Ocean (Site U1334, IODP Expedition 320)	IODP	48
A. Francke,B. Wagner, K. Lindhorst, H. Baumgarten, S. Krastel, T. Wonik, and the SCOPSCO Science Team	The ICDP SCOPSCO project at Lake Ohrid (Macedonia, Albania)	ICDP	49
O. Friedrich, J. Erbacher, R.D. Norris, B. Beckmann	Long-term evolution of Cenomanian to Campanian black shale formation at Demerara Rise	IODP	51
André Friese, Jens Kallmeyer, Aurèle Vuillemin	Inspecting the biogeochemistry of Lake Towuti surficial sediment: Implications for microbial communities.	ICDP	51
Ángela Garcia Gallardo, Patrick Grunert, Werner E. Piller, Barbara Balestra, Marlies van der Schee, Francisco Sierro Sanchez, José-Abel Flores, Carlos Alvarez-Zarikian, F. Javier Hernández-Molina, Dorrik A.V. Stow, and IODP Expedition 339 Scientists	The impact of Mediterranean Outflow Water on the Pliocene North Atlantic	IODP	52
J. Geldmacher, S. Li, F. Hauff, D. Garbe-Schönberg, S. Yu, S. Zhao, S. Rausch	Composition and timing of carbonate vein precipitation within the igneous basement of the Early Cretaceous Shatsky Rise, NW Pacific	IODP	52
J. Gose, E. Schmädicke, T. M. Will	Contrasting water contents and equilibrium conditions of abyssal peridotite from the Mid-Atlantic Ridge	IODP	53
J. Groeneveld, and Exp. 347 Scientists	Holocene bottom water variability in the Baltic Sea: The impact of atmospheric processes	IODP	54
J. Gruetzner, G. Uenzelmann-Neben	Changes in deep ocean circulation of the South Atlantic inferred from depositional processes at the eastern Agulhas Ridge	IODP	55

Patrick Grunert, David Hodell, Carlos Alvarez-Zarikian, F. Javier Hernández-Molina, Dorrik A.V. Stow, and IODP Expedition 339 Scientists	Impact of paleoceanographic changes at glacial/interglacial transitions on benthic foraminiferal faunas of the eastern North Atlantic (IODP Expedition 339, Site U1385)	IODP	55
N. Gussone, O. Friedrich	Calcareous dinoflagellates as archives for fluctuations in ocean chemistry and temperature changes	IODP	56
M. Gutjahr, A. N. Meckler	Gulf of Mexico Pb isotopic evidence for temporally elevated deglacial freshwater runoff from the Laurentide Ice Sheet	IODP	57
N. Hallmann, G. Camoin, A. Eisenhauer, C. Vella, E. Samankassou, A. Botella, G.A. Milne, J. Fietzke, P. Dussouillez, J. Plaine	Late Holocene sea-level changes in French Polynesia, South-Central Pacific: extending the last deglacial sea-level record from IODP Expedition #310	IODP	58
J.O. Herrle, C.J. Schröder-Adams, D. Selby, A. Du Vivier, S. Flögel, A. McAnena, W. Davis, A. Pugh, J. Galloway, P. Hofmann, T. Wagner	High Arctic and low latitude Atlantic paleoenvironmental and paleoclimatic changes in the Mid-Cretaceous (Axel Heiberg and Ellef Ringnes Island, DSDP Site 545, ODP Sites 1258, 1049)	IODP	58
K. Hesse, E. Schmädicke, J. Gose	Petrological and Geochemical Characterization of Abyssal Peridotites from the East Pacific Rise and Incorporation of Water in Nominally Anhydrous Orthopyroxene (ODP Leg 147: Hess Deep)	IODP	59
V.B. Heuer, S. Xie, M. Bowles, Y.-S. Lin, Y. Morono, F. Inagaki, and K.-U. Hinrichs	Molecular-isotopic studies of microbial processes and organic matter in the subseafloor coalbed biosphere of Shimokita (IODP Exp. 337).	IODP	60
K. Hockun, G. Mollenhauer, E. Schefuß and the Pasado Science Team	PASADO Lipids'- paleoenvironmental reconstruction in Southern Patagonia	ICDP	62
P. Hofmann, T. Wagner, J.O. Herrle, A. McAnena, S. Flögel	Gateway opening of the South Atlantic Ocean: New high resolution insights from the Aptian to Albian Falkland Plateau (DSDP Site 511)	IODP	64
Christian Hübscher, Angelo Camerlenghi, Vanni Aloisi, Johanna Lofi, Gert deLange, Rachel Flecker, Daniel Garcia-Castellanos, Christian Gorini, Zohar Gvirtzman, Wout Krijgsman, Stefano Lugli, Yizhaq Makowsky, Vinicio Manzi, Terry McGenity, Giuliana Panieri, Marina Rabineau, Marco Roveri, Francisco Javier Sierro, and Nicolas Waldmann	Uncovering a Salt Giant. Deep-Sea Record of Mediterranean Messinian Events (DREAM) multi-phase drilling project	IODP	65
A. Husen, R. Almeev, F. Holtz	Experimental petrology of the Shatsky Rise ocean plateau basalts	IODP	66
M. Inoue, N. Gussone, Y. Koga, A. Iwase, A. Suzuki, K. Sakai, H. Kawahata	Controlling factors of Ca isotope fractionation in *Porites* corals evaluated by temperature, pH and light controlling culture experiments	IODP	68
Sofie Jehle, André Bornemann, Arne Deprez, Robert P. Speijer	The impact of the Latest Danian Event on planktic foraminifera faunas at ODP Site 1210 (Shatsky Rise, Pacific Ocean)	IODP	69
G.Jung, M. Prange, M. Schulzlic	Causes of Neogene intensification of the Benguela Upwelling	IODP	71

J. Kallmeyer	Putting age into the equation: A new look at microbial distribution in subseafloor sediments	IODP	72
C. Karas, J.O. Herrle, D. Nürnberg, R. Tiedemann, A. Bahr	Pliocene Atlantic Ocean interhemispheric seesaw and the role of the constrictions of the Panama and the Indonesian seaways	IODP	72
U. Kotthoff, D.R. Greenwood, F.M.G. McCarthy, K. Müller-Navarra, S.P. Hesselbo	Palynomorph-based reconstructions of ecosystem and climate development on the North American Atlantic Coastal Plain between 33 and 13 million years before present	IODP	74
N. Kukowski, K. U. Totsche, M. Abratis, A. Habisreuther, T. Ward and INFLUINS Drilling Team	Drilling the centre of the Thuringian Basin, Germany, to decipher potential interrelation between shallow and deep fluid systems	IODP	75
W. Kurz, P. Vannucchi, Y. Yamamoto, C. Millan	Multiple reverse and normal faulting along the Costa Rica erosive plate boundary – results from IODP Expedition 344 (CRISP 2)	IODP	76
Robert M. Kurzawski, Michael Stipp, André Niemeijer, Jens C. Grimmer, Agnes Kontny, Christopher J. Spiers and Jan H. Behrmann	Magnetic fabrics and frictional behaviour of subduction zone input material from the erosive continental margin offshore Costa Rica (Costa Rica Seismogenesis Project, IODP expeditions 334 and 344)	IODP	77
S. Kutterolf, A. Schwalb	Tephrochronology of lacustrine ash layers in Lake Petén Itzá sediments: Implications for regional volcanology and Central American palaeoclimate	IODP	80
V. Lay, S. Buske, A. Kovacs, A. Gorman, E. Donner	Seismic site characterization for the Deep-Fault-Drilling-Project Alpine Fault	ICDP	81
O. Lehnert, G. Meinhold, U. Berner , M. Ahmed, A. Arslan, M. Calner, J. O. R. Ebbestad	Palaeogeographic setting of Upper Ordovician and Silurian source rocks preserved in the Siljan impact structure (central Sweden)	ICDP	81
K.Lindhorst, S.Krastel, Thomas Wonik , B. Wagner	Correlation of physical properties of sediments and seismic data: first results from the SCOPSCO ICDP campaign	ICDP	84
D. Loroch , A. Deutsch, J. Berndt, A. Bornemann and Expedition 342 Scientists	Geochemical impact evidence and trace element distribution at the K-Pg event bed, J Anomaly Ridge, Newfoundland – IODP Hole U1407B	IODP	85
N. Lübke, J. Mutterlose, C. Bottini	Habitat-dependant size variations of early Aptian coccoliths	IODP	86
L. Macario, S. Cohuo, L. Pérez, S. Kutterolf, A. Schwalb	Effects of Abrupt Climate Change on Ice Age Ecosystem of Lake Petén Itzá, Guatemala and on Distribution Patterns of Ostracodes across the Yucatán Peninsula	ICDP	87
C. März, A.C. Mix, E. McClymont, A. Nakamura, G. Berbel, S.P. Gulick, J.M. Jaeger, L. LeVay, Expedition 341 Scientists	Variations of marine pore water salinity and chlorinity in Gulf of Alaska sediments (IODP Expedition 341)	IODP	88
Patrick Meister, Bo Liu, Arzhang Khalili, Bo Barker Jørgensen	Modelling carbon isotope composition of dissolved inorganic carbon and methane in marine porewaters	IODP	88

P. Methe, A. Goepel, N. Kukowski	Downhole geophysical data from recent deep drilling in the centre of the Thuringian Basin, Germany	ICDP	89
I. Moebius, O. Friedrich, K.M.Edgar, H. Scher, P.F. Sexton	Bottom water changes in the subtropical North Atlantic and the Southern Ocean associated to the Middle Eocene Climatic Optimum	IODP	90
T. Mohr-Westheide, J. Fritz, A. Hofmann, R. Tagle, C. Koeberl, W.U. Reimold, D. Mader, T. Schulz, and D. Hoehnel	Petrographic and geochemical study of archean spherule layer occurrences in the BARB 5 ICDP drill core, Barberton Greenstone Belt, South Africa.	ICDP	92
A. Montinaro, H. Strauss, P. Mason, A. Galic	Peering into the Cradle of Life:multiple sulfur isotopes reveal insights into environmental conditions and early sulfur metabolism some 3.5 Ga ago	ICDP	93
S. Mousavi, M. Korn, K. Bauer	P and S wave tomography of the earthquake swarm area W-Bohemia/Vogtland and the relation between velocity structure and possible fluid migration	ICDP	95
J. Müller, M.L. Sanchez Montes, E. McClymont, R. Stein, K. Fahl, K. MAngelsdorf, H. Wilkes and Expedition 341 Scientists	Biomarker based reconstruction of Plio- and Pleistocene climate and environmental conditions in the Gulf of Alaska: Preliminary results obtained from Expedition 341 sediments	IODP	96
T. Müller, J. Koepke, D.Garbe-Schönberg, H. Strauss	Formation of fast-spreading oceanic crust: Petrological and geochemical investigation of the „Wadi Gideah“ cross section in the Oman ophiolite	ICDP	97
N. Mullick, S. Buske, S. Shapiro, P.Wigger	Reflection seismic investigation of the geodynamically active West-Bohemia/Vogtland region	ICDP	99
I. Neugebauer, A. Brauer, M.J. Schwab, P. Dulski, U. Frank and DSDDP Scientific Party	Interglacial climate variability recorded in the Dead Sea sediments	ICDP	101
John O'Connor, Bernhard Steinberger, Marcel Regelous, Anthony Koppers, Jan Wijbrans Karsten Haase, Peter Stoffers, Wilfried Jokat and C-Dieter Garbe-Schoenberg	Past plate and mantle motion from new ages for the Hawaiian-Emperor Seamount Chain	IODP	103
M. Oeser, S. Weyer, R. Dohmen, I. Horn, S. Schuth	Time scales of magma evolution derived from diffusion modeling of Fe-Mg chemical and isotopic zoning in natural olivines	IODP	104
A. H. Osborne, Derrick R. Newkirk, J. Groeneveld, Ellen E. Martin, Ralf Tiedemann and Martin Frank[1]	The neodymium and lead isotope record of the final stages of Central American Seaway closure	IODP	106
St. Pabich, N. Gussone, K. Rabe, Ch. Vollmer, B.M.A. Teichert	$\delta^{44/40}$Ca isotope fluctuations of the Cenozoic calcium isotope budget and investigations of benthic foraminifer test preservation	IODP	109
N. Pickarski, T. Litt and the Paleovan scientific team	Vegetation and climate history during the last 130 ka BP at Lake Van, Eastern Anatolia (Turkey)	ICDP	111

Frank Preusser, Flavio S. Anselmetti, Milos Bavec, Christian Crouzet, Markus Fiebig, Gerald Gabriel, Cesare Ravazzi, Christoph Spötl	Drilling overdeepened Alpine Valleys (DOVE)	ICDP	112
F. Preuss, T. Engelhardt, BjØrn Steinsbu , H. Cypionka, B. Engelen	Bacteriophages in sediments of the South Pacific Gyre	IODP	113
O. Preuss, M. Nowak, S. Ulmer	Simulation of magma ascent prior to the high-risk caldera forming eruptions of Campi Flegrei using continuous decompression experiments and different starting materials	ICDP	115
J. Raddatz, A. Rüggeberg, S. Flögel,V.Liebetrau, and C. Dullo	Paleo seawater pH dynamics in cold-water corals reefs along the European continental margin	IODP	117
P. Rammensee, I. Horn, S. Weyer, N. J. Beukes, S. Aulbach	A multiple isotope and trace element approach to constrain the oxygenation and metal cycling of 3.5 to 3.2 Ga paleo-oceans	ICDP	118
S. Rausch, W. Bach, A. Klügel	Carbonates and zeolites in seamounts trace seawater-basement interactions: results from IODP Exp330, Louisville Smt. Chain		145
A. Regelous, A. Renno, e.Schmädicke[1], K. Haase	Composition and evolution of the lithospheric mantle below the Eger Rift, Central Europe	ICDP	120
J. Renaudie, D. B. Lazarus	A quantitative review on Cenozoic marine diatom deposition history	IODP	120
A. Rüggeberg, S. Flögel, J. Raddatz, C. Dullo	Density reconstruction of intermediate waters along the European continental margin	IODP	121
S. Schächinger, O. Beermann, D. Garbe-Schönberg, L. Arzi, A. Holzheid	Time resolved alteration of gabbro at high temperature hydrothermal systems at slow-spreading mid ocean ridges: An experimental study	IODP	121
J.C. Schindlbeck, S. Kutterolf, A. Freundt	Miocene to Recent tephrostratigraphy offshore Central America: Evolution, Provenance and Cyclicities	IODP	124
T. Schwenk, H.R. Kudrass, V. Spiess, L. Palamenghi and Proponents	IODP Proposal 823-full: Records of geohazards and monsoonal changes in the northern Bay of Bengal	IODP	127
H. Simon, S. Buske, R. Giese, C. Juhlin, C. Schmelzbach, H. Maurer, J. Robertsson	Seismic site characterization in and around the COSC-1 drillhole	ICDP	127
V. Spiess, H. Keil, I. Sauermilch, Azat Said, K. Abdrakhmatov, C. Gebhardt, H. Oberhänsli	An Airgun Seismic Survey for Preparation/Support of ICDP Drilling at Lake Issyk-Kul, Kyrgyztan - Opportunities for Tectonic and Sedimentary Process Studies	ICDP	128
L. Steinmann, V. Spiess, M. Sacchi	The interplay of volcanic, tectonic and sedimentary processes in the offshore sector of the Campi Flegrei caldera (Gulf of Naples, Italy): Preliminary results of a multi-channel seismic Pre-Site Survey for combined IODP and ICDP drilling campaigns	ICDP	129

Michael Stipp, Kai Schumann, Bernd Leiss, Jan. H. Behrmann, Klaus Ullemeyer	Preferred mineral alignment promotes great strength variability in soft sediments from the Nankai accretionary prism offshore SW-Japan	IODP	130
M. Sumita, H.-U. Schmincke, J. Paleovan Scientific Team	Lake Van tephra: periodicity vs. episodicity, climate control of eruption frequency and seismic eruption triggering	ICDP	131
B.M.A.Teichert, N.Gussone, L.M.Wehrmann, C.März, H.Strauss	Constraining the dynamics of fluid flow and authigenic mineral formation at the northeastern Pacific continental margin – A multiproxy approach	IODP	131
M.J. Timmerman, R. Oberhänsli, U. Altenberger, M. Sudo	$^{40}Ar/^{39}Ar$ mica and amphibole ages for high-grade rocks exhumed along the Alpine Fault, South Island, New Zealand	ICDP	132
V. Vandieken, B. Engelen	Impact of salinity changes on viruses during the paleoenvironmental history ofBaltic Sea sediments	IODP	133
A. H. L. Voelker, A. Bahr, F. J. Jimenez-Espejo, G. D. Acton, U. Röhl	Surface and upper Mediterranean Outflow Water signals during the Mid-Pleistocene Transition: the IODP Site U1387 record (Faro Drift)	IODP	134
J.Voigt, E.C. Hathorne, A. Eisenhauer and H. Pälike	Marine stable Sr record of the last 50 Myrs	IODP	135
A. Vuillemin, D. Ariztegui, P.R. Leavitt, L. Bunting, the PASADO Science Team	Environmental DNA studies applied to the climatic record of Laguna Potrok Aike (Argentina): Examining Holocene and Last Glacial Maximum microbial assemblages.	ICDP	136
D. Wagner, J. Görsch, M. Alawi and the El'gygytgyn Scientific Party	Insights into the deep biosphere of the El'gygytgyn Crater Lake sediments	ICDP	136
M.E. Weber	Late Neogene ice-sheet, ocean, and atmosphere history in the Drake Passage and the Weddell Sea – current drilling proposals within IODP	IODP	137
L.M. Wehrmann, S. Arndt, C. Ockert, P. Meister, B. Brunner, C. März, N. Gussone, B.M.A. Teichert, T. Ferdelman	The evolution of early diagenetic signals in Bering Sea sediments in response to varying organic carbon deposition over the last 4.3 Ma (IODP Exp. 323, Site U1341)	IODP	138
T. Westerhold, U. Röhl, T. Frederichs, S.M. Bohaty, J.C. Zachos	An integrated geochemical and cyclostratigraphic framework for the Eocene South Atlantic Ocean	IODP	139
S. Wiesmaier, D. Morgavi, C. Renggli, D. Perugini, C. De Campos, K.-U. Hess, Y. Lavallée, D. Dingwell	Diffusional equilibration of distinct magmas aided by bubble ascent	ICDP	140
S. Wilke, C. Klahn, D. Mock, R. Almeev, F. Holtz	Effects of Anorthite on the phase relationship in granitic systems: Experimental calibrations for rhyolite geobarometry and application to Snake River Plain rhyolites	ICDP	140
D.G. Yirgaw, E.C. Hathorne, L. Giosan, T.S. Collett , M. Frank	History of the Indian Monsoon recorded in Andaman Sea sediments	IODP	141

C. Zhang, J. Koepke, M. Godard, L. France	Insight into the origins of SiO_2-rich magmas at mid-ocean ridges: Evidence from IODP Hole 1256D at equatorial Pacific	IODP	142
C. Zhang, J. Koepke, C. Kirchner, N. Götze, H. Behrens	Rapid hydrothermal cooling at fast-spreading mid-ocean ridges: Evidence from intra-plagioclase diffusion in the granoblastic dikes of IODP Hole 1256D (equatorial Pacific)	IODP	143
J. Zirkel, J.O. Herrle, H. Pälike, D. Liebrand ,S. Batenburg[1]	Mid-Oligocene climate dynamics using benthic foraminifera from the Central Eastern Pacific Ocean	IODP	144
A. L. K. Zirner, C. Ballhaus, R. Fonseca, C. Müncker	Experimental approach to form anorthositic melts: phase relations in the system $CaAl_2Si_2O_8$ – $CaMgSi_2O_6$ – Mg_2SiO_4 at 6 wt.% H_2O	IODP	145

Fahrtberichte

Expedition Report - IODP Expedition 341 Southern Alaska Margin Tectonics, Climate and Sedimentation

H. BAHLBURG[1], J. MÜLLER[2], IODP EXPEDITION 341 SCIENCE PARTY

[1]Institut für Geologie und Paläontologie, Westfälische Wilhelms-Universität Münster, Germany; hbahlburg@uni-muenster.de
[2]Alfred Wegener Institute for Polar and Marine Research, Potsdam, Germany; Juliane.Mueller@awi.de

The Gulf of Alaska borders the accretionary St. Elias orogen, the highest coastal mountain range on Earth. Mt St. Elias reaches an altitude of c. 5500 m at 55 km from the coast. Formation of the mountain belt since the middle Miocene is connected to oblique collision of the Yakutat terrane with the North American plate. Exhumation of the windward, Gulf of Alaska side of the orogen accelerated dramatically at c. 1 Ma, during the Mid-Pleistocene Transition (MPT). Sediment is being generated by glacial erosion throughout this high relief coastal mountain range and is subsequently being transported to the Aleutian subduction zone. While the formation of the orogen is plate-tectonically driven, exhumation rates and the development of high relief topography are strongly linked to the presence of large ice sheets in the Pleistocene, and highly erosive temperate glaciers in the Holocene combined with high precipitation rates on the orogen's windward side. Changing global climate together with the evolution of the orogen also influenced paleoceanographic patterns in the Gulf of Alaska.

Integrated Ocean Drilling Program Expedition 341 drilled a five site transect across the Gulf of Alaska margin of North America with Site U1420 on the shelf, Sites U1419 and U1421 on the slope, and Sites U1418 and U1417 on the proximal and distal Surveyor Fan, respectively (Fig. 1; IODP Expedition 341 Scientists, 2013). Complete recovery of 3240 m of high quality sediment cores and development of spliced sedimentary records of the Pleistocene through Holocene were achieved at the distal, proximal, and slope sites because of exceptional piston core recovery coupled with real-time stratigraphic correlation (Fig. 2).

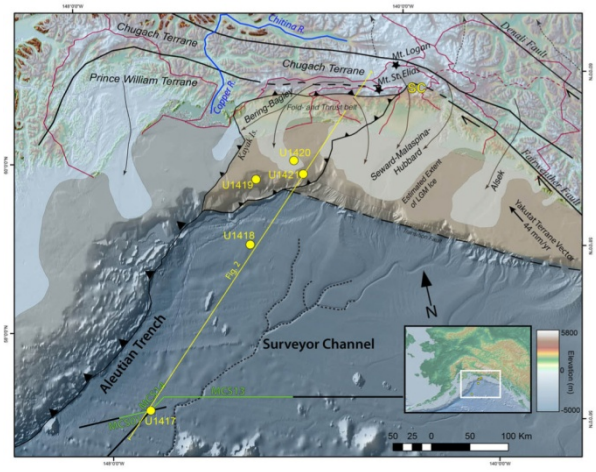

Figure 1. Gulf of Alaska study area with glacial extent estimated for the Last Glacial Maxima (blue, Manley and Kaufman, 2002), glacial flow paths (black arrows), modern watershed drainage basins (red; dashed where glacial divide differs from modern divide, Stroeven et al., 2010), and glacially fed deep-sea channels (black dashed). Yakutat Terrane shaded in tan. SC=Seward Corner. Seismic traverse shown in green and IODP Exp. 341 drillsites shown in yellow (Gulick et al, in review).

The obtained exemplary record allows us to address the main objectives of drilling in the Gulf of Alaska including to (i) document the tectonic response of an active orogenic system to late Miocene to recent climate change; (ii) establish the timing of advance/retreat phases of the northern Cordilleran ice sheet to test its relation to dynamics of other global ice sheets; (iii) implement an expanded source-to-sink study of the interactions between glacial, tectonic, and oceanographic processes responsible for creation of one of the thickest Neogene high-latitude continental margin sequences; (iv) understand the dynamics of productivity, nutrients, freshwater input to the ocean, and ocean circulation in the northeast Pacific and their role in the global carbon cycle.

More than 750 m of Miocene to Holocene sediments were recovered from Site U1417. A 30 m-thick interval of thin-bedded diamict interbedded with bioturbated mud is the earliest visible occurrence of ice-rafted debris (IRD) near the Plio-Pleistocene boundary. The diamict contains gravel size, subangular to subrounded clasts in a muddy matrix with gradational lower contacts. Deposition in the early Pleistocene is marked by mud interbedded with turbidite sand and silt beds, overlain by early to middle Pleistocene reoccuring intervals of diatom ooze and barren gray mud. IRD occurs as dispersed lonestones. Site U1418 recovered early Pleistocene to Holocene sediments. Diamict deposition dominated from the early to middle Pleistocene, followed by deposition of interbedded silt and mud with lonestones. Diamict ranges from massive clast-poor beds up to 150 cm thick to thin beds of coarse sand and granules that are interbedded with laminated mud. Laminated sequences have gradational contacts and range from sub-millimeter (a few coarse silt grains) to 2 mm thickness.

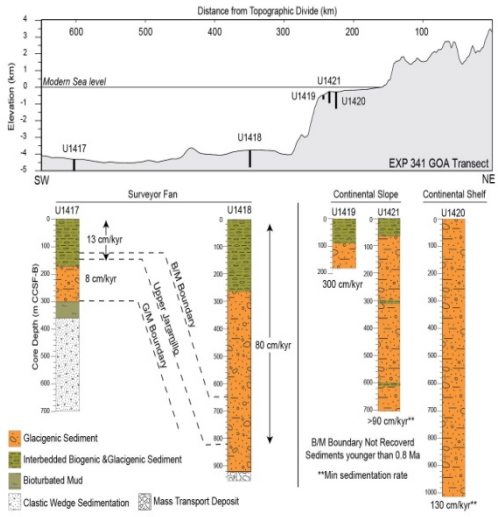

Figure 2. Representative topography through the IODP Expedition 341 drill sites (see Fig. 1 for location), showing the principle lithologies at each Site along with chronologies and accumulation rates in cm/kyr (Gulick et al., in review). Depths are in meters of core composite depth below the seafloor (CCSF-B) that approximates the drilled interval. B/M= Brunhes/Matuyama. G/M= Gauss/Matuyama. Vertical exaggeration ~18x.

Packages of laminae are bounded by regularly spaced thin layers of coarse sand and granules. One interpretation is that the laminated portion is formed by suspension settling from meltwater plumes whereas the thin coarse-grained beds are deposited by rafting from sea ice.

The thin granule layers may represent periods of enhanced sea-ice rafting. Diamict interbedded with mud containing IRD is the primary facies observed in the middle Pleistocene to Holocene sediments recovered from Sites U1419, U1420, and U1421. Diamict beds are thicker, more clast-rich, and have a coarser grained matrix than those deposited at other sites, reflecting their proximity to glaciers on the shelf. Some beds are interstratified with mud containing diatoms. This facies is interpreted to result from iceberg rafting and meltwater plumes.

Sediment accumulation rates vary from <100 m/Ma at the distal site to >1000 m/Ma on the proximal fan, slope and the continental shelf. At Site U1417, the onset of glaciation at the Plio-Pleistocene boundary resulted in a doubling of accumulation rates to ~100 m/Myr, the highest accumulation rates in the fan were recorded at Site U1418 with >1200 m/Myr in the late Pleistocene. All five sites include the middle Pleistocene to Holocene and demonstrate exceptionally high accumulation rates.

Provenance analysis is a key instrument for elucidating the denudation history of source terranes and for quantifying their respective contributions to sedimentary routing systems and the detrital composition of sedimentary systems. Through time and from the distal to the proximal sites the lithological variety of lonestones and diamict clasts gradually changes from a dominance of metamorphic clasts (argillite, meta-basalt) to one of sedimentary and igneous clasts, namely sand- and siltstones, granitoids and basalt. Noteworthy are also coal clasts contained in upper Miocene strata at Site U1417 which are interpreted as being derived from the Eocene Kulthieth Formation exposed in the onshore thrust belt.

These preliminary results indicate that the sources and oceanographic dispersal mechanisms of clasts delivered to all sites varied in space and time. The metamorphic clasts recovered from the distal fan including its Neogene parts were likely derived primarily from the Chugach terrane in the coastal part of the St. Elias orogen. The sites on the Quaternary proximal fan, the upper slope and the distal shelf display a wider range of lithologies indicative mainly of the more interior parts of the convergent margin including the Wrangellia and Alexander terranes. Post-cruise analyses of sediment provenance will constrain the changing loci of erosion linking them back to onshore patterns of exhumation. This will permit the ultimate test whether rapid erosion has the potential to cause a positive feedback in exhuming an active orogen.

References:

IODP Expedition 341 Scientists, 2013. Southern Alaska margin: Interactions of tectonics, climate, and sedimentation. IODP Prel. Rept., 341. doi:10.2204/iodp.pr.341.2013.

Gulick, S.P.S., Jaeger, J., Mix, A., and Expedition 341 Scientists, in review. Nonlinear feedback between tectonic uplift and glacial erosion constrained by Gulf of Alaska sedimentary record. Nature.

Manley, W., Kaufman, D.S., 2002. Alaska Paleoglacier Atlas: Boulder, CO (Inst. Arct. Alp. Res., Univ. Colorado).

http://instaar.colorado.edu/QGISL/ak_paleoglacier_atlas/

Stroeven, A.P., Fabel, D., Codilean, A.T., Kleman, J., Clague, J.J., Miguens-Rodriguez, M., Xu, S. 2010. Investigating the glacial history of the northern sector of the Cordilleran Ice Sheet with cosmogenic 10Be concentrations in quartz. Quaternary Sci. Rev. 29, 3630–3643.

Report from IODP Expedition 346 "Asian Monsoon": Onset and evolution of millennial-scale variability of Asian monsoon and its possible relation with Himalaya and Tibetan Plateau uplift

A. HOLBOURN[1], M. SAAVEDRA-PELLITERO[2], R. TADA[3], R.W. MURRAY[4], C. ALVAREZ ZARIKIAN[5] & EXPEDITION 346 SHIPBOARD SCIENTISTS[6]

[1]Institute of Geosciences, Christian-Albrechts-University, D-24118 Kiel, Germany
[2]Department of Geosciences, FB5, University of Bremen, D-28359 Bremen, Germany
[3]Earth and Planetary Science, University of Tokyo, Tokyo 113-0033, Japan
[4]Department of Earth Sciences, Boston University, Boston MA 02215, USA
[5]International Ocean Discovery Program Texas A&M University, College Station, TX 77845-9547, USA
[6]IODP Expedition 346 scientists: Anderson, W., Bassetti, M-A., Clemens, S., Dickens, G., Dunlea, A., Gallagher, S., Giosian, L., Gurgel, M., Henderson, A., Ikehara, K., Irino, T., Itaki, T., Karasuda, A., Kinsley, C., Kubota, Y., Lee, G-S., Lee, K-E., Lofi, J., Lopes, C., Peterson, L., Sagawa, T., Singh, R., Sugisaki, S., Toucanne, S., Wan, S., Xuan, C., Zheng, H., and Ziegler, M.

IODP Expedition 346 (29 July-27 September 2013) from Valdez, Alaska to Pusan, Korea recovered from the Sea of Japan/East Sea and the northern East China Sea an unparalleled sedimentary archive of fundamental changes in atmospheric and oceanic processes relating to the East Asian monsoonal system. The original scientific objectives of the expedition were:

1) to address the timing of onset of orbital- and millennial-scale variability of the East Asian summer monsoon (EASM) and East Asian winter monsoon (EAWM) and their relation with variability of Westerly Jet circulation;

2) to reconstruct orbital- and millennial-scale changes in surface and deepwater circulation and surface productivity in the Sea of Japan/East Sea during at least the last 5 m.y.;

3) to reconstruct the history of the Yangtze River discharge using cores from the northern end of the East China Sea, as it reflects variation and evolution in the EASM and exerts an impact on the paleoceanography of the Sea of Japan/East Sea;

4) to examine the interrelationship among the EASM, EAWM, nature and intensity of the influx through the Tsushima Strait, intensity of winter cooling, surface productivity, ventilation, and bottom water oxygenation in the Sea of Japan/East Sea and their changes during the last 5 m.y.

To meet these objectives, IODP Expedition 346 drilled seven sites located over a wide latitudinal and water depth range in the Sea of Japan/East Sea and two closely positioned sites in the northern East China Sea (Figure 1). A total of 6135.3 m of core was recovered with an average recovery of 101%, which set a new record of core recovered during any single IODP expedition (Figure 2). In addition, the newly engineered half advanced piston corer enabled recovery of the deepest piston core in Deep Sea Drilling Project/Ocean Drilling Program/IODP history (490.4 m in IODP Hole U1427A) and of the deepest continuously recovered piston cored sequence, penetrating to ~500 m core depth below seafloor. Multiple timescales

were targeted to assess climate variability on orbital to millennial timescales and to tease out forcing mechanisms and amplifying feedbacks related to changing climatic boundary conditions from the late Miocene to Holocene. Based on the shipboard biostratigraphy and magnetostratigraphy, the retrieved sedimentary records extend continuously down to ~12 Ma at Sites U1425 and U1430, to ~5 Ma at Sites U1423, U1424, and U1426, to ~4 Ma at Site U1422, to ~1.2 Ma at Site U1427 and to ~0.45 Ma at Sites U1428 and U1429.

One of the highlights of Expedition 346 was the recovery of centimeter- to meter-scale (and often millimeter-scale) alternating dark and light sediment layers that could be correlated across the six sites (IODP Sites U1422-U1426 and U1430) drilled in the Sea of Japan/East Sea (Figure 3). Shipboard analyses confirmed that these spectacular light and dark layers started at ~2.6 Ma and increased in frequency from ~1.2 Ma to the present. In general, darker (with lower color reflectance L* values) layers are poorly bioturbated and/or finely laminated, suggesting oxygen-poor conditions, whereas the lighter layers are more bioturbated, indicating more oxic conditions. Some of the dark layers are brownish and rich in microfossils such as diatoms, nannofossils, radiolarians, and foraminifers, suggesting high surface biological productivity. Orbital-scale dark-light color cycles were also detected in the Miocene interval (~12 to ~8 Ma) at Sites U1425 and U1430, but are generally not as distinct as Pleistocene millennial-scale cycles, except for intervals with pristine dark-light laminae at ~12 Ma at IODP Sites U1425 and U1430. A preliminary interpretation of these light/dark sedimentary cycles is that they reflect the ventilation and oxygenation history of the basin, which responds to changes in the EASM and EAWM. In addition, temporal changes in ice rafted debris at the most northerly sites and eolian dust accumulation appear to provide sensitive recorders of the EAWM's evolution. Postcruise investigation of the high quality sediment cores recovered in the Sea of Japan/East Sea during Expedition 346 will, thus, provide new insights into the Miocene to Holocene evolution of the EASM and EAWM and their relationships to atmospheric and oceanic processes and high-latitude climate change.

The recovery of a continuous sequence of biocalcareous mud in Sites U1428 and U1429 in the northern East China Sea that was ~137 and ~179 m thick, respectively, and that spanned the last ~0.45 m.y. will allow reconstruction of regional hydrographic changes at ultra high temporal resolution in this highly sensitive climate region. Five separate holes were drilled at these two sites with excellent stratigraphic correlations between adjacent holes and between the two sites. The sea surface salinity and sedimentary deposition at this location are closely linked to the seasonal discharge of fresh water and fine detrital material from the Yangtze River, which will enable to closely monitor changes in the intensity of the EASM. Temperature and salinity reconstructions through the water column will be integrated with parallel investigations of ventilation and productivity (based on Ba/Ca, $\delta^{13}C$ and microfossil assemblages) and monsoonal run-off (based on X-ray fluorescence scanning and provenance studies) and will be correlated with monsoon proxy records from mainland China to explore the sensitivity of individual proxies and to unravel regional and global climatic responses. In addition, the combination of Sites U1427 (Sea of Japan/East Sea), U1428, and U1429 (East China Sea) with extremely high sedimentation rates will allow detailed reconstruction of changes in the Tsushima Warm Current in relation to the Yangtze River discharge in order to assess the Sea of Japan/East Sea's response to external climate-related forcing through the late Pleistocene. The Tsushima Warm Current is the only current flowing into the Japan Sea and, thus, has a crucial impact on the primary productivity and stratification of this vast, semi-enclosed marginal sea, which is only connected with other seas by shallow and narrow straits (130 m water sill depth or less). Ultimately, collaborative research efforts will enable to link up the climatic hydrology on the Asian continent (traced through reconstruction of Yangtze River discharge and correlation to speleothem records) to atmospheric and oceanic processes (traced through the Sea of Japan/East Sea and East China Sea site locations).

References:

Expedition 346 Scientists, 2013. Asian Monsoon: onset and evolution of millennial-scale variability of Asian monsoon and its possible relation with Himalaya and Tibetan Plateau uplift. *IODP Preliminary Report*, 346. doi:10.2204/iodp.pr.346.2013.

Tada, R., Murray, R.W., and Alvarez Zarikian, C.A., 2013. Asian Monsoon: onset and evolution of millennial-scale variability of Asian Monsoon and its possible relation with Himalaya and Tibetan plateau uplift. *IODP Scientific Prospectus*, 346. doi:10.2204/iodp.sp.346.2013.

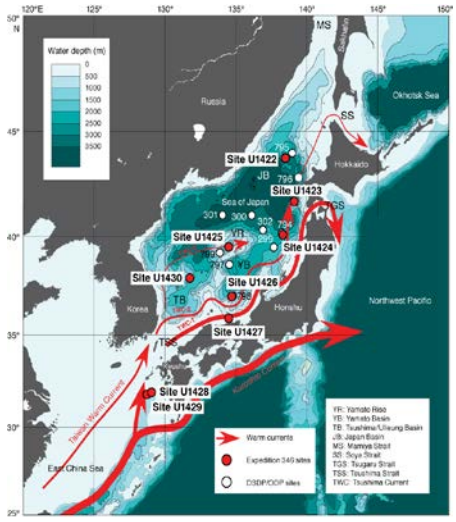

Figure 1. Bathymetric map of Expedition 346 sites (red circles) in the Sea of Japan/East Sea and the East China Sea during IODP Expedition 346 "Asian Monsoon" (from Tada, Murray and Alvarez Zarikian, 2013). Sites previously drilled by the Deep Sea Drilling Project (DSDP) and Ocean Drilling Program (ODP) are indicated by white circles. Also illustrated are surface current systems within and surrounding the Sea of Japan.

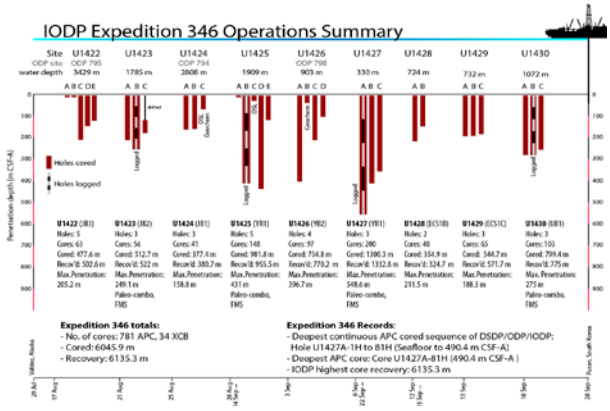

Figure 2. Summary of drilling and logging activities at the seven sites drilled in the Sea of Japan/East Sea and at the two sites drilled in the East China Sea during IODP Expedition 346 "Asian Monsoon" (Expedition 346 Scientists, 2013).

Figure 3. Representative dark and light layers in Lithological Subunit IA, Holes U1422C and U1422D (Expedition 346 Scientists, 2013). Note that the contrast in the core images has been enhanced to highlight sedimentary structures.

IODP Expedition 347 – Baltic Sea Paleoenvironment

T. ANDRÉN, B.B. JORGENSEN, J. GROENEVELD, T. BAUERSACHS, M. KENZLER, U. KOTTHOFF, C. COTTERILL, D. MCINROY, AND EXP. 347 SCIENTISTS

The 5th mission-specific platform expedition of the IODP, **Baltic Sea Paleoenvironment,** set sail from Kiel on September 12, 2013 and ended in Kiel on November 1, 2013. Using the *Greatship Manisha* equipped with a Geoquip Marine coring rig, the expedition recovered cores that will aid the investigation of environmental changes in the Baltic region during the last glacial cycle as the Scandinavian Ice Sheet waxed and waned. A total of ~1900 m has been drilled, with ~200 m of open holing and ~1600 m of core recovered (average recovery 98.7%). From January 22, 2014 till February 21, 2014, the Onshore Science Party assembled at the MARUM Bremen Core Repository to open the cores, describe, scan, and sample them.

After departing Kiel, the expedition visited site **M0059 (BSB-3)** in the Little Belt area**.** At this site, black mud and greenish-gray clay with weak cm-scale colour lamination was recovered, which down to 20 meters below seafloor (mbsf) displayed benthic foraminifera, diatoms and remains of coastal marine fauna and flora. The sediments in the lowermost part of the sequence were silty sands. At 89 mbsf a hard diamicton of sand and stones with little silt was encountered. Tills with this composition are known to have a northeasterly provenance and can be attributed to the main ice advance over the area reaching the Last Glacial Maximum (LGM) at around 23 to 21 kyr BP. It seems likely that the recovered diamicton can be assigned to this ice advance. The diamicton presented problems for the coring equipment, so open holing was conducted down to anticipated Eemian deposits at 160 mbsf, with spot-sampling on the way to confirm the lithology. From the core-catcher material it was concluded that an Eemian sequence might not be present at this site.

The next site was **M0060 (BSB-1)** southeast of Anholt in the Kattegat. The top 4.5 m of sediment consisted of very well sorted sand with only a few foraminifers, below which silty clay was recovered. From 18.6 mbsf, mostly stiff late Glacial clay was fully recovered, which gradually changed from lighter to darker grey with depth. The lithologies at this site are hard deposits of mixed clay and sand with variable composition, ranging from almost pure sand to silty clay. At several depths the sand layer had apparent overpressure and formation water with suspended sand, which shot up through the drill pipe. The occurrence of shell fragments of marine bivalves, snails and foraminifera, together with the grain-size succession, indicate that the depositional environment changed several times from shallow water to deeper water and then back again to more shallow water. Charcoal fragments were abundant at several horizons. The expedition also recovered 5-10 mm large, thin sheets of amorphous black plant material with fibrous imprints of cellular plant structure and with indications of initial pyritization. A number of such pieces were collected and frozen at -80°C for later DNA analysis. Such material also constitutes excellent samples for ^{14}C dating and the possibility to achieve an accurate timescale is very promising. Below 200 mbsf the sediment is increasingly hard and sandy. At about 10 m short of the target drilling depth, further coring was prevented due to a strong flow of formation water that carried large amounts of sand up into and around the drill string and locked the bottom hole assembly, causing the hole to be abandoned.

After a 3-day transit, the expedition arrived at **M0061 (BSB-10)** in the Ångermanälven Estuary. The uppermost part of the sequence consisted of a greenish clay on top of a black sulphidic clay, turning into weakly varved clay with weak sulphide banding. Some shell fragments and plant remnants were recorded. From 13.3 mbsf the sediment became increasingly rich in silt and was pure, well sorted silt at 20.7 mbsf. Due to the high water content it was not possible to determine from the material in the core catcher whether the sediment was varved or not. The last cores had been difficult to retrieve as sands became increasingly abundant. At the bottom of the sequence a hard layer was reached where hammer coring brought back a granite rock of about 5 cm diameter.

Coring operations then moved to site **M0062** (**BSB-11)** further up the river. The upper ca. 15 mbsf were pure clay

and are expected to be well suited for varve analyses when the cores are split in Bremen during the Onshore Science Party. Below that depth the sediment was coarser-grained, varying between clayey silt and silty sand. Drilling continued down to 35.9 mbsf to make sure that the borehole had penetrated through the clay deposits.

Site **M0063 (BSB-9)** in the Landsort Deep northeast of Gotland was partly completed before a port call was made at Nynäshamn, near Stockholm, Sweden. With a water depth of 437 m, this site was the deepest of Expedition 347 and also the deepest area in the Baltic Sea.

The first piston cores brought back a black gyttja (a lacustrine mud containing abundant organic material) strongly smelling of sulfide and with fine layers that were difficult to distinguish in the surface core due to the strong sulfidization and the very fluid sediment. The gyttja was highly charged with methane gas and developed large bubbles, cracks and voids in the cores. The gyttja contained

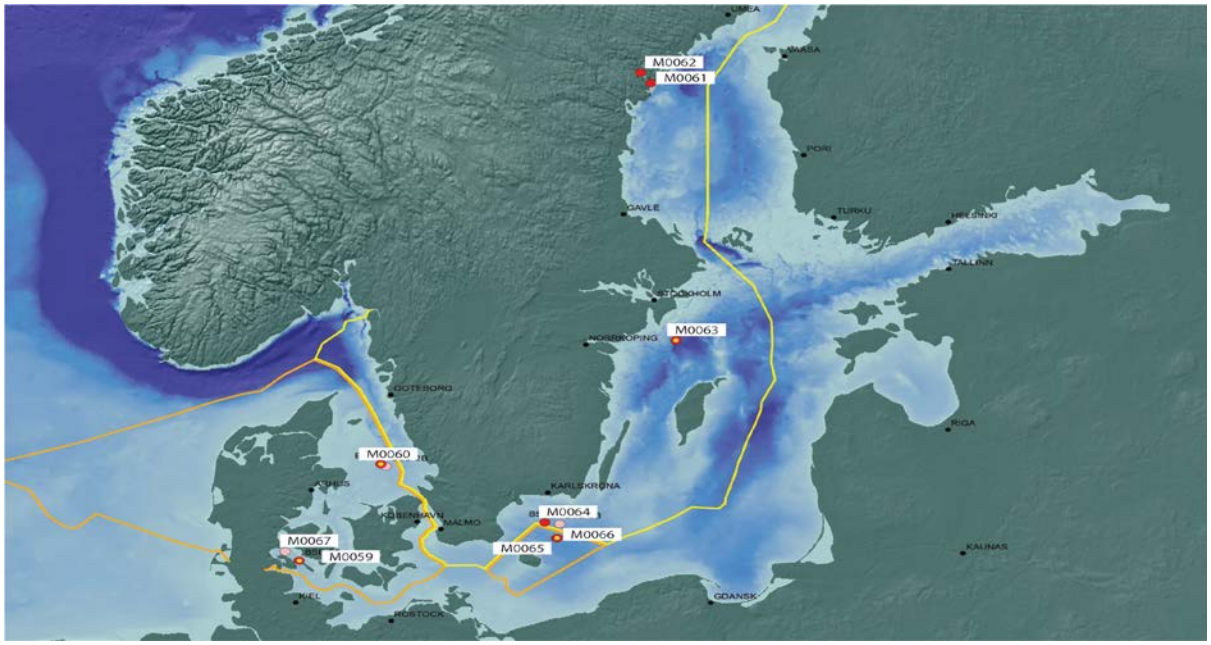

foraminifera, diatoms and pollen grains in varying densities. Below ca. 18 mbsf the sediment changed into a dark greenish gyttja with a small amount of silt. From 30 mbsf, varves were no longer recognizable and below 40 mbsf the sediment was grey, homogenous clay without foraminifera, typical for sediments deposited in the Ancylus Lake. Below 50 mbsf the clay was pale brownish and thinly varved. The varves became more variable and thicker (1-5 cm) in the deep glacial clay sequence below, which had no detectable foraminifera or other microfossils. At 90 mbsf the sediment became slightly coarser and a horizon of clayey sand was found. A tentative estimate based on the visible varve thicknesses points towards a sequence of glacially varved clay that represents ca. 2200 years of varve deposition. This varve deposition took place during the Baltic Ice Lake and Yoldia Sea stages of the Baltic Sea.

A clayey, sandy, and gravely diamicton was present from 92 to 102 mbsf, below which the sediment was pale brown, well-sorted silt. Coring continued into hard, very well sorted gravel by open-holing with intermittent hammer coring. At 106 mbsf and 116 mbsf hammer coring brought up only a small amount of well sorted gravel with no fine-grained sediment. This probably represents glacio-fluvial gravel resulting from a strong flow of melt water from the ice sheet. Due to the risk of getting stuck in the unstable gravel, Hole M0063A was terminated at a depth of 116 mbsf and logged.

Site **M0064 (BSB-5)** in Hanöbay and nearby sites **M0065 (BSB-7C)** and **M0066 (BSB-7D)** in the Bornholm Deep are located close to each other just southeast of the Swedish mainland close to the island of Bornholm. In Hanöbay a thin top layer of clay was followed by 10 m of varved, brown clays. Below that a diamicton occurred to nearly 40 mbsf, after which some gravel and then the Cretaceous bedrock followed. At the two Bornholm sites the first two meters of the sediment were open-holed due to the risk of chemical contaminants. At M0065 a dark greenish clay layer occurred down to 10 m, followed by a 30 m thick section of varved clays. Down to nearly 70 m sand and occasionally silty sand continued till the bedrock was encountered. At M0066 8 m of clay and then another 8 m of sand were followed by a diamicton, which can possibly be linked to the diamicton from Hanöbay. Below the diamicton interchanging layers of sand, silt, and clay were recovered down to 28 m.After completing the Bornholm area the Greatship Manisha sailed back to the Little Belt to drill site **M0067 (BSB-4)**. After an initial 3 m of dark green clays with abundant microfossils, gravel was encountered down to 10+ m, which caused instability of the two attempted holes. Due to the risk of losing equipment while continuing drilling it was decided to abandon the site and head back to Site M0059. Here, another paleo- and microbiology hole were drilled in addition to the previous holes. After completion the expedition was called to an end and everything was prepared for the short transit back to Kiel where Expedition 347 ended November 1, 2013

Report from IODP Expedition 348: Nankai Trough Seismogenic Zone Experiment Stage 3 - Plate Boundary Deep Riser 3

S. HAMMERSCHMIDT[1], H. SONE[2] AND THE IODP EXPEDITION 348 SCIENTISTS[3]

[1] MARUM - Center for Marine Environmental Sciences, University of Bremen, Bremen, Germany
[2] GFZ German Research Centre for Geosciences, Helmholtz Centre Potsdam, Potsdam, Germany
[3] D/V Chikyu, SE offshore Kii Peninsula, Japan

The Integrated Ocean Discovery Program (IODP) Nankai Trough Seismogenic Zone Experiment (NanTroSEIZE) is an international drilling project targeting the Nankai Trough subduction complex, SE offshore Japan. While Stage 1 of NanTroSEIZE focused on intense coring and logging-while-drilling (LWD) of the Kumano transect, Stage 2 added *in situ* long-term monitoring and riser drilling. The latter is essential for accomplishing deep drilling, and therefore, riser drilling was again the method of choice during Stage 3. Starting with IODP Exp. 326, riser drilling at Site C0002 above a presumably locked portion of an out-of-sequence splay fault system allowed deepening Hole C0002F from 856 meters below seafloor (mbsf) to 2005 mbsf. As a follow-up, the primary goals of IODP Expedition 348 with D/V *Chikyu* (14 September 2013 - 31 January 2014) were to further deepen the hole to 3600 mbsf using riser drilling technology, including LWD, lithological/structural description of cuttings, drilling mud gas monitoring, and coring from 2300 to 2400 mbsf. Prior to riser drilling, a new coring tool was tested by drilling and coring Hole C0002M to a depth of ca. 513 mbsf. After re-entering Hole C0002F, sidetracking at ca. 850 mbsf commenced for Hole C0002N, which was drilled to 2330 mbsf. Unfortunately, borehole conditions required again sidetracking at ca. 1950 mbsf, leading to a new borehole (C0002P). Drilling stopped at 2163 mbsf, and after coring from 2163 mbsf to 2218.5 mbsf, drilling continued smoothly to ca. 3060 mbsf. At that point, borehole conditions and time constraints made it necessary to complete the borehole and to make it ready for re-entry on upcoming IODP expeditions.

In total, preliminary results from both Hole C0002M and C0002N confirmed interpretations and unit boundaries from previous expeditions. In Hole C0002M, Unit II was encountered from 475 – 512.5 mbsf, and based on the predominance of hemipelagic mud with intercalations of turbidites, was again interpreted as lower Kumano forearc basin sediment. Biostratigraphic ages confirms a Pleistocene age. LWD and lithological data from Hole C0002N correspond to data from IODP Exp. 338, which point to syn-depositonal erosional processes in the lower part of Kumano forearc basin (Unit III). The unconformity between forearc basin sediments and the upper accretionary prism was defined at 915.0 mbsf based on changes in gamma ray response seen in the LWD data and 975.5 mbsf based on a sudden change from mainly silty-claystone to a more sand-dominated lithology observed in the cuttings. Calcareous assemblages point to Pliocene to Miocene age. The LWD gamma ray response and the cuttings-based sand content was used to further divide Unit IV into five different subunits, following those identified in Hole C0002F (Exp. 338) at overlapping depth ranges. The increase in LWD gamma ray at 1656.3 mbsf marks the start of Univ V in Hole C0002N, consistent with LWD responses observed in Hole C0002F. The distinct decrease in sand-content and dominance of (fine silty) claystone observed from cuttings collected below 1665.5 mbsf is consistent with the gamma ray increase, thus Unit V is interpreted as trench or Shikoku basin hemipelagic deposits of Miocene age, and can be correlated with Unit III at Sites C0011 and C0012 on the Phillippine Sea Plate. LWD data and cuttings lithology observations from the remaining deeper portions of Hole C0002N and Hole C0002P indicate that in general only a gradual increase in gamma ray or fining of claystones is observed further below, suggesting possible continuation of hemipelagic deposits.

Evidence for mechanical deformation and compaction was observed through structural observations and physical properties measurement of cuttings and core material. Only preliminary insights are currently available as interpretation and confirmation of these results requires comparison with detailed examination of sonic and borehole image log data which only became available after the Expedition. In addition to the deformational structures observed in the drilling cuttings, fault-related rocks associated with a brittle fault zone were encountered in the core recovered from Hole C0002P. The frequency of the occurrence of such major structures outside of the cored interval is unclear and awaits results from borehole image analyses. While onboard density measurements of hand-picked cuttings suggest porosity loss and mechanical compaction with depth, compressional wave velocity from the LWD data in Hole C0002P so far does not show an obvious increasing trend associated with sediment compaction. Whether this suggests abnormally high pore pressure or not shall be investigated together with further log data analyses and core laboratory measurement studies.

For all boreholes, TOC/TN ratios point to a dominance of marine organic matter. Methane predominated headspace gas samples from cores in Hole C0002M and C0002P. Concentrations found in headspace gas samples were up to two orders of magnitude higher than the drilling mud gas samples from the same interval, indicating an underestimation of hydrocarbons by real-time monitoring. The Bernard parameter and $\delta^{13}C_{CH4}$ of the drilling mud gas indicated a shift to a thermogenic regime at depths greater 1700 mbsf. Non-hydrocarbon gases showed mainly an atmospheric composition.

In conclusion, Expedition 348 results provide new insights into the Nankai subduction system. LWD data, core, cuttings, pore water and drilling mud gas were successfully collected, and will be subject to later onshore analysis for composition, geochemistry, microstructures, transport properties, and mechanical properties.

Abstracts:

ICDP

Core processing during the INFLUINS scientific deep drilling campaign, Thuringian Basin, Germany

M. ABRATIS, M. AEHNELT, C. KUNKEL, D. BEYER, P. METHE, N. KUKOWSKI, K. U. TOTSCHE

Friedrich Schiller Universität Jena, Institut für Geowissenschaften, Burgweg 11, 07749 Jena, michael.abratis@uni-jena.de

Deep drilling of the central Thuringian Basin was carried out in order to gather substantial knowledge of subsurface fluid dynamics and fluid rock interaction within a sedimentary basin. The final depth of the borehole was successfully reached at 1179 m, just a few meters above the Buntsandstein – Zechstein boundary. One of the aspects of the scientific drilling was obtaining sample material from different stratigraphic units for insights in genesis, rock properties and fluid-rock interactions. Parts of the section were cored whereas cuttings provide record of the remaining units. Coring was conducted in aquifers and their surrounding aquitards, i.e. parts of the Upper Muschelkalk (Trochitenkalk), the Middle Muschelkalk, the Upper Buntsandstein (Pelitrot and Salinarrot) and the Middle Buntsandstein.

In advance and in cooperation with the GFZ Potsdam team "Scientific Drilling" core handling was discussed and a workflow was developed to ensure efficient and appropriate processing of the valuable core material and related data. Core curation including cleaning, fitting, marking, measuring, cutting, boxing, photographing and unrolled scanning using a DMT core scanner was carried out on the drilling site in Erfurt. Due care was exercised on samples for microbiological analyses. These delicate samples were immediately cut when leaving the core tube and stored within a cooling box at -78°C. Special software for data input was used developed by smartcube GmbH. Advantages of this drilling information system (DIS) are the compatibility with formats of international drilling projects from the IODP and ICDP drilling programs and thus options for exchanges with the international data bases. In a following step, the drill cores were brought to the national core repository of the BGR in Berlin Spandau, where the cores were logged for their physical rock properties using a GeoTek multi sensor core logger (MSCL). After splitting the cores into a working and archive half, the cores were scanned for compositional variations using an XRF core scanner at the BGR lab and scan images of the slabbed surfaces were performed. The average core recovery rate was very high at nearly 100%. Altogether, we gained 533 m of excellent core material including sandstones, siltstones and claystones, carbonates, sulfates and chlorides. This provides valuable insight into the stratigraphic column of the Thuringian Basin.

ICDP

Online gas monitoring and sampling during drilling of the INFLUINS borehole EF-FB 1/12, Thuringian Basin, Germany

M. ABRATIS[1], M. GÖRLITZ[1], T. WIERSBERG[2], N. KUKOWSKI[1], K. U. TOTSCHE[1]

[1]Friedrich Schiller Universität Jena, Institut für Geowissenschaften, Burgweg 11, 07749 Jena, michael.abratis@uni-jena.de

[2]Helmholtz-Zentrum Potsdam, Deutsches GeoForschungsZentrum GFZ, Wissenschaftliches Bohren, Telegrafenberg A69, 14473 Potsdam

Online monitoring and sampling of drill mud gas (OLGA) was conducted during standard rotary drilling and core drilling of the INFLUINS borehole EF-FB 1/12 to gain information on the composition of gases and their distribution at depth within the Thuringian Basin (Germany). The method can help to identify areas of enhanced permeability and/or porosity, open fractures, and other strata associated with gases at depth.

The gas-loaded drill mud was continuously degassed in a modified gas-water separator, which was installed in the mud ditch in close distance to the drill mud outlet. The extracted gas phase was pumped in a nearby field laboratory for continuous on-line analysis. First information on the gas composition (H_2, He, N_2, O_2, CO_2, CH_4, Ar, Kr) was available only few minutes after gas extraction. More than 40 gas samples were taken from the gas line during drilling and pumping tests for further laboratory studies.

Enhanced concentration of methane, helium, hydrogen and carbon dioxide were detected in drill mud when the drill hole encountered gas-rich strata. Down to a depth of 620 m, the drill mud contained maximum concentration of 55 ppmv He, 1400 ppmv of CH_4, 400 ppmv of hydrogen and 1.1 vol-% of CO_2.

The drilling mud gas composition is linked with the drilled strata. Buntsandstein and Muschelkalk show different formation gas composition and are therefore hydraulically separated. Except for helium, the overall abundance of formation gases in drilling mud is relatively low. We therefore consider the INFLUINS borehole to be dry. The correlation between hydrogen and helium and the relatively high helium abundance rules out any artificial origin of hydrogen and suggest a radiolytic origin of hydrogen. Values $CH_4/(C_2H_6/C_3H_8)<50$ imply that hydrocarbons are thermogenic. Stable isotope and noble gas isotope studies are planned to better understand origin and migration processes of fluids at depth.

ICDP

Late Pliocene and Early Pleistocene environments inferred from the Lake El'gygytgyn pollen record

A.A. ANDREEV[1], P.E. TARASOV[2], V. WENNRICH[1], E. RASCHKE (MOROZOVA)[3], N.R. NOWACZYK[4], J. BRIGHAM-GRETTE[5], M. MELLES[1]

J. BRIGHAM-GRETTE[5], M. MELLES[1]

[1]Institute of Geology and Mineralogy, University of Cologne, Zülpicher Str. 49a, 50674, Cologne, Germany
[2]Free University Berlin, Institute of Geological Sciences, Paleontology Section, Malteser Str. 74-100, Haus D, 12249 Berlin, Germany
[3]Arctic and Antarctic Research Institute, Bering St. 38, St. Petersburg, 199397 Russia
[4]Helmholtz Centre Potsdam, GFZ German Research Centre for Geosciences, Section 5.2 - Climate Dynamics and Landscape Evolution, Telegrafenberg, 14473 Potsdam, Germany
[5]Department of Geosciences, University of Massachusetts, North Pleasant Str. 611, Amherst, MA 01003, USA

The Arctic is known to play a crucial, but not yet completely understood, role within the global climate system. The Middle Pliocene (3-3.5 Ma) is considered to be the most probable scenario of the future climate changes. Therefore, the development of possible scenarios of future climate changes in the Arctic is a major scientific challenge. However, reliable climate and environmental projections are hampered by the complexity of the underlying natural variability and feedback mechanisms. An important prerequisite for the validation and improvement of the future projections is a better understanding of the long-term environmental history of the Arctic. Unfortunately, formation of continuous, non-interrupted paleoenvironmental records in the Arctic was widely restricted due to repeated glaciations, limiting information predominantly to the Holocene and in a few cases to the last glacial/interglacial cycles (e.g. Andreev et al., 2011 and references therein). Continuous sequences that penetrates the entire Quaternary and further into the Pliocene, with a temporal resolution at least as good as the marine record, are highly desired and would enable to validate the absolute temperature rise during the mid-Pliocene that was proposed by former studies. Such a record has now become available from Lake El´gygytgyn (67º30'N, 172º05E') located in a meteorite impact crater in north-eastern Siberia (Melles et al., 2011).

The crater was created nearly 3.6 Ma ago in volcanic target rocks. The impact formed an 18 km wide hole in the ground that then filled with water. The modern lake is 170 m deep and has a roughly circular shape with a diameter of 12 km. The retrieved lake sediments are trapped pollen from a several thousand square-kilometer source area providing reliable insights into regional and over-regional millennial-scale vegetation and climate changes of the Arctic since the Pliocene (for details see Melles et al., 2011, 2012; Brigham-Grette et al., 2013 and references therein).

The German-Russian-American ''El´gygytgyn Drilling Project" of ICDP has completed three holes in the center of the lake between October 2008 and May 2009, penetrating about 318 m thick lake sediments and about 200 m of the impact rocks below. Because of its unusual origin and high-latitude setting, scientific drilling at Lake El´gygytgyn offered unique opportunities for paleoenvironmental and paleoclimate research, allowing the time-continuous reconstruction of the climatic and environmental history of the terrestrial Arctic back into the Pliocene for the first time (Melles et al., 2012; Brigham-Grette et al., 2013). We received the first relatively high-resolution (varying between ca 0.5 to ca 1.5 ka for the available part of the cores) pollen record which reflects paleoenvironmental and paleoclimate changes during the Late Pliocene and transition to the Early Pleistocene inferred from the lower 200 m of Lake El'gygytgyn lacustrine sediments (Fig 1 and 2, Andreev et al., 2013).

Revealed pollen assemblages can be subdivided into 55 main pollen zones, which reflect the main environmental fluctuations in the region during the Late Pliocene and Early Pleistocene, approximately 3.58-2.15 Ma BP. Pollen-based climate reconstructions show that conditions in the study area were the warmest about 3.58-3.4 Ma BP when spruce-pine-fir-hemlock-larch-Pseudotsuga forests dominated in nowadays treeless tundra area. After ca 3.4 Ma BP dark coniferous taxa gradually disappeared from the vegetation cover. Very pronounced environmental changes are revealed about ca 3.35-3.275 Ma BP when treeless tundra and steppe habitats dominated. Large amounts of coprophilous fungi spores indirectly imply a permanent presence of numerous grazing animals like bison, mammoth, horse etc around the lake, thus confirming that open habitats became broadly distributed in the study area. Interestingly this episode corresponds to the so-called Mammoth paleomagnetic subchron coinsiding with (MIS M2).

Since ca 3.087 Myr BP (ca 163 m of the sediment core) extremely numerous, small (ca 12 μm), round and transparent cysts occur in many sampled intervals. The origin of these cysts is not completaly clear. Most likely they are hypnozygote spores of algae from Chlamydomonas genus, which commonly produce such thick-walled cysts under unsuitable environmental conditions. Moreover, these cysts might be produced by the so-called snow-algae. According to Dr T. Leya (Fraunhofer IBMT, CryoCulture Collection of Cryophilic Algae) the found cysts may belong to Chlamydomonas or Chloromonas representatives (personal communication). Dr R. Below (Institute of Geology and Mineralogy, University of Cologne) also suggests that the cysts most likely hypnozygote spores of Chlamydomonas (personal communication). The presence of numerous hypnozygotes in the El'gygytgyn sediments younger than ca. 3.087 Myr BP (upwards 163.5 m core depth), therefore may indirectly reflect a longer persistence of large snow fields in the study area during the cyst-dominated intervals. Air temperatures are supposed to have varied between 0 and 10°C during their growing season (spring).

Treeless and shrubby environments are also indicative for the beginning of the Pleistocene, ca 2.6 Ma. Dry and cold climate conditions were similar to those during the Late Pleistocene. The Early Pleistocene sediments contain pollen assemblages reflecting alternation of treeless intervals with cold and dry climate and warmer intervals when larch forests with stone pines, shrub alders and birches were also common in the region. Very dry environments are revealed after ca 2.175 Ma BP. High amounts of green algae colonies (Botryococcus) in the

studied sediments point to a shallow water conditions ca 2.55, 2.45, and ca 2.175 Ma BP.

Thus, our pollen studies show that lacustrine sediments accumulated in Lake El´gygytgyn are an excellent archive of vegetation and climate changes since ca 3.58 Ma BP (Andreev et al., 2013; Brigham-Grette et al., 2013). The record well reflects main paleoenvironmental fluctuations in the region. However, the record does not only provides a means for deciphering changes in the regional vegetation and climate histories over the last 3.58 Ma at fairly high resolution, but also allows a variety of pollen-based reconstruction approaches to be tested across a wide range of paleoenvironmental conditions. Quantitative reconstruction of changes in vegetation cover near Lake El'gygytgyn presented in this paper were obtained using the biome reconstruction method (Tarasov et al., 2013), which provides time series of the dominant vegetation types (biomes) and -quantitative evaluations of landscape openness between ca. 3.58 and ca. 2.15 kyr BP

As work progresses with the El'gygytgyn sediments, the temporal resolution of the record will be substantially improved as future studies focus on specific intervals or questions of interest determined by the coarse-resolution analyses, thereby providing additional details to the observed shifts in climate and vegetation and opportunities for further applications of modeling and biome/analog techniques.

References:

Andreev, A., Schirrmeister, L., Tarasov, P., Ganopolski, A., Brovkin, V., Siegert, C., Hubberten, H.-W. Vegetation and climate history in the Laptev Sea region (arctic Siberia) during Late Quaternary inferred from pollen records. 2011. Quaternary Science Reviews 30, 2182-2199.

Andreev, A.A., Wennrich, V., Tarasov, P.E., Brigham-Grette, J., Nowaczyk, N.R., Melles, M., El'gygytgyn Scientific Party. 2013. Late Pliocene/Early Pleistocene environments of the north-eastern Siberian Arctic inferred from Lake El'gygytgyn pollen record. Climate of the Past. Discussion. 9, 4599-4653, doi:10.5194/cpd-9-4599-2013.

Brigham-Grette, J., Melles, M., Minyuk, P., Andreev, A., Tarasov, P., DeConto, R., Koenig, S., Nowaczyk, N., Wennrich, V., Rosén, P., Haltia-Hovi, E., Cook, T., Gebhardt, C., Meyer-Jacob, C., Snyder, J., Herzschuh, U. 2013. Pliocene warmth, extreme polar amplification, and stepped Pleistocene cooling recorded in NE Russia. Science 340, 1421-1427.

Melles, M., Brigham-Grette, J., Minyuk, P., Koeberl, C., Andreev, A., Cook, T., Gebhardt, C, Haltia-Hovi, E., Kukkonen, M., Nowaczyk, N., Schwamborn, G., Wennrich, V., El'gygytgyn Scientific Party. 2011. The Lake El'gygytgyn scientific drilling project - conquering Arctic challenges in Continental Drilling. Scientific Drilling 11, 29-40.

Melles, M., Brigham-Grette, J., Minyuk, P.S., Nowaczyk, N.R., Wennrich, V., DeConto, R.M. Anderson, P.M., Andreev, A.A., Coletti, A., Cook, T.L., Haltia-Hovi, E., Kukkonen, M., Lozhkin, A.V., Rosén, P., Tarasov, P., Vogel, H., Wagner, B. 2012. 2.8 million years of Arctic climate change from Lake El'gygytgyn, NE Russia. Science 337, 315-320.

Tarasov, P.E., Andreev, A.A., Anderson, P.M., Lozhkin, A.V., Haltia-Hovi, E., Nowaczyk, N.R., Wennrich, V., Brigham-Grette, J., Melles M. 2013: A pollen-based biome reconstruction over the last 3.562 million years in the Far East Russian Arctic – new insights climate-vegetation relationships at the regional scale. Climate of the Past 9, 2759-2775, doi:10.5194/cp-9-2759-2013.

IODP

Comprehensive analysis of Atlantic Circulation during Heinrich-Event 1 & 2

B. ANTZ[1], J. LIPPOLD[2], H. SCHULZ[3], N. FRANK[1], A. MANGINI[1]

[1]Institute of Environmental Physics, University of Heidelberg, Germany
[2]Institute of Geological Sciences, University of Bern, Switzerland
[3]Department of Geosciences, University of Tübingen, Germany

Introduction

The dynamic of the Atlantic Meridional Overturning Circulation (AMOC) is one of the key players in the global climate system [Rahmstorf 2002]. It crucially influences the redistribution of heat and carbon from surface into the deep sea and vice versa. Therefore, assessing the sensitivity of the AMOC is a major challenge for paleoclimatology.

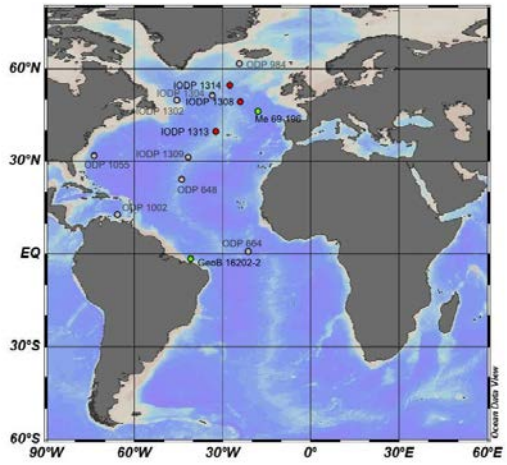

Fig. 1: Map of core samples, red: IODP -accomplished, green: non-IODP –accomplished, grey: ODP/IODP -in preparation. grey: ODP/IODP -in preparation.

Here the focus is set on how excessive freshwater input through melting of continental ice can affect its overturning vigour and, hence, heat supply to high northern latitudes. Such forcing can be tested by investigating its behaviour during extreme iceberg discharge events into the open North Atlantic during the last glacial period, so called Heinrich-Events [Heinrich 1988; Hemming 2004].

^{231}Pa and ^{230}Th are produced in the ocean through radioactive decay of their parent isotopes ^{235}U and ^{234}U at a constant rate (activity ratio = 0.093). Subsequently both isotopes are scavenged by sinking particles. The exploration of the temporal variability of the sedimentary ratio has been increasingly used as a kinematic circulation proxy in the Atlantic Ocean over the past years [Gherardi et al. 2009; McManus et al. 2004; Lippold et al. 2012]. The basis for the use of this proxy is an advective export of less particle reactive ^{231}Pa over ^{230}Th. Due to the unequal residence times of ^{231}Pa and ^{230}Th in the ocean the ratio ^{231}Pa/^{230}Th (Pa/Th in the following) indicates the strength of AMOC in the past.

Pa/Th cannot be used as a stand-alone proxy since it is also affected by changes in bioproductivity especially biogenic opal [Anderson et al. 1983A; Bradtmiller et al. 2007; Chase et al. 2002]. Besides this potential complication of the Pa/Th method, it is important to note that the response of sedimentary Pa/Th on AMOC in the Atlantic Ocean is a function of water depth and latitude [Francois 2007; Gherardi et al. 2010].

In this project we have measured Pa/Th in numerous sediment cores across Heinrich events 1 and 2 thus strongly augmenting the available database of Pa/Th for the investigation of the Atlantic Ocean deep circulation studies (Fig.1). These measurements are accompanied by the determination of the biogenic opal content of the sediment samples. Strength and geometry of the AMOC before, during and after the Heinrich-Events 1 and 2 can be derived from this new database in an inverse model approach [Luo et al. 2010]. By this we are aiming for answering the question if Heinrich-Events either caused cessations of AMOC or if maybe in contrast Heinrich-Events are the result of AMOC changes. Thus, in the context of potential ice shield melting and increasing precipitation in the northern North Atlantic, Heinrich-Events may display a model scenario improving our understanding of the upcoming response of AMOC on climate changes.

Experimental progress/Laboratory work

In total 76 sediment core samples have been selected and investigated regarding ^{231}Pa/^{230}Th.

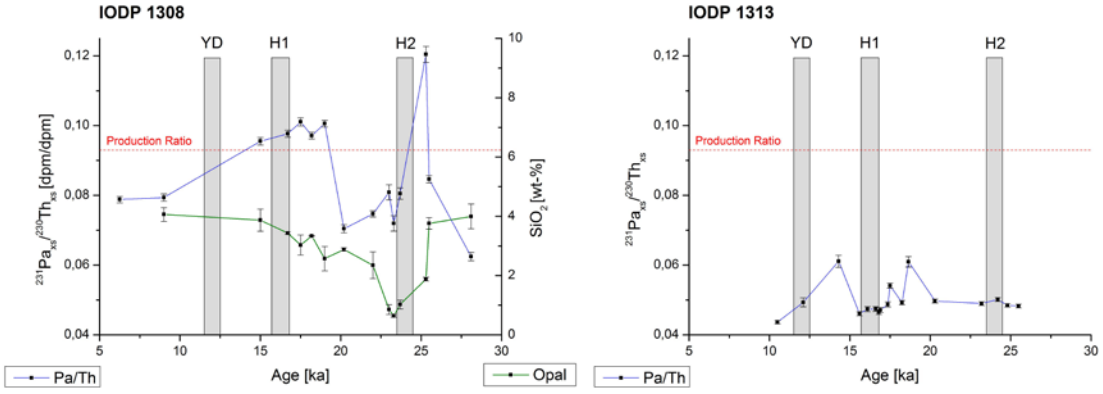

Fig. 2: Left: Measurements of Pa/Th (blue) and biogenic opal (green) on the core IODP 1308.
Right: Pa/Th of core IODP 1313. The red dotted line indicates the acticity ratio 0.093. Water depth are 3871 m (IODP 1308) resp. 3412 m (IODP 1313).

The new data stack contains so far samples of the cores IODP 1308, IODP 1313 and IODP 1314. In addition cores Me 69-196 (original "Heinrich-core") and GeoB 16202-2 were studied in the same way. All of those samples became investigated to an age back to at least 24 ka (Heinrich Event 2). They will be accompanied by measurements of biogenic opal in order to exclude local particle composition effects.

In general a Pa/Th signal close to the production ratio of 0,093 points to a weakened AMOC and/or influence of biogenic opal. Signals above the production ratio are an indicator for an opal-influence on protactinium scavenging. At IODP 1308 around Heinrich-Event 2 opal content in the sediment reaches a minimal influence followed by a strong increase. Here we found a distinct peak in Pa/Th (Fig.2, left) unrelated to biogenic opal. In contrast, site IODP 1313 shows an almost continous, very low signal of Pa/Th (Fig.2, right), significantly differing from the IODP 1308 profile. The comparison of both profiles demonstrates the potential pitfalls interpreating a single Pa/Th down-core profile. Instead it is necessary to build up a comprehensive and spatially well resolved data base in order to tap the full potential of Pa/Th.

Outlook

As shown in figure 1, numerous locations still need to be analysed. Approximately 150 sediment samples will be analysed for Pa, Th, U and biogenic opal in the next 12-18 months, many of those being in process. For some of the proposed sediment cores ^{14}C measurements are planned to improve or generate improved age models. First steps for modeling in comparison with the measurement data are currently underway to explore the experimental results and their significance in terms of ocean dynamics.

References:

Anderson, B., M. Bacon and P. Brewer, 1983A. Removal of 230Th and 231Pa at ocean margins. Earth and Planetary Science Letters, 66, 73-90.

Bradtmiller, L., R. Anderson, M. Fleisher and L. Burckle, 2007. Opal burial in the equatorial Atlantic Ocean over the last 30 kyr: implications for glacial-interglacial changes in the ocean silicon cycle. Paleoceanography, 22, PA4216.

Chase, Z., R. Anderson, M. Fleisher and P. Kubik, 2002. The influence of particle composition and particle flux on scavenging of Th, Pa and Be in the ocean. Earth and Planetary Science Letters, 204, 215-229.

Delworth, T., P. Clark, M. Holland, W. Johns, T. Kuhlbrodt, J. Lynch-Stieglitz, C. Morrill, R. Seager, A. Weaver and R. Zhang, 2008. Chapter 4. The Potential for Abrupt Change in the Atlantic Meridional Overturning Circulation. Synthesis and Assessment Product 3.4 Report by the U.S. Climate Change Science Program, U.S. Geological Survey (USGS).

Francois, R., 2007. Paleoflux and paleocirculation from sediment ^{230}Th and $^{231}Pa/^{230}Th$. Proxies in Late Cenozoic Paleoceanography. C. H.-M. a. A. d. Vernal, Elsevier, 681-716.

Gherardi, J.-M., L. Labeyrie, S. Nave, R. Francois, J. F. McManus, *and* E. Cortijo, 2009. Glacial-interglacial circulation changes inferred from 231Pa/230Th sedimentary record in the North Atlantic region, Paleoceanography, 24, PA2204.

Gherardi, J., Y. Luo, R. Francois, J. McManus, S. Allen and L. Labeyrie, 2010. Reply to comment by S. Peacock on "Glacial-interglacial circulation changes inferred from $^{231}Pa/^{230}Th$ sedimentary record in the North Atlantic region". Paleoceanography. 25, PA2207.

Heinrich, H., 1988. Origin and Consequences of Cyclic Ice Rafting in the Northeast Atlantic Ocean during the Past 130,000 Years. Quaternary Research, 29, 142-152.

Hemming, S. R., 2004. Heinrich events: Massive late Pleistocene detritus layers of the North Atlantic and their global climate imprint, Rev. Geophys., 42, RG1005.

Hodell, D., J. Channell, J. Curtis, O. Romero and U. Röhl, 2008. Onset of "Hudson Strait" Heinrich events in the eastern North Atlantic at the end of the middle Pleistocene transition (~ 640 ka)? . Paleoceanography. 23, PA4218.

Keigwin, D. and E. Boyle, 2008. Did North Atlantic overturning halt 17,000 years ago? Paleoceanography. 23, PA1101.

Lippold, J., J. Grützner, D. Winter, Y. Lahaye, A. Mangini and M. Christl, 2009. Does sedimentary 231Pa/230Th from the Bermuda Rise monitor past Atlantic Meridional Overturning Circulation?, Geophyscial Research Letters 36: L12601

Lippold, J., Y. Luo, R. Francois, S. Allen, J. Gherardi, S. Pichat, B. Hickey and H. Schulz, 2012. Strength and Geometry of the glacial Atlantic Meridional Overturning Circulation. Nature Geoscience, 10.1038/NGEO1608.

Luo, Y., R. Francois and S. Allen, 2010. Sediment $^{231}Pa/^{230}Th$ as a recorder of the rate of the Atlantic meridional overturning circulation: insights from a 2-D model. Ocean Science, 6, 381–400.

Lynch-Stieglitz, J., J. Adkins, W. Curry, T. Dokken, I. Hall, J. Herguera, J. Hirschi, E. Ivanova, C. Kissel, O. Marchal, T. Marchitto, I. McCave, et al., 2007. Atlantic Meridional Overturning Circulation During the Last Glacial Maximum. Science. Vol. 316, no. 5821, 66 - 69.

McManus et al., 2004. Collapse and rapid resumption of Atlantic meridional circulation linked to deglacial climate change, Nature, 428, 834-837.

Rahmstorf, S., 2002. Ocean circulation and climate during the past 120,000 years. Nature 419, 207-214.

Rahmstorf, S., 2005. Thermohaline circulation hysteresis: A model intercomparison. Geophys. Res. Lett. 32.

Yu, E., R. Francois and M. Bacon, 1996. Similar rates of modern and last-glacial ocean thermohaline circulation inferred from radiochemical data, Nature 379: 689-694.

IODP

Expedition Report - IODP Expedition 341 Southern Alaska Margin Tectonics, Climate and Sedimentation

H. BAHLBURG[1], C. MÄRZ[2], J. MÜLLER[3], IODP EXPEDITION 341 SCIENCE PARTY

[1]Institut für Geologie und Paläontologie, Westfälische Wilhelms-Universität Münster, Germany; hbahlburg@uni-muenster.de

[2]School of Civil Engineering & Geosciences, Newcastle University, Newcastle upon Tyne, UK

[2]Alfred Wegener Institute for Polar and Marine Research, Potsdam, Germany; Juliane.Mueller@awi.de

The Gulf of Alaska borders the accretionary St. Elias orogen, the highest coastal mountain range on Earth. Mt St. Elias reaches an altitude of c. 5500 m at 55 km from the coast. Formation of the mountain belt since the middle Miocene is connected to oblique collision of the Yakutat terrane with the North American plate. Exhumation of the windward, Gulf of Alaska side of the orogen accelerated dramatically at c. 1 Ma, during the Mid-Pleistocene Transition (MPT). Sediment is being generated by glacial erosion throughout this high relief coastal mountain range and is subsequently being transported to the Aleutian subduction zone. While the formation of the orogen is plate-tectonically driven, exhumation rates and the development of high relief topography are strongly linked to the presence of large ice sheets in the Pleistocene, and highly erosive temperate glaciers in the Holocene combined with high precipitation rates on the orogen's windward side. Changing global climate together with the evolution of the orogen also influenced paleoceanographic patterns in the Gulf of Alaska.

Integrated Ocean Drilling Program Expedition 341 drilled a five site transect across the Gulf of Alaska margin of North America with Site U1420 on the shelf, Sites U1419 and U1421 on the slope, and Sites U1418 and U1417 on the proximal and distal Surveyor Fan, respectively (Expedition 341 Scientists, 2013). Recovery of 3240 m of high quality sediment cores and development of spliced sedimentary records of the Pleistocene through Holocene were achieved at the distal, proximal, and slope

sites because of exceptional piston core recovery coupled with real-time stratigraphic correlation.

The obtained exemplary record allows us to address the main objectives of drilling in the Gulf of Alaska including to (i) document the tectonic response of an active orogenic system to late Miocene to recent climate change; (ii) establish the timing of advance/retreat phases of the northern Cordilleran ice sheet to test its relation to dynamics of other global ice sheets; (iii) implement an expanded source-to-sink study of the interactions between glacial, tectonic, and oceanographic processes responsible for creation of one of the thickest Neogene high-latitude continental margin sequences; (iv) understand the dynamics of productivity, nutrients, freshwater input to the ocean, and ocean circulation in the northeast Pacific and their role in the global carbon cycle.

More than 750 m of Miocene to Holocene sediments were recovered from Site U1417. A 30 m-thick interval of thin-bedded diamict interbedded with bioturbated mud is the earliest visible occurrence of ice-rafted debris (IRD) near the Plio-Pleistocene boundary. The diamict contains gravel size, subangular to subrounded clasts in a muddy matrix with gradational lower contacts. Deposition in the early Pleistocene is marked by mud interbedded with turbidite sand and silt beds, overlain by early to middle Pleistocene reoccuring intervals of diatom ooze and barren gray mud. IRD occurs as dispersed lonestones. Site U1418 recovered early Pleistocene to Holocene sediments.

Diamict deposition dominated from the early to middle Pleistocene, followed by deposition of interbedded silt and mud with lonestones. Diamict ranges from massive clast-poor beds up to 150 cm thick to thin beds of coarse sand and granules that are interbedded with laminated mud. Laminated sequences have gradational contacts and range from sub-millimeter (a few coarse silt grains) to 2 mm thickness. Packages of laminae are bounded by regularly spaced thin layers of coarse sand and granules. One interpretation is that the laminated portion is formed by suspension settling from meltwater plumes whereas the thin coarse-grained beds are deposited by rafting from sea ice. The thin granule layers may represent periods of enhanced sea-ice rafting. Diamict interbedded with mud containing IRD is the primary facies observed in the middle Pleistocene to Holocene sediments recovered from Sites U1419, U1420, and U1421. Diamict beds are thicker, more clast-rich, and have a coarser grained matrix than those deposited at other sites, reflecting their proximity to glaciers on the shelf. Some beds are interstratified with mud containing diatoms. This facies is interpreted to result from iceberg rafting and meltwater plumes.

Sediment accumulation rates vary from <100 m/Ma at the distal site to >1000 m/Ma on the proximal fan, slope and the continental shelf. At Site U1417, the onset of glaciation at the Plio-Pleistocene boundary resulted in a doubling of accumulation rates to ~100 m/Myr, the highest accumulation rates in the fan were recorded at Site U1418 with >1200 m/Myr in the late Pleistocene. All sites include the middle Pleistocene to Holocene and record exceptionally high accumulation rates.

Provenance analysis is a key instrument for elucidating the denudation history of source terranes and for quantifying their respective contributions to sedimentary routing systems and the detrital composition of sedimentary systems. Through time and from the distal to the proximal sites the lithological variety of lonestones and diamict clasts gradually changes from a dominance of metamorphic clasts (argillite, meta-basalt) to one of sedimentary and igneous clasts, namely sand- and siltstones, granitoids and basalt. Noteworthy are also coal clasts contained in upper Miocene strata at Site U1417 which are interpreted as being derived from the Eocene Kulthieth Formation exposed in the onshore thrust belt.

These preliminary results indicate that the sources and oceanographic dispersal mechanisms of clasts delivered to all sites varied in space and time. The metamorphic clasts recovered from the distal fan including its Neogene parts were likely derived primarily from the Chugach terrane in the coastal part of the St. Elias orogen. The sites on the Quaternary proximal fan, the upper slope and the distal shelf display a wider range of lithologies indicative mainly of the more interior parts of the convergent margin including the Wrangellia and Alexander terranes. Post-cruise analyses of sediment provenance will constrain the changing loci of erosion linking them back to onshore patterns of exhumation. This will permit the ultimate test whether rapid erosion has the potential to cause a positive feedback in exhuming an active orogen.

References:

Expedition 341 Scientists, 2013. Southern Alaska margin: Interactions of tectonics, climate, and sedimentation. IODP Prel. Rept., 341. doi:10.2204/iodp.pr.341.2013

IODP

Highly variable MOW flow speed during MIS 1-5 inferred from XRF scanning of contourite deposits in the Gulf of Cadiz (IODP Exp. 339)

A. BAHR[1], F. JIMENEZ-ESPEJO[2], N. KOLASINAC[1], P. GRUNERT[3], U. RÖHL[4], C. ESCUTIA[5], J. HERNÁNDEZ-MOLINA[6], D.A.V. STOW[7], D. HODELL[8], C. ALVAREZ-ZARIKIAN[9], IODP EXP. 339 SCIENTISTS[10]

[1]Institute of Geosciences, University Frankfurt, Altenhöferallee 1, 60438 Frankfurt, Germany
[2]Institute of Biogeosciences, Japan Agency for Marine-Earth Science and Technology, Yokosuka 237-0061, Japan.
[3]University of Graz, Institute for Earth Sciences, Heinrichstraße 26, A-8010 Graz, Austria
[4]MARUM, University of Bremen, Leobener Str., 28359 Bremen, Germany
[5]Instituto Andaluz de Ciencias de la Tierra (CSIC-UGR), Av. de las Palmeras, 4, 18100 Armilla (Granada), Spain
[6]Facultad de Ciencias del Mar, Universidad de Vigo, 36310 Vigo, Spain
[7]Institute of Petroleum Engineering, Heriot-Watt University, Edinburgh, EH13 4AS, UK
[8]Department of Earth Sciences, University of Cambridge, Downing Street, Cambridge, Cambridgeshire, CB2 3EQ, UK
[9]Department of Oceanography, Texas A&M University, 1000 Discovery Dr. College Station, TX 77845-9547, USA
[10]Acton, G., Balestra, B., Ducassou. E., Flood, R., Flores, J.A., Furota, S., Grunert, P., Kim, J. K., Krissek, L., Kuroda, J., Li, B., Llave, E., Lofi, J., Lourens, L., Miller, M., Nanayama, F., Nishida, N., Richter, C., Roque, C., Sanchez Goñi, M., Sierro Sanchez, F., Singh, A., Sloss, C., Takashimizu, Y., Tzanova, A., Voelker, A., Williams, T., Xuan, C.

During IODP Expedition 339 complete sequences of Pliocene and Quaternary contourite deposits were drilled in the Gulf of Cádiz. Since the build-up of these contourites is tightly linked to the Mediterranean Outflow Water (MOW)

they provide a unique archive of MOW variability and its influence on global circulation and climate. We performed high-resolution XRF scanning on spliced sections of two sites: 1) U1387, located on Faro Drift in 559.1 m water depth in the upper branch of the MOW, and 2) U1389, in 644 m water depth on Huelva Drift ~90 km W of Cádiz, located more proximal to the Gibraltar Gateway. Due to their different water depths, both sites can be used to infer vertical shifts of the MOW. The high sedimentation rates (25 cm/kyr for U1387 and ~40 cm/kyr for U1389) permit high-resolution reconstruction of MOW strength in millennial-scale resolution.

Based on the good correlation of the Zr/Al ratio with grain size changes we propose that Zr/Al can be used to reconstruct bottom current strength, hence, MOW activity. For correlating both sites by means of XRF data Br appears to be most valuable, as the Ca signal, typically reflecting climate-driven carbonate production, is severely compromised by reworking. For the investigated interval of MIS 1 to 5 we identify a strong link to high northern latitude climate signals. High MOW is generally inferred during glacial terminations and high latitude cold phases (Last Glacial Maxiumum and Greenland Stadials during MIS 3-5). Heinrich-Events are also elevated in Zr/Al but show reduced MOW strength during the so-called "Sierro-Events". Minimum MOW strength has been reconstructed for the early Holocene and MIS 5e, concomitant to sapropel formation in the Mediterranean Sea. Hence, there is a tight link to deep water production in the Mediterranean. While most of these changes occur rather synchronously at both sites, we observe a more complex behavior of the MOW during MIS 5b-e. In particular during MIS 5b-c a shoaling of the MOW core occurs synchronously to the intensification of the subtropical gyre circulation in the Northern Atlantic. The accompanying salt accumulation in the subsurface of the mid latitudes might have altered the density gradient in the Gulf of Cádiz and thereby forced the migration of the MOW into shallower water depths.

ICDP

Resolving sedimentary sulfur cycling during the Shunga Event (early Palaeoproterozoic) with sulfur isotopes

D. BANNING[1], H. STRAUSS[1], V.A. MELEZHIK[2], A. LEPLAND[2], M.J. WHITEHOUSE[3]

[1]Westfälische Wilhelms-Universität Münster, Institut für Geologie und Paläontologie, Münster, Germany
[2]Geological Survey of Norway (NGU), Trondheim, Norway
[3]Swedish Museum of Natural History, Box 50007, SE-104 05 Stockholm, Sweden

Early Earth's ocean - atmosphere system experienced fundamental global events during the early Palaeoproterozoic including the unprecedented accumulation of organic matter during the Shunga event in the aftermath of the Lomagundi-Jatuli Event (e.g. Melezhik et al., 1999a, b) ~2.05 billion years ago (Hannah, 2008) and the Great Oxidation Event (GOE, 2.3 Ga) (Holland, 1999) causing enhanced terrestrial sulfide weathering and subsequent delivery of sulfate to the ocean (Reuschel et al., 2012). The enhanced input of sulfate into the ocean water most likely resulted in an increased role of sulfate reducing bacteria in the microbial turnover of sedimentary organic matter which is archived in the isotopic signature of sulfur bearing minerals embedded in the Palaeoproterozoic sediments.

The data presented here are based on analyses of drillcore material from the Fennoscandia Arctic Russia – Drilling Early Earth Project (FAR DEEP). The drilling location is situated near Shunga, which is north of Petrozavodsk near the Onega Lake in NW Russia. Some 744 m of "shungite" drillcore from three drillholes within the c. 2.05 Ga old Zaonega Formation (ZF) were recovered. The main objective of this project is to resolve sedimentary sulfur cycling during the early Palaeoproterozoic with sulfur isotopes and related

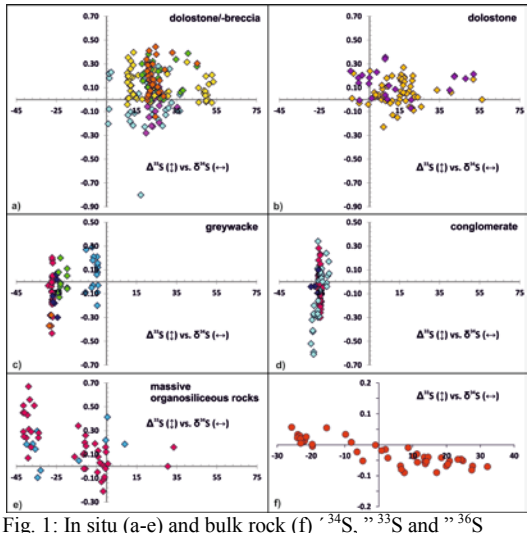

Fig. 1: In situ (a-e) and bulk rock (f) ´^{34}S, ” ^{33}S and ” ^{36}S

geochemical markers.

The rhythmically bedded sedimentary rocks of the ZF were deposited in a low-energy, non-euxinic environment (Melezhik et al., 1999a) and are of typically black to grey colour due to the great amount of organic matter which is most likely of algal or bacterial origin (Melezhik et al., 1999a). The rocks deposited during the Shunga Event underwent metamorphic alteration under greenschist facies conditions during the 1.8 Ga Svecofennian orogeny (Melezhik et al., 1999a). Iron sulfides are very common in these sedimentary rocks and show a high variability in their habitus with pyrite and pyrrothite being the most prevalent iron monosulfides and disulfides. The complex pattern of the iron sulfide morphologies and their geochemical characteristics relate to the nature of marine sulfur cycling, to different sulfide or sulfate generation stages, late-

diagenetic processes (e.g. migration of solutes) and organic matter degradation accompanying the generation and migration of bitumen within the sediments of the ZF (Melezhik et al., 2009; Strauss et al., 2013) as a result of postdepositional processes.The migrated hydrocarbons, now petrified (locally termed as shungite) complicate the interpretation of the collected dataset in terms of primary versus secondary pyrite formation. Therefore, it is of major interest to assess the different aforementioned processes.

Initially, sulfur and carbon contents were measured, in the following expressed as total sulfur (TS), total carbon (TC) and total inorganic carbon (TIC) abundances in bulk

rock samples with a CS MAT 5500 in Münster. Results are outlined in ICDP-IODP abstract volume 2013.

Stable sulfur isotopic data were obtained via sequential extraction procedure (SEP) after Canfield et al. (1986) and subsequent mass spectrometry. Based on highly variable $\delta^{34}S$ values of the chromium reducible fraction (CRS; disulfides; mainly pyrite) with -28.10 to +33.9 ‰ VCDT and of the acid volatile fraction (AVS; monosulfides) within the same range, differences in microbial sulfur cycling can be deduced. Although no clear correlation between $\delta^{34}S$ values and TOC or TIC contents could be observed, samples displaying the highest values for TOC (24.19 to 45.32 wt.%) show preferentially negative $\delta^{34}S$ signals, which is consistent with bacterial sulfate reduction (-5.0 and -28.1 ‰ VCDT). Up-section of the drillcore a general positive shift of $\delta^{34}S$ is discernible, which can be interpreted as a change towards a limited sulfate supply and subsequently, successively heavier $\delta^{34}S$ signatures of the residue. A positive correlation between $\delta^{34}S$ and total sulfur content in the uppermost massive organic matter rich rocks could be observed (TS 0.64 to 23.23 wt.%; +12.5 to +24.8 ‰ VCDT), whereas the deeper ones show negative signatures (-5.0 ‰ to -19.6 ‰ VCDT) with relatively constant TS values of 2 wt.% on average. Below 315 m in drillcore 12B two magmatic rock members occur whose bulk rock samples show a less negative isotopic signature of sulfur than for the intercalated greywacke siltstones and organic matter-rich rocks.

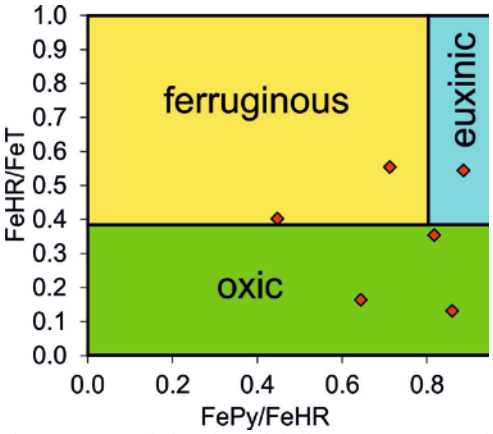

Fig. 2: Iron speciation data of drillcores 12A, 12B and 13A.

High-spatial in situ isotopic measurements on single sulfide grain scale were conducted on the Nordsim ion probe facility in Stockholm and yielded extreme values for $\delta^{34}S$ between -41.62 ‰ and +84.98 0 and for $\Delta^{33}S$ of -0.61 ‰ to +0.97 ‰ VCDT. A maximum fractionation within one sample of 75.10 0 for $\delta^{34}S$ and 1.18 ‰ for $\Delta^{33}S$ (organosiliceous rock) could be determined. Mass independent fractionation (MIF) of stable sulfur isotopes is commonly accepted as a proxy for a oxygen free atmosphere (Farquhar et al., 2000). The MIF signature in $\Delta^{33}S$ of -0.34 ‰ to -0.30 ‰ in the conglomerates (Fig. 1d) and of -0.43 ‰ to -0.30 ‰ in the greywacke (Fig. 1c) are interpreted as inherited signal of older source rocks deposited in a pre-GOE atmosphere. A high variability in $\Delta^{33}S$ in contrast to a relatively narrow range of $\delta^{34}S$ values (Fig.1c and d) was measured with variations on average of 4.10 ‰ for the conglomerates and 3.22 ‰ for the greywackes. Samples taken from a massive organosiliceous rock member (Fig. 1e; middle member) show a very wide range of values with $\delta^{34}S$ -41.62 ‰ to +33.48 0 and $\Delta^{33}S$ -0.21 ‰ to +0.97 ‰. The dolostone samples are characterized by a wider range in $\delta^{34}S$ values with most values plotting in the positive field.

Moreover, multiple sulfur isotope analysis ($\Delta^{33}S$) on 43 bulk rock CRS samples have been performed are illustrated in figure 1f. In general the samples show an average $\Delta^{33}S$ value of -0,027 ‰ with a maximum range from -0.090 to +0.057 ‰. These results are in good agreement with literature data for other post-GOE sediments (e.g. Whitehouse et al., 2005, Young et al., 2013)

Abundances of different iron species within the sedimentary framework can reveal ancient redox conditions in the marine water column. A set of 23 samples was selected in respect to their depositional character. All of them show mostly primary bedding with minor influence of secondary mobilization of organic material (e.g. shungite) or conglomeratic, becciated or volcanic compartments (dykes, etc.). They also exhibit graded bedding as an additional evidence for subsequently less reworked sediments. Sequential iron extraction procedure on these bulk rock samples was conducted following the specifications outlined in Poulton and Canfield (2005) for carbonate assiciated iron (Fe_{Carb}), (dithionite-) reducible iron (FeD), magnetite iron (Fe_{Mag}) and total iron which is the sum of these first 3 steps (Fe_{Tot}). Disulfide iron (Pyrite; FePy) and monosulfide iron were derived from aforementioned sulfur SEP. As a significant amount of the sulfides are preserved as iron-monosulfides (pyrrothite; Fe_{Po}), the assumptions of Poulton and Canfield (2005) have to be modified as followes: $FeS=Fe_{Py}+Fe_{Po}$ and therefore $FeHR=FeD+Fe_{Py}+Fe_{Po}$ and $FeT=Fe_{Tot}+Fe_{Py}+Fe_{Po}$. In modern environments oxic conditions can be found in the field FeHR/FeT <0.38 and the transition between euxinic and ferruginous conditions lies on the line of FeD/FeHR = 0.8 (Li et al., 2010). As illustrated in figure 2, most data plot in the field for euxinic sediments and range from FeHr/FeT 0.48 to 0.99 and FePy/FeHR 0.82 to 1.00. Two samples plot in the fields of ferruginous conditions and three approximately plot in the field of oxic conditions.

Acknowledgements: Financial support through the Deutsche Forschungsgemeinschaft (STR281/35) is gratefully acknowledged.

References:

Canfield, D.E., Raiswell, R., Westrich, J.T., Reaves, Berner, R.A. (1986). The use of chromium reduction in the analysis of reduced inorganic sulfur in sediments and shales. Chemical Geology 54: 149-155.

Farquhar, J.; Bao, H.; Thiemens, M. (2000). Atmospheric influence of Earth's earliest sulphur cycle. Science 289:756-758.

Hannah, J.L. (2008). Re-Os geochronology of a 2.05 Ga fossil oil field near Shunga, Karelia, NW Russia. Abstract, 33rd International Geological Congress, Oslo, 2008, 6-14 August

Holland, H.D. (1999). When did the Earth's atmosphere become oxic? The Geochemical News 100: 20-22.

Li, C.; Love, G.D.; Lyons, T.W.; Fike, D.A.; Sessions A.L.; Chu, X. 2010.A Stratified Redox Model for the Ediacaran Ocean. Science 328: 80-83.

Melezhik, V.A., Fallick, A.E, Filippov, M. M. Larsen, O. (1999a). Karelian shungite - an indication of 2.0-Ga-old metamorphosed oil-shale and generation of petroleum: geology, lithology and geochemistry. Earth-Science Reviews 47: 1-40.

Melezhik, V.A., Fallick, A.E., Medvedev, P.V., Makarikhin, V.V. (1999b). Extreme $^{13}C_{carb}$ enrichment in ca. 2.0 Ga magnesite-stromatolite-dolomite-`red beds´ association in a global context: A case for the world-wide signal enhanced by a local environment: Earth-Science Reviews 48: 71–120.

Melezhik, V.A., Fallick, A.E, Filippov, M.M., Lepland, A., Rychanchik, D.V., Deines, Y.E., Medvedev, P.V., Romashkin, A.E., Strauss, H.

(2009). Petroleum surface oil seeps from a Palaeoproterozoic petrified giant oilfield. Terra Nova 21: 119–126.
Poulton, S.W.; Canfield, D.E. (2005) Development of a Development of a sequential extraction procedure for iron: implications for iron partitioning in continentally derived particulates. Chemical Geology 214: 209-221.
Reinhard, C.T.; Lyons, T.W.; Rouxel, O.; Asael, D.; Dauphas, N.; Kump, L.R. (2012) Iron Speciation and Perspectives on Palaeoproterozoic Water Column Chemistry. In: Reading the archive of Earth´s oxygenation, Vol.3, pp. 1483-1492.
Strauss, H.; Melezhik, V.A.; Lepland, A.; Fallik, A.E.;.Hanski, E.J.; Filippov, M.M.; Deines, Y.E.; Illing, C.J.; • rne, A.E.; Brasier, A.T. (2013) Enhanced accumulation of organic matter: The Shunga Event. In: Reading the archive of Earth´s oxygenation, Vol.3, pp. 1195-1273.
Whitehouse, M.; Integrated Pb- and S-isotope investigation of sulphide minerals from the early Archaean of southwest Greenland
Young, S. A.; Loukola-Ruskeeniemi K., Pratt L.M. (2013), Reactions of hydrothermal solutions with organic matter in Paleoproterozoic black shales atTalvivaara, Finland:Evidencefrom multiple sulfur isotopes. Earth andPlanetaryScienceLetters 367: 1-14.

IODP

Evolution of deep-ocean circulation during the opening of the Atlantic Ocean in the latest Cretaceous and Paleocene

S. BATENBURG[1], S. VOIGT1[1], O. FRIEDRICH[2], M. FRANK[3]

[1]Goethe University Frankfurt
[2]University Heidelberg
[3]GEOMAR Kiel

This project aims at the identification of different intermediate- and deep-water masses within the Atlantic Ocean during latest Cretaceous to Paleocene times (75-55 Ma) by recognition of their potential source regions and detection of the time when deep-water connections between the oceanic sub-basins were established.

During Year 1, the main focus of work was the generation of the data as listed below:

Generation of a ´13C record for the Maastrichtian of Site U1403, Newfoundland margin, which is biostratigraphically calibrated to calcareous nannofossil events (Expedition 342 Scientists, 2012).

Completion of Nd isotope analyses at Sites U1403 and 525 (Walvis Ridge) for the 75-65 Ma time interval (Fig. 1).

Nd isotope analyses at sites across the Walvis Ridge-Rio Grande Rise structure (Site 1267) and the Cape Verde Basin (Site 369) are currently in progress.

Stratigraphy: The new ´^{13}C record for the Maastrichtian interval at Site U1403 can be tied into the global carbon-isotope stratigraphic framework with its prominent events, the mid-Maastrichtian Event (MME) and the Cretaceous-Paleogene transition (KPgE). The observed ´^{13}C pattern at Site U1403 allows for unprecedentedly detailed correlation with ´^{13}C variations at Gubbio (Italy; Voigt et al., 2012), ODP-Site 1210 (Voigt et al., 2012) and the orbitally-tuned ´^{13}C record of Zumaia-Sopelana, northern Spain (Batenburg et al., 2012, 2014) thus providing excellent age control for this site.

Work on ferromanganese coatings: Authigenic ferromanganese coatings of sediment particles acquire bottom-water μNd signatures during their early diagenetic formation near the sediment–water interface and are generally robust to later alteration (Gutjahr et al., 2007; Martin et al., 2010). However, during our work on samples of Site 525 we observed in parts very similar $\mu_{Nd(t)}$ values for coatings and the total dissolved detrital sediment (Voigt et al., 2013). This pattern is conspicuous to be caused by partial dissolution of detrital components. The detrital fraction may contain a reactive acid-extractible fraction, which might alter the $\mu_{Nd(t)}$ of the coatings (Wilson et al., 2013). Based on the distinct separation of $^{87}Sr/^{86}Sr$ ratios in the coatings and dissolved sediments and the good agreement of the $^{87}Sr/^{86}Sr$ ratio of coatings with the seawater strontium isotope signal, we concluded that the ferromanganese coatings at Site 525 represent a seawater signature (Voigt et al., 2013).

Another still not well constrained effect possibly responsible for similar $\mu_{Nd(t)}$ values in coatings and detrital fraction is the elemental release from basaltic sediments to bottom waters on ocean margins by boundary exchange (Lacan and Jeandel, 2005). Recent experimental studies have shown this process to exert a major control on the isotopic composition of seawater (Pearce et al., 2013). With this projectl we want to address this issue in more detail, in particular for the interval of highly radiogenic $\mu_{Nd(t)}$ values at Walvis Ridge in the early Maastrichtian. Concomitant measurements of $\mu_{Nd(t)}$ values in three different archives, fish teeth, ferromanganese coatings of bulk sediments and of foraminifera, will provide a test for the partial influence of detrital particles on the isotopic composition of coatings given that fish teeth and foraminifera are independent from the release of Nd from the particles during extraction procedures.

Latest Cretaceous to early Cenozoic Atlantic water mass characterization: Based on the new μNd(t) data obtained from Sites U1403 and 525, we make the following first observations (Fig. 1):

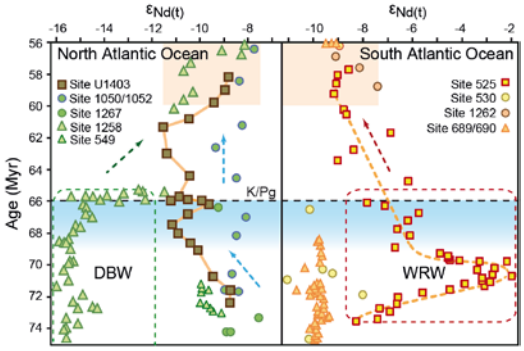

Figure 1: Preliminary Nd isotope data of coatings for Sites U1403 and 525 in comparison to published data (MacLeod et al., 2008, 2011; Martin et al., 2012, Robinson and Vance, 2012; Robinson et al., 2010; Thomas et al., 2003; Via and Thomas, 2006; Voigt et al., 2013).

The extension of the $\mu_{Nd(t)}$ record at Site 525 into the Paleocene clearly shows that the occurrence of highly radiogenic values only reflected a brief interval in the Maastrichtian prior to the MME (72-70 Ma), which seems to have been related to a period of increased hot-spot related volcanism. This answers one of the questions addressed in the original proposal: How long did intermediate water with a highly radiogenic Nd signature prevail in the South Atlantic? Whether this signal was caused by increased syndepositional leaching of ash particles, elemental release from the sediments or partial dissolution of the detrital fraction will be addressed by additional measurements. Furthermore, we hypothese here, that combined $\mu_{Nd(t)}$ data in coatings and fish teeth might be a tool to decipher volcanic events in the oceanic record, in

particular, since similarly radiogenic excursions were reported for the C/T and K/Pg boundaries at Demerara Rise (MacLeod et al., 2008; Martin et al., 2012).

From 69 Ma onwards, $\mu_{Nd(t)}$ values at the crest of Walvis Ridge (Site 525) continuously decreased until 60 Ma ago, when they reached values of ~-9. This long-term trend likely reflects cessation of magmatic activity with subsequent cooling of oceanic crust and deepening of the Walvis Ridge from shallow to deep bathyal depths.

The μNd(t) record at Site U1403 displays a decrease towards unradiogenic values in the Maastrichtian between 72 and 67 Ma and relatively negative values between 67 and 62 Ma (μNd(t) -10.5 to -11.5) followed by a rise up to -9 until 60 Ma.

The seawater μNd(t) signatures in the 67-62 Ma interval at Site U1403 were clearly distinct from those recorded further south in the North Atlantic at Blake Plateau (Sites 1050 and 1052), which rather constant values near -8. Possible explanations are still a matter of debate but could include a period of elevated non-radiogenic weathering inputs from the North American craton. This idea is testable by the analysis of seawater radiogenic Pb-isotope compositions, a proxy that reflects the weathering provenance and intensity in the hinterland (e.g. Gutjahr et al., 2009).

In the latest Maastrichtian, the Site U1403 $\mu_{Nd(t)}$ record displays a short-term positive excursion towards the K/Pg boundary (67-66 Ma) followed by a sudden drop to unradiogenic values at the K/Pg boundary itself. We speculate that there was a link to changes in ocean circulation related to climatic changes observed in the pre-extinction interval followed by a sudden ventilation of the entire North Atlantic as a consequence of the impact. Here, we plan to enhance the resolution of the $\mu_{Nd(t)}$ record across the K/Pg boundary to obtain a clearer picture of the exact stratigraphic level of this excursion and its relation to available paleoclimatic data.

The most important finding so far from the first data of the two sites, U1403 and 525, is the occurrence of a common deep-water neodymium isotope signature ($\mu_{Nd(t)}$ -9) in the North and South Atlantic since 60 Ma ago. This period might thus represent the time when the sub-basins of the deep Atlantic became fully connected and a deep-water mass with a common source and $\mu_{Nd(t)}$ signature prevailed over a broad range of water depths indicating vigorous deep ocean circulation. A possible site of deep-water formation located somewhere in the high southern latitudes has previously been proposed and is consistent with the $\mu_{Nd(t)}$ signature observed in our new records.

References:

Batenburg, S.J. et al. 2012. Earth and Planetary Science Letters 359-360, 264–278.
Batenburg, S.J. et al. 2014. Journal of the Geological Society, doi: 10.1144/jgs2013-015.
Expedition 342 Scientists, 2012. IODP Preliminary Report, 342. doi:10.2204/iodp.pr.342.2012
Lacan, F., and Jeandel, C., 2005. Earth and Planetary Science Letters 232, 245–257.
MacLeod, K.G. et al. 2011. Nature Geoscience 4, 779–782.
MacLeod, K.G., Martin, E.E., and Blair, S.W., 2008. Geology 36, 811–814.
Martin, E.E. et al. 2010. Chemical Geology 269, 414-431.
Martin, E.E. et al. 2012. Earth and Planetary Science Letters 327, 111–120.
Gutjahr, M. et al. 2007. Chemical Geology 242, 351–370.
Gutjahr, M. et al 2009. Earth and Planetary Science Letters 286, 546–555.
Pearce, C.R. et al. 2013. Earth and Planetary Science Letters 369-370, 138-147.
Robinson, S.A.,Vance, D.,2012. Paleoceanography 27, PA1102, http://dx.doi.org/10.1029/2011PA002240.
Robinson, S.A. et al. 2010. Geology 38, 871–874.
Thomas, D.J., 2004. Nature 430, 65–68.
Thomas, D.J., Bralower, T.J., and Jones, C.E., 2003. Earth and Planetary Science Letters 209, 309–322.
Via, R.K., Thomas, D.J., 2006. Geology 34, 441–444.
Voigt, S., Gale, A.S., Jung, C., Jenkyns, H.C., 2012. Newsletters on Stratigraphy 45, 25–53.
Voigt, S. et al. 2013. Earth and Planetary Science Letters, 369–370,169-177.
Wilson, D.J., Piotrowski, A.M., Galy, A., Clegg, J.A. 2013. Geochimica et Cosmochimica Acta 109, 197–221.

IODP

Climate evolution and terrestrial vegetation changes in the NW Pacific from the Holcene to the late Miocene

T. BAUERSACHS[1], A.S. JONAS[1], L. SCHWARK[1]

[1]Christian-Albrechts-University, Institute of Geosciences, Department of Organic Geochemistry, Ludewig-Meyn-Str. 10, 24118 Kiel, Germany

The late-Miocene to Holocene is a time period of severe perturbations of the global carbon cycle associated with significant changes in ocean circulation patterns and climate evolution, including the transition from the mid-Pliocene climate optimum to the Pleistocene ice-age era. While detailed climate records are available for the North Atlantic and the central Pacific, only little information on the climate evolution of the NW Pacific Ocean from the Miocene to the present-day is available. In this study, we investigated a ca. 8 Ma spanning sequence of deep-sea sediments recovered from sites C0011 and C0018 off the coast of Japan using stable carbon isotopes and lipid biomarkers in order to determine climate variation of the NW Pacific and associated vegetation changes on the East Asian continent. Our results demonstrate that TEX_{86} – based sea surface temperatures (SST) in this area show a long-term warming trend with temperatures ranging from 17 ºC during the Pleistocene to almost 30 ºC in the late Miocene. An overall similar pattern of SST variation for our study sites was deduced from the $U^{K'}_{37}$ and the long-chain diol index (LDI). Both lipid paleothermometers show an overall increase in SSTs over time with values ranging from ca. 21-27 °C for the $U^{K'}_{37}$ and ca. 19-26 °C for the LDI, respectively. $U^{K'}_{37}$- and LDI-based temperature estimates usually exceed TEX_{86}-reconstructed temperatures by 2-6 °C except in the lower part of the core where the opposite trend is observed. Offsets between the TEX_{86}- and $U^{K'}_{37}$-derived temperatures with the former yielding lower temperatures have previously been reported from the South China Sea (Jia et al. 2012) and it was posited that the TEX_{86} proxy records temperatures below the photic zone near the mix-layer-thermocline. Interestingly, the change in TEX_{86} and $U^{K'}_{37}$ as well as LDI reconstructed temperatures occurs around 3.3 Ma ago, which agrees with the closing of the Indonesian Seaway leading to the reorganization of the Pacific Ocean circulation (Nathan and Leckie 2009). It has been proposed that the closing of the Indonesian Seaway has resulted in the deepening of the thermocline depth, which is supported by our observations. When viewed in concert with previous SST estimates from the Western Pacific Warm Pool (LaRiviere et al. 2012), our new SST record of the NW Pacific also reveals that late Miocene meridional SST gradients were significantl reduced relative to those of the Pliocene.

Preliminary MBT/CBT-data indicates that mean annual air temperatures (MAATs) are well correlated with changes

in SST and significantly decrease during the Pleistocene while they maximize around 3.0 Ma, corresponding to the mid-Pliocene climate optimum. Both bulk stable carbon isotopes and distribution pattern of long-chain *n*-alkyl lipids suggest that the observed long-term warming trend was associated with a reorganization of the terrestrial vegetation on the Japanese mainland and the East Asian continent. The average chain-length (ACL) of odd-numbered C_{27}-C_{31} *n*-alkanes and even-numbered C_{28}-C_{32} *n*-fatty acids, which originate from epicuticular waxes of vascular plants, significantly increased during glacial periods of the Pleistocene. In contrast, the ACL of long-chain *n*-alkyl lipids generally decreased during interglacial periods and showed lowest values during the Pliocene climate optimum. *n*-Alkyl lipid distributions with comparatively high abundances of the C_{31} homologue have been reported from various families of Monocotyledons (Schwark et al. 2002; Duan et al. 2011) and the elevated concentrations of this component during glacial periods suggests a proliferation of a grass-like vegetation in the NW Pacific region. This finding is sustained by a general increase in sedimentary $\delta^{13}C_{org}$ values during glacial compared to interglacial periods, which may suggest an increased loading of organic matter derived from plant sources using the C_4 photosynthetic pathway. In addition, periods characterized by significant cooling show increased abundances of nonacosane-10-ol, a biological marker for representatives of the *Picea* (Jetter et al. 2006), suggesting a proliferation of conifer species during the glacial periods of the Pleistocene. This is in agreement with the reported spread of an open *Larix-Picea* forest on the northern Japanese islands based on pollen distributions (Inagaki et al. 2009). Our results thus contribute to a better understanding of the long-term ocean history of the NW Pacific, for which so far only limited information is available.

References:
Duan, Y., He, J. (2011) Distribution and isotopic composition of n-alkanes from grass, reed and tree leaves along a latitudinal gradient in China. Geochemical Journal 45: 199-207
Inagaki, M., Yamamoto, M., Igarashi, Y., Ikehara, K. (2009). Biomarker records from Core GH02-1030 off Tokachi in the northwestern Pacific over the last 230,000 years: Environmental changes during the last deglaciation. Journal of Oceanography 65: 847-858
Jetter, R., Kunst, L., Samuels, A.L. (2006). Composition of plant cuticular waxes. In: Riederer, M., Müller, C. (eds.) Annual plant reviews, biology of the plant cuticle. Blackwell Publishing Ltd, Oxford, pp. 145-181
Jia, G., Zhang, J., Chen, J., Peng, P.A., Zhang C.L. (2012). Archaeal tetraether lipids record subsurface water temperature in the South China Sea. Organic Geochemistry 50: 68-77
LaRiviere, J.P., Ravelo, A.C., Crimmins, A., Dekens, P.S., Ford, H.L., Lyle, M., Wara, M.W. (2012). Late Miocene decoupling of oceanic warmth and atmospheric carbon dioxide forcing. Nature 486: 97-100
Nathan, S.A., Leckie, R.M. (2009). Early history of the Western Pacific Warm Pool during the middle to late Miocene (similar 13.2-5.8 Ma): Role of sea-level change and implications for equatorial circulation. Palaeogeography Palaeoclimatology Palaeoecology 274: 140-159
Schwark, L., Zink, K., Lechterbeck, J. (2002) Reconstruction of postglacial to early Holocene vegetation history in terrestrial Central Europe via cuticular lipid biomarkers and pollen records from lake sediments. Geology 30: 463-466

ICDP

Seismic reflection profiling of the Baza Basin (Southern Spain) – Preliminary results

M. BAUMANN-WILKE[1], CH. HABERLAND[1], M. STILLER[1], L. GIBERT[2], M. J. JURADO[3], G. SCOTT[4]

[1]GeoForschungsZentrum Potsdam, Germany
[2]Universitat de Barcelona, Spain
[3]Institute of Earth Sciences Jaume Almera, CSIC, Barcelona, Spain
[4]Berkeley Geochronology Center, United States of America

The Baza Basin is an intra-mountain evaporitic basin in the Betic Cordillera (Southern Spain). The basin is formed by Pliocene to Pleistocene sediments. It can be distinguished into three lithological zones corresponding to different paleo-environments (Alfaro et al., 2010). The inner zone, interpreted as a central saline lake, is dominated by an alternation of gypsum and carbonate laminae. The intermediate zone is characterized by cyclic carbonate beds. This zone is interpreted as a mosaic of shallow lakes surrounding the inner zone. The marginal zone consists of lacustrine deposits which are surrounded by an alluvial belt. In the marginal zone, distal fan deposits and shallow lake sediments alternate as a result of fluctuations in the lake water level which are related to changes in climate (Gibert et al., 2007). Therefore, up to 2.5 km thick lacustrine and ancillary continental deposits are found in this part of the basin which provide an unique archive of climatic changes and paleo-climatic events. An ICDP drilling project (LARSEI – LAcustrine Record of SE Iberia) proposes to drill the marginal zone of the Baza Basin to analyze the sedimentary record with regard to the paleo-climate in the Mediterranean as well as on a global scale.In preparation for the future drilling activities, controlled-source seismic measurements are used to investigate the structure of the Baza Basin and to find local zones of neo-tectonic deformation bounding the basin to the west (Baza fault). The aim of the seismic work is to provide structural information for the planned scientific drilling project.End of October 2013 a seismic reflection experiment was carried out in the center of the Baza Basin. A net of three 2D seismic profiles was arranged crossing the basin and the bounding fault system. A vibroseis source (two vibrators with 200 kN peak force each) was used with a source point distance of 60 m along each of the 18 km long profiles. Eight sweeps with a frequency range of 8 – 100 Hz were conducted at each source point. The seismic wavefield was recorded by a cable-free acquisition system of more than 330 continuously operating digital data recorders. The receivers were spread along the currently active profile with a spacing of 20 m. They were moved in a roll-along-configuration to mainly cover the near-field offsets of the source points.

The seismic data of the three profiles were conventionally processed so far. We present current results of the ongoing seismic reflection processing with regard to the structure of the Baza Basin and the Baza fault system.

References:
Alfaro, P., Gibert, L., Moretti, M., García-Tortosa, F. J., Sanz de Galdeano, C., Galindo-Zaldívar, J. and Á. C. López-Garrido (2010) The significance of giant seismites in the Plio-Pleistocene Baza palaeo-lake (S Spain). Terra Nova, Vol. 22, No. 3, p. 172-179.
Gibert, L., Ortí, F. and L. Rosell (2007) Plio-Pleistocene lacustrine evaporites of the Baza Basin (Betic Chain, SE Spain). Sedimentary Geology, Vol. 200, No. 1-2, p. 89-116.

ICDP

First results from downhole logging in the ICDP project SCOPSCO at Lake Ohrid (Macedonia, Albania)

H. BAUMGARTEN[1], T. WONIK[1], A. FRANCKE[2], B. WAGNER[2], K. LINDHORST[3], S. KRASTEL[3] AND THE SCOPSCO SCIENCE TEAM

1 Leibniz Institute for Applied Geophysics (LIAG), Stilleweg 2, 30655 Hannover, Germany
2 Institute of Geology and Mineralogy, University of Cologne, Zülpicher Str. 49a, 50674 Köln, Germany
3 Institute of Geosciences, Christian-Albrechts-Universität zu Kiel, Otto-Hahn-Platz 1, 24118 Kiel, Germany

Ancient Lake Ohrid is located at the border between Macedonia and Albania (40°702 N, 20°42 E) and is assumed as the oldest lake in Europe. The lake with a surface area of 360 km² has trapped sediments and volcanic ashes over a long period and hence, contains essential information of major climatic and environmental change. The age estimates vary between 2 to 10 Ma, whereas age estimates from endemic species (molecular clock analysis) indicate a minium age of 1.5 Ma. Therefore, the lake is considered as extraordinary climate archiv of the central northern Mediterranean region.

Several scientific questions are adressed within the SCOPSCO project: age and origin of the lake, paleoclimatic change during the Quaternary, tephrostratigraphy, and driving forces for the outstanding biodiversity in Lake Ohrid.In the frame of the ICDP project SCOPSCO (Scientific Collaboration on Past Speciation Conditions in Lake Ohrid), sediments of Lake Ohrid have been targeted for a deep drilling campaign in spring 2013. Four sites (DEEP, CERAVA, GRADISTE, PESTANI) have been cored multiple timesup to a depth of ~568 m below lake floor (blf).

High-quality continuous downhole logging data have been achieved at all drill sites by the use of the following tools: spectral gamma ray, magnetic susceptibility, resistivity, dipmeter, borehole televiewer and sonic. Additionally, vertical seismic profiling was conducted at the DEEP site. Seismic investigations indicate a sediment fill of the lake basin up to a thickness of 700 m. First results from cores revealed, that the bottom part is characterized by coarser grained deposits while the upper part, above 430 meter blf, yields fine grained pelagic sediments.

The borehole logging data at the DEEP site shows strong contrasts in all physical properties, in particular in spectral gamma ray (gamma ray, K, U, Th-contents), magnetic susceptibility, resistivity and seismic velocity (vp). The bottom part (below 430 m blf) is characterized by higher gamma ray values of 70 gAPI compared to the pelagic sediments (above 430 m blf) showing mean values of 45 gAPI. Furthermore, the lacustrine facies show an cyclic alternation of low (20 gAPI) and high gamma ray values (65 gAPI). Numerous aspects will be investigated by use of information from downhole logging data. This includes an objective construction of a continuous lithological log whereby lithological units (electrofacies) will be interpreted by means of sedimentological information from cores. The physical properties from downhole logging data of the lacustrine facies will be analyzed focusing on changing sediment characteristics during glacial and interglacial periods. Furthermore, periodicities in the data will contribute to the construction of an age model together with chronological control (e.g. tephrostratigraphy and paleomagnetic information) spanning the younger 600,000 years. The spectral analysis will be applied with special emphasis on compaction of the sediment record and its effects on the analysis. The further characterization of the lacustrine sediment facies as well as their spatial distribution will be done by an integrated interpretation of physical properties from downhole logging and hydroacoustic data sets.

IODP

Fast response drilling and instrumentation of the 2011 Tohoku-Oki earthquake fault: a review of present accomplishments of IODP Expeditions 343 and 343T

JAN H. BEHRMANN[1], FREDERICK M. CHESTER[2], PATRICK M. FULTON[3], KOHTARO UJIIE[4], , WEIREN LIN[5], JAMES J. MORI[6], NOBUISHA EGUCHI[7], SEAN TOCZKO[7] AND EXPEDITION 343 AND 343T SCIENTISTS

[1]GEOMAR, Kiel, Germany
[2]Texas A&M University, College Station TX, U.S.A.
[3]University of California, Santa Cruz CA, U.S.A.
[4]Tsukuba University, Tsukuba, Japan
[5]Kochi Institute for Core Sample Research, Kochi, Japan
[6] Kyoto University, Kyoto, Japan
[7]CDEX JAMSTEC, Yokohama, Japan

Integrated Ocean Drilling Program (IODP) Expeditions 343 and 343T were conducted as a fast response to the great (moment magnitude = 9.0) 11th March 2011 Tohoku-Oki earthquake. The event produced very large displacements of about 50 meters near the Japan Trench, causing a devastating tsunami. Objectives accomplished on the expeditions were to drill, core and instrument boreholes (IODP Site C0019) targeted at the plate-boundary fault. Logging-while-drilling and core-sample observations showed that the large slip of the earthquake rupture was accommodated on a single slip zone hosted by a pelagic clay layer of less than five meters thickness, derived from the incoming Pacific Plate (Chester et al., 2013). This smectite-rich pelagic clay is the defining characteristic of the shallow earthquake fault, and implies a regionally important stratigraphic control on tsunamigenic earthquakes.

As frictional resistance on a fault during slip controls earthquake dynamics, the fault temperature after an earthquake offers important insight into the friction coefficient. The borehole temperature observatory was installed sixteen months after the earthquake across the fault, and the sensor string was successfully retrieved after nine months of operation. A 0.31°C temperature anomaly at the plate boundary fault was recorded. This corresponds to about 27 megajoules of energy per square meter dissipated during the earthquake (Fulton et al., 2013). The resulting apparent friction coefficient is 0.08. This is a value considerably lower than static friction coefficients known for most rocks.

High-velocity (1.3 meters per second) friction experiments on core samples of smectite-rich clay from the plate-boundary fault show very low peak and steady-state shear stresses, low friction coefficients, and very low stress drops (Ujiie et al., 2013). The low resistance to shear can

be attributed to the abundance of weak clay minerals (smectite) and thermal pressurization effects, which can facilitate fault slip. Extremely low coseismic strength of the plate-boundary fault is consistent with the inference of nearly total stress release during the earthquake from the post-seismic in situ stress determined from image logs and measurements of uniaxial compressive strength of sediments (Lin et al., 2013).

References:
Chester, F.M., Rowe, C., Ujije, K. et al., (2013) Science, 342, 1208-1211, doi: 10.1126/science. 1243719
Fulton, P.M., Brodsky, E.E., Kano, Y. et al. (2013) Science, 342, 1214-1217, doi: 10.1126/ science.1243641
Ujiie, K., Tanaka, H., Saito, T. et al. (2013) Science, 342, 1211-1214, doi: 10.1126/science. 1243485
Lin, W., Conin, M., Moore, J.C. et al. (2013) Science, 339, 687–690. doi:10.1126/science. 1229379

IODP

Eruption environments and subsidence of Louisville seamounts

C. BEIER[1], A.R.L. NICHOLS[2], P.A. BRANDL[1], S. KRUMM[1]

[1]GeoZentrum Nordbayern, Universität Erlangen-Nürnberg, Schlossgarten 5, D-91054 Erlangen
[2] Institute for Research on Earth Evolution (IFREE), Japan Agency for Marine Earth Science and Technology (JAMSTEC), 2-15 Natsushima-cho, Yokosuka, Kanagawa, 237-0061, Japan

The geochemical variability and the geochemical and petrological changes observed in oceanic intraplate volcanoes can be used to better constrain the origin and evolution of oceanic intraplate volcanoes. The along-chain temporal variability observed in long-lived seamount chains may be the result of changes in the conditions of melting, the composition of the mantle sources but may also arise from changes and interaction with the oceanic lithosphere. The two primary examples of long-lived seamount chains, the Hawaiian and the Louisville Seamount Chain in the Pacific Ocean both preserve more than 70 Ma of age progressive volcanism and thus allow the processes that may influence their compositions to be better determined. The Louisville Seamount Chain extends 4200 km from the youngest seamount ~300 km west of the Pacific-Antarctic spreading centre, dated at 1.11 Ma (Koppers et al., 2004), to Osbourn Guyot (~80 Ma) close to the Tonga trench. During IODP Expedition 330 five guyots along the westernmost 1500 km were drilled. Volcanic glass was recovered from four of these: Canopus (Site U1372), Rigil (Site U1374), Burton (Site U1376) and Hadar (Site U1377B) from north to south. The glasses were analysed for major (including Cl, F, S), trace and volatile elements by electron microprobe, laser ablation inductively coupled mass spectrometry (LA-ICP-MS) and Fourier-transform infrared (FTIR) spectroscopy.

In agreement with previously published whole rock data (Beier et al., 2011; Hawkins et al., 1987) and on-board whole rock data (Koppers et al., 2012) all glass samples belong to a suite of alkali basalts, basanites and trachybasalts. The major elements in the glasses from Canopus and Rigil define a liquid line of descent indicative of a significant fractional crystallisation of olivine, clinopyroxene and plagioclase in agreement with shipboard observations (Koppers et al., 2012). The overall variability of the drill samples is significantly less than that of the dredge samples. Major and trace elements for the volcanic glasses indicate that volcanism was geochemically extremely homogenous from ~85 Ma to 50 Ma, both along-chain and within a single volcanic edifice. In addition, the available samples provide no evidence of the tholeiitic shield stage seen in Hawaiian volcanoes. The trace elements show that the degrees and depth of partial melting within a single seamount, i.e. over the 1-3 Ma period of volcanism represented by the drill holes and along-chain over several million years remain constant, with the exception of Hadar Guyot that suggests preferential melting of an enriched source, possibly because it erupted on the oldest and thickest lithosphere along the Louisville seamount chain.

The H_2O contents of the glasses from volcaniclastic breccias in the igneous basement of Canopus, Rigil and Burton range from 0.07-0.12 wt.%. Glass on the chilled margins of intrusive sheets towards the bottom of the holes in Rigil and Burton have H_2O contents of 0.68 and 0.51-0.58 wt.%, respectively. Glass from the late-stage volcaniclastics in the sediment covering Rigil and Burton Guyots contains 0.47 and 0.29-0.30 wt.%, respectively. The only volcaniclastic sample from Hadar has a H_2O content of 0.09 wt.%, glass on chilled margins of intrusive sheets increase systematically downhole from 0.37-0.57 wt.%. None of the measured volatile phases (Cl, F, S and H_2O) vary systematically along-chain and, with the exception of H_2O in Hadar, downhole. However, a significant difference in glass volatile contents is observed between the various lithologies drilled. Low volatile contents in glass from the volcaniclastic breccias indicate that these glasses are degassed and have formed during shallow submarine eruptions or as subaerial flows that entered the sea. As these are now found throughout the igneous basement, the drilled depths may no longer reflect the relative age due to post-quench downslope movement of material. The slightly elevated volatile contents in the late-stage volcaniclastics suggest that these formed in submarine eruptions in water depths of 118 to 258 m below sea level. This implies that the volcanoes had subsided below sea level by the time they erupted. The glass from intrusion margins in Rigil, Burton and Hadar imply emplacement ~100 m below the surface. The paleo-quenching depths estimated from the volatile contents can be used to infer the subsidence that each seamount has experienced since formation. The required uplift to achieve these paleo-quench depths and the subsequent subsidence to reach their current depth exceeds that expected for normal oceanic lithosphere.

Lithosphere under the influence of a hot spot is expected to initially experience an enhanced rate of subsidence as it migrates away from the thermal anomaly, however, the subsidence observed in the Louisville seamounts is not as high as would be expected if the hot spot had reheated and thinned the lithosphere. Combined with the requirement of some dynamic uplift the subsidence anomalies of the drilled Louisville seamounts indicate, assuming all uplift and subsequent subsidence are caused by excess heat, that the temperature anomaly associated with the Louisville mantle plume is <100°C at 50-70 Ma, similar to those for other intraplate settings (Herzberg and Asimow, 2008). If dynamic flow or compositional buoyancy from the mantle plume also contributes, then the temperature anomaly may even be

smaller. Thus, the Louisville melting anomaly may be taken as a primary example of an extremely long-lived hotspot with a small temperature anomaly; however, contributions from compositional heterogeneities, such as volatiles, to melting cannot be ruled out at this stage.

References:
Beier, C., Vanderkluysen, L., Regelous, M., Mahoney, J.J., Garbe-Schönberg, D., (2011). Lithospheric control on geochemical composition along the Louisville Seamount Chain. Geochemistry, Geophysics, Geosystems, 12: Q0AM01. doi:10.1029/2011gc003690.
Hawkins, J.W., Lonsdale, P.F., Batiza, R., 1987. Petrologic evolution of the Louisville seamount chain. In: Keating, B.H. (Ed.), Geophysical Monograph Series. AGU, Washington D.C., pp. 235-254.
Herzberg, C., Asimow, P.D., (2008). Petrology of some oceanic island basalts: PRIMELT2.XLS software for primary magma calculation. Geochemistry, Geophysics, Geosystems, 9(Q09001). doi:10.1029/2008GC002057.
Koppers, A.A.P., Duncan, R.A., Steinberger, B., (2004). Implications of a nonlinear 40Ar/39Ar age progression along the Louisville seamount trail for models of fixed and moving hot spots. Geochemistry, Geophysics, Geosystems, 5(6): Q06L02. doi:10.1029/2003gc000671.
Koppers, A.A.P., Yamazaki, T., Geldmacher, J., Scientists, E., 2012. Proceedings of the Integrated Ocean Drilling Program. In: Integrated, 749 Ocean Drilling Program Management International, I. (Eds.), Tokyo.

ICDP

Metasomatic epidote veins, diopsidite and rodingite dikes: witnesses of fluid flow in the history of formation and emplacement of the Oman Ophiolite

B. BIESELER[1], N. JÖNS[1,2], W. BACH[1,2]

[1] University of Bremen, Department of Geosciences, Klagenfurter Straße (GEO), 28359 Bremen
[2] MARUM Zentrum für Marine Umweltwissenschaften, Leobener Straße, 28359 Bremen

The accretion of oceanic crust along mid-ocean ridge spreading centers is an essential part of Earth's tectonic cycle. However several details of this fundamental process remain poorly understood. For instance, the efficient cooling of fast spreading oceanic crust observed in seismic investigations (Dunn *et al.,* 2000) requires a larger amount of cooling than proposed. This deficit can be explained by deep seawater circulation into the hot gabbroic lower crust (Cherkaoui *et al.*, 2003). Detailed investigations of the lower 2/3 of the crust and the upper mantle remain inconclusive, because of a lack of sampling of in situ ocean lithosphere. Thus researchers have been looking for evidence of deep seawater circulation in ophiolite complexes such as the Oman Ophiolite (Nehlig & Juteau, 1988; Nicolas *et al.*, 2003).

Included in the long chain of Tethyan ophiolites, the Oman Ophiolite is a 500 km long, 50 km - 100 km wide and 10 - 15 km thick thrust sheet of oceanic lithosphere, located in the east of the Arabian Peninsula along the coastline of the Gulf of Oman. Evidence for the interpretation that the Oman Ophiolite represents obducted fast spreading oceanic crust, can be derived out of the combination of observations of a thick continuous volcanic sequence, almost no evidence for plastic deformation (Pallister & Hopson, 1981; MacLeod & Rothery, 1992), nearly no variation in radiometric ages throughout the entire ophiolite (Tilton *et al.*, 1981) and magmatic flow fabrics in the lower gabbroic crust (Nicolas *et al.*, 1988; Boudier *et al.*, 1996).

In this project we focus on different metasomatic lithologies: epidote veins from Wadi Gideah, rodingites from Samra and diopsidites at Shamad. Therefore we use a combined geochemical/fluid inclusion/thermodynamic modeling approach on these metasomatic rock types to (1) test hypotheses for their formation, (2) decipher the nature and sources of fluids causing the metasomatic reactions, and (3) learn about the timing of metasomatic events and their relation to the tectonic evolution of the Oman Ophiolite.

Epidote veins in the Wadi Gideah:

In the Wadi Gideah, located in the Wadi Tayin Massif in the southern Oman Ophiolite, the entire crustal sequence from the sheeted dikes to the mantle-crust transition zone is exposed. The Wadi Gideah stretches almost perpendicular to the mantle crust transition. Epidote veins are developed in reoccurring zones along the entire profile. Epidote (X_{Fe}=0.19 - 0.23) predominates as vein fill, and can be associated with quartz, and later interstitial calcite. Pink selvages of clinozoisite are common. Based on field observations we hypothesize that these epidote veins reflect channeled hydrothermal fluid percolation throughout the oceanic crustal section exposed (cf. Coogan et al., 2006). The implications of these veins for the cooling of the lower oceanic crust remain to be worked out. We have started a combined microthermometry, isotope (Sr, O), and trace element (LAICPMS) study to determine the conditions of water-rock reaction and the nature of the interacting fluids.

Rodingites from Samra:

Along a fault zone system in the area of Samra in the Sumail Massif, rodingite dikes crosscut the exposed mantle. The mostly harzburgitic mantle in the Sumail Block shows a higher degree of serpentinization than the mantle section in the Wadi Tayin Massif. Rodingites are metasomatic products of gabbroic dikes brought in contact with the serpentinization fluid during mantle alteration at temperatures between 200 and 350°C (e.g., Bach and Kein, 2009). The former gabbroic textures of these dikes are completely obliterated. The secondary mineral assemblages include hydrogrossular, diopside, zoisite, chlorite and prehnite. In contact to the serpentinized host rock, a blackwall of chlorite formed. Oxygen isotope thermometry and thermodynamic computation will be employed to estimate the formation temperatures and fluid fluxes. Raman-spectroscopy studies are planned to examine the compositions of the abundant fluid inclusions, with particular focus on reduced carbon species.

Diopsidites at Shamad:

Located in the serpentinized mantle section of the Sumail Massif (Shamad area), monomineralic diopsidite dikes and large pods of diopsidite with associated nephrite (a tremolite fels) are observed. These dikes occur in several smaller cataclastically deformed shear zones and are cm to dm wide and several meters in length. They are composed of diopside (X_{Mg}= 0.98 - 1.00), appear pale green to whitish in color, are irregular in shape and locally contain fragments of serpentinized mantle. Similar diopsidite dikes containing anorthite or garnet, and diopsidites with nephrite selvages were described in literature (Python *et al.*, 2007). The occurrences near Shamad are unusual with regards to the number of size, featuring numerous large bodies, which are tens of meters long and several meters wide. These large diopsidite pods show a larger variability in texture, from fine grained hornfels to coarse granular

textures. These rocks are clearly metasomatic in origin and thin section observations indicate that the olivine of the harzburgitic mantle was first replaced by tremolite and afterwards the tremolite was replaced by diopside. These reactions preceded serpentinization of the mantle.

We use isotope geochemistry (O, Sr) as well as LA-ICP-MS trace element analyses of these rocks and minerals together with fluid inclusion microthermometry to characterize the metasomatically formed phases and fingerprint the metasomatizing fluids. We combine petrographic observations, geochemical data and thermodynamic reaction path models to develop plausible formation scenarios of these different metasomatic lithologies.

References

Bach, W. & Klein, F. (2009): The petrology of seafloor rodingites: insights from geochemical reaction path modeling. Lithos, 112, 103-117.

Boudier, F., Nicolas, A., Ildefonse, B. (1996): Magma chambers in the Oman ophiolite: fed from the top and the bottom. Earth and Planetary Science Letters, 144, 239-250.

Cherkaoui, A. S. M., Wilcock, W. S. D., Dunn, R. A., Toomey, D. R. (2003): A numerical model of hydrothermal cooling and crustal accretion at a fast spreading mid-ocean ridge. Geochemistry Geophysics Geosystems, 4, 8616.

Coogan, L. A., Howard, K. A., Gillis, K. M., Bickle, M. J., Chapman, H., Boyce, A. J., Jenkin, G. R. T., Wilson, R., N. (2006): Chemical and thermal constraints on focussed fluid flow in the lower oceanic crust. American Journal of Science, 306, 389-427.

Dunn, R. A., Toomey, D. R., Solomon, S. C. (2000): Three-dimensional seismic structure and physical properties of the crust and shallow mantle beneath the East Pacific Rise at 9°30'N. Journal of Geophysical Research, 105, 23537-23555.

MacLeod, C. J. & Rothery, D. A. (1992): Ridge axial segmentation in the Oman ophiolite: evidence from along-strike variations in the sheeted dyke complex. Geological Society of London Special Publications, 60, 39-63.

Nehlig, P. & Juteau, T. (1988): Deep crustal seawater penetration and circulation at ocean ridges: Evidence from the Oman ophiolite. Marine Geology, 84, 209-228.

Nicolas, A. (1989): Structures of ophiolites and dynamics of oceanic lithosphere. Kluwer Academic Publishers, Boston, 367.

Nicolas, A., Mainprice, D., Boudier, F. (2003): High-temperature seawater circulation throughout crust of oceanic ridges: a model derived from the Oman ophiolite. Journal of Geophysical Research, 108, 2371.

Nicolas, A., Reuber, I., Benn, K. (1988): A new magma chamber model based on structural studies in the Oman ophiolite. Tectonophysics, 151, 87-105.

Pallister, J. S. & Hopson, C. A. (1981): Samail ophiolite plutonic suite: field relations, phase variation, cryptic variation and layering, and a model of a spreading ridge magma chamber. Journal of Geophysical Research, 86, 2593-2644.

Python, M., Ceuleneer, G., Ishida, Y., Barrat, J.-A., Arai, S. (2007): Oman diopsidites: a new lithology diagnostic of very high temperature hydrothermal circulation in mantle peridotite below oceanic spreading centres. Earth and Planetary Science Letters, 255, 289-305.

Tilton, G. R., Hopson, C. A., Wright, J. E. (1981): Uranium-lead isotopic ages of the Samail ophiolite, Oman, with applications to Tethyan ocean ridge tectonics. Journal of Geophysical Research, 86, 2763-2775.

IODP

Ocean circulation in transition between glacial and interglacial – measurements of neodymium isotopes on Atlantic IODP/ODP cores.

P. BLASER[1], N. FRANK[1], J. LIPPOLD[2], E. BÖHM[1]

[1]Ruprecht-Karls-Universität Heidelberg, Germany
[2]Universität Bern, Switzerland

The Atlantic circulation is dominated by the production of deep water in either the North or the South, which has a considerable impact on the heat budget of the respective hemisphere. Although significant effort has been made in order to reconstruct the past of the climatically relevant Atlantic Ocean, it is still uncertain whether the ocean circulation is driven by or the driver of the partly dramatic climate variations of the past 100,000 years. The branch of research, which considers these questions, namely palaeoceanography, faces two fundamental problems: On the one hand the methods used are often flawed and have limited scopes of application. This applies in particular to tracers which take part in the nutrient cycle or are subject to diagenetic processes. On the other hand the spacial and temporal coverage of the measurements in most cases only allows for limited conclusions, which may deliver local information, but do not facilitate inference in a global context. In order to deduce reliable statements about the oceanic past of heat transport and the distribution of carbon and nutrients, it is necessary to generate and analyse comprehensive data sets. The material provided by the IODP/ODP core repositories presents a unique foundation in this respect. As the method of choice for analysis the measurement of ratios of the neodymium isotopes $^{143}Nd/^{144}Nd$ has recently emerged. The distinct isotopical signature of water masses from the Pacific and of North Atlantic Deep Water render neodymium a unique tracer for deep water mass provenance in the Atlantic ocean. The neodymium signature and thus the mixing proportion of the water masses prevailing in the past is archived in Fe-Mn accretions in the sediment. By carefully leaching of these authigenic metal accumulations and the subsequent analysis of neodymium isotopes there is a method at hand that is very promising if used on large scale. It is applicable wherever marine sediment cores exist, it is reliably measurable and the preparation of the samples is cost as well as time efficient, if the respective expertise is available.

This project persues the question of deep water mass provenance in the Atlantic ocean by applying the Nd leach method to sediments from selected IODP/ODP cores. This question includes how fast the changes of water masses took place and which circulation patterns prevailed in which climatological phases. With the help of box models and by comparison with further tracers ($^{231}Pa/^{230}Th$, $d^{13}C$) a comprehensive picture of the last glacial-interglacial cycle shall be drawn, allowing for conclusions about the most critical feedbacks and interactions in the climate system, which are imperatively needed for the validation of climate models.

In this presentation the general idea as well as first analytical results will be depicted. A series of tests preceding the actual study and carried out on twelve core top sediments around the Atlantic is being conducted at the moment. These tests shall deliver information on how the leaching method could be improved in order to be used on a greater variety of sedimentological settings and comprises the extraction of multiple successive leaches from the same sample and their analyses on the chemical composition as well as the distribution of rare earth elements.

IODP

Characterization of metabolically active microorganisms in an active hydrothermal field in the Okinawa Trough (IODP Exp. 331)

MARCO BLÖTHE, ANJA BREUKER AND AXEL SCHIPPERS

Bundesanstalt für Geowissenschaften und Rohstoffe, Stilleweg 2, D-30655 Hannover

The objective of the BGR project, as part of the post-cruise research of IODP Expedition 331, Deep Hot Biosphere, was to test the hypothesis that the quantitative microbial community composition and the cultivable microorganisms in hydrothermally influenced deeply-buried marine sediments are significantly different from those in cold and temperate deeply-buried marine sediments. The previously successfully applied molecular techniques real-time PCR (qPCR) and catalyzed reporter deposition - fluorescence in situ hybridisation (CARD - FISH) have been used as well as cultivation to proof the existence of a deep hot biosphere, to describe it and to isolate novel microorganisms. The domains Archaea, Bacteria and Eukarya as well as the JS1 candidate group, Chloroflexi, Geobacteraceae, Crenarchaeota and the functional genes dsrA, mcrA, aprA, and Rubisco (cbbL) have been quantified via qPCR (see Fig 1).

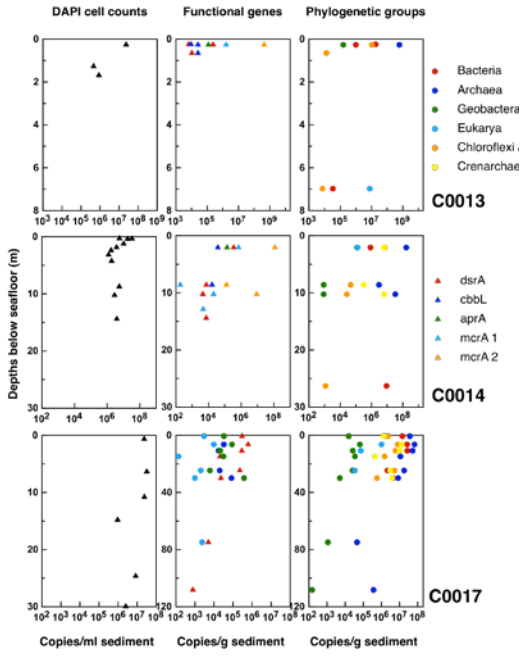

Fig. 1. Cell numbers and copy numbers of functional or 16S rRNA genes for specific phylogenetic groups at different depths from sites C0013, C0014 and C0017.

All genes have been detected in different copy numbers. The overall order of abundance is Archaea > Bacteria > Eukarya. Directly after IODP Expedition 331 in October 2010, culture media were inoculated with IODP samples at different temperatures and the enrichment cultures are maintained since then. Growth is continuously checked about every three months and in case of growth, colonies are picked and transferred to fresh media (Table 1). Several aerobic and anaerobic enrichments have been obtained so far. Based on partial 16S rRNA gene sequencing, isolates from the manganese oxidizing enrichment cultures reveal similarity to Bacillus aquimaris (94%) and Bacillus oceani (93%). Isolates obtained under aerobic conditions with a mix of organic polymeres as carbon source revealed similarities to cultivated species of Halobacillus litoralis (92%), Marinobacter salsuginis (90%), Shewanella benthica (89%) and Cytophaga fermentans (92%). Microcalorimetric measurements with the original samples showed a considerable heat production due to exothermic reactions at 90°C which was partly attributed to microbial activity. The microcalorimetric measurements revealed activity of thermophilic microorganisms in the IODP Exp. 331 samples.

		Enrichments anaerob		Isolates aerob		
Sample	Depth [m]	Monomere	Polymere	Mn-Oxidizer	Monomere	Polymere
331-C0013D	3.3	x	x			
331-C0013D	7	x	x			
331-C0013E	0.2				3	
331-C0013F	0.3	x	x	10		6
331-C0014B	8.8	x	x	11		
331-C0014B	15.3				1	6
331-C0014D	2.1	x	x	11	1	0
331-C0014D	10.2	x	x			
331-C0014D	11.5	x	x		3	2
331-C0014D	12.9	x	x			
331-C0017A	6.4	x	x		6	6
331-C0017B	10.9				3	4
331-C0017B	14.9	x	x		4	7
331-C0017C	30.1	x	x		6	12
331-C0017D	75				2	3
331-C0017D	108.5	x	x			

Table 1. Cultivation assays with different media. The aerobic isolates were obtained from arobic enrichment cultures by agar plate technique. Isolation of pure cultures from the anaerobic enrichments is still in progress. All cultures were incubated at 30°C.

ICDP

Downhole Seismic Monitoring in the Istanbul/Eastern Sea of Marmara Region: Recent Results from the ICDP-GONAF Project

MARCO BOHNHOFF[1,2], GEORG DRESEN[1], FATIH BULUT[1], CHRISTINA RAUB[1], TUGBAY KILIC[3], RECAI F. KARTAL[3], FILIZ TUBA KADIRIOGLU[3], MURAT NURLU[3], PETER E. MALIN[4] , HISAO ITO[5]

1 GFZ German Research Center for Geosciences, Helmholtz-Centre Potsdam, Germany
2 Freie Universität Berlin, Department of Earth Sciences, Germany.
3 AFAD, Disaster and Emergency Management Presidency, Earthquake Department, Ankara, Turkey.
4 Institute of Earth Science and Engineering, University of Auckland, Auckland, New Zealand.
5 Jamstec, Center for Deep Earth Exploration (CDEX), Japan Agency for Marine-Earth Science and Technology (JAMSTEC), Kanagawa, Japan.

The North Anatolian Fault Zone (NAFZ) below the Sea of Marmara represents a ‘seismic gap’ where a major earthquake is expected to occur in the near future. The Marmara segment of the NAFZ is located between the 1912 Ganos and 1999 Izmit ruptures and is the only segment that has not ruptured since 1766. The ICDP-GONAF project (Geophysical Observatory at the North Anatolian Fault; www.gonaf.de) involves the installation of a high-resolution borehole seismic observatory at the NAFZ consisting of several 300m deep vertical boreholes

in the broader Istanbul / eastern Sea of Marmara region to monitor the Princes Islands segment at the transition from the 'seismic gap' to the recent 1999 Izmit rupture. GONAF is an international collaboration and co-funded by the International Continental Scientific Drilling Programme (ICDP), GFZ Potsdam and the Disaster and Emergency Management Presidency in Ankara/Turkey (AFAD). Further principal partners are IESE/New Zealand, JAMSTEC/Japan, MIT and UNAVCO/both US,. The principal scientific objective of GONAF is to study physical processes acting before, during and after the expected M>7 earthquake along the Princes Islands segment by long-term monitoring microseismic activity at significantly reduced magnitude detection threshold and improved hypocentral resolution. By the end of 2013 three GONAF boreholes were successfully implemented and arrays of borehole seismometers were installed for permanent operation. Vertical 1Hz seismometers at 75m spacing as well as several different 3-component borehole seismometers at 300m depth are installed and are completed by a set of surface sensors. The benefit of seismic waveforms recorded at depth in a low-noise environment is shown and first results of microseismic activity along the Princes Islands segment are presented and will be discussed in the seismotectonic context.

IODP

A new surface-water temperature record for the Oligocene-Miocene Transition from the western North Atlantic (IODP Site U1405

ANDRÉ BORNEMANN[1], IRIS MÖBIUS[2], OLIVER FRIEDRICH[2,3], DIEDERIK LIEBRAND[4], PAUL A. WILSON[4], EXPEDITION 342 SCIENTISTS

[1] Institut für Geophysik and Geologie, University Leipzig, Germany,
[2] Institut für Geowissenschaften, Universität Frankfurt, Germany,
[3] Institut für Geowissenschaften, Universität Heidelberg, Germany,
[4] National Oceanography Centre, Southampton, University of Southampton, UK

The Oligocene represents an early stage of the Cenozoic icehouse world and is characterized by a high variability in the ´^{18}O of deep-sea benthic foraminifera and high-amplitude sea-level fluctuations probably related to southern hemisphere ice sheet instability. This variability culminates in a major glaciation event during the earliest Miocene ~23 Million years ago (Mi-1 event). High-quality data sets based of well-preserved planktic foraminifera across the Mi-1 event are scarce and limited to the low-latitudes and southern hemisphere. During IODP Expedition 342 expanded sequences covering the Oligocene to early Miocene transition have been drilled at J-Anomaly Ridge off Newfoundland. These sediments contain exceptionally well-preserved calcareous microfossils and are characterized by high sedimentation rates. Pristinely preserved, "glassy" planktic foraminiferal tests were analyzed at a resolution of H20 kyrs to unravel the long-term climate evolution during the magnetochron interval C6AAr.2n/C6AAr.3r to C6Cn.3n/C6Cr across the Oligocene-Miocene Transition. To achieve this goal, a dual-proxy approach (´^{18}O, Mg/Ca) has been employed to estimate sea-surface and thermocline temperatures based predominantly on *Globigerinoides primordius* and *Catapsydrax dissimilis*, respectively. This approach allows for the reconstruction of North Atlantic surface ocean response to the Mi-1 event and how it has been influenced by global climate dynamics. First results show a very high variability in ´^{18}O and Mg/Ca for both mixed-layer and thermocline dwelling taxa pointing towards highly variable climatic and oceanographic conditions in the northwestern Atlantic. Both habitats record a distinct shift to heavier ´^{18}O and lower Mg/Ca values across the Mi-1 event, implying decreasing temperatures.

IODP

Coccolithophores paleoproductivity for Marine Isotopic Stages 11 and 12 in the North Atlantic

CATARINA CAVALEIRO[1,2], MICHAEL KUCERA[2], KARL-HEINZ BAUMANN[2], ANTJE VOELKER[1,3], HEATHER STOLL[4]

[1]Interdisciplinary Center of Marine and Environmental Research, CIIMAR (Oporto), Portugal (cdcavaleiro@marum.de)
[2]Center for Marine Environmental Science, MARUM, Germany
[3]Div. Geologia e Georecursos Marinhos, IPMA, Lisbon, Portugal
[4]University of Oviedo, Spain

Coccolithophores are primary producers and the most important calcifying organisms in the ocean. Coccolithophores play a key role not only in the ecosystem, as primary producers, but also in the global carbon cycle by photosynthesis and calcification. The coccolith Sr/Ca ratio is linked to calcification rates, growth rates and ultimately productivity (Stoll and Schrag, 2000). Higher coccolith Sr/Ca ratios indicate higher productivity (Stoll et al, 2007a, b). Fluctuations on coccolithophores paleoproductivity can be related with oceanographic, atmospheric and ecological changes. Characterize coccolithophores productivity can give us a better understanding of how these important marine algae reacted to changes in the North Atlantic thermohaline circulation and atmospheric CO2.

This study is part of my PhD research. In the mid Northe Atlantic, near Azores, the paleoproductivity was clearly higher during MIS12 than 11. We took the same question to the Iberian margin where coastal influence and regional changes might lead to different results.

References:

Stoll, H., and D. P. Schrag (2000), Coccolith Sr/Ca as a new indicator of coccolithophorid calcification and growth rate., Geochem. Geophys. Geosyst., 1(1999GC000015).

Stoll, H., P. Ziveri, N. Shimizu, M. Conte, and S. Theroux (2007a), Relationship between coccolith Sr/Ca ratios and coccolithophore production and export in the Arabian Sea and Sargasso Sea, Deep Sea Research Part II: Topical Studies in Oceanography, 54(5-7), 581-600.

Stoll, H., A. Arevalos, A. Burke, P. Ziveri, G. Mortyn, N. Shimizu, and D. Unger (2007b), Seasonal cycles in biogenic production and export in Northern Bay of Bengal sediment traps, Deep Sea Research Part II: Topical Studies in Oceanography, 54(5-7), 558-580.

ICDP

New insights into the formation of shallow sedimentary structures in Lake Van, eastern Turkey: A joint analysis of high-resolution seismic and hydroacoustic data

D. CUKUR[1], S. KRASTEL[2], N. CAGATAY[3], D. WINKELMANN[1], AND BATHYVAN SCIENTIFIC TEAM

[1]GEOMAR | Helmholtz Centre for Ocean Research Kiel, Wischhofstr.1-3, 24148 Kiel, Germany
[2] Institute of Geosciences, Christian-Albrechts-Universität zu Kiel, Otto-Hahn-Platz 1, 24118 Kiel, Germany
[3]Istanbul Technical University, EMCOL and Department of Geological Engineering, 34469 Maslak, Istanbul, Turkey

Lake Van in Eastern Anatolia (Turkey) is the fourth largest terminal lake in the world with a surface area of ~3,560 km², a volume of ~650 km³, a maximum depth of 450 m, and a maximal length of 130 km WSW-ENE (Fig. 1). Annually laminated sediments for major parts of the sedimentary succession in Lake Van harbor an excellent high-resolution paleoclimate archive.

Therefore, an international drilling campaign was successfully conducted in summer 2010 in the frame of the International Continental Scientific Drilling Program (ICDP). Preliminary results from sedimentary cores show that the drilled sediments contain 600,000 years of paleo-environmental and volcanic/geodynamic history.

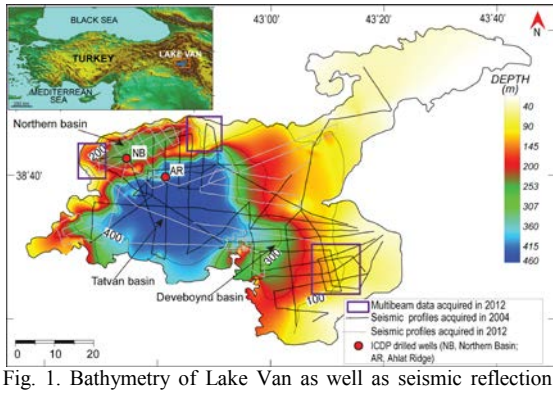

Fig. 1. Bathymetry of Lake Van as well as seismic reflection profiles, multibeam data, and drilled wells.

Multibeam bathymetry as well as shallow and high resolution seismic data from Lake Van has revealed various shallow sediment structures including submerged channels, submarine gullies, and microbialites (carbonate towers). The submerged channels are v-shaped in cross section, 0.5-1 km wide and 10 m deep an average (Fig. 2). They occur in water depths between 40 and 150 meters. Towards the west, at a water depth of about ~100 m, they are all joined to a westward draining channel (Fig. 2).

We interpret that the submerged channels represent fluvial-deltaic systems that have been formed subaerially during a low stand of the lake level, and have subsequently been submerged. Seismic reflection profiles from Lake Van show that the water levels of the lake has fluctuated significantly since the formation of the lake ca. 600 ka ago (Cukur et al., 2013). The last low of the water level in Lake Van occurred about ~14 ka ago during the Last Glacial Maximum (LGM). At this time, water level dropped to ~220 m below current lake level (Cukur et al., 2013). A drop of ~220 m water level would expose the shelf and could lead to the rivers incise the fluvial valleys. The subsequent rapid transgression of the lake drowned these valleys making the channels abandoned over time as suggested by deposition of well-stratified sediments on top of the channel floor. Erosion along the channel walls is probably still ongoing as evidenced by the truncation of the flat-lying reflections.

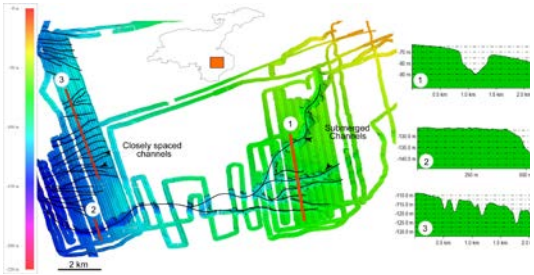

Fig. 2. Multibeam bathymetry map of eastern shelf showing numerous channels on the lake floor. These channels were probably formed during low lake levels when the shelf was subaerially exposed.

The multibeam data also show several small closely-spaced channels in the eastern part of Lake (Fig. 2). They are 5-10 m deep and 10-30 m wide. They occur in water depths of between 100 to 200 m. These channels were probably formed during the Last glacial Maximum (LGM), when the lake level was much lower and the present day submerged channels were part of subaerial fluvial systems. Some show truncation of flat-lying reflections on their walls, suggesting erosion is still active today.

Multibeam data, for the first time, delineates hundreds of microbialites and/or carbonate towers on the lakefloor in the northern part of Lake Van (Fig. 3). The heights of these features above the lakefloor range from less than 2 m to over 40 m. They occur both in very shallow (< 5 m deep) and deep waters down to a depth of 130 m. Acoustically, they are characterized by strong positive top reflections with their reflection-free or very low-amplitude character. Our data suggest that the occurrence of microbilites are mainly controlled by tectonics. The influence of tectonic control on microbialite distribution is evidenced by the abrupt occurrence of microbilaites in areas of structural faults and or cracks (Fig. 3). These faults/cracks are probably providing fluid pathways from the Miocene limestone below, seeping the calcium-rich groundwater into the alkaline lake water.

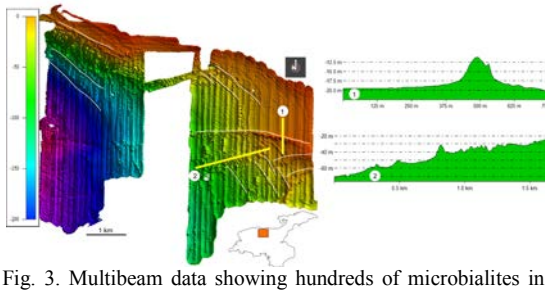

Fig. 3. Multibeam data showing hundreds of microbialites in the northern part of of Lake Van. The immdiate occurrence of these structures in areas of structural faults suggests they are controlled by tectonics. White solid lines indicate faults and/or cracks.

The multibeam data provides a detailed morphology of the submarine gullies on the western slope of the Northern basin. The canyons are v-shaped in cross-section and extend down to 170 m water depths. They are about 10-30

m deep, 50-200 m wide, and up to 1.5 km long. The existence of the canyons suggests subaerial erosion, probably during low lake levels. Cukur et al. (2013) show that the lake level in the Northern basin was about 200 m lower than the present day water depths during the LGM. They were then probably drowned with waters during the latest interglacial period.

References:
Cukur, D., Krastel, S., Schlüter, F.D., Demirba•, E., Imren, C., Niessen, F., Toker, M., PaleoVan-Working Group., 2013. Sedimentary evolution of Lake Van (Eastern Turkey) reconstructed from high resolution seismic investigations. International Journal of Earth Sciences 102 (2), 571–585.10.1007/s00531-012-0816-x

IODP

Seawater densities and cold-water coral carbonate mounds in the northeast Atlantic through time

C. DULLO[1], A. RÜGGEBERG[1,2], S. FLÖGEL[1], J. RADDATZ[1]

[1] GEOMAR, Helnholtz Zentrum für Ozeanforschung Kiel, Wischhofstr. 1-3, 24148 Kiel (cdullo@geomar.de)
[2] Dept. of Earth Sciences University of Fribourg, Chemin du Musée 6, CH-1700 Fribourg

Cold-water coral (CWC) reefs are marine benthic ecosystems acting as important hot spots of biodiversity and living resources. In the northeast Atlantic, the reefs form giant coral carbonate mound structures of up to 300 meters in height. The development of these coral carbonate mounds is paced by Northern Hemisphere climate variability since their occurrence started at about 2.7 Ma in the NE Atlantic. In this study we demonstrate that cold-water coral ecosystems only thrive under specific oceanographic conditions, among which seawater density plays an important role. It is based on the observation that CWC reefs along the European continental margin thrive under seawater densities of 27.5 ± 0.15 kg/m3 (Dullo et al., 2008).

Recent calibration based on seawater stable oxygen isotope ratios (´18O) and past application using benthic foraminifera ´18O values (Lynch-Stieglitz et al., 1999) allows the reconstruction of paleo-seawater densities at different times for three coral carbonate mound records in the Porcupine Seabight, southwest off Ireland: i) IODP Expedition 307 site Challenger Mound, ii) Galway Mound, both from the Belgica Mound province, and iii) Propeller Mound of the Hovland Mound province.

Our results indicate that the development of CWC reefs on the carbonate mounds is closely linked to mid-depth bottom water densities. Thriving coral growth is predominantly found at seawater densities (sigma-theta, Ã˜) between 27.2 and 27.7 kg/m3. In comparison to present-day conditions, we interpret the reconstructed density values relative to the pycnocline at ~27.5 kg/m3 serving as boundary layer, on which horizontal currents develop, carrying nutrients and enabling the possible distribution of larvae. Thus, the determination of past seawater densities has a great potential in paleoceanographic reconstructions of intermediate water-mass dynamics, in this study of the past 2.7 Ma. Furthermore, it provides a tool to study the sensitivity of CWC ecosystems with respect to environmental changes and, finally, highlights the importance of pycnoclines as a controlling factor favoring CWC growth on carbonate mounds.

References:
Dullo, W.-C., Flögel, S., Rüggeberg, A., 2008. Cold-water coral growth in relation to the hydrography of the Celtic and Nordic European continental margin. Marine Ecology Progress Series 371, 165–176.
Lynch-Stieglitz, J., Curry, W.B., Slowey, N., 1999. A geostrophic transport estimate for the Florida current from the oxygen isotope composition of benthic foraminifera. Paleoceanography 14 (3), 360–373.

ICDP

Mechanisms of palagonite formation on subsurface basaltic and rhyolithic glass alteration from ICDP sites Hawaii and Snake River Plain

S. DULTZ[1], H. BEHRENS[1], C. DUPONT[2] AND M. PLÖTZE[3]

[1]Institute of Mineralogy, Leibniz Universität Hannover, Callinstr. 3, D-30167 Hannover
[2]Institute of Soil Science, Leibniz Universität Hannover, Herrenhäuser Str. 2, D-30419 Hannover
[3]Institute for Geotechnical Engineering, ETH Zürich, Ch-8093 Zürich, Switzerland

Glass alteration, also called `palagonitization´ results from the low stability of the glass in aqueos solutions. It is a two stage process of glass dissolution and palagonite formation, which is controlled by many different factors, including temperature, microbial colonisation, solution chemistry and feedback mechanism between glass and secondary phases. All these factors affect kind, quantity, and micromorphology of palagonite formed, which can have highly variable properties (Stroncik and Schmincke 2002). At present the `leached layer theory´ (Grambow and Müller 2001) is the most accepted model for glass alteration. However observations on a rather distinct contact between palagonite and fresh glass are not compatible with this theory. The knowledge of the relevant mechanism of glass alteration is of substantial importance for modeling of element turnover, as results will strongly depend on the kind of mechanism. Bioalteration of volcanic glass was described for many different geological settings worldwide (Staudigel et al., 2008). Hence the impact of biological factors on glass alteration has to be considered too.

Micromorphological patterns on basaltic glass samples from the Hawaii Scientific Drilling Project (HSDP) were determined in thin sections applying petrographic and scanning electron microscopy. For visualisation of voids and Fe-rich secondary phases 3-D computed tomography was used. Topographic features of original surfaces were analyzed with a laser microscope. Visualization of connective porosity was done by the intrusion of a molten alloy called “Wood`s metal”. An argon pressure of 4 kb was realized which is just the same pressure as used for Hg-porosimetry. For verification of biogenic weathering and better understanding of the palagonite phase formed, the chemistry and degree of structural order of secondary mineral phases was investigated using electron microprobe and Raman microscopy. Mineralogical composition of palagonite was determined by X-ray diffraction. Fluid-glass experiments with different leaching fluids for analysis of ionic effects on glass dissolution were performed on two basaltic and rhyolithic synthetic glasses representing compositions from Snake River Plain as well as Hawaii.

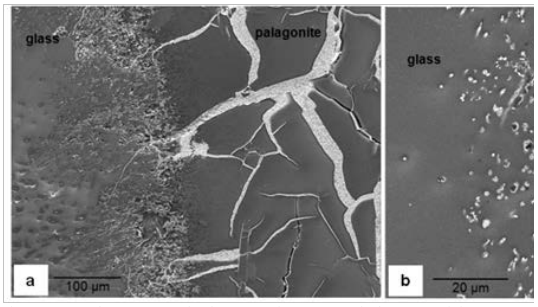

Fig. 1: Back scattered electron images of the transition zone between basaltic glass and palagonite in pillow lava at 8,808 ftbsl, Hawaiian drill core sample, where the bright shining alloy marks connective pores (a). At higher magnification (b) microtunnels due to microorganisms are visible.

Hereby also the zeta potential as the key electrochemical parameter of the solid-liquid interface was determined, which is an important for the sorption of ions from solution but also characterizes the ability of glass surfaces for the adsorption of dissolved organic matter and bacterial cells.

In thin sections, palagonite formation can clearly be seen for samples from HSDP. In the zone between the primary glass and the palagonite where bioalteration is observed, the molten alloy was intruded in the tubules of the microorganisms as well as in spaces of secondary porosity (Fig. 1). Open spaces at the glass palagonite interface in the region of microtunneling may act as conduits for fluid exchange with circulating waters, which are important for the nutrition of the microorganisms and may enhance abiotic glass alteration too.

A free space in vicinity of the outer rim of bioaltered glass with formation of microtubules and the palagonite was observed (Fig. 1b). The formation of voids indicates a marked loss of elements during palagonitization. It can be assumed that in an open system with sea water at pH 8.3 the release of Si from the glass is favored which is lost to the surrounding solution. Recently congruent dissolution of the glass that is spatially and temporally coupled to the reprecipitation of amorphous silica and other glass compounds at an inward moving reaction front was described by Geisler et al. (2010) for a borosilicate glass at low pH. The authors proposed an `interface-coupled dissolution-reprecipitation mechanism´. The distinct interface of the glass, broad open spaces between the glass and palagonite and porosity in the secondary phase clearly point towards a dissolution-reprecipitation mechanism during glass alteration in our samples under investigation. Hereby the palagonite surface moves in the direction of the parent glass phase with the progress of alteration. A sheme of this alteration mechanism is given in Figure 2. Further it was shown that this corrosion mechanism leads to a sharp drop of hardness due to initially high-porous corrosion products while clogging of these reprecipitates result in densification and decreasing porosity towards the outer parts of the alteration layer (Hasdemir et al. 2013).

Broad fractures are visible in the palagonite (Fig. 1a), where smectite was clearly identified by XRD. The fractures are filled with the bright shining alloy and their formation is most probably due to shrinkage of the smectite-rich palagonite upon drying. The matrix of palagonite itself was not intruded by the molten alloy indicating the presence of very small pores. Pore volume of palagonite samples included in Hg-porosimetry are strongly dependent on the amount of glass preserved and the presence of phenocrysts and quench crystals. In more strongly altered samples high shares of pores are between pore radii in the range from 2 to 10 nm which is due to the presence of smectites. A marked redistribution of elements during glass dissolution and formation of secondary phases in the fracture filling palagonite sheet can be deduced from microprobe analysis. Based on the assumption of isovolumetric alteration, in the HSDP sample from 7524 ftbsl FeO and TiO_2 are strongly enriched in palagonite as compared to the basaltic glass, 20 vs. 11.5 wt.% for FeO, 5.4 vs. 2.8 wt.% for TiO_2, whereas P_2O_5 is slightly enriched. In contrast Si^{4+}, Al^{3+}, Mn^{4+}, Mg^{2+}, Ca^{2+}, K^+ and Na^+ are depleted during alteration.

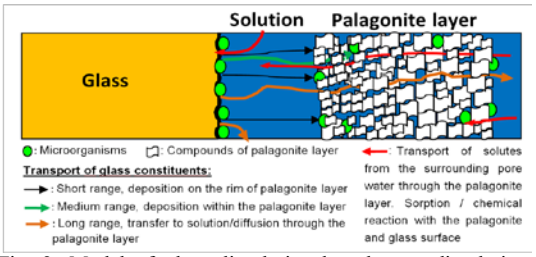

Fig. 2: Model of glass dissolution based on a dissolution-reprecipitation mechanism. Due to strong losses of glass compounds to the surrounding solution, an open space is formed between the glass and the inward moving reaction front of the palagonite layer.

Measurement of zeta potential combined with determination of element release gave insights on ionic effects on glass dissolution, which may control the principal course of palagonite formation. By the addition of divalent cations charge reversal of the zeta potential of basaltic glass from negative to positive values was observed. This is an interesting issue as bacterial cells have a negative surface charge (Wilson et al., 2001) and will be attracted by positively charged surface sites. The electrostatic stabilization of microorganisms on glass surfaces is likely to explain the generation of dissolution cavities on glass surfaces by bacteria to some part. The generation of positive charge on glass surfaces was traced at different temperatures with different cations including Ca^{2+}, which is a common cation in the pore solutions of many rocks. Temperature had strong effects on the absolute value as well as the time needed for reaching point of zero charge and generation of positive charge. Highest values for the zeta potential were obtained for basaltic glass exposed to 105°C indicating that the process inducing positive surface charge is most extensive at the highest temperature of the experiment. It is thought the observed charge reversal is due to the formation of Fe-oxides/hydroxides on the outer surface of the glass, as the content of FeO in the basaltic glass is relatively high (12.19 wt.%) and the point of zero charge of goethite and hematite, two common Fe-oxides is between pH 6-8. For clarification X-ray absorption spectroscopy (XAS) measurements will be performed for the extraction of short range structural and chemical information.

For the anions under investigation some increase was obtained for Cl^- and SO_4^{2-}, whereas oxalate ($C_2O_4^{2-}$), which is known to form stable complexes with Fe has the strongest effect on Si-release, highly dependent on concentration. During the runtime of the experiments the

pH of the suspensions was controlled and found to be stable between pH 6.0-6.5 due to the wide solution/solid ratio. Neutralization of deprotonated Si-O^- sites by monovalent cations might accelerate polymerization, leading to smaller Si release in comparison with absences of electrolytes. It is likely that anions can attack Si-O-Si bonds in a similar way as OH^-. Additives containing chemical groups that are strongly anionic, such as $C_2O_4^{2-}$ may react with Si centers in Si-O-Si bonds and increase solubility of the glass.

Glass chemistry was found to have a marked effect on the tendency of generation of positive zeta potential in $Ca(NO_3)_2$ solution. Values for zeta potential of the high K basaltic glass were in the whole time sequence of the experiment below the zeta potential values of the typical basaltic glass, which might be due to some stabilisation of the glass due to higher content of monovalent cations K^+ and Na^+. For the rhyolithic glass with a relatively low content of FeO, positive zeta potential was observed in experiments with deionized water and $Zn(NO_3)_2$ solution.

Our investigations on ICDP drilling cores from Hawaii and Snake River Plain show evidence for strong glass alteration at both localities. Palagonite formation is common at site Hawaii. In contrary palagonite was absent at sites Snake River Plain, indicating that high shares of glass compounds released are removed by solution. For samples from Hawaii, the formation of open spaces between glass and palagonite and microtunnels in the adjacent glass was observed easing conditions for fluid exchange and hence glass alteration. These observations as well as the sharp interface between the pristine glass and altered layers point to a dissolution-reprecipitation mechanism. Variations of chemical composition along the transect from the glass into the palagonite support this hypothesis, i.e. high concentrations of iron near the glass/palagonite transition are unlikely in presence of a leaching mechanism prevalent at glass alteration.

References:

Geisler, T., Janssen, A., Scheiter, D., Stephan, T., Berndt, J., Putnis, A. (2010) Aqueous corrosion of borosilicate glass under acidic conditions: A new corrosion mechanism. Journal of Non-Crystalline Solids 356, 1458-1465.

Grambow B, Müller R. 2001. First order dissolution rate law and the role of surface layers in glass performance assessment. J. Nucl. Mat. 298:112-124.

Hasdemir I, Striepe S, Deubener J, Schmidt BC. 2013. Micromechanical properties of banded alterations of archaeological glass fragments. Journal of Non-Crystalline Solids 376:126-132.

Staudigel, H., Furnes, H., McLoughlin, N., Banerjee, N.R., Connell, L.B., and Templeton, A. (2008) 3.5 billion years of glass bioalteration: Volcanic rocks as a basis for microbial life. Earth-Science Reviews, 89, 156-176.

Stroncik, N.A., and Schmincke, H.-U. (2002) Palagonite – a review. International Journal of Earth Sciences, 91, 680-697.

Wilson, W.W., Wade, M.M., Holman, S.C., and Champlin, F.R. (2001) Status of methods for assessing bacterial cell surface charge properties based on zeta potential measurements. Journal of Microbiological Methods, 43, 153-164.

IODP

Bestimmung der Magnetostratigraphie aus Bohrlochmessungen

S. EHMANN[1], A. HÖRDT[1], M. LEVEN[2], M.NEUHAUS[1], C. VIRGIL[1]

[1]Institut für Geophysik und extraterrestrische Physik, TU Braunschweig

[2]Institut für Geophysik, Universität Göttingen

Geophysikalische Messungen in Bohrlöchern haben den Vorteil, dass sie auch aus Teilen des Bohrlochs Daten liefern, in denen aus verschiedensten Gründen keine Bohrkerne gewonnen werden konnten. Messungen des Magnetfeldes in einer Bohrung können hierbei mehrere Zwecke erfüllen. In der einfachsten Form können sie dafür genutzt werden, verschiedene lithologische Einheiten auf Grund ihrer magnetischen Eigenschaften voneinander abzugrenzen.

Weiterhin ist es möglich, Aussagen über die Polarität der Magnetisierung der durchteuften Schichten zu treffen, wodurch die Bohrlochmessungen auch zur Datierung geeignet sind. Sofern orientierte dreikomponentige Magnetfeldmessungen durchgeführt werden, ist es unter bestimmten Bedingungen auch möglich, die genaue Richtung der Magnetisierung, also Inklination und Deklination zu bestimmen. Dies ist ein großer Vorteil gegenüber Messungen an Bohrkernen, da diese meist unorientiert entnommen werden, wodurch nur die Inklination der Magnetisierung bestimmbar ist.

Wir zeigen Anhand von vektoriellen Magnetfeldmessungen, die mit dem Göttinger Bohrlochmagnetometer während IODP Expedition 330 zu den Louisville Seamounts durchgeführt wurden, welche Schritte nötig sind um die Magnetisierungsrichtung zu bestimmen. Ausgehend von einem einfachen horizontalen Schichtmodell berechnen wir eine scheinbare Magnetisierung des Untergrunds. Über ein von uns entwickeltes Näherungsmodell können wir den Einfluss von nicht horizontalen Schichten mit beliebiger Neigung und Azimut auf die scheinbare Magnetisierung bestimmen und so zeigen, dass die geometrischen Schichtparameter eng mit den magnetischen Parametern verknüpft sind. Durch zusätzliche Informationen über mögliche Schichtgeometrien aus Bildern der Bohrlochwand können wir schließlich für ausgewählte Schichten die Deklination bestimmen. Hierbei ist es über unser Näherungsmodell auch möglich, eine Fehlerabschätzung zu treffen, wobei insbesondere die Genauigkeit der Bestimmung der Deklination stark von der Genauigkeit der Bestimmung des Schichtazimuts abhängt.

IODP

Viruses in subsurface sediments: predator or prey?

B. ENGELEN[1], T. ENGELHARDT[1*], J. KALLMEYER[2], H. CYPIONKA[1],

[1] Institut für Chemie und Biologie des Meeres, Carl-von-Ossietzky Universität Oldenburg, Carl-von-Ossietzky Str. 9-11, 26129 Oldenburg, Germany, www.pmbio.icbm.de

[2] Deutsches GeoForschungsZentrum GFZ, Telegrafenberg, 14473 Potsdam, Germany

[*] Present adress: Center for Geomicrobiology, Department of Bioscience, Arhus University, Ny Munkegade 116, 8000 Arhus C, Denmark

Throughout the last years, we recognised that " the deep subsurface biosphere is alive and well" (Teske, 2005). However, one aspect that was so far mainly overlooked, but is now being investigated, is the viral inventory of deep-subsurface sediments (Engelhardt et al., 2011, 2013, 2014). As grazers probably play only a minor role in anoxic and highly compressed deep sediments, viruses

might be the main "predator" for indigenous microorganisms.

Viral lysis of prokaryotic biomass does not only control microbial numbers, non-infected microorganisms could take advantage of nitrogen- and phosphorous-rich organic compounds that are released by lysed cells. This process is known as "the viral shunt" and was estimated to account for 35% of the total benthic prokaryotic metabolism at the sediment surface (Danovaro et al., 2008). Thus, we hypothized that the viral shunt could have a major impact on the deep biosphere in providing labile organic compounds to the microbial community in this generally nutrient depleted habitat.

To test this hypothesis, we have analysed the abundance of viruses in a comprehensive set of globally distributed sediments (Engelhardt et al., 2014). We found that virus counts always exceeded the cell numbers even in deep, ancient and the most oligotrophic sediments of the world´s oceans. The number of viruses varied by several orders of magnitude from one region to another, in correlation with the prokaryotic activity and abundance. At all investigated sites, the virus-to-cell ratio increased with depth, indicating an ongoing viral production throughout the sediment columns. Thus, prokaryotic subsurface communities are able to maintain viral populations.

The enormous number of viruses in subsurface sediments is a strong indicator for their impact as controlling factor for prokaryotic communities. Moreover, our quantification opens a novel view on the role of virus particles wihin extreme oligotrophic subsurface sediments. If viral biomass equals or even exceeds the prokaryotic biomass, it would represent a so far not considered pool of organic carbon. Particularly in the oldest sediments, the quality of organic carbon is highly recalcitrant and hard to degrade. A virus particle that is composed of proteins and nucleic acids might become a food source for indigeneous microorganisms. However, all quantification methods are close to their detection limits and the results must be judged carefully. Variations in numbers, sizes and carbon content of cells and viruses would affect the virus-to-cell ratios and their biomass, respectively. However, by applying the best available conversion factors of 0.2 fg per marine virus (Suttle, 2005) and 14 fg per cell (Kallmeyer et al., 2012), virus-bound organic carbon would exceed cellular carbon at virus-to-cell ratios greater than 70. For the extremely oligotrophic South Pacific Gyre with a virus-to-cell ratio of up to 225, viral biomass therefore exceeds the amount of prokaryotic biomass. Even with a lower ratio of up to 20, which we have found at continental margin sites, viral-bound carbon would still represents up to 30% of the total biomass. Thus, phage particles might represent a reservoir of relatively easily available carbon. When indigenous microorganisms are capable to utilize slowly decaying phage particles, their building blocks (e.g. proteins) would become "prey" and the pool of bioavailable carbon would substantially be changed.

References:

Danovaro R, Dell'Anno A, Corinaldesi C, Magagnini M, Noble R, Tamburini C et al (2008). Major viral impact on the functioning of benthic deep-sea ecosystems. Nature 454: 1084-1027.

Engelhardt T, Sahlberg M, Cypionka H, Engelen B (2011). Induction of prophages from deep-subseafloor bacteria. EMI Rep. 3: 459–465

Engelhardt T, Sahlberg M, Cypionka H, Engelen B (2013) Biogeography of *Rhizobium radiobacter* and distribution of associated temperate phages in deep subseafloor sediments. ISME J 7: 199-209

Engelhardt T, Kallmeyer J, Cypionka H, Engelen B (2014). High virus-to-cell ratios indicate ongoing production of viruses in deep subsurface sediments. ISME J, doi:10.1038/ismej.2013.245

Kallmeyer J, Pockalny R, Adhikari RR, Smith DC, D´Hondt S (2012). Global distribution of microbial abundance and biomass in subseafloor sediment. Proc Natl Acad Sci 109: 16213–16216.

Suttle CA (2005). Viruses in the sea. Nature 437: 356-361.

Teske, AP (2005). The deep subsurface biosphere is alive and well, Trends in Microbiology, 13(9): 402-404.

IODP

IODP Expedition 345: Slow cooling of the lowermost gabbroic crust from the fast-spreading East Pacific Rise determined from Mg-in-Pl and Ca-in-Ol geospeedometry.

K. FAAK[1,2], K. GILLIS[2] AND THE IODP EXPEDITION 345 SCIENCE PARTY

[1]Ruhr-Universität Bochum, Universitätsstr. 150, D-44870 Bochum, Germany
[2]School of Earth and Ocean Science, University of Victoria, Victoria, B.C., Canada

Models of crustal accretion along fast-spreading mid-ocean ridges differ in the proportion of crystallization at different depths within the lower oceanic crust. Therefore, these models predict different thermal evolution, and most significantly, different depths to which hydrothermal fluids circulate in the oceanic crust. As a consequence, this implies different rates of cooling as a function of depth. *'Gabbro glacier'* type models require most of the latent heat of crystallization to be removed by hydrothermal circulation at the top of the axial magma chamber, leading to fast cooling rates in the upper gabbros. With increasing depth, heat conduction becomes the dominant process of heat removal. Since heat conduction is a less efficient mechanism of heat removal than hydrothermal circulation, it is expected that cooling rates decrease with increasing depth. In contrast, in *'sheeted sill'* type models, the mechanism for heat removal (hydrothermal circulation) is the same over the entire depth of the gabbroic crust and, therefore, cooling rates are not expected to change as a function of depth. The determination of cooling rates of rocks from different depths within the oceanic crust therefore provides insights in the processes involved in its formation.

IODP Expedition 345 recovered primitive layered gabbroic rocks that originated in the lower half to two thirds of the plutonic crust at the fast-spreading East Pacific Rise and exposed at the Hess Deep Rift (HDR). The freshest gabbroic rock samples from Site U1415 were chosen to obtain subsolidus cooling rates using the recently developed Mg-in-Plagioclase geospeedometer and the well-established Ca-in-Olivine geospeedometer. Geospeedometers make use of the temperature dependence of the diffusive exchange of elements between different phases and thus allow the determination of cooling rates from diffusion modeling. Both methods were carried out in the same samples and yield results that are in very good agreement with each other. The obtained cooling rates of these lower plutonic rocks are 2-3 orders of magnitude slower than cooling rates that were determined previously (using the same methods) from shallow-level gabbros exposed at HDR. These preliminary data support models of

crustal accretion that require faster cooling at the top of the plutonic crust and slower cooling at deeper levels.

ICDP

Investigation and monitoring of seismic velocity change related to earthquake swarms in West Bohemia/Vogtland

M. FALLAHI[1], M. KORN[1], C. SENS-SCHOENFELDER[2]

[1] Institut für Geophysik und Geologie, Universität Leipzig, Talstraße 35, 04103 Leipzig
[2] Deutsches Geoforschungszentrum Helmholtz-Zentrum Potsdam

The West Bohemia/Vogtland region is characterized by earthquake swarms with a typical source depth of 6-12 km. During the swarmquakes, several thousand events occur in a small volume in a period of one to several months. Degassing of upper mantle derived fluids, correlating with seismicity, is observed as well as temporal variations in the amount and composition of the emitted gas, isotope composition, and in earthquake source processes. Evidence for the triggering of earthquakes by fluids were found by earthquake source studies and inter-event relationships. Fluid reservoirs in the upper crust and at the crust-mantle boundary have been proposed as an explanation, though it is indeed *still* a hypothesis and *lacks direct observation*. Epicentres and gas springs are spatially separated and the pathways of fluids to the surface remain unresolved as are their relations to the crustal seismic structure. The unknown processes and relationships make the Eger Rift/Vogtland area an outstanding place for scientific drilling.

In this study, we analyzed temporal variations in seismic velocity in the area of the swarm earthquakes in west Bohemia/Vogtland during an earthquake swarm in October 2008 using Passive Image Interferometry (PII). In this method the correlation of ambient seismic noise is used to obtain Green functions that include multiply scattered coda waves. Three-component data allow a redundant measurement of six independent trace pairs for each station pair. Additionally the autocorrelation functions were examined. Here, the idea is that due to fluid intrusions in the source area, cracks will open and the fluid contents in cracks will change. This in turn will change the seismic velocity in the source area. Another cause for velocity variations may be the change in the stress field due to the stress drop in the souce area.

So far, using this method, we could not observe significant seismic velocity variations related to earthquake swarms in this area. This result is in accordance with earlier results by Keyser et al., (personal communication) who investigated the waveforms of earthquake doubletts with the method of coda wave interferometry. They excluded velocity changes larger than 0.12%.

Our conclusion is that possible velocity changes in the hypocentral area during an earthquake swarm is too small to be detected from the surface. Installation of seismic sensors in boreholes around the epicentral area coudl increase the sensitivity of the interferometric methods.

ICDP

Fluid inclusion record of chert and quartz vein formation in ultramafic crust of the Mesoarchaean Barberton Greenstone Belt, South Africa

K.FARBER[1], A. DZIGGEL[1], F.M. MEYER[1],W. PROCHASKA[2]

[1]Institute of Mineralogy and Economic Geology, RWTH Aachen University, Wüllnerstr. 2, 52062 Aachen, Germany
[2]Department for Applied Geosciences and Geophysics, University of Leoben, Peter-Tunner-Straße 5, 8700 Leoben, Austria

Strongly silicified volcano-sedimentary sequences are a common feature in Archaean greenstone belts. In the Onverwacht Group in the Barberton Greenstone Belt, South Africa, silification predominately occurs at the top of mafic to ultramafic lava flows at the contact with sedimentary chert horizons, and has been interpreted as a result of fluid circulation in shallow subseafloor convection cells (Hofmann & Harris, 2008). This study aims to better constrain (1) the conditions of chert formation, and (2) the sources and the physico-chemical evolution of interacting fluids that might have been responsible for the alteration.

56 surface samples from the uppermost unit of the Onverwacht Group, the Mendon Formation, were investigated. These include silicified ultramafic rocks, overlying banded cherts and chert veins (Fig.1a, b). The silicified komatiites consist of quartz, Cr-muscovite, Cr-spinell, and locally chlorite, carbonate, and/or tourmaline. Primary igneous features, such as spinifex texture, are locally preserved. The banded cherts are silicified sedimentary rocks that are made up of microcrystalline quartz and carbonaceous matter with minor amounts of mica and carbonate. Both rock types include abundant cherty veinlets and veins, which are either bedding parallel or crosscutting (Fig.1b). The chert veins are up to 10 cm in diameter and many of them contain coarse crystalline quartz (up to 4 mm crystal size) in their interior. The chert veins consist of microcrystalline quartz with minor Fe-hydroxides along cracks or weathered surfaces.

Eight samples from the coarsed grained interior of chert veins in silicified komatiite (4) and banded cherts (4) were used for fluid inclusion microthermometry to constrain the temperature and salinity of the fluid(s). Crush-leach analyses were done of 18 samples to determine the composition of the fluid that was trapped during quartz formation. The samples analyzed include six pairs of chert veins and associated coarse-grained interiors, and six samples from the banded cherts. The samples used for both analyses cover a range of outcrops of the Mendon Formation such as the Barite Valley Syncline, the Power Line Road and Msauli Gorge (Fig.1a). Fluid inclusions from the crystalline vein interiors of mainly bedding parallel, syntaxial veins were investigated. Primary fluid inclusions occur as intragranular clusters with an average size of 5-15 µm. No daughter minerals are observed. Most samples contain homogeneous 2-phase (L + V) inclusions at room temperature with a relatively constant vapor fraction of 10-20 %. Two samples of the banded cherts additionally contain 3-phase inclusions with H_2O (L) and CO^2 (L+V). These CO^2-rich inclusions are, on average, slightly larger than the aqueous ones. Other fluid inclusions are found in transgranular trails that often crosscut several crystals. Inclusions in the trails are morphologically similar

to inclusions present in the 2-phase intragranular clusters. CO_2-inclusions have minor amounts of CH_4 and therefore melting temperatures (Tm) of -57.0 ± 1.0°C. Clathrate melting was observed at 7.7 ± 0.8°C. Homogenization of CO^2 occurred at ~ 30°C and total homogenization (Th) between 230-240°C.

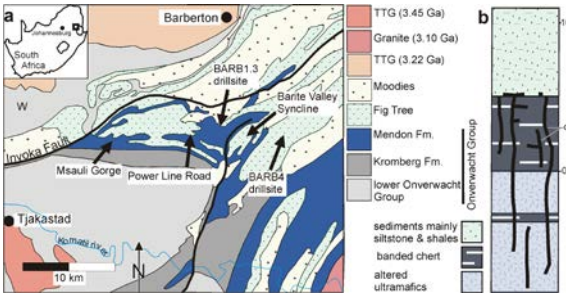

Figure 1:a) simplified geological map of the Barberton Greenstone, showing sample locations, and b) stratigraphic column of the Mendon Formation-Fig Tree contact on the wester limb of the Barite Valley Syncline (modified from Hofmann & Bolhar, 2007).

Melting temperatures in aqueous intragranular clusters and trails vary between ~ -15°C and 0°C. Most Tm values range between -2°C and 10°C, corresponding to a salinity of 3-11 mass% NaCl equiv.. One sample (M35a) contains a group of inclusions with significantly lower Tm values, pointing to a second type of fluid with a salinity of 18-30 mass% NaCl equiv.. In few samples, metastable fluid inclusions are observed in which Tm cannot be determined due to bubble disappearance during freezing. Homogenization into the liquid phase occurrs mainly at 150-200°C, whereas sample M35a shows lower Th of 110 - 150°C. The transgranular trails have the same microthermometric characteristics as the intragranular inclusions. The aqueous inclusions in veins from the silicified komatiites and the banded chert show similar microthermometric properties.

Crush-leach analyses show compositional differences between the crystalline interiors of the veins and the surrounding chert veins. The element ratios in the crystalline vein interior partly follow the seawater evaportation trend line, but are also similar to metamorphic fluids. In contrast, the chert veins and the sedimentary, banded cherts are more similar to Proterozoic seawater (Channer et al., 1997; Gutzmer et al., 2003; Foriel et al., 2004). Based on low Cl/Br ratios compared to modern seawater, these authors argued that Archaean seawater was buffered by the mantle and lacked organic matter. However, our samples show a high variability in Cl and Br and also resemble organic-rich fluids such as those observed in oilfield brines, which is probably due to an organic component of the carbonaceous matter. We therefore follow the interpretation of Hofmann & Bolhar (2007) that carbonaceous matter in cherts of the Mendon Formation represents material that originated in biogenic processes in the Archaean ocean. Although the source of the fluids has not been contrained unequivocally, a seawater component during chert precipitation is generally consistent with the field and geochemical evidence. However, the vein fluids analysed are also characterized by low Mg-concentrations that point to a hydrothermal component. In modern ultramafic-hosted seafloor hydrothermal fields, the low Mg content of the fluid is a result of serpentinisation reactions. Thus, some of the Mg that was leached from the silicified komatiites may have been removed from the fluid due to serpentinisation in the deeper parts of the crust (Fig.2).

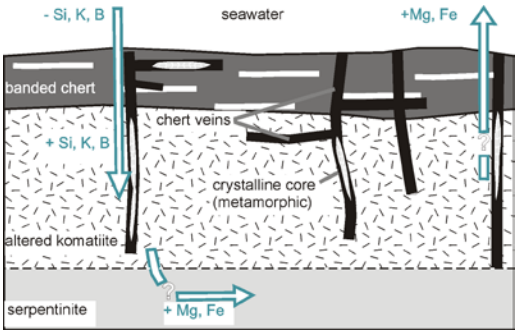

Figure 2: Preliminary model illustrating potential sources of fluids and elements during seafloor hydrothermal alteration in the Mendon Formation (not to scale).The crystalline cores in some chert veins formed after the developtment of the hydrothermal system.

Indepentend temperature estimates using chlorite thermometry and the Kübler illite cristallinity index are at 250-350°C, indicating greenschist facies conditions. The minimum temperature derived by microthermometry is much lower than the temperatures from the external thermometers. Using calculated isochores, the depths of vein formation is calculated to be between 5-8 km. These values argue against a shallow water deposition of the chert veins, yet likely mean that the crystalline interiors may have formed during a later deformation or fluid infiltration event. Evidence for this is given by the different element ratios obtained from crush-leach analyses, the greenschist facies metamorphic overprint, as well as the microthermometric properties of the late-stage transgranular fluid inclusions trails which are indistinguishable from the primary, intragranular clusters. Thus, the crystalline parts of chert veins in the Barberton Greenstone Belt are not suited for Archaean seawater reconstruction by fluid inclusion analysis, as they were formed by a later deformation and/or fluid infiltration event (Fig.2). This event may be related to the regional metamorphism during the main accretion event at c. 3.23 Ga (e.g. Dziggel et al., 2010 and references therein). The microcrystalline chert veins, however, still appear to retain the original signature of the fluid that was trapped during shallow water deposition, and indicate that both Archaean seawater and hydrothermal fluid have been involved in the silicification.

References:

Channer, D.M. de R., de Ronde, C.E.J., 1997. The Cl-, Br-,I- composition of 3.23 Ga modified seawater: implications for the geological evolution of ocean halide chemistry. Earth and Planetary Science Letters, 150, 325–335.

Dziggel, A., Poujol, M., Otto, A., Kisters, A.F.M., Trieloff, M., Schwarz, W., Meyer, F.M., 2010. New U-Pb and 40Ar/39Ar ages from the northern part of the Barberton greenstone belt, South Africa: implications for the formation of Mesoarchaean gold deposits. Precambrian Research, 179, 206-220.

Foriel, J., Philippot, P., Rey, P., Somogyi, A., Banks, D., & Ménez, B., 2004. Biological control of Cl/Br and low sulfate concentration in a 3.5-Gyr-old seawater from North Pole, Western Australia. Earth and Planetary Science Letters, 228(3), 451-463.

Gutzmer J., Banks, D.A., Lüders, V., Beukes, N.J., von Benzing, K.L., 2003. Ancient sub-seafloor alteration of basaltic andesites of the

Ongeluk Formation, South Africa: implications for the chemistry of Paeleoproterozoic seawater. Chemical Geology, 201, 37-53.
Hofmann, A., Bolhar, R., 2007. Carbonaceous cherts in the Barberton Greenstone Belt and their significance for the study of early life in the Archean record. Astrobiology, 7(2), 355-388.
Hofmann, A., Harris, C., 2008. Stratiform alteration zones in the Barberton greenstone belt: a window into subseafloor processes 3.5–3.3 Ga ago. Chemical Geology 257, 224-242.

IODP

Hydrothermal fluids from the ocean crust support microbial life in deeply buried sediments (IODP Exp. 301)

K. FICHTEL[1], H. CYPIONKA[1], B. ENGELEN[1]

[1]Institut für Chemie und Biologie des Meeres, Universität Oldenburg, Carl-von-Ossietzky Straße 9-11, D-26129 Oldenburg, Germany

Huge amounts of seawater circulate through the upper porous layers of the ocean crust. This crustal fluid flow contains electron acceptors such as sulfate for microbial respiration. Molecular biological analysis of crustal fluids have revealed several indigenous microorganisms to be present in the basaltic basement (Cowen et al., 2003, Huber et al.,2005). However, it is supposed that these hydrothermal fluids do not only fuel the crustal biosphere but also microbial populations within the deeply buried sediments by providing electron acceptors from below via diffusion (DeLong, 2004).

To examine this hypothesis, we studied the influence of diffusive flows, especially of sulfate, on the abundance, activity and diversity of deep-biosphere microbial populations. Samples were analysed from a 265 m long sediment column of IODP Site U1301 drilled at the eastern flank of the Juan de Fuca Ridge, northeastern Pacific (water depth: 2650 m). The sampling site is characterized by a steep temperature gradient of 2 to 62°C towards the basement. Geochemical depth profiles indicate that sulfate diffuses into the sediment column from both sides, the seafloor (27 mM) and the basement (16 mM). This results in the formation of two sulfate-methane transition zones, potential hot spots of high microbial activity.

Contamination-free subsamples (Lever et al., 2006) were used for cell quantification, molecular biological analyses, radiotracer- and exoenzyme activity measurements. Enrichments cultures were analyzed for their composition by molecular biological screening using PCR, DGGE and subsequent sequencing. They were further used for isolation of abundant populations with special emphasis on sulfate-reducing bacteria. Physiological investigations of these isolates were performed to unravel adaptations to this nutrient-limited habitat. Finally, temperature and pressure adaptations of a piezothermophilic isolate obtained from crust-near layers, were examined.

In our investigations, we found several evidences for crustal fluids stimulating the deep biosphere. Elevated cell numbers, most-probable number (MPN) counts and exoenzyme activities towards the sediment-basement interphase indicated the presence of a vital and metabolically active microbial community near the bedrock. The diffusion of sulfate from below into the methanogenic zone substantially stimulated sulfate reduction rates and rates of anaerobic oxidation of methane (Engelen et al., 2008).

Molecular biological analysis of initial enrichment cultures from the different sulfate-containing zones revealed shifts in the microbial diversity. The isolation of solely non-sporeforming sulfate-reducing Deltaproteobacteria from 3.5 My old basement-near layers indicated viable populations to thrive in fluid-influenced layers. Physiological tests demonstrated their capability to grow either chemoheterotrophically, chemolithoautotrophically or by fermentation. Interestingly, one Desulfovibrio-affiliated isolate (strain P23) even grew autotrophically on sulfate, carbon dioxide and hydrogen (Fichtel et al., 2012). This finding supports the assumption, that hydrogen may act as the key electron donor in deep subseafloor sediments and basaltic environments (Stevens and McKinley, 1995).

In situ, the bacteria living in crust-near sediments are exposed to both, high temperature and high hydrostatic pressure. Strain P23 was analyzed representatively to study the influence of pressure on the maximum temperature for growth. Complementary analysis of membrane lipids and fatty acids helped to identify cellular responses as adaptation mechanism to changing incubation conditions. Strain P23 turned out to be a moderately piezothermophilic bacterium, stabilizing its membrane viscosity and function by regulating the ornithine content, and by structural changes of main phospholipids (Fichtel et al., in prep.).

In conclusion, our studies confirm the hypothesis that crustal fluids support microbial life in marine subseafloor sediments. Mirobial abundances, metabolic activities and community structures are influenced by fluids from the ocean crust. Regarding the worldwide expansion of the crustal fluid aquifer, we assume that this impact is one major driving force for marine deep biosphere populations on a global scale and over geological time scales.

References:

Cowen, J. P, Giovannoni, S. J., Kenig, F., Johnson, H. P., Butterfield, D., Rappé, M. S., Hutnak, M., Lam, P., 2003. Fluids from aging ocean crust that support microbial life. Science 299, 120-123.
Huber, J. A., Johnson, H. P., Butterfield, D. A., Baross, J. A., 2006. Microbial life in ridge flank crustal fluids. Environ Microbiol 8, 88-99.
DeLong, E. F., 2004. Microbial life breathes deep. Science 306, 2198-2200.
Lever, M. A., Alperin, M., Engelen, B., Inagaki, F., Nakagawa, S., Steinsbu, B. O., Teske, A., IODP Exp. 301 Scientists, 2006. Trends in basalt and sediment core contamination during IODP Expedition 301. Geomicrobiol J 23, 517-530.
Engelen, B., Ziegelmüller, K., Wolf, L., Köpke, B., Gittel, A., Cypionka, H., Treude, T., Nakagawa, S., Inagaki, F., Lever, M. A., Steinsbu, B. O., 2008. Fluids from the oceanic crust support microbial activities within the deep biosphere. Geomicrobiol J 25, 56-66.
Fichtel, K., Mathes, F., Könneke, M., Cypionka, H., Engelen, B., 2012. Isolation of sulfate-reducing bacteria from sediments above the deep-subseafloor aquifer. Front Microbiol 3, 1-12.
Stevens, T. O., McKinley, J. P., 1995. Lithoautotrophic microbial ecosystems in deep basalt aquifers. Science 270, 450-455.

IODP

Sub-millimeter structure and internal architecture of ODP 204 (Hydrate Ridge) gas hydrates revealed by Synchroton Radiation X-Ray Cryo-Tomographic Microscopy

DAVID FISCHER[1,2], GERHARD BOHRMANN[1], THOMAS PAPE[1], STEPHAN A. KLAPP[1,3], FRIEDER ENZMANN[3], WERNER F. KUHS[4], THOMAS HUTHWELKER[5]

[1]MARUM – Center for Marine Environmental Sciences and Department of Geosciences at the University of Bremen, Leobener Straße, D-28359 Bremen, Germany
[2] Alfred Wegener Institute Helmholtz Centre for Polar and Marine Research, Am Handelshafen 12, D-27570 Bremerhaven, Germany
[3] Springer, Tiergartenstraße 17 | 69121 D-Heidelberg, Germany
[4] GZG, Abt.Kristallographie, Georg-August-Universität Göttingen, Goldschmidtstr.1, D-37077 Göttingen, Germany
[5] Swiss Light Source, Paul Scherrer Institute, CH-5232 Villigen, Switzerland

Although recognized worldwide in different environmental settings including the seafloor, natural hydrocarbon gas hydrates remain rather exotic materials whose interplay between chemical and physical parameters is still not fully understood. We radiographed gas hydrate specimen obtained during ODP Leg 204 to the renowned Hydrate Ridge offshore Oregon with Synchroton radiation provided by the Swiss Light Source in Villingen, Switzerland, in order to gain insight into their sub-millimeter scale internal structure. The project was conducted in the frame of the DFG-Schwerpunktprogramm "IODP".

In contrast to earlier studies focussing on shape parameters of hydrocarbon gas hydrates, our approach enabled us to investigate specific areas of interest within small samples and to identify internal, architectural particularities of single gas hydrate grains, grain boundaries and matrix materials in the µm- to several hundreds of µm- range. We identified three distinct materials within the samples, that are discernible based on density differences: gas hydrates, free gas, matrix material (probably water ice). Certain constituents feature typical three-dimensional shapes: Gas hydrate grains often appear as irregularly shaped bulky entities almost always surrounded by a thin layer of pore networks consisting of free gas. We additionally identified tube-like structures generally of few µm in diameter and several hundreds of µm in length within the gas hydrates that contained a very low density material, probably free gas. Such tubes almost always occur in "swarms" of several to several tens of single tubes often with the same or very similar orientations. The presence of the tubes, which were in some cases connected to the thin layer of pore networks surrounding the gas hydrate grains, is tentatively interpreted as ex situ phenomena representing degassing features produced during sample retrieval, when the samples were removed from the gas hydrate stability field that is constrained by high pressures and low temperatures. During this process the gas hydrates decomposed and separated into free gas and water. While the gas remained in the gas hydrates and was still identifiable due to its low density compared to surrounding materials, the released water likely recrystallized into water-ice that remained in the samples as the matrix material. Additional features related to gas hydrate decomposition are boundary pore-networks arranged in a cubic fashion that show reminescences of the expected cubic structure of gas hydrates. The amount, relative thickness, and preservation of such cubic pore networks may provide insights into the development and stability of the sample over time.

With this study we provide a new and unique dataset of the sub-millimeter scale internal structure of gas hydrates from Hydrate Ridge and show that Synchroton raditation is very helpful in investigating the architecture of natural hydrocarbon gas hydrates. Future investigations are needed to 1) adapt, establish and refine the used method for examining gas hydrates and 2) compare samples from different environmental settings and samples of different crystallographic compositions (e.g., sI and sII hydrates).

ICDP

WET-DRY SHIFTS IN THE SOURCE REGION OF MODERN MAN:

A Late Quaternary climate record from Chew Bahir, southern Ethiopia

V. FOERSTER[1], A. JUNGINGER[2], R. VOGELSANG[3], A. ASRAT[4], H.F. LAMB[5], V. WENNRICH[6], M. WEBER[6], J. RETHEMEYER[6], U. FRANK[7], M.C. BROWN[7], M.H. TRAUTH[2], AND F. SCHAEBITZ[1]

[1] University of Cologne, Seminar for Geography and Education; Gronewaldstrasse 2; 50931 Cologne; Germany
[2] University of Potsdam, Institute of Earth and Environmental Science; Karl-Liebknecht-Str. 24-25; 14476 Potsdam; Germany
[3] University of Cologne, Institute of Prehistoric Archaeology; Bernhard-Feilchenfeld-Str. 11; 50969 Cologne; Germany
[4] Addis Ababa University, Department of Earth Sciences; P. O. Box 1176, Addis Ababa, Ethiopia
[5] Aberystwyth University, Institute of Geography and Earth Sciences, Aberystwyth SY23 3DB, U.K.
[6] University of Cologne, Institute of Geology and Mineralogy; Zülpicher Str. 49A; 50674 Cologne; Germany
[7] Helmholtz-Zentrum Potsdam, Deutsches GeoForschungsZentrum – GFZ, 14473 Potsdam; Germany

Climatic variability and a rapidly changing environment are considered to have had a significant influence on human evolution, cultural and technological innovation, and human migration within and beyond the African continent. However, to evaluate the impact that climatic shifts on different timescales might have had on the living conditions of prehistoric humans, an understanding and continuous reconstruction of these climatic wet-dry variabilities and their underlying driving mechanisms are essential. Here we present a high-resolution (up to 3 years) and well-dated terrestrial record of the last 46,000 years from the paleo-lake Chew Bahir in southern Ethiopia.

The Chew Bahir basin, as a newly explored reliable climatic archive, lies in a biogeographically highly sensitive transition zone between the Main Ethiopian Rift and the Omo-Turkana basin, the region where the fossils of the oldest known anatomically modern human were found. The climate record is based on the multi-proxy data from six cores (9–18.8 m) along a NW-SE transect across the basin. This data-set combined with the comparison between the different transect coring sites provide initial insight into intra-basin dynamics and major mechanisms controlling the sedimentation of the proxies. Out of this we

developed a basic proxy concept for Chew Bahir for the last two wet-dry cycles.

The Chew Bahir record provides insights into the velocity and character of late-Quaternary wet-dry transitions on different time scales: three different modes were identified showing variability on precessional, millennial as well as decadal time scales all characterised by either abrupt or gradual changes of different magnitudes. All those factors, significantly shaping climatic transitions, would of course had important implications for humans to survive, adapt to or to be dislodged by a changing environment. As a contribution towards a better understanding of this more then complex human-climate interaction, we also present here a match between the last 20 ka of the Chew Bahir climate record and the settlement history of adjacent refugia.

IODP

Calcareous nannofossil response to paleoceanographic changes recorded during the Mid-Oligocene in the Central Eastern Pacific Ocean (Site U1334, IODP Expedition 320)

A. FRAGUAS[1], J. ZIRKEL[1,2], J.O. HERRLE[1,2], J. BOLLMANN[3], H. PÄLIKE[4]

[1]Institute of Geosciences, Goethe-University Frankfurt, D-60438 Frankfurt am Main, Germany
[2]Biodiversity and Climate Research Centre (BIK-F), D-60325 Frankfurt am Main, Germany
[3]Department of Geology, Earth Sciences Centre, University of Toronto, 22 Russell Street, Toronto, Ontario, M5S 3B1, Canada
[4]MARUM/Center for Marine Environmental Sciences, University of Bremen, D-28359, Bremen, Germany

Semiquantitative analyses were performed on Mid-Oligocene calcareous nannofossil assemblages from the Central Eastern Pacific Ocean (Site U1334, IODP Expedition 320) in order to determine their response to the paleoceanographic and paleoclimatic changes recorded during this time interval, charactirized by the maximum glaciation event Oi-2b (Miller et al., 1991). A total of 142 samples, between 26.6 and 27.04 Ma, were collected from the core at about 5 cm intervals and sprayed on aluminum stubs using the SMS-method described by Bollmann et al. (1999). This method guarantees homogeneous distribution of particles, a prerequisite for assemblage and diversity analyses. An automated Zeiss SIGMA field emission scanning electron microscope was used to capture about 600 images of calcareous nannofossils in each sample at a magnification of x4000, using a custom made imaging software. 300 nannofossils were counted per sample. The relative abundances of the species identified were expressed as percentages and the diversity was assessed using the Shannon diversity index (Shannon and Weaver, 1949). All these results are compared to benthic foraminifera accumulation rates (BFAR, indicator for surface water productivity of Herguera and Berger (1991)), the fragmentation index (FI, dissolution indicator of Berger (1970)) and $\delta^{18}O_{grimsdalei}$ data as preliminary record for major ice volume changes (e.g. Lea et al., 2002).

The calcareous nannofossil assemblages are dominated by *Cyclicargolithus floridanus*, *Sphenolithus* spp., *Coccolithus pelagicus* and *Discoaster* spp., which account for more than 95% of the total calcareous nannofossil assemblages. *C. floridanus* is the most abundant species, with relative abundances >60%. The calcareous nannofossil assemblage are well- to moderately-preserved, although partial dissolution of some elements on the distal shield can be frequently observed, especially in *C. floridanus*. Shannon diversity index shows high values at the onset and at the end of the Oi-2b glaciation event, between 26.6 and 26.9 Ma. During the Oi-2b, the Shannon diversity index is positively correlated with the BFAR, indicating that decreasing surface water productivity is accompanied by decreasing nannofossil diversity. A major shift in the relative abundances of the counted species can be observed during the onset of the Oi-2b (26.84 Ma), characterized by a sharp decrease of *C. floridanus* percentages and an increase of *C. pelagicus*, *Sphenolithus* spp. and *Discoaster* spp.. During the Oi-2b glaciation event, *C. floridanus* shows higher percentages and is negatively correlated with BFAR and positively correlated with the benthic foraminifera $\delta^{18}O$ record. The higher percentages of *C. floridanus*, often referred as indicator of cooler surface waters (e.g. Aubry, 1992), might support the idea of cooler equatorial Pacific sea surface water temperatures during the Oi-2b glaciation event. *Sphenolithus* spp. display a peak in the percentage around 27 Ma coinciding with lower $\delta^{18}O_{grimsdalei}$ values, supporting the idea that these species probably thrived in warm waters (e.g. Tremolada and Bralower, 2004). There are no evident correlations between the relative abundances of *C. floridanus*, *C. pelagicus*, *Sphenolithus* spp. and *Discoaster* spp. and FI.

Our preliminary results indicate a clear relationship between changes in sea surface water temperatures and productivity during the Oi-2b and the changes recorded in the calcareous nannofossil assemblages, especially in the most abundant species *C. floridanus*.

References:

Aubry, M.P., 1992. Paleogene Calcareous nannofossils from the Kerguesen Plateau, Leg 120. In: Wise Jr., S.W., Schlich, R., et al. (Eds.), Proc. ODP. Sci. Results, vol. 120, pp. 471-491.

Berger, W.H., 1970. Planktonic foraminifera: selective solution and the lysocline. Marine Geology 8, 111-138.

Bollmann et al., 1999. Bollmann, J., Brabec, B., Corte.s, M.Y., Geisen, M., 1999.Determination of absolute coccolith abundances in deepsea sediments by spiking with microbeads and spraying (SMS-method). Marine Micropaleontology 38, 29-38.

Herguera, J. C., Berger, W. H., 1991. Paleoproductivity from benthic foraminifera abundance: Glacial to postglacial change in the west-equatorial Pacific. Geology 19, 1173-1176.

Lea, D. W., Martin, P. A., Pak, D. K., Spero, H. J., 2002. Reconstructing a 350 ky history of sea level using planktonic Mg/Ca and oxygen isotopic records from a Cocos Ridge core. Quaternary Science Reviews 21, 283-293.

Miller, K.G., Wright, J.D., Fairbanks, R.G., 1991. Unlocking the Ice House – Oligocene – Miocene oxygen isotopes, eustasy, and margin erosion. Journal of Geophysical Research 96, 6829-6848.

Shannon, C.E., Weaver, W., 1949. The Mathematical Theory of Communication. University of Illinois Press, Urbana. 125 pp.

Tremolada, F., Bralower, T.J., 2004. Nannofossil assemblage fluctuations during the Paleocene–Eocene Thermal Maximum at Sites 213 (Indian Ocean) and 401 (North Atlantic Ocean): palaeoceanographic implications. Marine Micropaleontology 52, 107-116.

ICDP

The ICDP SCOPSCO project at Lake Ohrid (Macedonia, Albania)

A. FRANCKE[1], B. WAGNER[1], K. LINDHORST[2], H. BAUMGARTEN[3], S. KRASTEL[2], T. WONIK[3], AND THE SCOPSCO SCIENCE TEAM

[1]Institute for Geology and Mineralogy, University of Cologne, Cologne
[2] Institute of Geosciences, Christian-Albrechts-Universität zu Kiel
[3]Leibniz Institute for Applied Geophysics (LIAG), Hannover

Lake Ohrid is located at the border of Macedonia and Albania (40°702 N, 20°42 E) in a tectonic active, N-S trending graben. Chronostratigraphic interpretation of prominent cyclic patterns of hydro-acoustic data imply that the lake is about 2 Ma years old (Lindhorst et al., in press) which coincides with age estimations derived from molecular clock analyses of DNA data from ancient lake species (summarized by Wagner and Wilke, 2011). The lake is approximately 30 km long, 15 km wide and has a relative simple bathtube-shape bathymetry with a mean water depth of 151 m. With about 212 described endemic species, Lake Ohrid is the most diverse lake in world if the number of endemic species is set in relation to the surface area.

Previous studies on short sediment cores (up to 15 m) from Lake Ohrid have demonstrated the potential of Lake´s Ohrid deposits to provide a valuable archive of environmental and climatological variability in the Balkan area (e.g. Wagner et al., 2009; Vogel et al., 2010a), and of the tephrostratigraphic history of volcanic eruptions in the central Mediterranean region (e.g. Wagner et al., 2008b; Sulpizio et al., 2010; Vogel et al., 2010b) during the last Glacial - Interglacial cycle. Moreover, several mass wasting deposits can be observed at Lake Ohrid, which potentially can be used to reconstruct the seismo-tectonic history of the area (Wagner et al., 2008a; Reicherter et al., 2011). In order to obtain more information about the history of the lake back to its formation, more than 2100 m of sediment were recovered from 5 different drill sites between 2011 and 2013 within the scope of the ICDP SCOPSCO project (Scientific Collaboration on Past Speciation Conditions in Lake Ohrid). The aims of the SCOPSCO project are (1) to reveal a precise age and origin of Lake Ohrid, (2) to unravel the seismotectonic history of the lake area including effects of major earthquakes and associated mass wasting events, (3) to obtain a continuous record containing information on volcanic activities and climate changes in the central northern Mediterranean region, and (4) to better understand the impact of major geological/environmental events on general evolutionary patterns and shaping an extraordinary degree of endemic biodiversity as a matter of global significance.

As part the SCOPSCO project, a 10.8 m long sediment sequence (“LINI”- site, core Co1262) was recovered close to the Lini Peninsula in 2011. This site was selected in order to unravel the seismo-tectonic history of the lake. Hydro-acoustic data indicate three mass wasting deposits (MWD) at the coring location. Core Co1262 from the “LINI” site is mainly formed by relatively homogenous clayey to silty mud of greyish to olive color (Fig. 1). The sediments appear massive, probably as a result of bioturbation, as it was observed in other sediment sequences from Lake Ohrid at least throughout the Holocene (Wagner et al., 2009; Vogel et al., 2010a). The most prominent horizon in core Co1262 occurs between 320 and 121 cm below sea floor (blf). This horizon is characterized by a 1 to 2 cm thick sandy horizon at the base and very homogenous sediments without major variations in most sediment proxies above. The coarse grained base and the overall homogenous facies identify this horizon as a MWD and likely corresponds to the uppermost MWD in the hydro-acoustic data. A 15 cm thick turbidite from 980 cm to 965 cm as well as several < 4 cm thick wasting deposits were identified by variations in water content and grain-size composition, but these events are too small to be visible in the hydro-acoustic data.

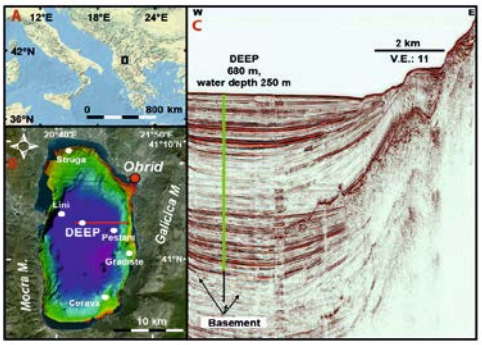

Fig. 1: A: Location of Lake Ohrid in the Balkan Region (black square). B: Bathymetric map of Lake Ohrid. Marked are the drill sites “DEEP”, “LINI”, “CERAVA”, “GRADISTE” and “PESTANI”. The “STRUGA” site in northern parts of the lake was canceled due to logistic reasons. Red line: Hydro-acoustic profile shown in Fig. 1 C. C: Hydro-acoustic profile from West to East in central parts of Lake Ohrid crossing the main drill site “DEEP”. The black bar marks the target drill depth, the green bar marks the recovered sediments.

A chronological control of the recovered sediments is based on tephrostratigraphy, radiocarbon dating and cross correlation with existing records from lakes Ohrid, Prespa, and Dojran (Fig. 1). Three cryptotephra layers at 709 cm, 517 cm and 320 cm (blf) were identified by XRF scanning and by microscopical and geochemical analyses. The cryptotephras could be assigned to the Mercato (8890 cal yr BP), to the FL (3370 cal yr BP) and to a mixture of the AD 512 and AD 472 Somma-Vesuvius tephras, respectively. In addition, the age control of core Co1262 was improved by five radiocarbon ages from terrestrial plant material fragments. A detailed discussion of the chronology of core Co1262 is presented by Wagner et al. (2012). The age-depth model was interpolated between the radiocarbon ages, the tephras and the cross correlation points by using a smooth spline function (Lacey et al., sub.). The calculations were carried out with the software package CLAM v.2.2 (Blaauw, 2010) operating with the IntCal 13.14C calibration curve (Reimer et al., 2013).

The established age model for core Co1262 can be used to determine the age of the uppermost MWD (MWD1). MWD1 directly overlays the 1mm thick greyish band, which was identified as the AD 472/512 tephra. According to the established age model, the sedimentation rate during the 6th century was about 0.1 cm*yr^{-1}. This implies that the mass movement occurred less than 20 years after the deposition of the AD 472/512 tephra. Potential triggers for a mass movement include delta collapses, rockfalls, lake

level changes, or earthquakes. Historical evidence revealed that three earthquakes affected the region of Ohrid during the 6th century at 518 AD, 526 AD, and 527 AD (summerized by Wagner et al., 2012). One of these earthquakes could have potentially triggered the deposition of MWD1, although the impossible differentiation between the AD 472 and AD 512 tephra do not allow a chronological discrimination between the three earthquakes (Wagner et al., 2012).

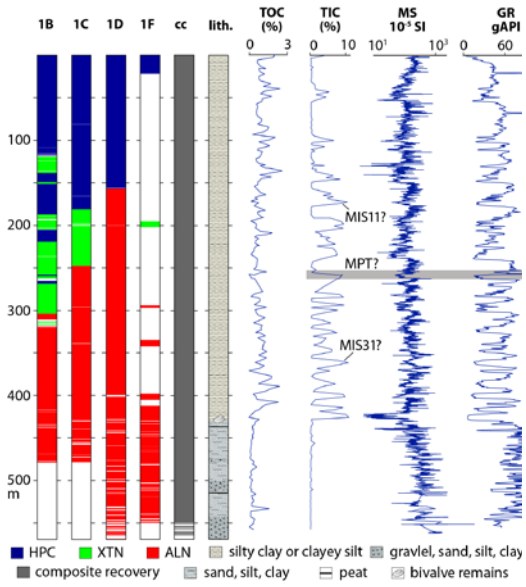

Fig. 2: Core recovery and lithology from "DEEP" site. Colours in the core recovery indicate the different coring tools (blue = hydraulic piston corer, green = extended nose, red = Alien). White parts indicate no core recovery due to gaps. The lithology and biogeochemical data (TIC, TOC) was obtained from core catcher samples, the magnetic susceptibility (MS) was measured in 2 cm resolution on-site in Ohrid on sediment cores from hole 1D. Gama ray (GR) values were achieved by borehole logging in hole 1D. Marked are Marine Isotope Stages 11 and 31 (MIS 11, MIS 31), and the Mid Pleistocene Transition (MPT).

In spring 2013, a deep drilling campaign at Lake Ohrid yielded about 2,100 m of sediment from 4 different drill sites (Fig. 1). The logistics for the coring equipment and the coring were operated by DOSECC (USA) with the DLDS (Deep Lake Drilling System). Logistics for scientific equipment, on-site initial core handling, magnetic susceptibility (MS) measurements at Lake Ohrid, and first biogeochemical analyses of core catcher samples were predominantly conducted by the University of Cologne and by the University of Kiel, respectively. At all 4 drill sites, high-quality continuous downhole logging data were achieved by the Leibniz Institute for Applied Geophysics (LIAG, Hannover). Spectral gamma ray was run through the drillpipe, and after having gradually pulled the pipes to maintain borehole stability, magnetic susceptibility, resistivity, dipmeter, borehole televiewer and sonic data were obtained. Additional vertical seismic profiling was conducted at the "DEEP" site.

At the "CERAVA" site in the southeastern part of the lake, two parallel cores were drilled with a maximum sediment depth of 90.5 m blf. The composite field recovery is ca. 97% (88 m). The basal sediments recovered consisted of lithified sediments and shell fragments or shells.

At the "GRADISTE" site in the eastern part of the lake, three parallel cores were drilled with a maximum sediment depth of 123 m blf. The composite core recovery is ca. 92% (114 m). Coarse-grained sediments dominated below ca. 82 m blf.

The originally planned "STRUGA" site in the northern part of the lake was skipped due to logistic reasons. Instead, a new site was selected, which, too, is located in the eastern part of the lake, about 3 km to the northeast of the "GRDAISTE" site. This "PESTANI" site had a water depth of 260 m and aimed at reaching sediments deposited directly above the bedrock at ca. 200 m blf. At this site, only one hole with a maximum sediment depth of 194.5 m blf was recovered. The composite field recovery is 91%.

At the "DEEP" site in the center of the lake, seismic data indicated a maximum sediment fill of ca. 700 m, of which the uppermost 569 m sediment were recovered with a composite field recovery of 95%. The sediment consists of fine-grained, pelagic deposits until about 430 m blf (Fig. 2). Between 430 and 569 m blf coarser material, fine-grained sediments with high organic content, peat, and sand or gravel layer indicate shallow water or even fluvial conditions at the coring location. Gravel and pebbles hampered a penetration deeper than 569 m blf. The initial biogeochemical data from the core catcher samples show distinct fluctuations of the Total Inorganic Carbon (TIC) and the Total Organic Carbon (TOC) contents above 430 m blf (Fig. 2). The fluctuations of the TIC content can likely be attributed to glacial / interglacial variability. Pre-site surveys between 2005 and 2009 and core Co1262 ("LINI"-site, Fig. 1), and first high-resolution XRF data from "DEEP"-site have shown that Ca counts (XRF data) are closely correlated to the amount of TIC and that both proxies are sensitive to short-term and long-term climate change (Wagner et al. 2010, Vogel et al. 2010). Over the last ca. 135 ka, TIC is high during interglacial periods and primarily originates from carbonate precipitation. During glacial periods, carbonate is almost absent as shown by negligible TIC contents and low Ca counts. TOC is very low throughout warm and cold periods, which probably indicates oligotrophic conditions in the lake throughout its entire history. The MS measured in 2 cm resolution and gamma ray values obtained by borehole logging show variations, which likely correlate with those of the TIC data above 430 m blf (Fig. 2). Low MS and high gamma ray values are associated with interglacial periods. In contrast, high MS and low gamma ray values persist during glacial time periods. Mutual dilution processes between endogenic carbonate and clastic sedimentation can probably partly explain low MS values during interglacial periods, such as also indicated by high K counts during glacial periods in the "LINI" record. Deposits below 430 m blf are characterized by higher MS and gamma ray values, respectively.

The high frequency variability of TIC and MS between ca. 430 and 315 m blf can probably be attributed to the 41 ka world of obliquity dominated cycles prior to 920 ka (Mudelsee and Schulz 1997, Tzedakis et al. 2006). The sequence between ca. 315 and 250 m indicates a decreasing frequency of TIC and MS, which probably corresponds with the Middle Pleistocene Transition (MPT) between 920 and 640 ka. The uppermost 250 m of sediment column

indicate a similar amplitude in TIC, with values between almost 0% and ca. 10%, but a less high frequency. This part of the sequence can probably be attributed to the 100 ka world cycles, which dominated during the last 640 ka. Applying this pattern to the "DEEP" site record, the Marine Isotope Stage (MIS) 5 sediments would occur at ca. 50 m blf, which is confirmed by the finding of tephra horizons observed already in the presite studies (Vogel et al. 2010b). 5 tephras could already be identified, which can likely be assigned to the known tephras Y3, Y5, X5, X6, and P11 (Wagner et al., 2008b; Vogel et al., 2010b). Further extrapolation downcore suggests that the TIC maximum at ca. 180 m blf could correspond with one of the warmest interglacials prior to the MPT, the MIS 11. Currently, core opening, core description, high-resolution XRF (2.5 mm resolution) and MSCL (1 cm resolution) – scanning, core correlation, and sub-sampling (16 cm resolution) of the sediment cores from the "DEEP" site is ongoing at the University of Cologne.

Overall, this first interpretation about glacial-interglacial variability of the data implies that the recovered sequence at the "DEEP" site covers at least the last 1.2 Ma. Until now, there is no evidence for major hiatuses or disturbed sequences, which implies that Lake Ohrid has the potential to provide an outstanding high-resolution, continuous record for paleoenvironmental and –climatological variability in the Balkan area. A robust age model will be established using paleomagnetic and tephrostratigraphic tie points and using climate-sensitive proxy data, such as the TIC content and MS data for tuning to global isotopic stacks (e.g. Lisiecki and Raymo, 2005) and orbital parameters. The already observed tephra layers and several peaks in K, Sr, Zr, and magnetic susceptibility indicate that the "DEEP" site sequence promise to provide a unique record of tephrostratigraphic history for the central Mediterranean Region.

IODP

Long-term evolution of Cenomanian to Campanian black shale formation at Demerara Rise

O. FRIEDRICH[1], J. ERBACHER[2], R.D. NORRIS[3], B. BECKMANN[4]

[1] *Institut für Geowissenschaften, Universität Heidelberg*
[2] *Bundesanstalt für Geowissenschaften und Rohstoffe, Hannover*
[3] *Scripps Institution of Oceanography, University of California, San Diego*
[4] *MARUM, Universität Bremen*

We present a 20 Million year record of benthic foraminiferal assemblage data spanning the Cenomanian to Campanian black shale sequence at Demerara Rise, tropical Atlantic (ODP Leg 207). This location is characterized by a continuous formation of organic-rich sediments (black shales) that have mean TOC values of 5-10 %, peaking at the OAE2 event (up to 30%). Interestingly, however, benthic foraminifera are present during a long time within these sediments, suggesting large fluctuations in bottom-water ventilation and oxygenation.

We combine this long-term benthic assemblage record with stable isotope, Nd isotope and TOC records from the same sites and can show that there are several periods of ventilation that occur, interestingly, during major events in the Cenomanian and Turonian (1) the OAE2 interval and (2) during a proposed glaciation event in the Late Turonian. From the Coniacian onwards, there is clear evidence for a stepwise change in bottom-water characteristics towards higher oxygen availability, that we interpret to reflect the beginning influence of opening the Equatorial Atlantic gateway and therefore the inflow of cooler, better oxygenated water masses. After a large hiatus in the early Campanian, the middle Campanian shows assemblages typical for the Late Cretaceous Atlantic, indicating normal marine conditions.

ICDP

Inspecting the biogeochemistry of Lake Towuti surficial sediment: Implications for microbial communities.

ANDRÉ FRIESE[1], JENS KALLMEYER[1], AURÈLE VUILLEMIN[1]

[1]GFZ German Research Centre for Geosciences, Section 4.5 Geomicrobiology, Telegrafenberg, 14473 Potsdam, Germany.

Lake Towuti is a tropical 200-m deep tectonic lake seated in ophiolitic rocks and surrounded by lateritic soils. Its location in central Indonesia allows to record paleoclimatic changes related to the tropical Western Pacific warm pool in its sedimentary sequence. As a result of this special climatic and geological setting, the sediment is very rich in iron and other metals, thus providing microbial communities with a wide range of metalliferous substrates (Crowe et al. 2004). A significant part of the sedimentary organic matter is remineralized in the water column via methanogenesis and, although lake water concentrations of nitrate and sulfate are extremely low, some of the produced methane appears to be oxidized anaerobically (Crowe et al. 2008a, 2010). Lake Towuti is thus ideal to look for mutual interactions between the iron and methane cycle, to inspect the influence of microbes on early diagenesis in iron-rich sediments and to compare these modern features with the conditions that generated banded iron formations during the Archaean (Crowe et al. 2008b).

During a pilot campaign in autumn 2013, several short (0.5 m) cores were retrieved from Lake Towuti. Oxygen concentrations measured at the sediment/water interface showed that Lake Towuti is anoxic in the deepest part of the basin. Thus, sediments from three different sites (60, 153 and 200 m water depth) corresponding to oxic, suboxic and anoxic bottom waters were sampled for pore water, cell count and genetic analyses. First results show that nitrate/nitrite is below detection limit (5 µM) in the pore water, whereas concentrations of SO_4 in the single µM range may indicate the presence of a cryptic sulfur cycle in the shallowest part of the sediment (Holmkvist et al. 2011). Cation pore water profiles show the presence of sodium, calcium and magnesium which are most probably derived from the mafic and ultramafic catchment of Lake Towuti. Except for alkalinity no other cations could be identified in appreciable amounts.

In parallel, DNA extractions were performed to retrieve the intracellular and extracellular fractions separately. A first DNA quantification shows that concentrations are systematically higher in sediments of the suboxic site compared to the oxic site. In both cases, the extracellular fraction constitutes more than 50% of the total DNA pool. The high iron content of the sediment is likely to foster the

preservation of extracellular DNA, which in turn may constitute a substantial source of nutrients for sedimentary microbial communities. Reducing conditions in anoxic Lake Towuti appear to limit issues associated with adsorption onto metal oxides while promoting the preservation of organic matter. The oxidation level of the bottom water may therefore have profound implications on the preservation of paleoclimatic and microbiological proxies.

Our pilot campaign, which is the first geomicrobiological work on Lake Towuti sediments, will provide a first dataset of the biogeochemistry in the upper part of the sediment and therefore be a valuable resource for the forthcoming Lake Towuti Drilling Project.

References:

Crowe SA, Pannalal SJ, Fowle DA, Cioppa MT, Symons DTA, Haffner GD, Fryer BJ, 2004. Biogeochemical cycling in Fe-rich sediments from Lake Matano, Indonesia, 13th International symposium on water-rock interaction, Saratoga Springs, USA, 1185-1189.

Crowe SA, O'Neill AH, Katsev S, Hehanussa P, Haffner GD, Sundby B, Mucci A, Fowle DA, 2008a, The biogeochemistry of tropical lakes: A case study from Lake Matano, Indonesia. Limnology and Oceanography, 53, 319-331.

Crowe SA, Jones CA, Katsev S, Magen C, O'Neill AH, Sturm A, Canfield DE, Haffner GD, Mucci A, Sundby B, Fowle DA, 2008b. Photoferrotrophs thrive in an Archean Ocean analogue. Proceedings of the National Academy of Sciences of the United States of America 105, 15938-15943.

Crowe SA, Katsev S, Leslie K, Sturm A, Magen C, Nomosatryo S, Pack MA, Kessler JD, Reeburgh WS, Roberts JA, Gonzalez L, Haffner GD, Mucci A, Sundby B, Fowle DA, 2010. The methane cycle in ferruginous Lake Matano. Geobiology, 9, 61-78.

Holmkvist L, Ferdelman TG, Jørgensen BB, 2011. A cryptic sulfur cycle driven by iron in the methane zone of marine sediment (Aarhus Bay, Denmark). Geochimica Et Cosmochimica Acta, 75, 3581-3599.

IODP

The impact of Mediterranean Outflow Water on the Pliocene North Atlantic

ÁNGELA GARCIA GALLARDO[1], PATRICK GRUNERT[1], WERNER E. PILLER[1], BARBARA BALESTRA[2], MARLIES VAN DER SCHEE[3], FRANCISCO SIERRO SANCHEZ[3], JOSÉ-ABEL FLORES[3], CARLOS ALVAREZ-ZARIKIAN[4], F. JAVIER HERNÁNDEZ-MOLINA[5], DORRIK A.V. STOW[6], AND IODP EXPEDITION 339 SCIENTISTS[*]

[1] Institute for Earth Sciences, University of Graz, Austria; patrick.grunert@uni-graz.at
[2] Institute of Marine Sciences, University of California Santa Cruz, USA
[3] Department of Geology, University of Salamanca, Spain
[4] Integrated Ocean Drilling Program, Texas A&M University, College Station, Texas, USA
[5] Department of Earth Sciences, Royal Holloway University London, United Kingdom
[6] Institute of Petroleum Engineering, Heriot-Watt University, Edinburgh, Scotland, United Kingdom

The opening and closing of ocean gateways play an important role amongst climate forcing mechanisms: along with paleogeography, surface and deep-water circulation are altered, and hence global heat transport. An important component of North Atlantic circulation patterns is the warm and saline Mediterranean Outflow Water (MOW) that enters the North Atlantic via the Gibraltar Strait. Its onset, that is strongly related to the opening of the Gibraltar Strait during the Late Miocene and Early Pliocene (c. 5.2 Ma), and early history are poorly constrained and its impact on oceanography and climate since the Pliocene are largely unexplored. The herein presented project, funded by the Austrian Science Fund FWF, is part of the research goals of Expedition 339 of the Integrated Ocean Drilling Program (IODP) that explores the environmental significance of the MOW and its role in global climate as a component of North Atlantic circulation since the Pliocene.

The project focuses on the reconstruction of the Pliocene history of MOW based on an approach that integrates micropaleontology and geochemistry: quantitative analysis of benthic foraminiferal assemblages is used for the reconstruction of MOW velocity and intensity; $\delta^{18}O$ and Mg/Ca from planktic and benthic foraminiferal shells are evaluated for changes in water-temperature and salinity; $\delta^{13}C$, TOC, S and $CaCO_3$ are applied as proxies for productivity and bottom-water ventilation.

Although the ultimate goal will be a MOW-record for the entire Pliocene, special emphasis will be put on two topics:

Paleoceanographic changes related to the opening of the Gibraltar Strait and the onset of MOW during Late Miocene – Early Pliocene. While the opening of the Gibraltar Strait is well-constrained to 5.23 Ma, the onset and early history of MOW remains poorly understood. The new proxy records will help to evaluate the impact of the new water source on the local Early Pliocene paleoenvironment.

Evaluation of variability in MOW intensity and its potential relation to the Middle Pliocene Thermal Optimum (MPTO) and Late Pliocene climate deterioration. The Early-Middle Pliocene world with its warm-house climate and elevated CO_2-levels is often referred to as a potential analogue to future climate change. However, the underlying mechanisms of the MPTO as well as the subsequent climate cooling are strongly debated. A strong focus of the project will thus lie on the variability of MOW intensity, the impact of these changes on North Atlantic circulation patterns and the potential impact on MPTO and the Late Pliocene climate transition.

References:

IODP Expedition 339 Scientists: Acton, G., Bahr, A., Ducassou. E., Flood, R., Furota, S., Jimenez-Espejo, F., Hodell, D., Kim, J. K., Krissek, L., Kuroda, J., Li, B., Llave, E., Lofi, J., Lourens, L., Miller, M., Nanayama, F., Nishida, N., Richter, C., Roque, C., Sanchez Goñi, M., Singh, A., Sloss, C., Takashimizu, Y., Tzanova, A., Voelker, A., Williams, T., Xuan, C.

IODP

Composition and timing of carbonate vein precipitation within the igneous basement of the Early Cretaceous Shatsky Rise, NW Pacific

J. GELDMACHER[1], S. LI[2], F. HAUFF[1], D. GARBE-SCHÖNBERG[3], S. YU[2], S. ZHAO[2], S. RAUSCH[4]

[1]GEOMAR Helmholtz Centre for Ocean Reserach Kiel
[2]College of Marine Geosciences, Ocean University of China, Qingdao, China
[3]Institute of Geosciences, Christian-Albrechts University Kiel
[4]Geosciences Department, University of Bremen

Shatsky Rise is an Early Cretaceous large igneous province located in the NW Pacific ca. 1500 km east of Japan and is the third-largest oceanic plateau on Earth (after Ontong Java and Kerguelen). Numerous calcium

carbonate veins were recovered from the igneous basement of Shatsky Rise during Integrated Ocean Drilling Program Expedition 324 (Expedition 324 Scientists, 2010). The chemical (Sr/Ca, Mg/Ca) and isotopic ($^{87}Sr/^{86}Sr$, $^{143}Nd/^{144}Nd$, $\delta^{18}O$, $\delta^{13}C$) compositions of these veins were determined to constrain the timing of vein formation and to provide valuable data for the reconstruction of past seawater composition. A dominant control of seawater chemistry on calcite composition is evident for most investigated vein samples with varying compositional contribution from the basaltic basement. The Sr/Ca ratio of the vein calcite is positively correlated with Mg/Ca and with $\delta^{18}O$, indicating warmer/colder precipitation temperatures with decreasing/increasing Sr/Ca (and Mg/Ca) ratios, respectively. Distinctly higher formation temperatures (as inferred from oxygen isotope ratios) indicative of hydrothermal vein formation are only observed at one site (Site U1350, drilled into the central part of Shatsky Rise). The highest $^{87}Sr/^{86}Sr$ ratios (least basement influence) of vein samples at each drill site range form 0.707264 to 0.707550 and are believed to best reflect contemporaneous Early Cretaceous seawater composition. In principle, age information can be deduced by correlating these ratios with the global seawater Sr isotope evolution. Since the Sr isotopic composition of seawater has fluctuated three times between the early and mid Cretaceous (McArthur et al., 2001) no unambiguous precipitation ages can be constrained by this method and vein precipitation could have occurred at any time between ~80 and 140 Ma. However, based on combined chemical and isotopic data and correlations of vein composition with formation depth and inferred temperature, we argue for a rather early precipitation of the veins shortly after basement formation at each respective drill site.

References:
Expedition 324 Scientists (2010) Testing plume and plate models of ocean plateau formation at Shatsky Rise, northwest Pacific Ocean. Integrated Ocean Drilling Program - Expedition Preliminary Report 324, doi:10.2204/iodp.pr.324.2010.
McArthur, J.M., Howarth, R.J., Bailey, T.R. (2001) Strontium isotope stratigraphy: LOWESS Version 3. Best-fit line to the marine Sr-isotope curve for 0 to 509 Ma and accompanying look-up table for deriving numerical age. Journal of Geology 109, 155-169.

IODP

Contrasting water contents and equilibrium conditions of abyssal peridotite from the Mid-Atlantic Ridge

J. GOSE[1], E. SCHMÄDICKE[2], T. M. WILL[3]

[1] University of Erlangen-Nürnberg, GeoZentrum Nordbayern, Schlossgarten 5a, D-91054 Erlangen, Germany, (Juergen.Gose@fau.de)
[2] University of Erlangen-Nürnberg, GeoZentrum Nordbayern, Schlossgarten 5a, D-91054 Erlangen, Germany (Esther.Schmaedicke@fau.de)
[3] University of Würzburg, Department of Geography and Geology, Geodynamics and Geomaterials Research Division, Am Hubland, D-97074 Würzburg, Germany

Water, precisely hydrogen, is stored in the Earth's mantle as OH defects in nominally anhydrous minerals such as orthopyroxene, clinopyroxene, and olivine (e. g. Miller et al. 1987). Even trace amounts of water in mantle minerals significantly influence the physical properties (viscosity, electric conductivity), melting behavior, mantle convection and even the stabilization of cratonic roots (e. g. Karato 1990; Asimow & Langmuir 2003; Peslier et al. 2010). Information on water contents in the sub-oceanic mantle is based on indirect evidence, such as the electrical conductivity or the composition of mid-ocean ridge basalt (MORB). Along the Mid-Atlantic Ridge, the water contents in MORB glass vary over one order of magnitude, ranging from less than 0.1 to 1.1 wt.-%; the majority of samples, however, typically has <0.5 wt.-% H_2O (e. g. Michael 1995; Dixon et al. 2002). This 'translates' into a content of 100-180 ppm H_2O for the sub-oceanic mantle (e. g. Michael 1988). However, because of the possibility of partial magma degassing, this value is far from certain.

Orthopyroxene (opx) is a very important container for water in the mantle. It may incorporate several hundred ppm H_2O in the uppermost mantle and even higher amounts in deeper parts, due to its pressure-enhanced storage capacity (Rauch & Keppler 2002). This mineral contains considerably more water than olivine, plus it is able to preserve mantle water contents during exhumation better than olivine rendering orthopyroxene a useful proxy for mantle water levels. Previous studies on opx were restricted to peridotite xenoliths from the sub-continental mantle. The first water data for sub-oceanic mantle opx are the result of own, DFG-financed investigations on abyssal peridotite from the Mid-Atlantic Ridge. This study yielded various unexpected results that have far-reaching consequences for models concerning (i) the distribution and re-distribution of water in the upper mantle and (ii) the processes that were involved in the exhumation of mantle rocks along mid-ocean ridges.

The novel investigations yielded contrasting water contents in peridotitic opx, comparing samples from near 15°N (IODP-Leg 209) and 23°N (ODP-Leg 153). Orthopyroxene from Leg 209 contains 15 ppm H_2O that is incorporated in the form of OH groups in the pyroxene structure. In contrast, H2O contents in opx from Leg 153 are one order of magnitude higher, with typical values of 270 ppm. This latter content agrees well with both the H_2O contents known from sub-continental spinel peridotite xenoliths and the water storage capacity of opx at pressures typical of the spinel peridotite facies. The water contents in opx from the sub-oceanic mantle at the Mid-Atlantic Ridge, ranging from 15 (= highly depleted) to 270 ppm (= water saturation in opx), compare well with the highly variable water contents of Atlantic MORB glass that also scatter over one order of magnitude.

Furthermore, mineral compositions imply different degrees of partial melting (18% for Leg 209, and 12% for Leg 153) and mantle equilibrium temperatures differing by 200 °C (1150-1200 °C for Leg 209, and 950-1000 °C for Leg 153). The opx water contents of Leg 209 are compatible with residual values after c. 18% partial melting of a peridotitic source with original bulk rock water contents of 120-130 wt.-ppm and original opx water contents of 300 wt.-ppm, respectively. In contrast, the water content of 270 wt.-ppm in opx of Leg 153 cannot be reconciled with residual amounts after 12% partial melting, because an unrealistic initial water content of 3500 wt.-ppm would be required for the original opx. This value exceeds the water storage capacity of opx by one order of magnitude. The data imply that – following melt depletion – the water contents of Leg 153 peridotite re-equilibrated in

the spinel-peridotite facies. This may have been facilitated by a longer mantle residence time of Leg 153 peridotite (compared to Leg 209) after partial melting and prior to tectonic exhumation from c. 60 km depth.

The recent results provide the first direct information on the water content in oceanic peridotite. The initial study (i) proved that water is present in sub-oceanic anhydrous mantle minerals, (ii) it yielded information on the content of water and its variation in the oceanic mantle, (iii) it showed that decompression-induced water loss did not occur, and (iv) it confirmed that partial serpentinization has no affect on structural water in orthopyroxene. The novel data are surprising because they document contrasting water contents in the sub-Atlantic mantle and comprise concentration levels typical for water saturation (ODP-Leg 153) as well as those that are one order of magnitude lower (ODP-Leg 209).

Acknowledgements. Financial support by DFG is gratefully acknowledged. This project used samples provided by ODP/IODP.

References:

Asimow PD, Langmuir CH (2003) The importance of water to oceanic mantle melting regimes. Nature 421, 815-820

Dixon JE, Leist L, Langmuir C, Schilling JG (2002) Recycled dehydrated lithosphere observed in plume-influenced mid-ocean-ridge basalt. Nature 420, 385-389

Karato S (1990) The role of hydrogen in the electrical conductivity of the upper mantle. Nature 347, 272-273

Michael P (1988) The concentration, behavior and storage of H2O in the suboceanic upper mantle: Implications for mantle metasomatism. Geochimica et Cosmochimica Acta 52, 555-566

Michael P (1995) Regionally distinctive sources of depleted MORB: Evidence from trace elements and H2O. Earth and Planetary Science Letters 131, 301-320

Miller GH, Rossman GR, Harlow GE (1987) The natural occurrence of hydroxide in olivine. Physics and Chemistry of Minerals 14, 461-472

Peslier AH, Woodland AB, Bell DR, Lazarov M (2010) Olivine water contents in the continental lithosphere and the longevity of cratons. Nature 467, 78-82

Rauch M, Keppler H (2002) Water solubility in orthopyroxene. Contributions to Mineralogy and Petrology 143, 525-536

IODP

Holocene bottom water variability in the Baltic Sea: The impact of atmospheric processes

J. GROENEVELD[1], AND EXP. 347 SCIENTISTS

[1]Center for Marine Environmental Sciences (MARUM), University Bremen, Leobener Strasse, D-28359 Bremen, Germany

With ongoing global climate change (IPCC, 2013) shelf areas and enclosed basins are seeing the largest environmental impacts including severe oxygen depletion, increased stratification and higher temperatures (Conley et al., 2011). As such, interest in how these environments have changed in the past is increasing. I sailed as one of the micropaleontologists (together with N. Quintana Krupinski) on IODP Expedition 347, Baltic Sea Basin Paleoenvironment, a Mission Specific Platform Expedition conducted by the European Consortium for Ocean Research Drilling (ECORD), which drilled the Baltic Sea Basin (BSB), one of the largest intercontinental basins, in autumn 2013 (Andrén et al., 2012). The past has shown extreme variations in the conditions of the BSB not only with repeated switches between freshwater and marine conditions but also between hypoxic and oxic conditions (e.g. Zillén et al., 2008). During Expedition 347 unique and continuous sequences of sediment covering the Eemian, the last deglaciation, and especially the Holocene were recovered. At several sites (i.e. Anholt (Site M59), Little Belt (M60), Bornholm (M63), and Landsort Deep (M65)) the Holocene (< 8 ka; 10-40 m long) contains abundant benthic foraminifera providing the opportunity to create unique high-resolution reconstructions of past bottom water conditions (Figure 1a).

Bottom water conditions in the BSB are characterized by strong variations in salinity and oxygen concentration. And although the reason for natural causes is consistently linked to changes related to atmospheric processes like the North Atlantic Oscillation (NAO), it is still unclear which phase of the NAO actually leads to a renewal of the bottom water masses (e.g. Gustafsson and Westman, 2002; Zillén et al., 2008). During a negative NAO phase winds and precipitation decrease over Scandinavia causing a decrease in relative sea level allowing the inflow of saline Atlantic water masses into the Baltic, while on the other hand a positive NAO phase leading to increased winds and precipitation over Scandinavia causes intensified mixing of the water column and hence a renewal of deeper waters.

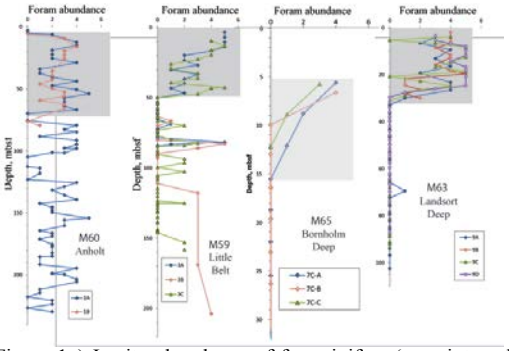

Figure 1a) In-situ abundance of foraminifera (grey intervals; abundance scaling 0-5) for Sites M59, M60, M63, and M65

In this proposed study I plan to use a high-resolution, multi-proxy approach to reconstruct variations in bottom water temperature (Mg/Ca), relative salinity ($\delta^{18}O_{water}$ and Ba/Ca), and oxygen concentration (Mn/Ca) along a transect from the Kattegat, via the Little Belt and Bornholm Deep, to the central Baltic Landsort Deep for the Littorina stage of the Holocene using samples from the previously mentioned cores of Exp. 347. The benthic foraminifera *Elphidium excavatum clavatum* is abundantly present at all four sites allowing direct comparison of the reconstructed records along the transect. This will reveal if changes in water mass conditions originated from the inflow of highly saline Atlantic water or were caused by increasing terrestrial runoff and mixing. As Ba/Ca as salinity proxy is controlled by variations in river runoff, the comparison with $\delta^{18}O_{water}$ will be an additional indication on bottom water influences.

As foraminifera in the BSB have hardly been used yet for the application of trace metal/Ca ratios it is going to have to deal with some potential issues (Groeneveld and Filipsson, 2013). Salinity gradients in the BSB are very large (up to 30 psu) which will significantly affect proxies like stable isotopes and Mg/Ca. Additionally, the hypoxic/anoxic setting of some of the basins, like Landsort Deep, results not only in the abundant occurrence of inorganic minerals being formed in the sediment, but also

in a low carbonate ion saturation state leading to dissolution of the tests (Figure 1b). Accordingly, it will be necessary to analyse the distribution of the different elements within the foraminiferal tests to determine what the impact of dissolution and possible inorganic coatings would be. The proposed methods to achieve these impacts are ion microprobe (distribution of elements) and Flow Through time resolved analysis.

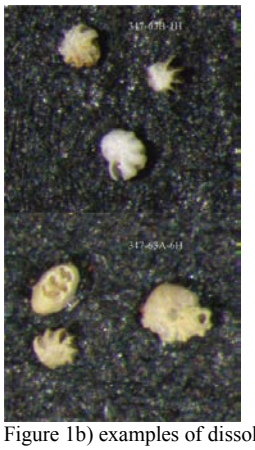

Figure 1b) examples of dissolution affected foraminifera.

References:
Andrén, T., Jørgensen, B.B., and Cotterill, C., 2012. Baltic Sea Basin Paleoenvironment: paleoenvironmental evolution of the Baltic Sea Basin through the last glacial cycle. IODP Sci. Prosp., 347. doi:10.2204/iodp.sp.347.2012.
Conley, D.J., et al., 2011. Hypoxia is increasing in the Coastal zone of the Baltic Sea. Environ. Sci. Technol., 45, 6777–6783.
Groeneveld, J., H.L. Filipsson, 2013. Mg/Ca and Mn/Ca ratios in benthic foraminifera: the potential to reconstruct past variations in temperature and hypoxia in
shelf regions. Biogeosciences 10, 5125-5138.
Gustafsson, B.G., P. Westman, 2002. On the causes for salinity variations in the Baltic Sea during the last 8500 years. Paleoceanography 17, 10.1029/2000PA000572.
Zillén, L., D.J. Conley, T. Andrén, E. Andrén, S. Björck, 2008. Past occurrences of hypoxia in the Baltic Sea and the role of climate variability, environmental
change and human impact. Earth-Sci. Rev. 91, 77- 92.

IODP

Changes in deep ocean circulation of the South Atlantic inferred from depositional processes at the eastern Agulhas Ridge

J. GRUETZNER[1], G. UENZELMANN-NEBEN[1]

[1]Alfred-Wegener-Institut, Helmholtz-Zentrum für Polar- und Meeresforschung, Bremerhaven, Germany (Jens.Grützner@awi.de)

The Agulhas Ridge forms an elongated part of the Agulhas-Falkland Fracture Zone (AFFZ) (43° S/9° E - 41° S/16° E) rising more than 2,000 m above the surrounding seafloor. Constituting a topographic barrier the ridge has a strong influence on the exchange of water masses between high and lower latitudes. While Antarctic Bottomwater (AABW) and Circumpolar Deepwater (CDW) originating in the Southern Ocean provide the inflow of cold water masses in larger water depths (Reid, 1989; Carter et al, 2008), the Agulhas leakage (Biastoch et al., 2008), is the main source of warm and salty waters carried towards the Subpolar North Atlantic as the upper limb of the Meridional Overturning Circulation (MOC). In order to track past changes in this circulation pattern 5400 km of high-resolution multichannel seismic reflection data were acquired during RV Maria S. Merian cruise MSM 19/2 (Uenzelmann-Neben, 2012) in the Agulhas Ridge area. Here we present processed profiles and a preliminary interpretation from the hitherto unexplored eastern plateau of the ridge and the area between the plateau and the Cape Rise Seamounts. Several hundred metres of sediments have accumulated since the onset of intrusion of Antarctic Bottom Water (AABW) derived water masses into the basins of the South Atlantic. Via crosscorrelation with ODP Leg 177 drillsites (e.g. Gersonde, et al., 1999) and a reconnaissance survey (Wildeboer Schut et al., 2002; Wildeboer Schut and Uenzelmann-Neben, 2005), prominent reflectors marking the early Oligocene, the middle Miocene and the base of the Pleistocene were identified. Sediment drifts deposited between these erosional surfaces indicate steady contour current acitivity at various depth levels. The chronological development of those drift structures studied both in 2d and 3d (depth to horizon and thickness maps) provide information on the displacement of depocenters and thus current pathways over time.

References:
Biastoch, A., Böning, C.W. and Lutjeharms, J.R.E., 2008. Agulhas leakage dynamics affects decadal variability in Atlantic overturning circulation. Nature, 456: 489-492.
Carter, L., McCave, I. N. and Williams, M. J. M., 2008. Circulation and Water Masses of the Southern Ocean: A Review, In: F. Florindo and M. Siegert (Editors), Antarctic Climate Evolution, Elsevier B.V., Amsterdam, pp. 85-114.
Gersonde, R. et al., 1999. Leg 177 summary; Southern Ocean Paleoceanography. In: R. Gersonde et al. (Editors), Proc. ODP, Init. Repts., 177. Ocean Drilling Program, College Station, TX pp. 1-67.
Reid, J.L., 1989. On the total geostrophic circulation of the South Atlantic Ocean: flow patterns, tracers and transports, Progr. Oceanogr., 23: 129-244.
Uenzelmann-Neben, G., 2012. Cruise Report RV MARIA S. MERIAN Cruise MSM19-2, Alfred Wegener Institut, Bremerhaven.
Wildeboer Schut, E. and Uenzelmann-Neben, G., 2005. Cenozoic bottom current sedimentation in the Cape Basin, South Atlantic. Geophysical Journal International, 161: 325-333.
Wildeboer Schut, E., Uenzelmann-Neben, G. and Gersonde, R., 2002. Seismic evidence for bottom current activity at the Agulhas Ridge. Global and Planetary Change, 34: 185-198.

IODP

Impact of paleoceanographic changes at glacial/interglacial transitions on benthic foraminiferal faunas of the eastern North Atlantic (IODP Expedition 339, Site U1385)

PATRICK GRUNERT[1], DAVID HODELL[2], CARLOS ALVAREZ-ZARIKIAN[3], F. JAVIER HERNÁNDEZ-MOLINA[4], DORRIK A.V. STOW[5], AND IODP EXPEDITION 339 SCIENTISTS[*]

[1] Institute for Earth Sciences, University of Graz, Austria;
[2] Department of Earth Sciences, University of Cambridge, United Kingdom
[3] Integrated Ocean Drilling Program, Texas A&M University, College Station, Texas, USA
[4] Department of Earth Sciences, Royal Holloway University London, United Kingdom
[5] Institute of Petroleum Engineering, Heriot-Watt University, Edinburgh, Scotland, United Kingdom

Communities of deep-sea foraminifera are sensitive recorders of environmental conditions. Consequently, the actualistic interpretation of fossil foraminiferal assemblages has become a valuable tool for the

reconstruction of paleoceanographic conditions at the sea-floor. For the present study, a quantitative data-set of benthic foraminifera >125µm from the eastern North Atlantic has been analysed to understand paleoceanographic changes (AMOC, ventilation, productivity) associated with glacial/interglacial transitions in more detail. The data-set consists of a series of samples from IODP Site U1385 spanning Terminations I, II and IV and several short-term (millennial-scale) climatic events including the Younger Dryas (YD), Heinrich (H) 1, and H 11.On the family and generic levels, a characteristic succession of foraminiferal assemblages can be recognized at all studied glacial/interglacial transitions: a glacial fauna with abundant occurrences of cassidulinids (Cassidulina, Globocassidulina); a fauna characterized by high abundances of buliminds (Bulimina, Globobulimina) and/or bolivinellids (Bolivinita) that is associated with H-events and the beginning of each termination; a fauna with high abundances of miliolids (mainly Pyrgo) and cibicidids at the end of the termination; an interglacial fauna composed of buliminds (Bulimina), gavellinellids (Gyroidinoides), and pseudoparrellids (Epistominella). For the glacial and interglacial endmembers, this succession indicates a moderately oxygenated environment at the seafloor with mesotrophic conditions due to moderate export productivity. For the early phase of the terminations as well as the short-term events, the dominance of infaunal taxa and high abundances of deep infaunal taxa indicate an environment with high export productivity that is mainly controlled by oxygen. Conversely, the absence of these taxa and the presence of miliolids suggests well-ventilated environments and decreasing export productivity during the later phase of the terminations.

While the evaluation on the generic level indicates repetitive paleoenvironmental changes for the studied transitions, the taxonomic analysis on the species level reveals significant differences between the terminations. These differences primarily concern the H-events and the early phase of the terminations. H 1 differs from other such events by showing the highest abundances of deep infaunal like Globobulimina affinis. In contrast, H 11 is characterized by high abundances of Bulimina marginata and Cassidulina laevigata/teretis which are rare to absent during H 1. A similar pattern is observed for a H-event associated with the onset of Termination IV. In contrast, the H-event preceding Termination IV shows high abundances of Bolivinita quadrilatera, a species absent all other samples.

The explanation of the faunal differences between the terminations despite a rather comparable environmental framework (poor ventilation and/or high export productivity) indicates that the nature of short-term events is fairly diverse and an individual perspective has to be put on each these events. E.g., in the case of H 1, increased primary productivity and/or severely reduced AMOC compared to other such events might provide explanations. For the other, less well known events new isotopic results are expected to help with the explanation.

References:
IODP Expedition 339 Scientists: Acton, G., Bahr, A., Balestra, B., Ducassou. E., Flood, R., Flores, J.A., Furota, S., Jimenez-Espejo, F., Hodell, D., Kim, J. K., Krissek, L., Kuroda, J., Li, B., Llave, E., Lofi, J., Lourens, L., Miller, M., Nanayama, F., Nishida, N., Richter, C., Roque, C., Sanchez Goñi, M., Sierro Sanchez, F., Singh, A., Sloss, C., Takashimizu, Y., Tzanova, A., Voelker, A., Williams, T., Xuan, C.

IODP

Calcareous dinoflagellates as archives for fluctuations in ocean chemistry and temperature changes

N. GUSSONE[1], O. FRIEDRICH[2]

[1] Institut für Mineralogie, Corrensstr. 24, 48149 Münster
[2] Institut für Geowissenschaften, Im Neuenheimer Feld 234-236, 69120 Heidelberg

Dinoflagellates are important marine primary producers, which can form cysts, composed of organic-material, silicate or calcium carbonate, which are used as stratigraphic and paleoenvironmental indicators. The calcium carbonate secreting dinoflagellates, the so-called calcareous dinoflagellates, provide an archive for long-term changes in the ocean chemistry and past environmental changes (Hildebrand-Habel, 2000). They are particularly useful as proxy archive recording ocean surface conditions (e.g. temperature, pH) due to their formation at the deep chlorophyll maximum depth in the water column (Zonneveld, 2004). Furthermore, they are comparatively insensitive to dissolution. It has been shown that the $\delta^{18}O$ of the dominant calcareous dinoflagellate species *Thoracosphaera* records reliable sea surface temperatures (SST) in specimens from laboratory cultures, surface waters and sediment samples (Zonneveld, 2004; Zonneveld et al., 2007).

Culture experiments on *T. heimii* revealed a significant dependence of Sr/Ca ratios of their cysts on temperature (Gussone et al., 2010). It might be applied as additional SST proxy and used to correct for changes in salinity, influencing the $\delta^{18}O$ of carbonate shells.

Furthermore, minor changes of Ca isotope fractionation in *T. heimii* have been shown in relation to the environmental parameters temperature, salinity and pH (Gussone et al., 2010), making it a promising archive for the reconstruction of $\delta^{44/40}Ca_{seawater}$.

In order to test the applicability and preservation potential of calcareous dinoflagellate cysts as recorders for Sr/Ca ratios as paleo-SST proxy and $\delta^{44/40}Ca$ as measure for changes in the oceanic Ca budget over geological time scales, we investigated sediments from IODP Hole 690C from the Weddel Sea (Southern Ocean), a site located close to the potential source region of Late Cretaceous southern component waters (e.g., Friedrich et al., 2009). We selected the abundant dinoflagellate species *Pirumella krasheninnikovii* and *Orthopithonella globosa*. Specimens were handpicked from the time interval 73-68 Ma (used size fraction 63-125 µm) and cleaned following the procedure for coccolithophores and dinoflagellates (Gussone et al. 2006, 2010).

Pirumella krasheninnikovii and *O. globosa* show a significant increase in $\delta^{44/40}Ca$ in the investigated time interval of about 0.3‰ and both calcareous dinoflagellate species exibit within uncertainty identical values. The same increase is revealed by benthic and planktonic foraminifers. However, the absolute $\delta^{44/40}Ca$ values for the late Cretaceous seawater are offset by about half a permill, applying the respective present day fractionation factors for dinoflagellates and foraminifers. In addition it emphesises the importance for careful selection of proxy archives and the need for a fundamental understanding of biomineralisation-related fractionation processes.

The trend of Sr/Ca ratios of *P. krasheninnikovii* and *O. globosa* show a decrease during the investigated period, sychronous to the temperature drop revealed by ´^{18}O (Friederich et al., 2009). However, the dinoflagellate Sr/Ca ratios suggest a significantly larger amplitude of temperature change compared to the ´^{18}O-based SST reconstruction, if the Sr/Ca vs. temperature calibration of *Thoracosphaera heimii* is applied. Possible explanations which will be discussed in the aim of this study include differences in the seawater chemical composition of the present and Cretaceous oceans and/or interference of several environmental parameters like temperature and carbonate chemistry of the water.

References:
Friedrich, O., Herrle, J.O., Cooper, M.J., Erbacher, J., Wilson, P.A. & Hemleben, C. (2009): The early Maastrichtian carbon cycle perturbation and cooling event: implications from the South Atlantic Ocean. Paleoceanography 24: PA2211, doi:10.1029/2008PA001654.
Gussone, N., Langer, G., Thoms, S., Nehrke, G., Eisenhauer, A., Riebesell, U., Wefer, G., 2006. Cellular calcium pathways and isotope fractionation in Emiliania huxleyi. Geology 34 (8), 625–628.
Gussone, N., Zonnefeld, K. and Kuhnert, H. (2010) Minor element and Ca isotope composition of calcareous dinoflagellate cysts of *Thoracosphaera heimii*. Earth and Planetary Science Letters 289, 180-188.
Hildebrand-Habel, T.,Willems, H., 2000. Distribution of calcareous dinoflagellates from the Maastrichtian to middle Eocene of the western South Atlantic Ocean. Int. J. Earth Sci. (Geol. Rundsch.) 88, 694–707.
Zonneveld, K.A.F., 2004. Potential use of stable oxygen isotope composition of *Thoracosphaera heimii* for upper water column (thermocline) temperature reconstruction. Mar. Micropaleontol. 50, 307–317.
Zonneveld, K.A.F., Mackensen, A., Baumann, K.-H., 2007. Stable oxygen isotopes of *Thoracosphaera heimii* (Dinophyceae) in relationship to temperature; a culture experiment. Mar. Micropaleontol. 64, 80–90.

IODP

Gulf of Mexico Pb isotopic evidence for temporally elevated deglacial freshwater runoff from the Laurentide Ice Sheet

M. GUTJAHR[1] AND A. N. MECKLER[2]

[1]GEOMAR Helmholtz Centre for Ocean Research Kiel, Wischhofstrasse 1-3, 24148 Kiel, Germany, mgutjahr@geomar.de
[2]Swiss Federal Institute of Technology Zürich (ETHZ), Geological Institute, Zürich, Switzerland , nele.meckler@erdw.ethz.ch

The disintegration of the North American Laurentide ice sheet during progressive warming throughout the last deglaciation provides an excellent opportunity to study changes in continental surface conditions and its effect on the dissolved runoff signal. The climate in interior North America shifted from glacial conditions dominated by intense (sub-) glacial physical and significantly reduced chemical weathering rates to wetter and warmer conditions in the transition to the Holocene. Various mineral phases in freshly exposed rock substrate weather relatively quickly, resulting in increased dissolved runoff fluxes for many major and trace elements during deglacial warming (cf. [1]). For tracing ice sheet retreat, isotopes of elements displaying incongruent chemical weathering behaviour are particularly useful as long as these elements have short residence time in seawater such as dissolved Pb (Ä~ 20-30 years). This incongruence is most clearly traceable during deglacial warming when incipient chemical weathering in near-glacial settings leads to highly elevated Pb isotopic runoff signals, significantly more radiogenic than the average drainage basin composition [2, 3].

At the NW Atlantic Laurentian Fan and deeper Blake Ridge, two Pb isotopic data sets suggest a significant increase in riverine input from proximal North American sources eastward during and after the Younger Dryas [3, 4]. The magnitude of change between these two sites suggests a proximal-distal relationship with the source of this radiogenic Pb signal most likely being located within the Gulf of St Lawrence. Together with Laurentide ice sheet margin retreat patterns presented from interior North America, oxygen isotope records derived from the Gulf of Mexico [5] and one multi-proxy data set from the outer St. Lawrence estuary [6], these Pb isotope records suggest that the signal recorded in the NW Atlantic traced major runoff reorganisations in interior North America during the mid-Younger Dryas.

Apart from [6], the identification of increased deglacial freshwater input into NW Atlantic sites by means of surface water ´^{18}O has proven difficult if not impossible [7]. Conversely, the supposedly preceding mid-deglacial Laurentide-derived freshwater runoff into the Gulf of Mexico was clearly recorded in surface-dwelling foraminifera in the open Gulf of Mexico [5, 8]. In order to complement the existing NW Atlantic Pb isotope records, we therefore present a new authigenic Fe-Mn oxyhydroxide derived Pb isotope record from within the Orca Basin in the Northern Gulf of Mexico. Our core has a well-dated deglacial section and contains oxygen isotopic and organic matter content-based evidence for enhanced freshwater runoff during this key interval [8], allowing direct comparison with the new Pb isotope records.

The authigenic Pb isotope trends seen throughout the deglaciation in the Gulf of Mexico are highly consistent and underline the high sensitivity of this as yet rarely used paleoclimatic archive. Radiogenic Pb isotopic excursions in the Gulf of Mexico record are dominantly seen (i) immediately following the end of the Last Glacial Maximum, as well as (ii) during Meltwater Pulse 1A (~14.9 ka). Strikingly, during times of elevated runoff as recorded in authigenic Pb isotope compositions outside the Gulf of St. Lawrence in the NW Atlantic [3, 4], the Gulf of Mexico record suggests no elevated Laurentide Ice Sheet derived runoff signal. Together, the various near-North American Pb isotope records sensitively trace spatially and temporally variable ice sheet retreat and runoff patterns.

References:
[1] Vance D., Teagle A. H. & Foster G. L. (2009) Nature 458, 493-496.
[2] Harlavan Y., Erel Y. & Blum J. D. (1998) GCA 62, 33-46.
[3] Gutjahr M., Frank M., Halliday A. N. & Keigwin L. D. (2009) EPSL 286, 546-555.
[4] Kurzweil F., Gutjahr M., Vance D. & Keigwin L. D. (2010) EPSL 299, 458-465.
[5] Leventer A., Williams D. F. & Kennett J. P. (1982) EPSL 59, 11-17.
[6] Carlson A. E., Clark P. U., Haley B. A., Klinkhammer G. P., Simmons K., Brook E. J. & Meissner K. J. (2007) PNAS 308, 1611-1615.
[7] Keigwin L.D. & Jones G. A. (1995) Paleoceanography 10, 973-985.
[8] Meckler A. N., Schubert C. J., Hochuli P. A., Plessen B., Birgel D., Flower B. P., Hinrichs K.-U. & Haug, G. (2008) EPSL 272, 251-263.

IODP

Late Holocene sea-level changes in French Polynesia, South-Central Pacific: extending the last deglacial sea-level record from IODP Expedition #310

N. HALLMANN[1], G. CAMOIN[1], A. EISENHAUER[2], C. VELLA[1], E. SAMANKASSOU[3], A. BOTELLA[4], G.A. MILNE[4], J. FIETZKE[2], P. DUSSOUILLEZ[1], J. PLAINE[1]

[1]Aix-Marseille Université, CNRS, IRD, CEREGE UM34, Europôle Méditerranéen de l'Arbois, BP80, 13545 Aix-en-Provence cedex 4, France
[2]Helmholtz-Zentrum für Ozeanforschung, GEOMAR, Wischhofstraße 1-3, 24148 Kiel, Germany
[3]University of Geneva, Rue des Maraîchers 13, CH-1205 Geneva, Switzerland
[4]University of Ottawa, Department of Earth Sciences, Ottawa, Ontario, K1N 6N5, Canada

Knowledge of the timing and course of sea-level changes provides an essential framework for conceptual models aimed at understanding the dynamics of melting of large ice sheets and their effects on the isostasy of the Earth.

The marked variability of local Holocene sea levels, responding both to ice-sheet unloading and the redistribution of water masses in the global ocean, demonstrates the need to constrain geophysical parameters (e.g., hydro-isostatic processes) affecting relative sea levels.

A regional reconstruction of Late Holocene sea-level changes (i.e., the last 6,000 yrs) is based on the accurate U-series dating and precise GPS positioning of coral microatolls and associated in situ coral colonies from five atolls (Fakarava, Hao, Manihi, Rangiroa, Tikehau) and five high islands (Bora Bora, Mangareva, Maupiti, Moorea, Raivavae) in French Polynesia. These islands provide the opportunity to accurately reconstruct Late Holocene sea-level changes that are well-suited to estimate eustatic and isostatic changes because: 1) they exhibit unique coral reef records including valuable sea-level indicators, such as corals and bivalves in growth position, emerged coral conglomerates and beachrocks, 2) their subsidence rates are negligible for the Late Holocene period, thus excluding any tectonic overprint, 3) they are affected by a low tidal amplitude, and 4) they are located far away from former ice sheets (‘far-field’ location), which minimizes the influence of the glacio-isostatic rebound. In addition, these islands cover a range of latitudes (14–23°S), and comparisons with adjacent sites on continental margins allow the reconstruction of sea-level curves that closely reflect the eustatic response and disengage this from the effects of other mechanisms.

This study extends the coral reef-based Tahiti sea-level curve (IODP Expedition 310) to improve the modelling of 1) the isostatic rebound during the last deglacial sea-level rise, and 2) regional geophysical processes (e.g., 'equatorial ocean syphoning') that dominate Late Holocene sea-level changes at 'far-field' sites.

IODP

High Arctic and low latitude Atlantic paleoenvironmental and paleoclimatic changes in the Mid-Cretaceous (Axel Heiberg and Ellef Ringnes Island, DSDP Site 545, ODP Sites 1258, 1049)

J.O. HERRLE[1,2], C.J. SCHRÖDER-ADAMS[3], D. SELBY[4], A. DU VIVIER[4], S. FLÖGEL[5], A. MCANENA[6], W. DAVIS[7], A. PUGH[3,8], J. GALLOWAY[9], P. HOFMANN[10], T. WAGNER[11]

[1]Institute of Geosciences, Goethe-University Frankfurt, D-60438 Frankfurt am Main, Germany
[2]Biodiversity and Climate Research Centre (BIK-F), D-60325 Frankfurt am Main, Germany
[3]Department of Earth Sciences, Carleton University, Ottawa, Ontario, K1S 5B6, Canada
[4]Department of Earth Sciences, Durham University, Science Labs, Durham, DH1 3LE, United Kingdom
[5]GEOMAR, Wischhofstr. 1-3, 24148 Kiel, Germany
[6]Institute of Marine and Coastal Sciences, Rutgers, The State University, USA
[7]Geological Survey of Canada, 601 Booth Street, Ottawa, Ontario K1A 0A8, Canada
[8]ConocoPhillips Canada, 2100, Bow Valley Square Four, 250-6th Avenue S.W., Calgary, Alberta, T2P 3H7, Canada
[9]Geological Survey of Canada, 3303-33 St. NW Calgary, Alberta, T2L 2A7, Canada
[10]Department of Geology and Mineralogy, University of Cologne, 50674 Cologne, Germany
[11]School of Civil Engineering and Geosciences, Newcastle University, Newcastle Upon Tyne, NE1 7RU, United Kingdom

Although major progress in Cretaceous (145-66 Ma) paleoclimate and paleoceanography has been made during the last decades (e.g., Hay, 2008, 2011; Föllmi, 2012 and references therein), our knowledge of high latitudinal environmental change remains largely unknown compared to low- and mid-latitude marine and terrestrial environments. Drilling the Arctic Ocean remains challenging and expensive, whereas the Sverdrup Basin provides excellent exposures on land. To fully understand the climate and paleoceanographic dynamics of the warm, equable greenhouse world of the Cretaceous Period it is important to determine polar paleotemperatures and to study paleoceanographic changes in a well-established and continuous bio- and chemostratigraphic context. Exceptional exposures of Cretaceous sediments on the central to southern part of Axel Heiberg Island at a Cretaceous paleolatitude of about 71°N (Tarduno et al., 1998) provide a unique window on the Cretaceous Arctic paleoenvironment and climate history (Schröder-Adams et al., 2014).

Here we present high-resolution records combining sedimentological studies, U-Pb zircon geochronology, marine organic carbon isotopes and initial 187Os/188Os data, TEX86-derived sea-surface temperatures (SST) and climate modelling, that constrain the timing and magnitude of major Oceanic Anoxic Events (OAEs) and climate events constructed from a ~1.8 km sedimentary succession exposed on Axel Heiberg and Ellef Ringnens islands in the Canadian Arctic Archipelago. The first high latitude application of initial 187Os/188Os data are agreeable with global profiles (Du Vivier et al., 2014) indicating the widespread magmatic pulse of the Caribbean Large Igneous Province (LIP) at the onset of OAE2 but also record the emplacement of local High

Arctic LIP prior to the OAE2 in the Sverdrup Basin. Initial SST data suggest a slightly lower meridional temperature gradient during the Middle/Late Albian compared to present and a similar to the present one during the OAE2 period which shades a new light on temperature gradients during different climate states of the Cretaceous. In contrast, to the Late Cenomanian to Early Turonian the distinct occurrence of several widespread glendonite beds in the Late Aptian to Early Albian support cool bottom waters of about 0°C in the Arctic Sverdrup Basin, consistent with much lower TEX86-SST ~28°C, McAnena et al., 2013) and bottom water temperatures (6°C, Huber et al., 2011) in the low latitude North Atlantic. This supports the global character of the proposed Late Aptian cold snap (Kemper, 1987; Herrle & Mutterlose, 2003; Mutterlose et al. 2009; McAnena et al. 2013) and perhaps a northern hemisphere high-latitude intermediate bottom water source.

References:
Du Vivier, A.C.D., Selby, D., Sageman, B.B., Jarvis, I., Gröcke, D.R., Voigt, S., 2014. Marine 187Os/188Os isotope stratigraphy reveals the interaction of volcanism and ocean circulation during Oceanic Anoxic Event 2. EPSL 389, 23-33.
Föllmi, K.B., 2012. Early Cretaceous life, climate and anoxia. Cretaceous Research 35, 230-257.
Hay, W.W., 2008. Evolving ideas about the Cretaceous climate and ocean circulation. Cretaceous Research 29,
725-753.
Hay, W.W., 2011. Can humans force a return to a "Cretaceous" climate? Sedimentary Geology 235, 5-26.
Herrle, J.O. , Mutterlose, J., 2003. Calcareous nannofossils from the Aptian - early Albian of SE France: Paleoecological and biostratigraphic implications. Cretaceous Research 24, 1-22.
Huber, B.T., MacLeod, K.G., Gröcke, D.R., Kucera, M., 2011. Paleotemperature and paleosalinity inferences and chemostratigraphy across the Aptian/Albian boundary in the subtropical North Atlantic. Paleoceanography 26, PA4221 doi:10.1029/2011PA002178.
McAnena, A., Flögel, S., Hofmann, P., Herrle, J.O., Griesand, A., Pross, J., Talbot, H.M., Rethemeyer, J., Wallmann, K., Wagner, T., 2013. Atlantic cooling associated with a marine biotic crisis during the mid-Cretaceous period. Nature Geoscience 6, 558-561.
Schröder-Adams, C.J., Herrle, J.O., Embry, A., Haggart, J.W., Galloway, J.M., Pugh, A.T., Harwood, D.M., 2014. Aptian to Santonian foraminiferal biostratigraphy and paleoenvironmental change in the Sverdrup Basin as re- vealed at Glacier Fiord, Axel Heiberg Island, Canadian Arctic Archipelago. Palaeogeography, Palaeoclimatology, Palaeoecology. (in press).
Tarduno, J.A., Brinkman, D. B., Renne, P. R., Cottrell, R. D., Scher, H., Castillo, P., 1998. Evidence for Extreme
Climatic Warmth from Late Cretaceous Arctic Vertebrates. Science 282, 2241-2244.

IODP

Petrological and Geochemical Characterization of Abyssal Peridotites from the East Pacific Rise and Incorporation of Water in Nominally Anhydrous Orthopyroxene (ODP Leg 147: Hess Deep)

K. HESSE[1], E. SCHMÄDICKE[1], J. GOSE[1]

[1]University of Erlangen-Nürnberg, GeoZentrum Nordbayern, Schlossgarten 5a, D-91054 Erlangen

A set of samples of serpentinized, plagioclase-free, abyssal spinel peridotite drilled during ODP cruise 147 of site 895 (2° 17.6' N, 101° 26.7' W) from the Hess Deep, a former triple junction of the fast-spreading East Pacific Rise, was investigated petrologically concerning their major and trace element concentrations and the incorporation of hydroxyl point defects in the crystal structure of nominally anhydrous orthopyroxene. Therefore, analyses were taken by electron microprobe, laser-ablation inductively-coupled-plasma mass-spectrometry, and Fourier-transform infrared spectroscopy.

The investigated rock type is harzburgite with a primary mineral assemblage of olivine, orthopyroxene, clinopyroxene, and spinel. The degree of serpentinization ranges from over 60 to over 95 %. Major secondary minerals are serpentine, bastite, and magnetite. Electron microprobe measurements reveal Mg# (=Mg/(Mg+Fe)) between 0.90 and 0.92 for olivine. The mean enstatite component in orthopyroxene varies between 78.6 and 85.5 % with Mg# ranging from 0.90 to 0.92 and Cr# (=Cr/(Cr+Al)) ranging from 0.15 to 0.24. Al_2O_3 varies between 0.49 and 2.88 wt. %. Clinopyroxene has Mg# of 0.91 to 0.96 and Cr# of 0.18 to 0.72. Al2O3 contents range from 0.07 to 3.58 wt. %. Analyses of spinel reveal Mg# of 0.44 to 0.54 and Cr# of 0.55 to 0.69. Mineral trace element data indicate an extreme depletion of the harzburgite, characteristic for the typical restitic nature of abyssal peridotites after the extraction of MORB melt. The water contents in orthopyroxene range from 80 to 240 wt. ppm H_2O.

Temperature and pressure conditions were evaluated using various geothermobarometric calibrations. Temperatures determined by two-pyroxene geothermometers are generally similar ranging from 962 to 1108 °C (Brey & Köhler, 1990), 914 to 1071 °C (Bertrand & Mercier, 1985), and 981 to 1134 °C (Taylor, 1998). Corresponding pressures range from 7.0 to 35.6 kbar (Köhler & Brey, 1990) resulting in equilibration depths between 23 and 117 km. Application of a pressure-independent thermometer yields lower temperatures varying between 865 and 991 °C (Witt-Eickschen & Seck, 1991). The degree of partial melting calculated after Hellebrand et al. (2001) amounts to 16 to 18 % of pure fractional melting in the spinel peridotite stability field. This value is consistent with the very depleted concentrations of trace and rare earth elements in the pyroxenes. Comparison of water contents in orthopyroxene to major and trace elements gives weak correlations ($R^2 < 0.4$) for SiO_2, TiO_2 and Ni, Zn, Ho, Er, Lu and stronger correlations ($R^2 > 0.7$) for to Li, Cr, and Zr. A correlation of water and temperature cannot be identified, however, comparing water contents to pressure results in a moderate correlation (R2 H0.5).

In contrast to peridotites from Legs 153 and 209 drilled at the Mid-Atlantic-Ridge previously investigated by Gose et al. (2009) and Schmädicke et al. (2011), the Leg 147 samples contain intermediate to high water concentrations, experienced a high degree of partial melting, and intermediate mean mantle equilibrium temperatures. The elevated water contents in Legs 147 and 153 as opposed to the high degrees of partial melting are notably conspicuous. Therefore, after melt removal, water must have been re-introduced into the orthopyroxenes. Re-equilibration of water contents took place under spinel-facies conditions before exhumation of the tectonite since elevated temperatures and pressures enhance diffusion and facilitate hydrogen uptake. We suggest that the residual mantle harzburgite formed during high degrees of fractional melting in the spinel peridotite field. Exhumation from spinel-facies depth was fast and accompanied by cooling during ascent. Therefore, re-equilibration of the spinel-facies mantle assemblage to

lower pressure assemblages and decompression-induced water loss were prevented (Schmädicke et al., 2011). The high variability of water contents in Leg 147 is explained by a combination of post melt extraction processes enhanced by slightly differing mineral chemistry, small-scale temperature and pressure variations during re-equilibration, and different initial water contents.

References:
Gose, J.; Schmädicke, E. & Beran, A. (2009): Water in enstatite from Mid-Atlantic Ridge peridotite: Evidence for the water content of suboceanic mantle? Geology 37: 543 - 546.
Schmädicke, E., Gose, J. & Will, T. (2011): Heterogeneous mantle underneath the North Atlantic: Evidence from water in orthopyroxene, mineral composition and equilibrium conditions of spinel peridotite from different locations at the Mid-Atlantic Ridge. Lithos 125: 308 – 320.

IODP

Molecular-isotopic studies of microbial processes and organic matter in the subseafloor coalbed biosphere of Shimokita (IODP Exp. 337).

V.B. HEUER[1], S. XIE[1], M. BOWLES[1], Y.-S. LIN[1,2], Y. MORONO[3], F. INAGAKI[3], AND K.-U. HINRICHS[1]

[1]MARUM – Zentrum für marine Umweltwissenschaften & Fachbereich Geowissenschaften, Universität Bremen, 28334 Bremen
[2]now: Department of Oceanography, National Sun Yat-Sen University, No. 70 Lienhai Rd, Kaohsiung 804, Taiwan
[3]Kochi Institute for Core Sample Research, Japan Agency for Marine-Earth Science and Technology (JAMSTEC), Kochi, Japan

Introduction - Marine subsurface hydrocarbon systems are among the most frequently exploited Earth systems. Nonetheless, the biological and abiotic processes associated with the transformation of organic matter in these systems are poorly understood. This is mainly due to the fact that drilling and sampling of subseafloor hydrocarbon systems requires costly riser-technology. IODP Expedition 337 was the first scientific initiative to drill and study a subseafloor hydrocarbon system using riser-technology. With Site C0020, the expedition targeted a natural gas field in the tectonically active forearc basin offshore the Shimokita Peninsula of Japan (Inagaki et al., 2010). When the upper 365 m of this site were explored by non-riser drilling in 2006, methane hydrates were found in combination with conspicuously high concentrations of microbial cells (Aoike et al., 2007) and suggested the existence of an active subseafloor biosphere that benefits from organic matter and nutrients expelled from deeper sources such as coalbeds (Inagaki et al., 2010). In 2012, Hole C0020A was deepened and spot-cored down to a total depth of 2466 meters below seafloor (mbsf) by riser-drilling. Thirteen coal layers with thicknesses >30 cm were identified and samples were recovered from seven of them at around 2000 mbsf, where in situ temperatures were around 50°C (Inagaki et al., 2012; 2013). The coal is of low maturity and embedded in an intertidal and wetland sequence that was deposited in a continuously subsiding basin from late Oligocene/early Miocene through early/middle Miocene, before the paleoenvironment gradually changed from a shallow-marine setting to an offshore continental shelf environment in the Pliocene (Inagaki et al., 2012). The ultra-deep drilling and recovery of coalbed samples provide unprecedented opportunities to assess the limits of life in the deep subseafloor, to study biological and abiotic processes in hydrocarbon reservoirs, and to elucidate the role of hydrocarbon reservoirs as energy and carbon sources for the deep biosphere. In our post-cruise research, we use a molecular-isotopic approach to study the processes and microbial communities associated with the deeply buried coalbed.

Research Approach – Our research employs both cultivation-independent and cultivation-dependent methods. The most prominent example for cultivation-independent methods is the identification of biogenic vs thermogenic methane sources (Whiticar, 1999) based on the stable carbon and hydrogen isotopic composition of methane in mud gas, sediment cores and formation fluids. Our cultivation-dependent methods comprise two types of isotope tracer experiments: (1) in order to investigate the role of specific substrates, we add ^{13}C-labeled organic compounds (n-hexadecane, vanillin, lignin) and track their remineralization by stable isotope analysis of CO_2 and methane. (2) In order to investigate the response of microbial communities to pulses of various organic substrates, we use a novel dual-isotope labeling approach with high concentrations of label in the form of ^{13}C-DIC and D2O (Wegener et al., 2012; Kellermann et al., 2012). In these experiments, analysis of ^{13}C and D incorporation into membrane lipids informs us on the growth, or absence thereof, of microbial communities in minimally perturbed samples. Due to the low concentration of microbial cells in very deep sediments, the detection of membrane lipids is analytically challenging. Therefore, method development is an essential part of our project.

Results and discussion of cultivation-independent molecular isotopic studies - Our shipboard and post-cruise gas analyses show unambiguously that microbial processes are the dominant source of methane in the deep subseafloor off Shimokita, even at 2466 mbsf. During drilling of Site C0020, on-line carbon isotope analysis of mud gas methane yielded a continuous down-hole record with ´^{13}C-values below -60‰ vs. VPDB. The results of on-line carbon isotope analysis of mud-gas methane by ring-down cavity laser spectroscopy were successfully verified by shore based isotope-ratio-monitoring gas chromatography/mass spectrometry (irm-GC/MS). The clear ^{13}C-depletion of methane is a strong indicator for the predominance of microbial methanogenesis at all depths (Whiticar, 1999). The down-hole ´^{13}C-methane profile has a distinct pattern and points to variations in methanogenic pathways and/or substrates with sediment depth that might be related to changes in depositional regime and organic matter input (Inagaki et al., 2013). ´^{13}C-values of methane were highest in the coal-bearing lithological unit. Further shore based analysis of mud gas showed little variation in the stable hydrogen isotopic composition methane with depth. ´D-values of methane average around -166 ± 10‰ vs. VSMOW and point to biogenic CO_2-reduction as dominant methane source. Shore based stable carbon isotope analysis of CO_2 in samples taken from sediment cores between 1606 to 2464 mbsf reveal an increase of ´^{13}C-CO^2 with depth from -18.2‰ to -7.2‰ vs VPDB as well as a distinct excursion towards heavier CO^2 with ´^{13}C-values of up to 0.2‰ vs VPDB in coal bearing horizons between 1900 and 2000 mbsf. The increasing

^{13}C-enrichment of the pore-water CO_2 pool is consistent with the preferential utilization of $12CO_2$ by biogenic methanogenesis. Overall, the results of our molecular isotopic studies agree well with shipboard results that rule out a predominant contribution of thermogenic methane sources at any depth of Hole C0020A (Inagaki et al., 2012; 2013): the abundance of higher hydrocarbon gases was low and C1/C2+ ratios were generally >200, thus indicating biogenic methane sources. Following a general trend related to early diagenesis (Pimmel and Claypool, 2001), C1/C2+ ratios decreased with increasing depth and temperature. However, the major coal-bearing horizons were striking exceptions from this trend. They showed a distinct peak of elevated C1/C2+ values (~1000) that point to elevated biogenic methanogenesis in coals compared to adjacent lithological units. Moreover, sedimentary organic matter was in a thermally immature to early mature state throughout the drilled formation, and the extent of sterene to sterane conversion suggests that even at the bottom of the hole temperatures have never exceeded 60°C (Inagaki et al., 2012).

Preliminary results and discussion of cultivation-dependent molecular isotopic studies – We initiated two series of cultivation-dependent studies onboard Chikyu. (1) In order to investigate metabolic activity in the presence of specific substrates, ^{13}C-labeled organic compounds were added to sediment samples, which were chosen to represent the different lithologies encountered between 1375 and 2461 mbsf, and incubated under anaerobic conditions at in situ temperatures. The remineralization of the labeled substrates was tracked by stable isotope analysis of CO_2 and methane. After 16 months of incubation, $'^{13}$C-values of CO_2 and methane had changed only slightly (< ±3‰) in the majority of all samples, with the notable exception of three samples that were taken from coal-bearing sediments between 1924 and 1993 mbsf. In the sample taken from 1924.5 mbsf, $'^{13}$C-values of methane had increased by 7.8‰ with the amendment of ^{13}C-labeled n-hexadecane or ^{13}C-labeled vanillin, thus suggesting metabolic activity and uptake of ^{13}C into the methane pool. At the same time, $'^{13}$C-values of CO_2 had increased by <2.0‰. In two samples taken from 1945 and 1993 mbsf, $'^{13}$C-values of methane showed only a slight increase (<4.0‰), while $'^{13}$C-values of CO_2 decreased by 11-13‰ in the presence of ^{13}C-labeled n-hexadecane and vanillin, respectively, thus suggesting that the remineralization of non-labeled substrates had been stimulated in this experiment. The preliminary results point to microbial activity in samples that were recovered from the organic-rich sandstone and shale associated with coalbeds at 1924 to 1993 mbsf. All incubation experiments with ^{13}C-labeled substrates are still in progress and monitoring of ^{13}C-uptake into the methane and CO_2 pool will continue. (2) In order to investigate the growth of microbial communities as response to the addition of organic substrates, we added non-labeled substrates in the presence of ^{13}C-DIC and D_2O to monitor the incorporation of ^{13}C and D into membrane lipids after 13 months of incubation at in situ temperatures. At the same time, the stable carbon isotopic composition of methane was analyzed to monitor methanogenic CO_2 reduction in the ^{13}C-DIC amended samples. We found evidence for active hydrogenotrophic methanogenesis only in the shallowest sample that was taken from 1375.3 mbsf, but not in samples taken from the coal-bearing lithologies. In the shallowest samples, the $'^{13}$C-values of methane had increased by 400‰ in the course of incubation. The analysis of membrane lipids is currently in progress.

Method development – Our preliminary analysis of membrane lipids in samples of Site C0020 revealed that the very low cell concentrations in the ultra deep sediments require development of trace analytical methods. On the one hand, the concentrations of intact lipids were below the detection limit of our current method (Wörmer et al., 2013), which corresponds to cell concentrations of 5×10^3~10^7 cells per injection. On the other hand, the analytical background that is caused by the processing of samples in the laboratory was critical. The amount of free fatty acids that derived from large volume extraction is around 16 ng per injection, this background corresponds to 10^6 bacterial cells per injection. Rather than scanning for unknown lipids, we will now focus on the identification of known compounds with high sensitivity using Triple-Quad mass spectrometry.

Conclusions and outlook – Our cultivation-independent molecular isotopic data show clearly that microbial processes are the dominant source of methane in the deep subseafloor off Shimokita, with a strong contribution of biogenic CO_2-reduction. However, while not excluding the possibility, our current data on methane stable isotopes and methane concentration do not provide support for the coalbeds as direct source of methane accumulating in shallow hydrates above 365 mbsf. The data are consistent with local processes dictating the isotope profiles rather than pointing to an upward flux from a deep point source, such as Eocene coal layers at greater depth. Our cultivation-dependent studies point to microbial activity in the coal-bearing lithologies at ~2000 mbsf, but so far we found evidence for active hydrogenotrophic methanogenesis only in the shallowest sample that was taken from 1375.3 mbsf (above the coal-bearing lithologies). The investigation of microbial activity in culture-dependent studies and the analysis of membrane lipids are still in progress.

Acknowledgements – We thank the crew and technical staff of the DV Chikyu for their support at sea. This research used samples provided by the Integrated Ocean Drilling Program (IODP), which is sponsored by the US National Science Foundation and participating countries under management of Joint Oceanographic Institutions (JOI), Inc. V.B.H. and K.-U.H. gratefully acknowledge funding of their research by the Deutsche Forschungsgemeinschaft (project grant HI 616/16).

References:

Aoike K. (ed.) (2007) CK06-06 D/V Chikyu shakedown cruise offshore Shimokita. Laboratory Operation Report: Yokahama, JAMSTEC-CDEX.

Inagaki F., Hinrichs K.-U., Kubo Y., and the Expedition 337 Project Team (2010) Deep coalbed biosphere off Shimokita: microbial processes and hydrocarbon system associated with deeply buried coalbed in the ocean. IODP Scientific Prospectus, 337.

Inagaki F., Hinrichs K.-U., Kubo Y., and the Expedition 337 Scientists (2012) Deep coalbed biosphere off Shimokita: microbial processes and hydrocarbon system associated with deeply buried coalbed in the ocean. IODP Preliminary Report, 337.

Inagaki F., Hinrichs K.-U., Kubo Y., and the Expedition 337 Scientists (2013) Deep coalbed biosphere off Shimokita: microbial processes and hydrocarbon system associated with deeply buried coalbed in the ocean. IODP Proceedings, 337. doi:10.2204/iodp.proc.337.2013.

Kellermann, M.Y., Wegener, G., Elvert, M., Yoshinaga, M.Y., Lin, Y.-S., Holler, T., Mollar, X.P., Knittel, K., Hinrichs, K.-U. (2012)

Autotrophy as a predominant mode of carbon fixation in anaerobic methane-oxidizing microbial communities. PNAS 109, 19321-19326.
Pimmel, A., Claypool, G., 2001. Introduction to shipboard organic geochemistry on the JOIDES Resolution. ODP Technical Note 30.
Wegener, G., Bausch, M., Holler, T., Thang, N.M., Prieto Mollar, X., Kellermann, M.Y., Hinrichs, K.-U., Boetius, A. (2012) Assessing sub-seafloor microbial activity by combined stable isotope probing with deuterated water and ^{13}C-bicarbonate. Environ. Microbiol. 14, 1517–1527.
Whiticar, M.J. (1999) Carbon and hydrogen isotope systematics of bacterial formation and oxidation of methane. Chem. Geol. 161, 291-314.
Wörmer, L-P., Lipp, J.S., Schröder, J.M., Hinrichs, K-U. (2013) Application of two new LC-ESI-MS methods for improved detection of intact polar lipids (IPLs) in environmental samples. Org Geochem. 59, 10-21.

ICDP

PASADO Lipids'-paleoenvironmental reconstruction in Southern Patagonia

K. HOCKUN[1], G. MOLLENHAUER[1,2], E. SCHEFUß[1] AND THE PASADO SCIENCE TEAM

[1]MARUM – Zentrum für Marine Umweltwissenschaften, Universität Bremen, Leobener Straße, 28359 Bremen
[2] Alfred Wegener Institut Helmholtz- Zentrum für Polar- und Meeresforschung, Am Handelshafen 12, 27570 Bremerhaven

Southern Patagonia is a key region for paleoclimatic reconstruction in the Southern Hemisphere as it is the only landmass located in the Southern Hemisphere westerly wind (SHW) region. Most paleoclimatic studies focused on the Chilean side of the Andes or the Andean region (Kilian and Lamy, 2012). Only a few promising sedimentary archives exist in the southeastern part of Argentina. Within the framework of the ICDP PASADO ("Potrok Aike Maar Lake Sediment Archive Drilling Project") drilling campaign, a core (51°58´S, 70°23´W) was drilled in 2007 in Laguna Potrok Aike (LPTA), a volcanic maar situated in the Pali Aike volcanic field in Southern Patagonia (Fig. 1). A high resolution sedimentary record was recovered. At present, the climate in our study area is mainly influenced by the SHW and the topography of the landmass (Mayr et al., 2007a,b).

Extensive studies with the focus on multiproxy approaches have been carried out within the framewort of the PASADO project. Regional calibrations for pollen, diatom and chironomid associations have been established in order to reconstruct temperature and precipitation changes in Southern Patagonia. In addition, several approaches have been taken to infer paleo-hydrological changes and associated lake-level variations (Haberzettl et al., 2007a; Haberzettl et al., 2005; Haberzettl et al., 2008), yielding, however, inconclusive results in comparison with the reconstructions based on archives in the Andean region. Furthermore, so far no quantitative paleoclimatic reconstructions exist for temperature and hydrological changes.

Therefore, the PASADO Lipids project started in 2011 aiming to provide new insights into the climate history of southern South America by using organic-geochemical proxies based on lipid biomarkers. We study abundances and compound-specific isotope compositions (´D, ´^{13}C) of biomarkers derived from terrestrial and aquatic plants including *n*-alkanes and n-fatty acids as well as temperature- and pH-sensitive abundance ratios of microbial membrane lipids (glycerol dialkyl glycerol tetraethers, GDGTs). Based on the GDGTs lake temperature changes using TEX_{86} (TetraEther index of GDGTs with 86 carbon atoms) shall be inferred, as well as soil temperature and soil pH changes using the MBT/CBT indices (methylation ratio/cyclization ratio of branched tetraethers). Compound-specific ´D values of biomarkers from aquatic and terrestrial sources are expected to reflect the local hydrology and changes in the lake water balance in particular. Combining all datasets will allow to develop an improved mechanistic understanding of terrestrial climatic conditions in the Southern Hemisphere.

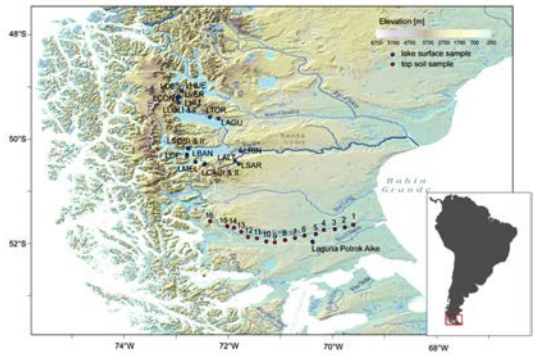

Figure 1: Map of Southern Patagonia with location of Laguna Potrok Aike, elevation map with core location.

To investigate the isotope signal in wax lipids derived from higher terrestrial plants in relation to moisture sources and fractionation effects during evaporation and transpiration we analysed 16 top-soil samples along a W-E transect along the same latitude as LPTA. Long-chain n-alkanes (n-C29 & n-C31) in the top soils show similar ranges of compound-specific ´D and ´13C compositions as in investigated sediment samples of LPTA. The ´D values of the n-C31 alkane vary from -225‰ to -195‰ and show an increase from W to E which might indicate the higher relative influence of the Atlantic (isotopically enriched) moisture over south-east Patagonia. The compound-specific ´^{13}C values of the *n*-C_{31} alkane (range: -34.9‰ to -32.7‰) also show an increase from W to E which is interpreted as higher water-use-efficiency of the C_3 plants in the east due to higher aridity, i.e., lower mean annual precipitation amounts. The positive correlation of ´^{13}C and ´D signals suggests that fractionation effects due to higher evapo-transpiration in the east partly cause the observed trend in long-chain *n*-alkane ´D values.

Furthermore, we characterized the lipid biomarker signatures of terrestrial plants, aquatic macrophytes, soils, dust traps, sediment traps and lake surface sediments from Laguna Potrok Aike to identify suitable tracers for paleo-reconstructions. We distinguished the *n*-alkane distribution of all samples and also the isotopic signature of the most abundant *n*-alkanes. The results show differences in the distribution as well as in the isotopic values of *n*-alkanes. The *n*-alkane distribution of the aquatic marcophyte samples show a predominance of *n*-C_{23} and *n*-C_{25}, while the distribution of *n*-alkanes from the terrestrial plants are predominated by *n*-C_{29} and *n*-C_{31}. The soil samples contain a mixture of these long and short chain compounds with *n*-C_{29} as most abundant contributor. The two sediment traps from 30 and 90 meter water depth

contain a mixture of *n*-alkanes from terrigenous and aquatic sources, the same applies for the surface sediment of LPTA. The terrestrial-derived long-chain *n*-C_{29} and *n*-C_{31} alkanes are consistently more depleted in deuterium (around -230 ‰ VSMOW) than the macrophyte-derived *n*-C_{23} and *n*-C_{25} alkanes (around -170 ‰ VSMOW). The same is true for ´^{13}C values. The macrophyte-derived *n*-C_{23} alkanes are more enriched in carbon (around -18 ‰ VPDB) as the terrestrially-derived *n*-C_{29} and *n*-C_{31} alkanes (around -30 ‰ VPDB). Isotopic signals in dust traps are limited to terrestrially-derived *n*-C_{29} and *n*-C_{31} alkanes and show ´^{13}C values around -33 ‰ VPDB and ´D values ranging from -200 to -210‰ VSMOW for *n*-C_{29} *n*-alkane. These results help us to identify the source of the different components and to understand their isotopic signal.

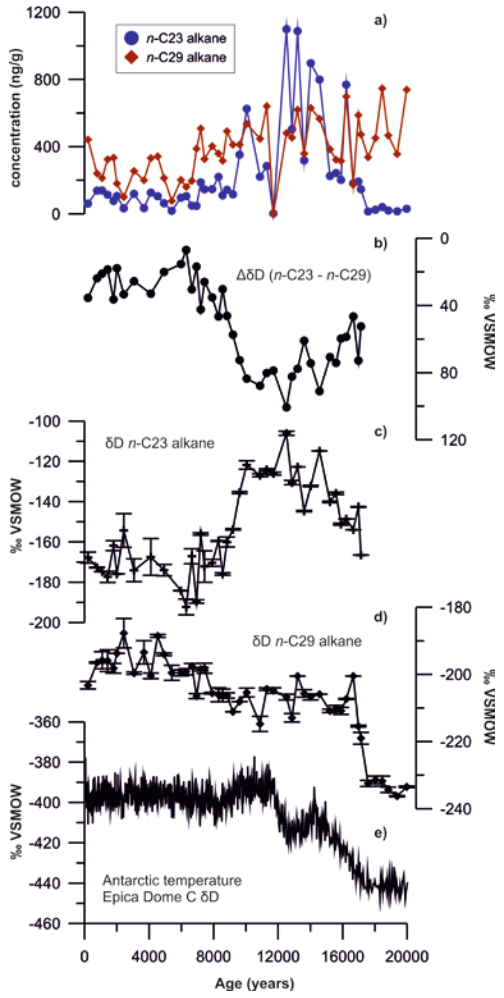

Figure 2: a) concentration of *n*-C_{23} and *n*-C_{29} downcore b) isotopic lake water balance of Laguna Potrok Aike, which is determined by the difference of *n*-C_{23} and *n*-C_{29} c) variations in ´D compositions of *n*-C_{23} alkane indicating isotopic changes of lake water d) variations in ´D compositions of *n*-C_{29} alkane reflecting isotope precipitation changes e) deuterium isotope changes of ice in Antarctica representing Antarctic temperature changes (Jouzel et al., 2007)

48 PASADO core samples of the last 20.000 years have been analyzed. The downcore data show high variability in the abundance of the n-alkyl lipids (Fig. 2a) with higher contributions of macrophyte-derived shorter-chain *n*-alkanes in the pre-Holocene section. Possibly, this indicates a more proximal position of shallow lake areas to the core site due to lower lake levels. ´D values of the *n*-C_{29} alkane, derived from higher plant leaf waxes and inferred to refelct the precipitation signal, range from -230 to -190 ‰ V-SMOW (Fig. 2d) in Laguna Potrok Aike sediments. The ´D values of the *n*-C_{29} alkane are much depleted (around -230 ‰ VSMOW) before 17,500 years before present (BP) consistent with cool glacial conditions. Starting at 17,500 years BP, parallel to Antarctic warming (Barbante et al., 2006) (Fig. 2e), *n*-C_{29} ´D values increase sharply to -200 ‰ VSMOW and range around -210 ‰ VSMOW afterwards (Fig. 2d). As the isotopic composition of precipitation at latitudes of about 50°S is largely controlled by temperature (Dansgaard, 1964) a change of about 20 0 in ´D would correspond to a temperature increase of about 5°C during deglaciation. The *n*-C_{29} ´D values remain at around -210 ‰ VSMOW until about 8,000 years ago and increased to values of around -190 to -200 until 200 years BP. This trend is different than the temperature trend observed in Antarctic ice cores (Barbante et al., 2006). Therefore, we ascribe this shift to a change in predominant moisture source. Atlantic-sourced rainfall events were found to be linked to enriched isotopic composition relative to Pacific-sourced precipitation in the LPTA region (Mayr et al., 2007a). We thus infer that from 8,000 years BP onward, the relative influence of Atlantic-derived moisture increased and that the relative influence of Pacific-derived moisture was higher before 8,000 years ago. This finding contradicts earlier interpretations of increasing westerly wind speeds over the Holocene (Mayr et al., 2007b). ´D compositions of the *n*-C_{23} alkane (Fig. 2c) range from -190 to -106 ‰ V-SMOW (Fig. 2d). Since *n*-C_{23} is derived from aquatic macrophytes (Ficken et al., 2000), its ´D values indicate isotopic changes of the lake surface water with the latter driven by isotopic changes of precipitation and evaporation. The difference in isotope values between these two compounds reflects the isotopic lake water balance, i.e., the hydrologic balance of the lake, mainly driven by evaporative processes (Fig. 2b)

.Results of GDGT distributions in the top soil samples as well as a series of lake surface samples (Fig. 1) confirm a correlation between GDGT index parameters (MBT/CBT indices) and soil temperature and pH in the study area. The predicted temperatures based on the global calibration (Weijers et al., 2007) are, however, lower than measured temperatures. Therefore, we developed a new calibration for the use of GDGT-based proxies in southern Patagonia based on the published MBT/CBT indices. The MBT-based reconstructed temperature values, however, differ (+/-2°C) from the measured mean annual temperatures in our study area (Fig. 2). The temperature estimates from the analysed lake surface sediments overestimate regional mean annual air temperatures by almost 10°C (Fig. 3). In situ production of several of the GDGTs used in the calibration appears to compromise the signals. For that reason, we are trying to avoid the questionable components for the new regional calibration. Therefore, additional samples covering a wider temperature range will be analysed to identify suitable temperature sensitive components and thus develop a calibration appropriate for Southern Patagonia. 30 additional top soil samples from a north-south transect and a few samples from the Andean region are provided for

this purpose from our cooperation partners from Argentina and Germany involved in the PASADO project.

40 further PASADO core samples are currently being processed to measure abundance and compound-specific isotope compositions (´D, ´^{13}C) of *n*-alkanes as well as temperature- and pH-sensitive abundance ratios of GDGTs covering a period from 20,000 to 55.000 years.

References:

Barbante, C., Barnola, J.M., Becagli, S., Beer, J., Bigler, M., Boutron, C., Blunier, T., Castellano, E., Cattani, O., Chappellaz, J., Dahl-Jensen, D., Debret, M., Delmonte, B., Dick, D., Falourd, S., Faria, S., Federer, U., Fischer, H., Freitag, J., Frenzel, A., Fritzsche, D., Fundel, F., Gabrielli, P., Gaspari, V., Gersonde, R., Graf, W., Grigoriev, D., Hamann, I., Hansson, M., Hoffmann, G., Hutterli, M.A., Huybrechts, P., Isaksson, E., Johnsen, S., Jouzel, J., Kaczmarska, M., Karlin, T., Kaufmann, P., Kipfstuhl, S., Kohno, M., Lambert, F., Lambrecht, A., Lambrecht, A., Landais, A., Lawer, G., Leuenberger, M., Littot, G., Loulergue, L., Luthi, D., Maggi, V., Marino, F., Masson-Delmotte, V., Meyer, H., Miller, H., Mulvaney, R., Narcisi, B., Oerlemans, J., Oerter, H., Parrenin, F., Petit, J.R., Raisbeck, G., Raynaud, D., Rothlisberger, R., Ruth, U., Rybak, O., Severi, M., Schmitt, J., Schwander, J., Siegenthaler, U., Siggaard-Andersen, M.L., Spahni, R., Steffensen, J.P., Stenni, B., Stocker, T.F., Tison, J.L., Traversi, R., Udisti, R., Valero-Delgado, F., van den Broeke, M.R., van de Wal, R.S.W., Wagenbach, D., Wegner, A., Weiler, K., Wilhelms, F., Winther, J.G., Wolff, E., Members, E.C., 2006. One-to-one coupling of glacial climate variability in Greenland and Antarctica. Nature 444, 195-198.

Dansgaard, W., 1964. Stable isotopes in precipitation. Tellus 16, 436-468.

Ficken, K.J., Li, B., Swain, D.L. and Eglinton, G., 2000. An n-alkane proxy for the sedimentary input of submerged/floating freshwater aquatic macrophytes. Organic Geochemistry, 31: 745-749.

Garreaud, R., Lopez, P., Minvielle, M., Rojas, M., 2013. Large-Scale Control on the Patagonian Climate. Journal of Climate 26, 215-230.

Haberzettl, T. et al., 2007a. Lateglacial and Holocene wet-dry cycles in southern Patagonia: chronology, sedimentology and geochemistry of a lacustrine record from Laguna Potrok Aike, Argentina. Holocene, 17: 297-310.

Haberzettl, T. et al., 2005. Climatically induced lake level changes during the last two millennia as reflected in sediments of Laguna Potrok Aike, southern Patagonia (Santa Cruz, Argentina). Journal of Paleolimnology, 33: 283-302.

Haberzettl, T. et al., 2008. Hydrological variability in southeastern Patagonia and explosive volcanic activity in the southern Andean Cordillera during Oxygen Isotope Stage 3 and the Holocene inferred from lake sediments of Laguna Potrok Aike, Argentina. Palaeogeography Palaeoclimatology Palaeoecology, 259: 213-229.

Jouzel, J., Masson-Delmotte, V., Cattani, O., Dreyfus, G., Falourd, S., Hoffmann, G., Minster, B., Nouet, J., Barnola, J.M., Chappellaz, J., Fischer, H., Gallet,J.C.,Johnsen,S.,Leuenberger,M.,Loulergue,L.,Luethi, D.,Oerter,H., Parrenin,F.,Raisbeck,G.,Raynaud, D.,Schilt, A.,Schwander,J.,Selmo, E., Souchez, R., Spahni, R., Stauffer, B., Steffensen, J.P., Stenni, B., Stocker, T.F., Tison, J.L., Werner, M., Wolff, E.W., 2007. Orbital and millennial Antarctic climate variability over the past 800,000 years. Science 317 (5839), 793-796.

Kilian, R. and F. Lamy (2012). "A review of Glacial and Holocene paleoclimate records from southernmost Patagonia (49-55°S)." Quaternary Science Reviews 53: 1-23.

Mayr, C., Wille, M., Haberzettl, T., Fey, M., Janssen, S., Lücke, A., Ohlendorf, C., Oliva, G., Schäbitz, F., Schleser, G., Zolitschka, B., 2007a. Holocene variability of the Southern Hemisphere westerlies in Argentinean Patagonia (52_S). Quat. Sci. Rev., 26, 579–584.

Mayr, C., Lücke, A., Stichler, W., Trimborn, P., Ercolano, B., Oliva, G., Ohlendorf, C., Soto, J., Fey, M., Haberzettl, T., Janssen, S., Schäbitz, F., Schleser, G.H., Wille, M., Zolitschka, B., 2007b. Precipitation origin and evaporation of lakes in semi-arid Patagonia (Argentina) inferred from stable isotopes (´18O, ´2H). Journal of Hydrology, 334, 53-63.

IODP

Gateway opening of the South Atlantic Ocean: New high resolution insights from the Aptian to Albian Falkland Plateau (DSDP Site 511)

P. HOFMANN[1], T. WAGNER[2], J.O. HERRLE[3,4], A. MCANENA[5], S. FLÖGEL[6]

[1]Department of Geology and Mineralogy, University of Cologne, 50674 Cologne, Germany
[2]School of Civil Engineering and Geosciences, Newcastle University, Newcastle Upon Tyne, NE1 7RU, United Kingdom
[3]Institute of Geosciences, Goethe-University Frankfurt, D-60438 Frankfurt am Main, Germany
[4]Biodiversity and Climate Research Centre (BIK-F), D-60325 Frankfurt am Main, Germany
[5]Institute of Marine and Coastal Sciences, Rutgers, The State University, USA
[6]GEOMAR, Wischhofstr. 1-3, 24148 Kiel, Germany

Young ocean basins developing as part of the geological Wilson Cycle in the wake of the breakup of supercontinents essentially contribute to global climate trends via evolving carbon sinks, both regional and global (e.g., Trabucho-Alexandre et al., 2012 and references therein). These young basins are important biogeochemical reactors, supported by their distinct bathymetry (i.e. high shelf-to-open ocean ratio) and often restricted ocean circulation, both deep and shallow. These properties turn young ocean basins into major drivers (or at least modulators) for long-term climate trends and probably also for short-term perturbations of the global carbon cycle.

Recent studies have argued that the young, evolving South Atlantic and Southern Ocean basins have acted as a primary site of organic carbon production, biotransformation and burial, as manifested by extensive black shale (e.g., Wagner et al., 2013) and prolific hydrocarbon provinces along both continental margins (e.g.; Cameron et al., 1999). Both basins are thought to have had a substantial impact on early Cretaceous global climate (Flögel et al., 2011, McAnena et al., 2013) via carbon sequestration in marine sediments based on geochemical and modeling results. Our own recent biogeochemical modelling work suggests that the South Atlantic and the Southern Ocean in combination sequestered ~35% of the total organic carbon on an area which represented only 5% of the mid-Cretaceous oceans (McAnena et al. 2013), emphasising the importance of these young oceanic sub-basins for the global carbon cycle.

During the Early Cretaceous the Falkland Plateau was part of the gateway allowing initial inflow of currents from the Southern Ocean into the South Atlantic, thereby fundamentally changing the conditions for carbon production and accumulation in the South Atlantic. New high resolution proxy records from DSDP Site 511 provide a significantly improved stratigraphic resolution of these important developments on the Falkland Plateau, based on bio- and carbon isotope stratigraphy. With this improved chronology we are able to precisely define the OAE 1a and the Late Aptian Cold Spell (LACS, McAnena et al., 2013) at this site and explore the relationships of these global climate perturbation with the opening history

of the southern gateway. Notably, both global climate perturbations are not characterized by high TOC values at Falkland Plateau, contradicting previous statements for the southern South Atlantic region. A second, new observation identifies a massive hiatus following OAE 1a, that lasted for about ~ 6 Myrs (top of the calcareous nannofossil zones NC7 to bottom of NC8). Notably, a similar hiatus, although far less well constrained, has been reported from DSDP Sites 327 and 330 on the Falkland Plateau (seismic reflector with overlying red bed successions, own observations) and DSDP Site 361 in the Cape Basin (Seismic Reflector Atlantis II; McLachlan and Pieterse, 1978). Such a hiatus at DSDP 511, 327, 330 and 361 supports a common mechanism that must have affected ocean circulation across the southern South Atlantic region, and probably beyond (Bover-Anal et al., 2014). The cause, exact stratigraphic extend, and near to far field consequences of this hiatus is currently not known, but we suggest that it was closely connected to the inflow of vigorous ocean currents from the Southern Ocean into the southern South Atlantic. As such, this hiatus may herald the initial opening of the South Atlantic-Southern Ocean (SO-SE) deep water gateway during the late Aptian (~120 Myrs). Such an inflow of cooler and probably better ventilated water masses from the Southern Ocean would have introduced well oxygenated waters into the southern South Atlantic, reducing the capacity to store carbon in this ocean basin.

References:

Bover-Arnal, T., Salas, R., Guimera, J., Moreno-Bedmar, 2014, Deep incision in an Aptian carbonate succession indicates major sea-level fall in the Cretaceous. Sedimentology (accepted; doi: 10.1111/sed.12105).

Cameron, N.R., Bate, R.H. and Clure, V.S., 1999, The oil and gas habitats of the South Atlantic. Geological Society Special Publication 153, The Geological Society, London, 474 pp.

Flögel, S., Wallmann, K. and Kuhnt, W., 2011, Cool episodes in the Cretaceous – Exploring the effects of physical forcing on Antarctic snow accumulation. Earth and Planetary Science Letters 307, 279-288.

McAnena, A., Flögel, S., Hofmann, P., Herrle, J.O., Griesand, A., Pross, J., Talbot, H.M., Rethemeyer, J., Wallmann, K., Wagner, T., 2013. Atlantic cooling associated with a marine biotic crisis during the mid-Cretaceous period. Nature Geoscience 6, 558-561.

McLachlan, I.R., Pieterse, E., 1978, Preliminary palynological results: Site 361, Leg 40, Deep Sea Drilling Project. In Bolli, H. M., Ryan, W.B.F., et al., 1978. Initial Reports of the Deep Sea Drilling Project, Volume 40: Washington (U.S. Government Printing Office), 857-811.

Trabucho-Alexandre, J., Hay, W.W., de Boer, P.L., 2012, Phanerozoic environments of black shale deposition and the Wilson Cycle, Solid Earth 3, 29-42.

Wagner,T., Hofmann, P., Flögel, S., 2013. Marine black shale deposition and Hadley Cell dynamics: A conceptual framework for the Cretaceous Atlantic Ocean. Marine and Petroleum Geology 43, 222-238.

IODP

Uncovering a Salt Giant. Deep-Sea Record of Mediterranean Messinian-Events (DREAM) multi-phase drilling project

CHRISTIAN HÜBSCHER (1), ANGELO CAMERLENGHI (2), VANNI ALOISI (3), JOHANNA LOFI (4), GERT DELANGE (5), RACHEL FLECKER (6), DANIEL GARCIA-CASTELLANOS (7), CHRISTIAN GORINI (3), ZOHAR GVIRTZMAN (8), WOUT KRIJGSMAN (5), STEFANO LUGLI (9), YIZHAQ MAKOWSKY (10), VINICIO MANZI (11), TERRY MCGENITY (12), GIULIANA PANIERI (13), MARINA RABINEAU (14), MARCO ROVERI (11), FRANCISCO JAVIER SIERRO (15), AND NICOLAS WALDMANN (10

(1) University of Hamburg, christian.huebscher@zmaw.de (2) OGS, Trieste, (3) Université Pierre et Marie Curie, Paris, (4) Université de Montpellier 2, (5) Utrecht University, (6) University of Bristol, (7) ICTJA-CSIC, Barcelona, (8) Geological Survey of Israel, Jerusalem, (9) University of Modena and Reggio Emilia, (10) University of Haifa, (11) University of Parma, (12) University of Essex, (13) University of Tromsø, (14) CNRS Plouzané Brest, (15) University of Salamanca

In May 2013, the DREAM MagellanPlus Workshop was held in Brisighella (Italy). The initiative builds from recent activities by various research groups to identify potential sites to perform deep-sea scientific drilling in the Mediterranean Sea across the deep Messinian Salinity Crisis (MSC) sedimentary record. In this workshop three generations of scientists were gathered: those who participated in formulation of the deep desiccated model, through DSDP Leg 13 drilling in 1973; those who are actively involved in present-day MSC research; and the next generation (PhD students and young post-docs). The purpose of the workshop was to identify locations for multiple-site drilling (including riser-drilling) in the Mediterranean Sea that would contribute to solve the several open questions still existing about the causes, processes, timing and consequences at local and planetary scale of an outstanding case of natural environmental change in the recent Earth history: the Messinian Salinity Crisis in the Mediterranean Sea.The product of the workshop is the identification of the structure of an experimental design of site characterization, riser-less and riser drilling, sampling, measurements, and down-hole analyses that will be the core for at least one compelling and feasible multiple phase drilling proposal. Particular focus has been given to reviewing seismic site survey data available from different research groups at pan-Mediterranean basin scale, to the assessment of additional site survey activity including 3D seismics, and to ways of establishing firm links with oil and gas industry.

The scientific community behind the DREAM initiative is willing to proceed with the submission to IODP of a Multi-phase Drilling Project including several drilling proposals addressing specific drilling objectives, all linked to the driving objectives of the MSC drilling and understanding . A series of critical drilling targets were identified to address the still open questions related to the MSC event. Several proposal ideas also emerged to support the Multi-phase drilling project concept: Salt tectonics and fluids, Deep stratigraphic and crustal drilling in the Gulf of Lion (deriving from the GOLD drilling project), Deep stratigraphic and crustal drilling in the Ionian Sea, Deep Biosphere, Sapropels, and the Red Sea.

A second MagellanPlus workshop held in January 2014 in Paris (France), has proceeded a step further towards the drafting of the Multi-phase Drilling Project and a set of pre-proposals for submission to IODP.

IODP

Experimental petrology of the Shatsky Rise ocean plateau basalts

A. HUSEN, R. ALMEEV, F. HOLTZ

Institute of Mineralogy, Leibniz University of Hannover, Germany (*a.husen@mineralogie.uni-hannover.de*)

Shatsky Rise IODP Expedition 324

Among the other large igneous provinces expressed on Earth, the Shatsky Rise ocean plateau was the only one which formed during a time of geomagnetic field reversals between Late Jurassic and Early Cretaceous. Its tectonic history recorded in magnetic lineations is relatively well reconstructed (Nakanishi et al., 1999), since its original morphology was not overprinted by later tectonic processes. The Shatsky Rise has a crustal volume of 4.3 x 106 km3 and an expected crustal thickness of 30 km (Sager et al., 1999, Sano et al., 2012). Three distinct massifs (Tamu, Ori and Shirshov Massif) were consecutively formed during different stages of the Shatsky Rise evolution which is directly linked with a progression of the triple junction northeastwards. All Massifs are mostly constructed by massive flows and pillow lava basalts, with intercalated sedimentary layers. Five cores were drilled on the three massifs of the Shatsky Rise during the IODP Expedition 324, providing samples of the igneous basement. Recent post-cruise geochemical investigations (Sano et al., 2012) of fresh glass samples from four sites (U1346, U1347, U1348, U1350) revealed an existence of tholeiitic basalts broadly clustered into three geochemical magma groups - normal, low-Ti and high-K. The chemical compositions of the normal group are similar to those of N-MORB with slight depletion in HREE. The low-Ti group has slightly lower Ti, Fe, and Mn contents at a given MgO. The high-K basalts are characterized by distinctively high contents in K, Nb, and REEs, indicating that they are likely affected by enriched source mantle components (Sano et al., 2012).

Objectives of This Study

Our project was focused on the petrography of the natural basalts and how those basaltic lavas were formed within the thick oceanic crust. We analyzed the natural minerals and glasses of the Shatsky basalts and investigated the differentiation mechanisms under different conditions. The project consisted of two main parts. At first, we investigated the characteristics of the natural samples from the core U1347A and used thermodynamic modeling to estimate the conditions, at which the basaltic magmas were stored and differentiated. In a second experimental part, we conducted crystallization experiments using the Shatsky Rise basaltic compositions, which provided detailed information on the influence of pressure, temperature and water content on the mineral stabilities and residual liquid evolution.

Petrography and Thermobarometry

The main results of petrographical study and the thermodynamic modeling are summarized in Husen et al. (2013). We demonstrate that the Shatsky Rise basalts are tholeiitic basalts within the array of natural East Pacific Rise mid ocean ridge basalts (EPR MORBs) having typically low melt volatile contents (H_2O: 0.18-0.6 wt%). However, they are extremely low in Na_2O (and SiO_2) and high in FeO, which indicates deep melt generation by high amounts of partial melting. Also the high Ca_8/Al_8 (back calculated values to 8wt% MgO after Niu & Batiza (1991)) supports the assumption of high degree of partial melting. The detailed study of the core samples from Site U1347 led to the discrimination of five groups along the profile, which correlate to the geochemical groups presented by Sano *et al.* (2012). They also correlate to the lithological profile, being bordered by sedimentary units or a change in the flow characteristics (pillow lavas vs. massive flows). They differ in their major element chemistry, representing different degrees of differentiation. The trace element chemistry (Sano *et al.*, 2012) was used to prove the genetic relation of all U1347 lavas.

Using the COMAGMAT model (Almeev & Ariskin, 1996, Ariskin, 1999, Ariskin & Barmina, 2004) and the method described in Almeev et al. (2008) we calculated the pressures and temperatures of multiple saturation (olivine+plagioclase+clinopyroxene+liquid) of each glass composition. This method is based on the assumption that the quenched natural glasses and their volatile contents (measured by FTIR) represent the last stage of equilibration before eruption.

Our calculations confirmed the assumption of low pressure differentiation beneath Shatsky Rise (Expedition 324 Scientists, 2010), but also show that polybaric differentiation (crystallization in the course of magma ascent) played a role and led to the formation of the different magmatic groups. The cored profile beneath Tamu massif contains two complete cycles of (1) initial magma refill of the reservoir, (2) subsequent differentiation followed by eruption, and finally (3) magmatic inactivity (represented by sedimentary layers).

Taking into account our calculations performed for samples from the younger massifs (Ori, Site U1350 and Shirshov, Site U1346), we found evidences that there were different levels in the oceanic crust where magma differentiation might have occurred: (1) low pressure (0-250 MPa) magma reservoir below 6 km depth, and (2) a deep reservoir at 18-25 km depth (~650 MPa).

Crystallization Experiments

Starting Materials

We used three synthetic starting materials which are analogues to natural basaltic glass compositions from Tamu and Ori Massif and represent different evolutionary stages of the Shatsky Rise (yellow stars in fig.1). The most primitive starting material AH6 (8.6 wt% MgO) is based on a melt inclusion found in fresh olivines from Site U1349 (Ori Massif). This melt inclusion in the olivine Fo_{87}, is expected to be a representative of the most primitive Shatsky Rise composition. The intermediate starting material AH3 (8.0 wt% MgO) is an analogue to a glass composition from Site U1350 (Ori Massif) and resembles one of the most magnesian basaltic glasses found on Shatsky Rise. The most evolved starting composition AH5 (6.4 wt% MgO) represents one of the highest magnesian compositions found on Tamu Massif (Site U1347), where only relatively evolved compositions were recovered.

Experimental Setups

All three compositions were investigated in internally heated pressure vessels (IHPV) at the Institute of Mineralogy, Leibniz University of Hannover. Crystallization experiments were performed isothermally

and isobarically in a range of pressures and temperatures with time duration varying from 40 to 90 hours. The experimental pressures were 100, 200, 400 and 700 MPa and the temperatures ranged between 1225 and 1075°C. To obtain conditions close to the natural system, we conducted the experiments at very low H_2O concentrations. In order to investigate the effect of small amounts of H_2O, we used two different capsule designs, simulating minimum and maximum H_2O concentrations observed in natural Shatsky Rise melts. In the first set of experiments (*dry*), the H_2O concentrations were controlled at very low values (~0.1 wt%) by using C-Pt double capsules. In the second set of experiments (*hydrous*) we used AuPd capsules, which were pre-saturated with Fe to avoid Fe-loss during the experiments. In these capsules H_2O is generated during the experiments leading to H_2O contents between 0.4 and 1 wt%.

Results and their Implication for Shatsky Rise

In general, our experiments reproduced the natural phase assemblage of the Shatsky Rise basalts (olivine+plagioclase+clinopyroxene). We observed major differences in the crystallization sequence and in the phase compositions depending on the starting composition and the pressure. Higher pressures lead to higher liquidus temperatures, whereas, when compared to dry experiments (<0.15 wt% H_2O) the slightly higher H_2O concentrations (0.4-1.1 wt%H_2O) in the *hydrous* experiments, led to a strong depression of the liquidus (~20-50°C) and the stability fields of the different minerals. Thus, the addition of H_2O has a major influence on the direction of the isobaric differentiation trends (Liquid Lines of Descent, LLDs).

In the most magnesian starting material AH6, olivine and plagioclase were the first phases which crystallized, followed by clinopyroxene. The stability of clinopyroxene showed a strong dependence on the experimental pressure. Higher pressures lead to earlier crystallization (at higher temperatures) of clinopyroxene. This explains why clinopyroxene was on the liquidus at 700 MPa in the intermediate starting material (AH3). At 400 MPa, olivine was the liquidus phase, and at the lower pressures (200, 100 MPa) olivine and plagioclase crystallized first. In the most evolved starting material (AH5) clinopyroxene was on the liquidus at all pressures, followed by plagioclase and late olivine crystallization close to the liquidus. Additionally, only in the *hydrous* experiments, we observed crystallization of a spinel in the most magnesian starting material (AH6) (200MPa, first 10% of crystallization). Magnetite was also stable in the two less evolved starting materials (AH6, AH3) during the very late differentiation stages (>60% crystal fraction) under *hydrous* conditions.

As shown in figure 1, there is a correlation between pressure and clinopyroxene liquidus temperature. Pressure favors the early appearance of clinopyroxene and affects the direction of isobaric LLDs, especially in CaO/Al_2O_3 ratio. Elevated pressures caused lower CaO/Al_2O_3 for given MgO content in the two less evolved starting compositions (AH6, AH3), due to earlier CaO extraction from the melt by clinopyroxene crystallization. Increased H_2O concentrations had a similar effect on the LLDs, because the plagioclase liquidus is most efficiently suppressed by H_2O (Danyushevsky, 2001, Almeev *et al.*, 2012), resulting in later Al_2O_3 extraction by plagioclase.

The comparison of the experimental and natural Shatsky Rise glasses (fig. 1) demonstrate that the natural glass compositions cannot be reproduced at 700 MPa using intermediate AH3 as a starting composition. Depending on the H_2O content, the natural differentiation trend can be reproduced at 200 MPa and *dry* or 100 MPa and *hydrous* conditions. In addition, using the most primitive composition (AH6), the range of natural Shatsky Rise basalts cannot be reproduced isobarically, because the less evolved compositions from Ori Massif (U1350) can only be reproduced at higher pressures (700 or 400 MPa depending on melt H_2O). In contrast, the evolved compositions from Ori and Tamu Massif (U1350, U1247) can be reproduced at lower pressures (200-400 MPa and 100-200 MPa for *dry* and *hydrous* experiments respectively). Regarding the most evolved starting material, the experimental glasses were all in the field of the natural Shatsky Rise basalts.

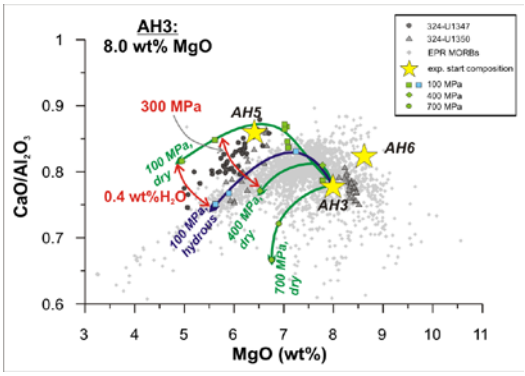

Figure 1: Selected "dry" (green arrows) and "hydrous" (blue arrow) LLDs experimentally produced at different pressures using the intermediate starting composition (AH3, 8 wt%MgO; all starting compositions are marked by yellow stars). EPR MORBs (grey diamonds) and Shatsky Rise basaltic glasses (grey dots and crosses) are shown for comparison.
The diagram illustrates the effect of pressure and small amounts of H2O (0.4 wt%) on multiple saturated basaltic liquid compositions.

It should be noted, that those compositions recovered at Tamu Massif (U1347) have slightly higher CaO/Al_2O_3 ratios, which were reproduced mainly by the low pressure (100, 200 MPa) experiments, whereas the higher pressures (400 MPa) led to experimental glass compositions close to those of Ori Massif (U1350).

Conclusions

The glass compositions of the samples from Site U1347 and U1350 follow typical MORB-type tholeiitic LLDs in the range of EPR MORBs, but they are distinctively lower in Na_2O and SiO_2, and higher in FeO as well as in CaO/Al_2O_3. Along the profile of core U1347A (Tamu massif), distinct groups of basalts with different geochemical characteristics were found. The results of geothermobarometry show that the Tamu Massif magmas were stored at relatively low pressures (1 atm-200 MPa), and that the different groups resemble polybaric differentiation of individual magma batches at different evolutionary stages of Tamu Massif. Also we found evidence that the magma plumbing system beneath Shatsky Rise is characterized by magma storage in different crustal levels (>6km and 18-25 km).

The experimental results support the assumption of low pressure fractionation beneath Tamu Massif leading to the more evolved basaltic glass compositions from Sites U1347 and U1350. In a more detailed view, it was observed that the formation conditions of Tamu and Ori Massif are slightly different, which correlates with the thermobarometry. Referring to the melt inclusion based starting material (AH6), which was expected to be representative for the parental melt of the Shatsky Rise lavas, the assumption of a multi level magma plumbing system was supported.

As displayed in figure 1, our crystallization experiments demonstrate the very strong effect of even small amounts of H_2O in magmatic liquids. In addition to pressure, the presence of small amounts of magmatic H_2O is responsible for the chemical evolution of residual liquids. Our experiments show that the addition of only 0.4 wt% of H_2O leads to the same decrease of the CaO/Al_2O_3 ratio which would be caused by a pressure increase from 100 MPa to ~300 MPa (corresponding to ~6 km difference in depth in the crust) at dry conditions. Thus, the effect of small amounts of H_2O needs to be accounted in geobarometric calculations of nominally "dry" MORB magmas.

References:

Almeev, R., Holtz, F., Koepke, J., Haase, K. & Devey, C. (2008). Depths of partial crystallization of H_2O-bearing MORB: Phase equilibria simulations of basalts at the MAR near Ascension Island (7-11 degrees S). *Journal of Petrology* 49, 25-45.

Almeev, R. R. & Ariskin, A. A. (1996). Mineral-melt equilibria in a hydrous basaltic system: Computer modeling. *Geokhimiya*, 624-636.

Almeev, R. R., Holtz, F., Koepke, J. & Parat, F. (2012). Experimental calibration of the effect of H_2O on plagioclase crystallization in basaltic melt at 200 MPa. *American Mineralogist* 97, 1234-1240.

Ariskin, A. A. (1999). Phase equilibria modeling in igneous petrology: use of COMAGMAT model for simulating fractionation of ferro-basaltic magmas and the genesis of high-alumina basalt. *Journal of Volcanology and Geothermal Research* 90, 115-162.

Ariskin, A. A. & Barmina, G. S. (2004). COMAGMAT: Development of a magma crystallization model and its petrological Applications. *Geochemistry International* 42, S1-+.

Danyushevsky, L. V. (2001). The effect of small amounts of H_2O crystallisation of mid-ocean ridge and backarc basin magmas. *Journal of Volcanology and Geothermal Research* 110, 265-280.

Expedition 324 Scientists (2010). "Testing plume and plate models of ocean plateau formation at Shatsky Rise, northwest Pacific Ocean." IODP Prel. Rept, 324.

Husen, A., Almeev, R. R., Holtz, F., Koepke, J., Sano, T. & Mengel, K. (2013). Geothermobarometry of basaltic glasses from the Tamu Massif, Shatsky Rise oceanic plateau. *Geochemistry, Geophysics, Geosystems* 14, 3908–3928.

Nakanishi, M., Sager, W. W. & Klaus, A. (1999). Magnetic lineations within Shatsky Rise, northwest Pacific Ocean: Implications for hot spot-triple junction interaction and oceanic plateau formation. *J. Geophys. Res.* 104, 7539-7556.

Niu, Y. L. & Batiza, R. (1991). An empirical method for calculating melt compositions produced beneath midocean ridges – Application for axis and off-axis (seamounts) melting. *Journal of Geophysical Research-Solid Earth* 96, 21753-21777.

Sager, W. W., Kim, J., Klaus, A., Nakanishi, M. & Khankishieva, L. M. (1999). Bathymetry of Shatsky Rise, northwest Pacific Ocean: Implications for ocean plateau development at a triple junction. *J. Geophys. Res.* 104, 7557-7576.

Sano, T., Shimizu, K., Ishikawa, A., Senda, R., Chang, Q., Kimura, J. I., Widdowson, M. & Sager, W. W. (2012). Variety and origin of magmas on Shatsky Rise, northwest Pacific Ocean. *Geochemistry Geophysics Geosystems* 13, 25.

IODP

Controlling factors of Ca isotope fractionation in Porites corals evaluated by temperature, pH and light controlling culture experiments

M. INOUE[1,2], N. GUSSONE[1], Y. KOGA[3], A. IWASE[3], A. SUZUKI[4], K. SAKAI[3], H. KAWAHATA [2]

[1] Institut für Mineralogie, Corrensstr. 24, 48149 Münster
[2]Ocean Research Institute, The University of Tokyo, 1-15-1 Minamidai, Nakano, Tokyo 164-8639, Japan
[3]Sesoko Station, Tropical Biosphere Research Center, University of the Ryukyus, 3422 Sesoko, Motobu, Okinawa 905-0227, Japan
[4]Geological Survey of Japan, National Institute of Advanced Industrial Science and Technology (AIST), 1-1-1 Higashi Tsukuba, AIST Tsukuba Central 7, Ibaraki 305-8567, Japan

Geochemical tracers such as $\delta^{18}O$ and Sr/Ca ratios in the skeleton of massive *Porites* coral have been well known as environmental proxies for sea surface temperature and/or salinity changes through time. For instance, paleoclimate during the last glacial termination has been reconstructed using fossil *Porites* corals collected from Tahiti by IODP Exp. 310 (e.g., Felis et al., 2012). On the other hand, knowing the mechanism of skeletal growth of *Porites* coral is crucial for the use of geochemical tracers as precise environmental proxies. Furthermore, to understand the controlling factors responsible for calcium isotope fractionation in marine calcifying organisms including scleractinian corals is critical to investigate the past evolution of Ca^{2+} concentrations in the ocean precisely. In this study, we cultured multiple colonies of *Porites* coral under temperature, pH and light controlled environments and investigated the relationship between $\delta^{44}Ca$ in skeleton grown during the cultured period and each environmental parameters. Variation of fractionation pattern of $\delta^{44}Ca$ in skeleton of different colonies growing under different environments would reveal information to understand coral biomineralization.

Culture experiments on *Porites* coral have been conducted at Sesoko Station, Tropical Biosphere Research Center, University of the Ryukyus, Okinawa, Japan. Temperature and pH controlled experiments were conducted inside for 6 and 3 months, respectively and settings of water temperature and pH were, 21, 23, 25, 27, 29˚C and 7.4, 7.6, 8.0, respectively. The light experiment was conducted in an outdoor tank of Sesoko Station for 18 months and light levels were maintained with high, middle and dark adjusted by partial shading with a sun-screen mesh. For temperature, pH and light experiments 3, 2 and 1 parallel colonies were analysed, respectively. Skeletal samples grown during the culture experiment, mostly < 1 mm from the surface of each colony, were taken after the experiments by micro-milling. For isotope measurements, 300-400 ng Ca were loaded on Re-single filaments with a tantalum activator after addition of a ^{42}Ca-^{43}Ca double spike. Calcium isotope ratios were determined on a Finnigan TRITON TI TIMS follwing the method described in Gussone et al. (2011). The isotope values are expressed relative to NIST SRM 915a as $\delta^{44}Ca=(({}^{44}Ca/{}^{40}Ca)_{sample}/({}^{44}Ca/{}^{40}Ca)_{SRM915a}$ -1) x 1000.

As a result of culture experiments, skeletal growth rate varied with the variation of each environmental parameter,

typically higher growth rate at higher temperature, pH and light conditions with a colony-specific variation especially in the temperature experiment. However, $\delta^{44}Ca$ showed negligible variation related to these variations of growth rate generated by differences of pH and light level, indicating that there are little or no relationships between pH and light and $\delta^{44}Ca$ in *Porites* coral. On the other hand, the temperature dependence of isotope fractionation of 0.02 ‰/°C which is similar to inorganic aragonite was found in this study, but the degree of isotope fractionation is about +0.4 ‰ offset in corals. The simple calculation based on the previously reported value of -1.0 ~ -2.0 ‰ fractionation during the function of Ca channels results in about 78% on average of Ca^{2+} used for the skeleton is that transported via paracellular pathways. Due to such coral-specific biomineralization processes, the overall mean $\delta^{44}Ca$ of scleractinian corals including results from previous studies are different from other biogenic aragonites like screlosponges and pteropods, which resemble inorganic aragonite. Apparently, coral Ca isotope ratios are more similar to those of calcitic coccolithophores. These results are important in order to investigate the evolution of Ca isotope in seawater during the Phanerozoic, as corals contribute significantly to the Ca export production. Indeed, as calcium isotope data of the dominant reef coral *Porites* spp. have been very limited, the present data of coral skeleton based on precise culture experiments contributes to the better understanding of their biomineralization and to define the average isotope composition of the the oceanic Ca sink.

References:

Felis, T., Merkel, U., Asami, R., et al. (2012) Pronounced interannual variability in tropical South Pacific temperatures during Heinrich Stadial 1. Nat. Commun. 3:965, doi: 10.1038/ncomms1973.

Gussone, N., Nehrke, G., Teichert, B.M.A. (2011) Calcium isotope fractionation in ikaite and vaterite. Chem. Geol. 285, 194–202.

IODP

The impact of the Latest Danian Event on planktic foraminifera faunas at ODP Site 1210 (Shatsky Rise, Pacific Ocean)

SOFIE JEHLE[1], ANDRÉ BORNEMANN[1], ARNE DEPREZ[2], ROBERT P. SPEIJER[2]

[1] Institut für Geophysik und Geologie, Universität Leipzig

[2] Department of Earth and Environmental Sciences, KU Leuven, Belgium

During the early Palaeogene global warmth several potential short-term climate events (<200 ky) have been documented over the last two decades. Paleocene events, bracketed by the Cretacous/Paleogene boundary (66 Ma) and the Paleocene-Eocene thermal maximum (PETM, 56 Ma) are the Dan-C2 Event (65.2 Ma ago, Quillevere et al., 2008)), the Latest Danian Event (LDE) or Top Chron 27n Event (61.75 Ma, e.g. Bornemann et al., 2009, Westerhold et al., 2011), and the Mid-Palaeocene Biotic Event (58.9 Ma, e.g. Bernaola et al., 2007; Petrizzo, 2005). The LDE is characterized by a prominent negative carbon isotope excursion (CIE) of <2‰ in different marine settings like the southern Tethyan shelf (Egypt, Bornemann et al., 2009), the western North Atlantic (Zumaia, Spain, Dinarès-Turell et al., 2010) and the Peri-Tethys (Bjala, Bulgaria, Dinares-Turell et al., 2012) Moreover, the LDE is characterized by the most negative $\delta^{13}C$ values for the entire Paleocene, thus, representing an extreme position in the secular changes of the global carbon cycle (Westerhold et al., 2011). In various ODP cores this event is marked by two prominent peaks in Fe intensities based on XRF core scanning and magnetic susceptibility. It correlates stratigraphically with an increase of both oceanic spreading rates and volcanic activity along the SE Greenland margin (Westerhold et al., 2008). Due to the supra-regional nature of the LDE and the associated paleoenvironmental changes that resemble those of the PETM (Bornemann et al., 2009) it has been hypothesized that the LDE may represent an additional Paleocene hyperthermal. So far, there are no detailed faunal data available for the LDE from the deep-sea. Here we present the first high-resolution planktic foraminiferal faunal data across this event from ODP Site 1210 (Shatsky Rise).

Shatsky Rise Plateau is a large igneous province that is situated on a triple-junction in the Pacific Ocean, formed between the Late Jurassic and the Early Cretaceous (149 Ma – 135 Ma, Sager, 2005). Drilled sedimentary successions are up to 1000 m thick representing a remarkable long-term record of Cretaceous to Neogene age. Site 1210 was drilled in a water depth of 2573 mbsl in the southern part of the Plateau. Paleodepth has been estimated as upper abyssal to lower bathyal based on benthic foraminiferal faunas. High carbonate values above 82 wt% suggest a deposition well above the calcite compensation depth during the Palaeocene (Bralower et al., 2002). The latest Danian is made up by homogeneous carbonate ooze, usually coloured in bright pale beige. Two prominent dark brown horizons are intercalated into this monotonous sequence that represent the “Latest Danian Event” (233.4–234.6 rmcd) as indicated by stratigraphic correlation with other ODP sites based on Fe XRF core scanning and magnetic susceptibility data (Westerhold et al., 2008).

The study interval covers about five metres of core (231.2–236.6 rmcd) that represent ~800 ky according to cyclostratigraphy (Westerhold et al., 2008). From this interval 73 samples, collected at a resolution of 2 to 15 cm steps, have been investigated for this study for $\delta^{13}C$ and $\delta^{18}O$ of planktic foraminifera calcite, calcium carbonate content, planktic foraminifera assemblages, planktic/benthic foraminifera ratio and other parameters like fragmentation, coarse fraction and absolute abundances. Faunal analysis was carried out at a sieve size fraction >125 µm. The overall objectives of studying a deep-sea record of the LDE were (1) to test the hyperthermal hypothesis (e.g. Bornemann et al., 2009), by studying the entire water column to reconstruct temperature changes, and (2) to assess the biotic response to the LDE using planktic foraminifera assemblages as an example.

Preservational bias of the faunal data was assessed, besides from visual criteria, by using a combined approach covering coarse fraction, absolute abundance of planktic foraminifera, P/B-ratios, planktic foraminiferal fragmentation and diversity changes. According to this method, only slight indications for dissolution have been observed during the event horizons, however, P/B-ratios never dropped below 96.2% and fragmentation never reached values above 17%, thus, indicating only minor

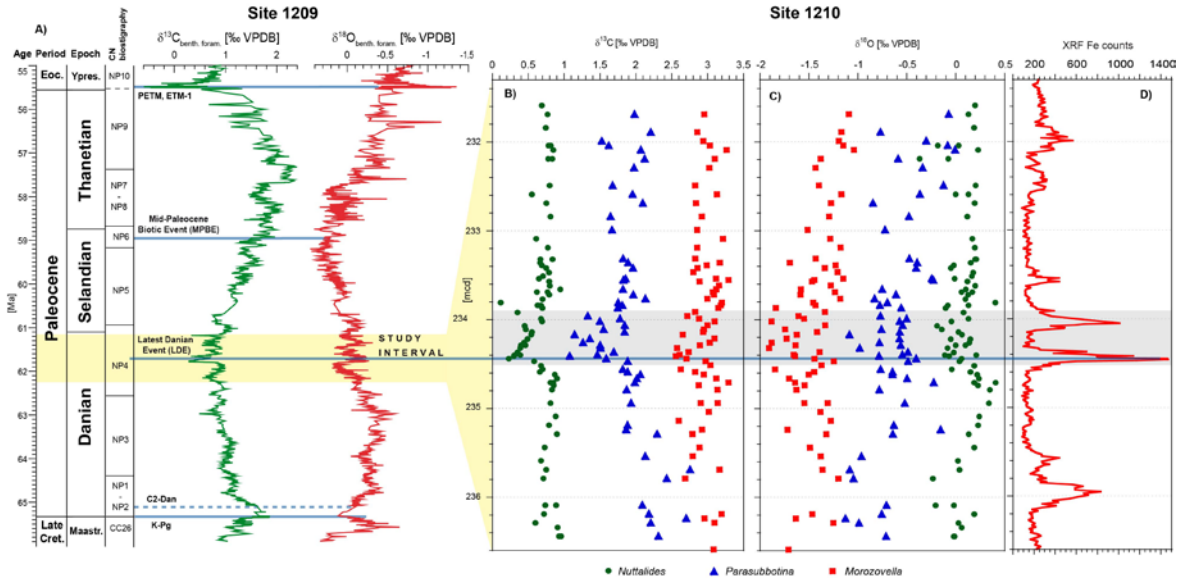

Figure 2: Stratigraphic overview of the study interval and new stable isotope results from ODP Site 1210. A) Paleocene stratigraphy with benthic foraminifera $\delta^{13}C$ and $\delta^{18}O$ of Site 1209 (Westerhold et al., 2011). B), C): $\delta^{13}C$ and $\delta^{18}O$ records for Site 1210. D) Fe XRF core scanning data (Westerhold et al., 2008). The blue line marks the main event horizon, indicated by a Fe peak and a negative CIE.

changes of the assemblage composition due to dissolution. However, more severe changes of the assemblages are indicated prior and after this event, probably due to enhanced recrystallization. Few samples have been removed from the faunal analysis due to a potential preservational bias of the assemblage data from the intervals below and above the LDE.

temperature changes of 3°, 2.5° and 2°C, respectively. Benthic foraminifera (Westerhold et al., 2011) of neighbouring Site 1209 show the magnitudes as observed at Site 1210. Our isotope data, specifically $´^{13}C$, suggest a higher gradient between surface and subsurface dwellers after the event, indicating a better stratified upper water column after the LDE. This difference in the offset

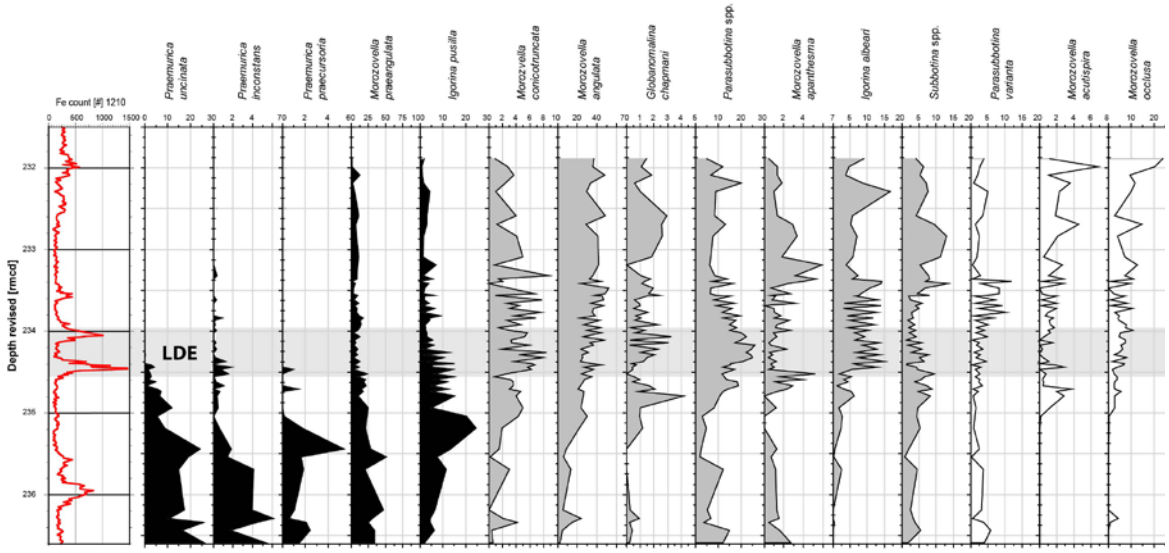

Figure 1: Relative abundance changes (percentages) of selected planktic foraminifera taxa ODP Site 1210, Fe XRF core scanning data (Westerhold et al., 2008) are used as a chemostratigraphic tool.

Planktic foraminiferal $´^{13}C$ and $´^{18}O$ of surface (*Morozovella angulata, M. praeangulata*) and subsurface dwellers (*Parasubbotina pseudobulloides, P.varianta*) show abrupt negative excursions for both isotope species of different amplitudes. $´^{13}C$ shows a drop of ~0.7‰ during LDE main peak for planktic surface dwellers, whereas subsurface ones decrease by ~0.9‰ and benthics by ~0.6‰ (Fig. 1). For surface dwelling taxa $´^{18}O$ decreases by ~0.6‰, at a subsurface position by ~0.5‰ and on the sea-floor by 0.4‰, which is interpreted as

between before and after the LDE makes 0.5‰ for $´^{13}C$ and 0.4‰ for $´^{18}O$.

Simple diversity varies between 13 and 23 species per sample, Shannon diversity H' ranges from 1.64–2.47 with a mean of 2.08. The lowest diversity is found at the beginning of the second peak. Planktic foraminifera faunas (Fig. 2) are dominated by nine taxa that make up ~86% of the total assemblage. *Morozovella angulata,* being the most abundant species, is constantly rising from 2 to 40% over the study interval with peaks of 52% and a strong

increase during the LDE. *M. praeangulata* decreases from 35 to 10% in pre-event time and shows a massive break-down at the beginning of the event. The LDE might have affected these two opposite appearances in enforcing evolutionary or morphological trends or adaptation capability of the two species to environmental changes.

Praemurica uncinata was a common component of planktic foraminifera faunas (c. 26%) before the LDE, but virtually disappears exactly at the first LDE horizon. A similar trend is observed in the less abundant *P. inconstans* and *P. praecursoria*. This suggests that this taxon is strongly affected by LDE-related environmental changes leading to a severe decline of the *Praemurica* genus. The disappearance of this group at this level has previously been documented in shelf successions from Tunisia (Guasti, 2005). *Morozovella occlusa* is practically absent before the onset of the LDE as values rise >5% 15 cm below event bed for the first time. The species is suggested to be closely related to *M. angulata*. During the LDE, *M. occlusa* has its highest values in the late part of the main event phase with 10.7% and minimum at the end after which it visibly increases from 10 to 25%. Abundance of *Parasubbotina* spp. shows a belly-shaped event-phase tipping 26% with 5–10% before and after the LDE. Highest values were found between the two LDE horizons which makes them profiteers of LDE-linked oceanic changes.

Igorina albeari is the marker species for the subzone P3b and occurs throughout the entire study interval, which implies that the base of P3b is well below the LDE at Shatsky Rise – a finding that has to be confirmed at other deep-sea sites. The surface mixed-layer water inhabitant *I. albeari* starts with 0.2–6%, to rise with the onset of the LDE to 14.8%. *I. pusilla* mainly peaks at 24.5% during pre-event phase to decrease with the onset of the LDE. Having strong oscillations like *I. albeari,* values rapidly go down from 15 to around 2% and disappears only shortly later, comparable in its course to *M. praeangulata.*

In conclusion, the entire water column has been warmed up by about 2-3°C during the LDE at Shatsky Rise, supporting the idea that this event is characterized by a temperature rise, albeit that the observed temperature rise is only slightly higher than the temperature changes observed on the bottom and the top of the studied interval. Only minor dissolution is apparent from the studied samples. We also observed major changes in the faunal assemblages specifically in photosymbiont-bearing taxa like *Praemurica* and *Morozovella*. A gradient between surface and subsurface dwellers in isotope measurements points to enhanced stratification of the upper water column in post-LDE times. Multivariate statistics indicate rather distinct faunal communities before, during and after the event, suggesting significant influence of temperature rise and accompanied oceanographic changes.

References:

Bernaola, G., Baceta, J.I., Orue-Etxebarria, X., Alegret, L., Martin-Rubio, M., Arostegui, J., Dinares-Turell, J., 2007. Evidence of an abrupt environmental disruption during the mid-Paleocene biotic event (Zumaia section, western Pyrenees). Geol. Soc. Am. Bull. 119, 785-795.

Bornemann, A., Schulte, P., Sprong, J., Steurbaut, E., Youssef, M., Speijer, R.P., 2009. Latest Danian carbon isotope anomaly and associated environmental change in the southern Tethys (Nile Basin, Egypt). J. Geol. Soc. 166, 1135-1142.

Bralower, T.J., Premoli Silva, I., Malone, M.J., al., e., 2002. Leg 198 summary. Proc. ODP Init. Reports 198, 1–148.

Dinares-Turell, J., Pujalte, V., Stoykova, K., Baceta, J.I., Ivanov, M., 2012. The Palaeocene "top chron C27n" transient greenhouse episode: evidence from marine pelagic Atlantic and peri-Tethyan sections. Terra Nova 24, 477-486.

Dinarès-Turell, J., Stoykova, K., Baceta, J.I., Ivanov, M., Pujalte, V., 2010. High-resolution intra- and interbasinal correlation of the Danian-Selandian transition (Early Paleocene): The Bjala section (Bulgaria) and the Selandian GSSP at Zumaia (Spain). Palaeogeogr. Palaeoclimatol. Palaeoecol. 297, 511-533.

Guasti, E., 2005. Early Paleogene environmental turnover in the southern Tethys as recorded by foraminiferal and organic-walled dinoflagellate cyst assemblages, Fachbereich Geowissenschaften. Univ. Bremen, 203 p. [PhD thesis].

Petrizzo, M.R., 2005. An early late Paleocene event on Shatsky Rise, northwest Pacific Ocean (ODP Leg 198): Evidence from planktonic foraminiferal assemblages. Proc. Ocean Drill. Program Sci. Res. 198, doi:10.2973/odp.proc.sr.2198.2102.2005.

Quillévéré, F., Norris, R.D., Kroon, D., Wilson, P.A., 2008. Transient ocean warming and shifts in carbon reservoirs during the early Danian. Earth Planet. Sci. Lett. 265, 600-615.

Sager, W.W., 2005. What built Shatsky Rise, a mantle plume or ridge tectonics? Geol. Soc. Am. Spec. Pap. 388, 721-733.

Westerhold, T., Röhl, U., Donner, B., McCarren, H.K., Zachos, J.C., 2011. A complete high-resolution Paleocene benthic stable isotope record for the central Pacific (ODP Site 1209). Paleoceanography 26, doi:10.1029/2010PA002092.

Westerhold, T., Röhl, U., Raffi, I., Fornaciari, E., Monechi, S., Reale, V., Bowles, J., Evans, H.F., 2008. Astronomical calibration of the Paleocene time. Palaeogeogr. Palaeoclimatol. Palaeoecol. 257, 377-403.

IODP

Causes of Neogene intensification of the Benguela Upwelling

G.JUNG[1], M. PRANGE[1,2], M. SCHULZLIC[1,2]

[1] MARUM - Center for Marine Environmental Sciences, University of Bremen, 28334 Bremen
[2] Faculty of Geosciences, University of Bremen, 28334 Bremen

Coastal upwelling off the West coast of southern Africa has, according to proxy evidence, progressively intensified during the past 12 million years. Contrasting hypotheses on the cause of this long-term change during the Miocene-Pliocene epoch have been proposed. These range from increasing Antarctic glaciation and global cooling to the northward movement of the African continent, and the closing of the Central American isthmus.

Geological evidence also suggests phases of major uplift in the East African Rift system as well as in South and South-West Africa during the Late Miocene and Pliocene but their potential climatic impact remains to be quantified.

We performed sensitivity experiments with the Community Climate System Model Version 3 (CCSM3) to test the effect of regional uplift of East and South Africa (in combination and separately) on the atmospheric and ocean circulation. The model is run with a resolution of T85 (~1.4°) for the atmosphere and land surface and a variable resolution for the computation of ocean and sea ice down to a meridional grid spacing of 0.3° around the equator.

The model results for South and East African uplift clearly indicate a strengthening of the low-level southerly Benguela jet along the southwestern African coast due to mountain uplift from half to full present-day altitude. This induces increased Ekman pumping and upwelling in the Benguela region. Consequently simulated temperature regionally decreases by up to 3.5°C in the surface ocean. The sensitivity runs show that only considering uplift of South-West Africa can not explain the entire magnitude of change, which indicates that also East African topography impacts upwelling intensity in the Benguela region.

Finally we analyzed two other model experiments regarding alternative hypotheses of 1) the closure of the Panama Isthmus and 2) Antarctic glaciation. The results indicate a minor impact of these processes on the strength of Benguela upwelling. We therefore conclude, that African uplift played a key role in strengthening the Benguela upwelling system during the late Neogene.

IODP

Putting age into the equation: A new look at microbial distribution in subseafloor sediments

J. KALLMEYER[1]

[1] GFZ German Research Centre for Geosciences, Section 4.5 Geomicrobiology, Telegrafenberg, 14473 Potsdam, Germany, kallm@gfz-potsdam.de

At any given depth cell abundance in subseafloor sediments varies by up to six orders of magnitude between sites. To a large extend this variability correlates with mean sedimentation rate and distance from land. This relationship can therefore be used to predict subseafloor cell abundance (Kallmeyer et al., 2013).

Usually, decrease in subseafloor microbial abundance at each site can be described by a logarithmic function. However, at some sites, e.g. IODP Exp. 320, Site U1334 from the equatorial Pacific Ocean, cell distribution strongly deviates from this trend and cannot be described by a simple equation.

In order to better understand why cell distribution at some sites exhibits such unusual patterns it is necessary to take a closer look at sedimentation rates and therefore sediment ages as well. The sites that were drilled by IODP Exp. 320 and 321 recovered a continuous Cenozoic record of the paleoequatorial Pacific by coring above the paleoposition of the highly productive equatorial upwelling zone at successive crustal ages on the Pacific plate (Pälike et al., 2010).

Although some of the unusual cell distribution is caused by strong geochemical gradients and diagenetic alteration fronts, the significant differences in sedimentation rates between within and outside the upwelling zone appear to be a major cause for the strong deviations in cell abundance from the expected logarithmic decline with depth.

Subseafloor microbial communities have to subsist without fresh supply of organic matter, which becomes increasingly recalcitrant with increasing age. When assigning ages to cell count data from different oceanic regions, these cells vs. age correlation show less variability between sites than correlations vs. depth.

These observations suggest that subseafloor microbial abundance is controlled by organic matter reactivity, which is largely controlled by sediment age. Using age instead of depth models might provide important clues about the finer details of subseafloor cell abundance, especially in areas that have not fitted into previous models.

References:

Kallmeyer, J., Pockalny, R., Adhikari, R. R., Smith, D. C., & D'Hondt, S. (2012). Global distribution of microbial abundance and biomass in subseafloor sediment. Proceedings of the National Academy of Sciences of the United States of America, 109(40), 16213-16216.

Pälike, H., Lyle, M., Nishi, H., Raffi, I., Gamage, K., Klaus, A., & Scientists, E. (2010). Proceedings of the Integrated Ocean Drilling Program, 320/321 Proceedings of the Integrated Ocean Drilling Program, Vol. 320/321.

IODP

Pliocene Atlantic Ocean interhemispheric seesaw and the role of the constrictions of the Panama and the Indonesian seaways

C. KARAS[1,2,3], J.O. HERRLE[1,2], D. NÜRNBERG[3], R. TIEDEMANN[4], A. BAHR[1]

[1] Goethe-University Frankfurt, D-60438, Frankfurt, Germany
[2] Biodiversity and Climate Research Centre (BIK-F), D-60325, Frankfurt, Germany
[3] GEOMAR Helmholtz Centre for Ocean Research Kiel, D-24148 Kiel, Germany
[4] Alfred-Wegener-Institute for Polar and Marine Research, D-27568 Bremerhaven, Germany

We here study the paleoceanographic effects of the constriction of the Central American Seaway (CAS) on the North and South Atlantic Ocean during the early Pliocene. Based on paleoceanographic proxy records from either side of the Panama landbridge it was assumed that the constriction of the CAS reached a critical threshold during ~4.8-4 Ma with distinct effects on the global ocean circulation and climate. Through this tectonic closure, model simulations predicted a significant increase of the Atlantic Meridional Overturning Circulation leading to higher sea surface temperatures (SST) and sea surface salinities (SSS) of up to 7°C and 3 (psu) in the Northern Atlantic Ocean, while the entire Southern Hemisphere would experience cooling and freshening through "heat piracy" of the Northern Hemisphere. To test this "Panama hypothesis" during ~4.8-4 Ma, we selected South Atlantic DSDP Site 516A (30°17'S; 35°17'W, 1313 m water depth) and North Atlantic DSDP sites 610A (53°13'N; 18°53'W, 2417 m water depth) and 552A (56°02'N; 23°13'W, 2301 m water depth), which should have been sensitive to the proposed interhemispheric changes in SST and SSS (Fig. 1).

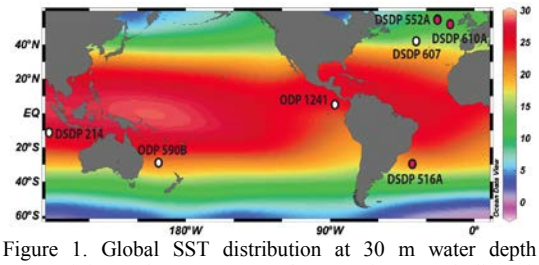

Figure 1. Global SST distribution at 30 m water depth (Locarnini et al., 2010). ODP/DSDP sites are indicated. Paleoceanographic proxy data were generated for South Atlantic DSDP Site 516A and North Atlantic sites 610A, and 552A (red).

We applied the combined measurement of Mg/Ca and $\delta^{18}O$ from planktic foraminifera *G. sacculifer* and *G. bulloides* to reconstruct (near)sea surface temperatures and to approximate (near)sea surface salinities. Our former results indicated a sea surface freshening and a distinct cooling of up to ~4°C during ~4.6-4 Ma in both South and North Atlantic oceans without any significant impact from

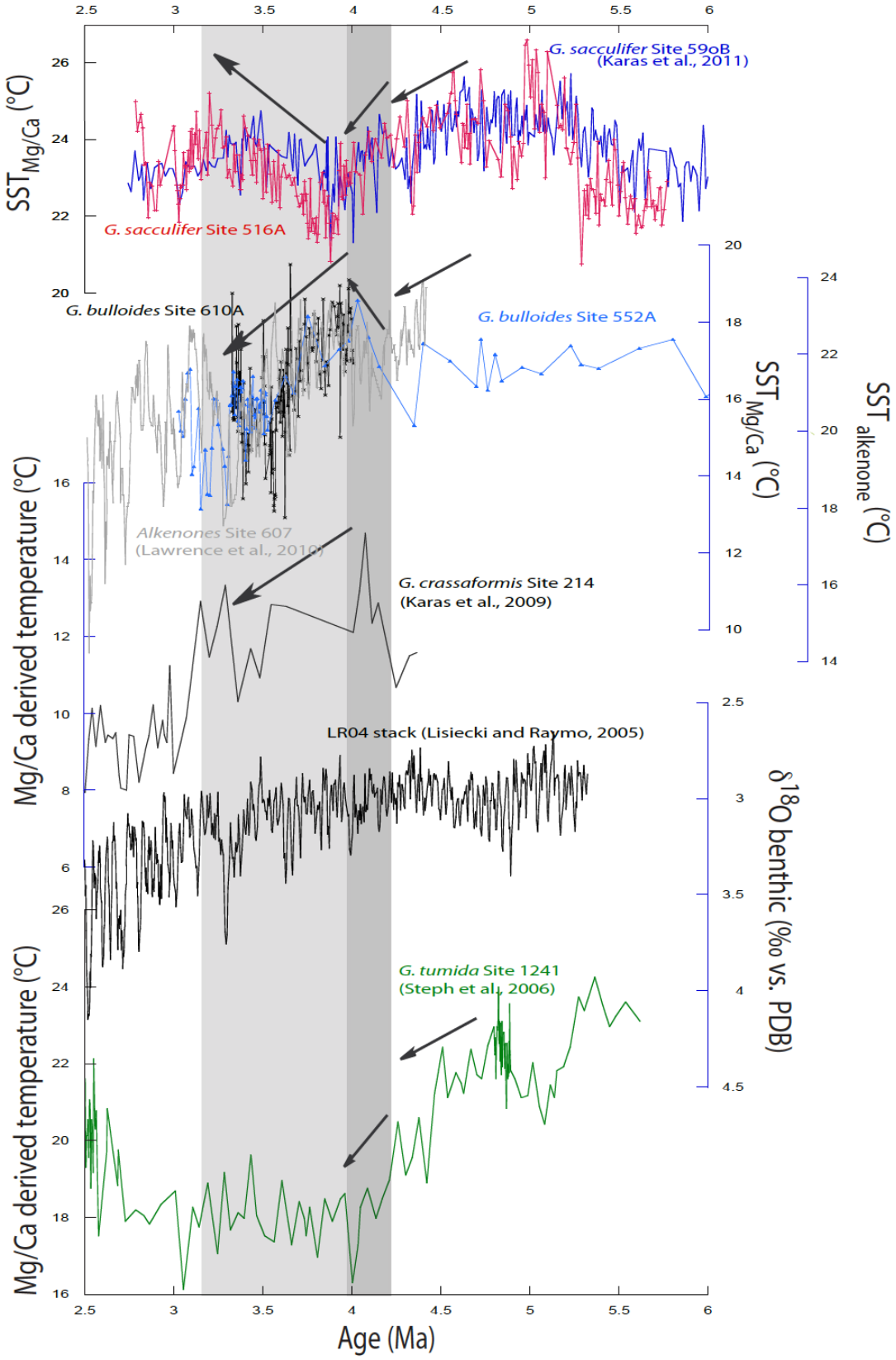

Figure 2. Pliocene paleoclimate conditions. (A) *G. sacculifer* $SST_{Mg/Ca}$ records from sites 516A (red; this study) and 590B (blue; Karas et al., 2011). (B) *G. bulloides* $SST_{Mg/Ca}$ record from Site 610A (black; this study), *G. bulloides* $SST_{Mg/Ca}$ record from Site 552A (light blue; this study), and alkenone derived SST from Site 607 (light gray; Lawrence et al., 2010). (C) *G. crassaformis* subsurface Mg/Ca derived temperatures from Site 214 (Karas et al., 2009). (D) Global benthic LR04 stack (Lisiecki and Raymo, 2005). (E) *G. tumida* subsurface Mg/Ca derived temperatures from Site 1241 (green; Steph et al., 2006). Shaded area indicate diverging North and South Atlantic SST records.

the constriction of the CAS. In combination with other SST reconstructions (LaRiviere et al., 2012), these data pointed to a global cooling of the mid-latitude oceans on both hemispheres. However, new foraminiferal Mg/Ca data from North Atlantic Site 552A and an updated age model for Site 610A modified our previous conclusions: Subsequent to a general cooling trend in both the northern and southern hemispheres during ~4.8-4.2 Ma, we observe diverging SST records since ~4.2 Ma: The North Atlantic Site 552A shows a warming of ~2°C during ~4.2-4 Ma, while the South Atlantic Site 516A shows the same amplitude of cooling. The establishing interhemispheric seesaw was most likely caused by both the strengthening of the North Atlantic Current and the related increasing formation of North Atlantic Deep Water. In this respect, the constriction of the CAS might have been crucial for the North Atlantic oceanographic and climatic development. After ~4 Ma, the SST development changed: The North Atlantic Sites 552A and 610A exhibit a distinct cooling of ~3-4°C, while the South Atlantic Site 516A indicate a warming of 2-3°C, which would contrast the conception of an ongoing constriction of the CAS.

We hypothesize that the constriction of the Indonesian Seaway, instead, might have been an active climate player by amplifying the cooling in the North Atlanic Ocean. The re-organisation of the Indonesian Throughflow (ITF) led to significant cooling and freshening of subsurface throughflow waters between 4 and 3 Ma (Karas et al., 2009), and most likely affected the upper thermocline in the E-Indian Ocean. As the ITF subsurface temperature record from Site 214 closely matches various North Atlantic SST proxy records (sites 552A, 610A, this study, Site 607, Lawrence et al., 2010), it may be speculated that the oceanographic re-organisation in line with the constriction of the Indonesian Seaway even affected the North Atlantic oceanography (Gordon, 1986; Karas et al., 2009).

References:

Gordon, A. L., 1986. Interocean exchange of thermocline water. J. Geophys. Res. 91,5037-5046.

Karas, C., Nürnberg, D., Gupta, A. K., Tiedemann, R., Mohan, K., and Bickert, T., 2009. Mid- Pliocene climate change amplified by a switch in Indonesian subsurface throughflow, Nat. Geosci., 2, 434–438, doi:10.1038/ngeo520.

Karas, C., Nürnberg, D., Tiedemann, R., Garbe-Schönberg, D., 2011. Pliocene climate change of the Southwest Pacific and the impact of ocean gateways. Earth Planet. Sci. Lett., 301, 117-124.

LaRiviere, J. P., Ravelo, A. C., Dekens, P. S., Ford, H. L., Lyle, M., Wara, M. W., 2012. Late Miocene decoupling of oceanic warmth and atmospheric carbon dioxide forcing. Nature, 486, 97-100, doi:10.1038/nature11200.

Lawrence, K.T., Sosdian, S., White, H.E., Rosenthal, Y., 2010. North Atlantic climate evolution through the Plio-Pleistocene climate transitions. Earth Planet. Sci. Lett., 300, 329-342.

Steph, S., Tiedemann, R., Groeneveld, J., Sturm, A., Nürnberg, D., 2006. Pliocene changes in tropical east Pacific upper ocean stratification: response to tropical gateways? In Proc. ODP, Sci. Results, 202 Tiedemann, R., Mix, A.C., Richter, C., Ruddiman, W.F. (Eds.) (College Station, TX 2006) pp. 1–51.

IODP

Palynomorph-based reconstructions of ecosystem and climate development on the North American Atlantic Coastal Plain between 33 and 13 million years before present

U. KOTTHOFF[1], D.R. GREENWOOD[2], F.M.G. MCCARTHY[3] K. MÜLLER-NAVARRA[1], S.P. HESSELBO[4]

[1]Institut für Geologie, Centrum für Erdsystemforschung und Nachhaltigkeit, Universität Hamburg, Bundesstraße 55, D-20146 Hamburg, Germany
[2]Department of Biology, Brandon University, 270 18th Street, Brandon, Manitoba, R7A 6A9, Canada
[3]Department of Earth Sciences, Brock University, 500 Glenridge Avenue, St. Catharines, Ontario, L2S 3A1, Canada
[4]Camborne School of Mines, College of Engineering, Mathematics and Physical Sciences, University of Exeter, Penryn Campus, Treliever Road, Penryn, Cornwall TR10 9EZ, United Kingdom

The major aims of IODP Expedition 313 were estimating rates, amplitudes, and mechanisms of sea-level change and the evaluation of sequence stratigraphic facies models that predict depositional environments, sediment compositions, and stratal geometries in response to sea-level change. Cores from three Sites (313-M0027, M0028, and M0029; 45 to 67 km off the coast) from the New Jersey shallow shelf (water depth approximately 35 m) were retrieved using an ECORD "mission-specific" jack-up platform. The recovery rate for the three sites exceeded 80%; in total, more than 1300 m core length were achieved. The oldest sediments were recovered from Hole M0027A, and dated as late Eocene/early Oligocene according to biostratigraphy, sequence-stratigraphy, and Sr-isotopy-based age estimates.

We have investigated the palynology of sediment cores from Sites M0027 and M0029, spanning 33 to 13 million years before present. Additionally, we examined a pollen assemblage from the Pleistocene. The palynological results were complemented with pollen-based quantitative climate reconstructions. Transport-related and preservational bias of the pollen assemblages was identified via analysis of the ratio of terrestrial to marine palynomorphs and of gonyaulacoid to protoperidinioid dinoflagellate cysts, and considered when interpreting palaeovegetation and palaeoclimate from the pollen data.

The palynofacies within each Miocene sequence reflects sea-level change through variation in terrigenous vs. authigenic flux. Very high ratios of terrigenous vs. marine palynomorphs are probably associated with seismic sequence boundaries. Comparison of palynomorphs-based ‘distance from shoreline’ estimates with paleodepth estimates derived from foraminiferal data allows relative sea level to be reconstructed at Sites M0027 and M0029. Milankovitch-scale periodicity is suggested for parasequences visible in thick sequences deposited in relatively deep water where substantial accommodation existed, such as during Miocene climatic optimum at Site M0029 (McCarthy et al., 2013).

The pollen data indicate that from the early Oligocene to the middle Miocene, the hinterland vegetation of the New Jersey shelf was characterized by oak-hickory forests in the lowlands and conifer-dominated vegetation in the highlands. Conifer forests expanded several times during

the Oligocene. These expansions were probably related to cooling events. The pollen-based climate data indicate an increase in annual temperatures from ~12 °C to more than 15 °C during the Oligocene (Fig. 1).

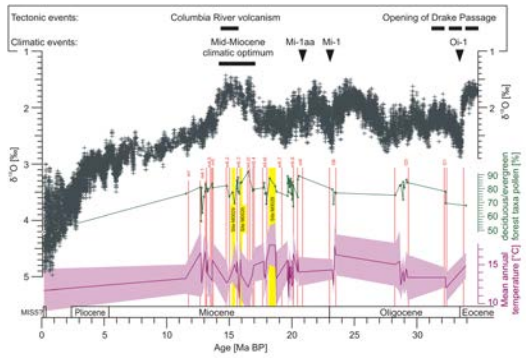

Fig. 1: Pollen-based mean annual temperature reconstruction and deciduous/evergreen forest taxa pollen percentages for Site M0027 (yellow bars mark samples from Site M0029) vs. age compared to global oxygen isotopes after Zachos et al. (2001, 2008), and global events. Age model for Eocene to Miocene samples after Browning et al. (2013), ages for sequence m4.1 are based on comparison with Site M0029. The age of the uppermost sample is based on Miller et al (2013). After Kotthoff et al. (2013).

An expansion of conifers and an annual temperature decrease from 15 °C to 12.5 °C around 23 million years before present represenst the local impact of the Mi-1 cooling event at the onset of the Miocene. Particularly low annual temperatures are also recorded for an interval around ~20 million years before present. This is probably a reflection of the Mi-1aa cooling event. Generally, Oligocene and Miocene ecosystems were similar each other in the hinterland of the New Jersey shelf. In opposite to other areas in the USA, a spread of grasslands during the Oligocene and Miocene is not evident for the hinterland of the New Jersey shelf (Kotthoff et al., 2013).

One of the most surprising findings is that the ecosystem and climate data for the hinterland of the New Jersey shelf do not show extraordinary changes during the Miocene climatic optimum at ~15 million years before present (Fig. 1), except for a minor increase in deciduous-evergreen mixed forest taxa and a decrease in swamp forest taxa. Furthermore, the carbon-isotope record (based on phytoclasts) from Site M0029 from the New Jersey shallow shelf lacks a positive excursion (as revealed in records from other regions) during this interval (Fang et al., 2013). An explanation could be that vegetation and regional climate in the hinterland of the New Jersey shelf did not react as sensitively to Miocene climate changes as other regions in North America or Europe. An additional explanation for the relatively low regional temperatures reconstructed for the Mid-Miocene climatic optimum, compared to other climate records, could be an uplift of the Appalachian Mountains during the Miocene. A Pleistocene pollen assemblage analyzed in the framework of the project derives from the Marine Isotope Chron 7 or 5e and shows vegetation and climate conditions similar to the present-day conditions in the region (Kotthoff et al. 2013).

References:

Browning, J.V., Miller, K.G., Barron, J., Katz, M.E., Kulhanek, D K., McCarthy, F.M.G., Feigenson, M.D., Olsson, R.K., Sugerman, P.J. (2013): Chronology of Eocene-Miocene sequences on the New Jersey shallow shelf: Implications for regional, interregional, and global correlations, Geosphere, 9, 1-23.

Fang, L., Bjerrum, C., Hesselbo, S.P., Kotthoff, U., McCarthy, M.F.G., Huang, B., Ditchfield, P.W. (2013): Carbon-isotope stratigraphy from terrestrial organic matter through the Monterey Event, Miocene, New Jersey margin (IODP Expedition 313). Geosphere, 9, 1303-1318.

Kotthoff, U., Greenwood, D.R., McCarthy, F.M.G., Müller-Navarra, K., Hesselbo, S.P. (2013): Vegetation and climate development on the North American Atlantic Coastal Plain from 33 to 13 million years ago (IODP Expedition 313). Climate of the Past Discussions, 9, 6551-6603.

McCarthy, F.M.G., Katz, M., Kotthoff, U., Browning, J., Miller, K., Zanatta, R., Williams, R., Drljepan, M., Hesselbo, S.P., Bjerrum, C., Mountain, G. (2013): Eustatic control of New Jersey margin architecture: palynological evidence from IODP Expedition 313, Geosphere, 9, doi:10.1130/GES00853.1.

Miller, K. G., Sugarman, P.J., Browning, J.V., Sheridan, R.E., Kulhanek, D.K., Monteverde D.H., Wehmiller, J.F., Lombardi, C., Feigenson, M.D. (2013): Pleistocene sequence stratigraphy of the shallow continental shelf, offshore New Jersey: Constraints of Integrated Ocean Drilling Program Leg 313 core holes, Geosphere, 9, 74-94, doi:10.1130/GES00795.1.

Zachos, J., Pagani, M., Sloan, L., Thomas, E., Billups, K. (2001): Trends, rhythms, and aberrations in global climate 65 Ma to present, Science, 292, 686-693, 2001.

Zachos, J.C., Dickens, G.R., Zeebe, R.E. (2008): An early Cenozoic perspective on greenhouse warming and carbon-cycle dynamics, Nature, 451, 279-283, 2008.

IODP

Drilling the centre of the Thuringian Basin, Germany, to decipher potential interrelation between shallow and deep fluid systems

N. KUKOWSKI, K. U. TOTSCHE, M. ABRATIS, A. HABISREUTHER, T. WARD AND INFLUINS DRILLING TEAM

Friedrich Schiller Universität Jena, Institut für Geowissenschaften, Burgweg 11, 07749 Jena

To shed light on the coupled dynamics of near surface and deep fluids in a sedimentary basin on various scales, ranging from the pore scale to the extent of an entire basin, is of paramount importance to understand the functioning of sedimentary basins fluid systems and therefore e.g. drinking water supply. It is also the fundamental goal of INFLUINS (INtegrated FLuid dynamics IN Sedimentary basins), a research initiative of several groups from Friedrich-Schiller University of Jena and their partners. This research association is focusing on the nearby Thuringian basin, a well confined, small intra-continental sedimentary basin in Germany, as a natural geo laboratory. In a multidisciplinary approach, embracing different fields of geophysics like seismic reflection profiling or airborne geomagnetics, structural geology, sedimentology, hydrogeology, hydrochemistry and hydrology, remote sensing, microbiology and mineralogy, among others, and including both, field-based, laboratory-based and computer-based research, an integral INFLUINS topic is the potential interaction of aquifers within the basin and at its rims. The Thuringian basin, which is composed of sedimentary rocks from the latest Paleozoic and mainly Triassic, is particularly suited to undertake such research as it is of relative small size, about 50 to 100 km, easily accessible, and quite well known from previous studies, and therefore also a perfect candidate for deep drilling.

After the acquisition of 76 km seismic reflection data in spring 2011, to get as much relevant data as possible from a deep drilling at the cross point between two seismic profiles with a limited financial budget, an optimated core sampling and measuring strategy including partial coring, borehole geophysics and pump tests as well as a drill hole design, which enables for later continuation of drilling

down to the basement, had been developed. Drilling Triassic rocks from Keuper to lower Buntsandstein was successfully realised down to a final depth of 1179 m from late June to mid-September 2013. Here, we give an introduction into the layout of INFLUINS deep drilling together with a summary of preliminary results, e.g. on the nature of the boundaries between Muschelkalk and Buntsandstein, and between upper and middle Buntsandstein, a complete core recovery of upper Buntsandstein saliniferous formations as well as unexpectedly low porosity and permeability of potential aquifers.

IODP

Multiple reverse and normal faulting along the Costa Rica erosive plate boundary – results from IODP Expedition 344 (CRISP 2)

W. KURZ[1], P. VANNUCCHI[2], Y. YAMAMOTO[3], C. MILLAN[4]

[1] Institute of Earth Sciences, University of Graz, Heinrichstrasse 26, A-8010 Graz, Austria; walter.kurz@uni-graz.at
[2] Department of Earth Sciences, Royal Holloway, University of London, Egham, Surrey TW20 OEX, United Kingdom; paola.vannucchi@rhul.ac.uk
[3] Institute for Research on Earth Evolution (IFREE), Japan Agency for Marine-Earth Science and Technology, 3173-25 Showaq-machi, Kanazawa-ku, Yokohama 236-0001, Japan; yuzuru-y@jamstec.go.jp
[4] School of Earth Sciences, Ohio State University, 275 Mendenhall Laboratory, 125 South Oval, Columbus OH 43210-1308, USA; millan.2@osu.edu

The primary objective of Integrated Ocean Drilling Program (IODP) Expedition 344 offshore the Osa Peninsula in Costa Rica was to sample and quantify the material entering the seismogenic zone of the Costarican erosive subduction margin. Fundamental to this objective is an understanding of the nature of both the subducting Cocos plate crust and of the overriding Caribbean plate. The subducting Cocos plate is investigated trying to define its hydrologic system and thermal state. The forearc structures recorded by the sediment deposited on the forearc, instead, document periods of uplift and subsidence and provide important information about the process of tectonic erosion that characterizes the Costa Rica margin.

Brittle structures within the incoming plate (sites U1381, U1414) are mineralized extensional fractures and shear fractures. The shear fractures mainly show a normal component of shear. Within the sedimentary sequence both types of fractures dip steeply (vertical to subvertical) and strike NNE-SSW. Deformation bands trend roughly ENE-WSW, sub-parallel to the trend of the Cocos ridge. Structures in the Cocos Ridge basalt mainly comprise mineralized veins at various orientations. A preferred orientation of strike directions was not observed. Some veins show straight boundaries, others are characterized by an irregular geometry. Vein mineralizations mainly consist of carbonate, quartz and pyrite. Quartz is often characterized by fibre growth of crystals perpendicular to the vein boundaries.

The top 150 m of the sediments in the prism-toe at about 2.5 km from the frontal thrust (Site U1412) are characterized by the presence of normal faults. These structures form distinct shear planes with little displacement and appear to form two conjugate sets with NW-SE and NNE-SSW trends. This reveals a sub-vertical orientation of the maximum principal stress axis, σ_1, and a sub-horizontal, ENE-WSE orientation of the minimum principal stress axis σ_3 indicating a stress regime characteristic of normal faulting. We interpret these faults as compaction-related features. As the stratigraphic age within this interval is Pleistocene, the deduced formation age of the normal faults is younger than Pleistocene. Deeper in the sediment sequence of the prism toe, fault zones are localized between 330 and 342 mbsf, and between 358 and 365 mbsf. Adjacent and within these fault zones, a well developed foliation with varying dip angles is observed.

Moving landward across the forearc, Site U1380 is located on the middle slope. There 154 fault planes were identified throughout the whole cored interval. Areas of particularly localized faulting and intense fracturing and brecciation were defined as fault zones. The brecciated domains are composed of cm- to sub-cm-sized angular fragments aligned along a preferred orientation and with polished surfaces. The lower part of Site U1380 is characterized by a downhole trend of decreasing bedding dip angles. Dip angles change from an average of 40° above 630 mbsf, to an average of 10° in the lower 100 m of the hole. The decrease of bedding dip value is not linear, but shows steps associated with brecciated zones. This interval also corresponds to a relative increased frequency of fault planes. Faults with both a normal and reverse sense of shear are common throughout the hole, equally present, and their abundance increases downhole. Strike slip faults increase in abundance downhole as well. This section also includes well consolidated/cemented sediments containing mineral veins. The veins indicate that high fluid pressure was generated just below the cemented interval.

Site U1413 is located on the upper slope of the Costa Rica forearc. Faulting-related deformation is abundant from approximately 180 mbsf to the bottom of the drilled section. Normal faulting is usually more abundant than reverse faulting. Dip angles of normal faults and reverse faults vary from subhorizontal to subvertical with a maximum dip of 75°. Both normal and reverse faults are not homogenously distributed along the entire hole. The deeper parts are additionally characterized by high-angle reverse faults with unusual steep dip angles (> 75°).

The structures within the mid- to upper slope of the Costa Rica forearc may therefore be associated with the development of an over-steepened slope margin, thrust-related anticlines, fault reactivation, structural inversion and over-printing, probably related to seamount impact. Faulting within the upper plate additionally controls the distribution of fluid seeps. Fluids released within the lower plate may migrate along the plate boundary and into the upper plate.

IODP

Magnetic fabrics and frictional behaviour of subduction zone input material from the erosive continental margin offshore Costa Rica (Costa Rica Seismogenesis Project, IODP expeditions 334 and 344)

ROBERT M. KURZAWSKI[1], MICHAEL STIPP[1], ANDRÉ NIEMEIJER[2], JENS C. GRIMMER[3], AGNES KONTNY[3], CHRISTOPHER J. SPIERS[2] AND JAN H. BEHRMANN[1]

[1]Department of Marine Geodynamics, GEOMAR Helmholtz Centre for Ocean Research Kiel, Kiel, Germany, (rkurzawski@geomar.de)
[2]HPT Laboratory, Faculty of Geosciences, Utrecht University, Utrecht, The Netherlands
[3]Institute of Applied Geosciences, Karlsruhe Institute of Technology (KIT), Karlsruhe, Germany

There are two general types of continental subduction zones which form either accretionary or erosive margins. Along accretionary margins, the forearc wedge of the overriding continental plate grows by the accretion of material tectonically detached from the downgoing oceanic plate. Along erosive margins comprising slightly more than half of the active margins worldwide, the forearc wedge of the overriding continental plate shrinks due to tectonic erosion by the downgoing oceanic plate. Two major endeavors of the International Ocean Discovery Program (IODP), the Nankai Trough Seismogenic Zone Experiment (NanTroSEIZE) and the Costa Rica Seismogenesis Project (CRISP), investigate the processes and controlling factors of deformation and seismogenesis at accretionary and erosive continental margins including the incidence of megathrust earthquakes. In our project focussing on the Costa Rica erosive margin we want to understand the material properties which promote either distributed and continuous deformation or localized and discontinuous deformation in the forearc wedge. Our results will also be compared to similar investigations on sediments from the Nankai accretionary prism.

Offshore Costa Rica, the Cocos plate is subducted towards NE beneath the Caribbean plate at the Middle America Trench. IODP expeditions 334 and 344 drilled into the shallow upper Caribbean plate at the upper slope (U1379, U1413), midslope (U1378, U1380) and the lower trench slope (U1412). Additionally, the entire sedimentary sequence covering the incoming Cocos plate as well as the uppermost part of the magmatic oceanic basement have been penetrated at two drill sites (U1381, U1414). We have experimentally deformed a set of 7 samples from these locations in a rotary shear apparatus in order to determine their frictional behavior at relatively slow sliding velocity (1-100 µm/s). Results can be compared to experiments on sample material from an adjacent drillhole (ODP legs 170 and 205, Ikari et al., 2013) and from the Nankai accretionary prism (den Hartog et al., 2012). Such experiments improve our understanding of earthquake nucleation and propagation and the influence of external parameters and material properties. For the extensive characterization of the latter we have carried out laser diffraction particle size analysis, backscattered electron imaging, electron microprobe analysis and measurements of the low-field anisotropy of the magnetic susceptibility (AMS). The first results of our study will be presented under consideration of various shipboard data including density and porosity measurements.

Methods

Thirty-one IODP samples recovered from NanTroSEIZE (Exp 315, 316, 333, 338) and CRISP (Exp 344) expeditions were selected to investigate the AMS in a low magnetic field of 300 Am^{-1}. The AMS reveals the crystallographic preferred orientation (CPO) of paramagnetic minerals so that magnetic fabrics correlate to bulk CPO analysis. If ferrimagnetic minerals are absent or can be extracted from the data set, pervasive planar anisotropies like bedding and fault planes can be identified and even quantified. The method is in particular useful to study fabric development of fine-grained sediments, such as the clayey sediments sampled in NanTroSEIZE and CRISP expeditions. We have measured the AMS of 14 original CRISP samples from a depth down to 365 mbsf, 8 original NanTroSEIZE samples from a depth range of 28 to 522 m and 9 NanTroSEIZE samples experimentally deformed to variable strain conditions (Stipp et al., 2013). 15 of the 17 NanTroSEIZE samples used here were previously analyzed by synchrotron texture (=CPO) analysis (Schumann et al., subm). A comparison of the naturally compacted and experimentally deformed samples is used here to evaluate the effect of compaction and triaxial deformation on magnetic fabrics of weakly consolidated sediments. In total 126 cylindrical specimens with a diameter of 14 mm and a heigth of 12 mm were prepared from the 31 samples. Due to the lack of orientation data a part of the magnetic fabrics are only rotationally symmetric to the core axis.

The AMS was measured using a KLY-4S Kappabridge (AGICO) in a field of 300 Am^{-1} and a frequency of 875 Hz at room temperature. The SUFAR software package (AGICO) was used to calculate the principal susceptibilities with K_{min} d K_{int} d K_{max} and the mean susceptibility K_{mean}. From these values the corrected degree of anisotropy P' and the shape factor T of the AMS ellipsoid can be derived (Jelinek, 1981). The shape of the ellipsoid is oblate if $0 < T$ d 1 and prolate if -1 d $T < 0$. Primary sedimentary fabrics commonly exhibit P'-values < 1.1. Higher P′-values are characteristic for deformation fabrics. One sample exhibiting a suspiciously high mean susceptibility was tested for the presence of ferrimagnetic minerals measuring the temperature dependence of magnetic susceptibility (š (T)) between -194 and 700 °C.

Seven samples from 4 different CRISP drilling sites (U1379: upper slope, U1378: midslope, U1412: lower trench slope, U1414: incoming plate) were experimentally deformed in a hydrothermal rotary shear apparatus described by (Niemeijer et al., 2008). Remolded sample material of a grain size < 125 µm simulating a fault gouge was evenly distributed between the confining rings and the two opposing internal pistons usually resulting in an initial layer thickness of about 2 mm. Experimental conditions were defined to suitably cover the expected conditions at the CRISP updip limit of seismogenesis in approximately 5-6 km depth. Three experiments were conducted on each sample: one at room temperature and two at elevated temperatures of 70 °C and 140 °C. During tempered experiments the pore fluid pressure was held constant at 60 MPa and 120 MPa, respectively. In each experiment, the effective normal stress was increased in steps of 20 MPa from 30 MPa to 110 MPa. Shear strength and

displacement were measured with a resolution of 0.2 MPa and 0.001 mm, respectively. At each of the applied normal stresses we performed an increasing velocity stepping to determine the velocity dependence of friction, quantified by the parameter (*a-b)* = ”¼lnV (e.g. (Marone et al., 1990). After reaching a steady state shear stress level during a first shear displacement of 1-3 mm at constant sliding velocity of 10 µm/s, sliding velocity was increased from 1 to 100 µm/s in half orders of magnitude. Assuming zero cohesion, the coefficient of sliding friction ($\mu = ÄÃ_n^{eff}$) was calculated. The total displacement of a successful experiment adds up to 45 mm. Finite layer thickness was usually approximately 400 µm. The deformed sample material was impregnated with epoxy resin for later microstructural analysis.

595 °C, revealed by temperature-dependent measurement of the susceptibility (š (T)). CRISP samples show lower K_{mean}-values than samples from the Nankai Trough (Fig. 1a,b; note the logarithmic scale). Experimentally deformed samples show the highest susceptibilies (Fig. 1c). In the absence of magnetite, magnetic fabrics of the clay-rich samples are controlled by the orientation of paramagnetic sheet silicates. The orientation of the principal susceptibility axes of the ferrimagnetic samples are coaxial with the paramagnetic samples. Nankai samples predominantly show oblate fabrics (Fig. 1b). Experimentally deformed samples consistently show oblate magnetic fabrics with T-values > 0.2 and P'-values of up to 1.15. Stereographic projections of the principal susceptibility axes nicely document the reorientation of

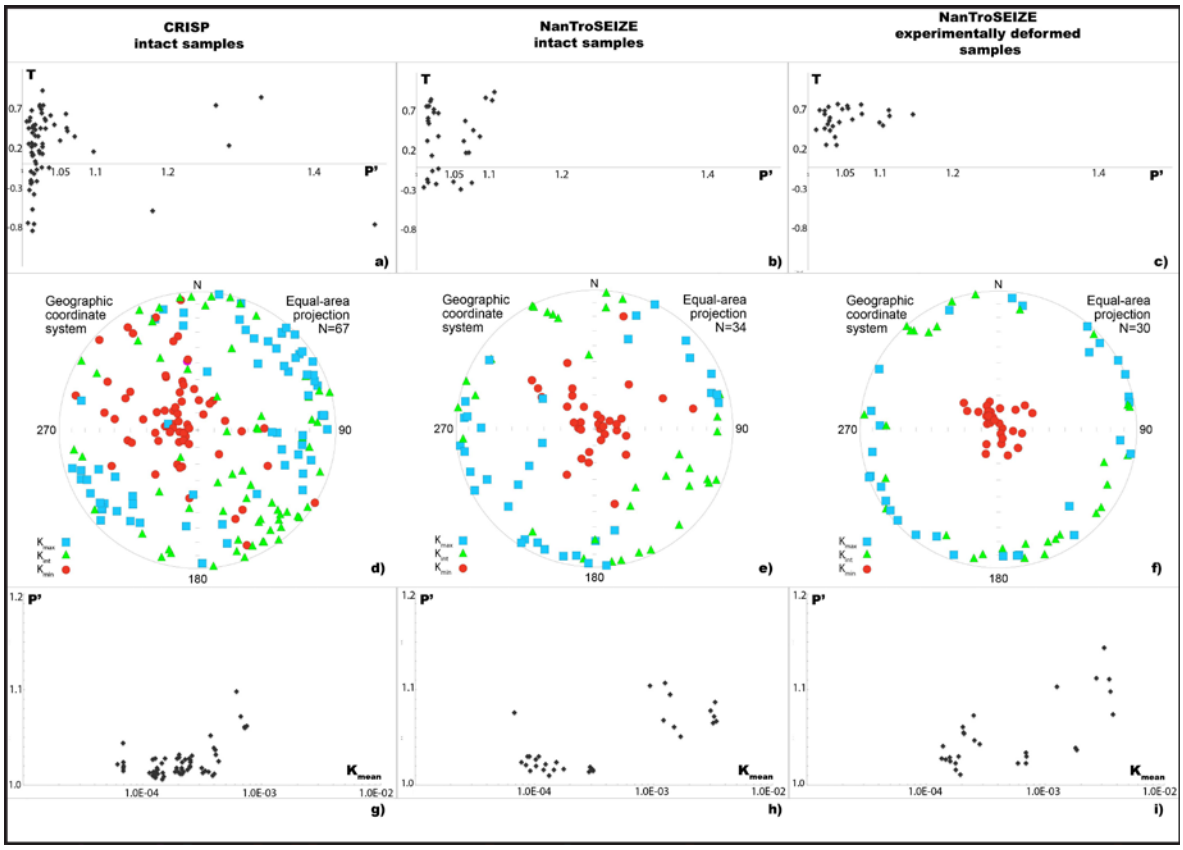

Figure 1
AMS data of Costa Rica (CRISP) and Nankai trench samples. T vs. P' plots show oblate and prolate magnetic fabrics for the CRISP samples (a) in contrast to triaxial and oblate fabrics for intact Nankai samples (b). Experimentally deformed samples exhibit stronger degrees of anisotropy and oblate magnetic fabrics (c). The formation of a new planar fabric is indicated by the reorientation of the principal susceptibility axes (f): K_{min} axes are oriented parallel to the axis of shortening. See text for further explanation.

Backscattered and secondary electron imaging was carried out using a JEOL JXA 8200 electron microprobe operated at a high Voltage of 20 kV and a low probe current of 1.4 nA in favour of a high imaging resolution. Intact CRISP samples were freeze dried and embedded in Araldite 2020 epoxy resin under vacuum to preserve the original pore space and microstructure. Ring-shaped experimental samples were cut tangentially, i.e. approximately parallel to the kinematic section.

Results

K_{mean}-values show a large variation ranging from 70 to 3700 x 10^{-6} SI units due to a heterogenous distribution of magnetite, which was identified based on a pronounced Verwey transition at -152 °C and a Curie temperature of

platy sheet silicates into an orientation perpendicular to the axis of shortening. The concentration of K_{min} axes (red dots) in the center, and K_{int} and K_{max} axes on the periphery of the diagram can be interpreted as the formation of a new subhorizontal planar fabric (foliation). In contrast to the Nankai material, samples from the CRISP area show both, oblate and prolate magnetic fabrics. The prolate fabrics occur predominantly at the lower trench slope (U1412) possibly indicating superposition of two sub-fabrics.

The frictional behaviour of the investigated CRISP samples varies distinctly with lithological differences. Frictional records of two representative samples, each deformed at room temperature and at an elevated

temperature, are exemplarily shown in Fig. 2. Sample 1414-30X7 is a nannofossil-rich calcareous ooze from the incoming plate. Consistent with a previous study (Ikari et al., 2013), frictional strength of this material is high at room temperature, where the apparent friction coefficient consistently shows values between 0.8 – 0.85 with little sensitivity to increasing stress, strain or sliding velocity (Fig. 2a). At 140 °C, however, a strong dependency on effective normal stress causes a significant weakening from values of about 0.9 at 30 MPa to 0.55 at 110 MPa. effective normal stress in excess of 70 MPa the frictional record is characterized by a slightly increasing friction coefficient towards higher normal stress, velocity strenghtening and a consistent strain hardening trend. This forearc material might enter the subduction channel by subduction erosion. Its velocity weakening behaviour at low normal stress might be important for rupture propagation at shallow levels and for earthquake nucleation at the updip end of the seismogenic zone.

The finite microstructures of the sheared sample

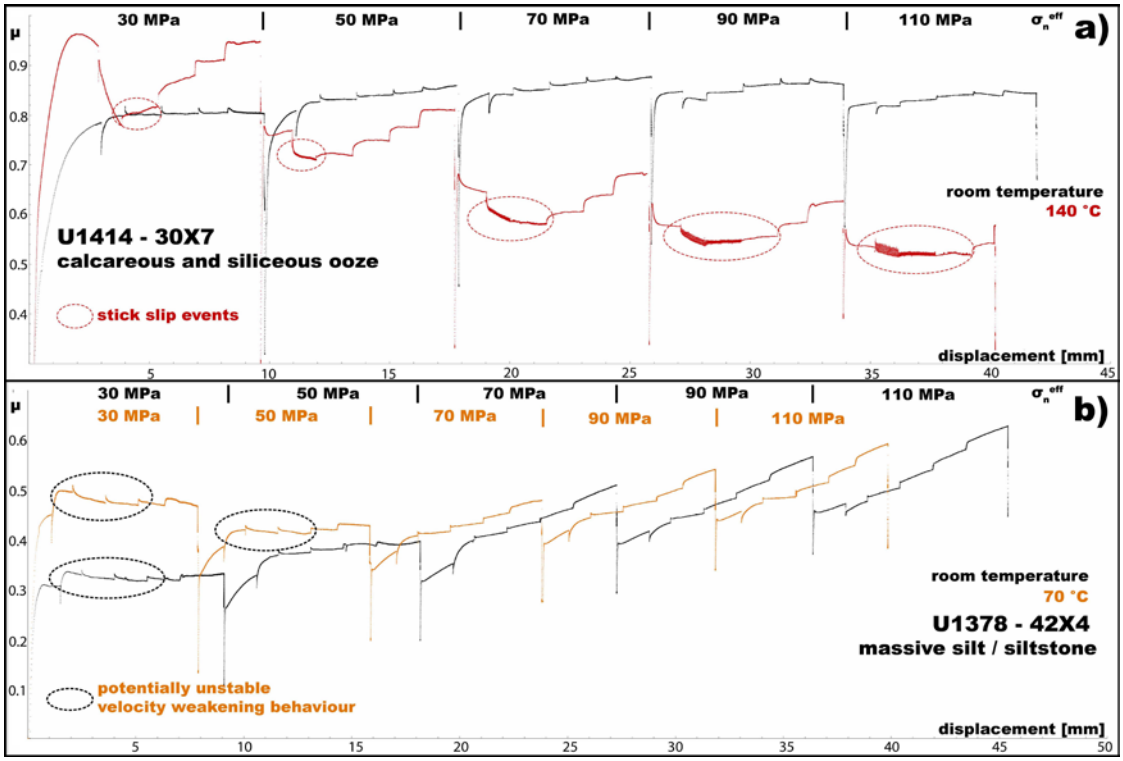

Figure 2.:
Evolution of friction with shear displacement during velocity-stepping experiments at different temperatures on (a) calcareous ooze from the incoming plate (IODP site U1414) and (b) a clayey silt from the upper plate midslope drill site (U1378). At each applied effective normal stress velocity is stepped in the following order: 10-1-3-10-30-100 µm/s. See text for further explanations.

This "normal stress weakening" is accompanied by velocity weakening at medium velocity steps and unstable slip (“stick-slip” events). Unstable slip occurs more frequently and with larger stress drop amplitudes when effective normal stress is increased. This behaviour was previously considered as a possible trigger for earthquake nucleation at low temperatures beneath 120 °C at the Middle America Trench (Ikari et al., 2013). As in the geological record the active margin off Costa Rica repeatedly changed from tectonic erosion to accretion (e.g.(Vannucchi et al., 2001) it can be assumed that this incoming plate sediment might be incorporated into the subduction channel and the seismogenic zone in the future. Indeed, similar pelagic sediments have been found in the paleo-forearc and might contribute to seismogenesis with a similar unstable behavior.

Sample U1378-42X4 is a silt/siltstone from the midslope drill site on the Caribbean plate. The friction coefficient displays intermediate values between approximately 0.3 at room temperature and 0.5 at 70 °C and 30 MPa effective normal stress (Fig. 2b). At low normal stress up to 50 MPa, the material shows potentially unstable (i.e. velocity weakening) behaviour. At higher exhibit a dense fabric and a considerably smaller grain size compared to the intact sediment cores indicating grain size reduction during deformation. A set of fractures with Riedel shear orientations demonstrates some shear localization within the clayey silts deformed at 70 °C. In contrast, at 140 °C the same material exhibits a rather homogeneous fabric indicating more distributed deformation.

References:

den Hartog, den, S.A.M., Peach, C.J., de Winter, D.A.M., Spiers, C.J., and Shimamoto, T., 2012, Journal of Structural Geology, v. 38, p. 156–171.

Ikari, M.J., Niemeijer, A.R., Spiers, C.J., Kopf, A.J., and Saffer, D.M., 2013, Experimental evidence linking slip instability with seafloor lithology and topography at the Costa Rica convergent margin: Geology, v. 41, no. 8, p.891-894.

Jelinek, V., 1981, Tectonophysics, v. 79, p. T63–T67.

Marone, C., Raleigh, C.B., and Scholz, C.H., 1990, Journal of Geophysical Research: Solid Earth, v. 95, p. 7007–7025.

Niemeijer, Spiers, Peach, 2008, Tectonophysics, v. 460, p. 16–16.

Stipp, M., Rolfs, M., Kitamura, Y., Behrmann, J.H., Schumann, K., Schulte-Kortnack, D., and Feeser, V., 2013, Geochemistry, Geophysics, Geosystems, v. 14, p. 4791–4810.

Vannucchi, P., Scholl, D.W., Meschede, M., and McDougall Reid, K., 2001, Tectonics, v. 20, p. 649–668.

IODP

Tephrochronology of lacustrine ash layers in Lake Petén Itzá sediments: Implications for regional volcanology and Central American palaeoclimate

S. KUTTEROLF[1], A. SCHWALB[2]

[1]GEOMAR Helmholtz-Zentrum für Ozeanfoschung, Kiel, Wischhofstr. 1-3, 24148 Kiel
[2]Technische Universität Braunschweig, Institut für Geosysteme und Bioindikation, Langer Kamp 19c, 38106 Braunschweig

Climate records from lacustrine systems have been established in the last years to improve our understanding of the regional and temporal expression of climate change on the continents, and how it influenced the human evolution. Lake Petén Itzá (120 m a.s.l., lake area 112 km^2, max. water depth 160 m), located in the center of the climatically sensitive Peninsula Yucatán, is a surficial closed basin lake located in the Petén District of the lowlands of northern Guatemala and has been drilled by ICDP in 2006. But one of the keys problems in interpolating and modeling past, partly linked, events in geosciences (volcanic eruptions, earthquakes, climate events, ecological crisis) into future scenarios is to establish robust chronologies larger than 40 ka since they exceed the range of ^{14}C dating. One tool to provide good age-constraints within sediments older than 40 ka is tephra layers. Both, with direct dating methods as well as correlation to well-dated deposits near their source volcanoes, ash layers in marine and lacustrine sediments can be used to develop an age model for an entire sediment sequence (e.g. Kutterolf et al. 2008a, Hodell et al. 2008, Child et al 1998, Fontaine et al. 2007). This is also true for the lake Petén Itzá sediments since numerous (#64) lacustrine tephras from the Central American volcanic arc (CAVA) have been found in the 1300 m of drilled Petén Itzá lake sediments (Mueller et al., 2010).

The Central American subduction zone is characterized by the subduction of the Cocos plate beneath the Caribbean plate. In the resulting CAVA, extending ~1400km from Guatemala in the northwest to Panama in the southeast, a number of large caldera volcanoes exist in Guatemala and El Salvador, which produced large-magnitude, widespread silicic eruptions during the Pleistocene and Holocene that could have contributed to the Petén Itzá area. Four Caldera systems in Guatemala and El Salvador have potentially produced large eruptions that had the capability to deliver their ash into the Petén area in the last 200 ka. Further back in time the tephra record is still incomplete although it is clear from field observations and older ODP/DSDSP cores offshore Central America that there have been a tremendous amount of large eruptions.

The pyroclastic sequence of the past 200 ka at Atitlán Caldera (Guatemala) comprises the W-tephra (WFT; 158±5 ka, Ar/Ar), and the deposits of the Los Chocoyos tephra (Kutterolf et al. 2008a). The ~84ka old Los Chocoyos tephra (LCY) is so far only dated indirectly from oxygen-isotope anomalies in ocean-sediment cores. With 100 and 800 km$_3$ tephra volume, respectively, W-Tephra and Los Chocoyos belong to the largest eruptions in the last 200 ka in Central America, can be traced until the Pacific and Gulf of Mexico (Kutterolf et al. 2008b), and first major element analyses indicate that they also reached the Petén Itzá area (LCY=PI and PI6, WFT=PI7). Similar the Amatilán caldera produced tephras potentially reaching the Petén Itzá region. The 191±11 ka old L-Tephra and ~50 ka old E-tephra can be traced until the Pacific (Kutterolf et al 2008b) and we correlate them preliminarily with major elements to PI 1 and PI 2, in the Petén Itzá cores. In El Salvador the Coatepeque Caldera and the Ilopango Caldera had the potential to distribute 5 tephras also over the Petén Itzá region but limited to major elements we have only be able to correlate the 72 ±5 ka old Arce tephra (ACT; PI1 and PI7) as well as the 53±3 ka old Congo tephra (CGT; PI1, PI2 and PI6) from Coatepeque Caldera to the Petén Itza cores.

The presence of lithological markers, stratigraphic boundaries and these tephra layers allowed layer-to-layer correlation between some sites and the respectively ages, yielding a first age-depth model for the entire sediment record of Lake Petén Itzá. Nevertheless, an irrevocable age model, especially in the older parts of the sequence, was not possible so far since 1) trace element analysis of the tephras, providing the best possible finger printing of tephras, have not been done, 2) tephras in the older sediment lacks in direct dating of tephras by Ar/Ar, and 3) even the 84 ka Los Chocoyos eruption has been dated so far only indirectly from oxygen-isotope anomalies in ocean-sediment cores (Rose et al. 1999). Therefore the overall goal of this project is to establish the longest paleo-record for climate proxies in Central America by building up a lacustrine tephrochronostratigraphy for Lake Petén Itzá sediment cores by inter-hole correlations and correlations to tephras from the source areas based on trace element analysis and direct dating. Next to the benefit for the paleooecology and paleoclimate the results will contribute greatly to the determination of the magnitude (eruptive volumes) and more precise eruption dates of those eruptions.

References:

Child, J.K., Begét, J.E., Werner, A., 1998. Three Holocene Tephras Identified in Lacustrine Sediment Cores from the Womder Lake Area, Denali National Park and Preserve, Alaska, U.S.A. Arctic and Alpine Research 30, 89-95.

de Fontaine, C.S., Kaufman, D.S., R. Anderson, S., Werner, A., Waythomas, C.F., Brown, T.A., 2007. Late Quaternary distal tephra-fall deposits in lacustrine sediments, Kenai Peninsula, Alaska, Quaternary Research 68, 64-78, doi.org/10.1016/j.yqres.2007.03.006.

Hodell, D.A., Anselmetti, F., Ariztegui, D., Brenner, M., Bush M. B., Correa-Metrio, A., Curtis, J.H., Escobar, J., Gilli, A., Grzesik, D.A., Guilderson, T.P., Kutterolf, S., Mueller, A.D., 2008. An 85-ka Record of Climate Change in Lowland Central America. Quatern. Sci. Rev. 27, 1152-1165.

Kutterolf, S., Freundt, A., Peréz, W., Mörz, T., Schacht, U., Wehrmann, H. and Schmincke, H.-U., 2008a. The Pacific offshore record of Plinian arc volcanism in Central America, part 1: Along-arc correlations. Geochem. Geophys. Geosyst., 9(2): doi:10.1029/2007GC001631.

Kutterolf, S., Freundt, A. and Peréz, W., 2008b. The Pacific offshore record of Plinian arc volcanism in Central America, part 2: Tephra volumes and erupted masses. Geochem. Geophys. Geosys., 9(2): doi:10.1029/2007GC001791.

Mueller, A.D., Anselmetti, F., Ariztegui, D., Brenner, M., Hodell, D.A., Curtis, J.H., Escobar, J., Gilli, A., Grzesik, D.A., Guilderson, T.P., Kutterolf, S., Plötze, M.L., Late Quaternary Palaeo-environment of Northern Guatemala: Evidence from Deep Drill Cores and Seismic Stratigraphy of Lake Petén Itzá. Sedimentology 57, 1220-1245.

Rose, W.I., Conway, F.M., Pullinger, C.R., Deino, A. and McIntosh, K., 1999. An improved age framework for late Quaternary silicic eruptions in nothern Central America. Bull. Volcanol., 61: 106-120.

ICDP

Seismic site characterization for the Deep-Fault-Drilling-Project Alpine Fault

V. LAY[1], S. BUSKE[1], A. KOVACS[2], A. GORMAN[21], E. DONNER[1]

[1]TU Bergakademie Freiberg, Institute of Geophysics and Geoinformatics, 09596 Freiberg, vera.glomb@geophysik.tu-freiberg.de
[2]University of Otago, Department of Geology, Dunedin 9054, New Zealand

The Alpine Fault in New Zealand (South Island) is one of the largest active plate-bounding continental fault zones on earth with earthquakes of magnitude 7.9 occuring every 200-400 years. Due to the surface exposure and the shallow depth of mechanical and chemical transitions it is a globally significant natural laboratory. Within the ICDP Deep-Fault-Drilling-Project Alpine Fault (DFDP-AF; https://wiki.gns.cri.nz/DFDP) a drill hole shall give insight into the geological structure of the fault zone and its evolution to understand the related deformation and earthquake processes.

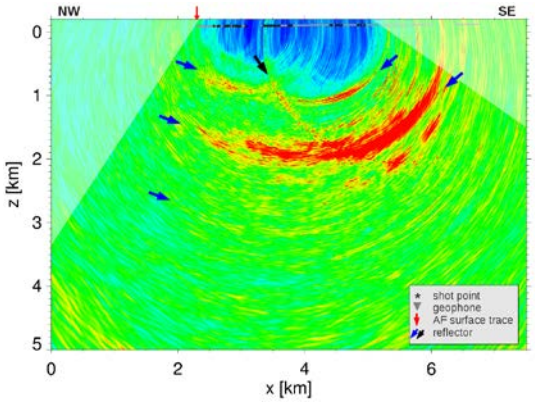

Fig. 1: Seismic reflection image obtained by Coherency-Migration.

With the help of advanced seismic imaging techniques, the shallow structure of the Alpine Fault is imaged to find the most suitable drill site location. A new seismic reflection profile has been acquired in 2011 by the WhataDUSIE project team consisting of partners from the University of Otago (New Zealand), TU Bergakademie Freiberg (Germany) and the University of Alberta (Canada). The reflection profile, located in the Whataroa river valley, has a total length of about 5 km. Up to 643 geophones with spacings between 4-8 m recorded 182 shots at approximately 100 shot point locations along the profile line.

The obtained data quality was in general very good. Nevertheless, extensive preprocessing of the data had to be performed to obtain shot gathers usable for imaging. Due to the field conditions the profile was divided into 5 parts with different features concerning geophone spacing and eigenfrequency of the geophones. To combine the single stations to one shot gather, we used overlapping geophones to derive the relative time corrections by crosscorrelating these particular traces. Additionally three Reftek 130 stations were recording continuously. By correlating the absolute Reftek time and the adjacent geophone trace we extracted the absolute shot time and applied the resulting time-shift to the corresponding traces. Finally the merged single shot gathers were further processed, including basic trace editing, bandpass filtering, trace equalization, FK-filtering and automatic gain control.

The single shot gathers already show various indicators of the Alpine Fault and the surrounding geology. Strong reflections and distorted first-arrival wavefields are clearly visible. A first arrival tomography with this data set delivered a shallow (< 1 km) macro-velocity model for migration. Beside 3D Kirchhoff prestack depth migration we also performed a focusing Cohereny-Migration. The result is shown in Fig. 1.

Beside some subhorizontal bands of high reflectivity a sharp and pronounced reflector is visible which dips at an angle of about 55 degrees to the SW. Its prolongation to the surface ends at the major mapped surface trace of the Alpine Fault, so we interpret this reflector as one branch of the Alpine Fault system at depth and correspondingly as the main drilling target.

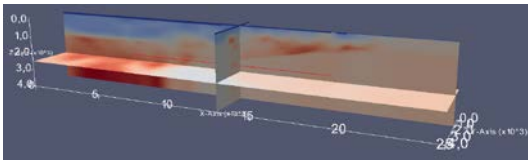

Fig. 2: 3D velocity model obtained by first arrival tomography of the Whataroa98 data set.

Further work concentrated on deriving a 3D velocity model for that region, in particular for greater depths (~ 1-3 km). For that we computed a velocity model by first arrival tomography of an older seismic reflection data set (Whataroa98) which has larger offsets of up to 25 km and therefore allows to derive velocity information for these greater depths. The result is show in Fig. 2. Currently we are merging the two obtained velocity models (for the WhataDUSIE2011 and the Whataroa98 data sets) and perform a final migration which will then enter the drill site selection process in spring 2014.

ICDP

Palaeogeographic setting of Upper Ordovician and Silurian source rocks preserved in the Siljan impact structure (central Sweden)

O. LEHNERT[1,2], G. MEINHOLD[3], U. BERNER[4], M. AHMED[5], A. ARSLAN[6], M. CALNER[2], J. O. R. EBBESTAD[7]

[1]GeoZentrum Nordbayern, Universität Erlangen, Schloßgarten 5, D-91054 Erlangen, Germany, oliver.lehnert@fau.de
[2]Department of Geology, Lund University, Sölvegatan 12, SE-223 62 Lund, Sweden
[3]Geowissenschaftliches Zentrum Göttingen (GZG), Abt. Sedimentologie/Umweltgeologie, Goldschmidtstr. 3, D-37077 Göttingen, Germany
[4]EXP BPSA PSA, Statoil ASA, Sandsliveien 90, Norway
[5]CSIRO Earth Science and Resource Engineering, 11 Julius Avenue, North Ryde, Sydney, NSW 2113, Australia
[6]Midland Valley Exploration Ltd, 144 West George Street, G22HG Glasgow, United Kingdom
[7]Museum of Evolution, Uppsala University, Norbyvägen 16, SE 752 36 Uppsala, Sweden

Exposures are very limited in the Siljan impact structure and contact relations of most units are not visible. Drill cores are the only useful tool to discover the

complex geological history of this area where the sedimentation on the Proterozoic basement started during the late Tremadocian and lasted at least until the Late Silurian with the deposition of the Orsa Sandstone (Lehnert et al. 2012, and references therein). The Siljan impact structure is a relict of a major bolide impact in the Late Devonian (e.g., Reimold et al. 2005; Jourdan et al. 2012) and has a ring-shaped depression (Siljan Ring; Juhlin & Pedersen 1987) around a central uplift of about 30 km in diameter.

In the Siljan Ring, Lower Palaeozoic sedimentary rocks have been preserved from post-impact erosion and represent the main focus of our drill core investigations which are linked to the Swedish Scientific Drilling Program (SSDP). The studied strata formed during the Early Palaeozoic on the western shelf of Baltica (present-day geography). Recent work has shown that the sediments were affected by Caledonian movements to the west already during the late Middle Ordovician (Lehnert et al. 2012, 2013) (Fig. 1A, B). During that time the Caledonian forebulge likely reached the Mora area and some backbulge deposcenter formed on the shelf towards

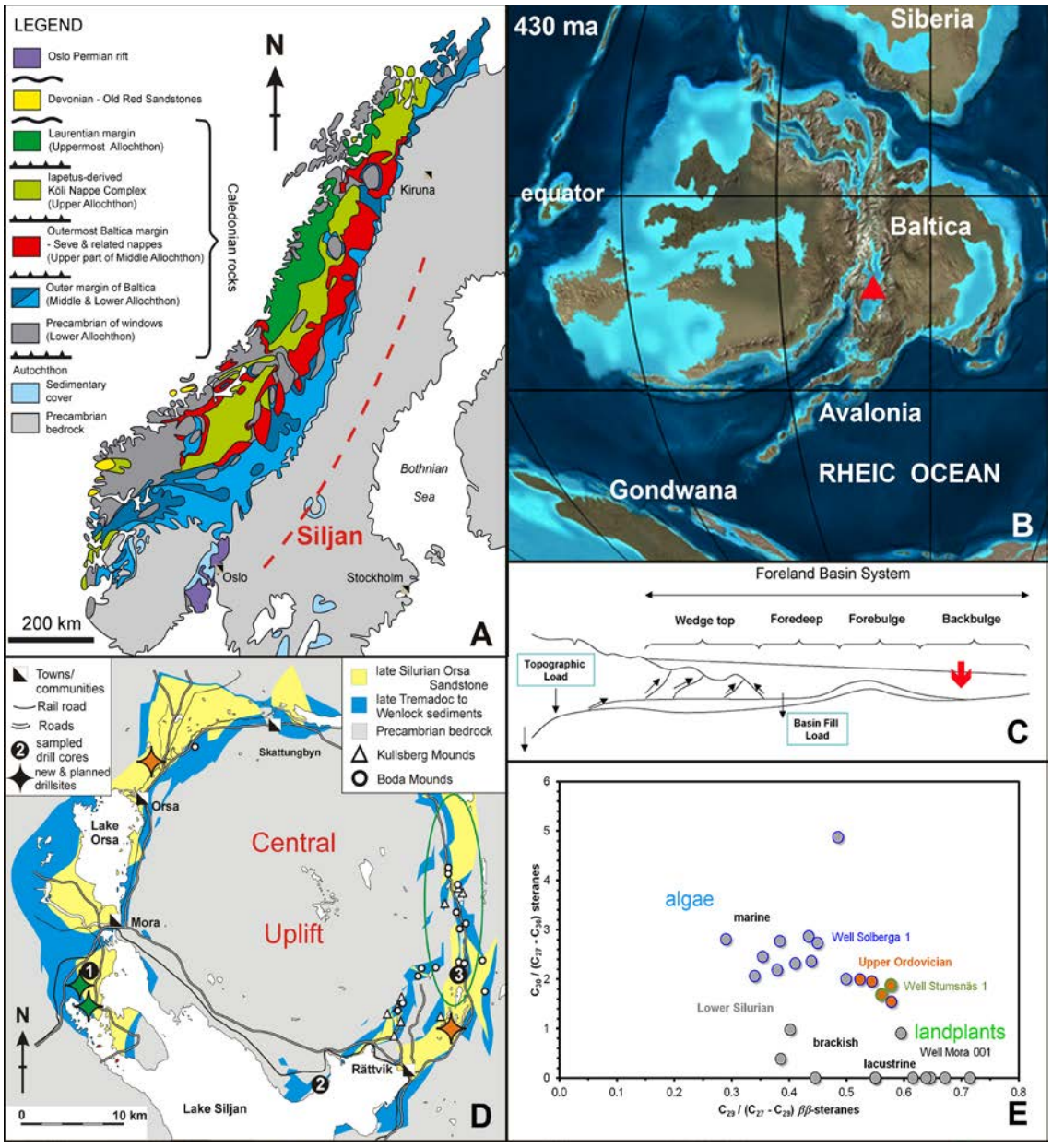

Figure 1: A - Location of the Siljan impact structure in relation to the Caledonian front to the northwest; red stippled line represents trace of the forebulge crest in the Caledonian foreland based on data by Garfunkel & Greiling (1998) and Lehnert et al. (2012) and adapted from Greiling et al (2013); B - Wenlock palaeogeographical reconstruction centred on Baltica and modified from a file of a Mollewide projection available at the website of Ron Blakey (http://www2.nau.edu/rcb7/), the location of the Siljan area is indicated by a red triangle; C - simplified scetch of the foreland basin model by DeDelles & Giles (1996) showing the palaeogeographic position of the Siljan shale depocenter in an early Silurian backbulge basin; D - Location of studied drillcores (1 – Mora 001, 2- Stumsnäs-1, 3 – Solberga 1), new cores to be studied in the future (green) and drilling locations planned for 2014 (orange); the green oval ring encircles an area with multiple core localities by SMA Mineral BA; E - Characterisation of depositional environments based on biomarker data from organic matter of samples from three drill cores in the Siljan ring structure ($C_{30}/(C_{27}$-$C_{30})$ regular steranes vs. $C_{29}/(C_{27}$-$C_{29})$ $\beta\beta$-steranes).

the east (Fig. 1C). The timing would fit with the early foreland basin development during the Darriwilian further to the northwest in Jämtland (Föllinge Basin; Greiling et al. 2013).

In the early Silurian, the forebulge moved further to the west due to tectonic loading by the Caledonian nappes and a backbulge basin filled by a more than 200 m thick siliciclastic succession formed in the Mora-Solberga region (Fig. 1C, D). After the westward migration of the forebulge due to tectonic loading of the Caledonian nappe system to the west, the shale and shale/mudstone succession displays unstable conditions exhibited by synsedimentary tectonic features, debris flows, turbidites, and megaslumps. The ingression of a delta system from the forebulge area to the west shown by the intercalation of a sandstone unit may reflect a strong regression in this shale basin related to an early Silurian glaciation (as indicated by a prominent delta$^{13}C_{org}$ excursion below the coarser grained sandstone unit). The sandstone deposition, however, may also indicate the uplift, exposure and erosion of the bulge area due to the additional loading in the foreland basin system further to the west. In a geodynamic context, the Silurian siliciclastic succession in Siljan was deposited during the time of the Scandian tectonic episode, the time of continent-continent collision and formation of an orogenic wedge and a molasse basin to the west (Greiling et al. 2013). In order to get some cohaerent picture, the Silurian deposits must be investigated with respect to timing of onlap on Ordovician strata, shifts in depocenters, synsedimentary tectonics, large scale slumping, debris flows in additional drill cores (Fig. 1D) and shallow seismic lines.

To support our hypotheses on the geodynamic evolution of the Siljan area in the frame of the Caledonian foreland basin development we have started studies on geochemistry and biomarkers in the organic-rich, fine-grained Upper Ordovician and Silurian siliciclastics. This will be completed by palynofacies research in the near future to distinguish between marine conditions and brackish to lacustrine environments at certain times. Furthermore, the geochemical and biomarker studies will be extremely useful to show that the hydrocarbons in the area derived from the organic-rich Lower Palaeozoic shales. This is important because for many years geochemical investigations in the Siljan impact structure focussed on abiogenic models (e.g., Gold 1999). In the early 1980s, Vattenfall started a large Deep Gas project (e.g., Donofrio et al. 1984) aiming the evaluation of possible abiogenic gas production from the Siljan structure. Vlierboom et al. (1986) however showed that hydrocarbon generation of the organic-rich sediments was induced by heating through the impact of the large meteorite leading to sufficient thermal maturation of the source rocks. This work is complemented by our studies focusing on the geochemical variability in sediments from three drill cores (Mora 001, Stumsnäs 1, and Solberga 1) to evaluate depositional environments and possible diagenetic alterations of organic matter (Fig. 1D).

Organic carbon and sulfur concentrations suggest changes between lacustrine and marine environments during Silurian times in Mora 001, and indicate that organic matter was likely affected by microbial sulfate reduction (diagenesis). Additional information on depositional environments and the organo-facies of the sediments are based on biomarker data (Fig. 1E), indicating a significant input from landplants and deposition of the shales at either fully lacustrine to slightly brackish conditions with no or low marine algal content.

At Solberga 1, organic carbon and sulfur concentrations in the upper Ordovician Fjäcka and lower Silurian Kallholn shales suggest deposition in marine settings, and diagenesis of the organic matter was obviously affected by sulfate reduction. Biomarker derived from marine algae are abundant and clearly support marine sedimentation. In addition, significant concentrations of landplant-derived biomarkers indicate likely coastal rather than open marine conditions (Fig. 1E). The geochemical results from Solberga 1 suggesting 'lacustrine' to brackish and marine palaeoenvironmental conditions are comparable to biomarker data from samples of crude oil and bitumen stored in large pores and vugs in the Ordovician carbonate succession (with the bulk concentrated in the Upper Ordovician mound facies) in the eastern part of the Siljan Ring (Ahmed et al. 2014). This study on seep oil and bitumen also displays different source characteristics for these hydrocarbons expelled from the Lower Palaeozoic shales and confirms that the Upper Ordovician and Silurian organic-rich sediments represent the source rock for oil and bitumen in the Siljan Ring. Biomarker studies showing lacustrine to brackish conditions for the sedimentation of the Silurian siliciclastic succession in the Mora area clearly support a depositional model for these in a backbulge basin of the Caledonian foreland basin system.

References:

Ahmed, M., Lehnert, O., Fuentes, D., Meinhold, G. (2014): Origin of oil and bitumen in the Late Devonian Siljan impact structure, central Sweden. Organic Geochemistry, 68, 13-26.

DeCelles, P.G., Giles, K.A. (1996): Foreland basin systems. Basin Research, 8, 105-123

Donofrio, R.R., Olsen, K.H., Vlierboom, F.W., Witschard, F., Petersson, G. (1984): Deep Gas, Swedish premises: the Siljan Ring project: independent expert evaluation. Vattenfall, Stockholm, 63 pp.

Gold, T. (1999): The Deep Hot Biosphere. Springer, New York.

Greiling, R.O., Oszczypko, N., Garfunkel, Z. (2013): A comparison of two orogenic margins: central Scandinavian Caledonides and western Outer Carpathians. Zeitschrift der Deutschen Geologischen Gesellschaft, 164, 9-32.

Jourdan, F., Reimold, W.U., Deutsch, A. (2012): Dating terrestrial impact structures. Elements, 8, 49-53.

Juhlin, C., Pedersen, L.B. (1987): Reflection seismic investigations of the Siljan impact structure, Sweden. Journal of Geophysical Research, 92, 14113–14122.

Lehnert, O., Meinhold, G., Bergström, S.M., Calner, M., Ebbestad, J.O.R., Egenhoff, S., Frisk, Å.M., Hannah, J.L., Högström, A.E.S., Huff, W., Juhlin, C., Maletz, M., Stein, H.J., Sturkell, E., Vandenbroucke, T.R.A. (2012): New Ordovician-Silurian drill cores from the Siljan impact structure in central Sweden – an integral part of the Swedish Deep Drilling Program. GFF, 134, 87-98.

Lehnert, O., Meinhold, G., Arslan, A., Ebbestad, J.O.R., Calner, M. (2013): Ordovician stratigraphy of the Stumsnäs 1 drill core from the southern part of the Siljan Ring, central Sweden. GFF, 135, 204-212.

Reimold, U., Kelley, S.P., Sherlock, S., Henkel, H., Koeberl, C. (2005): Laser argon dating of melt breccias from the Siljan impact structure, Sweden: Implications for a possible relationship to late Devonian extinction events. Meteoritics & Planetary Science, 40, 1-17.

Vlierboom, F.W., Collini, B., Zumberge, J.E (1986): The occurrence of petroleum in sedimentary rocks of the meteor impact crater at Lake Siljan, Sweden. Organic Geochemistry, 10, 153-161.

ICDP

Correlation of physical properties of sediments and seismic data: first results from the SCOPSCO ICDP campaign

K.LINDHORST[1], S.KRASTEL[1], THOMAS. WONIK[2], B. WAGNER[3]

[1]Christian-Albrechts-Universität zu Kiel, Institut für Geowissenschaften, Abteilung Geophysik, Otto-Hahn-Platz 1, 24118 Kiel
[2] Leibniz-Institute for Applied Geophysics (LIAG), Stilleweg 2, 30655 Hannover, Germany
[3] Institute für Geologie und Mineralogie, Universität Köln, Germany

Ancient Lake Ohrid (Macedonia/Albania), located within the Dinaride-Albanide-Hellenide mountain belt on the Balkan Peninsula, is often referred to as a hotspot of endemic biodiversity with more than 200 endemic species described (Albrecht and Wilke, 2008). Interpretation of seismic lines that were collected during several pre-site surveys in between 2004 and 2009 revealed up to 700 m thick undisturbed sediments in the central basin providing a long and continuous sediment record for studying the impact climatic, geological and environmental changes to the biodiversity pattern over a long time period and as a matter of global significance.

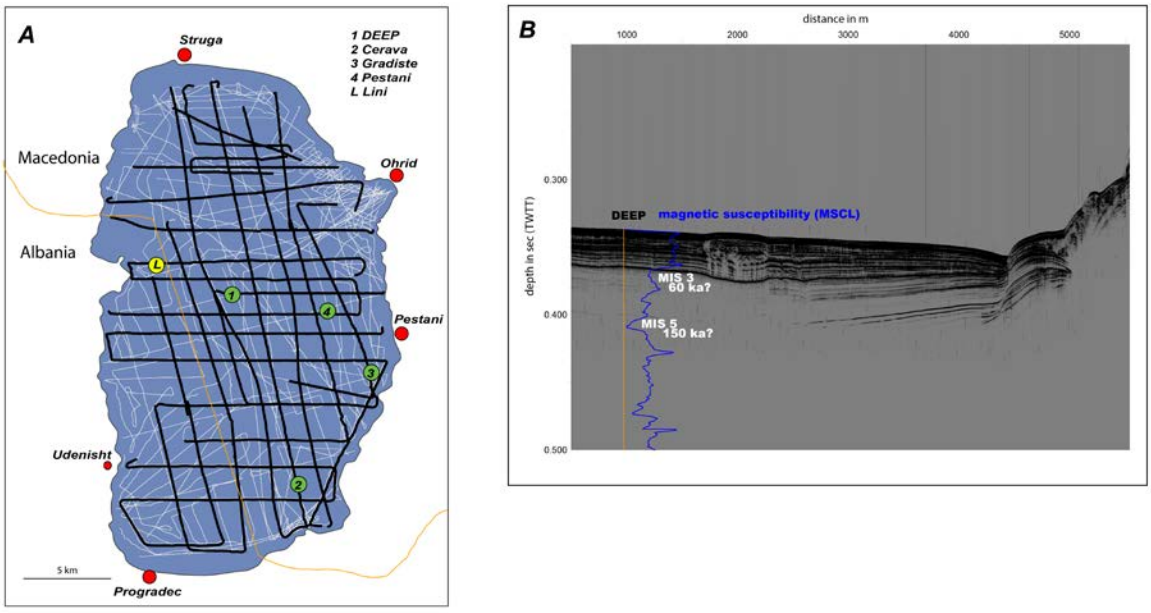

Figure1: A: Track line map of Lake Ohrid illustrating the dense grid of sediment echo-sounder lines (white) and multichannel seismic lines (black). Green and yellow points mark drill sites. B: High resolution seismic line crossing the DEEP site (orange). Overlain (blue) is the magnetic susceptibility curve as measured from sediment core sections in a MCSL lab onsite. Age estimations are given in white.

Intensive work has been done prior to the drilling campaign focusing on the sedimentary and tectonic evolution of Lake Ohrid Basin. It is situated in a tectonically active region influenced by mainly E-W extension explaining the two main boundary normal faults on each side of the basin. An analysis of the basement structure revealed a rhomboidal shape associated with the early stage geometry of the basin interpreted as a pull-apart basin in a transtensional phase in Late Miocene time (Lindhorst et al accept. for publ.). Interpretation of bathymtric and multichannel seismic cross section resulted in a reconstruction of the sedimentary history of Lake Ohrid, which has been found to be continuous and climatically influenced. The oldest lacustrine sediments in the deepest part of the lake were calculated to be around 2 Ma based on a first seismo-chronological model (Lindhorst et al. accept. for publ).

A successful ICDP campaign took place from April 1st to June 2nd, 2013 that recovered more than 2000 m sediment cores at four drill sites (Fig. 1A, Wagner et al., 2014). Magnetic susceptibility (MS) was measured at all sections by a Multi Sensor Core Logger (MSCL) device in a lab onshore immediately after cores were brought back from the barge and then stored in a reefer container. The major site DEEP was penetrated four times up to a sediment depth of 568 m. In addition down-hole logging was carried out at each site by the LIAG group from Hannover. A Vertical Seismic Profile (VSP) shot gather conducted at site DEEP hole 1C is now available and enables us to get valuable information of sediment velocities in order to calculate a time-depth-chart that is essential for the integration of sediment cores and hydro-acoustic data sets.

First results of correlating physical properties data (especially MS) and seismic data clearlry show a cyclicity most likely associated to climatic, geological, and environmental changes in the surrounding area.

A high resolution seismic line crossing the DEEP site is shown in B. In a first step we correlated the MS curve with a ´18O curve resulting in an age estimation for the MS data. In a second step we plotted the MS curve on top of our seismic line. Two reflectors within the seismic data have been chosen to demonstrate that changes in the intensity of magnetic susceptibility parameters are correlating with changes in seismic characteristics such as amplitude (Fig. 1B). In a sediment depth of about 50 m (calculated using a sediment velocity of 1500 m/s similar to water for the upper most sediments) a pair of reflectors are visible in the east with a decreasing amplitude toward west. This reflector has been interpreted to mark the transition from the penultimate Glacial (MIS 6) to the last Interglacial (MIS 5, Lindhorst et al. 2010) and hence would mean that is is about ~150 ka. A strong reflector can be observed below the uppermost sediments marking a

change in seismic character from low amplitude reflectors to high amplitude reflectors. By comparing this seismic characteristic of reflectors to the MS curve a change from high MS values to lower ones takes place at that sediment depth (Fig. 1B). Therefore we can estimate an age of about 60 ka for this strong reflector. Due to the dense grid of high resolution seismic lines within the central part of the basin we can now expand our ages to develop a 3D model

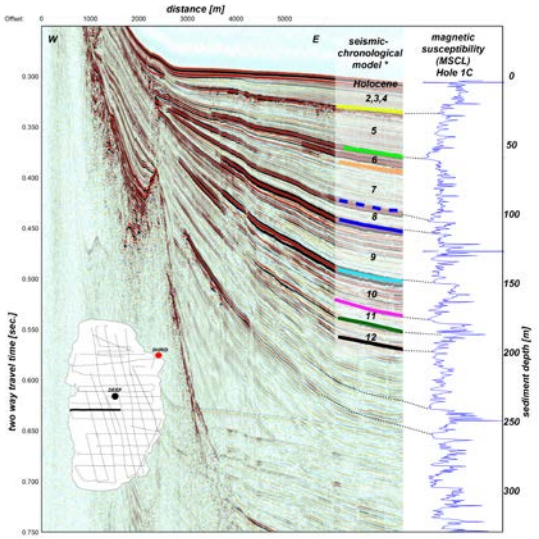

Figure 2: Seismic cross section, seismo-chronological model (numbers are Marine Isotope Stages –MIS see Lindhorst et al. accept. f. publ. for details), and magnetic susceptibility data of sediments cores measured onsite (blue curve). Dashed lines indicate correlation of interpreted MIS stages of the chronological model with major changes in the magnetic susceptibility.

of the basin.

Furthermore we extracted our correlation of MS and seismic data up to a depth of more than 300 m sediment depth (Fig. 2) because below multiples as primary reflectors. During the drilling campaign, at a depth of 420 m blf an increase in grain size up to pebbles hampered the drilling progress and is interpreted as the transition of lacustrine and fluvial sediments. A comparison of the preliminary seismo-chronological model developed by interpretation of seismic lines and the newly aquired MS curve suggest that they are in a good agreement to each other as major reflectors assigned to MIS stages can be correlated with specific highs or lows in the MS data (Fig. 2).

References:

Albrecht, C. And Wilke, T. (2008) "Ancient Lake Ohrid: Biodiversity and Evolution." Hydrobiologia, Vol. 615, p.103-140.

Lindhorst, K., S. Krastel, et al. (accepted for publication). "Tectonic and Sedimentary Evolution of Lake Ohrid (Albania/Macedonia)." Basin Research.

Lindhorst, K., H. Vogel, et al. (2010). "Stratigraphic analysis of lake level fluctuations in Lake Ohrid: an integration of high resolution hydro-acoustic data and sediment cores." Biogeosciences Vol. **7,** (in: Evolutionary and geological history of Balkan lakes Ohrid and Prespa

Wagner, B., Wilke, T., Krastel, S., Zanchetta, G., Sulpizio, R., Reicherter, R., Leng, M., Grazhdani, A., Trajanovski, S., Levkov, Z., Reed, J., Wonik, T. (2014) "More than one million years of history in Lake Ohrid cores." Eos, 95 25-26.

IODP

Geochemical impact evidence and trace element distribution at the K-Pg event bed, J Anomaly Ridge, Newfoundland – IODP Hole U1407B

D. LOROCH [1], A. DEUTSCH[2], J. BERNDT[1], A. BORNEMANN[3] AND EXPEDITION 342 SCIENTISTS

[1] Institut für Mineralogie, Westfälische Wilhelms-Universität Münster (WWU), Corrensstraße 24, D-48149 Münster
[2] Institut für Planetologie, WWU Münster, Wilhelm-Klemm-Straße 10, D-48149 Münster
[3] Institut für Geophysik und Geologie, Universität Leipzig, Talstrasse 35, D-04103 Leipzig

The Cretaceous-Paleogene (K-Pg) boundary is one of the best studied stratigraphic boundaries in Earth history. Each new sample location generates a dataset of information that helps to better understand formation processes but also results in new questions.

The IODP Expedition 342 Hole U1403B (J Anomaly Ridge, Newfoundland) core shows well preserved K-Pg Boundary sequence (Core 28X-1W, 43-57 cm) which contains an ~1 cm thick, graded, green-greyish spherule horizon. Due to the fact that this sample consists of soft clayey material with a high fluid content, sample preparation with Epo Thin® for in-situ analysis turned out to be quite tricky, especially because we paid particular attention to preserve the delicate textural features. We analysed the sample with electron microscopy, electron microprobe, and Laser Ablation – Inductively Coupled Plasma – Mass Spectrometry (LA-ICP-MS) at the Institute of Mineralogy, WWU. Trace element distribution was continuously measured at 144 spots along a cross section, spot-size was 235 µm. In total, 46 trace Elements were measured in-situ and compared to NIST standards (for analytical details, see Berndt et al., 2011).

The in-situ measurements located the Ir-anomaly below the ejecta layer with the altered glass spherules, based on a sharp increase in concentration to up to 50 ppb. This high concentration was determined for a small area of only few hundred µm which is characterized by a change in color from light beige to greenish, and which corresponds to the boundary between the Maastrichtian and K-Pg event bed. Concerning other PGE, we also found remarkable high concentrations of Pt d 2.79 ppm, Pd d 1.64 ppm, Rh d 0.348 ppm, and Au d 0.856 ppm at the bottom of the spherule horizon and some minor spikes in single spots below this horizon.

Compared to the average composition of the upper continental crust (Rudnick and Gao, 2003), and our reference samples from the uppermost Maastrichtian, and the lower Danian, the K-Pg bed is depleted by up to three orders of magnitude in Ba, Y, and the REE, whilst Pb, U, the HFSE, and Ti are significantly enriched.

The position of the Ir-anomaly below the spherule layer indicates a mobilization of PGE and several other trace elements towards the underlying Maastrichtian, obviously as corollary of the hydratization of the glass spherules in an acid milieu. This assumption is supported by a similar but near total depletion of REE that was recently reported for those parts of the black impact glass at Beloc, Haiti, which are altered to smectite (Ritter et al., 2014). Element mobility as result of alteration has been published for a number of K-Pg sites (Schulte et al., 2010;

Smit, 1999). In most cases, however, this effect is observed almost down to the uppermost 10 cm of the Maastrichtian beds, and not, like in our case, just at a small scale of only some hundred µm.

In conclusion, our data for the K-Pg event bed offshore Newfoundland compares well the characteristics of other distal K-Pg sections (e.g. Goderis et al., 2013; Berndt et al., 2011; Schulte et al., 2010; MacLeod et al., 2007; Smit, 1999; Montanari, 1991). The K-Pg sample from IODP Hole U1407B, however, provides an exceptional opportunity to document and understand alteration effects at the scale of 10s of µm.

Acknowledgements: This research used samples provided by IODP. We acknowledge the BCR curator Walter Hale for making the samples available. U. Heitmann (WWU) is thanked for technical support.

References:

Berndt, J., Deutsch, A., Schulte, P., Mezger, K., 2011. The Chicxulub ejecta deposit at Demerara Rise (western Atlantic); dissecting the geochemical anomaly using laser ablation-mass spectrometry. Geology 39, 279-282.

Goderis, S., Tagle, R., Belza, J., Smit, J., Montanari, A., Vanhaecke, F., Erzinger, J., Claeys, P., 2013. Reevaluation of siderophile element abundances and ratios across the Cretaceous-Paleogene (K-Pg) boundary; implications for the nature of the projectile. Geochim. Cosmochim. Acta 120, 417-446.

MacLeod, K.G., Whitney, D.L., Huber, B.T., Koeberl, C., 2007. Impact and extinction in remarkably complete Cretaceous-Tertiary boundary sections from Demerara Rise, tropical western North Atlantic. Geological Society of America Bulletin 119, 101-115.

Montanari, A., 1991. Authigenesis of impact spheroids in the K/T boundary clay from Italy; new constraints for high-resolution stratigraphy of terminal Cretaceous events. J. Sediment. Petrol. 61, 315-339.

Ritter, X., Deutsch, A., Berndt, J., Robin, E. 2014. Glass spherules in the Chicxulub K-Pg event bed at Beloc, Haiti: alteration patterns. In preparation for Meteoritics & Planetary Science

Rudnick, R. L., Gao, S., 2003. 3.01 - Composition of the Continental Crust, in Editors-in-Chief: Heinrich D. Holland, Karl K. Turekian (Eds.), Treatise on Geochemistry. Pergamon, Oxford, pp. 1-64.

Schulte, P., Alegret, L., Arenillas, I., Arz, J.A., Barton, P. J., Bown, P. R., Bralower, T. J., Christeson, G. L., Claeys, P., Cockell, C. S., Collins, G. S., Deutsch, A., Goldin, T. J., Goto, K., Grajales-Nishimura, J. M., Grieve, R. A. F., Gulick, S. P. S., Johnson, K. R., Kiessling, W., Koeberl, C., Kring, D. A., Macleod, K. G., Matsui, T., Melosh, J., Montanari, A., Morgan, J. V., Neal, C. R., Nichols, D. J., Norris, R. D., Pierayyo, E., Ravizza, G., Rebolledo-Vieyra, M., Reimold, W.-U., Robin, E., Salge, T., Speijer, R. P., Sweet, A. R., Urrutia-Fucugauchi, J., Vajda, V., Whalen, M. T., Willumsen, PI S. (2010) The Chicxulub Impact and Mass Extinction at the Cretaceous-Paleogene Boundary. Science 327, 1214-1218.

Smit, J., 1999. The global stratigraphy of the Cretaceous-Tertiary boundary impact ejecta. Annu. Rev. Earth Planet. Sci. 27, 75-113.

IODP

Habitat-dependant size variations of early Aptian coccoliths

N. Lübke[1], J. Mutterlose[1], C. Bottini[2]

[1]Institute for Geology, Mineralogy and Geophysics, Ruhr-Universität Bochum, Universitätsstr. 150, 44801 Bochum, Germany

[2]University of Milano, via Mangiagalli 34, 20133 Milano, Italy

Coccolithophorids, a group of calcifying haptophyte algae, are one of the main primary producers of the oceans. These unicellular organisms cover their cell with minute but complex calcite plates called coccoliths; the entire cell coverage is called coccosphere. Fossil coccoliths are widely used for biostratigraphic dating and for reconstructing the paleoenvironment. Entire coccospheres are rarely preserved in sediments. Biometrical studies on coccoliths offer the opportunity to understand species-specific responses of coccolithophorids to ecology.

We obtained and analyzed size data of three common coccolith species (Biscutum constans, Zeugrhabdotus erectus, Watznaueria barnesiae) in a stratigraphically very well-defined interval of the early Aptian (~126 Ma; Cretaceous). Material is derived from five sites (northwest Germany, North Sea, Tethys, Pacific Ocean) covering coastal to open-oceanic settings. The outcrop Alstätte 1 is located in northwest Germany and covers lower Aptian mudstone and marlstone. This coastal site was located at approximately 36°N at the southern margin of the Lower Saxony Basin during the early Aptian. Two cores from the North Sea (North Jens-1, Adda-2) represent the hemipelagic signal of the Boreal Realm. Both cores expose limestone and claystone, which were deposited at approximately 40°N in the early Aptian. The Cismon core (Italy) recovered lower Aptian carbonaceous limestones with radiolarian beds and chert lenses/layers. These sediments were deposited at approximately 20°N under pelagic conditions in the Tethys. DSDP Site 463 was located at approximately 13 to 20°S during the early Aptian. It exposed pelagic limestones, marlstones, claystones and volcanic ashes. The data of the Cismon core and of DSDP Site 463 reflect a low latitudinal signal. All studied samples can stratigraphically be attributed to nannofossil zone BC18 (Boreal sites; 36-40°N) or the agewise corresponding NC6 (low latitudinal sites; 13°S-20°N).

Nannofossil preservation is moderate to good in all studied samples. Coccoliths were studied in settling slides using a transmitted light microscope mounted with a CCD camera. Images of coccoliths were taken using an image editing software. Length and width measurements of more than 1500 specimens were raised and evaluated. The ellipticity of the coccoliths was calculated as the coccolith length over coccolith width ratio. Statistical test were applied to verify whether the data are normally distributed.

B. constans and Z. erectus have small sizes at the coastal site in the Boreal Realm, larger ones at the two North Sea sites and largest dimensions in the Pacific and in the Tethys. The size data for W. barnesiae are less clear, indicating a rather uniform size distribution at the sites studied. Previous studies (e.g. Henderiks, 2008) show that there are universal basic principles in coccolithophorid cell geometry. One of these principles is the positive correlation of coccolithophorid cell size (and coccosphere size) and coccolith size. The coccolith size variations of B. constans and Z. erectus are therefore most likely related to different cell sizes. The cell site is directly linked to the buoyancy of the specific species and thus to its habitat depth. The coccolithophorids of B. constans and Z. erectus were small and are thus thought to have occupied shallower water depths with reduced light availability. Alternatively an increased nutrient flux (shallow nutricline) may explain for the shallow habitat. The nutricline depth appears to be the main driving force for the depth habitat of B. constans and Z. erectus as the distribution of these species was controlled by nutrient availability. Less important factors are the light attenuation in surface waters due to turbidity and the generally less intense solar radiation at non-tropical latitudes. The low-latitudinal sites (Cismon, DSDP Site 463) were characterized by a deep nutricline and strong

solar radiation, forcing coccolithophorids to dwell deeper. W. barnesiae is an ecologically more tolerant species, suggested by its stable size pattern.

References:
Henderiks, J., 2008. Coccolithophore size rules — Reconstructing ancient cell geometry and cellular calcite quota from fossil coccoliths. Marine Micropaleontology, 67, 143-154.

ICDP

Effects of Abrupt Climate Change on Ice Age Ecosystem of Lake Petén Itzá, Guatemala and on Distribution Patterns of Ostracodes across the Yucatán Peninsula

L. MACARIO[1], S. COHUO[1], L. PÉREZ[2], S. KUTTEROLF[3], A. SCHWALB[1]

[1]Institut für Geosysteme und Bioindikation, Technische Universität Braunschweig, Langer Kamp 19c, 38106 Braunschweig, Germany
2Instituto de Geología, Universidad Nacional Autónoma de México, Ciudad Universitaria, 04510 México, D.F. Mexico
[3]GEOMAR Helmholtz-Zentrum für Ozeanfoschung, Kiel, Wischhofstr. 1-3, 24148 Kiel, Germany

Lake Petén Itzá is the largest and deepest lake of the Yucatán Peninsula (YP) and holds the oldest sedimentary record (~200 ka) known for the entire lowland northern Neotropics. Lacustrine ostracodes, small crustaceans (0.2-5mm) that have their entire body enclosed in a calcite carapace, provide one of the best fossil records and are thus well-suited proxies for paleoenvironmental change including water depth, temperature, conductivity, environmental energy and changes in hydrology, if their autecology is known. Pérez et al. (2011) established a first training set based on ostracode species sampled from 63 aquatic ecosystems (Guatemala, Belize and Mexico) that provided transfer functions for conductivity and water depth. This allowed to quantitatively reconstruct these environmental variables since the Last Glacial Maximum (LGM) from Petén Itzá sediments. For the past 85 ka, Hodell et al. (2012) showed extreme cooling in the Neotropics up to 10°C during Heinrich events. Escobar et al. (2012) and Pérez et al. (2013) found that the variations in oxygen and carbon isotope values registered in ostracode shells are distinctly correlated with hydrological change coinciding with Heinrich stadials, LGM and the Deglacial. Previous work, however, was restricted to the past 85 ka. .

We will thus analyze the consequences of abrupt climate change on the stability of aquatic ecosystems of Lake Peten Itza beyond 85 ka and back to about 200 ka, and consequently on the paleobiogeography of the YP, by using ostracodes as model bioindicators interlinking three major research topics: (1) Quantitative assessment of lake level changes during the past 200 ka. This will be achieved by extending the existing training set of recent ostracodes in order to refine transfer functions for water depth and conductivity. Hydrological changes will also be inferred using stable isotope signatures of ostracode shells. (2) Reconstruction of the ultrastructure of Late Pleistocene climates extremes using fossil ostracode assemblages. (3) Analysis of the effects of climatic variability on the aquatic ecosystem and elucidation if and to what extend these variations have shaped the actual distribution patterns of species by using morphological and molecular analysis of extant species (phylogeny, phylogeography).
The original training set has been extended by sampling 100 additional aquatic ecosystems during the rainy season along the YP and southern Central American countries (El Salvador, Honduras and Nicaragua) in summer/fall 2013. For all aquatic ecosystems physico-chemical parameters (temperature, conductivity, oxygen content, pH, etc.) were measured in situ, water samples and sediments were taken for further nutrient and chemical analysis, and aquatic bioindicators (diatoms, chironomids, thecamoebians, cladocerans, etc.) to improve interpretation of the fossil record. Sampling of Lake Petén Itzá sediments beyond 85 ka was carried out during a joint US-Swiss-Mexican-German core sampling party at LacCore, University of Minnesota. Preliminary tephrachronology of lacustrine ash layers in these recovered and sampled sediments, established by chemical fingerprinting to well-dated proximal tephras (e.g. L-Fall tephra from Amatitlán Caldera, Guatemala, 191 ka; W-Fall tephra from Atitlán Caldera, Guatemala, 159 ka), indeed suggests that the stratigraphic sequence in these holes extends back to at least 200 ka.

References:
Escobar, J., Hodell, D.A., Brenner, M., Curtis, J.H., Gilli, A., Müller, A.D., Anselmetti, F.S., Ariztegui, D., Grzesik, D.A., Pérez, L., Schwalb, A., Guilderson, T.J., 2012. A ~43-ka record of paleoenvironmental change in the Central American lowlands inferred from stable isotopes of lacustrine ostracods. Quaternary Science Reviews 37, 92-104.
Hodell , D. A., Turchyna, A.V., Wisemana, C.J., Escobar, J., Curtis, J.H., Brenner, M., Gilli, A., Mueller, A.D., Anselmetti F., Ariztegui D., Brown, E.T., 2012. Late Glacial temperature and precipitation changes in the lowland Neotropics by tandem measurement of ´18O in biogenic carbonate and gypsum hydration water. Geochimica et Cosmochimica Acta 77, 352-368.
Pérez, L., P. Frenzel, P. Hoelzmann, J. Escobar, M. Brenner, B. Scharf, A. Schwalb, 2011. Late Quaternary (24-10 ka BP) environmental history of the Neotropical lowlands inferred from ostracodes in sediments of Lago Petén Itzá, Guatemala. Journal of Paleolimnology 46, 59-74.
Pérez, L., J., Curtis, M. Brenner, D. Hodell, J. Escobar, S. Lozano, A. Schwalb. Stable isotope values (´ ^{18}O & ´ ^{13}C) of multiple ostracode species in a large Neotropical lake as indicators of past changes in hydrology. Quaternary Science Reviews 66, 96-111.

IODP

Variations of marine pore water salinity and chlorinity in Gulf of Alaska sediments (IODP Expe-dition 341)

C. MÄRZ[1], A.C. MIX[2], E. MCCLYMONT[3], A. NAKAMURA[4], G. BERBEL[5], S.P. GULICK[6], J.M. JAEGER[7], L. LEVAY[8], EXPEDITION 341 SCIENTISTS

[1]School of Civil Engineering & Geosciences, Newcastle University, Newcastle upon Tyne, UK (christian.maerz@ncl.ac.uk)
[2]College of Earth, Ocean, and Atmospheric Sciences, Oregon State University, Corvallis, Oregon, USA
[3]Department of Geography, Durham University, Durham, UK
[4]Atmosphere and Ocean Research Institute, The University of Tokyo, Kashiwa, Chiba, Japan
[5]Departamento de Oceanografia Física, Química e Geológica, Instituto Oceanográfico, Universidade de São Paulo, São Paulo, Brazil
[6]Institute for Geophysics, Jackson School of Geosciences, University of Texas at Austin, Austin, Texas, USA
[7]Department of Geological Sciences, University of Florida, Gainesville, Florida, USA
[8]International Ocean Discovery Program, Texas A&M University, College Station, Texas, USA

Pore waters of marine sediments usually have salinities and chlorinities similar to the overlying sea water, ranging around 34-35 psu (Practical Salinity Units) and around 550 mM Cl^-, respectively. This is because these parameters are conservative in the sense that they do not significantly participate in biogeochemical cycles. However, pore water studies carried out in the frame of the International Ocean Discovery Program (IODP) and its predecessors have shown that salinities and chlorinities of marine pore waters can substantially deviate from the modern bottom water composition in a number of environmental settings, and various processes have been suggested to explain these phenomena. Also during the recent IODP Expedition 341 that drilled five sites in the Gulf of Alaska (Northeast Pacific Ocean) from the deep Surveyor Fan across the continental slope to the glaciomarine shelf deposits, several occurrences of pore waters with salinities and chlorinities significantly different from respective bottom waters were encountered during shipboard analyses.

At the pelagic Sites U1417 and U1418 (~4,200 and ~3,700 m water depth, respectively), salinity and chlorinity maxima occur around 20-50 m sediment depth, but values gradually decrease with increasing drilling depths (down to 30 psu in ~600 m sediment depth). While the pore water freshening at depth is most likely an effect of clay mineral dehydration due to increasing burial depth, the shallow salinity and chlorinity maxima are interpreted as relicts of more saline bottom waters that existed in the North Pacific during the Last Glacial Maximum (Adkins et al., 2002).

In contrast, the glaciomarine slope and shelf deposits at Site U1419 to U1421 (~200 to 1,000 m water depth) are characterised by unexpectedly low salinitiy and chlorinity values (as low as 16 psu and 295 mM Cl^-, respectively) already in very shallow sediment depths (~10 m), and their records do not show systematic trends with sediment depth. Freshening of pore waters in continental margin settings has been reported in association with dissociating gas hydrate deposits (Hesse, 2003), but neither seismic profiles nor sediment records showed any indications for the presence of gas hydrates at the Gulf of Alaska sites. An alternative and intriguing explanation for these almost brackish waters in the glaciomarine shelf and slope deposits is the presence of glacial meltwater that could either be “fossil” (stored in the glaciomarine sediments since the last glacial termination) or “recent” (i.e., actively flowing from currently melting glaciers of the St. Elias Mountain Range along permeable layers within the shelf deposits).

As these relatively fresh waters are found at three distinct drill sites, it can be assumed that they are distributed all along the Gulf of Alaska shelf and slope, and similar findings have been reported at other glaciated continental margins, e.g., off East Greenland (DeFoor et al., 2011) and Antarctica (Mann and Gieskes, 1975; Chambers, 1991; Lu et al., 2010).

While a recent review has highlighted the importance of fresh and brackish water reservoirs in continental shelf deposits worldwide (Post et al., 2013), we suggest that climatic and depositional processes affecting glaciated continental margins (e.g., the release of huge amounts of fresh water from ice sheets and glaciers during glacial terminations, and the rapid deposition of unconsolidated sediments on the adjacent shelf) are particularly favourable for the storage and/or flow of meltwater below the present sea floor.

References:

Adkins JF, McIntyre K, Schrag DP (2002) The salinity, temperature, and d18O of the glacial deep ocean. Science 298, 1769-1773.

Chambers SR (1991) Solute distributions and stable isotope chemistry of interstitial waters from Prydz Bay, Antarctica. Proceedings of the Ocean Drilling Program 119, 375-392.

DeFoor W, Person M, Larsen HC, Lizarralde D, Cohen D, Dugam B (2011) Ice sheet–derived submarine groundwater discharge on Greenland’s continental shelf. Water Resources Research 47, W07549.

Hesse R (2003) Pore water anomalies of submarine gas-hydrate zones as tool to assess hydrate abundance and distribution in the subsurface: What have we learned in the past decade? Earth-Science Reviews 61, 149-179.

Lu Z, Rickaby REM, Wellner J, Georg B, Charnley N, Anderson JB, Hensen C (2010) Pore fluid modeling approach to identify recent meltwater signals on the West Antarctic Peninsula. Geochemistry, Geophysics, Geosystems 11, doi: 10.1029/2009GC002949.

Mann R, Gieskes JM (1975) Interstitial water studies, Leg 28. Deep Sea Drilling Project Initial Reports 28, 805-814.

Post VEA, Groen J, Kooi H, Person M, Ge S, Edmunds M (2013) Offshore fresh groundwater reserves as a global phenomenon. Nature 504, 71-78.

IODP

Modelling carbon isotope composition of dissolved inorganic carbon and methane in marine porewaters

PATRICK MEISTER[1], BO LIU[1], ARZHANG KHALILI[1,2], BO BARKER JØRGENSEN[1,3]

[1] Max Planck Institute for Marine Microbiology, Celsiusstrasse 1, 28359 Bremen; email: pmeister@mpi-bremen.de
[2] Center for Geomicrobiology, Aarhus University, Ny Munkegade 114, 8000 Aarhus, Denmark
[3] Earth & Space Sciences Program, School of Engineering and Science, Jacobs University, 28725 Bremen, Germany

Carbon isotope compositions of dissolved inorganic carbon (DIC) and methane (CH_4) in marine porewaters show some of the largest stable isotope fractionations in nature with $\delta^{13}C$ values varying between -100 and +35 ‰ (VPDB) and more. This fractionation is essentially the result of microbial activity, but the mechanisms and

factors controlling this fractionation and the distribution of isotopic compositions are still incompletely understood. Carbon isotopes in DIC and CH_4 were intensively investigated during the first few Legs of the Deep Sea Drilling Project (DSDP; see Claypool and Kaplan, 1974, for a review), and later during the discovery of early diagenetic dolomite layers carrying a wide range of $\delta^{13}C$ values within organic carbon-rich sediments of the Gulf of California (ODP Legs 63 and 64). But unfortunately $\delta^{13}C$ values of both DIC and CH_4 have not been systematically measured as part of the ODP/IODP since then. In the meantime, strongly varying carbon isotopes measured in dolomite from the Peru Margin were suggested to have formed as a result of a dynamic deep biosphere (Meister et al., 2007, 2008, 2011; Contreras et al., 2013; Wehrmann et al., in press). Despite these findings, the idea that carbon isotopes could be reproduced by relatively simple modelling has been viewed with scepticism. The extreme complexity of reactivities of different organic species and the many competing microbial pathways involved in this system are considered impossible to be simulated by numerical modelling of simplified chemical reactions for sulphate reduction and methanogenesis.

During the last four years, the authors made a considerable effort to provide a reaction transport model approach (see also Meister et al., 2013, and Contreras et al., 2013) to reproduce a dynamic sulphate methane transition zone. As part of this work, they also evaluated the effects of the most important processes and factors on carbon isotope distribution with the goal to better understand carbon isotope distribution in modern sediment porewaters and in the geological record. The model relies on the finding that organic matter in marine sediments decays as a function of time and burial depth that can be described by a reactive continuum model (Boudreau and Ruddick, 1991), and production and consumption of DIC and CH_4 are stoichiometrically coupled to this decay following several different pathways. The model further includes diffusive transport and degassing of CH_4.

Model results show that kinetic fractionation during methanogenesis, both through the acetoclastic and autotrophic pathways, results in ^{13}C-enriched DIC and ^{13}C-depleted CH_4 with a nearly symmetrical distribution of $\delta^{13}C$ values in DIC and CH_4 with respect to the isotope value of buried organic matter. An increased fractionation factor during methanogenesis leads to a larger difference between $\delta^{13}C_{DIC}$ and $\delta^{13}C_{CH4}$. Near the sulphate methane transition (SMT) zone, DIC is more depleted in ^{13}C due to diffusive mixing with DIC produced by anaerobic oxidation of methane (AOM) and organoclastic sulphate reduction. The model also shows that strongly decreased $\delta^{13}C_{CH4}$ values near the SMT, as commonly observed in measured profiles, can only be caused by equilibrium fractionation during AOM due to a "leakage" in the enzymatic pathway. However, this effect of reversibility has no influence on the DIC pool as long as methane is completely consumed at the SMT. Only a release of methane at the sediment-water interface, due to a fraction of the methane escaping re-oxidation, results in a small shift towards more positive $\delta^{13}C_{DIC}$ values. Methane escape at the SMT is possible if either the methane flux is too high to be entirely oxidized by AOM, or if bubbles of methane gas by-pass the sulphate reduction zone and escape episodically into the water column. A small but significant isotope effect is also caused by differential diffusion of the ^{12}C and ^{13}C isotopes of CH_4 leading to somewhat more positive $\delta^{13}C_{CH4}$ values below the SMT, while DIC remains unaffected by this process.

The consideration of all these effects allows a relatively good reproduction of $\delta^{13}C_{DIC}$ and $\delta^{13}C_{CH4}$ profiles in marine sediments in diffusive systems. However, the model cannot reproduce profiles measured in seep environments, where CH_4 and DIC profiles are perturbed by upward advecting, possibly thermogenic methane from greater depth. The model is now available to be applied for non-steady state systems, which ultimately will help to understand past dynamics of $\delta^{13}C$ compositions and their diagenetic records as a result of changing microbial activity.

References:

Boudreau, B.P., Ruddick, B.R., 1991, On a reactive continuum representation of organic matter diagenesis. American Journal of Science 291, 507–538.

Claypool, C.E., Kaplan, I.R., 1974, The origin and distribution of methane in marine sediments. In: Natural Gases in Marine Sediments (Ed. Kaplan, I.R.) Plenum Press, New York, 99–140.

Contreras, S., Meister, P., Liu, B., Prieto-Mollar, X., Hinrichs, K.-U., Khalili, A., Ferdelman, T.G., Kuypers, M., Jørgensen, B.B., 2013, Strong glacial-interglacial variation of sub-seafloor microbial activity on the Peruvian shelf. PNAS 110, 18098–18103, doi: 10.1073/pnas.1305981110.

Meister, P., Bernasconi, S., McKenzie, J.A., Vasconcelos, C., Frank, M., Gutjahr, M., Schrag, D., 2007, Dolomite formation in the dynamic deep biosphere: Results from the Peru Margin (ODP Leg 201). Sedimentology 54, 1007-1032.

Meister, P., Bernasconi, S., McKenzie, J.A., Vasconcelos, C., 2008, Sea-level changes control diagenetic dolomite formation in hemipelagic sediments of the Peru Margin. Marine Geology 252, 166-173.

Meister, P., Gutjahr, M., Frank, M., Bernasconi, S., McKenzie, J.A., Vasconcelos, C., 2011, Dolomite formation within the methanogenic zone induced by tectonically-driven fluids in the Peru accretionary prism. Geology 39, 563-566.

Meister, P., Liu, B., Ferdelman, T.G., Jørgensen, B.B., Khalili, A., 2013, Control of sulphate and methane distributions in marine sediments by organic matter reactivity. Geochim. Cosmochim. Acta. 104, 183-193.

Wehrmann, L.M., Ockert, C., Mix, A., Gussone, N., Teichert, B.M.A., Meister, P., Multiple onset of methanogenic zones, diagenetic dolomite formation, and silicate alteration under varying organic carbon deposition in Bering Sea sediments (Bowers Ridge, IODP Exp. 323 Site U1341). Special Issue in Deep Sea Research II, in press.

ICDP

Downhole geophysical data from recent deep drilling in the centre of the Thuringian Basin, Germany

P. METHE, A. GOEPEL, N. KUKOWSKI

Friedrich Schiller Universität Jena, Institut für Geowissenschaften, Burgweg 11, 07749 Jena

In the framework of the INFLUINS (Integrated Fluid Dynamics in Sedimentary Basins) project, a 1.179 meter deep scientific borehole was drilled in summer 2013. The drill site is situated in the north of Erfurt, in the center of the Thuringian Basin on the crossing point of two seismic reflection profiles, which were acquired in 2011. An almost complete sequence from Keuper to the base of the Buntsandstein was drilled. Drilling, geophysical measurements and well construction were conducted for three depth intervals. First, drilling was undertaken to a depth of 313 m down to the top of the Middle Muschelkalk. Then, the Middle and Upper Muschelkalk were drilled to a depth of 515 m and the third part of the drilling campaign was finished at a depth of 1.179 m at the base of the Lower Buntsandstein. Coring was done in the depth intervals of 285 m to 420 m and 520 m to 914 m. With the help of the borehole geophysical measurements, which were done along the entire depth, stratigraphic information obtained through core samples can be

extrapolated from cored sections into those depth sections, where no coring was done.

Immediately after finishing drilling through a certain depth interval, borehole geophysical measurements were conducted in the open hole. Using the caliper and inclination instruments, the geometry of the well was determined. In addition, milieu, gamma-ray, spectral gamma-ray, acoustic borehole television, sonic, susceptibility, dipmeter, gamma-gamma, neutron-neutron and the dual latero-log were measured to get information about rock properties. Within rock-salt bearing depth intervals, embedded cm-thin layers of clay can be geophysically resolved. This will e.g. enable to determine and contrast the physical properties of these alternating sequences with high accuracy. Besides the in-situ well measurements rock-physical parameters of the cores were acquired with a Multi-Sensor Core Logger (MSCL).

Here, we present the new data set and discuss some preliminary results. Unexpectedly and contrary to them being prominent aquifers like at the edges of the Thuringian Basin, the Middle Muschelkalk and Middle Buntsandstein sequences are characterized by very low porosities and no macroscopically recognizable fluid transport here.

IODP

Bottom water changes in the subtropical North Atlantic and the Southern Ocean associated to the Middle Eocene Climatic Optimum

I. MOEBIUS[1], O. FRIEDRICH[1,2], K.M.EDGAR,[3] H. SCHER[4], P.F. SEXTON[5]

[1] Institut für Geowissenschaften, Goethe Universität Frankfurt, Germany
[2] Institut für Geowissenschaften, Universität Heidelberg, Germany
[3] School of Earth and Ocean Science, Cardiff University, United Kingdom
[4] Department of Earth and Ocean Sciences, University of South Carolina, Columbia, USA
[5] Centre for Earth, Planetary, Space & Astronomical Research, The Open University, Milton Keynes, UK

The Eocene (55 to 34 Ma) is characterized by significant global climate change. Following the greenhouse climate of the Cretaceous, a warm climate was sustained during the Paleocene-Eocene Thermal Maximum (PETM) and Early Eocene, culminating in the Early Eocene Climatic Optimum (EECO, 52-50 Ma). Thereafter, a gradual cooling took place during the middle and late Eocene (49-34 Ma) that eventually resulted in the growth of the first continental-scale ice caps on Antarctica during the Eocene-Oligocene-transition (Miller et al., 1991; Zachos et al., 1996). Superimposed on the long-term Eocene cooling trend are a series of transient global warming events as well as longer-lived warming events like the Middle Eocene Climatic Optimum (MECO; e.g. Bohaty and Zachos, 2003; Bohaty et al., 2009). The latter is a prominent ~650 kyr long warming event that interrupts the middle to late Eocene cooling at ~40 Ma. Bulk and benthic foraminiferal carbonate $\delta^{18}O$ values indicate a gradual 1.0 – 1.5 ‰ decrease during the MECO. Assuming an absence of significant continental ice sheets at this time (Bijl et al., 2010; Bohaty et al., 2009; Burgess et al., 2008; Edgar et al., 2007), this $\delta^{18}O$ excursion likely corresponds to a temperature increase of 4 – 6 °C in surface and intermediate deep waters (Bohaty and Zachos, 2003; Bohaty et al., 2009; Edgar et al., 2010). This inferred warming culminates in a $\delta^{18}O$ minima for ~50 kyrs at ~40 Ma (MECO peak warming). The MECO is also accompanied by a transient increase in atmospheric pCO_2 (~2000 to 3000 ppmv; Bijl et al., 2010) as well as a brief, global shoaling of the Carbonate Compensation Depth (CCD) on the order of 500 to 1500 m (Bohaty et al., 2009; Pälike et al., 2012). The termination of the MECO is marked by an inferred abrupt increase in $\delta^{18}O$ values and cooling of up to 6°C in surface and intermediate deep waters to return to the pre-MECO long-term cooling trend. This is accompanied by a global deepening of the CCD and a proposed rapid decrease in pCO_2 (Bijl et al., 2010; Bohaty et al., 2009). The rapid nature of the cooling suggests enhanced organic carbon burial as the most likely driver for pCO_2 drawdown, while increased silicate weathering rates at this time as a possible additional

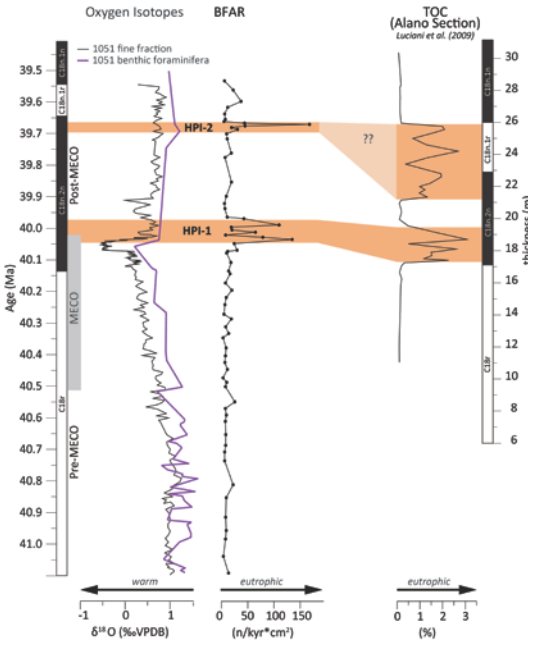

Figure 3: Fine fraction (black line, Bohaty et al., 2009) and benthic foraminiferal (purple line, Edgar et al., 2010) oxygen isotopes from Site 1051 show the MECO warming (gray bar). Benthic foraminiferal accumulation rates increase at peak warming at ~300 kyrs afterwards, suggesting 2 intervals of elevated productivity (HPI-1 and HPI-2, orange boxes). Intervals of increasing total organic carbon content (TOC) in the sediments of Alano Section (Luciani et al., 2010) imply carbon burial at the termination of the MECO and appear to be synchronous to (and might be correlated with) the HPIs.

(smaller) contributor (Pälike et al., 2012).

Because of dramatic temperature and ocean chemisty changes it is to be expected that the marine ecosystems was affected by the MECO. Furthermore, such ecological changes can be used to trace regional and global export productivity and bottom-water oxygenation, as well as deep-water circulation patterns. Therefore, we investigate two sites in the subtropical North Atlantic (ODP Site 1051) and the Southern Ocean (ODP Site 738).

Specifically, we employ benthic foraminiferal assemblages, benthic foraminiferal accumulation rates and fossil fish teeth Cerium to reconstruct paleoecological and paleoceanographic changes associated with the MECO.

At Site 1051 we use benthic foraminiferal assemblages and benthic foraminiferal accumulation rates (BFAR) to evaluate ecological and bottom water changes in the North Atlantic. The investigated record spans the MECO and post-MECO interval (41.1 to 39.5 Ma). Within this succession, 52 samples were analyzed based on the >125 µm size fraction. Classification was carried out to the species level whenever possible, mainly following Bolli et al. (1994) and Tjalsma and Lohman (1983). Benthic foraminifera accumulation rates (BFAR) were calculated following Herguera and Berger (1991) and are calculated by assuming that sedimentation rates remained constant between magnetochron datums. The age model employed in this study is based on the revised ODP Site 1051 magnetostratigraphy by Edgar et al. (2010). A total of 48 benthic foraminiferal taxa have been identified, with 20 genera having an average relative abundance of >1% in the samples. Across the investigated 2 million year long time interval, benthic foraminiferal assemblages are typical of tropical Eocene environments but we note little changes in the species composition. The muted biotic response implies that benthic foraminifera were relatively insensitive to the environmental changes that were occurring during the MECO. This may imply that the gradual rate of environmental change that accompanied the MECO allowed benthic foraminifera to adapt.

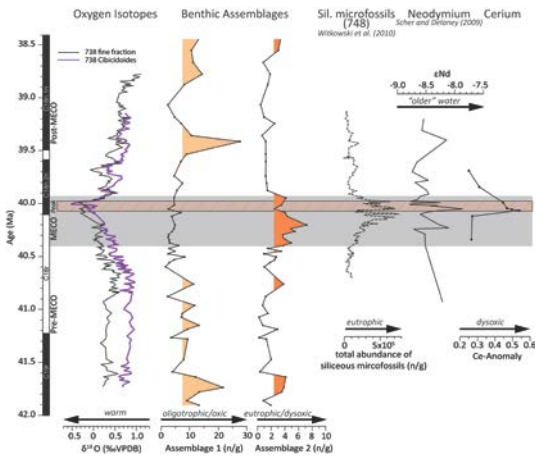

Figure 4: Fine fraction (black line) and benthic foraminiferal (purple line) oxygen isotopes (Bohaty et al., 2009) show the MECO warming (~40.65 – 39.95 Ma, gray box). Benthic foraminifera separate into an epifaunal and an infaunal assemblage that are dominant in the Pre- and Post-MECO, and during the MECO, respectively. In combination with the increase in siliceous microfossil abundance (Witkowski et al., 2012) this indicates eutrophication during the MECO. Peaks in fossil fish teeth μ_{Nd} (Scher and Delaney, 2010) and Ce-Anomaly suggest dysoxic bottom water conditions during the peak warming (shaded orange box).

However, we observe two transient intervals of BFARs increasing by one order of magnitude associated with peak warming (~ 40.25 Ma and 39.66 Ma) (Fig. 2). BFARs are traditionally employed as an indicator of export productivity from surface waters with high BFAR values reflecting enhanced food availability (e.g. Herguera and Berger, 1991; Jorissen et al., 2007; Van der Zwaan et al., 1999). Therefore, we interprete these two transient intervals of elevated BFARs during the final stages of and following the MECO as intervals of increased productivity. In addition, it appears that these intervals of elevated productivity occur synchronous to episodes of enhanced total organic carbon content in marine sediments of the Tethys (Luciani et al., 2010; Spofforth et al., 2010) (Fig. 2). We suggest that these intervals may be correlated and represent periods of widespread or even global (rather than local) eutrophication.

At Southern Ocean Site 738 we use benthic foraminiferal assemblages in combination with fossil fish teeth Cerium analyses (Moebius et al., submitted). We investigated 51 samples across a section spanning 41.9 - 38.5 Ma, using the same size fraction, counting technique and literature as for samples from Site 1051. The age model employed in this study is that of Bohaty et al. (2009), based on the correlation of tie points with Site 702. A total of 113 taxa have been identified among 45 genera, with 21 taxa accounting for an average abundance of > 1% each. In contrast to Site 1051, benthic foraminiferal communities experience a significant faunal turnover during the MECO. With a correspondence analysis based on species-specific counts using the Paleontological Statistics Tool PAST we separate two statistically different assmeblages. Assemblage 1 dominates the Pre- and Post-MECO intervals, as well as the first ~200 kyrs after the onset of the MECO (41.9 – 40.4 Ma; 39.9 – 38.5 Ma) and consists mainly of epifaunal species that prefer oligotrophic and well-oxygenated bottom-water conditions. Assemblage 2 dominates during the majority of the MECO (41.9 and 40.4 Ma) and is comprised of infaunal taxa (Fig. 3) that are well adapted to eutrophic and dysoxic bottom waters. Consequently, this turnover suggests eutrophication and/or a decrease of bottom-water oxygen concentrations during the MECO. Witkowski et al. (2012) investigated siliceous microfossil abundances and note a dramatic increase synchronously to the benthic foraminiferal assemblage composition change. High abundances of siliceous microfossils are an indicator of enhanced surface productivity and we thus suggest that the MECO is accompanied by an increase in surface and export productivity. Superimposed on this trend, a drop in Assemblage 2 abundances occurs during the peak warming (40.10 – 39.97 Ma). Synchronously, fossil fish teeth record a small excursion in μ_{Nd} (Scher and Delaney, 2010) and a low Cerium-anomaly (Fig. 3), both of which are indicative of dysoxic bottom-water conditions. Thus, we suggest a decrease in bottom-water oxygenation during MECO peak warming, potentially caused by the high productivity and/or the transient influence of an older, oxygen-depleted water mass.

Overall, our data suggest that the extent and rate of environmental change associated with the MECO varies in different ocean basins and that the processes influencing bottom waters are subject to large latitudinal differences.

References:

Bijl, P.K., Houben, A.J.P., Schouten, S., Bohaty, S.M., Sluijs, A., Reichart, G.-J., Sinninghe Damsté, J.S., Brinkhuis, H., 2010. Transient Middle Eocene Atmospheric CO2 and Temperature Variations. Science 330, 819-821.

Bohaty, S.M., Zachos, J.C., 2003. Significant Southern Ocean warming event in the late middle Eocene. Geology 31, 1017.

Bohaty, S.M., Zachos, J.C., Florindo, F., Delaney, M.L., 2009. Coupled greenhouse warming and deep-sea acidification in the middle Eocene. Paleoceanography 24, PA2207.
Bolli, H.M., Beckmann, J.P., Saunders, J.B., 1994. Benthic foraminiferal biostratigraphy of the south Caribbean region. Cambridge Univ Pr, Cambridge.
Burgess, C.E., Pearson, P.N., Lear, C.H., Morgans, H.E.G., Handley, L., Pancost, R.D., Schouten, S., 2008. Middle Eocene climate cyclicity in the southern Pacific: Implications for global ice volume. Geology 36, 651-654.
Edgar, K., Wilson, P., Sexton, P., Gibbs, S., Roberts, A., Norris, R., 2010. New biostratigraphic, magnetostratigraphic and isotopic insights into the Middle Eocene Climatic Optimum in low latitudes. Palaeogeography, Palaeoclimatology, Palaeoecology 297, 670–682.
Edgar, K.M., Wilson, P.A., Sexton, P.F., Suganuma, Y., 2007. No extreme bipolar glaciation during the main Eocene calcite compensation shift. Nature 448, 908-911.
Herguera, J.C., Berger, W., 1991. Paleoproductivity from benthic foraminifera abundance: Glacial to postglacial change in the west-equatorial Pacific. Geology 19, 1173-1176.
Jorissen, F.J., Fontanier, C., Thomas, E., 2007. Paleoceanographical proxies based on deep-sea benthic foraminiferal assemblage characteristics, in: Hillaire-Marcel, C., de Vernal, A. (Eds.), Proxies in Late Cenozoic Paleoceanography: Pt. 2: Biological tracers and biomarkers. Elsevier, pp. 263-326.
Luciani, V., Giusberti, L., Agnini, C., Fornaciari, E., Rio, D., Spofforth, D.J.A., Pälike, H., 2010. Ecological and evolutionary response of Tethyan planktonic foraminifera to the middle Eocene climatic optimum (MECO) from the Alano section (NE Italy). Palaeogeography, Palaeoclimatology, Palaeoecology 292, 82-95.
Miller, K.G., Wright, J.D., Fairbanks, R.G., 1991. Unlocking the Ice House: Oligocene-Miocene Oxygen Isotopes, Eustasy, and Margin Erosion. J. Geophys. Res. 96, 6829-6848.
Moebius, I., Friedrich, O., Scher, H.D., submitted. Changes in Southern Ocean bottom water environments associated with the Middle Eocene Climatic Optimum. submitted to: Palaeogeography, Palaeoclimatology, Palaeoecology.
Pälike, H., Lyle, M.W., Nishi, H., Raffi, I., Ridgwell, A., Gamage, K., Klaus, A., Acton, G., Anderson, L., Backman, J., 2012. A Cenozoic record of the equatorial Pacific carbonate compensation depth. Nature 488, 609-614.
Scher, H.D., Delaney, M.L., 2010. Breaking the glass ceiling for high resolution Nd isotope records in early Cenozoic paleoceanography. Chemical Geology 269, 329-338.
Spofforth, D.J.A., Agnini, C., Pälike, H., Rio, D., Fornaciari, E., Giusberti, L., Luciani, V., Lanci, L., Muttoni, G., 2010. Organic carbon burial following the middle Eocene climatic optimum in the central western Tethys. Paleoceanography 25, PA3210.
Tjalsma, R.C., Lohmann, G., 1983. Paleocene-Eocene bathyal and abyssal benthic foraminifera from the Atlantic Ocean, Micropaleontology, Spec. Publ., no 4. Micropaleontology Pr.
Van der Zwaan, G., Duijnstee, I., Den Dulk, M., Ernst, S., Jannink, N., Kouwenhoven, T., 1999. Benthic foraminifers: proxies or problems? A review of paleocological concepts. Earth-Science Reviews 46, 213-236.
Witkowski, J., Bohaty, S.M., McCartney, K., Harwood, D.M., 2012. Enhanced siliceous plankton productivity in response to middle Eocene warming at Southern Ocean ODP Sites 748 and 749. Palaeogeography, Palaeoclimatology, Palaeoecology 326, 78-94.
Zachos, J.C., Quinn, T.M., Salamy, K.A., 1996. High-Resolution (104 Years) Deep-Sea Foraminiferal Stable Isotope Records of the Eocene-Oligocene Climate Transition. Paleoceanography 11, 251-266.

ICDP

Petrographic and geochemical study of archean spherule layer occurrences in the BARB 5 ICDP drill core, Barberton Greenstone Belt, South Africa.

T. MOHR-WESTHEIDE[1], J. FRITZ[1], A. HOFMANN[2], R. TAGLE[3], C. KOEBERL[4,5], W.U. REIMOLD[1,6], D. MADER[4], T. SCHULZ[4], AND D. HOEHNEL[1]

[1] Museum für Naturkunde Berlin, Invalidenstrasse 43, 10115 Berlin, Germany.
[2] Department of Geology, University of Johannesburg, Johannesburg, South Africa.
[3] Bruker Nano GmbH, Am Studio 2, 12489 Berlin, Germany.
[4]University of Vienna, 1090 Wien, Austria.
[5]Natural History Museum, 1010 Vienna, Austria.
[6]Humboldt-Universität zu Berlin, Unter den Linden 6, 10099 Berlin, Germany.

In the Barberton Greenstone Belt (BGB), four distinct spherule horizons (S1-S4) with ages between about 3.5 and 3.2 Ga have been considered amongst the oldest remnants of large bolide impacts onto Earth [1,2] and allow to investigate the early Archean impact record on Earth. Spherules in these layers are interpreted as molten impact ejecta and condensation products from impact plumes or ejecta that were melted during atmospheric re-entry [2,3]. Primary signatures preserved in the spherule layers may provide insights regarding the impact event(s) and the projectiles involved. However, the spherule layers were extensively modified by sedimentary, diagenetic, and metamorphic processes [4], leaving, for example, questions regarding the number of individual spherule layers or the nature of primary versus secondary spinel and primary versus secondary projectile signatures [5].To discriminate between primary and secondary (alteration) geochemical characteristics of the spherule layers, a comprehensive study of sedimentary, petrographic, mineralogical, and geochemical characteristics from spherule layers in the ICDP drill core BARB 5 from the Barite Valley Syncline of the BGB is carried out.

All samples were studied by transmitted and reflected light microcopy, scanning electron microscopy (SEM), with the Bruker M4 Tornado micro-XRF scanner, and by instrumental neutron activation analysis (INAA).

In a 20 cm thick core interval (511.31-511.51 m) in BARB 5 0.3 to 2 mm sized spherules occur densely packed in four layers each about 4 cm thick. A further, 4 cm thick, intersection of a spherule layer occurs at 512.30 m depth, results for which will be disussed elsewhere. Layers 1-4 are separated by <1.5 cm thick shale beds. Cross-lamination is observed in the interval between layers 1 and 2. This spherule-layer-bearing interval correlates either with spherule layer S3 or S4 [6] or represents a different unit. Spherules on top of layer 1 are strongly sheared, in stark contrast to the generally un- or slightly deformed spherules in layers 2-4. In general, all spherule beds are comprehensively altered to assemblages of quartz, phyllosilicates, K-feldspar, Mg-siderite, barite, and calcite. The spherule layers in BARB 5 core show sulfide mineralization increasing from layer 1 to layer 4, with main ore minerals being pyrite, chalcopyrite, and gersdorffite. Sulfide mineralization often affects both matrix and spherules. Statistical analysis of spherule size did not show sorting of the individual spherule beds, but a slight increase of average spherule size from top to bottom was observed.

The X-ray elemental maps showed a comparatively low Cr abundance in the matrix and even less in the spherules for bottom layer 1. Chromium is highly concentrated in the sheared spherule zone enriched in chlorite and colored green. Nickel does not correlate with chromium and is only abundant in the zone straddling the transition from the green layer into the shale interbed above. Ni abundances in spherule layers may or may not be correlated with S and As contents. Chromite grains are well visible in a few undeformed sperules on top of the sheared zone. In contrast to layer 1, layers 2-4 contain zircon and nickel-rich chrome-spinel. Such Ni-rich chromites have been reported from layers S2 and S3 [5,6]. Scanning electron microscopy indicates that spinel in BARB 5 has distinct multiple types of zonation, mainly reflected in their Fe, Ni, Zn, and Cr contents. A major

spinel type involves cores rich in NiO (up to 19 wt%), changing to rims rich in ZnO (up to 7.9 wt%). Another main type is characterized by moderate NiO (up to 7.5 wt%) and relatively high Cr_2O_3 (up to 50 wt%) contents without zonation. The contents of Cr_2O_3 and NiO display, in general, a negative correlation. Where abundant, Co correlates well with nickel. In some cases V is abundant (up to >3.1 wt%). Highest Zn concentrations are often observed around the rims of Ni-rich spinels. Internally broken spinel frequently shows marginal Zn-enrichment on all fragments, indicating that this is likely secondary alteration late in the evolution of these materials.

The INAA trace element analyses showed distinctly elevated contents of the siderophile elements, such as Ni, Co, Ir, and Os, but also of Cr and Au, over the whole sample section. The lowest contents were found in the bottom layer 1 of the section, with about 0.3 to 10 ppb Ir, 7 to 22 ppm Co, and 120 to 470 ppm Ni. The highest amounts were found in spherule layer 2 with about 600 ppb Ir, 250 ppm Co, and 3800 ppm Ni, and at the top of spherule layer 3 with 730 ppb Ir, 530 ppm Co, and 5400 ppm Ni. In other parts of the section, the siderophile element contents were lower, with Ir in the 150-400 ppb range.

The presence of four closely spaced spherule beds with intermittent thin sedimentary layers is suggestive of aquatic deposition after a single impact event, with multiphase currents affecting sedimentation. However, grain size statistics do not significantly indicate regular decrease of spherule sizes from layers 1 to 4, which one would expect to occur with deposition under waning current activity. Our preliminary petrographic and geochemical findings indicate strong hydrothermal overprint for all lithologies in the studied section of the BARB 5 core. Primary characteristics include spherule size and shapes, and presence of Ni-rich chromite (projectile related formation), as well as zircon (terrestrial source) – both of which are, however, noticeably absent in layer 1. Sulfide mineralization, (e.g., pyrite, gersdorffite, and other sulfides) is of secondary origin and may be related to chemical alteration and metamorphism. High Zn concentrations frequently observed along cataclased spinel grains likely relate to late overprint. High abundances of the siderophile elements (Ni, Co, Ir, Os, Cr, and Au) are thought to reflect extraterrestrial components. However, as already observed by [7], these abundances are on the same level, or even exceeding, the contents of these elements in chondritic meteorites, which remains puzzling.

References:
[1] Lowe D. R. et al. (1989) *Science*, 245, 959-962. [2] Lowe D. R. et al. (2003) *Astrobiology*, 3, 7-47. [3] Johnson B. C. and Melosh H. J. (2014) *Icarus,* 228,
347-363. [4] Hofmann A. et al. (2006) *Geol. Soc. Amer. Spec. Pap. 405, 33-56.2* [5] Reimold W. U. et al. (2000) In: *Impacts and the Early Earth*, 117-180. [6]
Byerly G. R. and Lowe D. R. (1994) *Geochim. Cosmochim. Acta*, 58, 3469-3486. [7] Koeberl C. and Reimold W. U. (1995) *Precambrian Research,* 74, 1-33.

ICDP

Peering into the Cradle of Life:multiple sulfur isotopes reveal insights into environmental conditions and early sulfur metabolism some 3.5 Ga ago

A. MONTINARO[1], H. STRAUSS[1], P. MASON[2], A. GALIC[2]

[1] INSTITUT FÜR GEOLOGIE UND PALÄNTOLOGIE, WESTFÄLISCHE WILHELMS-UNIVERSITÄT MÜNSTER

[2] DEPARTMENT OF EARTH SCIENCE, UTRECHT UNIVERSITY

One of the most intriguing questions in earth and life sciences is where, when and under what conditions life emerged on our planet. Traces of early life on Earth comprise microfossils, stromatolites and chemofossils, i.e. chemical and isotopic signatures related to metabolic pathways. In particular, the stable isotopes of key elements of life, i.e. C, N and S have been utilized successfully for tracing life in Earth's respective archive, i.e. the sedimentary rock record.

Well-preserved rock of the Archean successions occur within the Barberton Greenstone Belt, South Africa, exhibiting a sequence of volcanic and sedimentary rocks that includes oceanic and continental lithofacies. The Barberton Supergroup comprises three major lithostratigraphic units. These are, in ascending order, the Onverwacht Group (3550–3260 Ma), mainly composed of ultramafic to mafic volcanic rocks, the Fig Tree Group (3260–3225 Ma), consisting of greywacke, shale, chert and dacitic volcanic rocks, and the Moodies Group (3225–3215 Ma), composed of conglomerate, sandstone, siltstone and shale (Visser, 1956; Lowe and Byerly, 1999). The Barberton Greenstone Belt was drilled in 2011 by the multinational and multidisciplinary ICDP project "Peering into the Cradle of Life", that aims to investigate under which environmental conditions life emerged and evolved on our planet. In general , during the early stages of Earth's evolution, environmental conditions were much different from today. The early Earth was characterized by a predominance of oceanic over continental crust (Rollinson, 2007) and presumably higher surface temperatures (Knauth, 2005). The early atmosphere was reducing with abundant carbon dioxide and methane but largely devoid of oxygen ($<10^{-5}$ PAL – present atmospheric level), while the ocean was anoxic (Holland, 2002). Hence, life emerged and evolved under seemingly inhospitable environmental conditions.

In this study, multiple sulfur isotopes are used in order to trace early metabolisms on Earth as well as to characterize the prevailing environmental and redox conditions. In particular, different sulfur sources and (bio)geochemical processes that governed the Archean sulfur cycle will be assessed through studying sulfide and sulfate minerals that potentially carry two different isotopic signals, i.e. mass-dependent and mass-independent sulfur isotopic fractionation. These different signals can be utilized to deduce terrestrial processes of sulfur cycling well as atmospheric sources of sulfur.

Mass-independent sulfur isotopic fractionation is thought to reflect the photochemistry of volcanogenic sulfur dioxide. Results are expressed as $\Delta^{33}S$ and $\Delta^{36}S$ values that represent a quantification of the deviation from the mass-dependent terrestrial fractionation line. The

preservation of distinctly different $\Delta^{33}S$ signals in the sedimentary realm is possible only under anoxic atmospheric conditions, with a maximum level of atmospheric oxygen of 10^{-5} PAL (Pavlov and Kasting, 2002), thus, anoxic conditions of Earth's atmosphere. Consequently, a systematic and comprehensive multiple sulfur isotope (^{32}S, ^{33}S, ^{34}S, and ^{36}S) study is being pursued for understanding the early sulfur cycle, prevailing overall environmental and redox conditions in particular, as well as for tracing life on Earth.

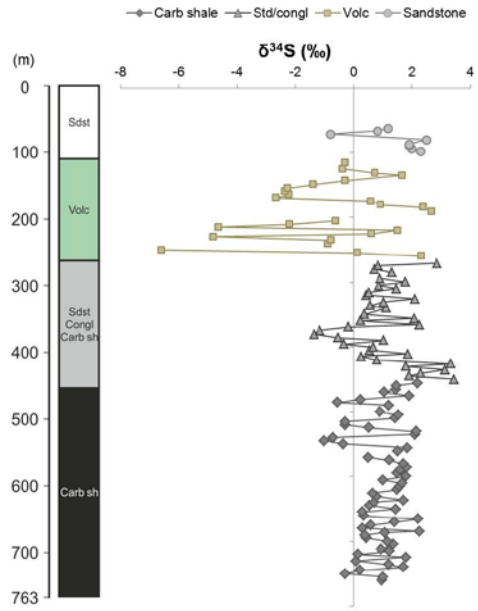

Fig. 1: $\delta^{34}S$ versus depth and lithologies plot.

Three different types of sulfur metabolism have been identified in the Paleoarchean: sulfate reduction (Shen et al., 2001; Ueno et al., 2008; Shen et al., 2009; Wacey et al., 2010; Wacey et al., 2011a; Roerdink et al., 2012), elemental sulfur disproportionation (Philippot et al., 2007; Wacey et al., 2010; Wacey et al., 2011a), and sulfide oxidation (Wacey et al., 2011b). In general, negative $\delta^{34}S$ values for sedimentary pyrite are thought to identify its biological origin because pyrite in modern marine sediments resulting from bacterial sulfate reduction usually displays negative sulfur isotope values (Strauss, 1997). However, sulfur isotopic fractionation is further controlled by additional environmental factors, like the reduction rate and the availability of sulfate (e.g., Leavitt et al., 2013). The principal product of bacterial sulfate reduction is hydrogen sulfide, which is depleted in ^{34}S, because bacteria preferentially utilize the lighter isotope ^{32}S for their metabolism, allowing the precipitation of ^{34}S-depleted pyrite.

We studied ICDP drill core BARB5 (Fig. 1) that was drilled in the Barite Syncline, specifically from the Mapepe Formation, Fig Tree Group. The lowest part is mostly composed of carbonaceous siltstone, the middle part of interbedded sandstone, conglomerate and siltstone, while the upper part comprises volcanoclastic rocks, carbonate, chert and barite. The uppermost sandstone is mostly alterated and weathered. Total core length is 763.23 m.

From powdered bulk samples total sulfur was measured via IR spectroscopy of SO_2 using a CS-MAT 5500 instrument. For isotope analyses, acid-volatile sulfide (AVS) and chromium-reducible sulfur (CRS) were extracted from bulk rock and precipitated as silver sulfide (Ag_2S). Resulting silver sulfides were subsequently subjected to multiple sulfur isotope measurements (^{32}S, ^{33}S, ^{34}S, ^{36}S) using a ThermoFinnigan MAT 253, following the fluorination of silver sulfide precipitates.

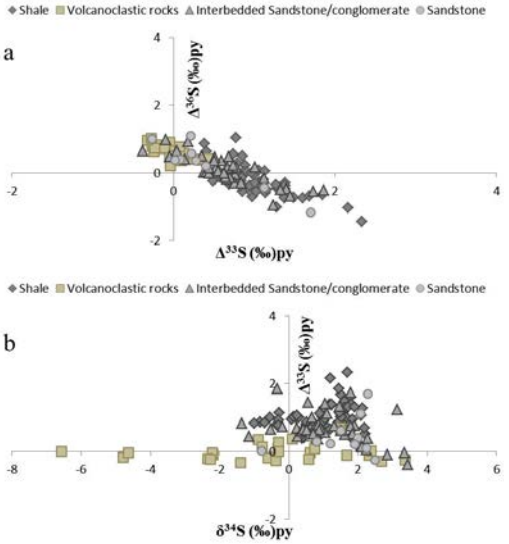

Fig. 2a: $\Delta^{33}S$ versus $\Delta^{36}S$ plot, with a linear negative correlation with a slope of -0.8.
Fig. 2b: $\delta^{34}S$ versus $\Delta^{33}S$ plot in different lithologies.

Total sulfur abundances range between 0.01 and 3.03 wt.% (avg. 0.26 wt.%, n=140; avg. for carbonaceous shale 0.34 wt.%, n=67; avg. for intercalated sandstone, conglomerate and shale 0.16 wt.%, n=35; avg. for volcanoclastic rocks 0.25 wt.%, n=30; avg. for upper sandstone 0.15 wt.%, n=9). The carbonaceous shale displays a sulfur isotopic composition ($\delta^{34}S$) between -1.0 and 2.3‰ (avg. 1.0‰; n=67). Samples from the interbedded sandstone, conglomerate and shale are characterized by $\delta^{34}S$ values between -1.3 and 3.4‰ (avg. 1.1‰; n=35). Volcanoclastic rocks show $\delta^{34}S$ values ranging from -6.5 to 3.4‰ (avg. 0.6‰; n=30), and the upper sandsone displays $\delta^{34}S$ values ranging between -0.8 and 2.5‰ (avg. 1.6‰; n=9).

Similar to $\delta^{34}S$, $\Delta^{33}S$ values are different for each lithofacies. Samples from the carbonaceous shale yielded a range between 0.02 and 2.33‰ (avg. 0.98‰, n=67), thus carbonaceous shale shows positive values. Interbedded sandstone, conglomerate and shale are characterized by $\Delta^{33}S$ values between -0.38 and 1.86‰ (avg. 0.67‰, n=35). Volcanoclastic rocks yielded $\Delta^{33}S$ values between -0.32 and 0.30‰ (avg. 0.01‰, n=28), whereas the upper sandstone displays $\Delta^{33}S$ values between -0.26 and 1.70‰ (avg. 0.42‰; n=9). Furthermore, samples reveal a linear negative correlation between $\Delta^{33}S$ and $\Delta^{36}S$ with a slope of -0.8, typical for Archean sedimentary sulfides (Fig. 2a) (Farquhar et al., 2000).

Each lithofacies is characterized by a different sulfur isotopic composition. $\delta^{34}S$ values are homogeneously distributed across the lower part of the core, while variable $\delta^{34}S$ values are discernible in the upper part of the core

(Fig. 1). ”^{33}S values in carbonaceous shale, in the interbedded sandstone, conglomerate and shale, and in the upper sandstone reflect mass-independent isotope fractionation, hence an atmospheric signature (Fig. 2b). In contrast, volcanoclastic rocks display rather small ”^{33}S values but substantial variability in ´^{34}S (Fig. 2a). Results we obtained are not consistent with results from Philippot et al. (2012), from a core drilled in the Barite Valley. Their results are more exotic, showing highly depleted ´^{34}S values and highly positive ”^{33}S values. Besides, they define a felsic volcanic array we cannot observe in our samples. Multiple sulfur isotope results from carbonaceous shale, interbedded sandstone, conglomerate and shale, and upper sandstone from the BARB5 drill core exhibit the mass-independent fractionation of sulfur isotopes, hence an atmospheric source signature. Data define a mixing line between two different pathways of S in pyrite: one reflecting the derivation from elemental sulfur (carrying positive ”^{33}S) and the other revealing pyrite formation following the bacterial reduction of atmospheric sulfate (carrying negative ”^{33}S). In contrast, volcanoclastic rocks in BARB5 show an extremely attenuated mass-independet fractionation signal, visible from the slope of -0.8 between ”^{33}S and ”^{36}S, that is typical for Archean sulfides (Fig. 2a)

Acknowledgements: Financial support from the Deutsche Forschungsgemeinschaft (DFG Str 281/36) is gratefully acknowledged.

References:

Farquhar, J., Bao, H., Thiemens, M., 2000. Atmospheric Influence of Earth's Earliest Sulphur Cycle. Science 289, 756–758.

Holland, H.D., 2002. Volcanic gases, black smokers, and the Great Oxidation Event. Geochim. Cosmochim. Acta 66, 3811-3826.

Knauth, L.P., 2005. Temperature and salinity history of Precambrian ocean: implications for the course of microbial evolution. Palaeogeography, Palaeoclimatology, Palaeoecology 219, 53-69.

Leavitt, W.D., Halevy, I., Bradley, A.S., Johnston, D.T., 2013. Influence of sulfate reduction rates on the Phanerozoic sulfur isotope record. Proc Natl Acad Sci USA, doi: 10.1073/pnas.1218874110.

Lowe, G.R., Byerly, G.R., 1999. Stratigraphy of the west-central part of the Barberton greenstone belt, South Africa. In: Lowe, G.R. and Byerly, G.R. (Eds.), Geologic Evolution of the Barberton Greenstone Belt, South Africa. Spec. Pap. Geol. Soc. Amer., 329, 1-36.

Pavlov, A.A., Kasting, J.F., 2002. Mass-independent fractionation of sulphur isotopes in Archaean sediments: strong evidence for an anoxic Archaean atmosphere. Astrobiology 2, 27-41.

Philippot, P., Van Zuilen, M., Lepot, K., Thomazo, C., Farquhar, J., Van Kranendonk, M.J., 2007. Early Archaean Microorganisms Preferred Elemental Sulfur, Not Sulfate. Science 317, 1534-1537.

Philippot et al 2012. Variations in atmospheric sulphur chemistry on early Earth linked to volcanic activity. Nature Geoscience: Volume 5, Pages 668-674.

Roerdink, D.L., Mason, P.R.D., Farquhar, J., Reimer, T., 2012. Multiple sulfur isotopes in Paleoarchean barites identify an important role for microbial sulfate reduction in the early marine environment. Earth and Planetary Science Letters 331-332, 177-186.

Rollinson, H.R., 2007. Early Earth Systems: A Geochemical Approach. Blackwell Publishing.

Shen, Y., Buick, R., Canfield, D.E., 2001. Isotopic evidence for microbial sulphate reduction in the early Archaean era. Nature 410, 77-81.

Shen, Y., Farquhar, J., Masterson, A., Kaufman, A.J., Buick, R., 2009. Evaluating the role of microbial sulfate reduction in the early Archean using quadruple isotope systematics. Earth and Planetary Science Letters 279, 383-391.

Strauss, H. 1997. The isotopic composition of sedimentary sulfur through time.

Palaeogeography, Palaeoclimatology, Palaeoecology 132, 97-118.

Ueno, Y., Ono, S., Rumble, D., Maruyama, S., 2008. Quadruple sulfur isotope analysis of ca. 3.5 Ga Dresser Formation: New evidence for microbial sulfate reduction in the early Archean. Geochimica et Cosmochimica Acta, 72, 5675-5691.

Visser, D.J.L. (Comp), 1956. The geology of the Barberton area. Spec. Publ Geol. Szrv. S. Afr., 15, 253.

Wacey, D., McLoughlin, N., Whitehouse, M.J., Kilburn, M.R., 2010. Two coexisting sulfur metabolisms in a ca. 3400 Ma sandstone. Geology 38, 1115-1118.

Wacey, D., Kilburn, M.R., Saunders, M., Cliff, J., Brasier, M.D., 2011a. Microfossils of sulphur-metabolizing cells in 3.4-billion-year-old rocks of Western Australia. Nature Geoscience 4, 698-702.

Wacey, D., Saunders, M., Brasier, M.D., Kilburn, M.R., 2011b. Earliest microbially mediated pyrite oxidation in ~ 3.4 billion-year-old sediments. Earth and Planetary Science Letters 301, 393-402.

ICDP

P and S wave tomography of the earthquake swarm area W-Bohemia/Vogtland and the relation between velocity structure and possible fluid migration

S. MOUSAVI[1], M. KORN[1], K. BAUER[2]

[1] Institut für Geophysik und Geologie, Universität Leipzig, Talstraße 35, 04103 Leipzig

[2] Deutsches Geoforschungszentrum Helmholtz-Zentrum Potsdam

The West Bohemia/Vogtland region is known for its complicated past and present geodynamical activities like repeated occurence of earthquake swarms, presence of mantle derived CO_2 and He isotopes, gas vents, mofettes, mineral waters, geothermal springs and quaternary volcanoes. At present there is no exact explanation for the concentration of many aspects of geodynamical phenomena in this small area. The commonly accepted hypothesis is the existence of an active magma reservoir in the upper mantle which is the source of upward fluid migration. Fluid upwelling causes stress changes on existing fault planes and triggers the periodic swarm quake activity at mid-crustal depths. The swarm quake epicenters and the gas escapement centers at the surface are not co-located, and the fluid pathways within the upper crust remain unclear.

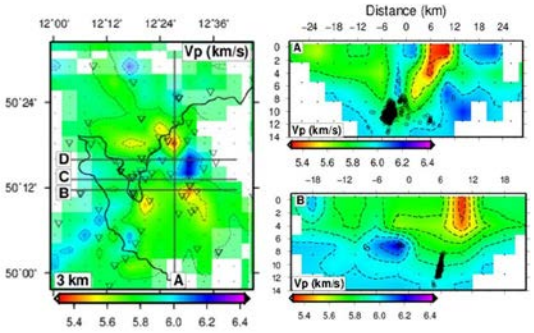

In this study we use local earthquake data to image the P- and S-velocity structure and the Vp/Vs ratio in a larger area around the prominent swarm quake region. Dense permanent and temporary seismic networks run by Czech and German institutions provide a sufficiently dense coverage to obtain a detailed 3D image of the velocity strucure and accurate hypocenter locations. Data from 543 spatially distributed events provided 13420 reliable picks of P and S onset times. A 3D model of Vp and Vp/Vs distribution was obtained using standard travel time inversion. Vertical cross sections of Vp and Vp/Vs distributions are presented in the figure.

To support the interpretation of the tomographic model, pattern recognition techniques were additionally applied using self-organizing maps. This kind of analysis reveals prominent features within the model, which show distinct anomalous petrophysical properties.

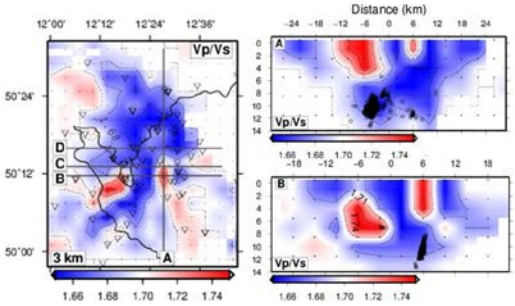

Fluid behavior in the subsurface of western Bohemia is still poorly understood, however, according to the results of this study, the tomographic images confirm the existence of two main fluid passages towards the Bad Brambach and the Bublak mofettes. These two anomalies with high Vp/Vs ratio, assumed to be highly fluid saturated fracture zones, were detected at the upper limit of swarm quakes focal zone. Another interesting result is the detection of a linear high Vp/Vs anomaly along the MLF in the shallow crust of Western Bohemia. This feature could be related to increased fluid saturation within the fractured surroundings of the seismically active fault plain. Ultimately, the distribution of re-located hypocenters corresponds to the regions with low Vp and low Vp/Vs ratio. The correlation between the detected Vp and Vp/Vs anomalies with the location of the earthquake swarm suggests a model in which CO_2 as part of magmatic fluids exists in the vast area beneath western Bohemia and frequently migrates up to the surface.

The results of this study could help to narrow the area of possible locations for an ICDP drilling project in view of direct observation of active fluid pathways.

IODP

Biomarker based reconstruction of Plio- and Pleistocene climate and environmental conditions in the Gulf of Alaska: Preliminary results obtained from Expedition 341 sediments

J. MÜLLER[1], M.L. SANCHEZ MONTES[2], E. MCCLYMONT[2], R. STEIN[1], K. FAHL[1], K. MANGELSDORF[3], H. WILKES[3], AND EXPEDITION 341 SCIENTISTS

[1]Alfred Wegener Institute Helmholtz Centre for Polar and Marine Research, Germany
[2]Department of Geography, Durham University, UK
[3]Helmholtz Centre Potsdam German Research Centre for Geosciences, Germany

A remarkable sedimentary record that extends from the Miocene to the late Pleistocene/Holocene has been drilled during IODP Expedition 341 (May - July 2013) in the Gulf of Alaska (Expedition 341 Scientists, 2013). The recovery and examination of sediments along a transect of five drill sites (U1417 - U1421) from the deep ocean towards the continental slope and shelf offshore the St. Elias Mountains enables the reconstruction of the palaeoceanographic and environmental development in the NE Pacific during a period of significant global cooling and directly addresses the overall research objectives of the IODP programme.

The knowledge about palaeo sea surface conditions and their relation to climate changes in the subpolar NE Pacific is relatively scarce and mainly confined to the past 17 ka BP (Addison, 2012; Davies, 2011; Barron, 2009). Within the framework of the PECA (Plio-**P**leistocene **E**nvironmental and **C**limatic conditions in the Gulf of **A**laska) project, biomarker based reconstructions of the sea surface conditions (i.e. sea surface temperature (SST), sea ice coverage, marine primary productivity) that characterised the subpolar NE Pacific during critical time intervals of Plio- and Pleistocene climate change will be carried out to provide new information on oceanic and atmospheric feedback mechanisms and further enable the identification of teleconnections between the palaeoceanographic evolution in the North Pacific and the North Atlantic.

Here we present preliminary biomarker data obtained from sediments from the distal deepwater site U1417 and the proximal site U1419 located at the Gulf of Alaska continental slope. At both sites, recovered lithofacies span biogenic ooze to clast-rich glacigenic diamict indicative of a highly variable Late Neogene depositional environment. Late Pliocene strata at Site U1417 are characterised by highly bioturbated (*Zoophycos* ichnofacies) diatom bearing mud, whereas Pleistocene strata are dominated by glacigenic sediments (i.e. containing abundant ice rafted detritus) at all sites. The intensification of the Northern Hemisphere Glaciation during the Plio-Pleistocene Transition (PPT) as well as the shift from a 41 ka to a 100 ka world during the Mid Pleistocene Transition (MPT) - two of the most prominent intervals of global Quaternary climate change - are clearly identifiable in Site U1417 sediments by means of shipboard lithostratigraphy and magnetostratigraphy data (Expedition 341 Scientists, 2013). In contrast to the long-term climate record preserved at Site U1417, exceptional high sedimentation

rates at Site U1419 allow for an ultra-high temporal resolution reconstruction of the late Pleistocene development of an ice-sheet proximal environment at the southern continental slope of Alaska during the last glacial cycle. Importantly, this site enables the detailed study of deglacial (including e.g. the Bølling-Allerød and Younger Dryas events), Last Glacial Maximum (LGM) and LGM preceding climate conditions and glacial oscillations (e.g. Heinrich events known from the North Atlantic realm).

The biomarker inventory of U1417 and U1419 sediments has been (and will be further) analysed to gain information on the Plio- and Pleistocene sea surface conditions and terrigenous organic matter input (e.g. via ice rafting or meltwater plumes). Variability in the distribution and abundance of short- and long-chain *n*-alkanes, sterols, and C_{25}-highly branched isoprenoids (HBIs) is interpreted to reflect changes in the environmental setting. These data provide insight into marine primary productivity changes (likely in response to cooling and warming intervals) and the variable input of terrigenous organic matter via meltwater and/or iceberg discharge events. The C_{25}-HBI diene/triene ratio - hitherto used as a sea ice proxy in the Southern Ocean (Masse et al., 2011; Etourneau, 2013) - is applied to examine the variability in polar water/sea ice extent in the study area. Previously, Rowland et al. (2001) documented that not only the degree of unsaturation in C_{25}-HBIs but also the *E*- to *Z*-isomerisation in the C_{25}-HBI trienes increases with increasing water temperature. Based on this observation we suggest that the ratio of the *Z*-isomer to the *E*-isomer in the C_{25}-HBI trienes might reflect SST changes and could be used as an additional qualitative SST proxy. The applicability of this approach, however, needs further evaluation (e.g. through comparisons with alkenone SST data obtained from Expedition 341 sediments).

References:

Addison, J.A., Finney, B.P., Dean, W.E., Davies, M.H., Mix, A.C., Stoner, J.S., Jaeger, J.M., 2012. Productivity and sedimentary $\delta^{15}N$ variability for the last 17,000 years along the northern Gulf of Alaska continental slope. Paleoceanography, 27 (1), PA1206.

Barron, J.A., Bukry, D., Dean, W.E., Addison, J.A., Finney, B., 2009. Paleoceanography of the Gulf of Alaska during the past 15,000 years: Results from diatoms, silicoflagellates, and geochemistry. Marine Micropaleontology, 72 (3–4), 176-195.

Davies, M.H., Mix, A.C., Stoner, J.S., Addison, J.A., Jaeger, J., Finney, B., Wiest, J., 2011. The deglacial transition on the southeastern Alaska Margin: Meltwater input, sea level rise, marine productivity, and sedimentary anoxia. Paleoceanography, 26 (2), PA2223.

Etourneau, J., Collins, L.G., Willmott, V., Kim, J.H., Barbara, L., Leventer, A., Schouten, S., Sinninghe Damsté, J.S., Bianchini, A., Klein, V., Crosta, X., Massé, G., 2013. Holocene climate variations in the western Antarctic Peninsula: evidence for sea ice extent predominantly controlled by changes in insolation and ENSO variability. Climate of the Past, 9 (4), 1431-1446.

Expedition 341 Scientists, 2013. Southern Alaska margin: Interactions of tectonics, climate, and sedimentation. IODP Preliminary Report., 341. doi:10.2204/iodp.pr.341.2013.

Massé, G., Belt, S.T., Crosta, X., Schmidt, S., Snape, I., Thomas, D.N., Rowland, S.J., 2011. Highly branched isoprenoids as proxies for variable sea ice conditions in the Southern Ocean. Antarctic Science, 23 (05), 487-498.

Rowland, S.J., Allard, W.G., Belt, S.T., Masse, G., Robert, J.M., Blackburn, S., Frampton, D., Revill, A.T., Volkman, J.K., 2001. Factors influencing the distributions of polyunsaturated terpenoids in the diatom, Rhizosolenia setigera. Phytochemistry, 58 (5), 717-728.

ICDP

Formation of fast-spreading oceanic crust: Petrological and geochemical investigation of the „Wadi Gideah“ cross section in the Oman ophiolite

T. MÜLLER[1], J. KOEPKE[1], D.GARBE-SCHÖNBERG[2], H. STRAUSS[3]

[1]Institut für Mineralogie, Leibniz Universität Hannover, Germany (t.mueller@mineralogie.uni-hannover.de)
[2]Institut für Geowissenschaften, Christian-Albrechts-Universität zu Kiel, Germany
[3]Institut für Geologie und Paläontologie, Westfälische Wilhelms-Universität zu Münster, Germany

Fast-spreading oceanic crust, which covers a large part of our planet, is regarded as layered and relatively homogenous, in contrast to oceanic crust generated at slow-spreading ridges. Theoretical models on magmatic accretion, thermal models, mass balance calculations or general alteration models related to the oceanic crust therefore only exist for fast-spreading systems. In spite of tremendous efforts by ship-based research, a complete modern chemical/petrological profile based on natural samples is still missing due to a lack of exposures and drilled sections of the deeper parts of fast-spread crust.

This study aims to establish a profile with reference character through fast-spreading crust by performing geochemical and petrological investigation of a crustal section of the Cretaceous Oman ophiolite, following the approach of Hopson et al. (1981). The Oman ophiolite is regarded as the best analogue of fast-spreading oceanic lithosphere on land and its southern massifs are regarded as the best area for studying “normal” fast-spreading ridge processes with the so-called “late-stage magmatism” being widely absent. For this study a complete section representative of approximately 6.5 km of fast-spreading oceanic crust was sampled at the Wadi Gideah in the Wadi Tayin massif. The profile includes 217 single samples of gabbro, dikes and basalts.

The project focuses on (1) petrography and major element studies, (2) trace and rare earth element studies, (3) quantifying the variations of crystallographic orientations with depth, (4) characterizing the evolution of hydrothermal alteration with depth by using strontium and oxygen isotopes, (5) characterizing the magmatic sources by Nd and Hf isotopes, and (6) quantifying sulfur cycling. In order to obtain data sets as coherent as possible, the concept is followed to perform all analytical investigations on the same single samples. This profile will be unique in terms of completeness of the crustal components and quality and coherence of analytical data to be obtained. Hence, it is well-suited for advancing our understanding of crustal accretion processes and the evolution of primary and secondary geochemical cycles in the environment of fast-spreading oceanic crust. The Oman profile will represent a reference section which is urgently needed for supporting the ICDP proposal "The Oman drilling project" lead by P. Kelemen (Columbia University, NY) in which the Wadi Gideah is a target for drilling key sections of the lower crust (e.g., the penetrating of the dike/gabbro transition). Moreover, our project provides scientific support for deep crust drilling projects of the Integrated Ocean Drilling Program (IODP, e.g., Site 1256 and Hess Deep Rift (equatorial Pacific), and on a longer term for the "MoHole to the Mantle" project).

With the structural data obtained during this project a layered stratigraphy of a virtually undeformed oceanic crust with a thickness of approximately 6.5 km was reconstructed. The Oman profile includes sheeted dikes (~1800m), varitextured gabbros (~700m), foliated gabbros (~1400m) and layered gabbros (~2600m) as main lithologies from top to bottom resting on a thin MOHO transition zone (~50m). The underlying upper mantle sequence (~300m) was sampled additionally but is not further considered for this project. Pillow basalts were sampled offset from the Wadi Gideah section and are used for petrological and geochemical investigations but not for calculation of the virtual profile length. Of special interest is to map and to characterize the frozen melt lens underlying the main part of the sheeted dike lithology.

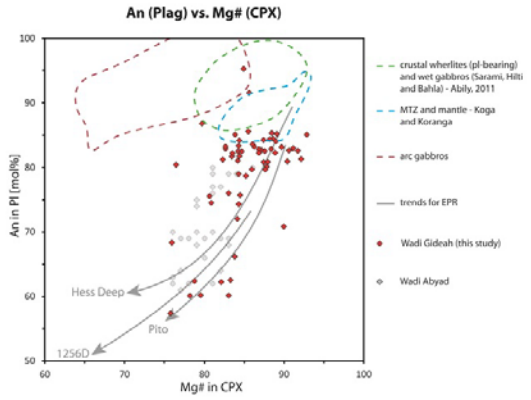

Fig. 1. An in plagioclase versus Mg# in clinopyroxene. Green dashed line represents field of data for plagioclase-bearing crustal wehrlites (Koepke et al., 2009) and gabbros assumed to be formed under high water activities ("wet gabbros") from Sarami, Hilti and Bahla (Abily, 2011). Blue dashed line represents field of data for gabbro sills within the mantle (Korenaga et al., 1997) and mantle transition zone (MTZ; Koga et al., 2003). Red dashed line represents field for arc gabbros (taken from Yamazaki et al., 2006). Grey arrows display differentiation trends of gabbros from the East Pacific Rise (EPR). Samples for this are from Hess Deep, IODP Leg 1256D and Pito Deep. Grey dots represent data for the Wadi Abyad profile within the Haylain block of the Oman Ophiolite (Browning, 1982). Red dots represent gabbros from the Wadi Gideah analyzed by electron microprobe.

We also focus on up to several 100 m wide fault zones cutting the layered gabbro at several places, which are characterized by the record of intense hydrothermal alteration at moderate (greenschist facies), high (amphibolite facies) and very high temperatures (magmatic regime). We identified these faults as zones were high hydrothermal flux was introduced into the lower crust, which were obviously responsible for cooling the deep crust. These zones are similar to those zones described as "focused fluid flow zones (FFFZ)" by Coogan et al. (2006), with the difference that the zones in the Wadi Gideah are much thicker (up to several 100 m; eventually multiple zones) and that their temperatures of formation reach the magmatic regime (formation of varitextured gabbro).

First results and conclusions are available after two third of the analytical investigation was done. The major mineral data of gabbroic rock follow a trend typical for normal mid-ocean ridge settings, very similar to trends recorded from the fast-spreading East Pacific Rise (EPR). This provides strong evidence, that this profile indeed correspond to a normal fast-spreading oceanic ridge situation (Fig 1), and not to a subduction zone setting which is characterized by quite different trends of gabbros ("arc gabbro trend" in Fig. 1). Electron probe micro analyses of the constituent mineral phases of the gabbro section reveal compositions of forsterite content in olivine from 0.75 to 0.82, XMg (Mg/(Mg+Fe), molar) in clinopyroxene from 0.82 to 0.92 and An in plagioclase from 72 to 85 mol% for the layered gabbro sequence. Foliated gabbros show compositions with forsterite content in olivine from 0.67 to 0.79, XMg in clinopyroxene from 0.76 to 0.87 and An in plagioclase from 60 to 85 mol%. Varitextured gabbros of the uppermost gabbro horizon show a forsterite content in olivine of 0.66, XMg in clinopyroxene from 0.76 to 0.84 and An in plagioclase from 67 to 85 mol%. The XMg for clinopyroxene and olivine vs. crustal depth displays a constant to slight negative trend for layered gabbros, changing to a distinct negative trend in foliated gabbros and fluctuations in varitextured gabbros. These trends clearly show that significant differentiation/fractionation was ongoing especially pronounced in the horizon of the foliated gabbros. These mineral trends are fully supported also be bulk chemical trends, both for major and trace elements.

First simple modeling using PETROLOG (Danyushevsky, L.V., Plechov, P., 2011) using a starting compositions corresponding to the bulk crust obtained recently from the Hess Deep Rift at equatorial EPR (Gillis et al., 2013) shows that the overall XMg trend with depth can be reproduced by a change of fractionation intensity in the middle of the plutonic crust at the horizon where the layered gabbros grade into the foliated gabbros. To summarize, the obtained major element trends with depth and the modeling performed so far provide strong evidence that the lower crust in the Wadi Gideah was accreted according to the "sheeted sill like" model and not to the "gabbro glacier model" which is favored as main accretion model for fast-spreading oceanic crust from many scientists. We suggest that the required deep crust cooling for the sheeted sill model was established via the observed focused fluid flow zones, like emphasized by Coogan et al. (2006). First results in isotopic composition for sampled FFFZ in the Wadi Gideah display increasing $^{87}Sr/^{86}Sr$ ratios compared to the surrounding gabbroic material, suggesting hydrothermal cooling down to the MOHO transition zone.

References:

Abily, B., 2011. Characteristiques petrographique, geochimique et structurale de la section crustale profonde del l'ophiolite d'Oman. Ph.D. Thesis, University of Toulouse, 686 pp.

Browning, P., 1982. The petrology, geochemistry, and the structure of the plutonic rocks of the Oman ophiolite. PhD Thesis Thesis, Open University, 404 pp.

Coogan, L.A., Howard, K.A., Gillis, K.M., Bickle, M.J., Chapman, H., Boyce, A.J., Jenkin, G.R.T., Wilson, R.N., 2006. Chemical and thermal constraints on focussed fluid flow in the lower oceanic crust. 306, 389-427.

Danyushevsky, L.V., Plechov, P., 2011. Petrolog3: Integrated software for modeling crystallization processes. Geochem. Geophys. Geosyst. 12, doi: doi:10.1029/2011GC003516.

Gillis, K.M, Snow, J.E., Klaus, A., Abe, N., Alden de Brito, A., Akizawa, N., Ceuleneer, G., Cheadle, M.J., Faak, K., Falloon, T.J., Friedman,

S.A., Godard, M.M., Guerin, G., Harigane, Y., Horst, A.J., Hoshide, T., Ildefonse, B., Jean, M.M., John, B.E.,Koepke, J., Machi, S., Maeda, J., Marks, N.E., McCaig, A.M., Meyer, R., Morris, A., Nozaka, T., Python, M., Saha, A., Wintsch, R.P., 2013 Primitive Layered Gabbros from Fast-Spreading Lower Oceanic Crust. Nature 505, 204-207

Koepke, J., Schoenborn, S., Oelze, M., Wittmann, H., Feig, S., Hellebrand, E., Boudier, F., Schoenberg, R., 2009. Petrogenesis of crustal wehrlites in the Oman ophiolite: Experiments and natural rocks. Geochem. Geophys. Geosyst. 10, doi:10.1029/2009GC002488.

Koga, K.T., Kelemen, P.B., Shimizu, N., 2003. Petrogenesis of the crust-mantle transition zone and theorigin of lower crustal wehrlite in the Oman ophiolite. Geochem. Geophys. Geosyst. 2, 2000GC000132.

Korenaga, J., Kelemen, P.B., 1997. Origin of gabbro sills in the Moho transition zone of the Oman ophiolite: Implications for magma transport in the oceanic lower crust. J. Geophys. Res.-Solid Earth 102, 27729-27749.

Pallister, J. S. & Hopson, C. A. (1981), Samail ophiolite plutonic suite: field relations, phase variation, cryptic variation and layering, and a model
of a spreading ridge magma chamber. Journal of Geophysical Research, 86 (B4), 2593–2644

Yamasaki, T., Maeda, J., Mizuta, T., 2006. Geochemical evidence in clinopyroxenes from gabbroic sequence for two distinct magmatisms in the Oman ophiolite. Earth Planet. Sci. Lett. 251, 52-65.

ICDP

Reflection seismic investigation of the geodynamically active West Bohemia-Vogtland region

N. MULLICK[1,2], S. BUSKE[1], S. SHAPIRO[2], P.WIGGER[2]

[1] Institute of Geophysics and Geoinformatics,TU Bergakademie Freiberg

[2] Institute of Geological Sciences, FU Berlin

The West Bohemia-Vogtland region in central Europe attracts much scientific interest due to recurrent earthquake swarms and continuous exhalation of CO2 dominated fluid from the subsurface. Seismological and geochemical studies reveal 1) significant upper mantle derived content of the emitted fluid (Weinlich et al., 1999), 2) an updoming of the MOHO below that area (Geissler et al.,2005) 3) possible existence of a magmatic fluid reservoir in the upper mantle (Weinlich et al., 1999) and 4) fluid activity as a possible trigger for the swarm earthquakes (Horalek and Fischer., 2008).

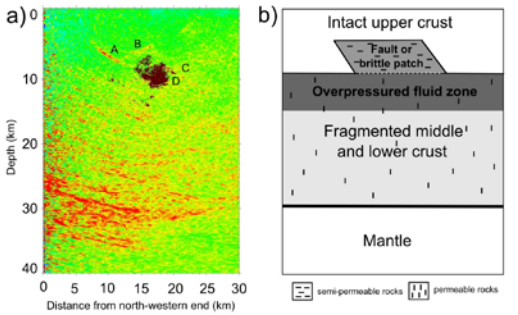

Figure 1: (a) The seismicity of the swarm area in the West-Bohemia/Vogtland region from year 1991 to 2011 (brown dots) plotted on top of the migrated section of 9HR profile. (b) Schematic sketch with the main interpreted features

In this study the subsurface beneath the region is investigated by reprocessing the deep reflection seismic profile 9HR (which runs almost directly across the swarm area (Figure 1)) with Kirchhoff prestack depth migration technique. Additionally, the waveforms of the swarm earthquakes recorded by local seismological station network KRASNET (1991-2008) has been used to image any structure directly above the swarm cluster that may act as a converter and produce converted waves recorded at a surface station.

The migrated image (Figure 1a)) confirms the upwelling of the MOHO known from receiver function studies. Directly below one of the major gas escape centres, channel like fault structures are observed which seem to have their roots at the MOHO. They may represent deep reaching degassing channels that allow direct transport of mantle-derived fluid.

Below the swarm earthquakes the crust is characterized by diffuse reflectivity (Figure 1a)). The diffuse reflectivity may be interpreted as highly fragmented permeable middle and lower crust below a rather intact less-permeable upper crust. Considering the nature of this reflectivity one can interpret this in terms of fluid from a source in the lower crust or upper mantle rising up through a strongly fragmented crust, hence producing even more diffuse reflectivity, and then getting blocked at some discontinuity. The high reflectivity and the laterally limited extent of bright spot A can be well explained by the presence of a fluid trap. This is also supported by the occurrence of many gas escape points adjacent to the swarm area (confirming active fluid flux below) but none directly above it. This way, fluids will accumulate at the bottom of the crustal units at a depth of approximately 10 km (Figures 1) and a highly pressured fluid zone may develop. After a critical pressure state is reached, this trapped fluid may then force its way up into the non-permeable medium above it by fracturing and generating swarms of earthquakes. Such a hypothesis is supported by the location of the main cluster of seismicity just above the strongly fragmented crust (upper edge marked by D), the influence of the swarm activity on the fluid activity (Bräuer et al., 2008) and also the results of modeling of hypocenter migration of the 2000 and 2008 swarms due to fluid movement (Fischer et al., 2013). Since the swarm seismicity is restricted mainly along a sub-vertical plane, the intrusion may possibly have taken place along a relatively permeable zone such as a fault or a brittle patch that extends from the fragmented permeable middle crust into the less-permeable units above (Figure 1b)). Bright spot (A) and the adjacent reflector (B) define the upper boundary of the seismicity and may therefore be identified as the upper edge of this semi-permeable zone.

In that context, the correlation of the seismic image (reflectivity) and the spatiotemporal evolution of the earthquake swarms in 2000 and 2008 additionally supports the above hypothesis. In both cases, the swarm activity initiates at the upper edge of the diffuse reflectivity zone marked by D with a sudden spontaneous upward movement of a large number of hypocenters (magenta dots in Figure 2a & 2e). This gives the impression of a release of highly pressurized trapped fluids into less permeable rocks above it by simultaneous fracturing and intruding into an overlying fault zone and redistributing the stress in the zone. Note that although the foci migration was rather complex in details, a prevailing upward spreading was observed in both swarms (Fischer at al., 2013). Then, the hypocenters ascend further with another sudden large number of events at bright spot C (blue dots in Figure 2b & 2f) followed by an immediate downward movement in case of year 2000 swarm (dark blue dots in Figure 2b). This may indicate the existence of a relatively strong

barrier that obstructs the ascent of the fluids. In the late periods of the swarms (since the second half of November 2000 and 2008, respectively) the hypocenter migration is stopped beneath an overlying bright spot B, and spreads in a cluster aligned with the local inclination of the bright spot B (black dots in Figure 2c & 2g). This may be interpreted as the ascending fluid being blocked by a non-permeable boundary and have no alternative but to turn and move along the boundary, further generating earthquakes until losing all of its energy.

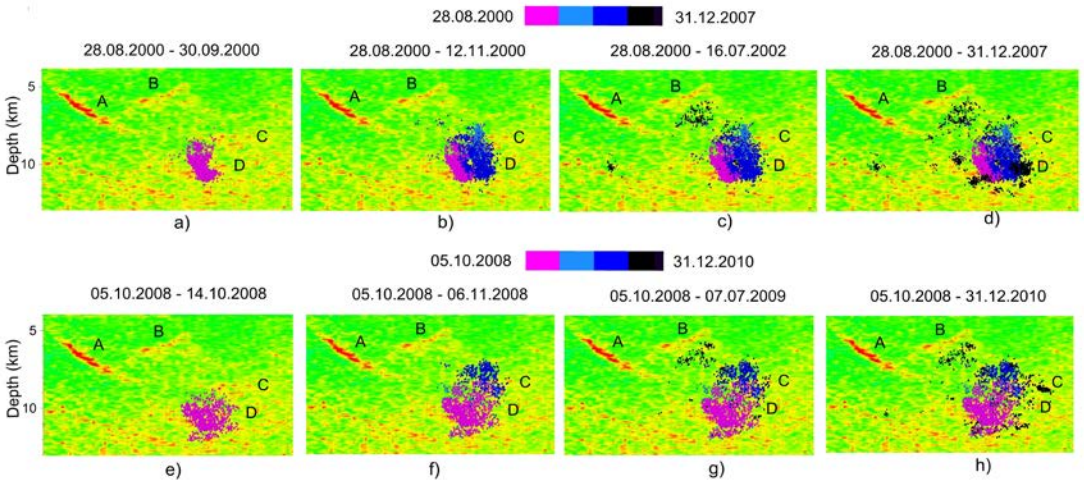

Figure 2. Spatiotemporal evolution of the swarms 2000 (top) and 2008 (bottom) with respective subsequent seismicity plotted on top of the reflectivity image (events plotted in a cumulative manner)

After the termination of both swarms, the seismicity appears randomly throughout the swarm volume (black dots in Figure 2d & 2h). This may represent additional earthquakes generated as the system returns slowly to equilibrium.

Based on the above arguments the following driving mechanism of the swarm activity may be hypothesized (Figure 1b). Fluids from a reservoir in the upper mantle rise through fragmented lower crust and are blocked by less-permeable upper crustal units developing an over-pressured fluid zone. After a critical pressure state is reached, fluid from this zone forces its way into a semi-permeable fault zone. This alters the stress distribution in the zone and produces swarms of micro-earthquakes. After relieving the critical energy this way, the system then returns to equilibrium until the critical pressure state is reached again due to continuous ascent of fluid from the reservoir below.

Supplementary to the above work, the waveforms of the swarm earthquakes recorded by local KRASNET network (consisting of five stations POCA, VACK, LUBY, BERN and JIND) have been used to image subsurface directly above the swarm seismicity using converted waves. A new imaging technique (Fresnel zone migration) is employed which is similar to the Kirchhoff migration of reflection seismic and consists of the primary steps, 1) calculation of P and S receiver functions from a swarm event, 2) migrating the same with restriction of the migration operators to Fresnel zone portions around the conversion points. This images any converting boundary between a swarm earthquake and a surface station.

With waveform data from KRASNET, many features seen in the reflection seismic image was also observed in the above-mentioned converted wave imaging method particularly the bright spots A and B (Figure 1a)). These were very likely target converters considering the locations of the swarm cluster and some of the stations e.g. POCA and BERN.

References:

Bräuer, K., Kämpf, H., Niedermann, S., Strauch, G., Tesar, J., 2008. The natural laboratory NW Bohemia — comprehensive fluid studies between 1992 and 2005 used to trace geodynamic processes. Geochemistry, Geophysics, Geosystems 9, Q04018.

Geissler, W.H., Kämpf, H., Kind, R., Bräuer, K., Klinge, K., Plenefisch, T., Horalek, J., Zednik, J., Nehybka, V., 2005. Seismic structure and location of a CO2 source in the upper mantle of the western Eger (Ohre) Rift, central Europe. Tectonics 24 (TC5001).

I lvfkhu

ICDP

Interglacial climate variability recorded in the Dead Sea sediments

I. NEUGEBAUER[1], A. BRAUER[1], M.J. SCHWAB[1], P. DULSKI[1], U. FRANK[1] AND DSDDP SCIENTIFIC PARTY*

[1] GFZ German Research Centre for Geosciences, Section 5.2 Climate Dynamics and Landscape Evolution, Telegrafenberg, D-14473 Potsdam, Germany

* The complete list of scientists involved in the DSDDP can be found at http://www.icdp-online.org

Introduction

In order to estimate the impact of global warming on natural systems, it is crucial to understand the natural climate variability in the past, especially during warm periods like the Holocene and the last interglacial. Lake sediments from the Dead Sea basin provide high-resolution records of climatic variability in the eastern Mediterranean region, which is considered, as is the entire Mediterranean region, being especially sensitive to changing climatic conditions.

Sediment profiles and characteristics

The ca 460 m long sediment profile 5017-1 from the deep Dead Sea basin (water depth ~300 m; Fig. 1a) is estimated to comprise about 200,000 years and hence two glacial-interglacial cycles (Neugebauer et al., in review). The record covers the upper part of the Amora (parts of MIS 7 and MIS 6; Torfstein et al., 2009), the last interglacial Samra (broadly corresponding to MIS 5; Waldmann et al., 2009), the last glacial Lisan (MIS 4-2; Stein, 2001) and the Holocene Ze'elim formations, including their transitions. Sediments composed of alternating aragonite and detrital marl (*aad*) characterize the more humid periods during glacials, whereas laminated detrital marl has been deposited during relatively drier and partly laminated halite during driest conditions. The latter is found within the interglacial Samra and Ze'elim formations, as well as at the MIS 6/5, 5/4 and 2/1 transitions, which are denoted as hiatuses in sediments outcropping on the present-day lake shores.

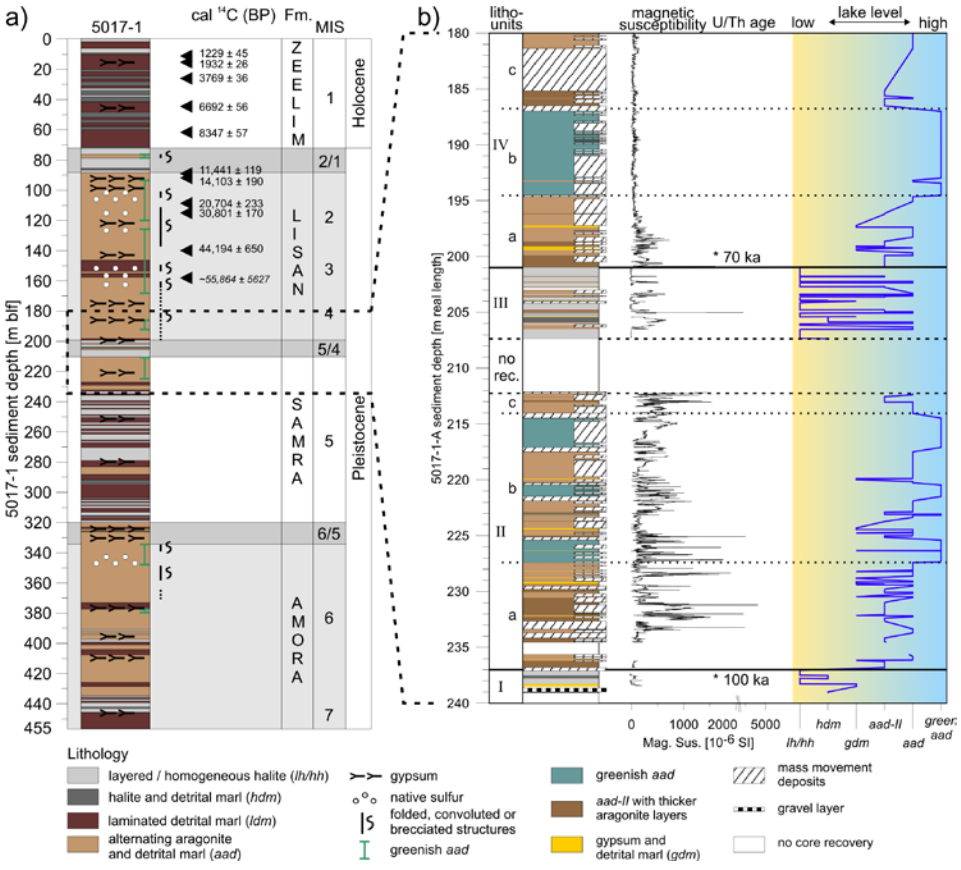

Figure 1: The last interglacial-glacial transition in the deep Dead Sea sediment record: a) lithological profile and stratigraphy of core 5017-1 (water depth ~300 m; Neugebauer et al., in review.); SU: sediment unit, Fm.: formation, MIS: marine isotope stage; b) detailed lithology of the last interglacial-glacial transition in core 5017-1, magnetic susceptibility data (1 mm resolution), relative lake level changes inferred from changes in sediment facies; U/Th dates from Torfstein et al., written communication.

In the study presented here, we aim to reconstruct palaeoclimatological changes during the last two interglacials as archived in the ICDP Dead Sea Deep Drilling Project (DSDDP) sediment cores and in exposed profiles from the lake's margin, using a combination of high-resolution sedimentological-mineralogical and geochemical analyses. Micro-facies analyses on large-scale petrographic thin sections, magnetic susceptibility measurements and µXRF element scanning allow depicting even single flood or drought events.

The Holocene interval of the 5017-1 deep core (i.e. the Ze'elim Formation) is compared to the DSEn and DSF sediment profiles from the western shore of the basin (Migowski et al., 2006). These profiles have been deposited under shallow-water conditions and are composed of laminated detrital marl, either dominated by clastic material or by evaporated layers (primary aragonite

and gypsum), and further characterized by occasional hiatuses during lower lake levels.

Last interglacial

The Samra Formation that corresponds to the marine isotope stage 5 encompasses ca 120 m in the deep 5017-1 profile (Fig. 1a). The lower ~85 m of the formation are mostly composed of laminated or homogeneous massive halite deposits that fingerprint a long period of aridity, most likely during the last interglacial MIS 5e. The finding of the thickest halite sequence (ca 40 m thick) of the entire 5017-1 profile at the upper part of this interval suggests the driest conditions rather at the end of MIS 5e, than in the beginning as was found e.g. in the pollen record of Lago Grande di Monticchio (central Italy; Brauer et al., 2007), among others.

time (probably MIS 5b), when the Northern Hemisphere experienced a somewhat colder climate. According to Waldmann et al. (2009) this might be attributed to a southern source of moisture. At the boundary between the Samra and Lisan formations (i.e. MIS 5/4 or MIS 5a) a ca 10 m thick halite sequence is observed in the deep 5017-1 profile, representing a most likely millenial-scale dry period at a time of major reorganization of the atmospheric circulation.

Holocene

In the Holocene interval, we focus on the middle to late Holocene period (~4000-2000 yrs BP) and compare the respective sequences from the western margin shallow-water DSEn and DSF sediment profiles with the deep 5017-1 profile (Fig. 2). The correlation is based on

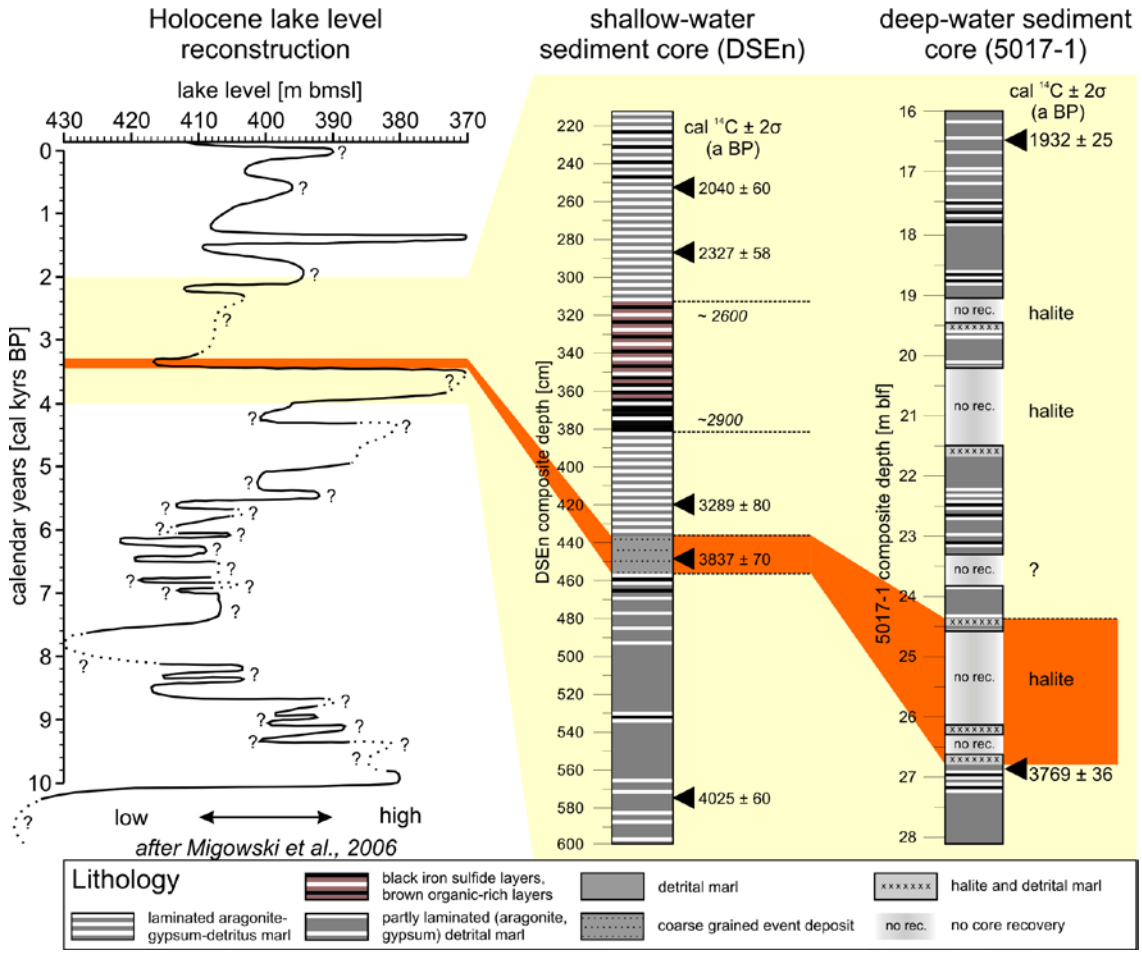

Figure 2: Holocene lake level reconstruction (after Migowski et al., 2006) and correlation of the mid- to late Holocene interval (~4000-2000 yrs BP; highlighted in yellow) in the DSEn and 5017-1 sediment profiles. The drastic lake level decline ~3800-3300 yrs BP is marked in orange.

The upper part of the stratigraphically defined Samra Formation in the 5017-1 profile has been deposited ca 100,000 to 70,000 yrs BP, based on preliminary U/Th ages of primary aragonite layers (Torfstein et al., written communication; Fig. 1b). This interval is characterised by a lower ca 25 m thick sequence of mainly alternating aragonite and detrital marl sediments that are similar to the sediments deposited during the early last glacial (MIS 4, the lower Lisan Fm.; Fig. 1b). This finding suggests an increase in precipitation in the Dead Sea region during that

radiocarbon dating and magnetic susceptibility data. This interval has been selected because of the nearly continuous lamination of that period in the DSEn profile, which enables to construct a precise chronology of flood and drought events. The analysed interval shows distinct facies changes between more clastic dominated sediments in the shallow environment (halite and detrital marl in the deep environment) during drier periods and laminated aragonite-gypsum-detrital marl sediments in both the shallow and deep cores during more humid phases. The most pronounced dry period occurred during the middle to

late Bronze Age ~3800-3300 yrs BP (Fig. 2), when the lake level declined almost 50 meters (Migowski et al., 2006) resulting in a hiatus in the shallow DSEn and DSF locations. A second, less pronounced dry period has been identified during the Iron Age at ~2900-2600 yrs BP in the DSEn profile. Despite the overall dry climatic conditions during that time, a strongly enhanced frequency of mostly graded, thick, organic-rich detrital layers is observed that are most likely due to flash-flood events.

Outlook

Both analysed intervals (the MIS 5/4 transition and the middle to late Holocene) have a great potential to better understand interglacial climate variability in the eastern Mediterranean region. Therefore, we will complement the established micro-facies and µXRF datasets with stable isotope, grain size and XRD measurements to develop high-resolution timeseries of climatic fluctuations and even single extreme events, like floods, droughts and dust storms.

References:

Brauer, A., Allen, J.R.M., Mingram, J., Dulski, P., Wulf, S. and Huntley, B., 2007. Evidence for last interglacial chronology and environmental change from Southern Europe. Proceedings of the National Academy of Sciences 104, 450-455.

Migowski, C., M. Stein, S. Prasad, Negendank, J.F.W., 2006. Holocene climate variability and cultural evolution in the Near East. Quaternary Research 66(3), 421-431.

Neugebauer, I., Waldmann, N.D., Schwab, M.J., Brauer, A., Enzel, Y., Kitagawa, H., Frank, U., Dulski, P., Agnon, A., Ariztegui, D., Ben-Avraham, Z., Goldstein, S.L., Stein, M. Lithologies and depositional environments of the last two climatic cycles in the deep hypersaline Dead Sea: New observations from the ICDP Dead Sea Deep Drilling Project (DSDDP). In review, Quaternary Science Reviews.

Stein, M., 2001. The sedimentary and geochemical record of Neogene-Quaternary water bodies in the Dead Sea basin – inferences for the regional paleoclimatic history. J. Paleolimnol. 26, 271-282.

Stein, M., Ben-Avraham, Z. and Goldstein, S.L., 2011. Dead Sea deep cores: A window into past climate and seismicity. Eos, Transactions American Geophysical Union 92, 453-454.

Torfstein, A., Haase-Schramm, A., Waldmann, N., Kolodny, Y., Stein, M., 2009. U-series and oxygen isotope chronology of the mid-Pleistocene Lake Amora (Dead Sea basin). Geochimica et Cosmochimica Acta 73, 2603-2630.

Waldmann, N., Stein., M., Ariztegui, D., Starinsky, A., 2009. Stratigraphy, depositional environments and level reconstruction of the last interglacial Lake Samra in the Dead Sea basin. Quaternary Research 72, 1-15.

IODP

Past plate and mantle motion from new ages for the Hawaiian-Emperor Seamount Chain

JOHN O'CONNOR (1,2,3), BERNHARD STEINBERGER (4,5), MARCEL REGELOUS (3), ANTHONY KOPPERS (6), JAN WIJBRANS (3),KARSTEN HAASE (1), PETER STOFFERS (7), WILFRIED JOKAT (2), AND C-DIETER GARBE-SCHOENBERG (7)

[1]GeoZentrum Nordbayern, University Erlangen-Nuremberg, Erlangen, Germany
[2]Alfred Wegener Institute, Bremerhaven, Germany
[3]Deep Earth & Planetary Sciences, VU University, Amsterdam,Netherlands
[4]Helmholtz Centre Potsdam, GFZ German Research Centre for Geosciences, Potsdam, Germany
[5]Physics of Geological Processes, University of Oslo, Oslo, Sweden
[6]CEOAS, Oregon State University, Corvallis, OR, United States
[7]Institute for Geosciences, Christian-Albrechts-University, Kiel, Germany

Estimates of the relative motion between the Hawaiian and Louisville hotspots have consequences for understanding the role and character of deep Pacific-mantle return flow. The relative motion between these primary hotspots can be inferred by comparing the age records for their seamount trails. Our new $^{40}Ar/^{39}Ar$ ages for 18 lavas from 10 seamounts along the Hawaiian-Emperor Seamount Chain (HESC) show that volcanism started in the sharp portion of the Hawaiian-Emperor Bend (HEB) at e47.5 Ma and continued for e5 Myr (O•Connor et al., 2013).The slope of the along-track distance from the currently active Hawaiian hotspot plotted versus age is remarkably linear between ~57 and 25 Ma in the central ~1900 km of the seamount chain, including the HEB. This model predicts an age for the oldest Emperor Seamounts that matches published ages, implying that a linear age-distance relationship might extend back to at least 82 Ma.

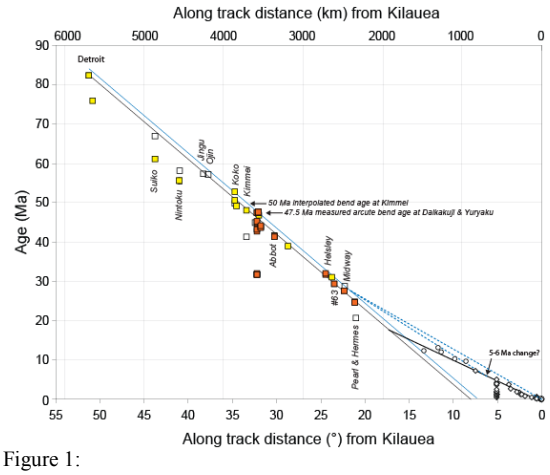

Figure 1:
New (red box symbols) and published (yellow box symbols for post-1995 and white for pre-1995) 40Ar/39Ar isotopic ages for the Hawaiian-Emperor Seamount Chain plotted against sample site distance from Kilauea. Great circle angular distances (in degrees) along the Hawaiian chain are measured with respect to Kilauea (19.2°N, 155.05°W). Great circle distances along the Emperor track are measured with respect to the HEB (32.546°N, 187.734°W) and summed with the distance between Kilauea and the HEB. The Hawaiian-Emperor Bend is 47.5 Ma, ~1 My older than the oldest existing isotopic age [Sharp & Clague, 2006]. Applying a regression fit to new and post-1995 40Ar/39Ar ages and pre-1995 40Ar/39Ar ages for Ljin and Jingk (see text for discussion), in the same ~1900 km section of the chain (i.e. between Ljin and Jingk and Pearl & Hermes Atoll) predicts a linear 57±2 km/Myr distance vs. age slope. This regression does not take into consideration the ~100 km width of the Hawaiian-Emperor chain. Extrapolating this regression fit (long black line) to the old end of the Emperor Seamount Chain predicts the oldest lava ages for Detroit seamount. Extrapolation to the young end of the Hawaiian Seamount Chain (same long black line) shows that age data for the young end of the Hawaiian seamount (small white spheres) and islands (small white diamonds) chain predicts roughly a doubling in the rate of age progression to ~100 km/Myr since at least 15 Ma to. The two dashed blue lines show the possibility that age progression increased to only about 80 km/Myr starting as early as 27 Ma. The long narrow solid blue line shows the linear trend shifted by 1.5 Myr such that it lays above all data points, consistent with the assumption that eruptions do not occur before a plate has passed over the plume.

In contrast, Hawaiian age progression was much faster since at least ~15 Ma and possibly as early as ~27 Ma. Linear age-distance relations for the Hawaii-Emperor and Louisville seamount chains predict ~300 km overall hotspot relative motion between 80 and 47.5 Ma, in broad agreement with numerical models of plumes in a

convecting mantle, and paleomagnetic data. We show that a change in hotspot relative motion may also have occurred between ~55 Ma and ~50 Ma. We interpret this changing in hotspot motion as evidence that the HEB reflects a combination of hotspot and plate motion changes driven by the same plate/mantle reorganization.

References:
O'Connor, J. M., B. Steinberger, M. Regelous, A. A. P. Koppers, J. R. Wijbrans, K. M. Haase, P. Stoffers, W. Jokat, and D. Garbe-Schönberg (2013), Constraints on past plate and mantle motion from new ages for the Hawaiian-Emperor Seamount Chain, Geochem. Geophys. Geosyst., 14, 4564–4584,

IODP

Time scales of magma evolution derived from diffusion modeling of Fe-Mg chemical and isotopic zoning in natural olivines

M. OESER[1], S. WEYER[1], R. DOHMEN[2], I. HORN[1], S. SCHUTH[1]

[1] Leibniz Universität Hannover, Institut für Mineralogie, Callinstr. 3, D-30167 Hannover
[2] Ruhr-Universität Bochum, Insitut für Geologie, Mineralogie und Geophysik, Universitätsstr. 150, D-44780 Bochum

Introduction

Modeling of chemical zoning in minerals, such as Fe-Mg in olivine, has been frequently used to estimate time scales for the thermal evolution of rocks and magmas, assuming that the observed chemical zoning was generated by diffusion (e.g. Pan and Batiza, 2002; Kahl et al., 2011). However, chemical zoning in magmatic crystals may also develop during crystal growth in an evolving magma without any diffusion-driven exchange between crystal and melt.

In this case, the chemical zoning provides no time information. Findings of recent studies indicate that diffusive exchange of Fe and Mg between olivine and melt during magmatic differentiation can result in isotope fractionation of Fe and Mg around 1‰ (e.g. Teng et al., 2011; Weyer and Seitz, 2012; Sio et al., 2013).

Accordingly, diffusion-generated Fe-Mg chemical zoning in olivine should be coupled with Fe-Mg isotopic zoning, and more reliable time information on magma evolution can be obtained by adequate modeling of both, chemical *and* isotopic zoning. In order to investigate this approach, we developed high-precision *in situ* Fe and Mg isotope analyses by femtosecond laser ablation (fs-LA) MC-ICP-MS on olivine crystals and basaltic glass. In a next step the technique was applied to olivine phenocrysts in mid-ocen ridge basalts (MORBs) to improve our knowledge on magma evolution at mid-ocean ridge settings. Additionally, we analyzed olivines in basanites from the Massif Central volcanic region, France, as these olivines are particularly suitable for testing and improving the *in situ* Fe- and Mg isotope analyses of chemically zoned crystals, as they show pronounced zoning in their forsterite (Fo) content.

Refinement of (*in situ*) Fe and Mg isotope analyses

In order to optimize the precision of *in situ* δ^{56}Fe analyses by fs-LA-MC-ICP-MS we tested the use of Ni as an external mass discrimination monitor. For this, a 5 ppm Ni standard solution (NIST SRM 986) was added via a quartz glass spray chamber and introduced into the plasma along with the ablation aerosol (i.e. simultaneously to laser ablation of the sample). Thus, Ni- and Fe isotope ratios can be determined simultaneously which is not possible with Cu as external mass bias monitor, however, essential for *in situ* analyses. After correction for the isobaric interference of ^{58}Fe on ^{58}Ni, the ^{60}Ni-^{58}Ni ratio was then used to correct for instrumental mass discrimination. This correction was extensively tested during *in situ* and solution nebulisation Fe isotope analyses of silicate reference glasses and powdered reference materials (e.g. BIR-1).

Our results indicate that Ni represents a suitable external mass discrimination monitor for Fe isotope analyses. For solution nebulisation analyses, we observed similar precision and excellent agreement between Ni- and Cu mass bias corrected data. Furthermore, reproducibility and accuracy of the *in situ* analyses are significantly improved by using Ni as an external mass discrimination monitor compared to data for which simply standard-sample standard bracketing was used as mass bias monitor. As yet no suitable reference material for *in situ* Fe- and Mg isotope analyses is available, we determined the Fe and Mg isotopic compositions of eight silicate reference glasses – for the first time – by *in situ* fs-LA-MC-ICP-MS and by conventional solution nebulisation MC-ICP-MS analyses. Furthermore, the comparison of solution and *in situ* analyses of these samples provides robust evidence for the accuracy of our laser ablation technique and ensures homogeneity of the glass standards. The precision of our *in situ* analyses is typically better than ±0.12‰ (2 SD) for δ^{56}Fe and δ^{26}Mg which is sufficient to investigate the fractionation of Fe and Mg isotopes in basalt-hosted olivines during magma evolution.

Chemical and isotopic zoning in natural olivines

We investigated MORB samples taken in drill cores from two DSDP holes (332A and 396B) at the slow-spreading Mid-Atlantic Ridge (MAR) and from one ODP hole (896A) at the intermediate-spreading Costa Rica Rift (CRR). About 50% of the MORB samples host fresh olivine phenocrysts with sizes from 0.5 mm to 2 mm across. About 40% of the analyzed fresh olivines in MORBs show distinct intra-mineral chemical gradients with respect to their Fo content (typically on the order of 2-4 mole percent), which is, however, rather small compared to the chemical zoning observed for olivines in the Massif Central basanites (MCBs; Fig. 1). As already observed in previous studies (Flower et al., 1976; Sato et al., 1976; McNeill and Danyushevsky, 1996; Pan and Batiza, 2002), forsterite contents of olivine cores in MORBs, even within one thin section (or sample), can vary significantly, in our samples up to 4 mole percent. These variations possibly reflect various olivine populations that were scavenged from diverse original magmas and mixed into one hybrid host magma which finally erupted (cf. Kahl et al., 2011). If a chemical disequilibrium existed between olivines and the new host, diffusive transport would generate chemical zoning in the crystals (cf. Pan and Batiza, 2002).

Several olivine phenocrysts from both, MORBs and the MCBs show "normally zoned" Fe and Mg isotope profiles, i.e. light iron and heavy magnesium isotopes are relatively enriched in a zone near the Fe-rich crystals' rims and the inversely correlated isotope profiles are coupled with the chemical zoning (Fig. 1). This negative correlation strongly indicates that the chemical zoning was generated by diffusion of Fe into and Mg out of the

olivine, driven by the chemical gradient between crystal and melt (Dauphas et al., 2010; Teng et al., 2011; Sio et al., 2013). The relatively small intra-mineral chemical gradients of olivines in MORBs correspond to the limited Fe-Mg isotope fractionation observed in these crystals. Nevertheless, modeling of the diffusion-generated chemical and isotopic zoning can provide information on the time scales of magma evolution beneath mid-ocean ridges (Fig. 2).

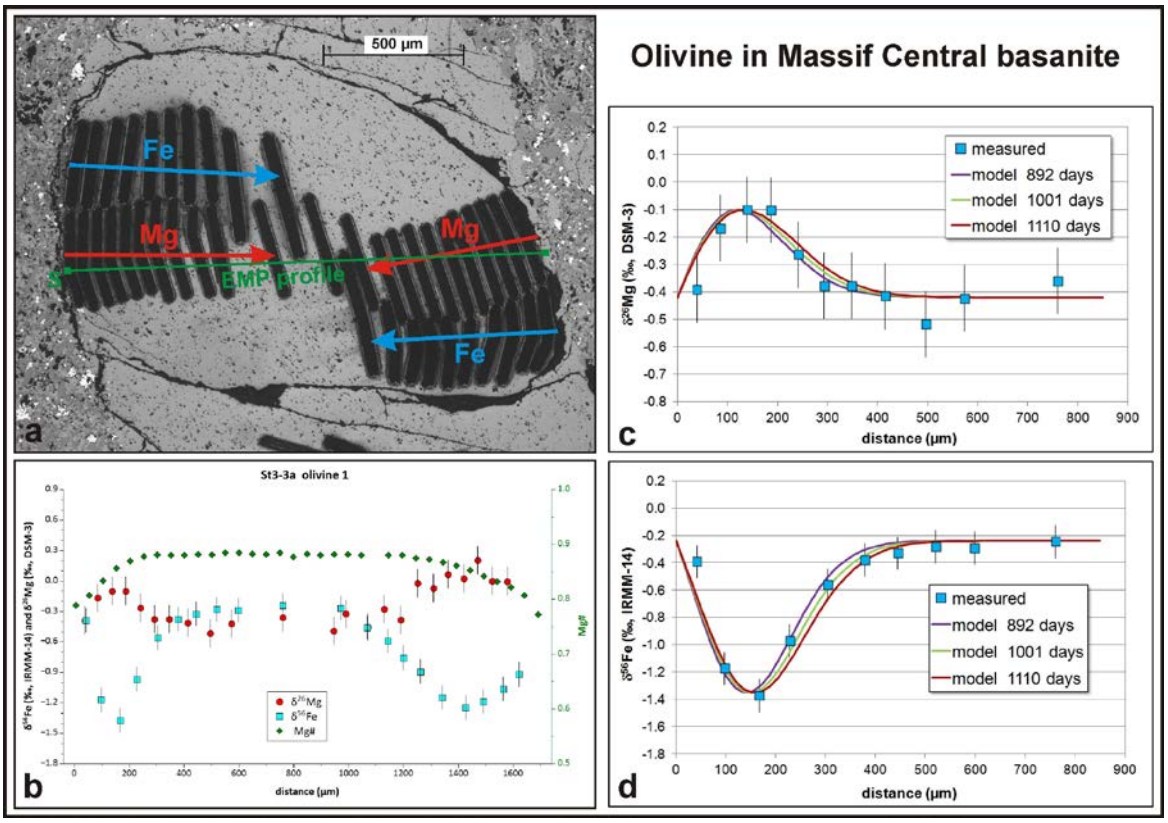

Fig. 1: Chemically and isotopically zoned olivine phenocryst in a basanite from the Massif Central (France). (a) Reflected-light image of the olivine after analyses using femtosecond laser ablation MC-ICP-MS. Ablation of sample material was performed along lines parallel to the crystal rim. The green line represents the profile analyzed by electron microprobe (EMP). (b) Fe and Mg isotopic profiles as well as variation of Mg# across the olivine. Error bars represent 2 standard deviations. (c) and (d) Simplified modeling of the isotopic diffusion profiles for the olivine shown in (a). Model parameters: T = 1212°C (constant; corresponding to 0.97·Tpeak and Tpeak = 1250°C); XFe = 0.165 (constant); fO2 at the NNO-buffer and calculated at the given temperature following the parameterizations of Schwab and Küstner (1981) and Herd (2008); P = 2000 bar; fixed boundary concentrations; crystallographic orientation of the analyzed profiles was considered; DFe-Mg = 1.0 · 10-16 m²/s;

Modeling of the diffusion zoning and time scales of magma evolution

As pointed out in Costa et al. (2008) the diffusion coefficient represents the key parameter in all diffusion models. It was calculated according to the parameterization of Dohmen & Chakraborty (2007). Durations of the diffusive processes were estimated at isothermal conditions following the simplification outlined by Ganguly (2002), which is based on a "characteristic temperature" (T_{ch}) defined as $T_{ch} = 0.97 \cdot T_{peak}$. Based on thermometry data from Sato et al. (1976), McNeill and Danyushevsky (1996), and Werling and Altherr (1997) T_{peak} was assumed to be 1210°C for MORBs and 1250°C for MCBs. The isotopic fractionation is modeled by using the empirical formula from Richter et al. (1999):

$$D_a/D_b = (M_b/M_a)^{\beta}$$

where D represents the diffusion coefficient, a and b are isotopes of a certain element (e.g. ^{54}Fe and ^{56}Fe), M is the atomic mass and β is a factor which can be estimated by fitting the observed extent of isotopic fractionation in the profiles. Further parameters that define our model for Fe-Mg inter-diffusion in olivine can be found in the figure captions.

Pan and Batiza (2002) and Costa et al. (2010) used Fe-Mg zoning in olivine and Mg zoning in plagioclase, respectively, to estimate the time scales either between a mixing event and eruption or between two mixing events within a magma chamber beneath mid-ocean ridges. We follow this approach by modeling the chemical zoning in olivines from the MAR. Additionally, we modeled the isotopic zoning which provides an additional check for the diffusion origin of the observed chemical zoning and the accuracy of the calculated time scales.

Especially for Fe, both the chemical and the isotopic profiles of the normally zoned olivines can be fitted quite well (Fig. 2), revealing time scales between 40 and 200 days as the duration of diffusion at around 1200°C. Pan and Batiza (2002) calculated similar time scales by modeling of the Fe-Mg zoning in olivines from the fast-spreading East Pacific Rise and interpreted these as the duration between a final magma mixing event and the eruption. Modeling of diffusion-generated Mg zoning in plagioclase in MORBs from the MAR and the CRR performed by Costa et al. (2010) also points to time spans of <1.5 years between magma mixing and eruption. Our

results for the MAR and the CRR support these findings as we observe indications of magma mixing processes (e.g. diverse olivine populations within one sample) and calculate times of <1 year as the duration between possible magma mixing (start of diffusion) and eruption ("freezing" the system).

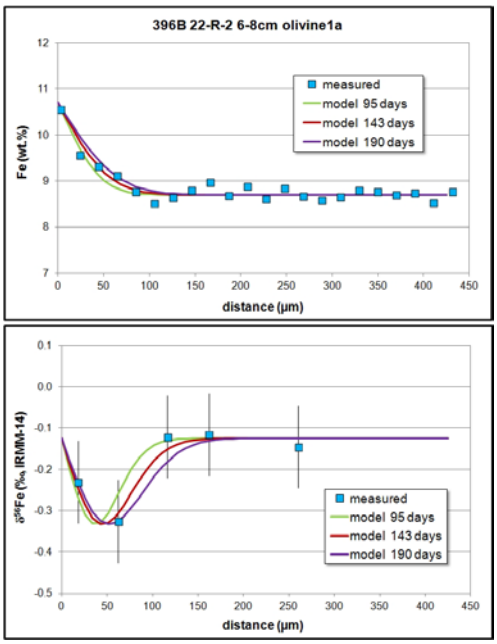

Fig. 2: Simplified modeling of chemical and isotopic diffusion profiles for an olivine from the Mid-Atlantic Ridge (DSDP Hole 396B). The diffusion coefficient D for Fe-Mg diffusion in olivine was calculated according to the parameterization of Dohmen and Chakraborty (2007). Model parameters: T = 1174°C (constant; corresponding to $0.97 \cdot T_{peak}$ and T_{peak} = 1210°C); X_{Fe} = 0.13 (constant); fO_2 at the NNO-buffer and calculated at the given temperature following the parameterizations of Schwab and Küstner (1981) and Herd (2008); P = 1000 bar; fixed boundary concentrations; crystallographic orientation of the analyzed

Our results suggest that sub-ridge magmatic systems appear to be very dynamic at slow-, intermediate- and fast-spreading ridges (Humler and Whitechurch, 1988; Pan and Batiza, 2002; Costa et al., 2010). Compared to olivines in MORBs, olivines in basanites from the Massif Central volcanic region record longer time scales of diffusive re-equilibration between 0.5 and 5 years, according to the diffusion modeling of Fe-Mg chemical and isotopic zoning for these samples.

Our findings show that *in situ* Fe- and Mg isotope analyses by femtosecond laser ablation MC-ICP-MS provide a powerful means to resolve small-scale isotopic variations in minerals and, therefore, allow to tracing diffusive processes that occur on the mineral scale during magma evolution. Furthermore, adequate diffusion modeling of chemical and isotopic profiles in olivines provides reliable time information on the evolution of sub-ridge and intra-plate magma chambers.

References:

Costa, F., Dohmen, R., Chakraborty, S., 2008. Time Scales of Magmatic Processes from Modeling the Zoning Patterns of Crystals. Rev. Mineral. Geochemistry 69, 545–594.

Costa, F., Coogan, L.A., Chakraborty, S., 2010. The time scales of magma mixing and mingling involving primitive melts and melt–mush interaction at mid-ocean ridges. Contrib. to Mineral. Petrol. 159, 371–387.

Dauphas, N., Teng, F.-Z., Arndt, N.T., 2010. Magnesium and iron isotopes in 2.7 Ga Alexo komatiites: Mantle signatures, no evidence for Soret diffusion, and identification of diffusive transport in zoned olivine. Geochim. Cosmochim. Acta 74, 3274–3291.

Dohmen, R., Chakraborty, S., 2007. Fe-Mg diffusion in olivine II: Point defect chemistry, change of diffusion mechanisms and a model for calculation of coefficients in natural olivine. Phys. Chem. Miner. 34, 409–430.

Flower, M.F.J., Ohnmacht, W., Schmincke, H., Gibson, I.L., Robinson, P.T., Parker, R., 1976. 8. Petrology and Geochemistry of Basalts from Hole 396B, Leg 46. Deep Sea Drill. Proj. - Initial Reports 46, 179–213.

Ganguly, J., 2002. Diffusion kinetics in minerals: Principles and applications to tectono-metamorphic processes. EMU Notes Mineral. 4, 271–309.

Herd, C.D.K., 2008. Basalts as Probes of Planetary Interior Redox State. Rev. Mineral. Geochemistry 68, 527–553.

Humler, E., Whitechurch, H., 1988. Petrology of basalts from the Central Indian Ridge (lat. 25°23'S, long. 70°04'E): estimates of frequencies and fractional volumes of magma injections in a two-layered reservoir. Earth Planet. Sci. Lett. 88, 169–181.

Kahl, M., Chakraborty, S., Costa, F., Pompilio, M., 2011. Dynamic plumbing system beneath volcanoes revealed by kinetic modeling, and the connection to monitoring data: An example from Mt. Etna. Earth Planet. Sci. Lett. 308, 11–22.

McNeill, A.W., Danyushevsky, L. V, 1996. 3. Composition and Crystallization Temperatures of primary melts from Hole 896A Basalts: Evidence from Melt Inclusion Studies. Proc. Ocean Drill. Program, Sci. Results 148, 21–35.

Pan, Y., Batiza, R., 2002. Mid-ocean ridge magma chamber processes: Constraints from olivine zonation in lavas from the East Pacific Rise at 9°30'N and 10°30'N. J. Geophys. Res. - Solid Earth 107, 9–13.

Richter, F.M., Liang, Y., Davis, A.M., 1999. Isotope fractionation by diffusion in molten oxides. Geochim. Cosmochim. Acta 63, 2853–2861.

Sato, H., Aoki, K., Okamoto, K., Fujita, B., 1976. 4. Petrology and Chemistry of Basaltic Rocks from Hole 396B, IPOD/DSDP Leg 46. Deep Sea Drill. Proj. - Initial Reports 46, 115–141.

Schwab, R.G., Küstner, D., 1981. The equilibrium fugacities of important oxygen buffers in technology and petrology. Neues Jahrb. für Mineral. 140, 111–142.

Sio, C.K.I., Dauphas, N., Teng, F.-Z., Chaussidon, M., Helz, R.T., Roskosz, M., 2013. Discerning crystal growth from diffusion profiles in zoned olivine by *in situ* Mg–Fe isotopic analyses. Geochim. Cosmochim. Acta 123, 302–321.

Teng, F.-Z., Dauphas, N., Helz, R.T., Gao, S., Huang, S., 2011. Diffusion-driven magnesium and iron isotope fractionation in Hawaiian olivine. Earth Planet. Sci. Lett. 308, 317–324.

Werling, F., Altherr, R., 1997. Thermal evolution of the lithosphere beneath the French Massif Central as deduced from geothermobarometry on mantle xenoliths. Tectonophysics 275, 119–141.

Weyer, S., Seitz, H.-M., 2012. Coupled lithium- and iron isotope fractionation during magmatic differentiation. Chem. Geol. 294-295, 42–50.

IODP

The neodymium and lead isotope record of the final stages of Central American Seaway closure

A. H. OSBORNE[1], DERRICK R. NEWKIRK[2,3], J. GROENEVELD[4], ELLEN E. MARTIN[2], RALF TIEDEMANN[5] AND MARTIN FRANK[1]

[1]GEOMAR Helmholtz Centre for Ocean Research, Kiel, Germany
[2]Department of Geological Sciences, University of Florida, Gainesville, Florida, USA
[3]Now at ExxonMobil Production Company, Houston, Texas, USA
[4]Center for Marine Environmental Sciences (MARUM) and Department of Geosciences, University of Bremen, Bremen, Germany
[5]Alfred Wegner Institute for Polar and Marine Research, Bremerhaven, Germany

The shoaling of the Central American Seaway (CAS) caused a major reorganisation of ocean circulation.

Competing hypotheses claim that disconnection of the Pacific and Atlantic at low latitudes contributed to either a warming or a cooling of global climate. A further hypothesis suggests that an increase in moisture supply to the northern hemisphere resulting from the closure was essential for the onset of major Northern Hemisphere Glaciation. Modeling reconstructions consistently link a closed seaway with increased strength of Atlantic Meridional Overturning Circulation (AMOC), although they differ in the magnitude of the change of the thermohaline circulation.

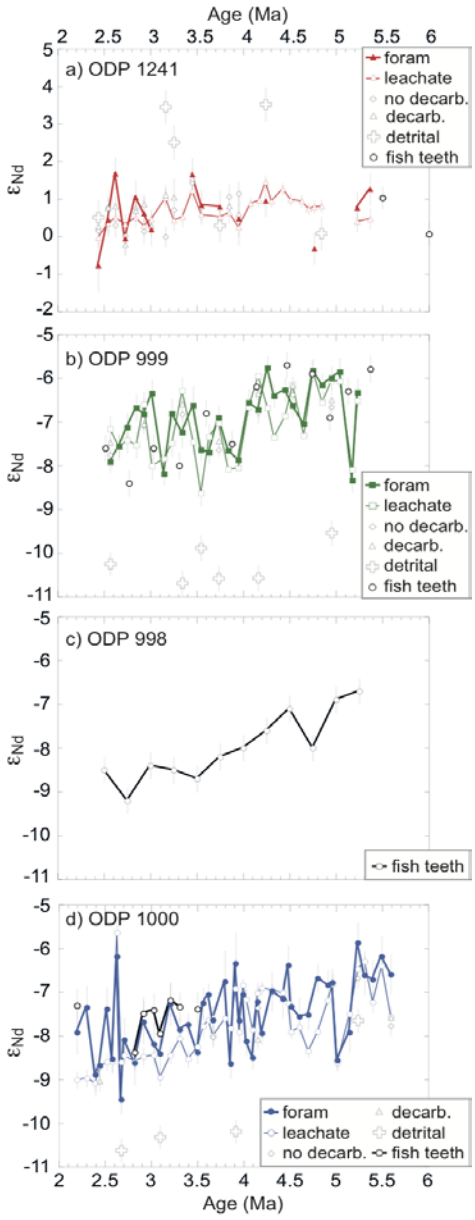

Figure 1 μ_{Nd} composition of uncleaned planktonic foraminifera (foram), full leachate procedure (leachate), hydroxylamine leach solution only (no decarb.), buffered acetic acid solution only (decarb), detrital fraction and fish teeth. Fish teeth data for ODP Site 1241 from Newkirk and Martin [2009].

A well-defined timeframe is central to understanding the direct and indirect consequences of the closure of this major ocean gateway. Here we use radiogenic isotopes of Nd and Pb in early diagenetic ferromanganese sediment coatings and fish teeth to reconstruct the history of intermediate and deep water circulation in the Caribbean Sea and the eastern equatorial Pacific Ocean from 5.6 to 2.2 million years ago (Ma).

The first eighteen months of the project were taken to validate the approach of using reductive-leaching to extract the seawater Nd and Pb signal from the ferromanganese coatings of bulk sediments and in producing reliable down core records for ODP Sites 1241 (2027 mbsl) in the Eastern Equatorial Pacific and ODP Sites 999 (2828 mbsl) and 1000 (916 mbsl) in the Caribbean. Ferromanganese coatings form from the ambient seawater and are an archive of the Nd and Pb isotope composition of bottom water at that location. Core-top results were initially encouraging, showing that there was indeed a large offset between the radiogenic Nd isotope composition (μ_{Nd}) in Pacific surface sediments samples and their less radiogenic counterparts in the deep and intermediate Caribbean, in line with present day seawater μ_{Nd} in the Pacific and Atlantic Oceans [*Lacan et al.,* 2012 and references therein]. This large offset in μ_{Nd} on either side of the Isthmus of Panama provided the basis for studying the closure history of the CAS.

Recent studies have shown that reductive-leaching may also release Nd from detrital material, thus overprinting the seawater signal [e.g. *Elmore et al.,* 2011; *Piotrowski et al.,* 2012]. To test this, repeat measurements were made of selected down core samples, using three different methods. The first was a modified version of the *Gutjahr et al*. [2007] reductive leaching method (without the $MgCl_2$ step), the second method was a weak buffered acetic acid leach only, and the third was a leaching method without the initial decarbonation step. The second and third approaches reduce the risk of partially dissolving detrital material [*Gourlan et al.,* 2008; *Wilson et al.,* 2013]. The down core results for the three ODP Sites showed no offset between the three approaches (Figure 1). Consequently the down core bulk sediment leach record was completed.

An alternative approach to leaching bulk sediments is to use fish teeth, because these rapidly incorporate bottom water Nd and are not altered during diagenesis [*Martin and Scher,* 2004]. As fish teeth are often scarce, a further option is to use the authigenic coatings that form on sedimentary planktonic foraminifera that have been shown to reliably record the Nd isotope composition (μ_{Nd}) of bottom waters [*Roberts et al.,* 2010]. Uncleaned planktonic foraminifera were measured for the three Sites and were found to be largely consistent with the leachate records of ODP Sites 1241 and 999. However, the majority of uncleaned planktonic foraminifera and fish teeth μ_{Nd} in the ODP Site 1000 record were more radiogenic than the leachate results and the Pliocene record showed a higher degree of variability superimposed on the trend towards less radiogenic μ_{Nd} described by the leachates (Figure 1).

The new μ_{Nd} records produced in the last eight months, along with additional fish teeth data for ODP Site 999 and 998 supplied by Derrick Newkirk and Ellen Martin of the University of Florida, show the history of seawater μ_{Nd}

during the final stages of CAS closure from 5.6 to 2.2 Ma. The narrow range of seawater μ_{Nd} in the Pliocene record at ODP Site 1241 (-0.03 to 1.45) is similar to that for fish teeth records from the Miocene [*Newkirk and Martin,* 2009] and indicates that ocean circulation in the deep eastern equatorial Pacific did not change significantly in response to CAS shoaling since at least 11.25 Ma, consistent with 3-D ocean circulation model reconstructions of a dominant Pacific to Caribbean flow. Short term variability in the leachate Pb (not shown) and Nd isotope signatures at Site 1241 is weakly correlated (R^2 = 0.39 for μ_{Nd} and $^{206}Pb/^{204}Pb$). The similarities of the weak trends suggest that both the Pb and Nd isotope records of deep waters at Site 1241 were mainly controlled by local weathering inputs. Comparison with the composition of rocks from the Pacific margins places Site 1241 seawater and detrital fraction Pb isotope compositions within the overlapping fields of the Andean Arc, the Galapagos and the Central American Arc, consistent with the probable transport of eolian material from the southeast.

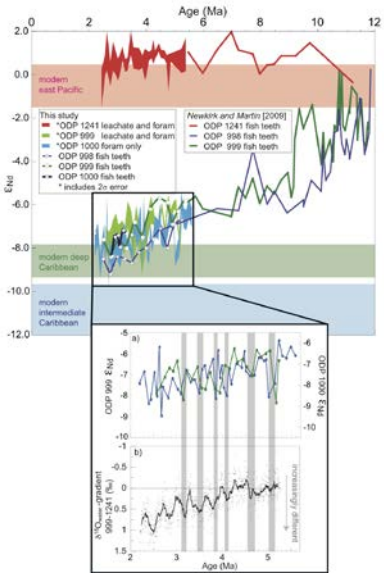

Figure 2 Compilation of μ_{Nd} data for ODP Sites 1241, 998, 999 and 1000 from this study and *Newkirk and Martin* [2009]. Inset shows: a) uncleaned planktonic foraminifera μ_{Nd} for Site 999 (green squares) and Site 1000 (blue circles). Note the scales are offset. Grey bars indicate episodes of less radiogenic μ_{Nd} in the Site 1000 record that correspond to maxima in the salinity-difference record. b) difference in salinity between the Caribbean and the eastern equatorial Pacific, line is the 25-point running average [*Groeneveld*, 2005].

The seawater μ_{Nd} signature at both Caribbean sites obtained from the coatings of the uncleaned planktonic foraminifera showed relatively large short term fluctuations (-5.8 to -8.3 μ_{Nd} for Site 999 and -5.9 to -9.5 μ_{Nd} for Site 1000) within an overall trend towards less radiogenic compositions. A similar trend is seen in the fish teeth records for Sites 999 and 998. When the Pliocene record is considered together with the Miocene record of *Newkirk and Martin* [2009] it is apparent that the major changes in deep Caribbean seawater μ_{Nd} away from radiogenic Pacific-like compositions had already taken place by ~ 7 Ma. Similarities between the Pliocene seawater μ_{Nd} signatures in all three Caribbean sites suggest that the deep and intermediate Caribbean waters were well mixed and that changes in μ_{Nd} were responding to the forcing. There was no trend or significant short term fluctuations in the leachate Pb isotope record from Site 999 (not shown); therefore it is unlikely that the variability in μ_{Nd} was the result of changes in weathering inputs.

The key question is: What caused the short term fluctuations Caribbean seawater μ_{Nd}. Evidence from planktic $\delta^{18}O$ records [*Haug et al.* 2001] and sea surface salinity reconstructions [*Groeneveld*, 2005; *Groeneveld et al*., 2006, 2008; *Steph et al*., 2006] indicate that the CAS had shoaled to a few hundred meters by ~ 4.2 Ma, therefore it is unlikely that contributions of radiogenic Pacific surface waters were influencing the intermediate and deep Caribbean. Plotting seawater μ_{Nd} with the temperature and ice volume-corrected $\delta^{18}O$ gradient between the Site 999 and Site 1241 [*Groeneveld,* 2005] reveals a possible mechanism for the change. Although our seawater μ_{Nd} records of Sites 999 and 1000 have a much lower time resolution than those of *Groeneveld* [2005], larger $\delta^{18}O$ gradients and thus closed CAS conditions were generally associated with less radiogenic μ_{Nd} signatures, particularly during the early and mid Pliocene (Figure 2). Our core-top calibration suggests that deep and intermediate water within the Caribbean is more radiogenic than incoming water from mid-depths in the Atlantic Ocean, possibly as a result of interaction with sediments from the surrounding volcanogenic terrain. The Pb isotope record does not indicate any change in weathering regime. Consequently, the less radiogenic μ_{Nd} signatures are consistent with an enhanced supply of water from the Atlantic and a shorter residence time of waters within the Caribbean. These variations in μ_{Nd} support a close link between periodic CAS closure and enhanced AMOC and advection into the Caribbean.

On going work for the remainder of this project is to produce a high resolution μ_{Nd} record from uncleaned planktonic foraminifera in ODP Site 999 at sub glacial-interglacial time scales to further investigate the possible link between complete CAS closure and strength of AMOC. Furthermore, the μ_{Nd} record at Site 1000 will be extended into the Miocene in order to establish whether there were major changes in ocean circulation at intermediate depth within the past 12 Myr.

An application will be made for a new project, which proposes to look specifically at the Gulf Stream during the Late Pliocene and Early Pleistocene. ODP Site 1006A, on the western slope of the Great Bahama Bank, is ideally situated to examine the history of the Gulf Stream, but has so far been vastly under-utilised. The proposed project would first produce an age model for the site, using benthic foraminifera stable isotope stratigraphy. Second, the hypothesis that CAS closure directly affected the salinity and temperature of the Gulf Stream would be tested, by measuring $\delta^{18}O$ and $\delta^{13}C$ in mixed layer and thermocline dwelling planktonic foraminifera. The third part of the proposed project would be to reconstruct intermediate depth ocean circulation at high resolution at both ODP Site 1006A and ODP Site 1000 using μ_{Nd} in

uncleaned planktonic foraminifera. A 12 Myr record of μ_{Nd} at Site 1006A has already been produced at low resolution and, although the age model is based only on biostratigraphy [*Kroon et al*., 2000; *Spezzaferri et al.,* 2002], there is a broad consistency with trends in the intermediate and deep Caribbean [this work and *Newkirk and Martin,* 2009], suggesting that the Site 1006A is suitable for examining the history of intermediate waters exiting the Caribbean.

References:
Elmore, A. C., A. M. Piotrowski, J. D. Wright, and A. E. Scrivner (2011) *Geochemistry Geophysics Geosystems*, *12, Q09008*, doi:10.1029/2011GC003741.
Gourlan, A. T., L. Meynadier, and C. J. Allegre (2008) *Earth and Planetary Science Letters*, *267*(1-2), 353-364.
Groeneveld, J. (2005) PhD thesis, Faculty of Mathematics and Natural Sciences, Christian Albrechts University, Kiel, Germany.
Groeneveld, J., D. Nürnberg, R. Tiedemann, G. J. Reichart, S. Steph, L. Reuning, D. Crudeli, and P. Mason (2008) *Geochemistry Geophysics Geosystems*, *9*, doi:Q01p23/10.1029/2006gc001564.
Groeneveld, J., S. Steph, R. Tiedemann, D. Garbe-Schoenberg, D. Nürnberg, and A. Sturm (2006) *Proc. ODP, Scientific Results*, *202*, 1-27.
Gutjahr, M., M. Frank, C. H. Stirling, V. Klemm, T. van de Flierdt, and A. N. Halliday (2007) *Chemical Geology*, *242*(3-4), 351-370.
Haug, G. H., R. Tiedemann, R. Zahn, and A. C. Ravelo (2001) *Geology*, *29*(3), 207-210.
Kroon, D., T. Williams, C. Primez, S. Spezzaferri, T. Sato, and J. D. Wright (2000) *Proc. ODP Sci. Res.*, *166*, 155-166.
Lacan, F., K. Tachikawa, and C. Jeandel (2012) *Chemical Geology, 300-301*, 177-184.
Martin, E. E., and H. D. Scher (2004) *Earth and Planetary Science Letters, 220*, 25-39.
Newkirk, D. R., and E. E. Martin (2009) *Geology*, *37*(1), 87-90.
Piotrowski, A. M., A. Galy, J. A. L. Nicholl, N. Roberts, D. J. Wilson, J. A. Clegg, and J. Yu (2012) *Earth and Planetary Science Letters*, *357-358*, 289-297.
Roberts, N.L., A.M. Piotrowski, J. F. McManus and L. D. Keigwin (2010) *Science, 327*, 75-78.
Spezzaferri, S., J. A. McKenzie, and A. Isern (2002) *Marine Geology, 185*, 95-120.
Steph, S., R. Tiedemann, M. Prange, J. Groeneveld, D. Nürnberg, L. Reuning, M. Schulz, and G. H. Haug (2006) *Paleoceanography*, *21*(4), doi:Pa4221/4210.1029/2004pa001092.
Wilson, D. J., A. M. Piotrowski, A. Galy and J. A. Clegg (2013) *Geochimica Et Cosmochimica Acta*, *109*, 197-221.

IODP

´ $^{44/40}$Ca isotope fluctuations of the Cenozoic calcium isotope budget and investigations of benthic foraminifer test preservation

ST. PABICH[1], N. GUSSONE[1], K. RABE[1], CH. VOLLMER[1], B.M.A. TEICHERT[2]

[1]Westfälische Wilhelms-Universität Münster, Institut für Mineralogie, Münster, Germany
[2]Westfälische Wilhelms-Universität Münster, Institut für Geologie und Paläontologie, Münster, Germany

In Earth science, one main aim is a better understanding of Earth´s climate changes by the reconstruction and understanding of the oceanic chemical and isotopic evolution over geologic time. In this context, Ca as one of the major elements in the oceans, is especially important because its variation in concentration are controlled by different factors including the CO_2 concentration of the atmosphere, continental weathering as well as hydrothermal input and Ca carbonate sedimentation. Imbalances in input and output to the ocean system will cause a shift in the isotopic composition of the ocean (cf. Skulan et al. 1997, Zhu and MacDougall 1998). Accordingly, the Ca isotope ratio of paleo-seawater that is recorded in biominerals like foraminifers is an ideal tool to study changes in the Ca budget of the ocean.

The PEAT drilling program (IODP Exp. 320 and 321) recovered a unique, well-preserved Cenozoic carbonate record (Pälike et al. 2010, Lyle et al. 2010), providing an archive of extreme Cenozoic climate variability, expressed in e.g. temperature changes and a rapidly shifting carbonate compensation depth (CCD) (Zachos et al. 2001, Pälike et al. 2012).

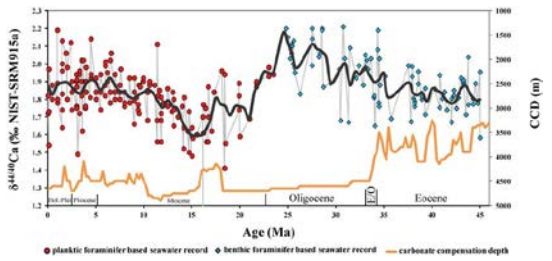

Figure 1: ´ $^{44/40}$Ca seawater record from the Eocene to present. The Neogene record is based on planktonic foraminifers (Heuser et al. 2005 and Sime et al. 2007); the Paleogene record is based on benthic foraminifers (this project). Black line: spline smoothed ´ $^{44/40}$Ca seawater reconstruction. Abbreviations are Hol, Holocene and Plei, Pleistocene.

With this record, we establish a ´ $^{44/40}$Ca paleo-seawater record for the late Paleogene between 45 Ma and 23 Ma and model changes in the Ca budget through time in response to major paleoceanographic fluctuations in the global carbonate cycle, as expressed in remarkable CCD fluctuations. We selected the most appropriate available micro fossils as archive for the Ca isotope measurements. Based on occurrence, isotope fractionation behavior and preservation, we chose the benthic foraminifers Nuttalides spp., Gyroidinoides spp. (G. soldanii and G. neosoldanii) and Cibicidoides sp. (C. grimsdalei, C. mundulus, C. subhaidingerii) from the size-fraction >63µm for ´ ^{44}/^{40}Ca measurements. Foraminifer tests were hand-picked under the binocular and cleaned following the method described in Gussone and Filipsson (2010). An aliquot of each sample was mixed with a ^{42}Ca/^{43}Ca double-spike to correct isotope fractionation during measurements (Gussone et al. 2011) prior to the isotope analysis by thermal ionisation mass spectrometry.

Our results suggest considerable differences in the Ca isotope record of benthic foraminifers during the Eocene and the Oligocene, which might be related to the dynamics of the CCD. The Eocene is characterized by a succession of carbonate poor and rich sediments with the occurrence of several carbonate accumulation events (CAE), reflecting a highly dynamic CCD and strong changes in bottom water calcite saturation. In contrast, the Oligocene shows a constantly deep CCD with carbonate rich sediments (c.f. Coxall et al. 2005, Pälike et al. 2010, Lyle et al. 2010, Pälike et al. 2012). Throughout the Eocene, the ´ ^{44}/^{40}Ca values show little variation with relatively constant values and no significant fluctuations during phases of large short term CCD fluctuations whereas the Oligocene is characterized by sediments with uniformly high carbonate content and a long term trend with increasing ´ ^{44}/^{40}Ca towards the late Oligocene by ~0.3‰. The lack of excursions during the Eocene to higher ´44/40Ca values during phases of low carbonate preservation (indicative for low calcite saturation of the bottom water) provides further evidence that at bottom water temperatures above 10°C, which are postulated for

the Eocene, a bias of the Ca isotope fractionation of benthic foraminifers can be excluded. Previous studies suggested that low calcite saturation in combination with low temperatures might result in anomalous Ca isotope fractionation pattern (Gussone and Filipsson 2010). There is also no offset between the different species visible, consequently no species-specific fractionation factors need to be applied.

changed according to different scenarios. In the second scenario, we modelled the Ca flux (input/output ratio) vs. time with constant boundary conditions (todays isotope composition of oceanic Ca sources and fractionation factor of the dominant Ca sink). Consequently, a shift in isotope fractionation caused by a change from a calcite to an aragonite ocean is not a likely explanation for the increase in Casw isotope values during the Oligocene. Therefore,

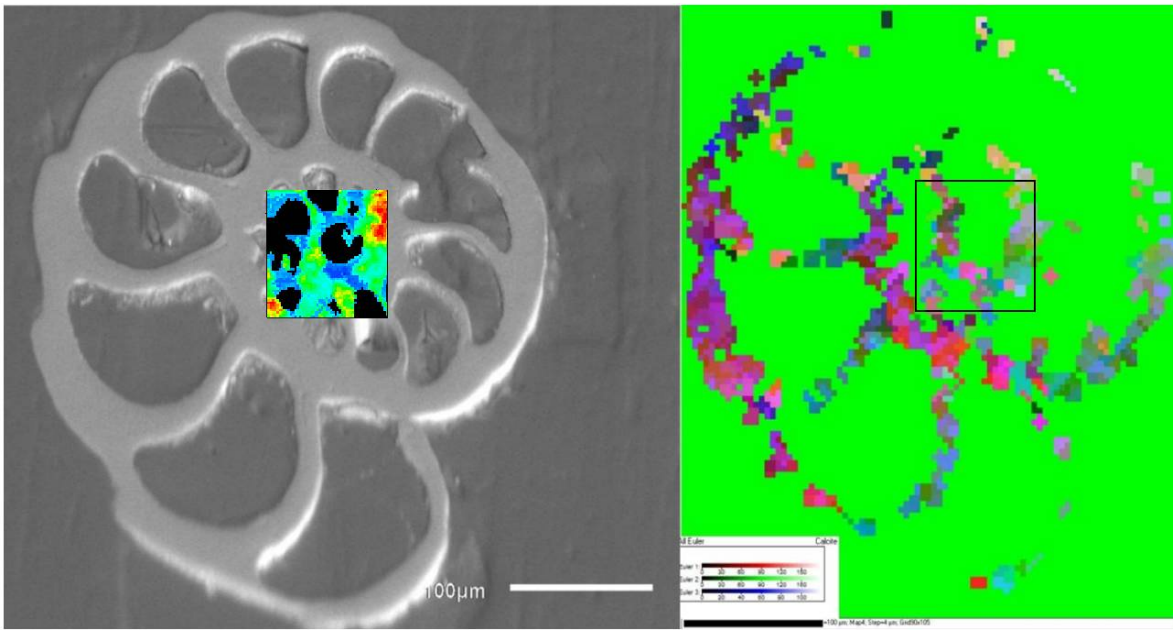

Figure 2: SEM image (left, with an additional Raman map) and corresponding EBSD map (right) of a recent C. *wuellerstorfi*, bright green shows resin, EBSD map shows colour-coded Euler angles, orientation differences between outer and inner chamber walls visible.

Past seawater $\delta^{44}/^{40}Ca$ was calculated from the benthic foraminifer record applying the calibration for Gyroidinoides spp. (1000ln± = -1.25 ‰) from Gussone and Fillipson (2010). The different analysed foraminifer tests reveal similar $\delta^{44}/^{40}Ca$ values, indicating that there is no species-specific offset in Ca isotope fractionation. The Ca budget during the Eocene seems to be relatively constant, indicating that the short term CCD fluctuations are too small to alter the isotopic Ca budget. The Oligocene on the other hand is characterized by a general increase in $\delta^{44}/^{40}Ca$ seawater values and a continuously deep CCD. This is consistent with a massive long term (> 1 Ma) Ca carbonate deposition and a decreasing Ca concentration in the ocean water. During carbonate formation, the lighter Ca isotopes are favoured over the heavier isotopes. As a consequence, the seawater isotopy will be depleted in light ^{40}Ca and the $\delta^{44}/^{40}Ca$ seawater increases. Combined with Neogene data from Heuser et al. (2005) and Sime et al. (2007) the data suggest an increase in values during the Oligocene with a maximum at the end of the Paleogene (Fig. 1).

Based on these observations, two different quantitative scenarios were modelled that could be responsible for the increase in Ca_{sw} isotope values during the Oligocene. In the first scenario, we modelled the effect of changing the fractionation between seawater and oceanic Ca sink in response to a shift from a calcite to an aragonite ocean. The model starts with the assumption of constant conditions (input = output) in the Eocene. At the Eocene/Oligocene transition the fractionation factor is

the Ca isotope record is most likely reflecting changes in the input/output ratio of Ca.

In addition, we investigate benthic foraminifer tests in terms of preservation and potential indicators for post depositional alteration. While recrystallization has a strong impact on paleoceanographic proxies based on trace element composition, the Ca isotope composition of foraminifers is relatively insensitive to diagenetic alteration. We test if the shell structure and crystal orientation remains intact over the 45 Ma PEAT record using Raman spectroscopy and EBSD (Electron Backscatter Diffraction) analysis.

Raman spectroscopy is a technique where a photon of light interacts with the sample and produces a scattered radiation of different wavelengths. This Raman shift is related to the mineralogy of the crystal, while the peak intensities also depend on crystal orientation. In EBSD a beam of electrons is directed onto a tilted sample in a scanning electron microscope (SEM). Some of the electrons emerge from the sample, forming a diffraction pattern, the so called Kikuchi lines, which symmetry and appearance are related to the crystal structure and orientation. We compare both methods in terms of applicability for the characterization of structures of foraminifer tests (Fig. 2).

References:

Coxall H. K.,Wilson P. A., Pälike H. Lear C. and Backman J. (2005) Rapid stepwise onset of Antarctic glaciation and deeper calcite compensation in the Pacific Ocean. Nature 433, 53 – 57.

Gussone N. and Filipsson H.L. (2010) Calcium isotope ratios in calcitic tests of benthic Foraminifers. Earth and Planetary Science Letters 290, 108 – 117.
Gussone N., Nehrke, G. and Teichert, B.M.A. (2011) Calcium isotope fractionation in ikaite and vaterite. Chemical Geology 285, 194-202.
Heuser, A., Eisenhauer, A., Böhm, F., Wallmann, K., Gussone, N., Pearson, P.N., Nägler T.F. and Dullo, W.-C. (2005) Calcium Isotope ($\varepsilon^{44/40}$Ca) Variations of Neogene Planktonic Foraminifera. Paleoceanography 20, PA2013, doi:10.1029/2004PA001048.
Lyle M., Pälike H., Nishi H., Raffi I., Gamage K., Klaus A. and the IODP Expeditions 320/321 Scientific Party (2010) The Pacific Equatorial Age Transect, IODP Expeditions 320 and 321: Building a 50-Million-Year-Long Environmental Record of the Equatorial Pacific Ocean. Scientific Drilling 9, 4 – 15.
Pälike H., Lyle M., Nishi H., Raffi I., Gamage K., Klaus A. and the IODP Expeditions 320/321 Scientists (2010) Expedition 320/321 summary. Proc. IODP, 320/321: Tokyo (Integrated Ocean Drilling Program ManagementInternational, Inc.)
Pälike H., Ridgwell A., and the Expedition 320/321 Scientists (2012) A Cenozoic record of the equatorial Pacific carbonate compensation depth. Nature 488, 609 – 615.
Sime N. G., De La Rocha C.L., Tipper E.T, Tripati A., Galy A., and Bickle M.J. (2007) Interpreting the Ca Isotope Record of Marine Biogenic Carbonates. Geochimica et Cosmochimica Acta 71, 3979 – 3989.
Skulan J., DePaolo D. and Owens T.L. (1997) Biological control of calcium isotopic abundances in the global calcium cycle. Geochimica et Cosmochimica Acta 61, 2505 – 2510.
Zachos J., Pagani M., Sloan L., Thomas E., Billups K. (2001) Trends, Rhythms, and Aberrations in Global Climate 65 Ma to Present. Science 292: 686 – 693.
Zhu P. and MacDougall J.D. (1998) Calcium Isotopes in the marine environment and the oceanic calcium cycle. Geochimica et Cosmochimica Acta 62, 1691 – 1698.

ICDP

Vegetation and climate history during the last 130 ka BP at Lake Van, Eastern Anatolia (Turkey)

N. PICKARSKI [1], T. LITT [1] AND THE PALEOVAN SCIENTIFIC TEAM

[1] University of Bonn, Steinmann-Institute, Nussallee 8, D-53115, Bonn, Germany; pickarski@uni-bonn.de

We investigated the first continuous high-resolution pollen record from Lake Van (38°38' N, 42°54' E), eastern Anatolia, documenting a series of paleoenvironmental and paleoclimate events during the last glacial-interglacial cycle. The reconstructed paleo-vegetation during the last 130 ka BP yields information about the vegetational succession in the Near East and the climate variability in the eastern Mediterranean region.

Palynological analyses were extracted from the lacustrine sedimentary record obtained during the ICDP drilling campaign in summer 2010. Based on several independent methods, a robust chronology of the sedimentary sequences was confirmed by Stockhecke et al. (subm.).

Lake Van is situated on the Eastern Anatolia high plateau (Turkey), in a climatically and tectonically highly sensitive region. Especially several earthquakes and volcanic eruptions (e.g. Nemrut and Süphan volcano) have affected the area significantly. With a surface area of 3,574 km² and with a maximum water depth of about 460 m, Lake Van is the largest soda lake (pH 9.8, salinity 21.4 ‰) and the fourth largest terminal lake (volume 607 km³) in the world.

Being located in a semi-arid region, the regional environment at Lake Van is characterized by a continental character with cold, wet winters and hot, dry summers resulting from the seasonal change of maritime subpolar and subtropical air masses. Therefore, the reconstruction of vegetation from the detailed palynological investigations (Fig. 1) reflects an alternation of an oak-steppe forest and a dwarf-shrub steppe/desert steppe vegetation. In general, cold and arid environmental conditions can be characterized by the dominance of Ephedra distachya-type, Artemisia, chenopods and grasses, whereas increased temperature and moisture availability suggest more favorable environmental conditions for the expansion of a warm-temperate steppe-forest (e.g. Quercus, Pistacia).

In eastern Anatolia the climate evolution within the last interglacial (~130-111 ka BP) can be described as a relatively stable warm period, but with several short-term climate setbacks (cooling events). The palynological sequence at Lake Van documents a vegetation succession with three climatic phases: (i) the Pistacia phase and the Quercus-Ulmus phase during the initial warming (130.9-127.2 ka BP) indicating summer dryness and mild winter conditions; (ii) the Carpinus phase (127.2-124.1 ka BP) suggesting slightly colder temperatures with higher moisture availability; and (iii) the increasing Pinus phase at ~124 ka, which marks the onset of colder/drier climate conditions, that extended into the interval of global ice growth. The major difference between the last interglacial at Lake Van in comparison to the Holocene is the relatively high amount of Pinus during the Eemian, indicating a considerably higher continentality index during the climate optimum as compared to the recent interglacial.

Throughout the last glacial (~74.7-14.7 ka BP), the detailed nature of the Lake Van pollen record allows the identification of several millennial-scale vegetational and environmental changes, which can be correlated with the stadial-interstadial patterns of the Dansgaard-Oeschger (D-O) events observed in the North Greenland ice core record (NGRIP). Relatively warm and humid climate conditions during the D-O interstadials enabled the emergence of an open steppe forest at Lake Van.

New insights of paleovegetation and climate variability at Lake Van demonstrate the great potential of paleoenvironmental reconstruction. It allows the comparison with other long continental pollen records from the Near East and the eastern Mediterranean region, to contribute to the discussion of climate change and to improve the understanding of vegetational changes in the eastern Anatolia region.

References:

Litt et al. (subm.). A 600,000 year long continental pollen record from Lake Van, eastern Anatolia (Turkey). Quaternary Science Reviews.
NGRIP members (2004). High-resolution record of Northern Hemisphere climate extending into the last interglacial period. Nature 431, 147–151.
Pickarski (subm.). Vegetation and climate history during the last glacial-interglacial cycle at Lake Van, Eastern Anatolia. Ph.D. thesis. University of Bonn.
Stockhecke et al. (subm.). Chronology of the 600 ka old long continental record of Lake Van: climatostratigraphic synchronization and dating. Quaternary Sciences Reviews.

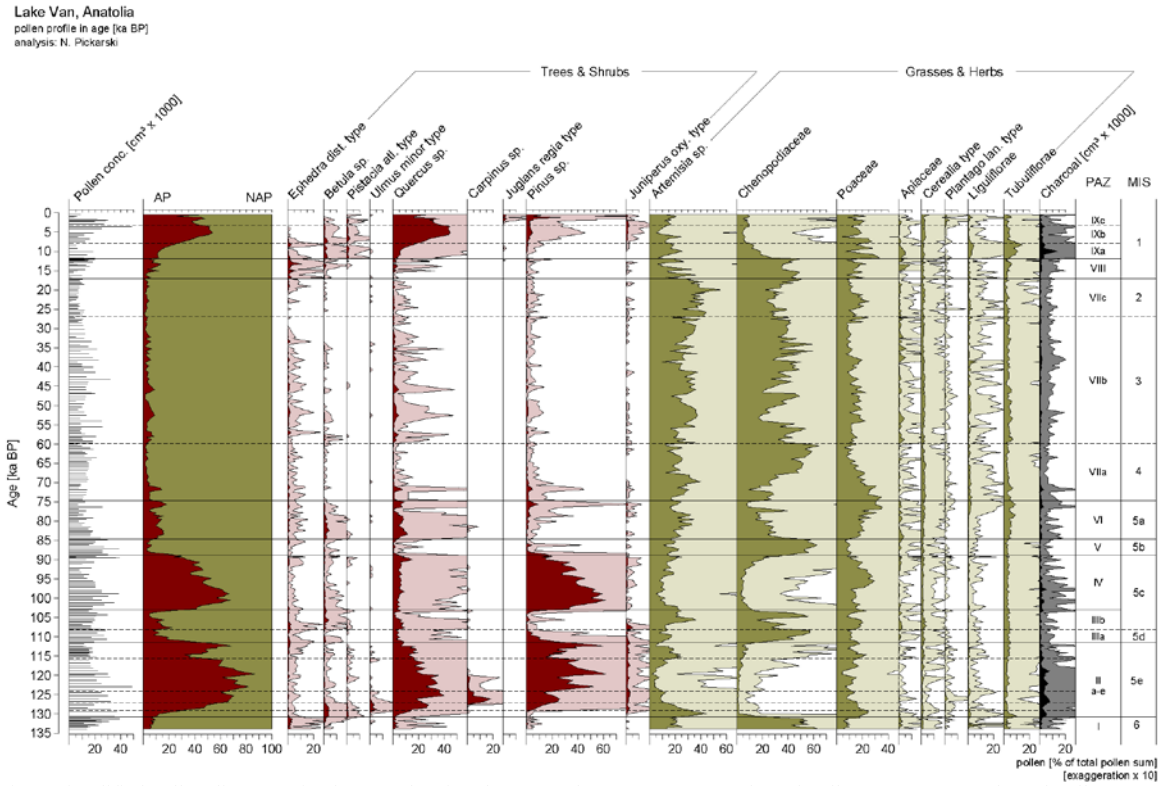

Fig.1: Simplified pollen diagram of Lake Van showing the most relevant taxa; AP = arboreal pollen; NAP = non-arboreal pollen; PAZ = pollen assemblage zones; MIS = marine isotope stages

ICDP

Drilling overdeepened Alpine Valleys (DOVE)

FRANK PREUSSER[1], FLAVIO S. ANSELMETTI[2], MILOS BAVEC[3], CHRISTIAN CROUZET[4], MARKUS FIEBIG[5], GERALD GABRIEL[6], CESARE RAVAZZI[7], CHRISTOPH SPÖTL[8]

[1] Department of Physical Geography and Quaternary Geology & Bolin Centre for Climate Research, Stockholm University, Sweden
[2] Institute of Geological Sciences & Oeschger Centre for Climate Change Research, University of Bern, Switzerland
[3] Geological Survey of Slovenia, Ljubljana, Slovenia
[4] Isterre, CNRS, Université de Savoie, France
[5] Institute of Applied Geology, University of Natural Resources and Life Sciences, Vienna, Austria
[6] Leibniz Institute for Applied Geophysics, Hannover, Germany
[7] C.N.R., Institute for the Dynamics of Environmental Processes, Milano, Italy
[8] Institute of Geology, University of Innsbruck, Austria

A recently submitted ICDP proposal targets formerly glaciated areas, which are often characterized by deeply incised, overdeepened structures filled by thick Quaternary deposits. These buried troughs and valleys were formed by glacial overdeepening, likely caused by pressurized subglacial meltwater below warm-based glaciers. The proposed multinational drilling initiative consists of 14 drill sites in six different countries, all linked by the fact that they surround a formerly glaciated, densely populated mountain range, the Alps. Being the best studied mountain range, the Alps will serve as textbook example allowing application of drilling results to other glaciated areas around the world.

The drill holes, to be cored all the way to bedrock, will explore the type and age of the infillings of these overdeepened troughs. Such drill cores, paired with matching geophysical and instrumental data, hold the keys to understand how and at which rates fast mountain ranges and their foreland are shaped by repetitive glaciations. The overarching goal will be to determine the age and extent of past glaciations and their connection to palaeoclimate, palaeoecology and landscape history. As of today, it is not known how these glaciations varied along and across the Alps during the past, and to what extent the ice build-up along and across the Alps reflects changes in atmospheric circulation patterns. First results of drill holes in similar settings have produced local knowledge of the timing of glacial activity. Only an alpine-wide drilling initiative, however, will allow to reconstruct the full spatial and temporal scale of glacier advances and erosion and related landscape-forming processes over several glacial-interglacial cycles.

Next to these palaeoglacial, palaeoecological and palaeoclimatic aspects, the thick valley fills hold large, untapped aquifers. In the light of an increasing demand for water resources likely amplified by the projected climate change, testing these aquifers in the framework of this project is of high relevance for future hydrogeological applications. Related to this role, these drill holes may be used for shallow geothermal applications, which, however, to date rely on poorly constrained physical properties of the infilling sections. In addition, the areas represent areas of high seismic hazards related to their unfavourable seismic site effects.

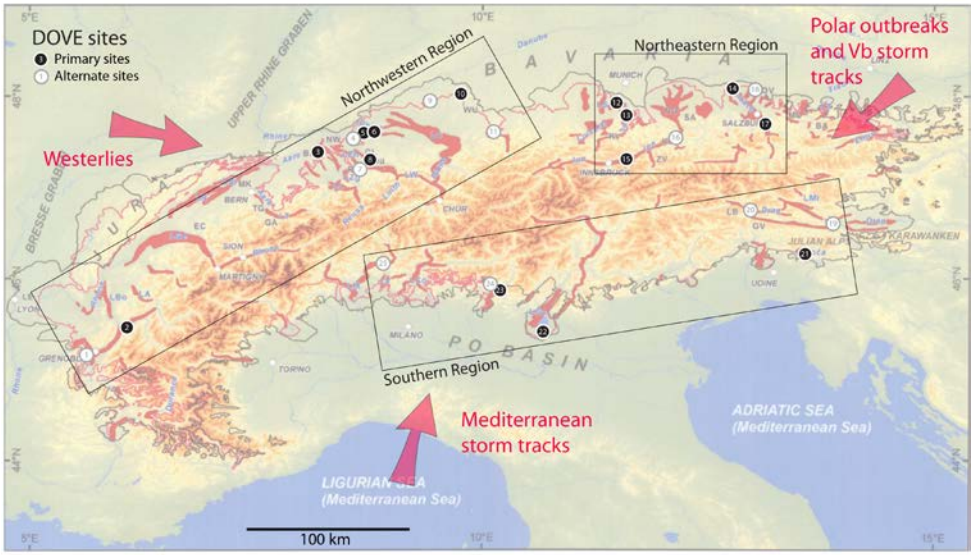

All these goals will be first addressed by state-of-the-art geophysical surveys that quantify the geometry of the overdeepenings. Drillholes will be analysed by downhole logging, groundwater sampling and subsurface biosphere testing. Sedimentological, geochemical and palaeobiological analyses will characterize the sediment cores, and a combination of different approaches (biostratigraphy, luminescence dating, cosmogenic nuclide dating, magnetostratigraphy, and tephrastratigraphy) will establish the chronological framework. Eventually, the results from the above approaches will be cross-checked with the outcome of modelling both glacial flow and erosion and atmospheric circulation.

IODP

Bacteriophages in sediments of the South Pacific Gyre

F. PREUSS[1], T. ENGELHARDT[2], BJØRN STEINSBU[3], H. CYPIONKA[1], B. ENGELEN[1]

[1] Institut für Chemie und Biologie des Meeres, Carl-von-Ossietzky Universität Oldenburg, Carl-von-Ossietzky Str. 9-11, D-26129 Oldenburg, Germany, www.pmbio.icbm.de
[2] Center for Geomicrobiology, Department of Bioscience, Arhus University, Ny Munkegade 116, 8000 Arhus C, Denmark
[3] Department of Biology, University of Bergen, Thormøhlensgt. 53 A/B, NO-5020 Bergen

Large oceanic provinces such as the mid-ocean gyres are characterized by extremely low microbial activities within the water column and the underlying sediments. The South Pacific Gyre (SPG) represents an extremely nutrient-depleted habitat in comparison to relatively more eutrophic continental margins. With a primary production of less than 0.03 mg/l in the centre of the SPG only traces of nutrients reach the underlying sediments. It was shown that sediments of the South Pacific Gyre contain 3-4 orders of magnitude lower cell densities than comparable ocean margin sites (D´Hondt et al., 2009). It is assumed that microbial activities are that low, that the oxygen penetration depth even exceeds the sediment coverage (Fischer et al., 2009). In this project, we hypothysize that viral lysis could provide labile organic compounds to this exteremely nutrient-depleted ecosystem and that viruses might be one main controlling factor for microbial abundance and diversity.

Viruses within the deep subsurface of the SPG outnumber prokaryotic cells

First evidence for this hypothesis is indicated by the phage-host relationships for different sedimentary regions of the marine deep biosphere. The viral impact in these distinct environments was elucidated by comparing the virus-to-cell ratios and viral decay rates (Fig. 1). For surface sediments and marine pelagic environments it was shown that the prokaryotic activity apparently controls viral productivity. Therefore, several sediments from the SPG (IODP Exp. 329), ODP Leg 201, IODP samples from the Bering Sea (IODP Exp. 323) and a North Sea tidal-flat were collected and analyzed. The sampling areas were chosen to comprise different characteristics in terms of sedimentation rate and total organic carbon content as well as sediment age and microbial activity. We could show that viruses outnumber prokaryotic cells in all subsurface sediments. We demonstrated that prokaryotic communities maintain a viral population even in deep, old and the

extreme oligotrophic sediments of the SPG. Accordingly, for sediments with high microbial activity, e.g. tidal flats, a virus-to-cell ratio of about 10 reflects a short-term balance of viral production and decay.

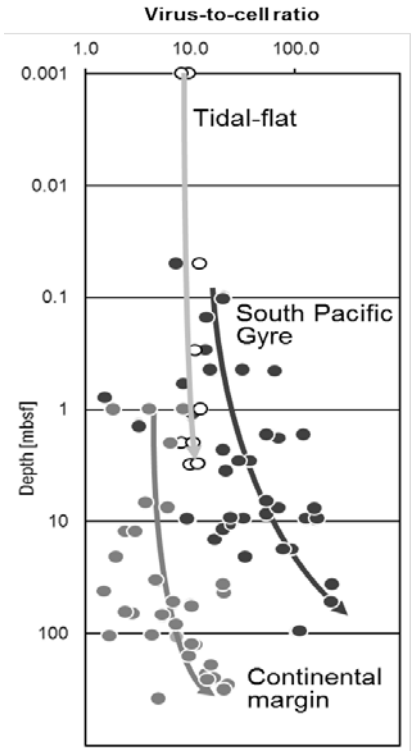

Figure 1. Virus-to-cell ratios (VCR) along the depth profiles of several sampling sites (North Sea tidal flat, South Pacific Gyre, continental margins). For tidal-flat sediments, the VCR remains constant with depth, indicating a balanced viral production and decay. Increasing VCR in oligotrophic and deep sediment layers points towards preservation and ongoing viral production. Graph redrawn after Engelhardt et al., 2014.

However, the consistent increase of the virus-to-cell ratio with sediment depth showed that environmental characteristics also influence the viral and prokaryotic population size. Better preservation of virus particles in deeper sediments or a diminished rate of viral decay in deeper sediment layers would increase the relative number of viruses with depth. Our calculations of viral community half-lives indicate that viruses are more persistent with sediment depth. However, apparent half-lives of tens of millions of years appear unrealistic and rather indicate that the diminished viral decay is overlaid by ongoing production of viruses (Engelhardt et al., 2014).

Induction experiments with isolated bacteria reveals the presence of functioning phages

In our previous investigations (Engelhardt et al., 2011), it turned out that temperate phages are more common in sediments than in the water column where the lytic life cycle is predominant. Hence, our first studies focused on the isolation of bacteria from SPG samples. Sediment samples were recovered from different sites and sediment horizons onboard the JOIDES Resolution (IODP Exp. 329). They were directly transferred into different cultivation media to target either aerobic or anaerobic heterotrophs or autotrophs. After some month of incubation we have obtained six isolates from a limited number of enrichments. Those isolates are affiliated to *Nocardioides basaltis* (99 % 16S rRNA similarity.), *Halomonas aquamarina* (100 %), *Erythrobacter vulgaris* (99 %), *Dietzia* sp. (100 %), *Pseudoalteromonas* sp. (99 %) and *Alteromonas* sp. (100 %). Their presence was confirmed by molecular screening of the enrichment cultures by DGGE.

Interestingly, all isolates came from aerobic enrichments which corresponds to the fact that the SPG sediments were oxic down to the basaltic crust. We now additionally investigate four aerobic strains of another cultivation study from the University of Bergen. Those strains belong to *Marinobacter* sp., *Saligentibacter* sp, *Micrococcus* sp. and *Pseudomonas* sp. First induction experiments with the antibiotic mitomycin C where performed and revealed an increase of phages in the induced cultures compared to non-induced controls (Fig. 2). The morphological visualisation with transmission electron microscopy (TEM) showed that these phages belong to the families of the *Podoviridae* and *Siphoviridae*. The phage size is currently determined by pulsed-field gel electrophoresis (PFGE). Furthermore, we are going to apply physiological tests with the isolates to determine putative adaptations to the low nutrient availability. This will help to understand why it was yet not possible to obtain isolates from the most oligotrophic centre of the SPG.

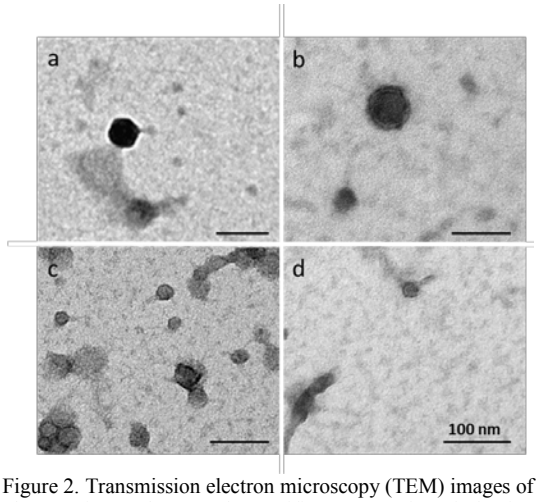

Figure 2. Transmission electron microscopy (TEM) images of phages from the South Pacific Gyre after induction experiments from bacterial host strains affiliated to: (a) Halomonas aquamarina, (b) Pseudomonas sp., (c) Nocardioides basaltis and (d) Erythrobacter vulgaris. Bars = 100 nm

Diversity of temperate phages and indigenous viruses

While first experiments were performed to characterize temperate and potentially active phages within our isolates by means of induction experiments, TEM and molecular analyses, the viral diversity of free viral particles within different sites and sediment horizons was of great interest. For this purpose molecular fingerprinting methods such as randomly amplified polymorphic DNA-PCR (RAPD-PCR) and PFGE will be done. In contrast to diversity studies on microbial communities, no conserved regions that are available within viral genomes to be used as molecular markers. Due to the low numbers of viruses within the sediments,

we additionally gain extremely low yields of DNA which is a limiting factor for the application of the described fingerprinting techniques. A solution for this methodological problem is a pre-amplification of the DNA by "whole genome amplification". To overcome this limitation, we will use the phi29 DNA polymerase, originally found in a phage that infects *E.coli* (Johne et al., 2009). This enzyme has the capability to amplify whole genomes of both, linear and circular viruses (Rector et al., 2004; Silander & Saarela, 2008). Until now, this technique has only been used for medical purposes and will be applied for the first time to environmental samples. To design a protocol and to identify possible bias by the pre-amplification step, control experiments are currently performed on subsurface sediments from the North Sea tidal-flat Janssand which was already used as a model site for the deep biosphere (Engelen et al., 2008). Several sediment horizons of a four meter long core were sampled and are now used for our approach.

References:
D'Hondt, S., Spivack, A.J., Pockalny, R., Ferdelman, T.G., Fischer, J.P., Kallmeyer, J., Abrams, L.J., Smith, D.C., Graham, D., Hasiuk, F., Schrum, H., and Stancine, A.M., 2009. Subseafloor sedimentary life in the South Pacific Gyre. Proc. Natl. Acad. Sci. U. S. A., 106(28):11651–11656.
Engelhardt, T., Kallmeyer, J., Cypionka, H. and Engelen, B. 2014. High virus-to-cell ratios indicate on-going production of viruses in deep subsurface sediments. ISME Journal, In Press doi: 10.1038/ismej.2013.245.
Engelhardt, T., Sahlberg, M., Cypionka, H. and Engelen, B. 2011. Induction of prophages from deep-subseafloor bacteria. EMIR 3:459–465.
Fischer, J.P., Ferdelman, T.G., D'Hondt, S., Røy, H., and Wenzhöfer, F., 2009. Oxygen penetration deep into the sediment of the South Pacific gyre. Biogeosciences 6:1467–1478.
Johne, R., Mueller, H., Rector, A., van Ranst, M. and Stevens, H. 2009. Rolling cycle amplification of viral DNA genomes using phi29 polymerase. Trends in microbiology Vol. 17 No. 5 205-211.
Rector, A., Tachezy, R. and van Ranst, M. 2004. A sequence-independent strategy for detection and cloning of circular DNA virus genomes by using multiply primed rolling-cycle amplification. J. Virol. 78, 4993-4998.
Silander, K. and Saarela, J. 2008. Whole genome amplification with phi29 DNA polymerase to enable genetic or genomic analysisof samples of low DNA yield. Methods Mol. Biol. 439, 1-18.

ICDP

Simulation of magma ascent prior to the high-risk caldera forming eruptions of Campi Flegrei using continuous decompression experiments and different starting materials

O. PREUSS[1*], M. NOWAK[1], S. ULMER[1]

[1]Eberhard Karls Universität Tübingen, Department of Geosciences, Wilhelmstr. 56, 72074 Tübingen

The Campanian Volcanic District is located in the middle-southern part of the Campanian plain with the Campi Flegrei Volcanic Field and the Monte Somma-Vesuvio strato-volcano (Mastrolorenzo and Pappalardo, 2006). The Campi Flegrei (CF) are an active volcanic field characterized by mainly explosive activity, both hydromagmatic and magmatic, and few effusive episodes. The main structural feature is a nested caldera that formed during two main collapse episodes, related to the two most powerful eruptions, the 39 ka Campanian Ignimbrite (CI) and the 14 ka Neapolitan Yellow Tuff events. This project focuses on the CI super-eruption yielding > 200-300 km^3 dense rock equivalent of trachytic-phonolitic material, distributed over ~30,000 km^2 synchronous with significant climate changes (De Vivo et al., 2010).

The Campi Flegrei Deep Drilling Project (CFDDP) offers a unique opportunity to sample a substantial sequence of volcanic rocks and ashes of the restless Campi Flegrei caldera. However, the dynamic magmatic processes prior to the 39 ka Campanian Ignimbrite eruption at Campi Flegrei, occurring during magma ascent, cannot be observed directly in nature. Nevertheless, there is a need to understand these processes that may lead to potentially catastrophic eruptions threaten millions of people in and around Naples (Italy). Experimental simulations of CI magma ascent are necessary to give detailed insight to the mechanisms of CF super eruptions. In combination with the textural and structural analysis of drilled natural samples, it will possibly serve as a tool for volcanic hazard assessment at the high risk Campanian Volcanic District and other comparable volcanic systems.

A pressure decrease during magma ascent accompanied with fluid oversaturation in the melt initiates bubble nucleation, growth, coalescence and decompression induced partial crystallization, which lead to a substantial density decrease and a change in viscosity in the ascending magma. These processes may act as driving forces for increased ascent rates and may lead to catastrophic eruption styles (e.g. Gonnermann and Manga, 2007). To investigate such processes occurring during CF magma ascent, a trachytic CI composition is used. This synthetic CI glass composition (Civetta et al., 1997) is chemically similar to the sampled natural ones in the Apennine Mountains near Avellino at the beginning of this project in May/June 2012, consisting of a sequence of pumice and tuff samples of the presumed first eruptive material of the 39 ka Campanian Ignimbrite eruption. The synthetic composition was already used for the investigation of phase relations and H_2O-CO_2 solubility by the coordinated ICDP project (BE 1720/28-1) of the *Leibniz Universität Hannover* and is therefore a reasonable choice of starting material for the decompression experiments. The glass was synthesized by mixing oxides and carbonates. These powders were homogenized and subsequently molten at 1600 °C under atmospheric fO_2 conditions for six hours in a platinum-rhodium ($Pt_{90}Rh_{10}$) crucible and quenched to a glass. Gold-Palladium alloy ($Au_{80}Pd_{20}$) was chosen as capsule material for the experiments, because of the temperature range of the experiments (1300 – 1050 °C) and to inhibit iron loss due to reactions between the melt and the capsule material. The design and the shape of the experimental container were carefully considered due to the particular requirements during decompression. The challenge was to create a capsule geometry, which allows a substantial volume increase during melt degassing. Based on these requirements, a 13 mm long capsule with a welded star on top and a welded lid at the bottom was used. Additionally, the capsule diameter was increased from 3 mm to 5 mm to minimize the influence of the capsule wall on degassing. Due to a preferred nucleation at the capsule melt interface, the undisturbed melt volume of bubble nucleation and growth is now significantly larger than in previous experiments.

So far, the experiments of this study were performed inside an internally heated argon pressure vessel (IHPV),

which can achieve pressures up to 900 MPa and temperatures up to 1500 °C. This installation is equipped with a rapid quench device reaching a cooling rate of approximately 150 K per second. All experiments were performed at intrinsic oxygen fugacity conditions using argon as a pressure medium. At H_2O-saturated conditions, the oxygen fugacity (fO_2) was determined to be 3.5 log units above the oxygen fugacity of the quartz-fayalite-magnetite (QFM) solid oxygen buffer (Berndt et al., 2002). The continuous pressure decrease is realized by using a novel high-pressure low-flow metering valve equipped with a piezoelectric nano-positioning system (Nowak et al., 2011). First experiments were successfully performed with a hydrous rhyodacitic melt. These experiments revealed that degassing during continuous decompression behaves different from single-step decompression (SSD) and multi-step decompression (MSD) inducing sudden H_2O supersaturation in the melt, due to an extremely shock-wave-like decompression corresponding to unrealistically high ascent velocities of about 300 – 1200 km·h^{-1} (2.5 – 10 MPa·s^{-1}).

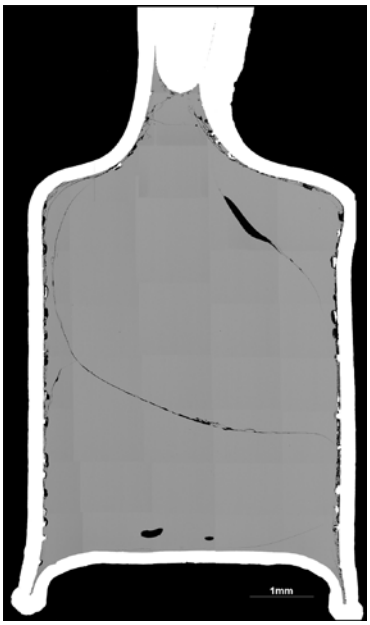

Figure 1
BSE-image showing a complete longitudinal section of experiment CF-TF-18 used a massive glass cylinder as starting material, which was saturated with 5 wt% H_2O. The sample was decompressed from 200 MPa to 100 MPa with a rate of 0.024 MPa·s^{-1}. It illustrates the onset of degassing documented by few nearly invisible bubbles < 10 µm in the undisturbed center of the melt.

Therefore, all conducted experiments in this study were performed with this new piezoactor-driven valve. It consists of a 1 GPa high-pressure valve where the position of the valve needle is controlled by a piezoelectric actuator connected to a high voltage power amplifier, which controls the extension of the piezoelectric actuator on a nanometer scale. Nearly infinitesimal low decompression rates in the range of Pa·s^{-1} can be realized by using this technique and fast decompression rates realized by opening the valve completely are only limited by the diameter of the high-pressure tubing of the autoclave. Lowering carefully the voltage at the amplifier via a potentiometer opens the low-flow metering valve with a precision on a nanometer scale to achieve a desired decompression rate. With progressing decompression the valve is slowly shutting, due to its elastic behavior accompanied with decreasing decompression rate. Thus, the needle has to be driven out of the valve seat periodically by lowering the voltage.

Up to now, H_2O is the only added volatile to the system to keep the identification of occurring processes simple. For melt hydration at 1300 °C (96 hours for glass cylinders and 24 hours for glass powder) prior to decompression, slightly fluid undersaturated conditions are important to inhibit the formation of a fluid filled big bubble prior to the degassing, which effects bubble nucleation and decompression behavior. Therefore, decompression experiments were performed at a starting pressure of 200 MPa and H_2O content of 5 wt%, close to saturation (S. Fanara, pers. Communication, ICDP project BE 1720/28-1). To test an upcoming hypothesis that the starting material influences the degassing behavior, a set of experiments with the same starting conditions for different grain size fractions of the glass powder was conducted. These experiments were compared to those using massive glass cylinders as a starting material under the same conditions. Series of experiments with two different decompression rates (0.024 and 0.17 MPa·s^{-1}) were performed above the liquidus at 1050 °C to ensure a crystal free melt and a homogenous bubble nucleation. After isobaric rapid quench at target pressure of 75 and 100 MPa, the capsules were cut longitudinal into two halves and then embedded in epoxy resin racks. The specimens were polished and afterwards analyzed by a scanning electron microscope (SEM). To generate high-resolution backscattered electron (BSE) images of the whole samples, 80 - 130 frames depending on magnification were taken for each specimen. For quantitative image analysis, it is important that even the smallest bubbles in the BSE images are visible. For this purpose, the magnification of the images was adjusted on the basis of bubble visibility. The calculation of the bubble size distribution (BSD) and bubble number density (BND) with the 2D to 3D crystal size distribution software „CSDCorrections“ (Higgins, 2000) is based on random 2D intersections of the specimen.

Based on the first continuous decompression experiments, it can be demonstrated that changes in decompression rate lead to a different degassing behavior of the magma. Faster decompression rates > 0.024 MPa·s^{-1} generate more and smaller bubbles than slower decompression rates, controlled by the diffusivity of H_2O in the melt. During slow decompression, there is sufficient time for H_2O to diffuse over longer distances to already nucleated bubbles to the benefit of bubble growth and/or ripening, whereas H_2O forms new smaller and more numerous bubbles during fast decompression due to supersaturation and new bubble nucleation.

Beside the results that decompression rate, H_2O content, fluid solubility and target pressure affect the degassing behavior of the melt, the influence of different starting materials (glass- cylinders and powders) on the degassing behavior was additionally compared. The advantages by using a glass powder are shorter H_2O diffusion paths and therefore a shorter equilibration time of 24 hours instead of 96 hours for massive glass cylinders

prior to the decompression. The disadvantages of using a glass powder are a possible preferred bubble nucleation on former glass grain boundaries during decompression and even more important the trapped air between the single grains, which dissolve under high pressure and temperature.

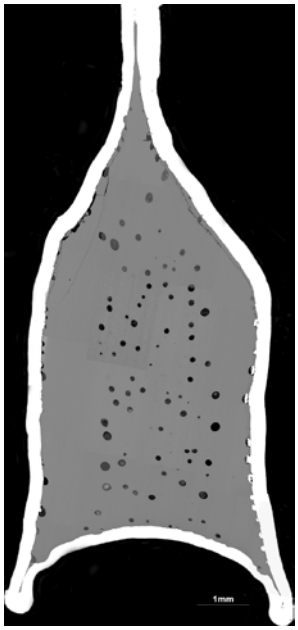

Figure 2
BSE-image of experiment CF-TF-13/2. A typical mixture of grain size fractions (500 µm – 200 µm and below 200 µm) at a ratio of 1:1 was used to attain a maximum possible packing density inside the capsule. The powder was saturated with 5 wt% H_2O prior to the decompression from 200 MPa to 100 MPa with a rate of 0.024 $MPa \cdot s^{-1}$. Here, a lot of bigger bubbles are visible throughout the whole sample showing a complete different degassing behavior (cf. Fig.1).

As a result this dissolved nitrogen (air), which has a low solubility in the melt (75-150 ppm per 100 MPa for silicate melts; Carroll and Webster, 1994), has the potential to initiate the first bubble nucleation at much higher pressure compared to pure dissolved H_2O. Assuming a free capsule volume of 30% in powder experiments leads to about 350 ppm atmospheric N_2 encapsuled during preparation. At 200 MPa maximum N_2 solubility is about 300 ppm. This will lead to initial N_2-rich fluid degassing during decompression. Experiments, comparing the two different starting materials, revealed that samples using massive glass cylinders (Fig. 1) degassed in a completely different way than powders (Fig. 2) supporting our suggestion that the nucleation of bubbles in the center of the melt using glass powder as starting material is effected by dissolved nitrogen. Iacono Marziano et al. (2007), who used a phonolitic Vesuvius 79AD composition for decompression experiments, also mentioned that the bubbles in powder experiments are characterized by larger sizes and by a broader size distribution in comparison with those using massive glass cylinders. That implies that one of the major controlling factors of previous degassing experiments was the usage of glass powder (e.g. Larsen and Gardner, 2004; Mastrolorenzo and Pappalardo, 2006; Suzuki et al., 2007). The dissolved N_2 in the hydrous melt determines the onset of degassing and serves as a source for preferred nucleation. Based on this major problem, glass cylinders have to be used as starting material for decompression experiments of H_2O bearing melts. Nevertheless, using a powder in future experiments might be practicable to dissolve mixed volatiles (e.g. H_2O, CO_2 Cl) in the melt prior to decompression experiments to shorten experimental run time needed for the homogenization of a glass cylinder.

References:

Berndt, J., Liebske, C., Holtz, F., Freise, M., Nowak, M., Ziegenbein, D., Hurkuck, W. and Koepke, J., 2002. A combined rapid-quench and H_2-membrane setup for internally heated pressure vessels: Description and application for water solubility in basaltic melts. American Mineralogist, 87(11-12): 1717-1726.

Carroll, M.R. and Webster, J.D., 1994. Solubilities of sulfur, noble gases, nitrogen, chlorine, and fluorine in magmas. Reviews in Mineralogy and Geochemistry, 30(1): 231-279.

Civetta, L., Orsi, G., Pappalardo, L., Fisher, R.V., Heiken, G. and Ort, M., 1997. Geochemical zoning, mingling, eruptive dynamics and depositional processes - The Campanian Ignimbrite, Campi Flegrei caldera, Italy. Journal of Volcanology and Geothermal Research, 75(3-4): 183-219.

De Vivo, B., Petrosino, P., Lima, A., Rolandi, G. and Belkin, H.E., 2010. Research progress in volcanology in the Neapolitan area, southern Italy: a review and some alternative views. Mineralogy and Petrology, 99(1-2): 1-28.

Gonnermann, H.M. and Manga, M., 2007. The Fluid Mechanics Inside a Volcano. Annual Review of Fluid Mechanics, 39(1): 321-356.

Higgins, M.D., 2000. Measurement of crystal size distributions. American Mineralogist, 85(9): 1105-1116.

Iacono Marziano, G., Schmidt, B.C. and Dolfi, D., 2007. Equilibrium and disequilibrium degassing of a phonolitic melt (Vesuvius AD 79 "white pumice") simulated by decompression experiments. Journal of Volcanology and Geothermal Research, 161(3): 151-164.

Larsen, J.F. and Gardner, J.E., 2004. Experimental study of water degassing from phonolite melts: implications for volatile oversaturation during magmatic ascent. Journal of Volcanology and Geothermal Research, 134(1-2): 109-124.

Mastrolorenzo, G. and Pappalardo, L., 2006. Magma degassing and crystallization processes during eruptions of high-risk Neapolitan-volcanoes: Evidence of common equilibrium rising processes in alkaline magmas. Earth and Planetary Science Letters, 250(1-2): 164-181.

Nowak, M., Cichy, S.B., Botcharnikov, R.E., Walker, N. and Hurkuck, W., 2011. A new type of high-pressure low-flow metering valve for continuous decompression: First experimental results on degassing of rhyodacitic melts. American Mineralogist, 96: 1373-1380.

Suzuki, Y., Gardner, J.E. and Larsen, J.F., 2007. Experimental constraints on syneruptive magma ascent related to the phreatomagmatic phase of the 2000AD eruption of Usu volcano, Japan. Bulletin of Volcanology, 69(4): 423-444.

IODP

Paleo seawater pH dynamics in cold-water corals reefs along the European continental margin

J. RADDATZ[1], A. RÜGGEBERG[1,2,3], S. FLÖGEL[1], V.LIEBETRAU, AND C. DULLO[1]

[1] GEOMAR Helnholtz Zentrum für Ozeanforschung Kiel,
[2] Renard Centre of Marine Geology, Dept. Of Geology and Soil Science, Ghent University, Krijgslaan 281, S8, B-9000 Gent, Belgium
[3] Dept. of Earth Sciences University of Fribourg, Chemin du Musée 6, CH-1700 Fribourg

The current increase in the pCO2 of seawater is a serious threat for marine calcifiers and alters the biogeochemistry of the ocean. Therefore, the reconstruction of paleo seawater properties and their impact on marine ecosystems is an important way to investigate the underlying mechanisms and to better constrain the effects of possible changes in the future ocean. Cold-water coral (CWC) ecosystems are biodiversity hotspots (Freiwald et al., 2004). Modern CWC reefs along the European continental margin are

thriving in a seawater pH range from 7.92 to 8.3 (Flögel et al. 2013 oder ist das offiziell 2014?). Recent studies have shown that past reef growth was controlled by enviromental changes such as temperature, nutrients and bottom currents. However, a study reconstructing the paleo carbonate system in CWC reefs is still missing. Therefore, the controlling meachnims remain unclear (e.g., Rüggeberg et al., 2007; Raddatz et al., 2014). The study of Raddatz et al. (2013) demonstrated that U/Ca ratios in the azooxanthellate scleractinian CWC *Lophelia pertusa* are controlled by the ambient seawater pH. This suggests that U/Ca ratios in *L. pertusa* may be a reasonable alternative to boron isotopes for the reconstruction of intermediate water mass pH and hence may help to constrain potential tipping points for ecosystem dynamics and evolutionary characteristics in a changing ocean. Here, we aim to reconstruct the paleo seawater pH using the method of Raddatz et al. (2013) to estimate changes in the carbonate system as crucial limitation of coral growth. We analyzed *Lophelia pertusa* samples from CWC reefs of the Norwegian Margin, Irish Margin (IODP Site 1317) and the Bay of Biscay extending back to ~3 Ma. Preliminary results indicate that active CWC reef growth always occured above the modern pH threshold of 7.9, with only a few exceptions. Hence, we suggest that even though if single corals may have developed adaptive strategies to not only thrive in cool waters but also to survive under low carbonate saturations states this does not account for the growth of flourishing CWC reefs.

References:

Flögel, S., Dullo, W.-C., Pfannkuche, O., Kiriakoulakis, K., & Rüggeberg, A. (2014). Geochemical and physical constraints for the occurrence of living cold-water corals. *Deep Sea Research Part II: Topical Studies in Oceanography*, doi:10.1016/j.dsr2.2013.06.006.

Freiwald, A., Fosså, J.H., Grehan, A., Koslow, T., Roberts, J.M. (2004). Cold-water coral reefs. UNEP-WCMC, Cambridge, UK, p. 84.

Raddatz, J., Rüggeberg, a., Flögel, S., Hathorne, E. C., Liebetrau, V., Eisenhauer, a., & Dullo, W.-C. (2013). The influence of seawater pH on U / Ca ratios in the scleractinian cold-water coral *Lophelia pertusa*. *Biogeosciences Discussions*, *10*(10), 15711–15733. doi:10.5194/bgd-10-15711-2013.

Raddatz, J., Rüggeberg, A., Liebetrau, V., Foubert, A., Hathorne, E. C., Fietzke, J., & Dullo, W.-C. (2014). Environmental boundary conditions of cold-water coral mound growth over the last 3 million years in the Porcupine Seabight, Northeast Atlantic. *Deep Sea Research Part II: Topical Studies in Oceanography*, doi:10.1016/j.dsr2.2013.06.009.

Rüggeberg, A., Dullo, C., Dorschel, B., Hebbeln, D. (2007) Environmental changes and growth history of Propeller Mound, Porcupine Seabight: Evidence from benthic foraminiferal assemblages. International Journal of Earth Sciences 96, 57–72.

ICDP

A multiple isotope and trace element approach to constrain the oxygenation and metal cycling of 3.5 to 3.2 Ga paleo-oceans

P. RAMMENSEE[1], I. HORN[2], S. WEYER[2], N. J. BEUKES[3], S. AULBACH[1]

[1]Goethe-Universität Frankfurt, Institut für Geowissenschaften, Germany
[2]Universität Hannover, Institut für Mineralogie, Germany
[3]University of Johannesburg, Department of Geology, South Africa

The complex redox evolution of the oceans prior to the great oxidation event ca. 2.45 Ga is a highly active field of research with regard to multiple aspects. The evolution of early life forms is closely linked to the redox state and availability of metabolically cycled elements. For example, oxygenic photosynthesis has been established long before the rise of oxygen levels in the atmosphere. The ICDP Project "Barberton Drilling Project: Peering into the Cradle of Life" has provided drill core covering successions of the 3.5 to 3.2 Ga Barberton Greenstone Belt and has attracted >50 scientists from 12 countries, with aims to resolve the details of environmental conditions on early Earth that led to the emergence and evolution of life [1]. At three of the project's drilling sites (BARB3, BARB4 and BARB5) sedimentary successions of deep to shallow marine environments were retrieved, consisting mostly of carbonaceous siltstone, chert and banded iron formation (BIF). We are investigating selected samples of theses cores by (a) platinum group element (PGE) and Re-Os isotopic compositions, (b) U isotope compositions and (c) Fe isotope compositions to fingerprint metal sources to the early oceans, to decipher modes of stable isotope fraction and for age constraints using the Re-Os radiogenic isotope system.

Quantifying PGE concentrations in carbonaceous shale is challenging due to their low abundances and the presence of interfering isotopes or molecules of matrix elements. The choice of digestion method and analyte concentration has strong effects on the precision and reliability of the results. We used the SDO-1 shale USGS reference material to develop a method for the precise and accurate determination of spiked samples by isotope dilution (ID) ICP-MS after digestion and matrix separation by cation exchange column chromatography, using single collector (SC) and multi collector (MC) instruments. The ID method relies strongly on an appropriate spike composition that has to be close to the relative concentrations in the sample. Two mixed spikes (Re-Os and Ru-Pd-Ir-Pt) were prepared from single calibrated concentrated spike stock solutions with relative composition similar to published values of Archaean carbonaceous shale.

For accurate analysis by ID complete dissolution and equilibration of PGE-Re in spike and sample is indispensable, which requires that the analytes have the same oxidation state. In carbonaceous shale this may be challenging due to the presence of organic carbon, carbonates and sulfides. The high-pressure asher (HPA-S) allows digestion in glass vessels at 300°C and 130 bar. Use of inverse aqua regia (AR_i: 2 HCl : 5 HNO_3) provides highly oxidizing conditions that lead to complete Os oxidization and volatilization. Hence, extraction with chloroform and further purification can be conducted. However, this reagent mix does not decompose all silicates. Because AR_i does not digest silica, we tested desilification steps involving HF. Severe problems occurred as the efficiency of the column chromatography decreased. Since no consistently or significantly different PGE or Re yield was observed, we concluded that the desilification step was not necessary and that AR_i is able to efficiently leach the analytes from the sample powder during re-precipitation of the silica component as a gel. Additional test runs with the Picotrace DAS pressure digestion system, which is less prone to break-down than the HPA-S and allows higher sample through-put, up to 170°C resulted in almost complete dissolution but loss of volatile Os and unacceptably high Ru and Ir blanks. We further tested a low temperature digestion in a hot bath at 80°C for 3h [2] and achieved very low total procedural

blanks and significantly lower Re concentrations. We selected to use HPA-S for total digestion to get information on the source of PGE to the ocean and low temperature digestion to isolate the hydrogenous component and authigenic enrichment.

Upon both digestion types cation exchange chromatography will follow to remove the matrix. Several column set ups were tested and calibrated, including variation of the molarities of the carrier solution (0.05 to 0.5M HCl), with and without the addition of acetone, variation of resin volume and single or two-column approaches. Separation efficiency of the matrix elements causing the most severe molecular interferences (Zr, Mo, Cd, Hf) is offset by a decrease in PGE yields. Introducing a subsequent step involving extraction of interfering elements into BPHA (organic solvent) resulted in significant improvements. As sample treatment that does not result in severe PGE loss does not allow for complete separation of the matrix, sample introduction and instrumental settings have to minimize reaction rates of interfering molecules (oxides). Monitoring and quantification in sample and standard (pure element solutions) is necessary to apply consistent corrections. We use the Aridus desolvating nebulizer for SC-ICP-MS that we setup to maximize sensitivity at tolerable oxide production rates.

Our various tests have now resulted in a sample preparation and analytical routine that will allow accurate determination of PGE and Re concentrations, with the exception of Pd, which suffers from severe molecular interferences that cannot be eliminated without compromising the yields of the other analytes. We are in the process of cleaning and powdering the first samples, from two intervals in core BARB5 from the Fig Tree Group and one interval in core BARB3 from the Buck Reef Chert, for determination of PGE-Re-Os isotopes, and aim to present results at this year's European Geosciences Union General Assembly.

As the formation of BIF is unresolved, the modes of Fe isotope fractionation in this setting are still a matter of discussion [3]. We use pristine Fe-rich layers in thin sections of the BARB4 core from depths of 230 to 354 m with the aim to determine the pathways of Fe isotope fractionation until early diagenesis. In order to enhance the isotopic constraints, the sections, which were made from sediments containing iron rich layers in contact with fine-grained sediments, were scanned, imaged and investigated by optical microscopy and scanning electron microprobe (SEM) in preparation for the analytical work. The optical appearance of Fe-rich layers is jaspilitic red, with aphanitic red chert layers and fine-grained, thicker layers of red siderite-magnetite-chert with visible hematite in chert and occasionally thin magnetite-rich layers. Internally, layers are composed of laminae noticeable by varying modal proportion of siderite and magnetite. Layers often are separated by gradual changes in mineral modes rather than a distinct boundary. However, contacts to surrounding sediments can be abrupt. Surrounding sediments are greenish, sericite-rich shale containing chert fractions, Fe-carbonate and minor chromite. Hematite varies from submicroscopic in chert bands to specularitic hematite. Magnetite occurs as idiomorphic grains in all red shale layers. Occasionally, magnetite overgrows chromite, suggesting approximately equal proportions of chromite in surrounding sediments and in siderite-magnetite-chert layers. Siderite appears as major disseminated component of shale layers or as veins inside chert layers, and nodules and SEM work reveals a broad spectrum of Fe content, varying on the tens of µm scale. Ankerite appears in contact of siderite rich layer to chert layers or nodules, shows small variation in Fe content and is always porous, enclosing Fe-rich chert.

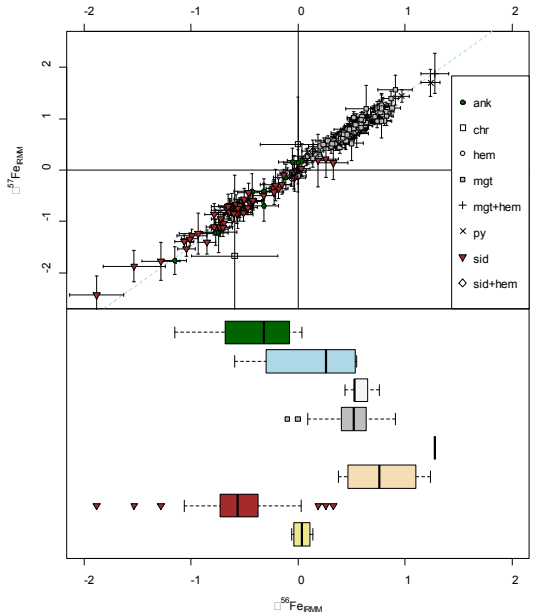

Fig. 1: $\delta^{56}Fe_{IRMM}$ of depths from 230 to 354 m BARB4 core; ank = Ankerite, chr = magnetite with $^{54}Cr/^{54}Fe > 0.001$, mgt = magnetite, mgt+hem = mixed analysis of magnetite and hematite, py = pyrite, sid = siderite, sid+hem = mixed analysis of siderite and hematite

In situ Fe isotope measurements were performed at Institut für Mineralogie at University of Hannover using a UV-femtosecond laser ablation system coupled with MC-ICP-MS [4]. To date, a total of n = 172 valid $\delta^{56}Fe$ values (relative to the IRMM-14 standard) from six thin sections were obtained in two sessions in July and December 2013. The overall range of measured $\delta^{56}Fe_{IRMM}$ is -1.88 ‰ to +1.28 ‰ with an average precision of 0.1 ‰. The majority of data represent single phase measurements of magnetite (n = 95) and siderite (n = 52). Furthermore, analyses of ankerite, hematite and pyrite were performed. Due to small grain size of hematite, the analysis of mixed phase could not be avoided (hematite and siderite, n = 4; hematite and magnetite, n = 1). In the future, the red chert matrix including fine grains of hematite will be analyzed to obtain pure hematite $\delta^{56}Fe$. Within errors, all measured values are consistent with mass-dependent fractionation [Fig. 1]. As several of the magnetites, analyzed in this study, had cores consisting of chromite and even chromite-free magnetites had traces of chrome abundances, precise correction for the mass interference of ^{54}Cr on ^{54}Fe was essential for high precision Fe isotope analyses. Implemented chrome correction has been reported to work well up to 0.0001 $^{54}Cr/^{54}Fe$ ratio [5]. In the current work, we show that we can perform high precision Fe isotope analyses for samples with significantly higher $^{54}Cr/^{54}Fe$, applying a technique of mass bias corrected interference correction. With this

technique, no correlation of $\delta^{56}Fe_{IRMM}$ with Cr/Fe was observed, up to $^{54}Cr/^{54}Fe$ of ca. 0.005.

Mean $\delta^{56}Fe_{IRMM}$ of magnetite of depths from 230 to 354 m is +0.53 ± 0.04 ‰ (student-t distribution 95 % confidence interval). The means of magnetite in each thin section are between +0.40 ± 0.08 ‰ (253 m) and +0.70 ± 0.07 ‰ (285 m). Furthermore, significant variation within thin sections and even between sets of siderite-magnetite lamination could be identified. Siderite $\delta^{56}Fe$ is on average lighter, and ranges between -1.88 and +0.33 ‰ for single analyses. Microprobe analysis work will be carried out to determine whether there is a connection between Fe content and $\delta^{56}Fe$. Hematite-siderite mixed analyses lead to $\delta^{56}Fe$ of +0.04 ± 0.14 0 , indicating hematite $\delta^{56}Fe$ of more positive value. Accordingly, the few hematite pure analyses are +0.58 ± 0.15 ‰. As siderite and magnetite concentrate almost the entire mass of Fe in many lamina and layers, an estimate of modal proportion will be used to constrain bulk isotopic compositions of laminas and layers. Fe-rich chert layers and nodules may be equilibrated with ankerite. Hence, hematite in chert and ankerite as dominating Fe phases are keys to bulk isotopic composition. Further Fe isotopes analyses of carefully selected Fe-rich laminas are necessary to understand the isotopic mass balance of these BIFs which will improve our understanding of the Archean ocean water column and of the iron mobilization during the genesis of BIF.

References:
[1] Arndt et al. (2013) Geophys Res Abstr 15: EGU2013-3909
[2] Xu et al. (2012) Chem Geol: 324, 132-147
[3] Steinhoefel et al. (2010) Geochim Cosmochim Acta: 74, 2677-2696
[4] Horn et al. (2006) Geochim Cosmochim Acta: 70, 3677-3688
[5] Schoenberg and Blanckenburg (2005) Int J Mass Spectrom: 242, 257-272

ICDP

Composition and evolution of the lithospheric mantle below the Eger Rift, Central Europe

A. REGELOUS[1], A. RENNO[2], E.SCHMÄDICKE[1], K. HAASE[1]

[1]GeOZentrum Nordbayern, Universität Erlangen-Nürnberg (FAU), Schlossgarten 5, 91054 Erlangen
[2]Institut für Mineralogie, Technische Universität Bergakademie Freiberg, Brennhausgasse 14, 09596 Freiberg

The buoyant continental mantle root plays an important role in stabilizing of the lithosphere, but its composition and age as well as its relationship to the crust are poorly understood. The crust is believed to be largely generated in subduction zones while several other geodynamic settings have been proposed to faciliate lithospheric mantle generation. The Eger region (Central Europe) is particularly interesting because it transvereses the boundary of two major lithospheric blocks (the Saxothuringian and the Moldanubian) and has been amalgamated during the Variscan orogeny (Babuska and Plomerova, 2006). The Eger rift region is situated in the Bohemian Massif and is supposed to have undergone a young lithosphere formation. Very few studies have yet investigated the region and representative accurate and precise trace elemental and isotopic data from the various levels of lithosphere are largely absent. The 400 km long, NE-SW striking Eger Rift has developed in the Cenozoic and transects the northern Saxothuringian and northern Moldanubian teconic units (Malkovsky, 1987)

Here we present mineral compositions of mantle xenoliths from 13 different outcrops from the Eger rift region, in order to compare the petrogenesis of the different parts of the lithosphere and to define possible relationships. Cr# in spinel vary from 0.29 to 0.76. Together, trace element content of cpx and Cr# in spinel of the xenoliths hint to a degree of melting ranging between 8 and 21%. Some of the spinel minerals show high TiO2 values up to 14%. Oxygen isotope data own a typical lithospheric mantle signature with an average of d18ol of 5.4 and d18cpx of 5.7. These values indicate that the lithospheric mantle here is in an equilibrium state.

Interestingly, the mineral data for olivines, cpx and spinel of western Eger rift samples show overall a smaller variation (e.g. Fo in olivine, Mg# in cpx, Cr# in spinel) in compositions compared with the eastern Eger rift samples.

References:
Babuska, V. and Plomerova, J., 2006. European mantle lithosphere assembled from rigid microplates with inherited seismic anisotropy. Physics of Earth and Planetary Interiors 158, 264-280.
Malkovsky, M., 1987. The Mesozoic and Tertiary basins of the Bohemian Massif and their evolution. Tectonophysics 137, 31-42.

IODP

A quantitative review on Cenozoic marine diatom deposition history

J. RENAUDIE[1], D. B. LAZARUS[1]

[1]Museum für Naturkunde, Leibniz-Institut für Biodiversitäts- unde Evolutionsforschung, Invalidenstraße 43, 10115 Berlin. johan.renaudie@mfn-berlin.de

Marine planktonic diatoms play an important role today as one of the world's main primary producers, as the main organic carbon exporter to the deep sea and also as the main silica exporter balancing global chemical weathering. They were however a very minor component of the plankton at the beginning of the Cenozoic. Studies to date have focussed mainly on the evolution of their taxonomic diversity. Studies of changes in their actual global abundance over the Cenozoic are few, qualitative, and based on limited amounts of data. Reviewing their depositional pattern during the Cenozoic is therefore of interest in order to understand the modality, the context and, eventually, the cause of their rise; and to understand how diatom evolution affected the Cenozoic functioning of the ocean pump, and as a proxy for silicate weathering.

We present here, based on a review of the literature coupled with a new data analysis of the full global DSDP-ODP Initial Reports smear slides descriptions, a quantitative synthesis of the depositional history of marine diatoms for the last 60 Myr. We also place these data in their paleogeographical context in order to understand the changes in diatom biogeography and what it says about Cenozoic paleoceanography.

Diatoms first became widespread during the Middle Eocene. Two temporary major high-abundance events, one at the Eocene-Oligocene transition, another during the Late Oligocene were followed by decreases in the Middle Oligocene and Early Miocene. Diatom abundance in sediments shifted in the Mid-Miocene to globally higher values which have largely persisted to the modern day.

Despite appearing initially during the Late Oligocene, the Southern Ocean circumpolar diatom accumulation belt only became a stable feature in the Mid-Miocene. At this time the main diatom deposition loci switched from the Atlantic to the Pacific and Indian Oceans, and mid-latitude upwelling zones appeared.

Our findings provide support for the idea that diatoms, through their ecological role in the ocean's carbon pump, are responsible at least in part for Cenozoic changes in atmospheric carbon dioxide pressure and therefore changes in global climate state. Additionally, correlations between diatom abundance peaks and shifts in seawater strontium and osmium isotope composition hint at a strong control of weathering on diatom deposition and therefore indicates that diatom abundance can be useful to reconstruct Cenozoic history of weathering intensity.

IODP

Density reconstruction of intermediate waters along the European continental margin

A. RÜGGEBERG[1,2,3], S. FLÖGEL[1], J. RADDATZ[1], C. DULLO[1]

[1]GEOMAR Helmholtz Centre for Ocean Research Kiel, Wischhofstr. 1-3, D-24148 Kiel, Germany.
[2]Renard Centre for Marine Geology, Department of Geology and Soil Science, Ghent University, Krijgslaan 281, S8, B-9000 Gent, Belgium.
[3]Present address: Department of Geosciences, University of Fribourg, Chemin du Musée 6, CH-1700 Fribourg, Switzerland, Email: andres.rueggeberg@unifr.ch.

The reconstruction of past ocean seawater densities can be helpful to understand benthic hydrodynamics and ecological processes important for ecosystems such as the cold-water coral (CWC) reefs along the European continental margin. Recent studies underline the environmental control (temperature, salinity, current strength, food supply, sedimentation rate, substrate) on the growth and development of these large CWC reef structures being able to form giant carbonate mounds of up to 300 m height (e.g., Freiwald, 2002; Rüggeberg et al., 2007). Within the DFG SPP-project INWADE (Cold-Water Coral Mound Development Related to INtermediate WAter DEnsity Gradient) we concentrates on the observation that the density of seawater is an environmental control factor for Northeast Atlantic coral reefs (Dullo et al., 2008). In the density range of 27.5 ± 0.15 kg/m^3, coherent with the position and stability of the thermocline for the Porcupine Seabight and Rockall Bank carbonate mounds (White and Dorschel, 2010), stable and favourable environmental conditions occur over longer time scales allowing CWCs to create large reef and mound ecosystems. These conditions involve a constant food supply by continuous or tidally controlled currents.

The possibility to reconstruct palaeo-densities (Lynch-Stieglitz et al., 1999) and palaeo-temperatures (e.g., Shackleton, 1974) gives us the opportunity to determine past environmental water mass characteristics in comparison to the recent setting and interpret these in relation to cold-water coral growth and carbonate mound development. A compilation of existing stable oxygen isotope data from DSDP, ODP and IODP sites combined with data from sediment cores are used for this reconstruction.

Here, we present three depth-transects at 37°N, 51°N and 65°N across the European continental slope for the upper 3000 m of water column. Along these transects palaeo-densities and palaeo-temperatures are calculated for the past 3 million years and oceanographic changes at intermediate water depth are interpreted with special focus of CWC reef development and decline during different periods in the Pleistocene.

References:

Dullo, W.-C., Flögel, S., Rüggeberg, A., 2008. Cold-water coral growth in relation to the hydrography of the Celtic and Nordic European continental margin. Marine Ecology Progress Series 371, 165–176.

Freiwald, A., 2002. Reef-forming cold-water corals, in: Wefer, G., Billett, D., Hebbeln, D., Jørgensen, B.B., Schlüter, M., van Weering, T. (Eds.), Ocean Margin Systems, Springer Verlag, Berlin, Heidelberg, New York, pp. 365–385.

Lynch-Stieglitz, J., Curry, W.B., Slowey, N., 1999. A geostrophic transport estimate for the Florida current from the oxygen isotope composition of benthic foraminifera. Paleoceanography 14 (3), 360–373.

Shackleton, N.J., 1974. Attainment of isotopic equilibrium between ocean water and the benthonic foraminifera genus Uvigerina: isotopic changes in the ocean during the last glacial. Colloquium International CNRS 219, 203–225.

White, M., Dorschel, B., 2010. The importance of the permanent thermocline to the cold water coral carbonate mound distribution in the NE Atlantic. Earth and Planetary Science Letters 296, 395–402.

IODP

Time resolved alteration of gabbro at high temperature hydrothermal systems at slow-spreading mid ocean ridges: An experimental study

S. SCHÄCHINGER[1], O. BEERMANN[1], D. GARBE-SCHÖNBERG[1], L. ARZI[1], A. HOLZHEID[1]

[1]Institut für Geowissenschaften (IFG), Christian-Albrechts-Universität zu Kiel (CAU)

Submarine hydrothermalism with extensive alteration of oceanic crust is a major process governing energy and mass fluxes from Earth's interior into the oceans. New estimates suggest that about fifty percent of hydrothermal crust alteration occurs along the slow and ultra-slow spreading Mid-Atlantic Ridge (MAR) [1]. In addition recent investigations revealed high fluid and high element fluxes discharging from the MAR [1, 2, 3] suggesting that hydrothermalism at slow and ultra-slow spreading ridges is the dominating process for mass transfer between lithosphere and ocean. For example the recently discovered hydrothermal system at 5° S MAR is hosted in young lava flows [4, 5] and it is suggested, that hydrothermal venting intensified after a volcanic eruptive event in 2002 [5]. Here vent fluids emanate with extreme temperatures above 400 °C [2] at high pressure (~300 bar at 3000 m water depth) containing high concentrations of dissolved gases (e.g., H_2), transition metals, and rare earth elements (REE) with 'atypical' REE-pattern. Geochemical models on mass transfer between oceanic lithosphere and ocean base upon time integrated mass balance between vent fluid and host rock geochemistry [e.g., 6, 7, 8]. But non of these models provide estimates for early-stage high-temperature hydrothermalism with unaltered host-rocks that obviously create high element fluxes in particular at slow-spreading mid ocean ridges (MOR) as evident from the 5° S MAR hydrothermal system.

Several experimental studies exist on seawater-rock interaction processes at pressure and temperature conditions representative for high-temperature

hydrothermalism at MOR with most of them dealing with fluid-rock equilibration [e.g., 9, 10, 11]. To outline the results, besides rock geochemistry and temperature, the water-to-rock ratio (w/r ratio) strongly affects fluid chemistry [e.g., 12, 10]. According to natural MOR vent fluids, experimental seawater reacted at high temperatures with mafic glasses or pyroxenes has lost mostly all of its magnesium [e.g., 9, 10, 11, 12] triggered by hydrolysis of the seawater MgCl-component: $MgCl_{2(aq)} <=> Mg(OH)_{2(s)} + HCl_{(aq)}$ (1).

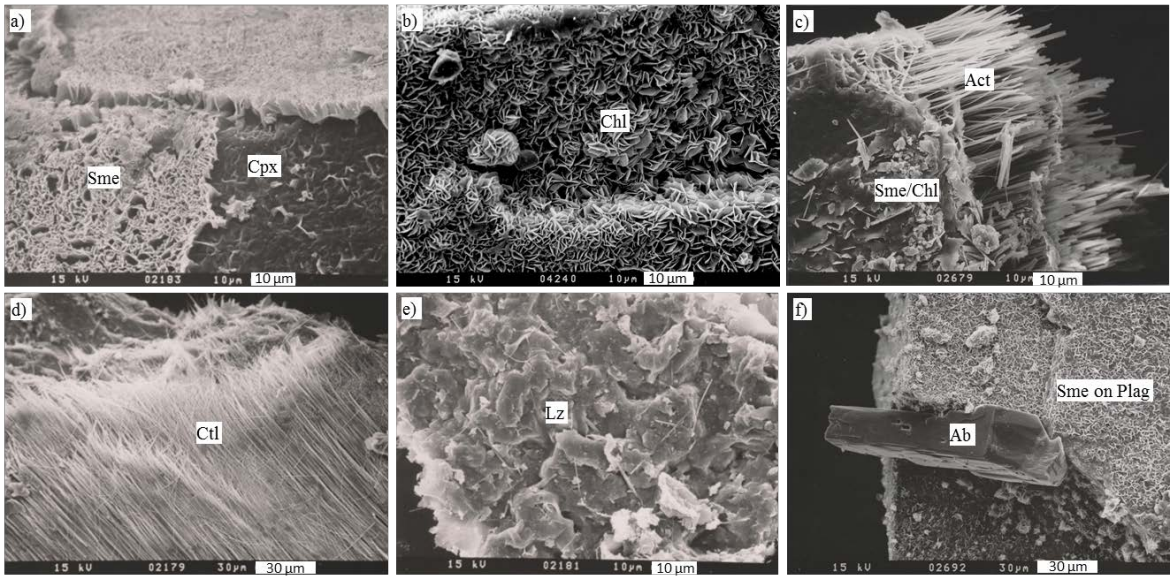

Fig. 1: SEM pictures of secondary mineral alteration products by seawater-rock interaction experiments at 425 °C and 400 bar; a) smectite (Sme) (montmorillonite, Mnt) layer on clinopyroxene (Cpx) (w/r = 5, run duration = 72 h); b) partly hexagonal chlorite (Chl) platelets on Cpx (w/r = 10, run duration 6 h); c) actinolite (Act) intergrown with smectite (montmorillonite) and chlorite replacing Cpx (w/r = 1, run duration 6 h); the serpentine-group minerals d) chrysotile (Ctl) replacing Cpx orientated along the Cpx <001> direction and e) lizardite (Lz) (both, Ctl and Lz at w/r = 1, run duration 72 h); f) secondary albite (Ab) grown together with smectite (probably as montmorillonite) on plagioclase (Plag) (w/r = 5, rund duration 72 h).

The hydrolysis reaction of Eq. (1) is strongly shifted to the right, if temperatures exceed more than 300 °C as it can be deduced from experiments of [13] and is therefore the fundamental process that causes heated seawater to be a high reactive fluid. It is evident from our preliminary results of our study that the Mg(OH)2 or brucite-component from the seawater will be subsequently fixed in silicate alteration phases within a few hours, if significant amounts of clinopyroxene are present, but this effect is more than 1000-fold slower for the reaction of seawater with olivine [11]. The reaction of $Mg(OH)_2$ with silica components that released from pyroxene dissolution during water-rock interaction processes further shifts the equilibrium constants for Mg-hydrolysis reactions strongly to HCl(aq) production. Thus, the reaction of $Mg(OH)_2(s)$ precipitated from seawater with silica-components counteracts re-dissolution of the brucite-component and "stabilizes" HCl in the aqueous solution. The fixation of $Mg(OH)^2(s)$ by the reaction with silica-component is also evident from an experimental study on the time-resolved alteration processes of basalt glass by seawater at run durations between ~2 and 23 hours at lower temperature (200 to 320 °C) and at a w/r mass ratio of 25 [14]. Here, Mg-rich clay minerals (saponite, $Ca0._{25}[Mg,Fe]_3[Si,Al]_4O_{10}[OH]_2$ * nH_2O) have been rapidly formed adjacent to amorphous silica layer on basalt glass rims.

Previous results of our study show, that Mg-fixation and the accompanied HCl production triggers rapid dissolution of REE and transition metals from the rock into the fluid indicating this process governs early-stage metasomatism and rock dissolution in particular at high fluid fluxes, i.e., at high water-to-rock ratios (w/r ratios). In order to unravel the temporal evolution and the impact of early-stage hydrothermalism on element mass transfer between seawater fluid and oceanic lithosphere dependent on the fluid flux we started a systematic time-resolved experimental study on high-temperature seawater-rock interaction processes at variable w/r ratios.

A series of experiments was conducted with mineral assemblage from fresh, unaltered gabbro (Atlantis Massif, 30°N MAR, IODP expedition 305, Site U1309D, core sample R211, 1020 m bsf) that reacted in gold capsules with natural bottom seawater collected at MAR 9°S. Mixtures of 125-500 µm-sized hand-picked plagioclase (Plag) and clinopyroxene (Cpx) with minor coherent olivine (Ol) grains reacted with the fluids in cold seal pressure vessels (CSPV) at 425 °C, 400 bar and at w/r ratios from 0.5 to 10 and run durations from 3 to 720 hours. Solid products were qualitatively analysed by scanning electron miscroscopy (SEM) and X-ray diffraction (XRD). Qualitative and quantitative phase analyses of solid alteration products were determined by XRD, so far without internal standards. It should be emphasized that in particular accurate XRD analysis of, in particular clay minerals and some amphiboles, which are commonly associated to hydrothermally altered basalts, require precise records of XRD pattern below 10° 2-theta. This has recently not been possible with the XRD ouf our laboratory and in the meanwhile, we obtained a new XRD that allow for modifications to record XRD pattern below

10° 2-theta. As mentioned below one experimental series (at a run duration of 72 h) has not been analysed by our new XRD and thus the determined phase proportions should be considered with caution.

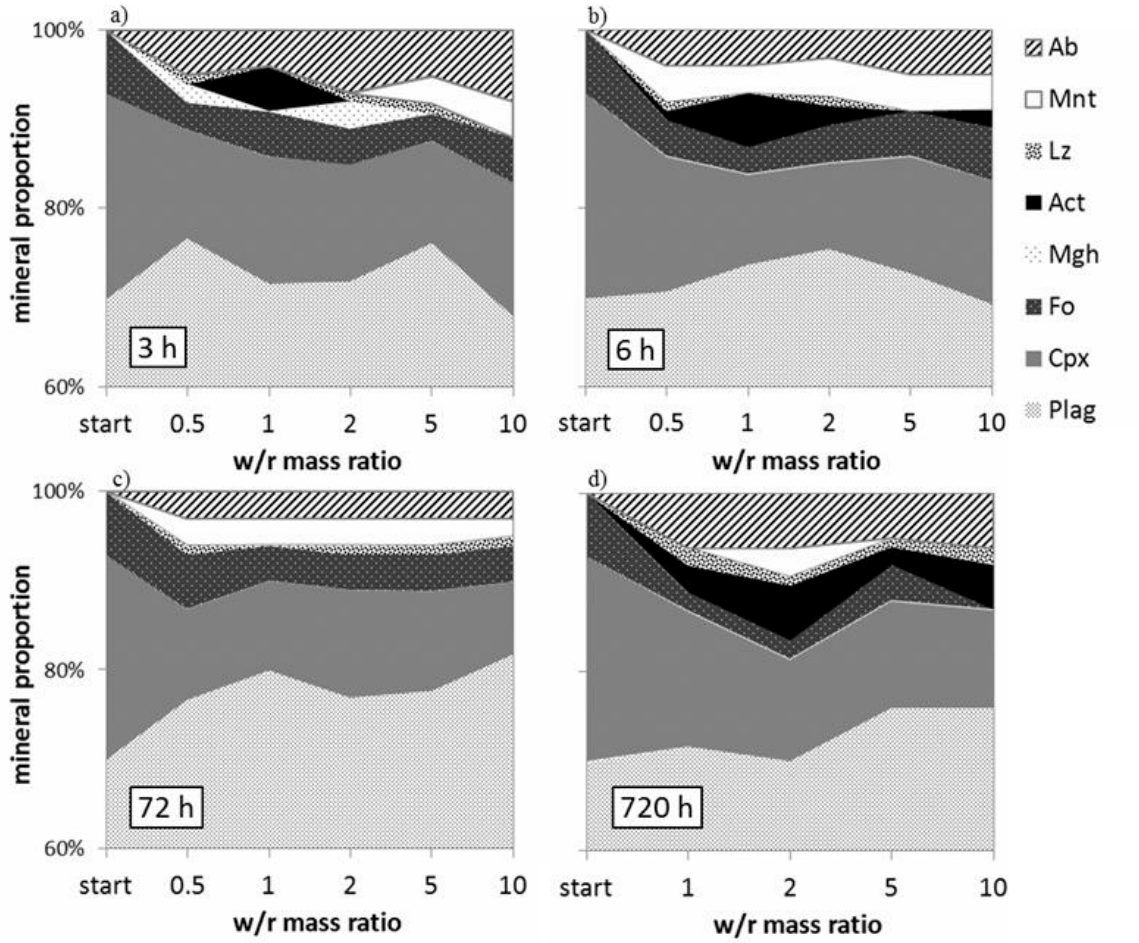

Fig. 2: Relative proportions of mineral phases determined by XRD of the gabbro starting mineral assemblage ("start" on x-axes) and the experimental mineral products depending on the water-to-rock mass ratio (w/r mass ratio) and run durations of the experiments in hours (h) with (a) 3 h, b) 6 h, c) 72 h, and d) 720 h. Note the mineral assemblage is composed of ~70 rel. % plagioclase (Plag), ~23 rel. % clinopyroxene (Cpx), and ~ 7 rel. % olivine as forsterite (Fo) (determined by XRD). All other phases are alteration products. However, actinolite (Act) present in the starting gabbro could not be excluded. In order to get a closer view on the proportions of secondary mineral phase, i.e., montmorillonite (Mnt), lizardite (Lz), and maghemite (Mgh), the y-axes cuts 60 rel. % of Plag. *It is noteworthy, there were difficulties in the determinations of actinolite from XRD from the series at a run duration of 72 h (further explanation is given in the text).

The starting mineral assemblage was composed of ~70 rel. % Plag, ~23 rel. % Cpx, and ~7 rel. % olivine as forsterite (Fo). In all experiments significant amounts of secondary mineral phases (~3 to 10 rel. %) mostly sized ~2-50 µm were primarily formed on Cpx. All Cpx grains were covered by honeycomb-structured smectites (Sme) (Figure 1a) with EDX pattern similar to montmorillonite (Mnt, $[Na,Ca]_{0.3}[Al,Mg]_2Si_4O_{10}[OH]_2 \cdot nH_2O$) and minor partly hexagonal chlorite (Chl, $[Fe,Mg,Al]_6[Si,Al]_4O_{10}[OH]_8$) platelets amongst (Figure 1b). Other widespread alteration products associated with Cpx were identified as actinolite (Act, $Ca_2[Mg,Fe]_5Si_8O_{22}[OH]_2$) often intergrown with smectites and chlorite (Figure 1c) and the serpentine-group minerals chrysotile (Ctl, $Mg_3Si_2O_5[OH]_4$) epitaxic to the Cpx ⟨001⟩ direction (Figure 1d), and lizardite (Lz, $Mg_3Si_2O_5[OH]_4$) that occurred as platy phase with irregular rims (Figure 1e). Secondary epitaxic albite (Ab, $NaAlSi_3O_8$) on Plag (Figure 1f), which was in general less extensively covered by smectites than Cpx. Besides the visually identified alteration phases the iron oxide maghemite (Mgh, Fe_2O_3) was detected by XRD analyses. As mentioned above, qualitative XRD analyses of actinolite was difficult, which was in particular the case for the experimental series at a run duration of 72 hours (Figure 2c, marked with "*"). Here, actinolite was not satisfactorily identified, but we're aware of the fact, that actinolite may have been present within the sample. It is noteworthy, that phase abundances determined in a first approximation by XRD (without internal standards) revealed in all experiments albite was the major alteration phase (~3-6 rel. %) followed by montmorillonite and actinolite (both up to 6 rel %), lizardite (up to 2 rel. %), and in only two samples with low run duration of 3 hours maghemite (2-3 rel. %) (Fig. 2). However, not all by SEM images identified phases, i.e., chrysotile and chlorite have been detected by XRD, probably because of the reasons described above. The proportions of secondary minerals showed distinct systematics depending on the w/r ratio and the run duration. From Figure 2 it is apparent, that in paticular Cpx proportions decreased during gabbro-seawater interactions even after short durations of 3 and 6 hours while secondary minerals were formed (note, in Figure 2 the start rock composition is shown at "start" of the x-

axis). The only detected iron oxide, maghemite, occured at low run duration of 3 hours and at relatively low w/r ratios (0.5 and 2, Figure 2a), but it disappeared as the Fe-bearing phase actinolite and smectite/montmorillonite probably along with Fe-bearing chlorite were formed. Albite was abundant in all experiments, but the albite proportions have been decreased between 3 and 720 hours while smectite/montmorillonite showed the largest abundances throughout all w/r ratios (cf. Figure 2a,d vs. Figure 2b,c). The proportion of forsterite has been decreased only after a long run duration of 720 h as the abundance of lizardite has been increased. Finally at a high w/r ratio (w/r = 10) forsterite not been detected (Figure 2d), most probably because it might have been completely serpentinized to lizardite at these conditions.

As a preliminary conclusion, it is evident from our results, that hydrothermal alteration of gabbro at high pressure and temperature (p-T) conditions is a very fast process with major changes in mineralogy within durations less than 3 hours. The observed extensive rapid formation of $Mg(OH)_2$-bearing secondary mineral phases adjacent to Cpx (i.e., smectites and chlorite, the serpentine-group minerals lizardite and chrysotile, and ± actinolite) points towards metasomatic delivery of Mg- and OH-components to the rock by the seawater. This rapid metasomatic process is in so far important as it produces $HCl_{(aq)}$ (Eq. 1), which in turn causes extensive rock leaching in particular at high w/r ratios, e.g., at high fluid fluxes. Our results reveal the importance of smectites during early metasomatic seawater-gabbro interactions in particular at higher w/r ratios (w/r > 5). Based on our preliminary study smectites disappeared during metamorphic gabbro-seawater equilibration, at which the major amounts of serpentine-group minerals were formed. Thus, smectites might be closely related to metasomatic processes of intense hydrothermal circulation. Due to the wide-spread abundance of smectites in basalts it is evident, that the magnitude of metasomatic non-equilibric processes within the oceanic crust is larger than previously thought.

In future experiments we will focus on the temperature and pressure dependence of seawater-rock interaction processes at variable mineralogy with more detailed quantitative and qualitative analyses of the obtained mineral phases and fluid chemistry to gain knowledge on element fluxes during early-stage hydrothermal alteration processes for various ocean crust lithologies.

References:

[1] German C. R., Thurnherr A. M., Knoery J., Charlou J.-L., Jean-Babtiste P., and Edmonds H. N. (2010) Deep Sea Res. 157, 518-527.
[2] Schmidt K., Garbe-Schönberg D., Bau M., and Koschinsky A. (2010) Geochim. Cosmochim. Acta 74, 4058–4077.
[3] Saito M. A., Noble A. E., Tagliabue A., Goepfert T. G., Lamborg C. H., and Jenkins W. J. (2013) Nat. Geosci. 5, 775-779.
[4] German C. R., Bennett S. A., Connelly D. P., Evans A. J., Murton B. J., Parson L. M., Prien R. D., Ramirez-Llodra E., Jakuba M., Shank T. M., Yoerger
D. R., Baker E. T., Walker S. L., and Nakamura K. (2008) Earth. Planet. Sci. Lett. 273, 332-344.
[5] Haase K. M., Petersen S., Koschinsky A., and M64/1, M68/1 Scientific Parties (2007) Geochem. Geophys. Geosyst. 8, Q11002, doi: 10.1029/2006GC001509.
[6] Elderfield H. and Schultz A. (1996) Annu. Rev. Earth Planet. Sci., 24, 191-224.
[7] German C. R., Thurnherr A. M., Knoery J., Charlou J.-L., Jean-Baptiste P., and Edmonds H. N. (2010) Deep Sea Res. 157, 518-527.
[8] Coogan L. A. and Dosso S. (2012) Earth. Planet. Sci. Lett. 323-324, 92-101.
[9] Mottl M. J. and Holland H. D. (1978) Geochim. Cosmochim. Acta 42, 1103-1115.
[10] Hajash A. and Chandler G. W. (1981) Contrib. Mineral. Petrol. 78, 240-254.
[11] Allen D. E. and Seyfried [Jr.] W. E. (2003) Geochim. Cosmochim. Acta 67, 1531-1542.
[12] Seyfried [Jr.] W. E. and Bischoff J. L. (1977) Earth. Planet. Sci. Lett. 34, 71-77.
[13] Bischoff J. L. and Seyfried [Jr.] W. E. (1978) Am. J. Sci. 278, 838-860.
[14] Berger G., Schott J., and Loubet M. (1987) Earth. Planet. Sci. Lett. 84, 431-445.

IODP

Miocene to Recent tephrostratigraphy offshore Central America: Evolution, Provenance and Cyclicities

J.C. SCHINDLBECK[1], S. KUTTEROLF[1], A. FREUNDT[1]

[1]GEOMAR, Helmholtz-Zentrum für Ozeanforschung Kiel

The Central American convergent margin is part of the Pacific "Ring of Fire" along which explosive volcanic eruptions and earthquakes frequently occur. At the same time, convergent margins are particularly attractive for human settlements because logistic advantages of coastal plains combine with natural resources at the arc and fertile volcanic soils. Thus there is strong motivation to understand the natural hazards represented by volcanoes and earthquakes in these regions by studying the processes that control eruption recurrence times and cyclicities in the volcanic record. Recent years have shown how vulnerable modern societies are to even relatively small volcanic eruptions (Grimsvötn 2011, Puyehue-Cordon Caulle 2011, Eyjafjallajökull 2010, Santa Ana 2004). Vulnerability in the face of subduction earthquakes has been dramatically demonstrated by the Fukushima 2011, Maule 2010, and Sumatra 2004 events. During the recent IODP drilling of the CRISP project (CRISP A1 and A2; IODP Leg 334 and 344) the relationships between physical properties, structural geology and sedimentology with seismicity at an erosional convergent margin offshore Costa Rica were investigated. Studying the nature and stratigraphic distribution of volcaniclastic material in the CAVA sediment record aims to investigate relationships between tectonic and volcanic processes as well as long-term changes in arc volcanism. The Central American Volcanic Arc (CAVA) extends from Panama to Guatemala and runs roughly parallel to, and 150-200 km away from, the Middle America Trench (MAT) where the Cocos plate subducts beneath the Caribbean plate at a convergence rate of 70–90 mm/year (Barckhausen et al., 2001; DeMets, 2001). Along the CAVA, variations in the nature of the incoming plate (Hoernle et al., 2002), in upper-plate crustal thickness and composition (Carr, 1984) and the tectonic setting, are paralleled by along-arc variations in the composition of the volcanic rocks (Carr, 1984; Carr et al., 2007; Feigenson et al., 2004; Hoernle et al., 2008; Patino et al., 2000) and the magnitudes of eruptions (Rose et al., 1999). A major change of subduction input occurred when material from the Galapagos Hot Spot arrived at the MAT, particularly the collision and subduction of the 2km thick Cocos Ridge offshore Costa Rica. Magmas of variable degrees of magmatic differentiation, ranging from normal calc-alkaline basalt to rhyolite but also comprising alkaline compositions, have been discharged by CAVA volcanoes ranging from cinder cones and maars through

stratocones to calderas. Upper Pleistocene (since ~500 ka) to Holocene large caldera volcanoes, which produced large-magnitude eruptions of highly evolved, silicic magmas, predominate at the northern CAVA (Rose et al., 1999) but also occur less commonly in Nicaragua and Costa Rica. Particularly the tephras of highly explosive, Plinian-type eruptions have been predominantly dispersed by the prevailing winds to the west across the Pacific where they provide excellent marker beds in the mostly non-erosive submarine environment.

A number of publications have therefore used this submarine reservoir to complement field work on land to investigate the Late Peistocene to Holocene tephrostratigraphic successions in middle to northern Central America (Drexler et al., 1980; Freundt et al., 2006; Hart and Steen-McIntyre, 1983; Koch and McLean, 1975; Kutterolf et al., 2008a-c; Kutterolf et al., 2007a; Newhall, 1987; Pérez et al., 2006; Pérez and Freundt, 2006; Peterson and Rose, 1985; Pullinger, 1998; Rose et al., 1999; Rose et al., 1987; Scott et al., 2006; Self et al., 1989; Wehrmann et al., 2006; Wundermann and Rose, 1984). However, very little is yet known about the volcanic stratigraphy for the Early Pleistocene and the Tertiary, is presently mainly based on lavas. Wiesemann (1975) and Weyl (1980) did a first study of the mostly Neogene rocks of Nicaragua and El Salvador. Ehrenborg (1996) provided an age framework for the laterally displaced Tertiary arc segments of Nicaragua. Reynolds (1980; 1987) and Jordan et al. (2006; 2007) extended this to Guatemala and Honduras but Carr et al. (2007) also stated that there is much to learn about timing and extent of the Tertiary volcanism. Although obviously large explosive eruptions from Nicaragua, Honduras, El Salvador and Guatemala are present the information and data regarding the older explosive arc volcanism is very sparse and cannot be studied continuously with field data alone. Volcaniclastic deposits preserved in the ocean floor provide an excellent opportunity to complement sampling and dating of remnant lavas on land. Fortunately, the Pacific submarine sediment successions sampled offshore Central America by the Ocean drilling programs (DSDP, ODP, IODP) do contain numerous ash beds from volcanoes of the Pliocene and Miocene arc. This tephra record provides answers for diverse geoscientific questions encompassing cyclic behavior of arc, or global, volcanism (see Kutterolf et al., 2013), marker horizons for paleontology and sedimentary basin reconstruction, hazard studies involving next to volcanogenic also tsunamogenic causes of risk, identification of hidden volcanic sources of the past, and compositional relationships between subduction input and arc output on a long term scale (e.g. Kutterolf et al., 2008a-c). The Ocean drilling at the Central American convergent margin revealed numerous marine tephra beds

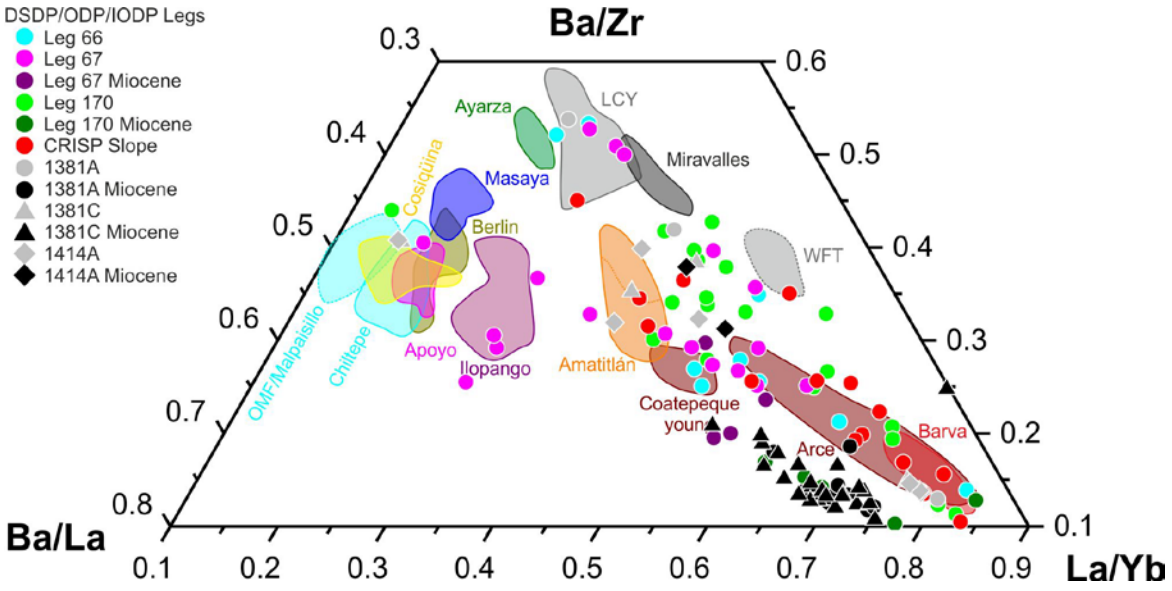

Quaternary through Tertiary ages from 69 Holes at 29 Sites during 9 Legs. We complement that data set by marine cores from former German Research cruises covering Holocene through Late Pleistocene ages (e.g. Kutterolf et al., 2008b; Kutterolf et al., 2007). The aims of our work in progress are:

1. establish a continuous tephrostratigraphy from the Holocene to the Miocene.

So far we identified several marker horizons on the basis of volcanic glass compositions (major and trace elements). We calibrated first points for the age models of the CRISP Sites for the late Pleistocene (Tiribi Tuff, 322 ka, Costa Rica; Los Chocoyos, ~84 ka, Guatemala; LFT, 191 ka, Guatemala; Figure 1) that are identified in all southern CAVA sediments.

2. provenance of marine volcaniclastics along the CAVA to reconstruct lateral variations in volcanism over time.

Systematic along-arc variations of trace-element characteristics documented by on-land studies (e.g. Zr/Nb, Ba/La and Ba/Zr; Figure 1) allow to constrain the source regions of marine tephras along the CAVA. Source regions of for example the CRISP tephras so far identified lie predominately in Costa Rica, but also in Nicaragua, and some in El Salvador, Honduras and Guatemala. Our results suggest much more abundant highly explosive volcanism situated in the southern part of Central America (Costa Rica/Panama) than previously thought.

3. revealing the history of very long-lived volcanic centers.

The geochemical correlation of marine ash beds to large volcanic centers at the CAVA suggests that these centers have been active for significantly longer times than previously known from work on land. Figure 1 shows similarities in trace element ratios of marine tephras to eruptive products from volcanic centers like Atitlán, Amatitlán (Guatemala), Coatepeque and Ilopango (El Salvador), and Apoyo (Nicaragua), as well as Barva (Costa Rica). Continued analyses and age datings promise to reveal long live cycles for these (and possibly other) volcanoes.

4. constraining the onset of Galapagos Hotspot Track subduction.

Subduction of Cocos crust modified by Galapagos magmatism has generated CAVA magmas carrying geochemical Galapagos tracers. There is discussion about the timing when Galapagos material arrived at the MAT (e.g. Abratis and Woerner, 2001; Gräfe et al., 2002; Kolarsky et al., 1995; Gazel et al. 2009).). The age at which the Galapagos signal first appears in CAVA ashes will help to constrain the timing of that event.

5. identifying cyclicities in the volcanic record.

Cyclicities have been observed in marine ash records on a range of time scales. For example, Kutterolf et al. (2013) relate cyclic periods of 10^4 to 10^5 years to global climate changes while Sigurdsson et al. (2000) observed periods 10^6 to 10^7 years probably related to geotectonic changes. So far we observe cyclic variations in the abundance of ash beds in the tephra record of Legs 170, 334, and 344. In the Miocene the incoming plate tephra records are dominated by compositional characteristics of the Galapagos Hot Spot Center, and we therefore suggest that cyclic ash abundances are related to processes modulating the hot spot volcanic activity.

References:

Abratis M and Woerner G (2001) Ridge collision, slab-window formation, and the flux of Pacific asthenosphere into the Caribbean realm. Geology, 29: 127-130.

Barckhausen U, Ranero CR, von Huene R, Cande S, Roeser H (2001) Revised tectonic boundaries in the Cocos Plate off Costa Rica: Implications for the segmentation of the convergent margin and for plate tectonic models. Geophys. Res. 106(19):207-220

Carr MJ (1984) Symmetrical and segmented variation of physical and geochemical characteristics of the Central American volcanic front. J. Volcanol. Geotherm. Res. Vol. 20:p. 231-252

Carr MJ, Saginor I, Alvarado GE, Bolge LL, Lindsay FN, Milidakis K, Turrin BD, Feigensohn MD, Swisher III CC (2007) Element fluxes from the volcanic front of Nicaragua and Costa Rica. Geochem Geophys Geosys 8:doi:10.1029/2006GC001396

DeMets C (2001) A new estimate for present-day Cocos-Caribbean plate motion: Implications for slip along the Central American volcanic arc. Geophysical Research Letters 28(21):4043-4046

Drexler JW, Rose jr. WI, Sparks RSJ, Ledbetter MT (1980) The Los Chocoyos Ash, Guatemala: A Major Stratigraphic Marker in Middle America and in the Three Ocean Basins. Quaternary Research 13:327-345

Ehrenborg J (1996) A new stratigraphy for the Tertiary volcanic rocks of the Nicaraguan highland. Geol Soc Am Bull 108: 830-842

Feigenson MD, Carr MJ, Maharaj SV, Bolge LL, Juliano S (2004) Lead Isotope Composition of Central American Volcanoes: Influence of the Galapagos Plume. Geochem. Geoph. Geosy. 5(6):1-14

Freundt A, Kutterolf S, Schmincke HU, Hansteen TH, Wehrmann H, Perez W, Strauch W, Navarro M (2006) Volcanic hazards in Nicaragua: Past, present, and future. In: Rose WI, Bluth GJS, Carr MJ, Ewert J, Patino LC, Vallance JW (eds) Volcanic hazards in Central America. Geol. Soc. Am. Spec. Publ., pp 141-165

Gazel E, Carr M, Hoernle K, Feigenson MD, Szymanski D, Hauff F, van den Bogard P, (2009) Galapagos-OIB signature in southern Central America: Mantle refertilization by arc–hot spot interaction. Geochem. Geophys. Geosys., 10(2): doi:10.1029/2008GC002246.

GräfeK, Frisch W, Villa IM and Meschede M (2002) Geodynamic evolution of southern Costa Rica related to low-angle subduction of the Cocos Ridge: constraints from thermochronology. Tectonophysics, 348(4): 187-204.

Hart WJE, Steen-McIntyre V (1983) Terra Blanca Joven Tephra from the AD 260 Eruption of Ilopongo Caldera. In: Sheets PD (ed) Archeology and Volcanism in Central America - The Zapotitán Valley of El Salvador. University of Texas Press, Austin, pp 15-34

Hoernle K, Abt DL, Fischer KM, Nichols H, Hauff F, Abers GA, van den Bogaard P, Heydolph K, Alvarado G, Protti M (2008) Arc-parallel flow in the mantle wedge beneath Costa Rica and Nicaragua. Nature 451(7182):1094-1097

Hoernle K, and von den Bogaard, P. et al (2002) Missing history (16-71 Ma) of the Galapagos hotspot: Implications for the tectonic and biological evolution of the Americas. Geology Vol. 30(No. 9):p. 795-798

Jordan BR, Sigudsson H, Carey SN, Rogers R, Ehrenborg J (2006) Geochemical correlation of Caribbean Sea tephra layers with ignimbrites in Central America. In: Siebe C, Macías JL, Aguirre-Díaz GJ (eds) Neogene-Quaternary Continental Margin Volcanism: A Perspective from México. pp 175-208

Jordan BR, Sigurdsson H, Carey SN, Rogers R, Ehrenborg J (2007) Geochemical variation along and across the Central American Miocene paleoarc in Honduras and Nicaragua. Geochimica et cosmochimica acta 71(14):3581-3591

Koch AJ, McLean H (1975) Pleistocene tephra and ash-flow deposits in the Volcanic Highlands of Guatemala. Geol. Soc. Am. Bull. 86:529-541

Kutterolf S, Freundt A, Peréz W (2008b) The Pacific offshore record of Plinian arc volcanism in Central America, part 2: Tephra volumes and erupted masses. Geochem. Geophys. Geosys. 9(2):doi:10.1029/2007GC001791

Kutterolf S, Freundt A, Peréz W, Mörz T, Schacht U, Wehrmann H, Schmincke H-U (2008a) The Pacific offshore record of Plinian arc volcanism in Central America, part 1: Along-arc correlations. Geochem. Geophys. Geosyst. 9(2):doi:10.1029/2007GC001631

Kutterolf S, Freundt A, Pérez W, Wehrmann H, Schmincke HU (2007) Late Pleistocene to Holocene temporal succession and magnitudes of highly-explosive volcanic eruptions in west-central Nicaragua. J. Volcanol. Geotherm. Res. 163(1-4):55-82

Kutterolf S, Freundt A, Schacht U, Bürk D, Harders R, Mörz T, Peréz W (2008c) The Pacific offshore record of Plinian arc volcanism in Central America, part 3: Application to forearc geology. Geochem. Geophys. Geosys. 9(2):doi:10.1029/2007GC001826

Kutterolf S, Jegen M, Mitrovica JX, Kwasnitschka T, Freundt A, Huybers PJ (2013) A detection of Milankovitch frequencies in global volcanic activity. Geology 41(2):227-230

Kolarsky RA, Mann P and Montero W (1995) Island arc response to shallow subduction of the Cocos Ridge, Costa Rica. In: P. Mann (Editor), Geologic and tectonic development of the Carribean plate boundary. Geological Society of America Special Paper, pp. 235-262.

Newhall CG (1987) Geology of the Lake Atitlàn region, Western Guatemala. J. Volc. Geo. Res. 33:23-55

Patino LC, Carr MJ, Feigenson MD (2000) Local and regional variations on Central American arc lavas controlled by variations in subducted sediment input. Contrib Mineral Petrol 138:265-283

Pérez W, Alvarado GE, Gans PB (2006) The 322 ka Tiribi Tuff: Stratigraphy, geochronology and mechanisms of deposition of the largest and most recent ignimbrite in the Valle Central, Costa Rica. Bull. Volcanol. 69:25-40

Pérez W, Freundt A (2006) The youngest highly explosive basaltic eruptions from Masaya Caldera (Nicaragua): Stratigraphy and hazard assessment. In: Geological Society of America, Special Paper 412. pp 189-207

Peterson PS, Rose WI (1985) Explosive eruptions of the Ayarza Calderas, Southeastern Guatemala. J. Volc. Geo. Res. 25:289-307

Pullinger CR (1998) Evolution of the Santa Ana volcanic complex,El Salvador. In: Michigan Technological University, p 145

Reynolds J (1980) Late Tertiary volcanic stratigraphy of northern Central America. Bulletin Volcanologique 43(3):601-607

Reynolds JH (1987) Timing and sources of neogene and quaternary volcanism in South-Central Guatemala. J. Volc. Geo. Res. 33:9-22

Rose WI, Conway FM, Pullinger CR, Deino A, McIntosh K (1999) An improved age framework for late quaternary silicic eruptions in nothern Central America. Bull. Volcanol. 61:106-120

Rose WI, Newhall CG, Bornhorst TJ, Self S (1987) Quaternary silicic pyroclastic deposits of Atitlàn Caldera, Guatemala. J. Volc. Geo. Res. 33:57-80

Scott W, Gardner C, Alverez A, Devoli G (2006) A.D. 1835 eruption of Volcán Cosigüina, Nicaragua: A guide for assessing hazards. In: Rose WI, Bluth GJS, Carr MJ, Ewert J, Patino LC, Vallance JW (eds) Volcanic hazards in Central America. Geol. Soc. Am. Spec. Publ., pp 125-140

Self S, Rampino MR, Carr M (1989) A reappraisal of the 1835 eruption of Coseguina and its atmospheric impact. Bull. Volcanol. 52:57-65

Wehrmann H, Bonadonna C, Freundt A, Houghton BF, Kutterolf S (2006) Fontana Tephra: A basaltic plinian eruption in Nicaragua. In: Rose WI, Bluth GJS, Carr MJ, Ewert J, Patino LC, Vallance JW (eds) Volcanic hazards in Central America. Geol. Soc. Am. Spec. Publ., pp 209-223

Sigurdsson H, Kelley S, Leckie RM, Carey S, Bralower T, King J (2000) History of circum-Caribbean explosive volcanism: 40Ar/39Ar dating

of tephra layers. In: Leckie RM, Sigurdsson H, Acton GD, Draper G (eds) Proceedings ODP, Scientific Results 165: 299-314
Weyl R (1980) Geology of Central America. 2nd ed., in: Beiträge zur regionalen Geologie der Erdepp. In: Bender Fea (ed) Gebr. Borntraeger. Berlin - Stuttgart, p.371
Wiesemann G (1975) Remarks on the Geologic Structure of the Republic of El Salvador, Central America. Geol. Paläont. Inst., Univ. Hamburg 44:557-574
Wundermann RL, Rose WI (1984) Amatitlán, an actively resurging caldera 10km south of Guatemala City. J. Geophys. Res. 89:8525-8539

IODP

IODP Proposal 823-full: Records of geohazards and monsoonal changes in the northern Bay of Bengal

T. SCHWENK[1], H.R. KUDRASS[2], V. SPIESS[3], L. PALAMENGHI[2] AND PROPONENTS

[1]Department of Geoscience, University of Bremen, Klagenfurter Str., D-28359 Bremen, Germany
[2]MARUM, University of Bremen

IODP Proposal 823-full propose to investigate the world's largest sedimentary system sustained by drainage from the Himalayas by the Ganges and Brahmaputra rivers. Three rapidly accumulated, high-resolution archives from the northern Bay of Bengal should be used to reconstruct the history and impacts of monsoonal variability and the record of cyclones and seismic geohazards. These archives will be collected from the diverse settings of a deeply incised shelf canyon, a shelf-edge sequence of low-stand deltas, and the hemipelagic cover of the upper continental slope.

The shelf canyon intersects the active deltaic clinoform and receives most of its sediment through mass failures and gravity flows generated by frequent tropical cyclones, depositing graded beds on both sides of the canyon with extremely high sedimentation rates of up to 30 cm/year. The 500 m-thick, Holocene to late Pleistocene graded beds preserve a record of tropical-cyclone frequency that can be related to monsoon intensity, ENSO, shifting ITCZ, and northern solar insolation. This archive also contains pollen, terrestrial biomarkers, weathering indicators, and marine diatoms, which can be used to reconstruct contemporaneous changes of monsoonal precipitation and paleoceanographic settings. In addition, the anthropogenic impacts of expanding agriculture and vanishing forest cover on the quality of terrigenous and organic sediment components can be addressed. Finally, dating the series of mass transport deposits accumulated on the central floor of the canyon will determine the recurrence interval of massive subduction related earthquakes.

The rapid sedimentation in the canyon is a great challenge for the microbial life. The microbial response to such an extreme anoxic environment with rapid and frequent burial events by gravity-driven flows and mass transport deposits is a main objective for deep biosphere research. The extremely high accumulation rates provide an end-member example of deep organic carbon burial and offer unique opportunities to study microbial controls on carbon sequestration.

These high-resolution records in the canyon are complemented by comparable coupled records preserved near the shelf edge, where eight stacked low-stand submarine deltas inform on timing of sea-level variations, subsidence patterns, and glacial-period sediment and water fluxes to the margin. Shifting to longer time scales of millennium years, the hemipelagic deposits, which will be drilled on the upper slope, contain the records of environmental evolution and sediment transport pathways back to the upper Miocene. Together, these three distinct archives complement one another by capturing the significant spatial and temporal variations of the environmental evolution in this densely populated area.

Three distinct depositional settings with annual sedimentation rates of 30 cm to 0.1 mm are targeted in the northern Bay of Bengal. These sedimentary archives contain coupled high-resolution records of the onshore environmental and the offshore paleoceanographic responses to monsoon variation, including a record of regional geohazards. The following main objectives are addressed:

Quantify and exactly date changes in monsoonal precipitation using contemporaneous Holocene/ Pleistocene/Upper Miocene records of vegetation, weathering intensity and paleoceanographic changes.

Define the shifting source areas and transport pathways for Himalayan detrital sediment through the Quaternary, as controlled by the positions of the ITCZ and the main areas of monsoonal precipitation.

Establish the relationship between tropical cyclone frequency, ENSO, and other Holocene global and regional climatic variations through the reconstruction of a detailed record of cyclone-generated deposits.

Reconstruct the Holocene history and recurrence interval of major subduction-related earthquakes from mass-transport deposits.Reconstruct the history of Late Quaternary low-stand deltas to determine glacial climate, water and sediment discharge, and to constrain long-term subsidence rates of the Bengal shelf.

Define the strategies of microbial life in rapidly accumulating anoxic marine sediments and the microbial controls on preservation of buried organic carbon.

Investigate the anthropogenic impacts of deforestation and expanding agriculture within the catchment area of the Ganges and Brahmaputra, particularly on the composition and quantity of organic carbon and sediment exported to the offshore depocenters.

ICDP

Seismic site characterization in and around the COSC-1 drillhole

H. SIMON[1], S. BUSKE[1], R. GIESE[2], C. JUHLIN[3], C. SCHMELZBACH[4], H. MAURER[4], J. ROBERTSSON[4]

[1]Institute of Geophysics and Geoinformatics, TU Bergakademie Freiberg
[2]Scientific Drilling, GFZ German Research Centre for Geosciences, Helmholtz Centre Potsdam
[3]Dept. of Earth Sciences, Uppsala University
[4]Institute of Geophysics, ETH Zurich

The project COSC (Collisional Orogeny in the Scandinavian Caledonides) focuses on the mid Paleozoic Caledonide Orogen in Scandinavia in order to better understand orogenic processes, both in the past and in recent active mountain belts (Gee et al. 2010). The Scandinavian Caledonides provide a well preserved example of Paleozoic plate collision, where the surface geology in combination with geophysical data provide control of the geometry of the Caledonian structure, both

of the allochthon and the underlying autochthon, including a shallow W-dipping décollement surface on a thin skin of Cambrian black shales beneath the Caledonian thrust sheets. The structure of the basement underneath the décollement is highly reflective and apparently dominated by mafic sheets intruded into either late Paleoproterozoic granites or Mesoproterozoic volcanics and sandstones. The COSC project will examine the structure and physical conditions of these units, in particular the Caledonian nappes ("hot" allochthon) and the underlying basement, with two approximately 2.5 km deep drillholes, located near Åre and Mörsil in western Jämtland (http://ssdp.se/projects/COSC). In addition to that, the drillholes will provide unique information about the present temperature gradient in the Caledonides, the porosity and permeability of the rock formations, and the petrophysical properties of the rocks at depth.

Existing regional seismic and magnetotelluric data have imaged the geometry of the upper crust, and pre-site seismic reflection surveys were performed in 2010 and 2011 to better define the exact drill site locations (Hedin et al. 2012). This project presented here is dedicated to complement these surface seismic measurements by drillhole-based investigations to better resolve and define the small-scale structures (including lithological boundaries, steeply dipping fault segments, fracture sets, etc.) around the drillhole COSC-1. This will be achieved by a combination of seismic transmission and reflection experiments using a 3-component (3C) borehole geophone system and complemented by 3C geophones at the surface, where sources and surface receivers will be aligned at different azimuths and centred around the borehole location.

A first reconnaissance survey has been performed in early summer 2013 at the COSC-1 drill site. Three profile lines have been defined, each approximately 10 km long and radially centered around the drill site. Because of the forested and mountainous terrain the profile lines are mostly bound to existing roads and paths. Along these lines the 3C receivers plus standalone data recorders as well as the source points will be distributed for multiazimuthal walkaway VSP (Vertical Seismic Profiling) measurements. Furthermore a 3C geophone chain with 10 m spacing will be installed in the ~2.5 km deep COSC-1 borehole and operated such that an almost complete depth profile for each source point will be obtained. The second part of the planned survey will be a zero-offset VSP measurement along the entire borehole length with very densely spaced receivers, with the source in the direct vicinity of the borehole. The start of drilling for the COSC-1 borehole is scheduled for end of April 2014. After the drilling is finished and the in-hole tests and loggings are done, our VSP survey will take place in late summer or autumn 2014.

In preparation for the survey and the following data processing we have performed finite-difference elastic wavefield modelling to investigate the effects of the survey geometry, such as the receiver ghost on borehole recordings, the influence of the free surface and of the significant topography. With these modelled synthetic data sets we are currently testing various methods for the processing of the drillhole-based data (e.g. wavefield separation).

The data processing after the survey will employ recently developed advanced imaging techniques and will focus on, amongst other things, the analysis of anisotropic effects caused by aligned fractures and faults and their relation to the stress regime.

The results of our investigations will be high-resolution images of the fine-scale structure of faults and fractures around the borehole. This information is vital not only for a reliable spatial extrapolation of the structural and petrophysical properties observed in the borehole, but also for a thorough understanding of the tectonic and geodynamic setting, including but not limited to, the past and present stress regime.

References:

Gee, D.G. et al., 2010. Collisional Orogeny in the Scandinavian Caledonides (COSC). GFF, 132(1), pp.29–44.

Hedin, P., Juhlin, C. & Gee, D.G., 2012. Seismic imaging of the Scandinavian Caledonides to define ICDP drilling sites. Tectonophysics, 554-557(0), pp.30–41.

ICDP

An Airgun Seismic Survey for Preparation/Support of ICDP Drilling at Lake Issyk-Kul, Kyrgyztan - Opportunities for Tectonic and Sedimentary Process Studies

V. SPIESS[1], H. KEIL[1], I. SAUERMILCH[1], AZAT SAID[2], K. ABDRAKHMATOV[2], C. GEBHARDT[3], H. OBERHÄNSLI[4]

[1] Department of Geosciences, University of Bremen, Klagenfurter Strasse, D-28359 Bremen, Germany
[2] Institute of Seismology, NAS KR, Bishkek, Kyrgyztan
[3] Alfred-Wegener Institut für Polar- und Meeresforschung, 27568 Bremerhaven, Germany
[3] Naturhistorisches Museum, Berlin

Lake Issyk-Kul became a potential target for the International Continental Drilling Program (ICDP), as it represents a huge depositional sink in the hinterland of the Indian-Eurasian collision zone, probably ranging back to Miocene times. It is located in the Tien Shan mountains in Kyrgystan at an elevation of 1607 meters and oriented in E-W direction responding to the main thrust belt formation..

Drilling had been proposed for the area of Lake Issyk-Kul, Kyrgystan to mainly investigate the tectonic history of the last 5-15 million years, as had been discussed during an ICDP-funded workshop at the lake in 2012. As part of this planning, drilling in the lake was considered as an option, and further investigations in the lake were suggested to gain a better understanding of regional sedimentary and tectonic processes imaged in presumably continuous sedimentary sections at the lake floor.

With the support of ICDP, a multichannel seismic survey had been carried out in early May, 2013, to collect deeper penetrating seismic data, complimentary to those data sets, which had been acquired by the Renard Centre of Marine Geology (RCMG, Gent). Partners of this enterprise were the Natural History Museum Berlin, Universität Bremen - Meerestechnik/ Umweltforschung and the Alfred Wegener Institute, Bremerhaven.

Main task were the acquisition deeper penetrating multichannel seismic data as well as the use of sonobuoys for a refraction seismic study along a selected profile. The 180 km long and 60 km wide lake reveals a depth of ~670

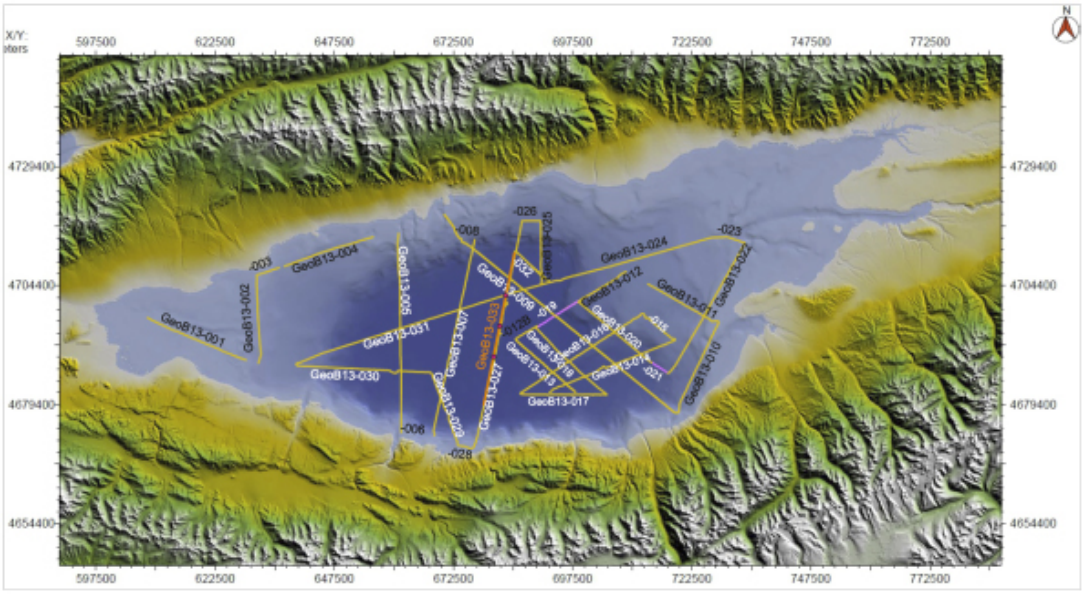

Figure 1: Sismic track lines of the Moltur 2013 cruise. The green circle marks the location of a tectonically induced anticline. Pink circles mark deployment locations of sonobuoys, the orange line the associated profile, shot with a 1,7 L airgun towed at 6m depth. The lake floor is between 600 und 700 m deep.

m, which in turn promotes a rich sedimentary environment with deltas, steep slope and a turbiditic plain. As long as evaporation and precipitation is in some balance, sedimentary records in the deeper lake are assumed to be continuous and to be therefore suitable, and besides terraces found at different depth levels, which indicate lower lake levels, the deep fill appears to be continuous.

Figure 1 shows the grid of seismic lines, which concentrate on the deep lake, complimentary to the shallow water data of RCMG. Preliminary data will be presented, which clearly reveal an evolving anticline, where a condensed section would allow an optimized drilling strategy (green circle). Several lines across the deep lake will also allow demonstrate a very thick filling. The base of the fill cannot be detected within raw data, but further processing will be required to both increase penetration, but also to reveal further details on the assumed bounding faults near the northern and southern slopes as well as basinwide fault pattern.

ICDP

The interplay of volcanic, tectonic and sedimentary processes in the offshore sector of the Campi Flegrei caldera (Gulf of Naples, Italy): Preliminary results of a multi-channel seismic Pre-Site Survey for combined IODP and ICDP drilling campaigns

L. STEINMANN[1], V. SPIESS[1], M. SACCHI[2]

[1] Department of Geosciences, University of Bremen, Klagenfurter Strasse, D-28359 Bremen, Germany
[2] Institute for Coastal Marine Environment (IAMC), Italian Research Council (CNR), Calata P.ta di Massa, Porto di Napoli, 80133 - Napoli, Italy

Large collapsed calderas are associated with exceptionally explosive volcanic eruptions, which are capable of triggering a global catastrophe second only to that from a giant meteorite impact. Therefore, active calderas have attracted a lot of attention in both scientific communities and governmental institutions worldwide. However, the mechanisms for unrest and eruptions at calderas are still largely unknown and, as demonstrated by ample volcanological research in the last decades, they may be very different from those characterizing the more commonly studied stratovolcanoes or shield volcanoes.

One prime example of a large collapsed caldera can be found in southern Italy, more precisely in the northern Bay of Naples within the Campi Flegrei Volcanic Area. The Campi Flegrei caldera covers an area of approximately 200 km² defined by a quasi-circular depression, half onland, half offshore, formed mainly by two huge ignimbritic eruptions. It has been the world's most active caldera for the last 40 years, a time period that has been characterized by episodes of unrest involving huge ground deformation (uplift) and seismicity, which have nevertheless not yet led to an eruption. Phases of remarkable uplift, as for instance observed in the period between 1982 and 1984 with uplift rates of 1 m/year, have a clear character of eruption precursors. Understanding the mechanisms for unrest and eruptions is of paramount importance as a future eruption of the Campi Flegrei caldera would expose more than 500,000 people to the risk of pyroclastic flows, rising to several millions in case of an ignimbritic eruption.

Despite the fact that the Campi Flegrei caldera has been extensively studied on land, the submerged part, which makes up half of the entire structure, still remains to a large extent unknown. In January 2008, a high-resolution multi-channel seismic survey on R/V URANIA was carried out in order to image the stratigraphic sequences inside and outside of the caldera structure.

The primary aim of the survey was to provide a robust site survey database for the proposed IODP drilling of the Campi Flegrei caldera as well as the now ongoing ICDP onshore drilling. Based on the seismic dataset, major stratigraphic units such as the Campanian Ignimbrite (CI)

and the Neapolitan Yellow Tuff (NYT) could be traced on regional scales. The spatial distribution of these volcanic units provides information about the eruptive processes and vent locations. Moreover, the preliminary results show first indications for a shallow ring fault system associated with the collapse of the NYT caldera. Furthermore, a dome-like structure associated with a cluster of faults was identified in the center of the supposed caldera, which indicates uplift that might be related to a magma intrusion, thereby suggesting the resurgence of the caldera. Particularly, a dense (semi-3D) grid of seismic reflection profiles provides an optimal foundation for a reliable reconstruction and understanding of the late Quaternary tectono-stratigraphic architecture and evolution of Naples Bay.

The main advantage of such marine investigations is that a complete record of volcanic activity can be studied without the challenges posed on land, by the subsequent destruction or burial of earlier features. Besides, the seismic data have the potential to build a bridge between deep tomographic observations and high-frequency boomer profiles that have already been acquired in this volcanic area.

In particular, the shallow water seismic reflection profiles may serve as a basis for the correlation of the recently completed onland ICDP pilot hole and the ongoing ICDP drilling with marine deposits and proposed IODP drill sites in the Gulf of Naples in order to develop a large scale picture of the study area.

IODP

Preferred mineral alignment promotes great strength variability in soft sediments from the Nankai accretionary prism offshore SW-Japan

MICHAEL STIPP[1], KAI SCHUMANN[1], BERND LEISS[2], JAN. H. BEHRMANN[1], KLAUS ULLEMEYER[3]

[1]GEOMAR, Helmholtz-Zentrum für Ozeanforschung Kiel, Wischhofstr. 1-3, D-24148 Kiel
[2]Geowissenschaftliches Zentrum, Universität Göttingen, Goldschmidtstr. 3, D-37077 Göttingen
[3]Institut für Geowissenschaften, Universität Kiel, Otto-Hahn-Platz 1, D-24118 Kiel

The Nankai Trough Seismogenic Zone Experiment of the International Ocean Discovery Program (IODP) is the very first attempt to drill into the seismogenic part of a subduction zone. Offshore SW-Japan the oceanic Philippine sea plate is subducted beneath the continental Eurasian plate causing earthquakes of magnitude 8.0 to 8.5 and related tsunamis with a recurrence rate of 80-100 years. For the tsunamigenic potential of the forearc slope and accreted sediments their mechanical strength, composition and fabrics have been investigated. 19 drill core samples of IODP Expeditions 315, 316 and 333 were experimentally deformed in a triaxial cell under consolidated and undrained conditions at confining pressures of 400-1000 kPa, room temperature, axial shortening rates of 0.01-9.0 mm/min, and up to an axial strain of 64% (Stipp et al., 2013). With respect to the mechanical behavior, two distinct sample groups could be distinguished. Weak samples from the upper and middle forearc slope of the accretionary prism show a deviatoric peak stress after only a few percent strain (< 10%) and a continuous stress decrease after maximum stress combined with a continuous increase in pore pressure. Strong samples from the accretionary prism toe display a constant residual stress at maximum level or even a continuous stress increase together with a decrease in pore pressure towards high strain (Stipp et al., 2013).

Synchrotron texture and composition analysis of the experimentally deformed and undeformed samples using the Rietveld refinement program MAUD indicates an increasing strength of the illite and kaolinite textures with increasing depth down to 523 m below sea floor corresponding to a preferred mineral alignment due to compaction. Experimentally deformed samples have generally stronger textures than related undeformed core samples, and they show increasing strength of the illite and kaolinite textures with increasing axial strain. Mechanically weak samples have a bulk clay plus calcite content of 31-65 vol.-% and most of their illite, kaolinite, smectite and calcite (001)-pole figures have maxima >1.5 mrd (multiples of a random distribution). Mechanically strong samples, which were deformed to approximately the same amount of strain (up to 40%) have no calcite and a bulk clay content of 24-36 vol.-%. Illite, kaolinite and smectite (001)-pole figure maxima are mostly <1.5 mrd, except for one sample which was deformed to a considerably higher strain (64%).

The higher clay and calcite content and the stronger textures of the mechanically weak samples can be related to collapsed pore space in the originally flocculated aggregates. Because there is no pore fluid loss in undrained experiments, there must be pore space realignment in the mechanically weak samples due to the clay mineral preferred alignment. Pores are increasingly flattened as experimental deformation proceeds, with short pore axes normal to horizontally oriented large illite grains. The synchrotron texture results indicate that the mineral fabric as a whole, i.e. especially clay and also calcite grains, become preferentially oriented. Re-orientation of the mineral alignment is an important cause of strain weakening and contraction, continuing to high compressive strains. Likewise sediments from the incoming Philippine Sea plate are mechanically weak and show a similar composition and texture development as the samples from the forearc slope. Such a re-orientation process is insignificant in the strong samples from the accretionary prism toe; they keep their microfabric until relatively high compressive strain, allowing for strain hardening and dilation. This different mechanical behavior may be caused by the much higher content of strong quartz and albite grains hampering grain rotation and alignment, as well as the collapse or flattening of pores due to angular shapes and minor cleavage planes of these minerals. Soft sediment hardening tends to involve increasingly large volumes of sediment into the imposed deformation allowing for strain dissipation as long as these sediments are homogeneous. This situation is given within the accretionary prism toe, and is characterized by folding and a distributed deformation pattern. If there were structurally weak sediments included in the lithological sequence, deformation would tend to localize within these. Such weak sediments, which soften further with increasing strain, predominate in the cover units of the forearc slope. Consequently, the zone of the megasplay fault cutting the

middle forearc slope, is characterized by fracturing and a more localized deformation pattern. Hence, these structurally weak samples from the forearc slope may provoke mechanical runaway situations allowing for earthquake rupture, surface breakage and tsunami generation. They are also more prone to slope destabilization and resulting submarine mass wasting.

Reference:
Stipp, M., Rolfs, M., Kitamura, Y., Behrmann, J.H., Schumann, K., Schulte-Kortnack, D. and Feeser, V. 2013. Strong sediments at the deformation front, and weak sediments at the rear of the Nankai accretionary prism, revealed by triaxial deformation experiments. - Geochem. Geophys. Geosys. 14/11, doi: 10.1002/ggge.20290.

ICDP

Lake Van tephra: periodicity vs. episodicity, climate control of eruption frequency and seismic eruption triggering

M. SUMITA[1], H.-U. SCHMINCKE[1], J. PALEOVAN SCIENTIFIC TEAM[3]

[1]GEOMAR Helmholtz-Zentrum für Ozeanforschung Kiel , Wischhofstr. 1-3, 24148 Kiel, Germany

The interpretation of the evolution of the system Nemrut and Süphan volcanoes-Lake Van-geodynamics, is based on ca. 500 tephra layers (ca. 25% reworked) emplaced over ca. 600 ky. The 4 sources for the ca. 350 primary tephras - well-defined by mineral and glass compositions - are: (1) peralkaline Nemrut, (2) subalkaline Süphan, the large systems, (3) basaltic Incekaya (Schmincke et al., 2013) and (4) many, mostly basaltic intralake volcanic centers. Nemrut volcano system, the main tephra supplier, erupts periodically with large magnitude rhyolitic at 30-40 ky intervals, followed by smaller trachytic eruptions reflecting steady long-term parent magma flux and no signs of decreasing activity (Sumita and Schmincke, 2013a, b). Explosive activity of nearly extinct Süphan, has been strongly waning over the past ca. 200 ky and typically erupts episodically in focussed tephra swarms, possibly triggered by seismic activity, basalt-rhyolite magma interaction and magma-glacier external forcing. Total eruptive activity of both large systems appears related to climate changes, complete absence of tephras e.g. during the cold period c. 14-30 ka being possibly due to lithosphere loading during glacial periods preventing or reducing mantle melting/magma reservoir activation. Other explanations for the striking tephra absence are dominance of the Siberian High and easterly winds, ice cover of Lake Van or temporary exhaustion of the central Nemrut magma reservoir following the large magnitude Nemrut Formation eruption at ca. 30 ka.

References:
Schmincke H-U, Sumita M, Cukur D, Paleovan Scientific Team (2013) Impact of volcanism on the evolution of Lake Van III: Incekaya – and exceptionally large magnitude (DRE > 1 km3) subaqueous/subaerial explosive basaltic eruption. Abst. IODP-ICDP Kolloquium 2013 (Freiberg)

Sumita M, Schmincke H-U (2013a) Impact of volcanism on the evolution of Lake Van II: temporal evolution of explosive volcanism of Nemrut Volcano (eastern Anatolia) during the past ca. 0.4 Ma. J Volcanol Geotherm Res 253: 15-34

Sumita M, Schmincke H-U (2013b) Impact of volcanism on the evolution of Lake Van I: Evolution of explosive volcanism of Nemrut Volcano (eastern Anatolia) during the past ca. 0.4 Ma. Bull Volcanol 75: 714-747

IODP

Constraining the dynamics of fluid flow and authigenic mineral formation at the northeastern Pacific continental margin – A multiproxy approach

B.M.A.TEICHERT[1], N.GUSSONE[2], L.M.WEHRMANN[3], C.MÄRZ[4], H.STRAUSS[1]

[1] Institut für Geologie und Paläontologie, Universität Münster, Corrensstrasse 24, D-48149 Münster, Germany
[2] Institut für Mineralogie, Universität Münster, Corrensstrasse 24, D-48149 Münster, Germany
[3] GEOMAR Helmholtz-Zentrum für Ozeanforschung Kiel, Wischhofstr. 1-3, D-24148 Kiel, Germany
[4] Newcastle University, School of Civil Engineering and Geoscience, Newcastle upon Tyne, NE1 7RU, United Kingdom

The sediments along the northeastern Pacific continental margin have been targeted by ODP (Legs 146 and 204) and IODP Expeditions (Exp. 311 and 341) as a natural laboratory with respect to early diagenetic biogeochemical processes. The pore water profiles at these locations exhibit a characteristic decrease of sulfate with depth. This concentration gradient results either from the microbially mediated organoclastic sulfate reduction (OSR) or from the anaerobic oxidation of methane (AOM). Authigenic carbonates occur widely in these continental margin settings. They provide important information about biogeochemical processes in the sediments like OSR, AOM and methanogenesis. By deriving their original depths and ages of formation it will be possible to relate them to global climate changes or also to more regional variations in productivity or methane discharge. The paragenesis of different carbonate phases within each carbonate sample also indicates that they bear information on a geochemical chronology. While carbonates get successively buried they pass through different geochemical zones. In each zone, a carbonate with a different mineralogy might precipitate and create, in the end, a very complex mineralogical mixture.

Constraining sulfate reduction in such settings has previously mainly been focused on the traditional $\delta^{34}S$ values when investigating the sulfur isotopic composition of pore water sulfate (combined with $\delta^{18}O$ analyses). However, a high degree of additional information can be obtained with respect to the process itself through studying the minor sulfur isotopes (^{33}S and ^{36}S). With this additional information, details concerning the sulfate flow during sulfate reduction and the recycling of sulfur intermediates within the environment can be much better constrained.

Sulfate reduction via OSR and AOM has a distinct effect not only on the carbon but also on the calcium isotopic composition of carbonates and pore waters. The ammonium that is being produced during organic matter remineralization releases isotopically light Ca from clay minerals. This effect has been observed at several locations. Only sites with vigorous carbonate formation, i.e. active methane seep sites, provide the opportunity to observe the effect of calcium isotope fractionation during carbonate formation on the pore water isotopic composition.

ICDP

$^{40}Ar/^{39}Ar$ mica and amphibole ages for high-grade rocks exhumed along the Alpine Fault, South Island, New Zealand

M.J. TIMMERMAN, R. OBERHÄNSLI, U. ALTENBERGER, M. SUDO

Institut für Erd-und Umweltwissenschaften, Universität Potsdam, Germany

The Alpine Fault, exposed on South Island of New Zealand, marks the Australian-Pacific plate boundary in which the western, Australian plate side constitutes the less deformed footwall and the eastern Pacific plate the strongly deformed and denuded hanging wall. The Fault started out as a strike-slip structure in the early Miocene (c. 23-35 Ma), but many aspects of its early evolution are unclear due to later, Pliocene to Recent, convergence. Convergent movements within the last 5 to 10 Ma are due to reorganization of plate motions and resulted in the present day oblique, dextral convergence across the Fault and distributed deformation of rocks of the Pacific plate east of it. Concomitant rapid uplift, deep exhumation and erosion of the latter removed rocks recording early movements and caused the formation of the Southern Alps. Since the last c. 5 Ma an estimated 50 +/- 35 km of shortening took place across the plate boundary, although regional variations in uplift and exhumation rates along the orogen are significant. The total strike-slip movement based on the separation of the Dun Mt. Belt amounts to c. 480 km and the maximum exhumation is 20–30 km (Cooper & Norris 2011). Presently, uplift along the Alpine fault accounts for c. 75% of relative velocity between the Australian and Pacific plates (Norris & Cooper 2000).

The mainly metasedimentary Otago Schists of the Pacific plate form a c. 150 km wide antiform with sub-greenschist facies rocks in the flanks and greenschist-facies rocks in the centre. $^{40}Ar/^{39}Ar$ dating of foliation defining white micas shows that it records an older geological history and is the result of juxtaposition at c. 120 Ma of predominantly metasedimentary terranes. Deformation and low grade metamorphism at 120 Ma was followed by exhumation and cooling until 100 Ma (Gray & Foster 2004). Westwards, K-Ar ages of the Otago Schists decrease markedly to 12-30 Ma (Neogene) within a c.10 km wide zone south-east of the Alpine Fault within the hanging wall (Adams & Gabites 1985). In addition to resetting of K-Ar ages, overthrusting of the Pacific plate resulted in exhumation of mid-crustal garnet-bearing amphibolites and garnet-biotite-oligoclase schists close to the Fault (Koons 1989). Within this 10-20 km wide Alpine Schist belt the grade of metamorphism increases from sub-greenschist facies in the Otago Schists to the east, to amphibolite facies in the west where foliations are steep and the isograds are truncated and distorted by the Alpine Fault (Grapes 1995; Grapes & Watanabe 1992, Cooper & Norris 2011). The high-grade rocks are intruded by white mica –bearing granitic pegmatites of probably anatectic origin that have c. 67-82 Ma U-Pb zircon and monazite crystallization ages (Chamberlain et al. 1995, Batt et al. 1999) and a c. 73 Ma $^{40}Ar/^{39}Ar$ white mica age (Batt et al. 2004). Therefore, the amphibolite-facies metamorphism is likely to be of late Cretaceous age or older.

Fission track, U-Th-He and K-Ar studies showed that the recent rapid uplift and exhumation is strongly concentrated against the Alpine Fault and disturbed the thermal structure of the leading edge of the Pacific plate immediately east of it, producing a strong thermochronologic signal. A c. 50 km long fault-parallel stretch centring on Aoraki/Mt. Cook in the central part of the Southern Alp records the youngest $^{40}Ar/^{39}Ar$, K-Ar and fission track ages, showing that maximum rates and amount of uplift focused here in the last 3 to 5 Ma (e.g. Batt et al. 2000, Little et al. 2005). During this Pliocene to Recent period, a 1 to 2 km wide, mid-crustal ductile shear zone (mylonite) that developed in the hanging wall amphibolite-facies rocks was exhumed along a current brittle fault marked by cataclasite and fault gauge (Norris & Cooper 2003, Toy et al. 2008, 2012).

For this study, amphibolite-facies metapsammites and (garnet) amphibolites were taken from near the Alpine Fault plane at two localities within the zone with the highest recent uplift rates: Gaunt Creek (site of the Deep Fault Drilling Project DFDP-1A and -B test boreholes) and Waikukupa River. The amphibolites are of various grain sizes and in addition often contain garnet, biotite and/or white mica. The primary aim is to determine the uplift and cooling history of the prograde, high grade metamorphic rocks that are actively being brought up along the Fault using the $^{40}Ar/^{39}Ar$ dating of small amounts of material to avoid possible contamination effects.

The first $^{40}Ar/^{39}Ar$ infra-red laser step-wise heating dating results show that biotite and white mica from hanging wall (proto)mylonitic garnet-biotite-muscovite schists at Gaunt Creek have plateau and near-plateau ages of 1.1 Ma (white mica) and 1.0 Ma (biotite). The $^{40}Ar/^{36}Ar_i$ intercept values (280-298) are close to that of air, showing that the micas contain no detectable amounts of excess argon. The young ages overlap with the youngest K-Ar ages of biotite (0.9 to 1.3 Ma) reported by Batt et al. (2000) from nearby Whataroa Valley and indicate that the rocks were rapidly exhumed through the nominal argon closure temperatures of white mica (muscovite, c. 400-450°C) and biotite (c. 300°C) c. 1 – 1.1 Ma ago. Thermometry of fluid inclusions in quartz veins at Gaunt Creek and nearby localities by Toy et al. (2010) show they were trapped at the onset of, or above, the brittle-ductile transition at temperatures of 325 ± 15 °C and pressures of c. 40 MPa. In combination with the age data, this suggests that c. 1 Ma ago the schists passed through the partial retention zone for argon in micas and through the brittle–viscous transition at an estimated depth of less than 8 km.

In contrast, amphibole (tschermakite to tschermakitic hornblende) from Gaunt Creek amphibolite shows a disturbed age spectrum in which the low temperature steps have anomalously old apparent ages (400 – 70 Ma) dominated by excess argon, and high temperature steps with minimum apparent ages in the range 7-10 Ma. Amphiboles from Waikukupa River shows similar decreasing age spectra with low temperature steps having apparent ages at high as 1.5 and 2.2 Ga, and high temperature steps around 40-50 Ma. The exception is a coarse-grained amphibole that yielded a c. 8 Ma weighted-mean age for the high temperature steps, but still shows evidence for extraneous argon. Previously, Chamberlain et al. (1995) and Batt et al. (2000) reported that excess argon in amphiboles from amphibolites exposed near the Alpine

Fault complicated the interpretation of their $^{40}Ar/^{39}Ar$ and K-Ar ages. The exact significance of these (apparent) ages is not clear as they do not correspond to any known tectonothermal event in New Zealand. Instead they may be the result of protracted cooling in combination with the uptake of argon from outside sources at an unknown time. One explanation may be that, compared to the micas, the relatively low K_2O contents of the amphiboles (0.3-0.5 wt%) may have left them more vulnerable to the effects of even small amounts of extraneous argon. The source(s) of the extraneous argon may have been the large amounts of fluids that invaded rocks near, and within, the fault plane after they passed through the brittle-ductile transition, as is clear from pervasive hydrothermal alteration (Sutherland et al. 2012). $^{40}Ar/^{39}Ar$ in situ UV laser ablation dating on selected amphiboles ("age mapping") may resolve whether the excess argon resides in the grain margins (as suggested by its release at low experimental temperatures) or in older cores. $^{40}Ar/^{39}Ar$ step-wise heating of late, discordant feldspar/adularia veinlets in DFDP-1B core samples is planned in order to establish the timing of late fluid flow in the Gaunt Creek locality.

References:

Adams, C.J. & Gabites, J.E., 1985. Age of metamorphism and uplift in the Haast Schist Group at Haast Pass, Lake Wanaka and Lake Hawea, South Island, New Zealand. New Zealand Journal of Geology and Geophysics, 28, 85-96.

Batt, G.E., Kohn, B.P., Braun, J., McDougall, I. & Ireland, T.R., 1999. New insight into the dynamic development of the Southern Alps, New Zealand, from detailed thermochronological investigation of the Mataketake Range pegmatites. In: Ring, U., Brandon, M.T., Lister, G.S. & Willett, S.D. (eds), Exhumation Processes: Normal Faulting, Ductile Flow and Erosion. Geological Society, London, Special Publications, 154, 261-282.

Batt, G.E., Braun, J., Kohn, B.P. & McDougall, I., 2000. Thermochronological analysis of the dynamics of the Southern Alps, New Zealand. Geological Society of America Bulletin, 112, 250-266.

Batt, G.E., Baldwin, S.L., Cottam, M., Fitzgerald, P.G., Brandon, M.T. & Spell, T.L., 2004. Cenozoic plate boundary evolution in the South Island of New Zealand: new thermochronological constraints. Tectonics, 23, TC4001, doi:10.1029/2003TC001527

Chamberlain, C.P., Zeitler, P.K. & Cooper, A.F., 1995. Geochronologic constraints of the uplift and metamorphism along the Alpine Fault, South Island, New Zealand- New Zealand Journal of Geology and Geophysics, 38, 515-523.

Cooper, A.F. & Norris, R.J., 2011. Inverted metamorphic sequences in Alpine fault mylonites produced by oblique shear within a plate boundary fault zone, New Zealand. Geology, 39, 1023-1026.

Grapes, R.H., 1995. Uplift and exhumation of Alpine Schist, Southern Alps, New Zealand: thermobarometric constraints. New Zealand Journal of Geology and Geophysics, 38, 525-533.

Grapes, R. & Watanabe, T., 1992. Metamorphism and uplifi of Alpine schist in the Franz Josef-Fox Glacier area of the Southern Alps, New Zealand. Journal of Metamorphic Geology, 10, 171-180.

Gray, D.R. & Foster, D.A., 2004. 40Ar/39Ar thermochronologic constraints on deformation, metamorphism and cooling/exhumation of a Mesozoic accretionary wedge, Otago Schist, New Zealand. Tectonophysics, 385, 181-210.

Koons, P.O., 1989. The topographic evolution of collisional mountain belts - a numerical look at the Southern Alps, New-Zealand. American Journal of Science, 289, 1041-1069.

Little, T.A., Cox, S., Vry, J.K. & Batt, G., 2005. Variations in exhumation level and uplift rate along the oblique-slip Alpine fault, central Southern Alps, New Zealand. Geological Society of America Bulletin, 117, 707-723.

Norris, R.J. & Cooper, A.F., 2000. Late Quaternary slip rates and slip partitioning on the Alpine Fault, New Zealand. Journal of Structural Geology, 23, 507-520.

Norris, R.J. & Cooper, A.F., 2003. Very high strains recorded in mylonites along the Alpine Fault, New Zealand: implications for the deep structure of plate boundary faults. Journal of Structural Geology, 25, 2141–2157.

Sutherland, R., Toy, V.G., Townend, J., Cox, S.C., Eccles, J.D., Faulkner, D.R., Prior, D.J., Norris, R.J., Mariani, E., Boulton, C., Carpenter, B.M., Menzies, C.D., Little, T.A., Hasting, M., De Pascale, G.P., Langridge, R.M., Scott, H.R., Reid Lindroos, Z., Fleming, B. & Kopf, A.J., 2012. Drilling reveals fluid control on architecture and rupture of the Alpine faults, New Zealand. Geology, 40, 1143-1146.

Toy, V.G., Prior, D.J. & Norris, R.J., 2008. Quartz fabrics in the Alpine Fault mylonites: Influence of pre-existing preferred orientations on fabric development during progressive uplift. Journal of Structural Geology, 30, 602-621.

Toy, V.G., Craw, D. Cooper, A.F. & Norris, R.J., 2010. Thermal regime in the central Alpine Fault zone, New Zealand: Constraints from microstructures, biotite chemistry and fluid inclusion data. Tectonophysics, 485, 178–192.

Toy, V.G., Prior, D.J., Norris, R.J., Cooper, A.F. & Walrond, M., 2012. Relationships between kinematic indicators and strain during syn-formational exhumation of an oblique slip, transpressive, plate boundary shear zone: The Alpine Fault, New Zealand. Earth and Planetary Science Letters, 282–292.

IODP

Impact of salinity changes on viruses during the paleoenvironmental history ofBaltic Sea sediments

V. VANDIEKEN, B. ENGELEN

Institut für Chemie und Biologie des Meeres, Carl von Ossietzky Universität Oldenburg,Carl-von-Ossietzky Straße 9-11, D-26129 Oldenburg, Germany, www.pmbio.icbm.de

Viruses are the most abundant biological entities in the oceans (Fuhrman, 1999). They have been detected in sediments as deep as 320 m and as old as 14 Ma (Middelboe *et al.*, 2011, Engelhardt *et al.*, 2014). These viruses may either represent an inactive reservoir with long decay rates or may contiuously be produced. We argue that increasing virus-to-cell ratios as well as unlikely long half-lives for viruses of estimated 10 to 100 million years (if no production is assumed) give good indications for viral production in deep subsurface sediments (Engelhardt *et al.*, 2014). However, viral production, to our knowledge, has never been measured in sediments deeper than 1 m (Mei & Danovaro, 2004), and it remains unclear how prokaryotes, living at energy fluxes that barely admit maintenance of the cell (Røy *et al.*, 2012, Hoehler & Jørgensen, 2013), can enable the production of viruses.

One possible life mode of virus production is the induction of lysogenic phages in their bacterial host. We showed that 6 out of 13 bacterial isolates of the deep biosphere contained mitomycin-inducible prophages and genes of lysogenetic phages are present down to 100 m depth in various sediments indicating that the capability of virus production exists in deep sediments (Engelhardt *et al.*, 2011, Engelhardt *et al.*, 2013). In general, prophages can be induced to become free phage particles when host cells are exposed to stress (Fuhrman, 1999). Thus, changes in salinity can constitute a stimulus for induction of prophages.

Sediments from the Baltic Sea, sampled during IODP Exp. 347, have undergone alterations between limnic, brackish and marine conditions due to repeated glaciations. Changes in salinity might have had major impacts on the prokaryotic and viral communities in sediments. We received fresh sediment samples of 4 stations that cover the complete salinity range from freshwater to brackish to marine water. We have started sediment incubations for viral production measurements and most-probable-number counts of viable prokaryotes in three media of different salinities.

In our new proposal we plan to address the following questions:

Are viruses produced in sediments of the Baltic Sea? We hypothesize that increasing virus-to-cell ratios point to continuous viral production in deeply buried sediments. For this part of the project, we will determine the virus-to-

cell ratio for sediments of IODP Exp. 347. Additionally, we will directly measure, to our knowledge for the first time, viral production rates in deep sediment samples that already were incubated with ^{3}H-thymidine and are currently stored in the freezer.

Were prokaryotic and viral community structures influenced by salinity changes in the past? We hypothesize that the paleoenvironmental history of the Baltic Sea significantly influenced the prokaryotic communities. We will investigate, whether changes in the prokaryotic and viral community can be correlated to changing salinity concentrations in the sediment with respect to 1) viable prokaryotic numbers (MPN counts), 2) prokaryotic community structure, 3) viral numbers, 4) viral community structure and 5) viral decay.

Can virus proliferation be induced by salinity changes in enrichments and isolates obtained from these sediments? Are respiration rates and carbon turnover influenced by salinity changes? We hypothesize that changes in salinity might have resulted in induction stimuli for prophages. If this was the case, this might have had significant impact on the prokaryotic community influencing prokaryotic physiology and biogeochemical processes in the sediments. We plan to investigate salinity changes as an incubation stimulus for lysogenic phages in enrichment and pure cultures. Viral production will be monitored by radiolabeling and pulsed-field gel electrophoresis (PFGE) analysis.

The overall goal of the project is to understand the role of viruses for biogeochemical cycling, microbial abundance and diversity in deep subsurface sediments. We will investigate if viruses are produced in deep sediments and if the induction of temperent phages is a potential source of these viruses. In the past, events of high virus production due to salinity changes might have had major impacts for the prokaryotic community and the biogeochemical cycles in Baltic Sea sediments.

References:

Engelhardt T, Sahlberg M, Cypionka H & Engelen B (2011) Induction of prophages from deep-subseafloor bacteria. Environmental Microbiology Reports 3: 459-465.

Engelhardt T, Sahlberg M, Cypionka H & Engelen B (2013) Biogeography of Rhizobium radiobacter and distribution of associated temperate phages in deep subseafloor sediments. ISME Journal 7: 199-209.

Engelhardt T, Kallmeyer J, Cypionka H & Engelen B (2014) High viruses-to-cell ratios indicate ongoing production of viruses in deep subsurface sediments. ISME Jounal, in press.

Fuhrman JA (1999) Marine viruses and their biogeochemical and ecological effects. Nature 399: 541-548.

Hoehler TM & Jørgensen BB (2013) Microbial life under extreme energy limitation. Nature Reviews Microbiology 11: 83-94.

Mei ML & Danovaro R (2004) Virus production and life strategies in aquatic sediments. Limnology and Oceanography 49: 459-470.

Middelboe M, Glud RN & Filippini M (2011) Viral abundance and activity in the deep sub-seafloor biosphere. Aquatic Microbial Ecology 63: 1-8.

Røy H, Kallmeyer J, Adhikari RR, Pockalny R, Jørgensen BB & D'Hondt S (2012) Aerobic microbial respiration in 86-million-year-old deep-sea red clay. Science 336: 922-925.

IODP

Surface and upper Mediterranean Outflow Water signals during the Mid-Pleistocene Transition: the IODP Site U1387 record (Faro Drift)

A. H. L. VOELKER[1], A. BAHR[2], F. J. JIMENEZ-ESPEJO[3], G. D. ACTON[4], U. RÖHL[5]

[1]Divisão de Geologia e Georecursos Marinhos, Instituto Português do Mar e da Atmosfera (IPMA), Av. de Brasília 6,1449-006 Lisbon, Portugal
[2]Institute of Geosciences, University Frankfurt, Altenhöferallee 1, 60438 Frankfurt, Germany
[3]Institute of Biogeosciences, Japan Agency for Marine-Earth Science and Technology, Yokosuka 237-0061, Japan
[4]Sam Houston State University, Department of Geography & Geology, P.O. Box 2148, Huntsville, TX 77341-2148, USA
[5]MARUM – Zentrum für Marine Umweltwissenschaften, Universität Bremen, Leobener Strasse, 28359 Bremen, Germany

During the Mid-Pleistocene transition (MPT; 500-1250 ka) the dominant pacing of glacial/ interglacial cycles changed from the 41 ky obliquity to the 100 ky eccentricity cycle. Superimposed on the orbital-scale changes are millennial-scale climate instabilities that in the mid-latitude Atlantic are linked to insolation (e.g., Weirauch et al., 2008). In the Mediterranean Sea, on the other hand, sapropel layers were formed during insolation maxima and the associated circulation changes in the basin also affected the water exiting through the Strait of Gibraltar and forming the Mediterranean Outflow Water (MOW). MOW's hydrographic history is unknown prior to 100 ka but this is changing now with the Plio-/Pleistocene contourite sequences recovered during IODP Exp. 339 (Hernandez-Molina et al., 2013). IODP Site U1387 (36.8°N; 7.7°W) was drilled in the Faro drift, southern Portuguese margin, at a water depth of 559 m. This Site records changes in the upper MOW core and the mud-rich Pleistocene sediments contain numerous contouritic layers related to MOW activity. Surface waters in the region are derived either from the Azores Current or the Portugal Current (upwelling season). Based on the shipboard bio- and magnetostratigraphy sediment rates are on average 25 cm/ ky, so that proxy records presented here have currently a temporal resolution of d1 ky; with the exception of the XRF records (3 cm resolution).

Hydrographic changes during Marine Isotope Stage (MIS) 16 to 32 (630-1100 ka) are being reconstructed using a multi-proxy approach. Variations in the surface waters are infered from the *G. bulloides* stable isotope data. Upper MOW core history is extracted from the benthic (*Cibicidoides pachyderma*; *Planulina ariminensis*) stable isotope records and the weight percent of the sand fraction, the XRF-derived Zr/Al ratio and the mean grain size of the bulk fraction <63µm, all of which mark contouritic layers and thus variations in bottom current flow strength. In this region with potential sediment advection, as indicated by the C/N data, the Ti/Ca and Fe/Ca ratios cannot be interpreted as reflecting purely the contributions of terrestrial (Ti, Fe) versus marine (Ca) sediment components, even though the records mirror the carbonate content. The ratios were, however, essential in correcting the shipboard splice because during the study it became obvious that some splice transitions need to be adjusted.

Besides the glacial/ interglacial cycles both surface water and MOW records show millennial-scale stadial/ interstadial oscillations, in particular during the glacial inceptions. Planktonic and benthic oxygen isotope records are strongly correlated on the orbital and millennial-scale level. Contourites were formed by the upper MOW core towards the end of an interglacial period; in agreement with the Holocene record, when the contouritic layer was formed around 4 ka (e.g., Voelker et al., 2006). Additional contouritic layers are associated with the interstadial oscillations. Ventilation in the upper MOW core varied significantly with better ventilation occurring during glacial and stadial intervals and periods of contouritic layer formation. Ventilation was at minimum during deglaciations and the beginning of the interglacial periods hinting to a link between MOW ventilation and sapropel formation in the Mediterranean Sea. The new U1387 records reveal that climate conditions were as variable during the early to mid Pleistocene as during the late Pleistocene. MOW was sensitive to abrupt climate instabilities during the MPT and, like during the last glacial cycle, provided an important component to the stability of the Atlantic's overturning circulation.

References:
Hernández-Molina, F.J., Stow, D., Alvarez-Zarikian, C., et al., 2013. IODP Expedition 339 in the Gulf of Cadiz and off West Iberia: decoding the environmental significance of the Mediterranean outflow water and its global influence. Sci. Dril. 16, doi: 10.5194/sd-16-1-2013.
Voelker, A.H.L., Lebreiro, S.M., Schönfeld, J., Cacho, I., Erlenkeuser, H., Abrantes, F., 2006. Mediterranean outflow strengthening during northern hemisphere coolings: A salt source for the glacial Atlantic? Earth and Planetary Science Letters 245 (1-2), 39-55.
Weirauch, D., Billups, K., Martin, P., 2008. Evolution of Millennial-Scale Climate Variability During the Mid Pleistocene. Paleoceanography 23, PA3216, doi: 10.1029/2007PA001584.

IODP

Marine stable Sr record of the last 50 Myrs

J.VOIGT[1], E.C. HATHORNE[1], A. EISENHAUER[1] AND H. PÄLIKE[2]

[1]GEOMAR Helmholtz-Zentrum für Ozeanforschung Kiel, Wischhofstr. 1-3, 24148 Kiel
[2]MARUM Zentrum für Marine Umweltwissenschaften, Universität Bremen, Leobener Str. 2, 28359 Bremen

Understanding the climate system and feedbacks in the past is highly important for modelling and thus for future projections of global climate change. The carbonate compensation depth (CCD), which is the depth where the rate of $CaCO_3$ accumulation equals the rate of carbonate dissolution, varies between ocean basins and changed over time. One large shift towards a deeper CCD, coincided with the Eocene/Oligocene transition, and marks a major step from the warm greenhouse climate of the Paleogene to the icehouse climate of the present (Pälike *et al.* 2012). Such variations of the CCD are caused by variations in ocean carbonate chemistry and atmospheric CO_2 concentrations as a function of volcanic outgassing and weathering (e.g. Ridgwell and Zeebe 2005, Pälike *et al.* 2012). Therefore, recording variations in the CCD help to understand past changes in the global carbon cycle. The silicate weathering flux, which controls atmospheric CO_2 on geological timescales, is thought to have increased at about 40 Ma as a result of the Himalayan uplift (Raymo and Ruddiman 1992). Carbonate weathering was enhanced during glaciations when carbonate shelves were exposed (e.g. Krabbenhöft *et al.* 2010). Traditionally, radiogenic Sr isotopes ($^{87}Sr/^{86}Sr$) are used to estimate weathering rates by variations of Sr input into the ocean. However, $^{87}Sr/^{86}Sr$ is not sensitive to changes in $CaCO_3$ accumulation rates, reflected by changed Sr fluxes, and variations in the CCD because Sr is homogenously distributed within the ocean. Moreover, the dissolution of carbonates produces a radiogenic $^{87}Sr/^{86}Sr$ value equal to the one in seawater (e.g. Richter and DePaolo 1988).

Paired radiogenic ($^{87}Sr/^{86}Sr$) and stable Sr ($\delta^{88/86}Sr$) isotopes have been applied to determine natural fractionation during calcification (Krabbenhöft *et al.* 2010, Böhm *et al.* 2012), diagenesis (Voigt *et al.* submitted) and precipitation of inorganic carbonates in hydrothermal systems (Chao *et al.* 2013). The $\delta^{88/86}Sr$ of seawater is mainly controlled by carbonate burial, continental weathering and recrystallisation (Vollstaedt *et al.* 2013). Therefore, it is possible to determine the Sr removal flux into carbonates and thus $CaCO_3$ accumulation rates by analysing the $\delta^{88/86}Sr$ of past seawater using biogenic carbonates since the stable Sr signature is different for seawater, hydrothermal inputs, rivers and carbonates (Krabbenhöft *et al.* 2010). For the Cenozoic stable Sr isotopes are novel and have not been published so far. Therefore, a $\delta^{88/86}Sr$ record of the last 50 Myrs would provide valuable information about changes in global $CaCO_3$ accumulation rates in particular for sensitive transitions in Earth's climate history like the Eocene/Oligocene transition.

Additionally, changes in the CCD and $CaCO_3$ accumulation influenced the preservation of biogenic carbonates such as foraminifera which are widely used for the reconstruction of past climate (e.g. Zachos *et al.* 2008). A better understanding of preservation and recrystallisation is therefore important for the reliability of proxy data used for climate reconstruction and modelling. Preliminary work (Voigt *et al.* submitted) suggests pore water $\delta^{88/86}Sr$ is a sensitive tracer of recrystallisation.

The aim of the proposed study is to reconstruct the $\delta^{88/86}Sr$ of seawater to detect changes in the $CaCO_3$ accumulation rates over the last 50 Myrs by analysing benthic foraminifera focusing on major shifts in the CCD like those at the Middle Eocene Climate Optimum and the Eocene/Oligocene boundary. Earlier work (Edgar *et al.* 2013) and our study suggest benthic foraminifera to be more resistant to recrystallisation and would be the most reliable carbonate fraction of the sediments. Moreover, the benthic foraminiferal assemblage has not changed essentially over the last 50 Myrs. Benthic foraminifera from sediments from the Pacific Equatorial Age Transect (IODP expeditions 320/321) will be analysed because these sediment cores comprise a continuous Cenozoic record and material from these Sites has been used for a detailed reconstruction of the Pacific CCD (Pälike *et al.* 2012). The determined $\delta^{88/86}Sr$ of benthic foraminifera will be compared with stable Sr measurements of the corresponding pore waters, planktonic foraminifera and bulk carbonates at the key intervals of CCD shifts and the preservation of these microfossils will be assessed by these multi-component analyses.

References:
Böhm F., Eisenhauer A., Tang J., Dietzel M., Krabbenhöft A., Kisakürek B., and Horn C. (2012) Strontium isotope fractionation of planktic foraminifera and inorganic calcite. Geochimica et Cosmochimica Acta 93, 300-314

Broecker W.S. and Peng T.-H. (1987) The role of CaCO3 compensation in the glacial to interglacial atmospheric CO2 change. Global Biogeochemical Cycles 1, 15-29
Chao H.-C., You C.-F., Liu H.-C. and Chung C.-H. (2013) The origin and migration of mud volcano fluids in Taiwan: Evidence from hydrogen, oxygen, and strontium isotopic compositions. Geochimica et Cosmochimica Acta 114, 29-51
Edgar K.M., Pälike H. and Wilson P.A. (2013) Testing the impact of diagenesis on the ´18O and ´13C of benthic foraminiferal calcite from a sediment burial depth transect in the equatorial Pacific. Paleoceanography 28, 468–480, doi:10.1002/palo.20045
Krabbenhöft A., Eisenhauer A., Böhm F., Vollstaedt H., Fietzke J., Liebetrau V., Augustin N., Peucker-Ehrenbrink B., Müller M.N., Horn C., Hansen B.T., Nolte N., and Wallmann K. (2010) Constraining the marine strontium budget with natural strontium isotope fractionations (87Sr/86Sr*, ´88/86Sr) of carbonates, hydrothermal solutions and river waters. Geochimica et Cosmochimica Acta 74, 4097-4109
Pälike H., Lyle M.W., Nishi H., et al. (2012) A Cenozoic record of the equatorial Pacific carbonate compensation depth. Nature 488, 609-61
Richter F.M. and DePaolo D.J. (1988) Diagenesis and Sr isotopic evolution of seawater using data from DSDP 590B and 575. Earth and Planetary Science Letters 90, 382-394
Raymo M.E. and Ruddiman W.F. (1992) Tectonic forcing of late Cenozoic climate. Nature 359, 117-122
Ridgwell A. and Zeebe R. (2005) The role of the global carbonate cycle in the regulation and evolution of the Earth system. Earth Planetary Science Letters 234, 299-315
Voigt J., Hathorne E.C., Frank M., Vollstaedt H. and Eisenhauer A., Variability of carbonate diagenesis in equatorial sediments deduced from radiogenic and stable Sr isotopes. to be submitted
Vollstaedt H., Eisenhauer A., Wallmann K., Böhm F., Fietzke J., Liebetrau V., Krabbenhöft A., Farkaš J., Tomašovych A., Raddatz J. and Veizer J., The Phanerozoic ´ 88/86Sr Record of Seawater: New Constraints on Past Changes in Oceanic Carbonate Fluxes. Geochimica et Cosmochimica Acta (2013), doi: http://dx.doi.org/10.1016/j.gca.2013.10.006
Zachos J.C., Dickens G.R., and Zeebe R.E. (2008) An early Cenozoic perspective on greenhouse warming and carbon-cycle dynamics. Nature 451, 279-283

ICDP

Environmental DNA studies applied to the climatic record of Laguna Potrok Aike (Argentina): Examining Holocene and Last Glacial Maximum microbial assemblages.

A. VUILLEMIN[1], D. ARIZTEGUI[2], P.R. LEAVITT[3], L. BUNTING[3], THE PASADO SCIENCE TEAM[4]

[1]GFZ German Research Centre for Geosciences, Section 4.5 Geomicrobiology, Telegrafenberg, 14473 Potsdam, Germany.
[2]University of Geneva, Earth and Environmental Sciences, rue des Maraîchers 13, 1205 Geneva, Switzerland.
[3]Limnology Laboratory, Department of Biology, University of Regina, Regina, Saskatchewan, Canada.
[3]http://www.pasado.uni-bremen.de.

Laguna Potrok Aike is an endorheic basin located in the southern hemisphere's mid-latitudes (52°S). Rainfall and geology of the catchment exert a dominant control on the lake inputs, resulting in different sedimentary sequences related to paleoenvironmental conditions. The interpretation of the limnogeological multiproxy record developed in the frame of the ICDP-PASADO project showed that oscillations in the Southern Westerly Winds were recorded through lake-level fluctuations resulting from their influence on the regional hydrological regime, which allowed for the identification of contrasting time windows (Zolitschka et al. 2013).

In the context of this project, a 100-m-long core was dedicated to a detailed geomicrobiological study in order to explore the subsurface biosphere (Vuillemin et al. 2010; 2013a). By combining a microbiological and geochemical approach, we identified the presence of living microbes in deep sediments and defined the substantial role of microbial processes in modifying the initial organic (Vuillemin et al. in press) and mineral (Vuillemin et al. 2013b) fractions. Moreover, compiled results pinpointed the role of environmental features upon microbial development and survival throughout the sedimentary sequence (Vuillemin et al. 2014).

In addition, because aquatic sediments provide a wide range of ecological niches for microbes, the genetic material of microorganisms preserved in the respective sediments is likely to be used in paleoclimatic reconstructions. To test this hypothesis, we selected two sedimentary horizons displaying *in situ* microbial activity and corresponding to the Holocene and Last Glacial Maximum times, where we extracted environmental DNA and established bacterial and archaeal 16S rRNA gene libraries. The sequences recovered from the productive Holocene record revealed a microbial community adapted to subsaline conditions producing methane with a high potential of organic matter degradation. In contrast, sediments rich in volcanic detritus from the Last Glacial Maximum showed a substantial presence of lithotrophic microorganisms and sulfate-reducing bacteria mediating framboidal iron sulfides.

Together, these patterns suggested that prevailing climatic conditions exert a hierarchical control on the microbial composition of lake sediments by regulating the influx of organic and inorganic material to the lake basin. This influx in turn determines water column chemistry, production and sedimentation of particulate material, resulting in different microbial communities at the time of sediment deposition. Moreover, it demonstrates that environmental DNA can constitute sedimentary archives of phylogenetic diversity and diagenetic processes over tens of millennia.

References:

Vuillemin A, Ariztegui D, Vasconcelos C, and the PASADO Scientific drilling party (2010). Establishing sampling procedures in lake cores for subsurface studies: Assessing in situ microbial activity. Scientific Drilling 10, 35-39.
Vuillemin A, Ariztegui D, and the PASADO Science Team (2013a). Geomicrobiological investigations in subsaline maar lake sediments over the last 1500 years. Quaternary Science Reviews 71, 119-130.
Vuillemin A, Ariztegui D, De Coninck AS, Lücke A, Mayr C, Schubert CJ, and the PASADO Science Team (2013b). Origin and significance of diagenetic concretions in sediments of Laguna Potrok Aike, southern Argentina. Journal of Paleolimnology 50, 275-291.
Vuillemin A, Ariztegui D, Lücke A, Mayr C, and the PASADO Science Team (2014). Paleoenvironmental conditions define current sustainability of microbial populations in Laguna Potrok Aike sediments, Argentina. Aquatic Sciences 76, 101-114.
Vuillemin A, Ariztegui D, Nobbe G, Schubert CJ, and the PASADO Science Team (in press). Influence of methanogenic populations in Holocene lacustrine sediments revealed by clone libraries and fatty acid biogeochemistry. Geomicrobiology Journal.
Zolitschka B, Ariztegui D, Francus P, Maidana N, Wastegård S (eds.) (2013). The Potrok Aike Maar Lake Sediment Archive Drilling Project (PASADO). Quaternary Science Reviews 71, 1-228.

ICDP

Insights into the deep biosphere of the El'gygytgyn Crater Lake sediments

D. WAGNER, J. GÖRSCH, M. ALAWI AND THE EL'GYGYTGYN SCIENTIFIC PARTY

GFZ German Research Centre for Geosciences, Telegrafenberg, 14473 Potsdam, Germany (dirk.wagner@gfz-potsdam.de)

Despite the progress that has been made in the field of microbiology in deep subsurface environments in recent

years, we still know very little about the diversity and function of deep biosphere microorganisms and their impact on the global geochemical cycles. For this reason, we studied the abundance and diversity of deep biosphere microorganisms in the sediments of the El'gygytgyn Crater Lake. The sediments and impact rocks were recovered from the El'gygytgyn Lake in the scope of the ICDP project "Scientific Drilling at El'gygytgyn Crater Lake" from November 2008 to May 2009. Of particular interest is the understanding of the development, survival and potential metabolic activity along the chronosequence from the oldest to the youngest lake sediments. Because the El'gygytgyn Lake was formed by a meteorite impact 3.6 million years ago, this impact should be taken into consideration to understand the development of microbial life since that time. For this purpose microbiological, molecular ecological and geochemical methods were applied to analyze the lake sediments. This includes the investigation of small-scale variations within the community structure and their potential metabolic activity along the lake sediment chronosequence. The acquired data will help deepen our knowledge about the development of microbial communities and variations within the communities in time and space since the meteorite impact.

Despite of low cell numbers and therefore of the low DNA contents, DNA was successfully extracted from all studied deposits along the more than 300 m long sediment chronosequence. Bacterial and archaeal abundances were determined using quantitative PCR (qPCR) for 16S rRNA genes. A higher bacterial than archaeal abundance was revealed over the entire sediment core. Interestingly, the copy number for both, archaeal and bacterial 16S rRNA genes, was increasing towards the deepest sediment layer (nearly 3.6 million years old). The extracted DNA was further used for DGGE fingerprint analyses to get an overview of the archaeal community structure over the entire lake deposits. Therefore, different primers were evaluated to enhance the coverage of the archaeal diversity. The DGGE fingerprints revealed high differences in the population structure according to different sediment depths. The differences might be interpreted as adaptations of the microbial communities to different environmental conditions. This is in accordance to the varying concentration of carbon over the whole chronosequence. However, the diversity cannot be strictly correlated to warmer periods in the lake history: there is a higher diversity in some interglacial periods (MIS 23 and 45), but also in some glacial periods (MIS 50 and 60). It is remarkable that a relatively high microbial diversity was found in a sediment sample of the largest cooling phase during the mid-Pliocene (M2). These first results show that the archaeal community was dominated by *Methanosarcinales*, *Methanomicrobiales*, and *Methanocellales*, but also *Crenarchaeota* were found in the sediment deposits. In contrast to a widespread appearance of *Methanosarcinales* in interglacial and glacial periods, representatives of the group *Methanocellales* seem to be adapted to warmer Marine Isotope Stages such as MIS 11 and 13.

Another aspect of the work was focussing on the different extractable DNA fractions of the core material. Beside of intracellular DNA from microorganisms we could also extract, even from the deepest and oldest samples, so-called extracellular DNA (eDNA), which is usually bound to the sedimentary matrix. This eDNA pool contains genetic informations of fossil microbial communities which might be preserved for hundreds of thousands of years. With special regards to the fact that the El'gygytgyn Crater Lake sediments are covering an enormous time record, we might retrieve valuable information about ancient microbial populations dominating the different glacial- and interglacial periods. Additionally, this approach is helping to distinguish between the recent, most likely active, microbial community and DNA relicts from ancient times. To obtain an overview and to compare the two extractable DNA pools, we again conducted DGGE analyses with PCR products from the 16S rRNA gene. First results are indicating that both pools are showing differences in the diversity and abundance of the microorganisms. Supplementary molecularbiological techniques are in progress to analyze the recent and ancient microbial communities more detailed.

Our results showed the successful application of our combined methodical approach to obtain first insights into the microbial abundance and diversity of the El'gygytgyn Crater Lake sediments. Based on this unique sediment material, we were able to present the first microbiological dataset of such an old lake ecosystem.

IODP

Late Neogene ice-sheet, ocean, and atmosphere history in the Drake Passage and the Weddell Sea – current drilling proposals within IODP

M.E. WEBER[1]

[1]Institute of Geology and Mineralogy, University of Cologne, Cologne, Germany, e-mail michael.weber@uni-koeln.de

According to the current IODP Science Plan, RV Joides Resolution offers drilling opportunities in the Southern Ocean 2017 – 2019. Therefore, we have submitted two drilling proposals in fall 2013 to study the Weddell Sea history (846-Pre, Weber et al., 2013a) and the Drake Passage paleoenvironment (847-Pre, Weber et al., 2013b). On their meeting in San Diego in January 2014, the IODP Science Evaluation Panel has evaluated both pre-proposals positively. Accordingly, we are currently putting together full proposals for both projects.

The 'Late Neogene ice-sheet and sea-level history of the Weddell Sea, Antarctica' (846-Pre) should address critical questions of East and West Antarcrtic Ice Sheet stability in a key area of Earth's past climate variability, where the majority of Antarctic Bottom Water is formed, and where one of the world's two largest ice shelves, the Filchner-Rønne Ice Shelf, drains into the ocean. Ice-sheet dynamics in the Weddell Sea sector of the EAIS are highly susceptible to far-field changes in sea level (Weber et al., 2011). Practically all icebergs from the East Antarcrtic Ice Sheet merge in the Weddell Sea before they exit Antarctica through the Scotia Sea, thereby providing a unique location to study Antarctic Ice Sheet dynamics.

We aim at achieving the first complete Late Neogene reconstruction for the Weddell Sea to study changing ice-sheet dynamics, the interhemispheric phasing of ice-sheet and climate events, ocean circulation, and bottom-water

production. Specifically, we wish to address the following questions: Was the formation of the contourite ridges north of Crary Fan associated with a sea-level drop initiated through intensification of Northern Hemisphere glaciation during the Pliocene? Did the drainage pattern change during the Mid-Pleistocene Transition? Can we decipher ice-sheet dynamics on glacial-to-interglacial time scales and during the Last Glacial Maximum? Can we detect far-field sea-level effects and rates of sea-level rise from Iceberg Alley? Can we relate varve thickness variations to external (solar) or internal (ocean-atmosphere) variability on decadal-to-centennial time scales?

We propose to drill three contourite drifts northeast of Riiser-Larson Ice Shelf that contain high-resolution sections necessary to reconstruct, for the first time, East Antarcrtic Ice Sheet dynamics through Plio-Pleistocene times. One additional test site should obtain a complete Cenozoic record from Polarstern Plateau. Alternate sites cover the ridges and one high-resolution Plio-Pleistocene site in the Scotia Sea. Sediment cores and high-resolution seismic data are available for all sites.

The 'Plio-Pleistocene reconstruction of ocean, atmosphere, and ice-sheet interactions through the Drake Passage' (847-Pre) offers the unique opportunity of reconstructing the exchange of heat, nutrients, and salt between the Pacific and the Atlantic Ocean. We propose three drill sites to recover 1000-m long Plio-Pleistocene sequences to reconstruct past changes in ocean and atmospheric circulation as well as Antarctic ice-sheet dynamics at unprecedented, decadal-to-centennial-scale sample resolution through stadial-to-interstadial, glacial-to-interglacial and warmer than present time intervals.

We will deliver the first detailed and chronologically well-constrained reconstruction of ice mass loss from the Antarctic Ice Sheet through climate terminations from a combined far-field deep-ocean record in the center of Iceberg Alley. This includes the study of provenance signatures to determine sources of Antarctic Ice Sheet mass loss (Weber et al., in review), the interhemispheric phasing of ice-sheet and climate events, and the relation of Antarctic Ice Sheet dynamics and global sea-level development through the ice ages.

We will also deliver critical information on paleoceanographic changes in Drake Passage throughflow, meridional overturning in the Southern Ocean, CO2 transfer via wind-induced upwelling, variability of oceanic and atmospheric fronts in the vicinity of the Antarctic Circumpolar Current by comparing N-S trends within the Scotia Sea and W-E trends between the Scotia Sea and the Chile margin. This includes studying the interaction with bottom water outflow from the Weddell Sea.

Comparing changes of the Patagonian Ice Sheet as the major dust source in the Southern Hemisphere, to proximal dust records in the Scotia Sea and distal dust records preserved in Antarctic ice cores, will provide the first detailed reconstruction on the history of the Southern Hemisphere westerlies and associated changes in atmospheric circulation in the Southern Ocean on millennial- and orbital time scales. This study will help to evaluate the climate-dust coupling in global glaciations since the Pliocene, its potential role in iron fertilization and atmospheric CO2 drawdown during glacials, and the effects of dust and Antarctic ice volume on the Mid-Pleistocene-Transition.

References:

Weber, M.E., Clark, P. U., Ricken, W., Mitrovica, J. X., Hostetler, S. W., and Kuhn, G. (2011): Interhemispheric ice-sheet synchronicity during the Last Glacial Maximum. – Science, 334, 1265-1269, doi: 10.1126:science.1209299

Weber, M. E., Clark, P. U., Kuhn, G., Timmermann, A., Sprenk, D., Gladstone, R., Zhang, X., Lohmann, G., Menviel, L., Chikamoto, M., Friedrich, T. (in review): Millennial-scale variability in Antarctic ice-sheet discharge during the last deglaciation. – Nature.

Weber, M.E., Kuhn, G., Clark, P.U., Smith, J., Williams, T., Channell, J., Jokat, W., Huang, X., Belt, S., (2013a): Late Neogene ice-sheet and sea-level history of the Weddell Sea, Antarctica. – IODP (848-Pre – Weddell Sea History).

IODP

The evolution of early diagenetic signals in Bering Sea sediments in response to varying organic carbon deposition over the last 4.3 Ma (IODP Exp. 323, Site U1341)

L.M. WEHRMANN[1, 2,*], S. ARNDT[3], C. OCKERT[4, 7], P. MEISTER[1], B. BRUNNER[1, 5], C. MÄRZ[6], N. GUSSONE[7], B.M.A. TEICHERT[8], T. FERDELMAN[1]

[1]Biogeochemistry Department, Max Planck Institute for Marine Microbiology, Celsiusstrasse 1, D-28359 Bremen, Germany
[2]Department of Earth Sciences, University of California, 900 University Ave., Riverside, CA 92521, USA
*present address: GEOMAR Helmholtz-Zentrum für Ozeanforschung Kiel, Wischhofstr. 1-3, D-24148 Kiel, Germany
[3]School of Geographical Sciences, University of Bristol, University Road Clifton, Bristol BS8 1SS, United Kingdom
[4]Forschungszentrum Jülich IBG-3, Wilhelm-Johnen-Straße, D-52428 Jülich, Germany
[5]Department of Geological Sciences, University of Texas at El Paso, 500 West University Avenue, El Paso, TX 79968, USA
[6]School of Civil Engineering and Geosciences (CEGS), Newcastle University, Newcastle upon Tyne, NE1 7RU, United Kingdom
[7]Institut für Mineralogie, Universität Münster, Corrensstrasse 24, D-48149 Münster, Germany
[8]Institut für Geologie und Paläontologie, Universität Münster, Corrensstrasse 24, D-48149 Münster, Germany

Deep subseafloor sediments at Bering Sea Site U1341 (2177 m water depth), drilled on Bowers Ridge during IODP Expedition 323, show large down-core variability in the distribution of geochemical paleoproxies, e.g., excess Si (Si_{xs}) and Ba/Al ratios (März et al., 2013). These records are evidence of prominent changes in opal export and likely also opal productivity over the last 4.3 Ma at this site, including a time period of very high opal deposition between ~2.6 and ~1.8 Ma BP (März et al., 2013). During this time period, the onset of North Pacific stratification likely caused leakage of nutrient-rich deep/intermediate North Pacific water into the Bering Sea via the Kamtchatka Strait (März et al., 2013). Transient geochemical signatures of microbially mediated early diagenetic processes in the pore-water and solid-phase reflect variability in the extent of organic carbon respiration in the sediments as a result of the changes in opal deposition and organic carbon flux at this site over time.

An inverse reaction-transport model, based on pore-water sulfate concentrations and solid-phase Ba/Al ratios, was used to examine the evolution of these diagenetic signals over time. Our results support the hypothesis that at ~2.58–2.51 Ma ago a high deposition flux of extremely labile organic matter affected this site (Wehrmann et al., 2013). Associated elevated organoclastic sulfate reduction rates led to low sulfate concentrations and the onset of methanogenesis. Sulfate depletion caused the dissolution of biogenic barite reflected by a sedimentary interval with low Ba/Al ratios. Two sulfate–methane transition zones (SMTZs) developed where high rates of anaerobic oxidation of methane (AOM) controlled sulfate consumption, which was sustained by the influx of sulfate from seawater above and a deep source below. The positions of both SMTZs shifted non-synchronously over the subsequent ~130,000 yrs, until methanogenesis and AOM declined. The present-day sulfate concentration and sulfur isotope profiles still reflect the impact of the reactive organic matter pulse (Wehrmann et al., 2013). They also record a period of very low reactive organic matter deposition during the middle to late Pleistocene, probably linked to very low primary productivity, resulting in little microbial carbon turnover in the sediment.

The minimum in sulfate concentrations is reflected in a minimum in magnesium concentrations, less radiogenic strontium and isotopically light calcium in the pore-water (Wehrmann et al., in press). We propose that magnesium was removed from the pore-water during carbonate precipitation and volcanic ash alteration which occurred in the former methanogenic zone. The latter process also released strontium with a less radiogenic isotope ratio and isotopically light calcium into the pore-water. The isotopic composition of pore-water calcium was additionally influenced by ammonium-calcium exchange on clay minerals (Wehrmann et al., in press).

Hard-lithified calcite-dolomite layers, and laminae of disseminated carbonate at 280-440 mbsf provide further insight into the diagenetic history of this site. These carbonates not only occur in association with the "high-productivity" interval between 2.58–2.51 Ma, but they document the frequent and episodic onset of higher organic carbon turnover rates and likely sulfate reduction coupled to AOM at a shallow SMTZ for short time periods (Wehrmann et al., in press).

Our studies represent new approaches to disentangle past and present biogeochemical processes in marine subseafloor sediments. With the help of the reaction-transport model we were able to hindcast the progression of the SMTZs and the duration of sulfate depletion, providing quantitative insight into the temporal geochemical evolution of this deep subsurface habitat. The careful assessment of the diagenetic mineral phases archived in the sedimentary record, and the concentration and isotope composition of pore-water calcium and strontium, additionally helped to unravel short time diagenetic changes and gave insight into additional processes linked to silicate alteration and element-exchange on clay minerals. We show that variations in biogeochemical processes in response to changes in oceanographic conditions, and a dynamic subseafloor biogeochemical zonation, also have to be taken into account at deep water sites such as U1341 for a global assessment of organic carbon burial fluxes, organic carbon remineralization, and marine carbonate burial.

References:
März C., Schnetger B., Brumsack H.J., 2013, Nutrient leakage from the North Pacific to the Bering Sea (IODP Site U1341) following the onset of Northern Hemispheric Glaciation? Paleoceanograpgy 28, 1–11, doi:10.1002/palo.20011.
Wehrmann L.M., Arndt S., März C., Ferdelman T.G., Brunner B., 2013, The evolution of early diagenetic signals in Bering Sea subseafloor sediments in response to varying organic carbon deposition over the last 4.3 Ma. Geochimica et Cosmochimica Acta 109, 175–196.
Wehrmann L.M., Ockert C., Mix A.C., Gussone N., Teichert B.M.A., Meister P., in press, Repeated occurrences of methanogenic zones, diagenetic dolomite formation and linked silicate alteration in southern Bering Sea sediments (Bowers Ridge, IODP Exp. 323 Site U1341). Deep-Sea Research II.

IODP

An integrated geochemical and cyclostratigraphic framework for the Eocene South Atlantic Ocean

T. WESTERHOLD[1], U. RÖHL[1], T. FREDERICHS[2], S.M. BOHATY[3], J.C. ZACHOS[4]

[1]MARUM – Center for Marine Environmental Sciences, University of Bremen, Bremen, Germany
[2]Fachbereich Geowissenschaften, University of Bremen, Bremen, Germany
[3]Ocean and Earth Science, University of Southampton, National Oceanography Centre, Southampton, SO14 3ZH, UK
[4]University of California, Santa Cruz, California, USA

For more than four and a half decades, scientific ocean drilling has successfully acquired composited drillcore material suitable for developing accurate astronomically calibrated timescales for the past 34 million years (Oligocene to Pleistocene) using high-resolution physical property, geochemical, magnetostratigraphic, and biostratigraphic records. For older time intervals (Cretaceous to Eocene), both the coverage and resolution of these datasets are still sparse, composed discontinuous records from numerous sites around the globe and characterised by a predominance of records from the Southern Ocean. High-resolution studies from multiple-hole cored sedimentary successions from the Atlantic (Ocean Drilling Program Leg 207, Demerara Rise; ODP Leg 208, Walvis Ridge) and the Pacific (ODP Leg 198, Shatsky Rise; ODP Leg 199 and Integrated Ocean Drilling Program Exp. 320/321, both East Equatorial Pacific) revealed spectacular new insights into climate dynamics of the Paleocene, early to middle Eocene, and Eocene/Oligocene Transition (EOT). Drillcores from these recent expeditions, however, have been underutilized for development of high-resolution, long-term stratigraphic and paleoceanographic proxy records through Eocene. Several bulk and benthic stable isotope records have been published from these sections at variable resolution indicating that a detailed reconstructed climate history requires a sampling resolution of 5 kyr and less to capture short-lived transient events and the full climate dynamics. Such studies have not been achieved yet for the Eocene in its entirety.

We have recently initiated a project aimed at establishing for the first time a complete cyclostratigraphic framework based on the identification of the stable long eccentricity cycle (405 kyr) for the entire Eocene (55 to 34 Ma) for both the Atlantic and Pacific Ocean. Our study will be focused on the development of high-resolution

XRF core scanning and paleomagnetic data with stable isotope records. This project is built on earlier projects and will both develop new records and synthesize large existing datasets to establish a fully integrated and astronomically calibrated bio-, chemo-, and magnetostratigraphy for the entire Eocene for the two major ocean basins, the Atlantic and Pacific. Here we present first data and preliminary interpretation of paleomagnetic and geochemical analysis from ODP Site 1263 (Leg 208, Walvis Ridge) covering the middle to late Eocene of the South Atlantic.

ICDP

Diffusional equilibration of distinct magmas aided by bubble ascent

S. WIESMAIER[1,2], D. MORGAVI[1], C. RENGGLI[3], D. PERUGINI[4], C. DE CAMPOS[1], K.-U. HESS[1], Y. LAVALLÉE[5], D. DINGWELL[1]

[1]Ludwig-Maximilians-Universität München, Earth and Environmental Sciences, Munich, Germany (sebastian.wiesmaier@min.uni-muenchen.de)
[2]Department of Physics (Geology), GEOVOL, University of Las Palmas, Gran Canaria, Spain
[3]Research School of Earth Sciences, Australian National University, Canberra ACT 0200, Australia
[4]Department of Earth Sciences, University of Perugia, Perugia, Italy
[5]School of Environmental Sciences, University of Liverpool, Liverpool, UK

Diffusional equilibration of compositional gradients in mingled magmas is a fundamental process for magmatic evolution. Detection of compositional gradients, or disequilibrium, in glassy volcanic rocks permits reconstruction of otherwise inaccessible processes in magmatic plumbing systems. Recently obtained drill cores from the Snake River Plain (SRP) show limited evidence for magma mingling, whereas older studies do have recorded a limited amount of outcrops where hybrid magmatic rocks have been found in the SRP [1]. At a viscosity contrast on the order of 10^4 Pa s between basaltic and rhyolitic SRP melts [2], efficent mingling is thought to occur under mechanical force (stretching and folding). As alternative mechanism, experiments with analogue materials demonstrated that ascent of bubbles from one magma into the other may play a role for mechanical mixtures of two distinct magmas [3]. Does this process play a role for SRP magmas?

Here, we experimentally investigated advection of basaltic SRP melt into a rhyolitic one by means of bubble ascent. At 1450 °C, bubbles were made to rise from basalt into overlying rhyolite, thereby dragging portions of basalt upwards. The resulting basaltic filaments, which resemble small plume tails in 3D, immediately commenced to equilibrate with the surrounding rhyolite, as shown by EMP analyses. At their most mafic composition in the centre, the resulting hybrid filaments are of dacitic to rhyolitic composition, sometimes trachytic. Filaments of basaltic composition have not been detected after an experimental run time of 3 hours.

Several qualitative indicators are evidence for multiple bubble ascent through the same pathway. Firstly, tomography shows single filaments that fan out into multiple smaller ones towards the bottom. Second, several bubbles are frozen in their path of ascent and appear to directly follow already existing filaments. Thirdly, this is consistent with values of concentration variance for individual filaments, which show that alkali elements Na and K homogenised efficiently, but are not correlated to filament thickness, counter to expected behaviour.

In-situ measurements of the compositional gradients surrounding the filaments have been employed for qualitative characterisation and to calculate diffusivities. From the experimental setup and the subsequent in-situ analyses, time, composition and distance along the gradient are known. The resulting diffusion coefficients are empirical and aid in comparison of distinct filaments and the understanding of the process of bubble advection. In theory, empirical diffusivities ought to be constant when compared to different filament thicknesses (all other variables being similar). Unsystematic variation of diffusivities, however, confirmed the notion that bubble-generated filaments can be complex structures, which experience intermittent replenishment of basaltic melt. The process of bubble ascent as mechanism for magma mixing may thus accelerate once a first generation of bubbles rose through the high-silica medium, creating lower viscosity pathways for subsequent bubbles.

References:

[1] Leeman, W. P. (1982). Evolved and hybrid lavas from the Snake River Plain, Idaho. In: Bonnichsen, B. & Breckenridge, R. M. (eds.) Cenozoic Geology of Idaho: Idaho Bureau of Mines and Geology Bulletin, 193-202.
[2] Morgavi, D., Perugini, D., De Campos, C. P., Ertl-Ingrisch, W., Lavallée, Y., Morgan, L. & Dingwell, D. B. (2013). Interactions between rhyolitic and basaltic melts unraveled by chaotic mixing experiments. Chemical Geology 346, 199-212.
[3] Thomas, N., S. Tait, and T. Koyaguchi (1993), Mixing of stratified liquids by the motion of gas bubbles: application to magma mixing, Earth Planet. Sci. Lett. , 115(1-4), 161-175.

ICDP

Effects of Anorthite on the phase relationship in granitic systems: Experimental calibrations for rhyolite geobarometry and application to Snake River Plain rhyolites

S. WILKE[1], C. KLAHN[1], D. MOCK[1], R. ALMEEV[1], F. HOLTZ[1]

[1]Leibniz Institute of Hannover, Institute for Mineralogy, Callinstraße 3, 30167 Hannover, Germany

General aim of the study

The Snake River Plain – Yellowstone (SRPY) volcanic system represents one of the best recent examples of hotspot volcanism, producing large amounts of bimodal – basaltic and rhyolitic – melts in the overlaying continental plate in the western US. Due to the shift of the plate over time, several large volcanic centers of highly silicic composition are distinguishable in time along the hotspot track. One of the goals of the ICDP proposal is to reveal the interactions between mantle hotspot and continental lithosphere. The rhyolitic magmas are formed as a result of these interactions and one of the problems is to constrain at which depth such interactions do occur and to which extend the depth of rhyolitic magma chambers change as a function of time and space along the hotspot track. Due to the high silica contents of the SRPY rhyolites, their mineral assemblage (e.g. two pyroxenes, Fe-Ti-oxides, two feldspars, Quarz) usually hosts no satisfying geobarometer. Amphibole, that could be used as a geobarometer, is absent (except for some of the youngest eruptions) because of the low water contents of the rhyolitic melts (less than 2.5 to 1.5 wt% H^2O, e.g. Almeev

et al., 2012). The experiments of Almeev et al. (2012) demonstrated that the effect of pressure on the silica content of cotectic rhyolitic melts (in equilibrium with quartz and feldspar) can be utilized as a geobarometer. However the effect of pressure (as well as water activity) on the composition of the cotectic melt is well calibrated in the ternary system SiO_2 – $NaAlSi_3O_8$ – $KAlSi_3O_8$ but for systems containing normative anorthite (An, $CaAl2Si_2O_8$). This project aims at determining the liquidus phase relationships in systems which are relevant for natural strongly water-undersaturated SRP rhyolites. The results would enable us to determine the storage depth of rhyolitic melts coexisting with quartz and at least one feldspar, a mineral assemblage which is often observed among SRP rhyolites.

Experimental outline

To create a robust dataset for pressure calibration, six experimental conditions where chosen to check for the shift of the eutectic point and cotectic compositions (when projected onto the ternary system SiO_2 – $NaAlSi_3O_8$ – $KAlSi_3O_8$) as a function of anorthite content of the melt, water activity and pressure. Our starting compositions host (1) 1.2 wt% H_2O and 3.5 wt% An, (2) 1.2 wt% H_2O and 7 wt% An and (3) 3 wt% H2O and 3.5 wt% An and the experiments are performed at 200 MPa and 500 MPa pressure. Starting glasses are created from oxide powders that are molten two times at 1600 °C under 1 atmosphere and afterwards pre-hydrated at 1200 °C in an internally heated pressure vessel (IHPV). These starting hydrous glasses are checked for their chemical composition by electron microprobe and for water content by infrared spectroscopy. The phase relationship experiments are performed in an IHPV at temperatures between 900 °C and 1050 °C. Oxygen fugacity is fixed close to QFM+0 and monitored by shaw-membrane during experiments. Although we apply techniques to enhance the nucleation of phases (e.g. finely ground powdered starting glass), the experimental duration is at least 7 days. This long duration is necessary to achieve near-equilibrium conditions in such highly viscous rhyolitic systems.

Preliminary results from this proposal

Ten months after the start of the project microprobe analysis of experimental products obtained at 200 MPa with starting materials (2) and (3) were performed as well as the analysis of some 500 MPa experimental products from starting material (2). The derived data do not yet allow the exact determination of all the eutectic point compositions but preliminary results show a significant increase of the quartz component in the presence of An at water-undersaturated conditions. The effect of pressure on the quartz component in systems containing An is comparable to that observed in the system SiO_2 – $NaAlSi_3O_8$ – $KAlSi_3O_8$.

Future objectives

As soon as the experimental calibration of the eutectic compositions will be at an advanced state, attempts will be made to apply the derived geobarometer to natural systems. Natural glasses coexisting with quartz anf feldspar collected from the ICDP drilling (kimberly core) and from other localities (cooperations with ICDP coordinators J. Shervais and E. Christiansen and with B. Nash) will be used to constrain pre-eruptive pressure. Glass inclusions in quartz and feldspar will also be analyzed. It is also planned to apply the thermobarometer Ti-in-Quartz (Huang and Audetat 2012) and to compare the data with the pressure estimated from the SiO_2 content in cotectic glasses. This thermobarometer may provide an additional tool for pressure determinations but there are still serious problems with its application (temperature and activity of TiO_2 need to be known). Our independent barometer may be usefull to calibrate the thermobarometer Ti-in-Quartz for natural high silica rhyolitic systems.

References:
Almeev, R. R., Bolte, T., Nash, B.P., Holtz, F., Erdmann, M., Cathey, H.E. (2012),High-temperature, low-H2O Silicic Magmas of the Yellowstone Hotspot: an Experimental Study of Rhyolite from the Bruneau-Jarbridge Eruptive Center, Central Snake River Plain, USA, Journal of Petrology 53 (9), 1837-1866
Huang, R., Audetat, A. (2012), The titanium-in-quartz (TitaniQ) thermobarometer: A critical examination and re-calibration, Geochimica and Cosmochimica Acta 84, 75-89

IODP

History of the Indian Monsoon recorded in Andaman Sea sediments

D.G. YIRGAW[1], E.C. HATHORNE[1], L. GIOSAN[2], T.S. COLLETT[3], M. FRANK[1]

1Helmholtz-Zentrum für Ozeanforschung Kiel (GEOMAR), Wischhofstr. 1-3, 24148 Kiel, Germany
2Woods Hole Oceanographic Institution, 360 Woods Hole Rd., Woods Hole, MA 02543, USA
3U.S. Geological Survey, Box 25046, MS-939 Denver, Colorado 80225, USA

The Asian monsoon is vitally important to billions of people while also posing a risk to human life through flooding. Despite the importance to so many the monsoon is difficult to predict and model while its evolution is not fully understood, making its future development in a changing global climate uncertain. Records of the East Asian monsoon have been generated from China and the South China Sea while past variability of the Indian Monsoon is mainly known from records of monsoon wind strength over the Arabian Sea. This project uses a unique long sediment core obtained by the IODP vessel *JOIDES Resolution* in the Andaman Sea to examine the past variability of the Indian monsoon revealing changes in continental weathering, runoff and precipitation on orbital timescales for the last 2 million years. Here we present new data examining variations during the last 60 kyrs with an age model constructed with 5 radiocarbon dates on planktonic foraminifera, benthic foraminifera oyxgen isotopes and the Toba ash layer.

The monsoon related influx of freshwater to the Bay of Bengal and Andaman Sea leads to a low salinity surface layer and a strong stratification of the upper 200 meters. Ocean atlas data (Antonov et al., 2010) indicate that this stratification is remarkably stable throughout the year while the salinity of the surface layer changes with the monsoon season. We utilise the depth habitat preferences of different foraminifera species to investigate the freshwater-induced stratification with paired Mg/Ca and $\delta^{18}O$ analyses of both *G. sacculifer* and *N. dutertrei*. Mg/Ca analyses suggest a 2 degree change in both the mixed layer and the thermocline temperature between the Last Glacial Maximum (LGM) and Holocene. Both *G. sacculfer* and *N. dutertrei* display a similar 2 ‰ glacial-interglacial change in $\delta^{18}O$ indicating relatively little change in the stratification of the water column during the last glacial and last deglaciation.

Additionally, we determined Mg/Ca temperatures and $\delta^{18}O$ of seawater from many single shells of *N. dutertrei* to

reconstruct past temperature and salinity conditions. Preliminary results of Mg/Ca results for thermocline dwelling *N. dutertrei* suggest little change in temperature variability during mid Holocene and LGM. Individual *N. dutertrei* $\delta^{18}O$ measurements reveal a large contrast between the mid Holocene and the core top and LGM samples. Samples from a nearby gravity core top and LGM samples exhibit a relatively small range although the absolute values differ mostly because of global ice volume changes. The mid Holocene individuals have a greater range of $\delta^{18}O$ values and a large skew toward more negative values indicating the greater influence of fresh water and strengthened monsoon. These data demonstrate the usefulness of individual shell analyses for the reconstruction of monsoon variability for intervals in the past.

References:
Antonov et al. (2010). World Ocean Atlas 2009 Volume 2: Salinity. S. Levitus, Ed., NOAA Atlas NESDIS 69, U.S. Government Printing Office, Washington, D.C., 184 pp.

IODP

Insight into the origins of SiO_2-rich magmas at mid-ocean ridges: Evidence from IODP Hole 1256D at equatorial Pacific

C. ZHANG[1], J. KOEPKE[1], M. GODARD[2], L. FRANCE[3]

[1] Institut für Mineralogie, Leibniz Universität Hannover, Callinstr. 3, D-30167 Hannover, Germany
[2] Géosciences Montpellier, CNRS, Université Montpellier 2, 34095 Montpellier, France
[3] CRPG, UMR 7358, CNRS, Universite de Lorraine, Vandoeuvre-le`s-Nancy France

The accretion of oceanic crust at mid-oceanic ridges is dominated by basaltic magmas which are derived by partial metling of mantle. However, SiO_2-rich magmas, although in a minor proportion, have also been observed, mostly as intrusions of so-called "oceanic plagiogranites" in the mid-crust, especially in the upper part of the gabbroic crust near the gabbro-dike transitions. The origin of these leucocratic lithologies has been controversially discussed for decades and remains an enigma. Previous models of formation of these rocks are mainly fractional crystallization of MORB and partial melting of altered crust, and combination of them. Here, we report the petrological and geochemical features of SiO_2-rich magmatic rocks recovered by drilling at IODP Hole 1256D (eastern equatorical Pacific), which has been performed via IODP multi-leg mission “Superfast Spreading Rate Crust”. The used samples were drilled by Expeditions 312 and 335. These in-situ data allow us to better constrain the origins invovling different endmember models in a quantitative way.

These SiO_2-rich magmatic rocks occur as dioritic-tonalitic centimeter-to-milimeter scale veins/dikelets intruding into background gabbros or sheeted dikes which were typically contactmetamorphicly convertet to the so-called "granoblastic dikes". They show largely varying textures and mineral assemblages and are divided into six types based on petrographic and geochemical criteria: (1) altered tonalite, (2) quartz-rich tonalite, (3) amphibole-rich diorite, (4) oxide-rich diorite, (5) pyroxene-rich diorite, and (6) ptchy plagioclase-rich leucocratic domains within gabbros. Collectivel, they have SiO_2 contents up to 71 wt% and MgO contents as low as 0.5 wt%, but with nearly constant K_2O content within 0.05-0.25 wt%. Except the altered tonalites which show distinctively high Al_2O_3 and Na_2O compared to other rock types, all groups generally show linear variation trends in major element plotted versus MgO except for TiO_2 and FeO^{total} . These oxides show a distinct peak at an intermediate MgO content. The general trend of major elements seems similar to a common crystallization trend of MORB, which is in aggrement with MELTS modeling (Ghiorso and Sack, 1995) using a primitive MORB composition with 0.1-0.5 wt% H_2O, but cannot fully explain many features of the trace element data. Generally, with increasing SiO_2 content, La/Yb and Eu/Eu* ratios increase slightly. The pyroxene-rich diorites are the most mafic rocks in the felsic series and thus similar with the gabbors in most major elements (such as high MgO and CaO contents), but the former show negative Eu anomalies and positve Zr-Hf anomalies which are in constrast to the gabbros. Although amphibole-rich diorites and oxide-rich diorites are clear different in petrography, their major and trace element compositions largely overlap with each other. Compared to other felsic rocks, the quartz-rich tonalites have charateristically high SiO_2 contents, strong enrichment in Zr and Hf but strong depletion in Ti.

In-situ mineral LA-ICP-MS analyses indicate that plagolcase in the quartz-rich tonalites generally have more enriched REE than other rock types, and amphibole in the quartz-rich tonlaites have enrichments in Nb and Ta but depletions in Zr and Hf relative to neighboring trace elements. Tiniate in the quartz-rich tonalites show much higher REE than those in the amphibole-rich diorites and the oxide-rich diorites, each of which exhibits different patterns in Nb-Ta, Zr-Hf and Eu anomalies. Quartz cathodoluminescence (CL) images reveal multiple generation/alteration stages, which implies reiterative penetrative fluid/melt activities concerning late magmatic evolution.

Comparison with modeled MORB differentiation trends and with compositions of melts produced by experimental hydous partial melting of sheeted dikes reveals that the various SiO_2-rich magmatic rocks recovered from the roof of the axial melt lens may be resulted from complicated mixing of differentiated MORB magmas and partial melts of altered sheeted dikes or gabbors with different mixing endmembers and ratios. The combination of the fast upward moving of axial melt lenses at fast-sprading mid-ocean ridges, and the rapid cooling by hydrothermal cicrulation might have triggered high-degree differentiation of gabbroic magmas and low-degree partial melting of hydrous prololiths, as well as immature mixing/assimilation which resulted in a large compositional range of SiO_2-rich magmas.

IODP

Rapid hydrothermal cooling at fast-spreading mid-ocean ridges: Evidence from intra-plagioclase diffusion in the granoblastic dikes of IODP Hole 1256D (equatorial Pacific)

C. ZHANG, J. KOEPKE, C. KIRCHNER, N. GÖTZE, H. BEHRENS

Institut für Mineralogie, Leibniz Universität Hannover, Callinstr. 3, D-30167 Hannover, Germany

Understanding the mechanism of crustal accretion at mid-ocean ridges requires information about magma generation, crystallization and cooling. According to the "gabbro glacier" model melt lenses sandwiched between the the lower oceanic crust and the sheeted dikes at fast-spreading mid-ocean ridges are the magma sources of crust formation (Detrick et al., 1987; Phipps Morgan and Chen, 1993). According to this model, the accretion of the lower oceanic crust requires fast and efficient cooling of the melt lens, resulting in partly crystallization of the melt lens, leading to cystal-melt mushes which may subside down to form the lower crust, a processes, which is believed to be controlled dominantly by hydrothermal circulation above the melt lens (Sleep, 1991).

In this study, we quantified the cooling rates above the melt lens, using the chemical zoning of plagioclase from former sheeed dikes, now recrystallized to the so-called granoblastic dikes in an contactmetamorphic aureole generated by the upmoving of a melt lens after repenishment.

These contactmetamorphic, hornfelsic horizon above the uppermost gabbros which are interpreted as part of the frozen melt lens system, were sampled from the Integrated Ocean Drilling Program (IODP) at Hole 1256D in the equatorial, eastern Pacific, where, for the first time, the dike-gabbro transition of an intact fast-spreading oceanic crust was penetrated (Expedition 312, 335). The measured zoning patterns should be a combined record of inter-zone diffusion processes during both on-ridge hydrothermal cooling and thermal conduction off-ridge cooling (Maclennan et al., 2005). While the off-ridge cooling is relatively easy to constrain and substracted mathematically from the total cooling contrution to the diffusion-induced element concentration patterns. We estimated the on-ridge cooling rate using a forward modelling approach based on CaAl-NaSi couple diffusion in plagioclase. The results show that the recrystallized sheeted dikes, which reached the peak contact metamorphism at 1000-1050 °C as heated by the underlying melt lens (Koepke et al., 2008), cooled to 700 °C within about 7-30 years as hydrothermal circulation proceeded accompanying the waning of melt lens, corresponding to a cooling rate of 10-50 °C/year. Two examples are shown below in Fig. 1, which corresponds two general types of zoning in plagiolcase.

The estimated cooling timescale is consistent to the decal fluctuation of melt lens (Mutter et al., 2008), and demonstrates a very efficient cooling effect of on-ridge hydrothermal circulation above the melt lens at fast-spreading mid-ocean ridges.

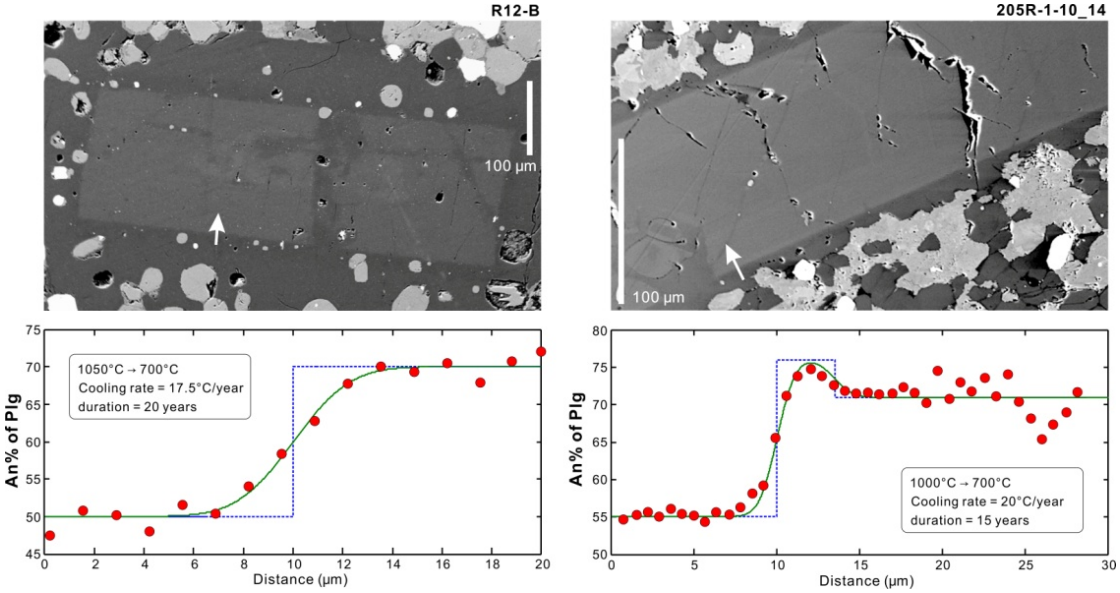

Figure 1. Two examples of concentration-distance profiles and modelling results for intra-plagioclase CaAl-NaSi couple interdiffusion. The measured An% contents along profiles (positions denoted as white arrows on back-scattered electron images) are shown as red dots. The best-fit final profiles after thorough cooling, including both on-ridge and off-ridge cooling, were calculated applying a finite difference equation and the diffusion coefficient for a hydrous condition detemined by Liu and Yund (1992), using estimated starting temepratures which have been estimated by two-pyroxene thermometry for individual samples. The diffusion coefficients

References:

Detrick, R.S., Buhl, P., Vera, E., Mutter, J., Orcutt, J., Madsen, J., Brocher, T., 1987. Multi-channel seismic imaging of a crustal magma chamber along the East Pacific Rise. Nature 326, 35-41.

Koepke, J., Christie, D.M., Dziony, W., Holtz, F., Lattard, D., Maclennan, J., Park, S., Scheibner, B., Yamasaki, T., Yamazaki, S., 2008. Petrography of the dike-gabbro transition at IODP Site 1256 (equatorial Pacific): The evolution of the granoblastic dikes. Geochemistry Geophysics Geosystems 9, Q07O09.

Liu, M., Yund, R.A., 1992. NaSi-CaAl interdiffusion in plagioclase. American Mineralogist 77, 275-283.

Maclennan, J., Hulme, T., Singh, S.C., 2005. Cooling of the lower oceanic crust. Geology 33, 357-366.

Mutter, J., Carton, H., Carbotte, S., Canales, J., Nedimovic, M., Newman, K., Marjanovic, M., Xu, M., Aghaei, O., Stowe, L., 2008. Searching for changes in AMC characteristics on the EPR using comparisons of reflection images obtained in 1985 and 2008, AGU Fall Meeting, pp. 0321.

Phipps Morgan, J., Chen, Y.J., 1993. The Genesis of Oceanic Crust: Magma Injection, Hydrothermal Circulation, and Crustal Flow. Journal of Geophysical Research 98, 6283-6297.
Sleep, N.H., 1991. Hydrothermal circulation, anhydrite precipitation, and thermal structure at ridge axes. Journal of Geophysical Research 96, 2375-2387.

IODP

Mid-Oligocene climate dynamics using benthic foraminifera from the Central Eastern Pacific Ocean

J. ZIRKEL[1,2], J.O. HERRLE[1,2], H. PÄLIKE[3], D. LIEBRAND[4] ,S. BATENBURG[1]

[1]Goethe-University Frankfurt, Institute of Geosciences, D-60438 Frankfurt, Germany
[2]Biodiversity and Climate Research Centre (BIK-F), D-60325 Frankfurt, Germany
[3]MARUM/Center for Marine Environmental Sciences, University of Bremen, D-28359, Bremen, Germany
[4]School of Ocean and Earth Sciences, University of Southampton, SO14 3ZH, United Kingdom

The Oligocene marks the onset of major Antarctic ice sheets and hence the first step into a "icehouse" world, which continues to the present day. To understand the evolution of the Antarctic ice sheet, it is fundamental to assess and quantify changes in the ocean circulation pattern and the intensity of Pacific equatorial upwelling (PEU) since the initiation of southern hemisphere ice caps during the Eocene-Oligocene transition.

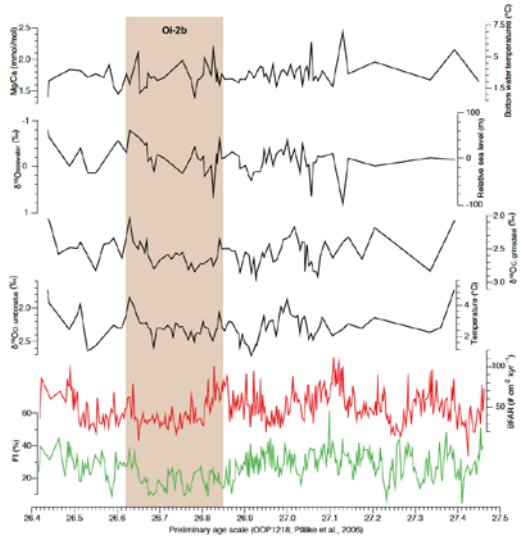

Figure 1. Preliminary Mg/Ca paleotemperatures, $^{18}O_{seawater}$ estimates and ^{18}O records of *O. umbonatus* and *C. grimsdalei* of Site U1334 plotted against BFAR and FI between 26.4 – 27.5 Ma. Estimated variation in $^{18}O_{seawater}$ composition, is calculated by substituting Mg-temperatures and benthic ´^{18}O of *O. umbonatus* data into ^{18}O paleotemperature equation. The brown interval indicates the duration of the Oi-2b maximum glaciation interval following (Wade & Pälike, 2004).

It is well known that combined variations in the eccentricity, obliquity and precession of Earth´s orbit influence long-term climate fluctuations, notably the build up and decay of ice volume. To unravel the importance of orbital forcing on ice volume changes and to estimate its impact on paleoproductivity in the Central Eastern Pacific Ocean, we focused on the Oi-2b event about 26.8 Ma ago, being the most important glacial episode in the mid-Oligocene (Pälike et al., 2006).

We calculated benthic foraminifer accumulation rates (BFAR) to reconstruct organic matter flux to the sea floor and hence surface water productivity. Furthermore, to assess and differentiate between changes in productivity and dissolution, a planktic foraminifera-based fragmentation index (FI) was calculated (Figs.1, 2).

BFAR values range between 16 and 217 NBF/cm^2/kyr (average: 65 NBF/cm^2/kyr). Increased BFAR indicate phases of higher supply of organic matter to the sea floor and thus enhanced surface water productivity. Our BFAR record indicates variable but generally lower productivity conditions during the glacial event compared to pre- and post-Oi-2b conditions. However, the transition into the Oi-2b event which is documented in heavier ´^{18}O of *Cibicidoides grimsdalei* (2.1 ‰ to 3.0 ‰) and *Oridorsalis umbonatus* (1.7 ‰ and 2.6 ‰) is characterized by a higher productivity, which is also supported by the assumption of increased productivity for the onset of Oi-2b based on ´^{13}C variations of planktic and benthic foraminifera from ODP Site 1218 (Wade & Pälike, 2004). The sample material is characterized by a good preservation which is documented in our FI record with constantly lower FI

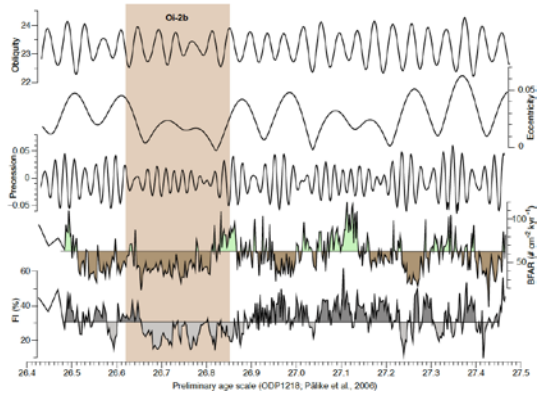

Figure 2. Preliminary benthic foraminifera accumulation rates (BFAR) and planktic foraminifera fragmentation index (FI) as an indicator for dissolution of the Oi-2b maximum glaciation event of Site U1334 of 26.4 - 27.5 Ma. Higher BFAR values indicate increasing organic matter flux to the sea floor and thus higher surface water productivity. Values <60 % of the FI are interpreted as an indicator for good preservation of the carbonate fraction (see detailed discussion in the text). Filters are shown for the precession, eccentricity, and obliquity cycles calculated from BFAR values using the time series analyzing tool AnalySeries 2.0.4.2. The Oi-2b glacial event falls within a low-amplitude of precession, obliquity and minimum eccentricity. BFAR indicating a higher variability of productivity as previously suggested for the Oi-2b interval (Wade & Pälike, 2004). The FI indicates a slightly better preservation of the carbonate fraction during the Oi-2b interval. The brown interval indicates the duration of the Oi-2b maximum glaciation interval following (Wade & Pälike, 2004).

percentages during Oi-2b. This assumption is also supported by the relatively high $CaCO_3$ content of >80 wt.% within the succession studied.

References
Pälike, H., Norris, R.D., Herrle, J.O., Wilson, P.A, Coxall, H.K., Lear, C.H., Shackleton, N.J., Tripati, A.K., Wade, B.S., 2006. The heartbeat of the Oligocene climate system. Science 314, 1894-1898.
Wade, B.S., Pälike, H., 2004. Oligocene climate dynamics. Paleoceanography 19, PA4019. doi:10.1029/2004PA001042.

IODP

Experimental approach to form anorthositic melts: phase relations in the system $CaAl_2Si_2O_8$ – $CaMgSi_2O_6$ – Mg_2SiO_4 at 6 wt.% H_2O

A. L. K. ZIRNER[1], C. BALLHAUS[1], R. FONSECA[1], C. MÜNCKER[1,2]

[1]University of Bonn, [2]University of Cologne

Massive anorthosite dykes are documented for the first time from the Limassol Forest Complex (LFC) of Cyprus, the LFC being a deformed equivalent of the Troodos ultramafic massif. Both the Troodos and LFC complexes are part of the Tethyan realm consisting of Cretaceous oceanic crust that formed within a backarc basin 90 Ma ago and was obduced during late Miocene.

From crosscutting relations with the sheeted dyke complex, it follows that the anorthosites belong to one of the latest magmatic events on Cyprus. In hand specimen, the rocks appear massive and unaltered, although in thin section magmatic plagioclase (An93) is partially replaced by albite and thomsonite (zeolite). Where magmatic textures are preserved, plagioclase forms cm-sized, acicular, radially arranged crystal aggregates that remind of spinifex textures. Six major types of anorthosite occurrences have previously been described, none of them matching with the above described anorthosite dykes [1]. The origin of these anorthosite dykes remains poorly understood. Even though they occur as intrusive dykes, it is evident that they cannot represent liquidus compositions, at least under dry conditions. Whole-sale melting of pure An93 would require temperatures in excess of 1450 °C, which is a quite unrealistic temperature of the modern Earth's crust.

The working hypothesis is that boninitic melts with approximately 4 wt.% H_2O, as found in the cyprian upper pillow lavas (UPL), could produce such rocks by olivine-pyroxene fractionation. Indeed, experiments indicate that such lithologies can be generated by medium-pressure fractional crystallization of hydrous basaltic melts followed by decompression-degassing. High pH_2O stabilizes olivine but tends to suppress plagioclase as the highest polymerized phase. Hence the An component is accumulated in the (late-stage) melt. When such a system experiences sudden decompression, the aqueous phase will exsolve and will trigger massive precipitation of anorthite.

Experiments at various temperatures are being performed in the ol-cpx-plag-H_2O system, with olivine from a xenolith (Fo95) and anorthite and diopside glasses as starting materials. The materials are ground and mixed in the desired proportions, then equilibrated with 6 wt. % H_2O at 0.5 GPa total pressure in a piston-cylinder press. A phase diagram of the Fo-Di-An-H_2O system at 0.5 GPa will be constructed to outline the precise phase relations and fractionation paths are high H_2O partial pressure. Aim is to delineate the anorthite saturation field in the ol-cpx-plag-H_2O system, and to assess to which extent plagioclase can be suppressed as a liquidus phase when a basaltic melt fractionates under hydrous conditions.

References:
[1] Ashwal, L. D. (1993). Anorthosites, Springer-Verlag.

IODP

Carbonates and zeolites in seamounts trace seawater-basement interactions: results from IODP Exp330, Louisville Smt. Chain

S. RAUSCH[1], W. BACH[1], A. KLÜGEL[1]

[1]Geoscience Department, University of Bremen, Germany; srausch@uni-bremen.de / wbach@uni-bremen.de / akluegel@uni-bremen.de

Seamounts emerge above the abyssal plains and are therefore less covered with sediments, which allows for prolonged seawater circulation (Fischer et al., 2003). To examine the importance of seamounts for seawater-crust chemical exchange and CO_2 uptake (Alt and Teagle 2003; Bach et al., 2003), we sampled void and fracture fills from IODP cores from the Louisville seamount chain (IODP Expedition 330), which is located on the Pacific plate north east of New Zealand (Koppers et al., 2012). These samples from four seamounts aged between 50 and 74.2 Ma comprise carbonates (calcite, aragonite, siderite and Fe-/Mn-rich calcite) and minor zeolites. The chemical and isotopic composition of these phases was used to trace seawater circulation through the oceanic lithosphere and associated ocean-basement exchange.

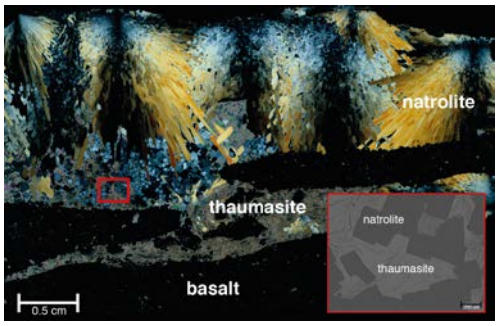

Fig. 1: Thin section image (polarized light) of a void-filling zeolite (natrolite) and a cement (thaumasite), hole U1374A.

Formation temperatures of carbonates were calculated from oxygen isotopic ratios and range between 2.2 and 18.4 °C. A slight downhole increase in temperature is indicated by carbonates from Holes U1372A (74.2 Ma, depth 232.9 m below seafloor (mbsf)) and U1376A (64.1 Ma, depth 182.8 mbsf). Samples from Hole U1374A (70.7 Ma, depth 522 mbsf) show temperatures from 3.0 to 9.7 °C with no systematic downhole trend. Carbonate-cemented volcanic breccias of Holes U1372A and U1374A have Sr isotopic values that indicate precipitation shortly (up to a few million years) after seamount formation. In contrast, samples from younger seamounts (Sites U1376 and U1377; 50.0 Ma) show evidence for precipitation from seawater-derived fluids that had exchanged Sr with the basement. Highly variable extents of fluid-basement interaction are also shown by the REE+Y concentrations of carbonates. Carbonates from the oldest seamounts (Holes U1372A, U1374A) are

characterized by negative Ce-anomalies and positive Y-anomalies, pointing to precipitation from pristine seawater. In contrast, the two younger seamounts (Holes U1376A and U1377A, B) show REE patterns that lack these seawater signatures and show subtle positive Eu anomalies, indicative of enhanced exchange with basement.

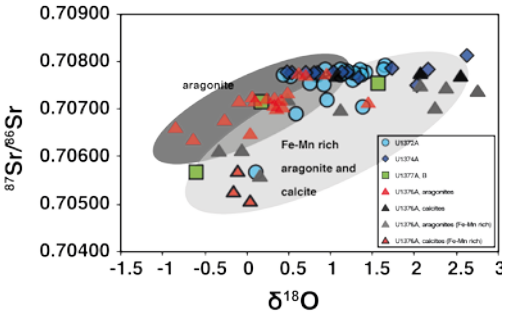

Fig. 2: In a Sr isotope ratio versus ^{18}O diagram the calcites and aragonites samples indicate two groups (dark grey field for "pure" aragonites; light grey field for Fe-Mn rich aragonite and calcites).

The magnitude and direction of elemental exchange seems to be strongly controlled by temperature. The isothermal gradient displayed by carbonates from Hole U1374A may suggest recharge of cold seawater deep into the basement, making the seamount a possible paleo-seawater-recharge site down to > 350 mbsf. From 350 to 522 mbsf in Hole U1374A, carbonates give way to low-temperature zeolites (gmelinite, tetranatrolite, phillipsite) and thaumasite as void-filling material in lithologic units with higher abundance of intrusive sheets and hyaloclastites (Fig.1). These minerals are interpreted to form at temperatures below 100 °C. The zeolites were characterized for their major and trace element contents (microprobe and LA-ICPMS) to obtain information about the fluid from which they precipitated. It can be shown that the Sr and Pb content is elevated in the gmelinite sample (up to 70 ppm and 3 ppm, respectly). Transition metals such as V, Cr, Cu and Zn reach concentrations of up to 1ppm. The REE element contents are very low in most zeolite samples (up to 0.5 ppm for the light REE, up to 0.1 for the heavy REE, many were below the detection limit of ca. 0.02 ppm). Nevertheless, the respective REE spectra (especially from analcime) provide relevant information, showing no seawater signature anymore but a rather basement-dominated pattern with flat LREE and a decrease towards the HREE and a positive Eu-anomaly.

Thaumasite, on the other hand is abundant as cementation phase in breccias from the lowermost section of Hole U1374A. It seems to be the last mineral to have crystallized during intense alteration of the volcanic hyaloclastites. Thaumasite is a hydrated Ca-Si carbonate sulfate hydroxide and is often found in association with low-temperature zeolites.

In general, a relatively rapid precipitation of carbonate in the seamount at Hole U1374A may have sealed the upper volcanic basement (upper 300 mbsf) and facilitated the development of closed-system circulation of slightly warmer and more evolved fluids in greater depths. In contrast, linear downhole decrease in $\delta^{18}O$ observed in carbonates from Holes U1372A and U1376A suggests roughly steady-state thermal gradients of 50°C/km, corresponding to a conductive heat flow of around 150 mW/m^2.

The most common carbonate species in Hole U1376A is aragonite (50 to 70 mbsf), followed by Fe- and Mn-rich (up to 4000 ppm) calcite and aragonite (70 to 170 mbsf) and calcite (3 to 45 mbsf). The latter veins are found extending up into the sediment cover. Additionally, sediment was lying above a massive white coralline algal boundstone, which separated the calcite from the other carbonate veins.

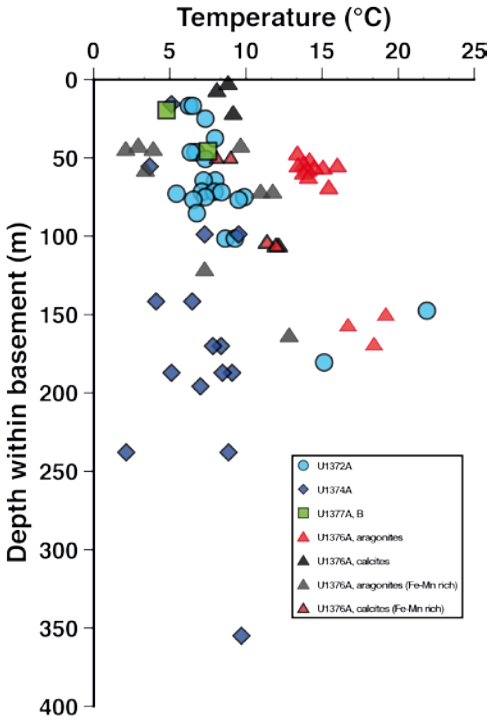

Fig. 3: Carbonate formation temperature calculated from ^{18}O values for calcites and aragonites versus depth within basement.

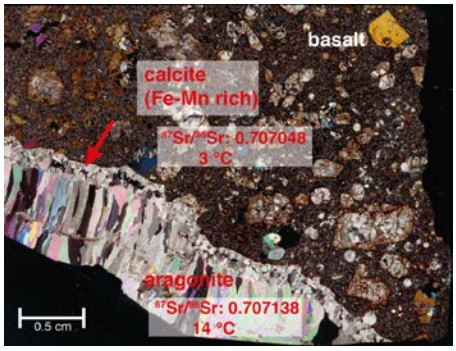

Fig. 4: Thin section image (polarized light) of a void-filling carbonate (calcite, aragonite) from core U1376A-7-2.

Unlike the other carbonate veins, the calcite samples show Sr isotope, $\delta^{18}O$ and $\delta^{13}C$ values pointing to a precipitation from seawater, which is further supported by a weak negative Ce anomaly are. In contrast, all other samples from Hole U1376A show enhanced exchange with the basement rocks. Aragonites and Fe-Mn rich carbonates seem to fall into two slightly different groups. In a diagram of $^{87}Sr/^{86}Sr$ versus $\delta^{18}O$ both groups show a similar positive correlation between $^{87}Sr/^{86}Sr$ and $\delta^{18}O$ (Fig. 2). These two groups are also indicated in a temperature versus basement depth plot (Fig. 3).

The larger-scale downhole mineralogical and geochemical differences are also displayed on the scale of a single vein. For example, in sample U1376A-7-2 (Fig. 4) we investigated a zoned vein, with a Fe-Mn rich calcite rim adjacent to the basalt host rock and a larger aragonite zone in the middle of the vein. The calcite is more radiogenic ($^{87}Sr/^{86}Sr$ = 0.707048) and heavier in $\delta^{13}C$ (-0.78 permil) than the aragonite ($^{87}Sr/^{86}Sr$ = 0.707138; $\delta^{13}C$ = -3.17 permil). The calcite precipitated from a colder fluid (ca. 3 °C), whereas aragonite formed at warmer temperatures (14 °C).

The carbonate and zeolite archive in the Louisville seamount chain provides new insights into the complex multi-stage seawater-basement exchange during ageing of the seamount basement. Our data indicate a pivotal role of temperature and volcanic facies in mediating the intensity of exchange between basement and circulating seawater.

References:

Alt, J.C. and Teagle, D.A.H. 2003. Hydrothermal alteration of upper oceanic crust formed at a fastspreading ridge: mineral, chemical, and isotopic evidence from ODP Site 801. Chemical Geology, 201:191-211.

Bach, W., Peucker-Ehrenbrink, B., Hart, S.R. and Blusztajn, J.S., 2003. Geochemistry of hydrothermally altered oceanic crust: DSDP/ODP Hole 504B – Implications for seawater-crust exchange budgets and Sr- and Pb-isotopic evolution of the mantle. Geochem. Geophys. Geosys., 4(3): 10.1029/2002GC000419.

Fisher, A. T. et al., 2003. Hydrothermal recharge and discharge across 50 km guided by seamounts on a young ridge flank. Nature, 421: 618-821.

Koppers, A. A.P., Yamazaki, T., Geldmacher, J., Gee, J. S., Pressling, N., Hoshi, H., at al. 2012, Limited latitudinal mantle plume motion for the Louisville hotspot. Nature Geoscience, 5: 911-917.